Strains in concrete beams subjected to climatic conditions similar to those of central Saudi Arabia

Rawaf, Abdallah Saad

STRAINS IN CONCRETE BEAMS SUBJECTED TO CLIMATIC CONDITIONS SIMILAR TO THOSE OF CENTRAL SAUDI ARABIA

By

ABDALLAH SAAD RAWAF

Master of Science

Stevens Institute of Technology

A thesis submitted for the Degree of Doctor of Philosophy

The Department of Engineering

University of Durham

June, 1985

To Hoda and Hadeel

Summary

The behaviour of reinforced and prestressed unsealed, partly sealed and fully sealed concrete beams was observed. Measurements of surface strains and of internal temperatures were recorded during daily cycles of imposed environmental conditions which modelled the summer and late spring climate of central Saudi Arabia. The boundary values for the temperature regimes modelling both summer and late spring were predicted using a finite element package with data appropriate to central Saudi Arabia.

Part of the experimental work reported here is concerned with comparing the elastic and creep deformations of reinforced beams subjected to daily cycles of raised temperature and low humidity values prior to loading with beams subjected to similar cycles after loading. It was found that diurnal environmental cycles imposed prior to loading reduced elastic deformation of partly sealed beams, but increased it for unsealed beams. On the other hand creep deformation of both partly sealed and unsealed beams was reduced when the daily cycles were imposed prior to loading.

The second part of the experimental work is concerned with investigating the effects of sealing on the elastic and creep deformations of beams.

It was found that sealing conditions had a marked influence not only on the elastic and final creep values but also on the chronological development of creep. Further the elastic and creep deformations of these beams were compared to elastic and creep deformations of all beams exposed to normal laboratory conditions. It was found that although early-age creep was significantly higher for beams subjected to cyclic temperature and humidity values, later creep values were either about equal or less than the comparable values for beams exposed to normal laboratory conditions.

Creep curvature values are compared with predicted values from the rate of creep method based upon specific thermal creep values and a step by step approach.

Correlation between measured and computed curvature was acceptable, even though the comparison between the various beams showed that the relation between temperature, humidity and creep is more complex than the simple assumption upon which this method is based.

Measured curvature due to the daily thermal cycle is compared to predicted curvature values using an iterative method based on the equilibrium of forces and moment change through the cross section. Close correlation was achieved by the use of an uncracked beam analysis to both uncracked and cracked beams. It was found that the correlation was dependent primarily on the coefficient of thermal expansion used in the analysis.

Finally, the behaviour of unsealed and partly sealed prestressed beams subjected to the daily environmental cycles has been observed and compared with behaviour of prestressed beams exposed to normal laboratory conditions. It was found that the loss in prestress force in beams subjected to these cycles was only marginally greater than the loss in prestress force in beams exposed to normal laboratory conditions.

ACKNOWLEDGMENTS

The author is indebted to Dr. A. R. Selby under whose supervision this research was conducted, for his most invaluable help, concern, and guidance throughout the course of this thesis.

Sincere thanks are extended to all workshop staff and laboratory technicians, in particular to Mr. B. Rosscamp, Mr. B. Scurr, T. Brown and F. Emery.

Finally the author wishes to thank King Saud University, Riyadh who sponsored his studies in this country.

CONTENTS

Page

Basic Notations

A = cross-sectional area

A_s = cross-sectional area of reinforcement

b = width of the section

c = specific thermal creep

d = Effective depth of section

E_c = Elastic modulus of concrete

E_s = Elastic modulus of steel

F_{CM} = modulus of rupture

h = thickness of section

h_c = convection heat transfer coefficients

I_C = moment of inertia of cracked

I_{uc} = moment of inertia of uncracked transformed section

K = thermal conductivity

L = Span between supports

M_{cr} = cracking moment

M^{max} = maximum moment ever put into the section

S_y = stress at layer y from origin

t_s = temperature of steel

$\bar{y}$ = vertical distance of centroid from origin

y_s = distance of steel from origin

ε = strain in general

σ = stress

α_c = coefficient of thermal expansion of concrete

α_s = coefficient of thermal expansion of steel

$\emptyset$ = creep coefficient

ρ = density

$[N]$ = linear shape function

$\{T\}$ = column vector

$[M]$ = square symmetric thermal mass

$[S]$ = square symmetric thermal condutivity

$\{Q\}$ = Vector heat fluxes which enter the structure at the nodes

$[\ ]^T$ = transpose matrix

$[B]$ = a matrix consisting of the first derivatives of the element shape functions

CHAPTER 1

INTRODUCTION

1.1 General

A large number of constructional activities in the past two decades involving concrete as the building material have taken place in the Middle East, particularly in the Arabian Peninsula using on the whole knowledge of concrete technology which already exists in the developed countries. Many concrete structures in the region however tend to deteriorate more rapidly than in temperate climates.

For example out of 42 recently surveyed concrete structures in the eastern province of Saudi Arabia with an age span of 15 to 20 years only eleven showed slight or no deterioration.(1)

The decrease in durability of concrete structures in the Arabian Peninsula could be attributed to several factors such as the quality of mix materials (aggregates, cement, water), the environmental conditions, design and detailing and the level of skill of workmanship.

The effects of the severe climatic conditions upon the durability of concrete are not fully understood, and further study is desirable.

The climate in the Arabian Peninsula can be divided into two categories:-

1. Hot and humid climate on the coast
2. Hot and dry climate, mainly inland.

The mean annual temperature is about 28°C. The shade temperature can exceed 50°C in the summer, with inland being on average hotter than on the coast. It can fall to 3°C near the coast and below zero inland.

Relative humidity averages 50% in summer and 70% in winter near the coast, and 30% in summer and 50% in winter inland.

High temperature can occur in many parts of the world, and there are some brief guidelines published in different countries dealing particularly with recommendations on placing of concrete during hot weather (2,3). Some specify a limit at which concrete can be placed. For example, the Institution of Civil Engineers,(4) U.K., recommend a limit of 32°C, and Brooks (5) quotes the U.S. Corps of Engineers as stating that all concrete placed during warm weather shall be delivered to the forms at the coolest temperature practicable but in any case not above 29°C. Some contracts had a clause specifying the maximum temperature of placing. For example, a maximum temperature of 32°C was specified for the temperature of concrete placed during a recent construction of a canal in Pakistan (5).

Rosenström (6) reported on his experience in the use of concrete in the salvage of ABU Simble Temples operation at Nubia desert in Egypt. The temperature during construction at the location occassionally exceeded 50°C with low humidity in the range of 10-20%. Faced with this he reported that the contractor had to go through an elaborate scheme in order to lower the temperature of the placed concrete by cooling both the aggregate and the mixing water.

In recent years there has been a number of published works (6-13) dealing with some aspects relating to concrete and concrete structures in hot climates which grew out of the recently gained experience of various international agencies working in these regions. However, these works, few as they are, deal mainly in a descriptive way with the short term aspects of cooling and curing concrete in the unique environmental conditions involved. There is a shortage of essential data about the behaviour of mature concrete and concrete structures under these conditions. Of particular importance, for example,are data relating to

the shape and magnitude of the temperature distribution within concrete roads, bridges and building elements when subjected to the high solar radiation present in hot climates, and stresses resulting from the gradient of these temperatures. For example, the recent failure of the not yet completed bridge (14) around Riyadh City, Saudi Arabia which involved a loss of around 100 million pounds is believed to be caused by stresses developed as a result of the nonlinear temperature distribution.

Another important area of research is to quantify the effects of the high temperatures when coupled with low humidity values on the long term behaviour of concrete structures.

1.2 Effects of Temperature

There exists a large body of literature dealing with the short and long term effects of high temperature on material and structural behaviour of concrete and concrete structures, particularly on the fire resistance (15) of concrete, and more recently its effects on prestressed concrete vessels. In nuclear pressure vessels the temperature can rise to around 400°C (16) which is maintained at steady gradient.

Another example occurs in the use of North sea oil storage cells which are subjected to cyclic temperature gradients with the inside face alternating between 50°C and 5°C while the outside may be at a steady 5°C (Clark)(17).

Temperature effects on structures due to severe climatic conditions are manifested in two respects. Non-linear temperature gradient through the structure leads to thermal stresses, and the long term redistribution of stresses in both statically determinate and indeterminate structures. Also the average temperature and temperature gradient of the concrete element may affect the short and long term performance of the concrete structure, if the element is partly restrained.

Some recent bridge failures in several countries (18) due in part to the stresses from nonlinear temperature distributions have prompted research into the effects of the nonlinear temperature distributions in several countries.

In the U.K. much of work was done by Emerson and others (19-29) on measurement and prediction of the temperature distributions caused by environmental conditions and stresses created by these distributions on concrete bridges and roads.

However the temperatures involved are generally less than temperatures observed in the Arabian Peninsula and thus the methods and conclusions arrived at cannot be used for these conditions. Further the influence of temperature on the structural properties of concrete is critically dependent on the moisture content and distribution in concrete (which is greatly influenced by the values of the environmental humidity) at the time of heating.

The moisture content has a marked influence on the thermal properties of concrete also. Hence a concrete member in which moisture is free to evaporate behaves very differently to concrete sealed against moisture loss.

1.3 Effects of Relative Humidity

Less has been published on the effects of relative humidity on concrete and concrete structures than on temperature effects. Changes in relative humidity affect the rate of drying of concrete. Shirley (3) reported that a decrease in relative humidity from 90% to 50% without change in any other weather condition, will increase fivefold the rate of evaporation of water from unprotected concrete. This effect is greatly

increased by an increase in temperature. ACI-305 (2) gives a table listing temperatures with minimum humidities below which concrete should not be placed. For example, at a temperature of 42°C, the humidity should not be below 90%.

Relative humidity affects greatly the long term deformation of concrete. Both drying shrinkage and drying creep values are increased by decrease in relative humidity values, although the relation is not linear. de La Pena (30) found that shrinkage values increased by six times for thin mortar specimens when the humidity values were dropped from 100% to 50% and that they only increased 1.23 times when the humidity was dropped from 50% to 10%.

1.4 Objective of the project

From the foregoing discussions and the cited experimental data it is clear that the need exists for investigation of the immediate effects of the nonlinear temperature distribution due to the solar radiation present in Central Saudi Arabia, and the effects of elevated surface temperatures coupled with low humidity values on the long term behaviour of concrete structures.

This project attempts to address these two points.

1.5 Overall Planning of the Project

Two possibilities were considered at the outset. One was to test the variation of several parameters (such as mix design, water cement ratio, type of aggregate etc.) under higher than normal temperature and low humidities values involving a large number of small specimens. The other was to conduct tests on structure - like models involving a limited number

of parameters. While small specimens can give reasonable information about concrete material properties such as strength, elasticity, their use in the prediction of the long term deformation is limited by the many factors involved, particularly the effect of the environmental conditions on the moisture movement and content which is related to the size and shape of the specimen. Thus it was decided to conduct tests on structure - like beams of 100mm x 200mm x 2800mm in dimension. This size was dictated partly by the practical limitation on the maximum transferable weight and partly by the size of the testing chamber.

The only parameters considered in the work were variable temperature and humidity regimes. Two environment conditions were chosen, one producing the maximum overall average temperature (thus representing summer) and the other producing the maximum temperature gradient through the section (thus representing late spring). Humidity variation as a boundary condition was studied through its effects on unsealed and partly sealed beams. Subsequently their behaviour was compared to the behaviour of completely sealed beams.

Two further 100mm x 200mm x 1000mm beams were cast with every test serving as shrinkage companions for the loaded beams, thus making it possible to separate creep effects from shrinkage effects.

Measurements of surface strains and of internal temperature were recorded during enforced environmental conditions which modelled the spring and summer climate of central Saudi Arabia.

CHAPTER 2

LITERATURE REVIEW

2.1 Review of the literature pertaining to the non-linear differential temperature distributions and temperature induced stresses in concrete bridge structures

A large body of literature has accumulated in the past twenty years dealing with measurements and predictions of the non-linear temperature distribution due to the solar radiation and stresses induced by these temperatures.

Here a short review is made of research pertaining to these two phenomenon.

2.1.1 Temperature distribution

There are basically two approaches for the prediction of temperature distribution inside a concrete section. The first one is concerned with the solution of the transient thermal equation:

$$\frac{K}{\rho c}\left(\frac{\partial^2 T}{\partial x^2} + \frac{\partial^2 T}{\partial y^2} + \frac{\partial^2 T}{\partial Z^2}\right) = \frac{\partial T}{\partial t} \qquad \ldots.2.1$$

where K is conductivity, ρ = density, C = specific heat.
T = temperature, x, y and Z = rectangular co-ordinates, t = time.

Since heat that flows through the depth of the beam is much greater than in the other two directions, eq.2.1can be reduced to a one-dimensional equation with its boundary conditions of the form:

$$\frac{K}{\rho c}\left(\frac{\partial^2 T}{\partial Z^2}\right) = \left(\frac{\partial T}{\partial t}\right) \qquad \ldots..2.2$$

As early as 1957 Barber (31) developed equations relating weather factors to maximum pavement temperature. Later Zuk (32) developed coefficients for use in Barber's equation for calculation of the maximum bridge surface temperature for two conditions in the Middle Atlantic states. The equations he used are of the form:-

$$T_m = T_a + 0.18L + 0.667(0.5\ T_r + 0.054L)$$

and $T_m = T_a + 0.027L + 0.65(0.5T_r + 0.081L)$

For normal concrete and bitumen covered deck respectively where

T_m = maximum surface temperature, in degrees °F

T_a = average daily air temperature, in degrees °F

T_r = daily range in air temperature, in degrees °F

L = solar radiation received on a horizontal surface w/m^2

Zuk also developed an approximate relation between top and bottom temperatures

$$\Delta T_m = T_m - \lambda T_r$$

where λ is a factor indicating the phase lag between the maximum surface temperature and the maximum ambient air temperature.

Then applying Carslaw and Jaegor's (33) solution of eq.2 as it applies to the special case for periodic temperature states on an infinite plate, Zuk developed equations relating the surface temperatures to the internal temperatures of the section. His theoretical results were within 10% of his experimental results.

Kehlbeck (34) in Germany observed that the atmospheric conditions acting on a structure could be approximated in terms of periodic functions. Thus by applying the property that harmonic boundary conditions yield harmonic functions, he developed a solution to eq.2.1 However his method is too impractical for most cases where much easier approximate methods are available. These approximate methods are the solution of eq.2.1 (in one or two dimensions) numerically by either the finite difference or the finite element methods.

Considerable research was done in the Transport and Road Research Laboratory in measuring and predicting temperature distribution in bridges and the overall range of temperature governing the longitudinal movement (19-28).

E merson (19) used the finite difference method to calculate the distribution of temperature in bridges. She divided the section into several layers, and assumed a starting time at which the governing external boundary conditions are applied. She assumed that the minimum temperature is most likely to occur at 05.00 $\pm$ 1 hour and the maximum temperature at 15.00 $\pm$ 1.

Further she assumed that the variation of temperature between these times is represented by a straight line. From experimental measurements she found that the minimum temperature gradient through the depth of the section occurs at 0800 $\pm$ hour, and 1600 for the heating and cooling phases respectively. By interpolation she found the temperature at these two times.

The disadvantage of Emerson's method was that it applies only to homogenous bridge decks. That is it does not allow for surfacing. However in a later report (21) she made some modification to the parameters used in the calculations. while still considering the surface/concrete

layered system as a homogenous concrete system. The values she obtained for various thicknesses of surfaces were in good agreement with measured values.

A formulation which considers two layers with different thermal properties was developed by Hunt and Cooke (35) using the finite difference method with Crank-Nicholson implicit scheme to solve the following equation

$$K_i \frac{\partial^2 T}{\partial 2} = \rho_i c_i \frac{\partial T}{\partial t} \quad i = 1,2$$

where the boundary conditions upon both top and bottom surface can be put in the form:

$$K_j \frac{dT}{dh} + h_i (T - T_s) = \alpha_i F_i (t) , i = 1,2$$

in which h_i = coefficient of surface heat transfer. $T_s(t)$ = shade temperature of the ambient air. α = absorptivity ($0< \alpha <1$) and $F_i(t)$ is the normal component of heat flux entering the bridge through the surface. The normal derivative has the value $\frac{dT}{dn} = - \frac{\partial T}{\partial y}$ and $\frac{dT}{dn} = \frac{\partial T}{\partial y}$ upon the top and bottom surfaces. respectively.

Boundary conditions at the inteface between the top and bottom layer require that both the temperature and heat flux be continuous across the interface thus

$T_+ = T_-$ upon the top and bottom side of the interface, respectively. And

$$K_1 \frac{\partial T}{\partial y}^+ = K_2 \frac{\partial T}{\partial y}^-$$

This equation results in discontinuity in temperature gradient at the interface unless $K_1 = K_2$.

Hunt and Cooke compared their results to those obtained experimentally by Priestley from a model box girder bridge. Good agreement was obtained. However Priestley (36) and Thurston indicated that good agreement was to be expected since experimental and theoretical deck temperatures were constrained to be the same values and the values of $\frac{K}{\rho c}$ and $\frac{h}{k}$ were assumed and not measured.

In TRRL 702 Jones (28) described a computer program to calculate the temperature distribution using Emerson's equations. However. because of the complexity of radiation at dusk and dawn. it cannot be used to cover a 24 hour period. Also it does not take into account the shape of the cross-section of a deck. unless the shape can be approximated to thick - thin slabs, box section, or any combination of all three.

More recently many researchers (37,38,39) have used the finite element method in the solution of the transient thermal equation (eq2.1) as it applies to concrete in two dimension for various boundary conditions. They obtained good correlations between measured and predicted temperature distributions.

Another approach is a simplified temperature depth approach for the temperature distribution. Priestley (40) compared the temperature distributions from tests carried out at the Ministry of Works at New Zealand and other available data at the time with power law temperature distribution of the form

$$t_y = T^n_y / d^n$$

where n is equal to 2,4 or 6. He found that the sixth-order curve represented the best fit for the available data. Later however Priestley (41) proposed a revised temperature distribution for New Zealand conditions consisting of a fifth power temperature decrease from a maximum T at the concrete deck surface to zero at a depth of 1200mm and a linear increase in temperature over the bottom 200mm of the section. BS5400 (42) gives a temperature-depth distribution which consists of a bi-linear section at the top and a linear distribution at the soffit as a simplification of Emerson's measured curves. Figure 2.1 gives a comparison of various temperature-depth distributions and Emerson's finite difference

Besides these basic approaches, Hambly (43) attempted to predict temperature distribution by assuming that the top and bottom surface temperatures are known and considering the temperature distribution inside the deck as a superposition of a steady state average heat flow between top and bottom surfaces and an hourly changing variation near the surfaces, by assuming that the surface temperatures changed sinusoidally with the time of the day. He used an equation given by Ingersoll for the temperature distribution within a large body which has a plane surface subjected to a temperature varying sinusoidally with time. The equation is of the form.

$$\Delta T = \hat{\Delta T} \exp(-x \, (y/2K)^{\frac{1}{2}} \sin (yt - x \, (y/2K)^{\frac{1}{2}})$$

where x = depth below surface. t = time. K = diffusivity of material = $\frac{K}{\rho c}$, k = conductivity. ρ = density. c = specific heat, y = diurnal frequency = $2\pi/24 \; ht^{-1}$

He further indicated that this equation can be used for slabs thinner than 600mm. For thin slabs he suggested drawing two curves for top and bottom which will overlap. and then drawing a third curve between the envelope and the sum of the two curves. This curve represents the design curve for thin slabs.

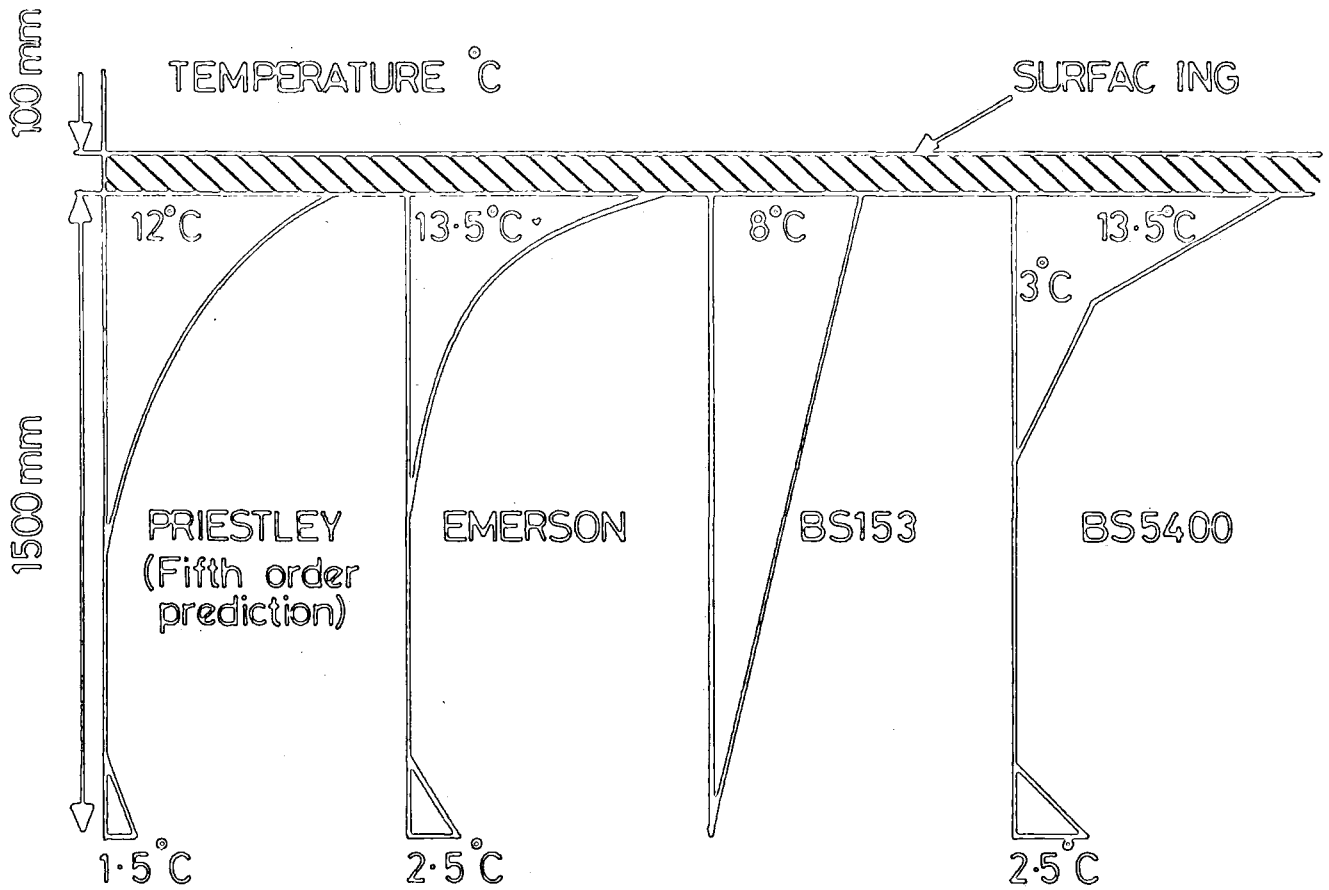

FIG. 2·1A Temperature distributions for a 1500 mm depth of section.

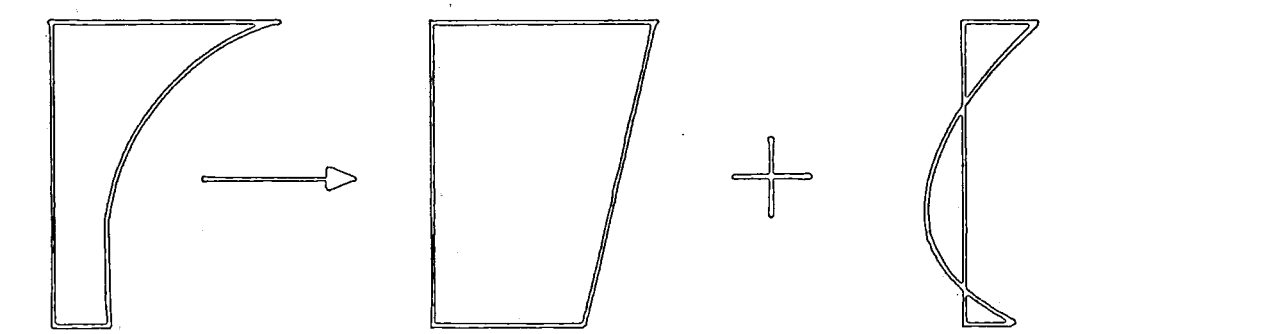

FIG. 2·1B

More recently Churchword and Sokal (44) attempted to establish analytical criteria for the prediction of the average temperatures which are responsible for the longitudinal deformation of the bridge, and of the vertical differential temperature profiles responsible for the bending deformations in the vertical plane. Comparing their results with temperatures measured on a section of a prestressed twin box concrete bridge and the environmental parameters outside, they found that the total temperature profile may be reasonably well predicted from the sum of two design variables: one having a constant value over the whole section and the second representing the maximum of the differential temperature profile. Then they formulated expressions which correlate these design variables with the environmenal parameters of maximum and minimum ambient temperatures and insulation. They found good correlation between their derived expressions and the magnitude of temperatures and the induced curvatures. However their results were derived only for a particular bridge section under particular environmental conditions, and has not been tested for other forms of sections at different locations.

Comments

In conclusion, it has to be pointed out, that there is not sufficient data available about temperature distribution for concrete in the Middle East, making it impossible to assess the use of any of these methods for predicting temperature distribution in the Middle East. However the use of the diffusion equation will of course give the correct prediction depending on the validity of the boundary conditions used.
Emerson deduced some of the boundary conditions applicable to the Gulf

region from the few available data and assumed values for those boundary conditions where data is lacking (45). Then she predicted the temperature distribution for some types of bridges using the boundary conditions she obtained with the computer program described by Jones (28)which is a numerical solution to the one dimensional diffusion equation using the finite difference approach. However, in view of the current absence of any experimental data, the accuracy of her calculations cannot be assessed until further in situ measurements are made.

2.1.2 Temperature - induced stresses

Stresses due to a temperature profile can be classified into two categories. The first is stresses that are functions of the boundary conditions, such as stresses arising from a restraint to axial or rotational movement. The second is self-equilibrating stresses that are not functions of the boundary conditions and are produced by the non-linear distribution of temperature through the depth of the section.(Fig. 2.1B).

If the beam is simply supported and not restrained axially or flexurally, then stresses due to the boundary conditions will be zero. However if the beam is continuous, then stresses will arise due to the partial restraint of the temperature-induced curvature called continuity stresses. Priestley (40) has proposed a simple method by which they can be calculated:-

1. Calculate the curvature due to the thermal loading, assuming that the beam is supported at its extreme ends only.
2. Calculate the forces necessary to reimpose compatibility at the internal supports.
3. Hence, calculate bending moments and stresses induced by these forces.

The calculation of the self-equilibrating stresses due to the nonlinearity of temperature considers cracked section and uncracked section and is based on simple beam-bending theory (46).

Priestley (40) calculated these stresses for crack-free prestressed section by imposing conditions of axial force and moment equilibrium on the section.

Hambly (138) explained his method by an example where he imposed a nonlinear temperature profile on a section and then he assumed that the section was totally constrained. Then he converted the temperature strains into stresses. By removing the constraints and imposing the two equilibrium conditions of forces and change of moment across the cross section he obtained values for the self equilibrating stresses.

Thurston et al.(47) considered a cracked section. They made the following assumptions:-

1. Concrete and steel stresses remain in the elastic range.
2. Uncracked concrete may support tensile stresses as high as the modulus of rupture f_t
3. Plane sections remain plane under thermal and force loading.

Using these assumptions, they estimated the average strain at the extreme tensile fibre as

$$\varepsilon_o = \left(\frac{M_D + M_L}{I_T E_C}\right) \bar{y}$$

where M_D = dead load moment, M_L = live load moment $\bar{y}$ = distance from neutral axis to extreme tensile fibre, I_T = transformed "all-concrete" moment of inertia of the cracked section.

They assumed a linear distribution of equivalent crack strain with distance from the crack.

Tensile stresses cannot develop in the cracked region, but compressive stresses will develop if the thermal compression strain exceeds the effective crack strain at this level.

They concluded that selfequilibrating stresses in simply supported reinforced concrete bridges are small and may be ignored for the temperature regime they considered. Curvature and deflection may be estimated using analyses based on uncracked section properties. Thermal continuity moments can be adequately estimated from the uncracked section thermal curvatures, and the cracked section stiffnesses at midspans and support locations. Continuity thermal moments in continuous structures are greatly reduced below the values applying for uncracked bridges, because of the reduction in moment of inertia that occurs with cracking. For a thermally loaded model bridge, the reduction in moments was more than 50 per cent, compared with uncracked moments.

Summary

From the foregoing discussion, we can conclude the following few points·

1) That stresses are produced in structure due to nonlinear temperature distribution even though the structure is not restrained axially or flex urally.
2) These stresses are normally calculated by imposing the equilibrium of forces and change of moments across the section.
3) Their magnitude depends on the shape and magnitude of the temperature distribution.

2.2 Effects of elevated temperature on the mechanical properties of concrete

Introduction

Although there exists a large body of published works dealing with the effects of elevated temperature on the properties of concrete. it is difficult to draw general conclusions. since the effects of temperature on the properties of concrete are influenced by many factors such as mix design, aggregates type. age of specimen at time of its exposure to heat, moisture condition of the specimen. level and duration of heating sealing conditions and test conditions. This makes it difficult to use any published results in a specific situation. However for a particular concrete, the most important variables are the level and duration of heating and the sealing and moisture conditions of the specimen (16.48-58). It has to be noted however that most of the published works deal with the effects of high temperatures such as in fires or in reactor vessels which are much higher than temperatures dealt with in the present experimental work.

2.2.1 The modulus of elasticity

Several investigators have reported that the modulus of elasticity decreases Figure 2.2with an increase in temperature (16,48.53,56). The amount of reduction varied between as low as 8% and as high as 70% and depending on several conditions such as duration of heating, mix design. aggregate type. specimen dimension, type of curing. sealing conditions etc. All reported that the decrease is irrecoverable except Hanant (58), who found that the elastic modulus had recovered slowly after two years at the higher temperature (77°C) to a value approaching that at normal temperatures.

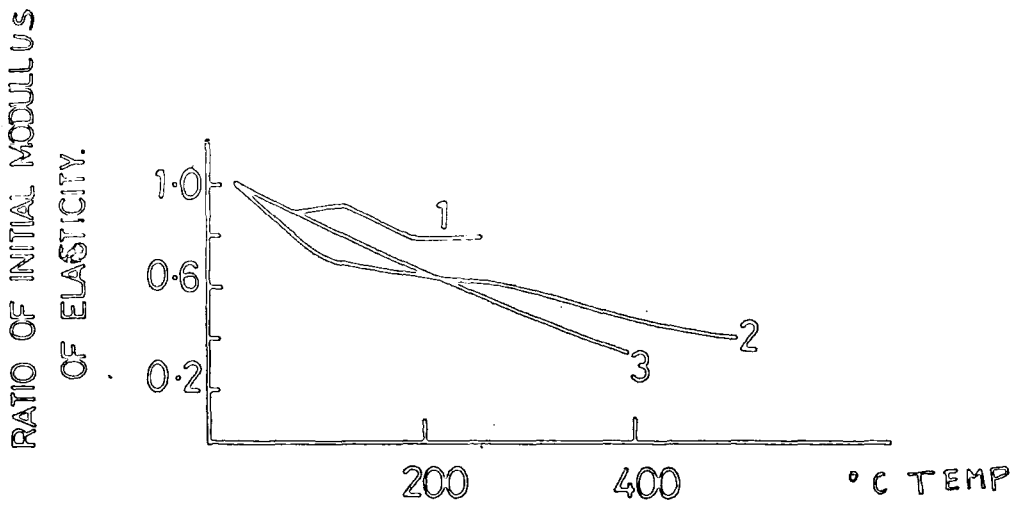

1. Gravel concrete heated at atmospheric pressure ω/c =0·4 Ref (16)
2. " " " " " " Ref (48)
3 Quartzite " " " " " " Ref (56)

FIG. 2·2

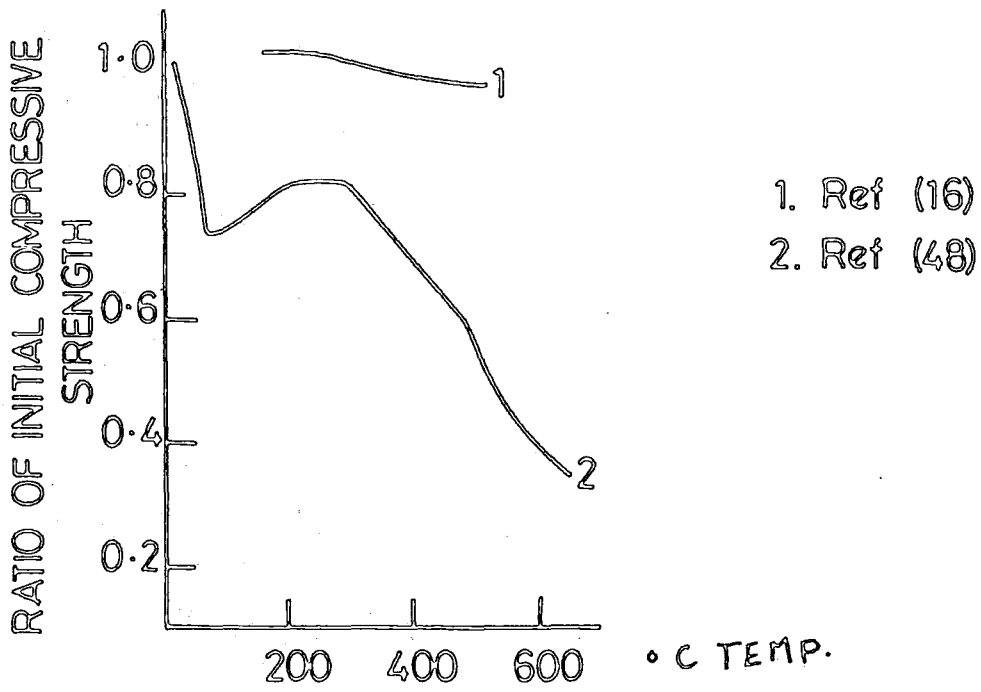

FIG. 2·3

2.2.2 Compressive Strength

Most researchers reported a reduction in compression strength with elevated temperature (Figure 2.3) with the reduction being a function of many factors and varying between 12 and 60% (48.49.50.54.56.59). Lankard et al.(16) reported that the compressive strength for unsealed specimen was either increased or was only very slightly decreased when stored at temperatures 79°. 121°. 190°. 260°C for time periods varying from 91 to 109 days. Also Hannant(60) reported that using a suitable mix design. no reduction in strength had occurred when specimen was stored in water at a temperature of 93°C for 18 months.

2.2.3 Tensile Strength

Again most researchers reported a reduction in tensile strength with heat (16.48.53.55.57) with the percentage reduction being more than in the compressive strength. Herada et al (48) found that the reduction also varied depending on the method of determination whether it was direct tensile or cylinder splitting.

2.2.4 Poisson's ratio

Published work is more scarce on this property. References (49.50,56) reported a reduction in Poisson's ratio with increasing temperature (Figure 2.4).

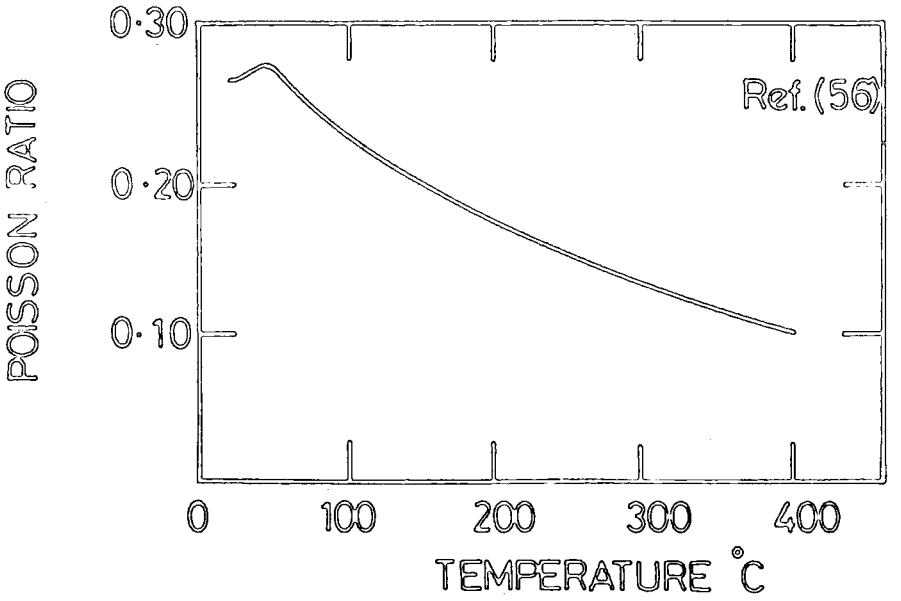
POISSON RATIO
0·30
0·20
0·10
Ref. (56)
0
100
200
300
400
TEMPERATURE °C

FIG. 2·4

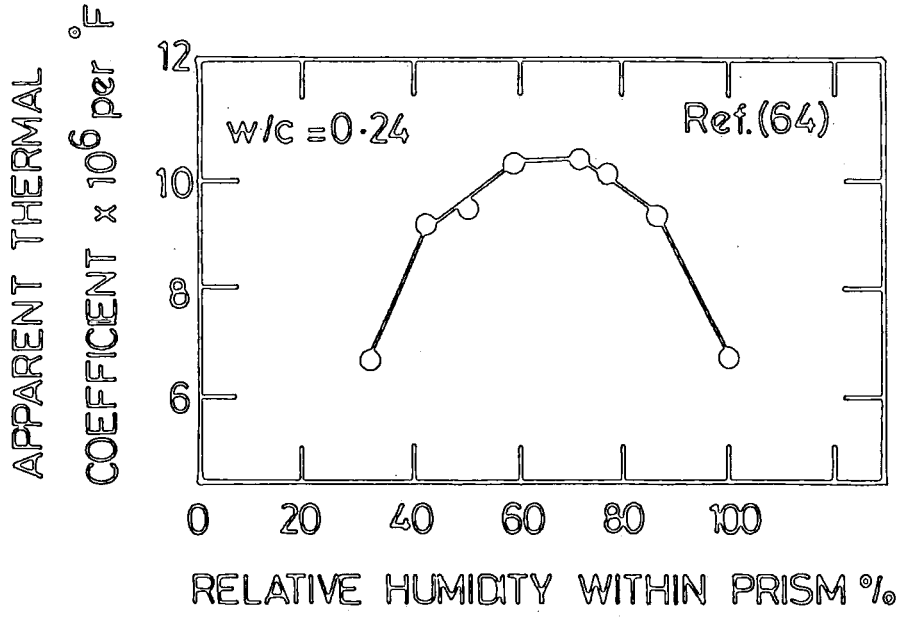
APPARENT THERMAL COEFFICENT x 10⁶ per °F
12
10
8
6
w/c =0·24
Ref. (64)
0
20
40
60
80
100
RELATIVE HUMIDITY WITHIN PRISM %

FIG. 2·5

2.3 Effects of elevated temperature on the thermal characteristics of concrete

The thermal properties of hardened concrete that are of particular interest are thermal conductivity (K). specific heat (C). thermal diffusivity (D) and coefficient of thermal expansion. Where

$$D = \frac{K}{\rho . c}$$

ρ is the density.

It is generally reported that these properties are greatly influenced by the mix design. the type of aggregates used. age and moisture conditions of concrete.

Aggregates properties are important. For instance quartz expands suddenly by 0.85 per cent at the temperature of 574°C(61). For a particular concrete age the environmental conditions affect the thermal properties of concrete. A fuller account of the thermal properties of concrete are given in references (51,61.62).

2.3.1 The thermal conductivity

Thermal conductivity is defined as the ratio of the flux of heat to temperature gradient and is measured in joules per second per square metre of area of body when the temperature difference is 1°C per metre of thickness of the body. Therefore it affects the gradient of temperature within the member. This in turn influences curvature and stresses in the structural member. It is a function of numerous factors the most important being the type and size of aggregates and mix design.

For a given composition the water contained in the material becomes an important factor of the thermal conductivity in relation to temperature (63). Cripino's (57) tests showed that for a limestone concrete, measured conductivity values exhibited an initial rise followed by a rapid decline with rising temperature. Marechal (63) reported similar results for the conductivity values of quartzite concrete specimens exposed to temperature of up to 400°C. He found that the maximum measured conductivity values were at 50° to 60°C and decreasing at higher temperatures. He further placed his dried specimen for several months in a 20°C and 98% relative humidity and measured their conductivity and found that the specimens showed no recovery in their initial conductivity values. He attributed this to the destruction of a large number of conductive bonds. On the other hand Herada et al.(48) reported a progressive decline in conductivity values with rise in temperature for their silica aggregate concrete.

2.3.2 The Thermal coefficient of expansion

This has a great influence on strains and stresses of concrete under temperature gradients and is a significant factor in the prediction of curvature of the structural member.

The thermal coefficient is made up of two movements : the true kinetic thermal coefficient. and an apparent expansion or contraction caused by hygrothermal volume changes associated with moisture movement.

Mayers (64) divided the thermal effects of temperature differences in concrete into four classifications:-

1. The effect of changes on the aggregate alone, many being non-uniform in composition. or made up of dissimilar crystals, as a granite, where each kind of crystal may have a different rate of thermal expansion.
2. The effect of changes on the cement paste; the magnitude of expansions of hardened cement paste varies with relative humidity and age.
3. The expansion of the mortar-cement matrix (paste plus sand or fine aggregate) and the stress set up at the contact of paste and fine aggregate due to differences in thermal coefficients of the two materials.
4. The exapansion of the concrete. considering the concrete to be made up of coarse aggregate and mortar (assuming the mortar to expand as a one-component material) and the thermal stress set up at the contact of mortar and coarse aggregate. The coarse aggregate-mortar bond appears to be very important in resisting stress due to thermal dissimilarities between the two materials.

Whilst it is not intended here to introduce a comprehensive survey of the various experimental results, the reader is referred to the following references (64-70), and for a comprehensive review is referred to (61,62). Some of the main points reported in these references are summarised as follows:

- The type and quantity of the aggregate plays a dominant role on the value of the coefficient of concrete.
- For a particular concrete and at a particular age. the coefficient of thermal expansion varies according to the hygral state of the cement paste.

- The coefficient of thermal expansion for the cement paste is a maximum at a relative humidity of 70%,Figure 2.5 and this being less for aged pastes.
- The coefficient of thermal expansion increases with an increase in temperature for high temperatures and being effectively constant in the range 0-60°C.
- The coefficient of thermal expansion increases with decrease in water/cement ratio.
- There is a contradiction in the references in relation to the effect of age on the coefficient of thermal expansion. for example while Wittman and Lukas (68) reported a decrease in its value with age. Berwanger and Sarkar (66) reported an incease of its value with age.

2.4 Effects of elevated temperature and changes of relative humidity on Moisture Transfer and Drying Shrinkage

Introduction

The deformations behaviour of concrete structures is greatly influenced by moisture content and distribution. Temperature and relative humidity are important factors in moisture distribution and moisture exchanges with the environment.

Because concrete continues to hydrate for a long time after casting and for the added reason of workability at casting. the amount of water originally added to the concrete mix is usually in excess of the quantity required for the hydration process of the cement paste. The state of water in a hardened concrete matrix has been arbitrarily classified according to its degree of fixity into(71):

1. Water of hydration of the cement gel, which can be termed non-evaporable water.
2. Gel pore water absorbed into the pores of the cement gel, this being evaporable over the range from 40% to 0% relative humidity.
3. Capillary pore water held outside the cement gel in the larger continuous channels or cavities. This water is more easily evaporable and will migrate out of the cement paste at a relative humidity of 40% to 50% and above.

2.4.1 Drying Shrinkage

Drying shrinkage comprises the deformational changes which are caused by the withdrawal of water from concrete stored in unsaturated air. Water gain on the otherhand causes swelling. Drying shrinkage of concrete is influenced by a large number of factors, which may be divided into intrinsic factors and extrinsic factors. The intrinsic factors are those material character istics which are fixed when concrete is cast. The extrinsic factors are those which vary after casting they include environmental conditions (temperature, humidity, carbonation, open surface to volume ratio, etc....). Drying shrinkage is a physical property of the hardened cement paste. However its measured value at any time is modified by the stresses that develop due to the continuous changes in moisture distribution inside the specimen resulting from the drying condition. Drying penetrates gradually inwards compressing the interior and creating tensile stresses in the outer layers. This often results in cracking. More cracks also develop at the cement paste-aggregate interface as a result of the differential shrinkage which is created in the hardened concrete matrix. Microcracks are thought to contribute to creep.

2.4.2 Influence of temperature gradient on moisture transfer and drying shrinkage

Temperature gradient has a significant influence on moisture transfer and its subsequent drying process and deformation in concrete.

Several experimental studies have been devoted to investigating the temperature-gradient moisture movement in concrete (72,73,74). However most of these were concerned with moisture movement within simulated thick wall structures, of the type used in prestressed concrete pressure vessels for reactors, and thus related to temperature regimes far removed from the ones used in the present experimental work. It is not intended to introduce a comprehensive survey, and the reader is referred to the following references - (72 ⇐ 76). However, some of the principal findings are reported here.

England and Sharp (74) conducted tests on a concrete cylinder subjected to a longitudinal temperature crossfall of 110°C and a maximum temperature of 150°C. They found that drying was encountered in the hottest regions of the concrete mass in addition to boundary areas associated with free evaporation of water to the atmosphere, and also that simple diffusion theory based on concentration of water was incapable of predicting these moisture distributions. A method of prediction was sought which recognised the pore air and vapour pressures as additional factors which caused moisture to migrate down the temperature gradient.

England and Ross (72) reported their results from several different types of experiments incorporating moisture paths of up to 10ft in length and maximum temperature of 150°C. Their findings can be summarised as follows:-

- Movement of moisture in concrete is a slow process and in thick sections permeability is a dominating factor.
- In thick sections, the normal evaporation behaviour at the boundary and forced migration of moisture in the hot regions are essentially isolated causes of drying due to the large distance the moisture must travel before reaching a zone where further movement is unimpeded.
- At thick sections and at temperatures below 100°C drying and pore pressures are unlikely to be a very important factors.

Similar results were reported by McDonald (73) where he found no significant changes in his specimen's moisture content after it had been subjected to a temperature gradient of 44°C for one year.

2.4.3 Influence of ambient relative humidity on moisture transfer and drying shrinkage:-

Environmental relative humidity greatly influences drying shrinkage and subsequently moisture migration inside concrete. Drying shrinkage increases when the relative humidity decreases. For example Troxell et al. (77) found that shrinkage at 50 per cent relative humidity was about 1.4 times that at 70 per cent relative humidity and about 8 times that of concrete stored in water. Although it is well established that low humidity leads to higher drying shrinkage, very little work has been done on the constitutive relationship of concrete shrinkage at various relative humidities (78). Bazant (79,80,) set up partial differential equation to model pore humidity variation with time using the environmental relative humidity as a boundary condition. However his model is too complicated for use in practical situations.

2.4.4 Prediction of deformation due to drying shrinkage

There are three established ways of predicting deformation due to drying shrinkage.

- From mix composition. strength and the operating conditions as used in the Codes of practice.
- From short time tests with the use of mathematical shrinkage-time expressions which are commonly expressed in exponential or hyperbolic power forms such as

$$\varepsilon_{sh}\,(t_1,t_o) = \varepsilon_\infty \{\, 1 - e^{\,A(t-t_o)}\,]$$

or

$$\xi(t_1 t_o) = \left[\, \frac{t-t_o}{A + B(t-t_o)}\, \right]^M$$

where $\xi(t,to)$ = shrinkage at time t measured from the start of drying (to)

ε_∞ = ultimate shrinkage

A, B and M are constants determined experimentally

The third method is using Fick's law of diffusion. The basic equation used in terms of shrinkage is·

$$\frac{\partial S}{\partial t} = K \left(\frac{\partial^2 S}{\partial x^2} + \frac{\partial^2 S}{\partial y^2} + \frac{\partial^2 S}{\partial z^2}\right) \qquad 2.3$$

where S = the true, unrestrained shrinkage strain,

t = time

K = shrinkage diffusivity or diffusion coefficient

x,y and z = rectangular co-ordinates

Hansen and Mattock (81) have shown that the linear diffusion theory (eq.2.3)which is based on constant diffusion coefficient K and the use of volume/surface ratio as a parameter for use in evaluation of shrinkage data obtained from members of differing size and shape adequately describes the drying shrinkage of concrete at ordinary temperature conditions. Hughes et al.(82) found that diffusion theory can describe the drying process in the temperatue range 50 - 90°C requiring however a temperature-dependent diffusion coefficient.

Lowe et al.(83) have shown that the diffusion coefficient for concrete dried at 30°C and a relative humidity of 70% is a function of the concentration of evaporable water. In an attempt to simplify this they determined an expression for the diffusion coefficient as a function of time.

Another method of predicting shrinkage was proposed by Carlson and Pickett and slightly extended by Bazant(80).. In this method shrinkage is treated as a material property rather than a specimen property, and shrinkage is modelled as a function of pore water content w(g of water per cm^3 of concrete), which is in turn a function of pore humidity h. Therefore

$$\varepsilon_s = \varepsilon_s^{o} \, f_s(h)$$

ε_s^{o} is the maximum shrinkage (for h = o).
The function $f_s(h)$ is empirical, approximated by $f_s(h) = 1 - h^2$.

Further Bazant and Naggar (84) modelled the change of pore humidity h with time by the following non-linear differential equation:

$$\frac{\partial h}{\partial t} = K \operatorname{div} \vec{J} + \frac{\partial h_s\,(t_e)}{\partial t} + K \frac{dT}{dt} \quad \vec{J} = - c \operatorname{grad} h \quad \ldots\ldots \qquad 2.4$$

where $\vec{J}$ is water flux: $K = \frac{\partial h_s}{\partial w}$ at constant temperature T and constant age; w is the specific pore water content; t_e is age and $\frac{\partial h_s(t_e)}{\partial t}$ is the rate of self-dessication.

Bazant (80) further proposed that moisture transfer in a heated environment or thermal moisture transfer can be modelled by considering that the driving force of the diffusion flux in eq.2.4 is not grad h or grad w but grad p where p is the vapour pressure in the pores.

It must be noted that shrinkage considered in this way will not be directly a function of age but a function of pore humidity or specific water content.

However it is very difficult to determine the different coefficients in eq.2.4 Thus very little experimental work is found to support the model proposed by eq.2.4

There are other simple methods of predicting shrinkage which involve the use of charts such as that produced by Hobbs and Parrott (85).

In conclusion however none of the methods mentioned predict closely the long-term deformation due to shrinkage, and any method has to be used with an assumed error coefficient. However, in general experimentally-based methods give better prediction than do the theoretical methods. Their complication lies in the dependence of shrinkage on size and open surface to volume ratio.

Comments

The importance of shrinkage to the engineer lies mainly in its contribution to the long-term curvature or deflection of the structural member. Its contribution has been estimated to lie between 5 and 30% of the total long-term deformation of the member. (86)

The use of results on plain concrete in predicting curvature or deflection for reinforced concrete involves the use of one of several expressions mostly empirical such as Miller's empirical expression and Branson's (87) method.

Branson's empirical method has an expression for curvature of uncracked section of the form

$$\frac{1}{r} = \frac{\rho_\beta \epsilon_{cs}}{h}$$

ρ_β is a tabulated coefficient dependent on the percentage of compression and tension steel. h is depth of the member, and ϵ_{cs} is the shrinkage of plain concrete. Another simple method is the theoretical equivalent tensile force method (86,88). It involves an expression of the form

$$\frac{1}{r} = \frac{(1 + \phi)\ \epsilon_{cs}\ Es\ A_s(d-x) - \acute{A}_s(x-\acute{d})}{E_c I_u}$$

For an uncracked section, where $\frac{1}{r}$ is the curvature, ϕ is the creep coefficient (ratio of creep strain to elastic strain), ϵ_{cs} is the shrinkage of plain concrete, E_c and E_s are the elastic modulus for concrete and steel respectively, As and $\acute{A}_s$ are the percentage of the tension and compression steel respectively, d and d' are the distances of tension and compression steel respectively, and I_u is the second moment of area for the uncracked section. A similar expression for the curvature of the cracked section is used by replacing I_u by I_c , where I_c is the second moment of area for cracked section.

2.5 Review of literature relating to Creep

Introduction

Concrete can be regarded as a two-phase material consisting of a graded mixture of naturally occurring sands and gravels or crushed rock, bonded together by a hydrate formed during the reaction of the cement with the mixing water. The aggregate can occupy up to 75% of the concrete by volume. The usual normal-weight aggregate used in concrete is not liable to creep to an apreciable extent, so that it is reasonable to assume that the seat of creep is in the cement paste (89). The influence of the aggregate can be effectively eliminated if one type of aggregate is used throughout a particular study.

The structure of hardened cement paste is complex. There is an almost infinite range of possible combinations of anhydrous cement compounds (C_3S, C_2S, C_2A, C_2AF, plus various minor compounds such as MgO, TiO_2) and amounts of water in cement paste, these parameters being subject to random variations due to the inconsistent quality of the raw materials and to methods of cement manufacture. The cement paste at any age consists of hydration products, in the form of collodial cement gel, of unhydrated cement grains, crystals of calcium hydroxide $Ca(OH)_2$ and free uncombined water. The gel is continuously developed at a decreasing rate depending on the progress of hydration of the cement grains. The gel has extremely small particle size. It has a large internal surface area and a pore size distribution ranging from 15 to 20Å diameter in the gel to capillaries of 5000 Å diameter.

2.5.1 Mechanisms and Theories of creep

The mechanism and prediction of creep is subject to considerable controversy. Evans and Kong (90) quote ACI Committee 209 "The difficulty is that a satisfactory theory of creep must explain in a unified way the behaviour of concrete under various environmental conditions and under various states of stress. It is hard to suggest definite conclusions on the mechanisms of creep. Perhaps the only non-controversial statement that can be made is that the presence of some evaporable water is essential to creep." Two types of creep are identified:

- Basic creep: Strain caused by load, that takes place without moisture exchange with the atmosphere.
- Drying creep: strain caused by load, in addition to shrinkage or swelling, that is associated with moisture exchange with the surroundings. Drying creep is assumed to be the total time-dependent strain measured in a loaded drying specimen minus shrinkage and minus basic creep.

Strains due to creep are usually divided into the following components

- Instantaneous strain on loading
- recovery upon unloading
- Creep strain
- Delayed elastic (creep recovery) strain
- Residual deformation (irrecoverable creep or flow)

There are several broad mechanisms of creep. The most important can be distinguished under the following categories:

1. Mechanical deformation theory
2. Plastic flow theory
3. Viscous flow theory
4. Seepage of gel water theory
5. Delayed elasticity theory

None of these mechanisms can account for all the observed phenomena. Accordingly there have been various hypotheses which ascribe creep to more than one mechanism(91,92,93).. These mechanisms are presented and discussed to the extent that they would explain the effect of elevated temperatures on the creep of concrete.

Mechanical Theory

Proponents of this theory assume that the creep phenomenon is a function of the surface tension of the water in the capillary pores of the specimen. It is assumed that under a compressive stress the capillaries are deformed and the water meniscus displaced outward to a point where the capillary diameter is larger so that the tension under which the capillary water is held is decreased. This would in turn induce creep. Creep is assumed to be completely recoverable, and mass cured concrete will not exhibit any creep strains under normal or elevated temperature. Both of these conclusions are contrary to available experimental evidence.

Plastic deformations theory:

Proponents of this theory suggest that creep of concrete is similar to that of metals, i.e. a result of slipping along planes within the crystal lattice. Such deformations would be irrecoverable, nonlinear with the applied stress and would occur only after a limiting stress is exceeded. According to this theory, if a specimen were loaded at elevated temperature, plastic flow would start at a lower stress since the yield point in a stress-strain diagram would be lowered due to the rise in temperature. But the total value of the plastic strain should be nearly equal to the corresponding strains at other temperature levels. Again experimental evidence is contrary to the conclusions of this theory.

However as has been suggested by Neville et al.(94) some form of plasticity may enter the deformational behaviour of concrete at stresses nearing failure but this is not of great significance to the creep behaviour of concrete under normal loads.

Viscous flow theories:

Proponents of this theory consider hardened cement paste as a viscous fluid, surrounding the relatively rigid aggregate particles. When the concrete specimen is loaded, the paste would flow gradually under stress, transferring a major part of the load to the aggregate skeleton which would resist that flow. This is one of the important theories. It does explain the linearity of creep strain with stress, the absence of a limiting stress for creep to occur and stress relaxtion at a constant deformation. It further postulates that if the temperature is raised, the viscosity of the paste would decrease, and hence its rate of flow would increase accordingly. The theory however does not explain some of the observed characteristics of creep, for example creep recovery on removal of applied stress, sensitivity of creep to moisture exchange, the reduction of the rate of creep with time and change of volume during creep.

Seepage theory:

This is possibly the most important theory of creep mechanism. It assumes that hardened cement paste is a limited swelling gel, whose equilibrium with its solid skeleton and external load is determined by the vapour pressure of the gel water. Upon loading, the vapour pressure of the adsorped water in the gel is increased, disturbing the hygral equilibrium. The gradual re-establishment of the equilibrium results in the exchange of moisture with the environment. The volume change accompanying the resulting moisture movement is identified with creep.

When the moisture movement is external into the ambient atmosphere a three-dimensional state of stress is created and the phenomenon is called shrinkage. Hence shrinkage and creep are inter-related phenomenon. This theory does explain many aspects of creep, including the increase in creep under the applied stress with simultaneous drying and the increase of creep at elevated temperature which can possibly be related to the faster rate of seepage due to the higher activity of the molecules. This theory predict (93) that the creeping specimen should suffer an additional gel moisture loss over an unloaded control specimen. Experimental evidence contradicts this.

Delayed Elasticity theories:

This theory proposes that the gel under load behaves as a composite body consisting of more or less elastic and viscous phases, and that creep of concrete is an elastic deformation which is delayed by the action of the viscous gel. An increase in temperature would result in a decrease in the viscosity of the gel and the water; this in turn would increase the rate of the delayed elastic deformation. This theory does not however offer an explanation to the observed influence of moisture exchange on creep.

2.5.2 Rheological models:

Rheological models basically represent idealised deformations for the elastic (Hookean), viscous (Newtonian) and plastic (St.Ven ant) types and are modelled by a spring, a dashpot and a friction element.

Mathematically the Hookean (Figure 2.6a) body is represented by the equation

$$\sigma(t) = K\epsilon(t)$$

where $\sigma(t)$ is the stress and $\epsilon(t)$ is the strain, K is the proportionality constant.

The Newtonian body (Figure 2.6b) is represented simply by

$$\sigma(t) = C \frac{d\varepsilon(t)}{dt}$$

C is a Newtonian liquid constant.

These basic elements can be built up into rheological models of varying complexities.

There are two basic models known as a Kelvin's model and Maxwell's model (Figure 2.6c,d). The difference between the two models is that in the Kelvin's model, the spring and the dashpot are parallel, while in the Maxwell's model, the spring and the dashpot are in series

(a)

Hookean

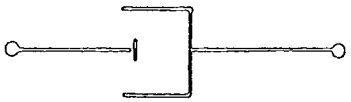

(b)

Newtonian

(c) Maxwell's model

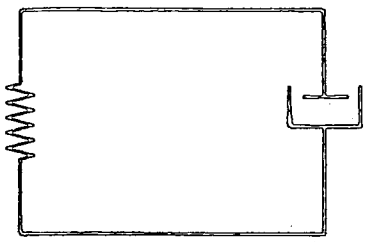

(d)

Kelvin's model

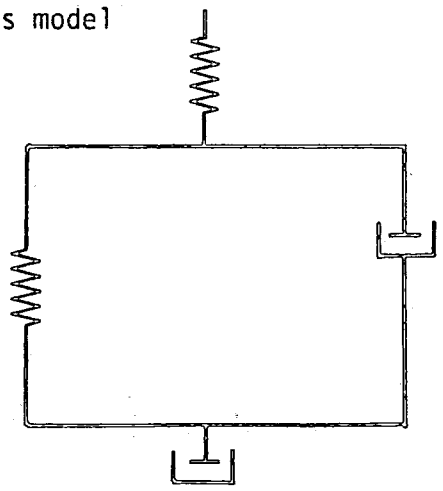

(e) Burger's Model

(Figure 2.6)

Thus the stress in the Kelvin's body is shared between the spring and the dashpot.

That is

$$\sigma(t) = K\varepsilon(t) + C\frac{d\varepsilon(t)}{dt}$$

if at $t = 0$, the body is unstrained, i.e.

$$\varepsilon_o = 0$$

$$\therefore \quad \varepsilon = \frac{\sigma}{K}\left(1 - e^{-\frac{K}{C}t}\right)$$

The immediate strain is zero and the final strain for $t = \infty$ is that of the perfectly elastic solid and is reached asymptotically.

In the Maxwell's model, the sress in the two elements is the same.

and the total deformation of the body is the deformation of the spring plus the deformation of the dashpot.

The differential equation of this model is

$$\frac{1}{k}\left(\frac{d\sigma(t)}{dt}\right) + \frac{\sigma(t)}{c} = \frac{d\varepsilon(t)}{dt} \quad \ldots\ldots \qquad 2.5$$

Two cases are considered

a) A constant stress producing a constant rate of strain

Thus 2.1 becomes

$$\dot{\varepsilon} = \frac{\sigma}{c}$$

and $\therefore \quad \varepsilon = \frac{\sigma}{c} t + \text{constant}$

where the constant is the elastic strain

b) A constant strain

$\therefore$ eq.2.5 becomes

$$\frac{1}{k} \dot{\sigma} + \frac{\sigma}{c} = 0$$

$$\sigma = \sigma_o e^{\frac{-k}{c} t}$$

which means that if the deformation is kept constant, the initially induced stress is gradually relaxed.

The Kelvin's model and Maxwell's model can be built-up into a more complex model. The most basic built-up model is the Burger model (Figure 2.6e).

A number of researches have used these models to represent the deformation of concrete (92,95). Figure 2.7 gives one of the models that represent the effects of temperature and is taken from reference (95).

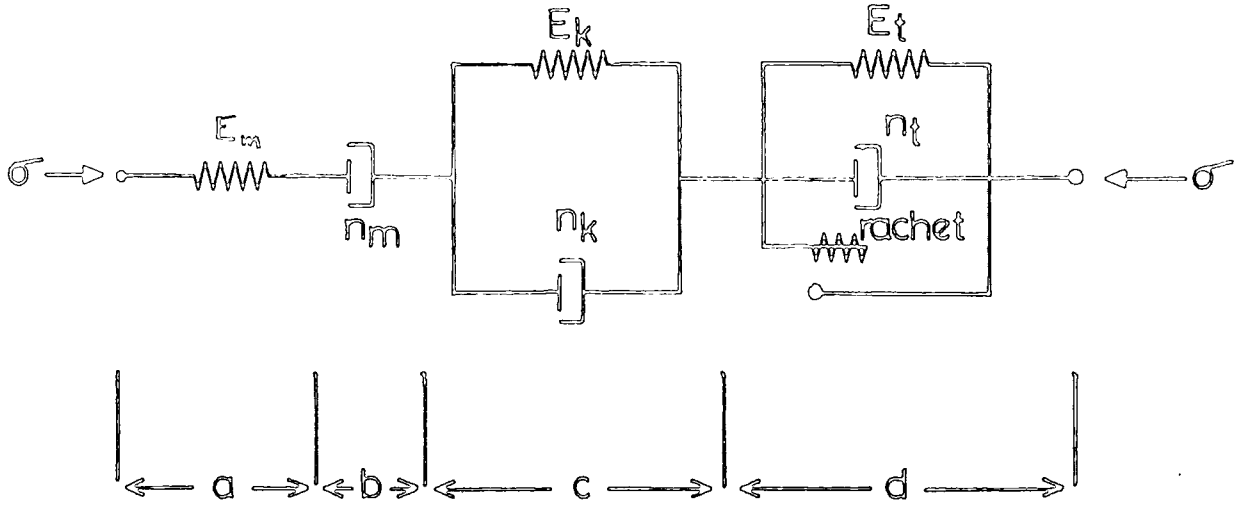

Model representation of uniaxial elastic and creep behaviour of concrete at elevated temperature (Ref.[95]).

Strain component:

a. Elastic

b. Non-recoverable creep, or flow

c. Recoverable creep, or delayed elastic

d. Temperature change component

E_m is elastic modulus corresponding to short-term stress application

E_K governs the magnitude of the delayed elastic strain

E_t is a temperature softening modulus and permits the temperature change creep component to develop for upward changes of temperature only. The rachet (d) prevents any creep recovery for falling temperature.

(Figure 2.7)

2.5.3 Factors affecting creep

The factors affecting creep can be divided into two categories:

1. Intrinsic factors, resulting from the internal state of the material.
2. Extrinsic factors, i.e. ambient conditions (relative humidity, temperature, carbonation) and the effect of member size.

Only the extrinsic factors will be dealt with in detail here, particularly the temperature and humidity factors. Intrinsic variables which may affect creep in general are numerous and they can be summarised briefly as follows:-

(1) Aggregate ratio and properties; (2) Cement and its properties; (3) Water and its relative ratio in the mix; (4) Mix proportions; (5) Entrained air; (6) Admixtures; (7) Mixing time and consolidation; (8) Curing conditions.

For a fuller account of the effect of these variables on the creep of the concrete, the reader is referred to references (61,89,94).

2.5.3.1 Influence of ambient relative humidity on creep

Numerous tests have shown that creep increases with decrease in the relative humidity. For example Troxell et al.(77) reported that at a relative humidity of 50 per cent creep may be two to three times greater than at a relative humidity of 100 per cent Figure 2.8. Their findings indicated further that, for the same time under load, the relation between creep and the relative humidity values they considered is generally linear However the statement that creep is higher the lower the relative humidity is misleading. Two conditions have to be distinguished. The influence of the ambient relative humidity affects creep if drying takes place while the specimen is under load. But if the concrete has reached hygral equilibrium prior to loading, the magnitude of creep is independent of the relative humidity of the surrounding medium.

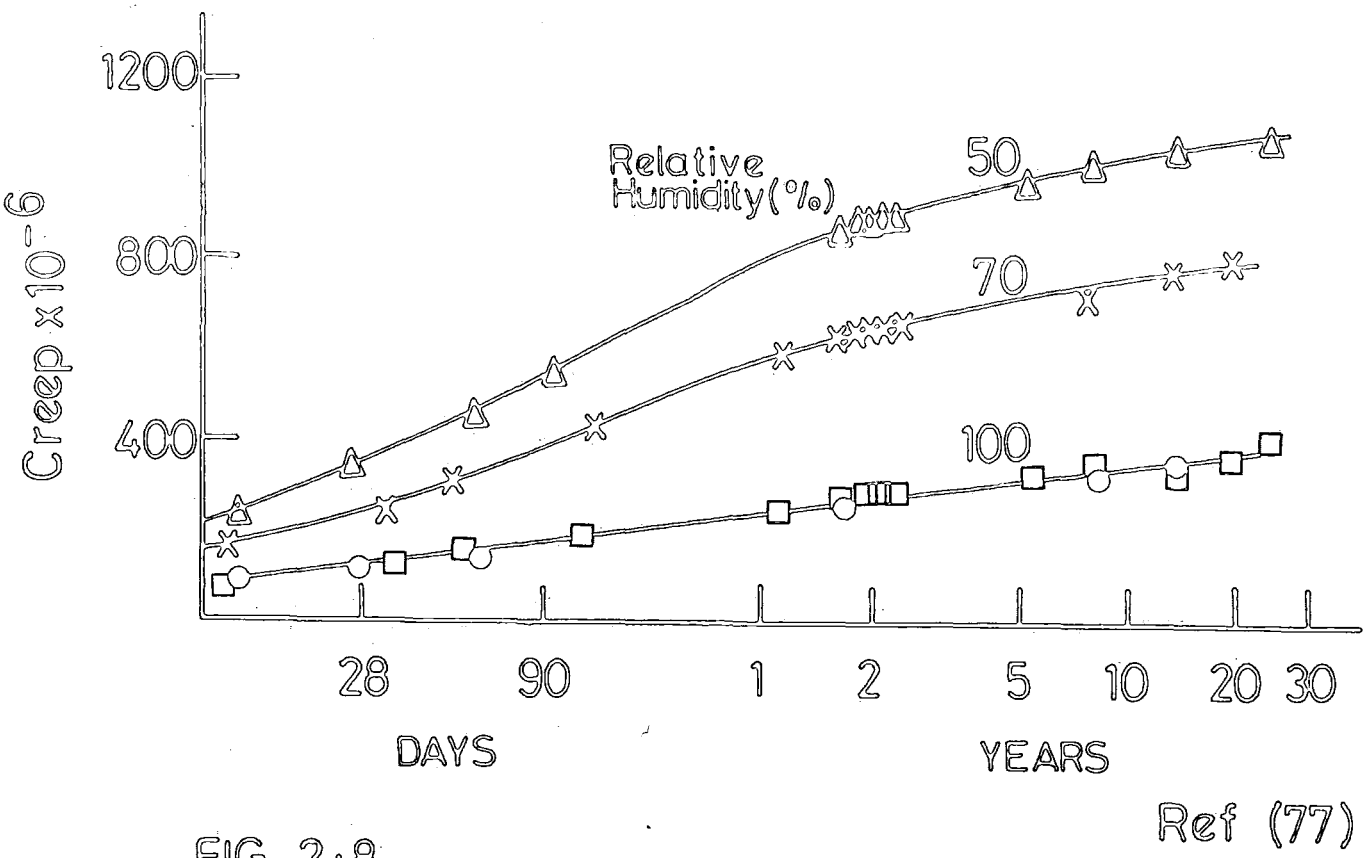

Ref (77)

FIG. 2·8

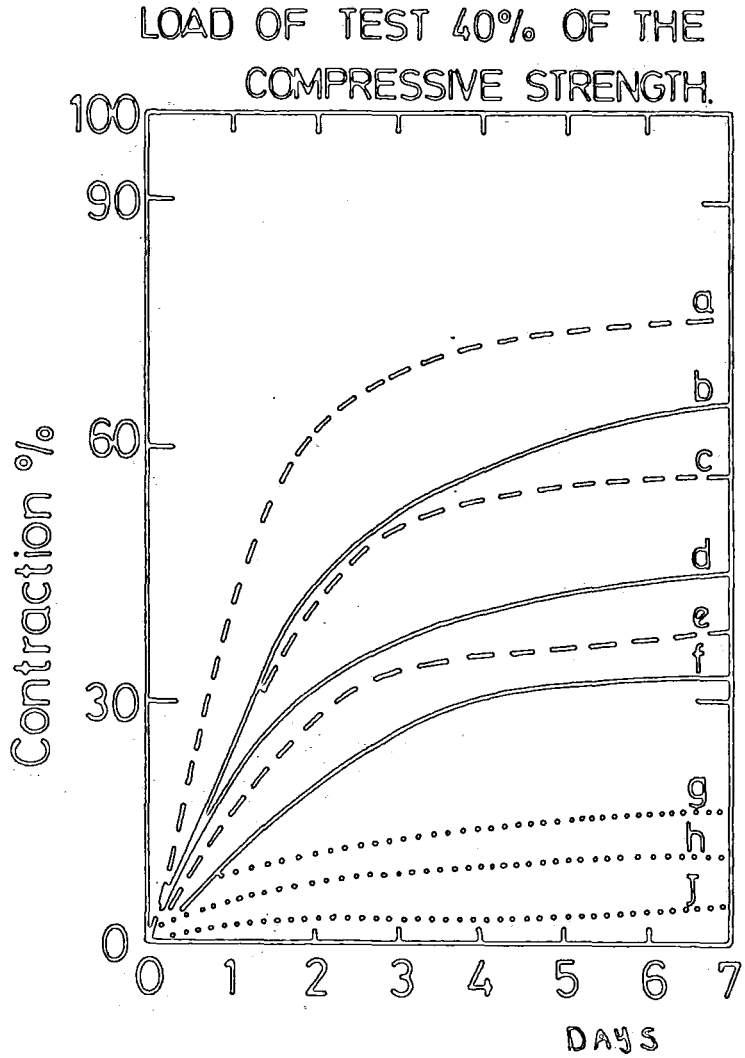

KEY

M8:2 = Mortar, 8 parts cement by 2 parts sand ω/c = 0·31

M6:4 = 6parts by 4, ω/c = 0·35

M4:6 = 4parts by 6, ω/c = 0·48

a	M=8:2 - H=10%
b	M 8:2 - H=50%
c	M 6:4 - H=10%
d	M 6:4 - H=50%
e	M 4:6 - H=10%
f	M 4:6 - H=50%
g	M 8:2 - H=100%
h	M 6:4 - H=100%
J	M 4:6 - H=100%

FIG. 2·9

Ref. (30)

Other investigations have indicated conflicting trends on the subject of the influence of relative humidity on creep. de La Pena (30) did not find proportionality using mortar specimens 2mm thick (Figure 2.9).. At 50 per cent relative humidity the relative shortening of the specimen was more than six times its value at 100 per cent relative humidity. However when the humidity was dropped to 10% the relative shortening was only 1.23 its value at 50%.

2.5.3.2 Alternating humidity

Hansen (96) investigated creep of cement mortar beams exposed to cyclic variations in the relative humidity of the surroundings. He found that the first period of drying greatly increases the creep over the amount which is observed when specimens are stored constantly under the average humidity. However during any subsequent period of drying after intermediate exposure to a higher relative humidity, the amount of creep is smaller than the creep observed when specimens are stored under constant average humidity.

Gamble (97) investigated the effect on creep and shrinkage on specimens stored in a constant environment of 70°F and 50% and specimens stored outdoors in central Illinois with an average annual humidity of 70. He found that shrinkage strains in the outdoor specimens were quite low, corresponding to strains expected at relative humidity values of 80-90%. However the creep strains in the outdoor specimens were much larger than normally would have been associated with the 70% relative humidity range and were of the same general magnitude as the creep of companion specimens stored indoors in a constant environment of about 45-50%. Gamble explained his results by the following proposal: At least part of the shrinkage is due to loss of water from the concrete to the atmosphere. This shrinkage is relatively slow since the water is contained in capillary pores and gel pores, and is subjected to high surface tension and capillary forces tending to hold the water within these pores. On the other hand, moist causing swelling will be taken into these same pores quite readily by the same capillary forces, each time moist is made available. The capillary forces might be compared to check valves, whose function it is to let water flow into the concrete but not back out. Thus the average moisture content of the concrete would always be higher than that of concrete stored under a similar, but constant, humidity condition.

If this is a valid picture of the behaviour, it should not be surprising that the shrinkage of the outdoor specimens was less than that normally associated with the average humidity.

Gamble and Parrot (98) found that when a specimen is exposed to a drying condition for the first time, its drying creep can be related to the concurrent shrinkage by the following expression:

$$C_d = \sigma K \epsilon_{sh} \qquad 2.6$$

where C_d is the drying creep and σ is stress, ϵ_{sh} is shrinkage and K is a constant for the particular concrete used, and is independent of age at loading, delays in drying, size of specimen and ambient relative humidity, and only slightly dependent upon stress within the normal working range.

2.5.3.3 Relative humidity of storage and the effect of water present at the time of loading

Previously the influence on creep of drying after the application of the load was considered. But creep as has been indicated depends not only on the loss of water under load but also on the actual amount present when the load is applied. The result of a reduction in the amount of evaporable water content before loading is twofold; basic creep is less, and drying creep is also reduced because the concurrent rate of shrinkage is less. Ruetz (91) reported a decrease in basic creep in specimens which were dessicated before sealing at the age at application of load, so that only basic creep occurred. G.Lucklish and Ishai (92) reported that no creep took place in concrete containing no evaporable water.

Meyers and Slate (99) found that the most important variables affecting the creep of concrete are: the degree of hydration at the time of loading; the amount of water present and not chemically combined at the start of loading and while the specimen is under load; and the amount of microcracking developed in the system before and during the time underload.

They found that in sealed concrete, basic creep decreases wth the age at application of load because the amount of evaporable water decreases with the progress of hydration. However at very early ages, an increase in basic creep with age can occur: this is due to the rapid increase in the quantity of gel, which dominates the effect of the decrease in evaporable water.

2.5.3.4 Wetting creep

Gamble and Parrott (98) related wetting creep to the concurrent swelling by an expression similar to that of eq.26, but, as with drying creep, the relation is limited to the first cycle of re-wetting.

2.5.3.5 Effect of Wind

Hansen (100) investigated the influence of wind velocity on creep, to see whether the rate of drying is influenced by the air velocity, when a hardened concrete structure is exposed to forced convection, and whether the velocity of wind over an exposed surface therefore has an influence on the creep and drying shrinkage of the structure. He used mortar specimens, 20 x 50mm in cross-section, which after water curing, were exposed to a relative humidity of 50 per cent at 20°C in still air and air with a velocity of 5m/sec. No difference was observed in weight change, shrinkage or creep under the two conditions.

2.5.3.6 Effects of carbonation

Parrott (101) reported an increase in creep on carbonation of prisms of cement paste (12.5 x 12.5 x 110mm) with a water/cement ratio of 0.47. The specimens were cured in water for three weeks and dried at a relative humidity of 65 per cent in a dessicator for 18 weeks. Ten of the

specimens were then loaded to about 10% of their strength. After three days under load, half of the specimens were removed from the dessicator and placed in the laboratory where carbonation occurred at 65 per cent relative humidity. The increase in creep of the carbonated specimens was 70 per cent after seven weeks under load. For tests, where carbonation began 29 days after loading, the increase in creep after three weeks of carbonation were 50%, 45% and 50% for the three experiments.

2.5.3.7 Influence of temperature and curing

Temperature is considered the second major environmental factor in creep after humidity. As in the case of humidity distinction must be made between the temperature during the period of curing preceding the application of load and the temperature while the concrete is under load.

Results on the influence of temperature on creep as reported by various researchers are variable and sometimes contradictory.

De La Pena found creep of 1:1 mortar specimens stored under water to be proportional to the temperature in the range 0 to 50°C. Serafim and Guerreiro (102) investigated the influence of temperature on creep of mass-cured concrete. Their tests were carried out on 8 prisms 20 x 20 x 60cm loaded at the age of three days. Four were kept at room temperature and four were kept at 45°C. They found that the rate of creep at 45°C was higher than at room temperature during the first four to seven days following loading. But thereafter the rate of creep was approximately the same for both temperatures.

Arthanari and Yu (103) carried out tests on sealed and unsealed concrete under uniaxial and equal biaxial stresses in the temperature range of 20° to 100°C at intervals of about 20C. They used specimens of the form of 12" x 12" x 4" slabs. They found that creep of sealed concrete

was less than that of unsealed concrete which was allowed to shrink simultaneously but the general trend showed that the ultimate creep may be greater in the sealed specimen. They found creep strain of stressed concrete appeared to increase rapidly whenever the temperature was stepped up. They observed higher creep values when the temperature was increased in stages than when the maximum temperature was continuously maintained.

England and Ross (104) reported results on shrinkage and creep of concrete at temperatures up to 140°C. They found that the influence of temperature was more pronounced for sealed concrete in the range 20° - 60°C than in the range 100 - 140°C, while the creep of unsealed concrete was only slightly greater than that of sealed concrete for similar conditions of temperature.

Nasser and Neville (105) investigated the influence of temperature on creep of concrete loaded at the age of one year and fifty years at temperatures ranging from 70°F (21°C) to 205°F(96°C). The concrete fifty years old was cored from a railway bridge and subjected to sustained loading after heating to various temperatures in water. They compared its creep to concrete which was loaded at the age of one year and stored under water and subjected to two temperature regimes. They found that concrete as old as 50 years was still liable to creep of substantial magnitude especially at temperatures above normal. (Figure 2.11) The general shape of creep-time curves was similar for moist-stored old and young concretes. They found that elevated temperature of storage while under load increased creep and rate of creep. The increase was linear up to about 160°F (71°C) but it became smaller at higher temperatures. At 205°F (96°C) creep was no greater than at 115°F(46°C). This behaviour applies to concretes with all ages at loading used in their investigation.

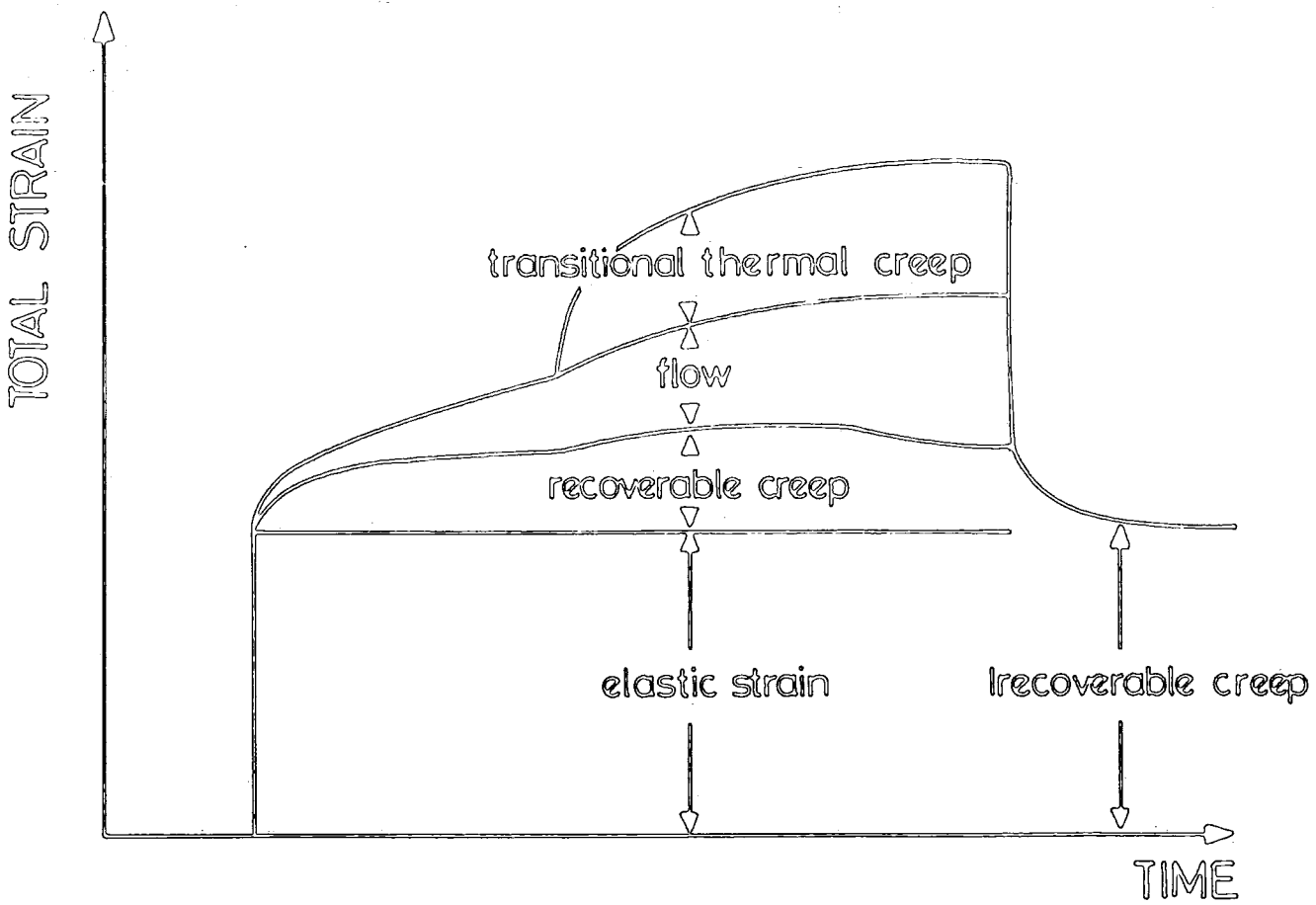

FIG. 2·10. Elastic and creep strain components.

Ref (109)

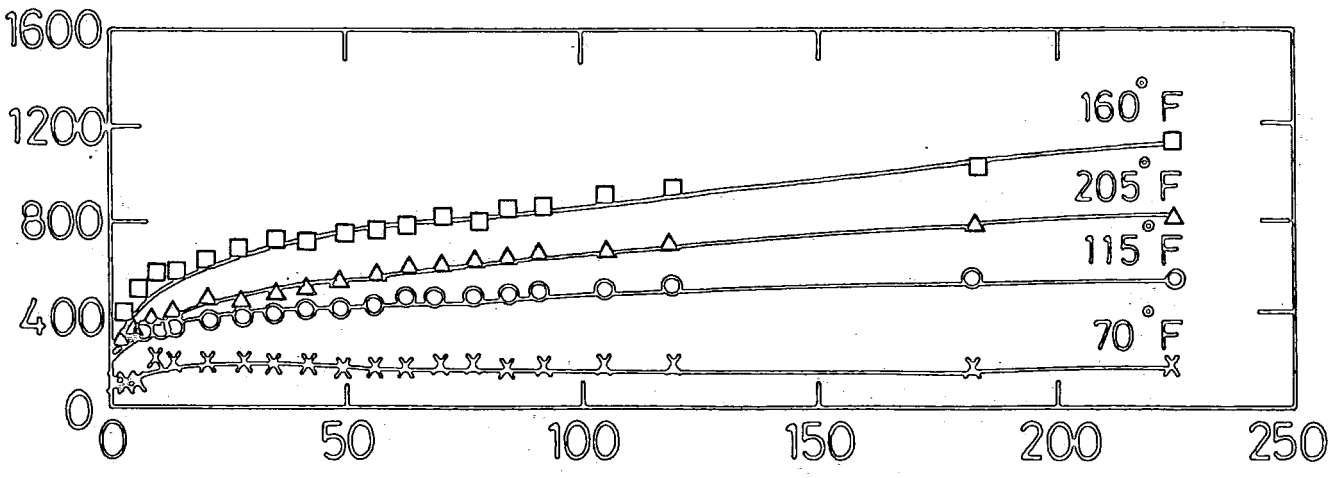

Relation between creep and time under load for concrete fifty years old. Ref (105)

FIG. 2·11

Hannant (58) carried out tests on 90 specimens with dimensions 10.5cm dia x 30.5cm long. He investigated both elastic and creep deformations under various uniaxial and multiaxial compressive stress combinations at temperatures between 27°C and 95°C for periods of loading up to 2 years. His tests showed that creep strain of sealed concrete subjected to uniaxial compressive stress increased with temperatures up to 93°C, and was linear in the temperature range 27°C to 77°C, but was not linear between 77°C and 93°C where the rate of increase of creep was greater above 77°C. The creep strain at 77°C under uniaxial stress was between 4.0 and 4.8 times the creep at 27°C. He found that creep of concrete which was dried before loading was a small fraction of the value for wet concrete, even at temperatures of 70°C.

The increase of creep with temperature was also reported by Zielinski and Sadowski (106) on concrete specimen made of crushed basalt with w/c of 0.46 and tested at various moisture content, at temperature 20° and 60°C. Hansen and Eriksson (107) carried out tests on cement paste and mortar beams
(2 x 5 x 40cm) stored under water to determine the effect of temperature changes between room temperature and 212F (100°C) on deflection. They found that deflections were greatly increased when heat was applied after loading, and that heating before loading gave lower deflection. That increase in deflection always took place when the temperature increased, never when the temperature decreases.

2.5.3.8 Creep under varying temperature and the occurrence of Transitional thermal creep

Illston and Sanders (108) divided strain of mortar stored in an environment with a varying temperature and subjected to a sustained load into four components. (Figure 2.10).

a) Elastic strain, taken as the first measured strain difference after loading or unloading.

b) Delayed elastic strain, which develops after loading to reach a limiting value, and appears as time-dependent recovery after unloading.

c) Transitional thermal creep, occurring rapidly and irrecoverably when the temperature of a loaded specimen is raised to the first time. (Transitional thermal creep is defined as the irrecoverable creep which occurs during the virgin heating of concrete that is stressed and is equal to the total creep strains minus flow and any recoverable creep.)

d) Flow, which is also irrecoverable and is observed as the long-term strain; for a given temperature, its rate is simply a function of the age of the mortar, and not of age of loading.

They carried out tests in which saturated tubular specimens of mortar were loaded in torsion and put through various temperature regimes within the range 20°C to 95C. The ages at loading varied between 30 and 60 days, and the maximum time under load was 40 days. They found that the expression that described their results for the limiting value of the specific transitional thermal creep C_t (in microstrain per N/mm^2) was given by

$$C_{t\infty} = 2.46\ (\theta - 20) - 0.0082(\phi - 20)^2$$

where ϕ is the particular temperature and is larger than 20.

Parrott and Symmons (109) carried out tests on concrete specimens (450mm x 100mm square) under various loadings and temperatures histories. Their experiments were designed to measure elastic, recoverable, flow, and transitional thermal creep.

They found that their results for the transitional thermal creep could be fitted to the following equation

Transitional thermal creep/unit stress/°C virgin temperature rise =

$$= 0.45 \times 10^{-6} \times \Delta T \times (0.3 + 0.7 (1 - e^{t_v/\theta_1}))$$

per N/mm^2 per degree C

where ΔT is the increase in temperature t_v is the virgin heating time.

In a later study Parrott (110) carried out tests on prisms of hardened cement paste 12 x 12 x 110mm loaded to a stress of 4 N/mm^2. The prisms were gradually heated from 20 to 60°C. He found that prisms exhibited large increases in creep when they were gradually heated for the first time from 20 to 60°C. Transitional thermal creep developed, but to a lesser extent in prisms which were subjected to preloading heating cycle. Cooling did not induce any transitional thermal creep.

Rainford and J.Timusk (111) carried out tests on sealed cement paste specimens (35.65 x 12.7 x 7.62cm) loaded at 28 days to a constant stress/strength ratio of 0.2 and were subjected to cyclic temperatures of 32.3° to -5°C, the period of cycling ranging from one to four days and they studied their creep behaviour in relation to the amplitude, and frequency and mean value of the cyclic temperature. They found that temperature cycling increased creep above that which occurred at the mean temperature and this creep may be greater than that which would occur at the highest temperature.

Fahmi et.al.(112) carried out tests on hollow cylindrical microconcrete specimens (15.24 O.D, 12.7cm I.D., 101.6 cm long) in

compression and torsion, at 50 and 100% relative humidity. They were subjected to a sustained load for 37 days at 23°C, and then heated to 60°C or exposed to thermal cycles between 23 and 60°C. They observed an increase in creep strain and rate of creep when the concrete was first heated and sustained at 60°C., and that after heating, the creep strain continued increasing with time for the 100% R.H. specimens, whereas for the 50% R.H. specimens the creep strain stablised in about 2 to 3 weeks. They explained it as due to irreversible changes in the structure of the cement gel caused by elevated temperature. They found that the first thermal cycle caused the largest increase in creep strain. Although each subsequent thermal cycle caused a further increase in creep for the 100% R.H. specimens, no appreciable increase in creep was observed on the 50% R.H. specimens. The specific creep in torsion was higher than that in compression at sustained normal elevated or cyclic temperatures. Most of the creep strain at elevated or cyclic temperature was irrecoverable.

2.5.4 Prediction of creep deformation

It is generally accepted that creep within the working normal load is proportional to stress. There are various methods for predicting long-term deformation of concrete structures due to creep, and they range in complexity from the simple design aids using charts (113) to the use of the finite elements with various complexities (depending on the number of factors involved). Here a short review is made for the relevant methods of predicting long-term deformation due to creep.

2.5.4.1 Prediction under constant stress

There are two approaches used in predicting long-term creep deformation: one using extropolation of short term results and the other based upon mix composition, strength and operating conditions such as employed by the codes.

Prediction of long-term creep from short term results is divided into those which assume that creep deformation tends to a limiting value and those which assume that creep deformation increases indefinitely.

The types of creep expressions which have a limiting value are the exponential and hyperbolic expressions, and those which do not have a finite limit are the power and logarthimic expressions.

Of these expressions, the most commonly used is the Ross Lorman hyperbola, which is in the form

$$C(t,to) = \frac{(t - t_o)}{A+B(t-t_o)}$$

where A and B are constants, and the limiting creep is thus equal to $\frac{1}{B}$ and can be obtained from experimental results, by plotting (t-to)/C(t,to) against (t-to) which give a straight line of slope B and the intercept on the ordinate is equal to A. Bazant criticised the use of this prediction method since the plot of results does not always give a straight line (114).

An example of this approach is given in Figure 2.12 using data from test 8.I.

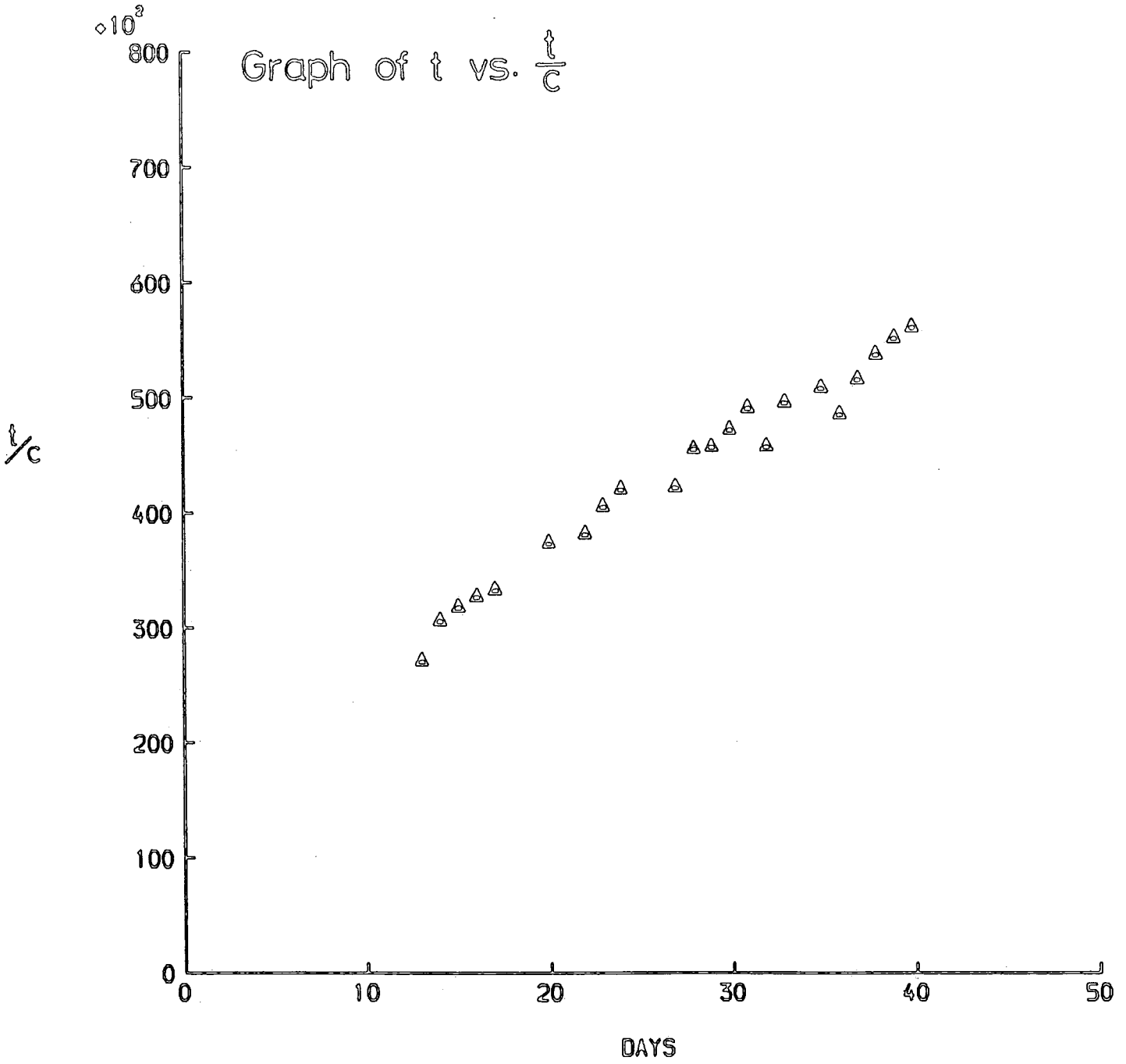
Graph of t vs. t/c
◇10³
800
700
600
500
400
300
200
100
0
t/c
0
10
20
30
40
50
DAYS

Fig. 2.12

2.5.4.2 Prediction under varying stress

There are many methods of calculating strain under varying stress. The simplest method is the effective modulus method, where the effective modulus is calculated as

$$E_t = \frac{Eo}{1+\phi(t,t_o)} \quad \text{or} \quad \epsilon(t) = \frac{\sigma(t)}{E(t_o)} \left[1 + \phi(t,t_o)\right]$$

$\phi(t,to)$ is the creep coefficient i.e. the ratio of creep strain at time t to elastic strain at the initial time t_o.

The effective modulus method underestimates strain under decreasing stress, and overestimates strain under increasing stress. For this reason it gives a good result if the stress does not vary significantly during the period under investigation. It also does not take in consideration, the ageing of concrete. Trost and Bazant modified the elastic modulus method to account for the ageing of concrete, where they introduced an ageing coefficient χ, which E_e is calculated as

$$E_e = \frac{E(t_o)}{1+\chi(t,t_o)\phi(t,t_o)}$$

where $\chi(t,to)$ is the ageing coefficient. This method is called, the age-adjusted effective modulus method.

The use of the effective modulus method in an elevated temperature and varying humidity environment leads to difficulties due to the changing of E with temperature, and the redistribution of stress due to the non uniform temperature.

Rate of creep method

The rate of creep method is based on the assumption that the rate of creep at any time is independent of the age of loading. This results in parallel creep curves for all ages at application of load. The rate of creep method can be given mathematically by the following relationship

$$\frac{d\varepsilon}{dt} = \frac{1}{E} \cdot \frac{d\sigma}{dt} + \sigma \cdot \frac{dc}{dt}$$

where ε is strain, σ is stress, E is the elastic modulus, which is assumed to be constant, c is the specific creep strain (Strain per unit stress).

The main deficiency of this method is that it neglects strain recovery that is strains in a decreasing stress environment.

In an elevated temperature environment, although the irrecoverable creep component (flow) is greatly enhanced, the recoverable (delayed elastic) is greatly diminished. This enhances the value of the rate of creep method in an elevated temperature environment. The method has been used successfully by many researchers when the temperature is elevated (115,116,117).

In their paper Ross et al.(116) further demonstrated that in general terms a prestressed beam subjected to a prolonged temperature crossfall will reach a stable stress distribution. This distribution which they referred to as steady-state stresses can be calculated without reference to the elastic modulus and coefficient of expansion of the concrete. However very few experimental data support this due to the fact that the structure needs a very long time to reach this state and might not reach it at all if the creep capacity of concrete involved is not sufficient to allow the process of redistribution to become complete.

Other methods of predicting creep include the use of the principle of superposition, the rate of flow method where creep is divided into two components, delayed elastic strain and flow. It requires more data than the rate of creep method. It is superior to the rate of creep method in predicting strain under a decreasing stress. The improved Dischinger method (118) is a simplification to the rate of flow method by assuming that the recoverable creep develops instantly after the stress is applied and therefore can be included with the initial elastic strain. In an elevated temperature however, because of the diminishing value of the recoverable strain, the required accuracy thus does not justify the added complexity resulting in the use of the rate of flow method or the improved Dischinger method as opposed to the rate of creep method.

More recently some researchers have used a statistical approach in predicting long-term deformation from design strength and concrete composition. This aproach is improved greatly by carrying out some short-time creep measurements. Thus using a Bayesian type statistic (119).

Comments

From the foregoing cited experimental data and the discussion on various methods of predicting creep, the following comment can be made.

Although there are a great number of predictive methods for creep deformation, with different degrees of mathematical complications, their use in any practical situation always necessitates some form of approximation by ignoring or idealising some relevant factors. Thus the use of elegant and sophisticated mathematical expressions should not mask the fact that any equation is not more reliable than the data used in its formulation (or fed in it to predict a particular situation). Even if

excellent agreement was occasionally reported, it was often found that data were used selectively, and did not include all information about test conditions making it difficult to reproduce results.

Thus from a designer's point of view, the use of a simple method is probably preferable to a complicated one for the good reason that it is simple. And that a method using physical and observable components is always preferable to one based on unproven and often arbitrary assumptions.

2.5.4.3 Creep, curvature and deflection

The preceding discussion concentratated on creep as a material property. However the engineer is interested in predicting creep deformation in actual structure. The two commonly used methods are the effective modulus method (or the modified age adjusted method) for unheated conditions and the rate of creep for heated conditions. The effective modulus approach involves predicting the creep coefficient (ϕ) either from mix information or through short term tests on small specimen. Then E_t (the effective modulus) is calculated from the equation

$$E_t = \frac{E_o}{1+\phi}$$

Then deflection can be calculated by replacing E_o (the initial modulus) by E_t in the standard expression for the elastic deflection

$$d = K \frac{M^{max} L^2}{E_o I_u}$$

Here K is a deflection coefficient depending on type of loadig and type of support, L is the span and I_u is the second moment of area of the transformed uncracked section.

If the section is cracked however, then the moment curvature relation will not be linear due to the variation of I. There are several methods of calculating I (and its variation with time for a loaded member) for partialy cracked section. They vary in complexity from the simple methods such as the commonly used Branson's (87) empirical exression to the use of the finite element method (120) (with differing degrees of complications). Branson's expression is of the form

$$I_e = \left(\frac{M_{CR}}{M^{max}}\right)^m I_g + \left[1 - \left(\frac{M_{CR}}{M^{max}}\right)^m\right] I_c$$

where I_e is the effective second moment of area, M_{cr} is the cracking moment and M^{max} is the maximum moment ever applied to the member. I_g is the second moment of area of the transformed uncracked section and I_c is the second moment of area of the cracked section. The exponent m was found from experiments to be equal to 3 for simply supported beam and 4 for individual sections in continuous members.

The second approach to computing long-term deflection is to multiply the initial elastic deflection d_o by factors representing the effect of creep in deflection

$$\Delta d(t) = d_o \; K \; \phi \; (t,to)$$

where $\Delta d(t)$ is deflection due to creep d_o is the initial (elastic) deflection, K is a reduction coefficient depending on the ratio of the compression steel area to the tension steel area, and $\phi(t,to)$ is creep coefficient(ratio of creep strain to elastic strain) at time to for concrete loaded at time to. The use of the rate of creep method in heated environment involves dividing the time into discrete intervals and the continuum of the structure into a number of discrete elements. By assuming that stress is constant through each time subinterval, strain distribution can be found using the specific thermal creep concept. However if the temperature distribution is non-linear, then the resulting strain distribution will not satisfy the compatability condition of plane sections remaining plane. This condition is satisfied by imposing the equilibrium conditions for forces and moment changes across the section (for fuller treatment of this see Chapter 3, section 2). Curvature then equals the slope of the strain distribution across the section. Thus deflection can be calculated using the moment-area theorem or any other method.

It must be noted however that these methods are approximate methods. That is, they assume that certain factors can be neglected, thus simplifying the calculations. For example redistribtuion of stresses can occur in reinforced concrete member under sustained load even with no temperature gradient due to the lowering of the neutral axis.

CHAPTER 3

THEORY AND ANALYSIS

Introduction

In this chapter. the theoretical basis for the computer programs used in the several analyses are established. They are discussed under the following headings:-

1) Stresses induced in a reinforced concrete cross section due to the nonlinear temperature distriution during a daily thermal cycle. This was programmed in the computer program AZ (listed in the appendix).
2) Long term analysis of creep curvature. This was programmed in the computer program CPCR (listed in Appendix).
3) Finite Element analysis of transient temperatures in a concrete deck by the use of the Package Program PAFEC (121,125).
4) Statistics : Programs SA (listed in Appendix) for finding the confidence interval and the package programs from NAG library to calculate a least square cubic spline fit for the data points.

3.1 Stresses induced in reinforced concrete cross section due to the non linear temperature distribution during a daily thermal cycle:-

In this section the analysis of the effects of the nonlinear temperature distribution during the daily thermal cycle is carried out on singly reinforced. simply supported concrete beams. The method is similar to the treatment employed by Priestley (40). for prestressed beams and is as follows·

If we consider a typical section as in Figure 3.1.a, subjected to a nonlinear temperature profile across its depth as in 3.1.b. These nonlinear temperature distributions will produce a free strain profile as in 3.1.c. This free strain if not restrained axially or flexurally will decompose into an axial strain as in 3.1.d and curvature as in 3.1.e plus a residual stress inducing strain as in 3.1.f. This residual stress inducing strain is due to the compatibility of strains condition that plane sections must remain plane.

For a single-span simply supported beam. two equilibrium conditions due to the thermal loading must be satisfied:

(i) The total axial force on the section induced by temperature distribtion in the concrete and steel must be zero.

(ii) The net moment on the section due to the foregoing forces must be zero.

From Figure 3.1 we have

$$\varepsilon_s = \varepsilon_a + \varepsilon_y - \alpha_c t$$

$$= \varepsilon_a + y\left(\frac{\varepsilon_c}{h}\right) - \alpha_c t$$

Converting this into stress. we have

$$S_y = E_c\left(\varepsilon_a + y\left(\frac{\varepsilon_c}{h}\right) - \alpha_c t_y\right) \qquad \ldots 3.1.1$$

in which compression strains are taken as positive.

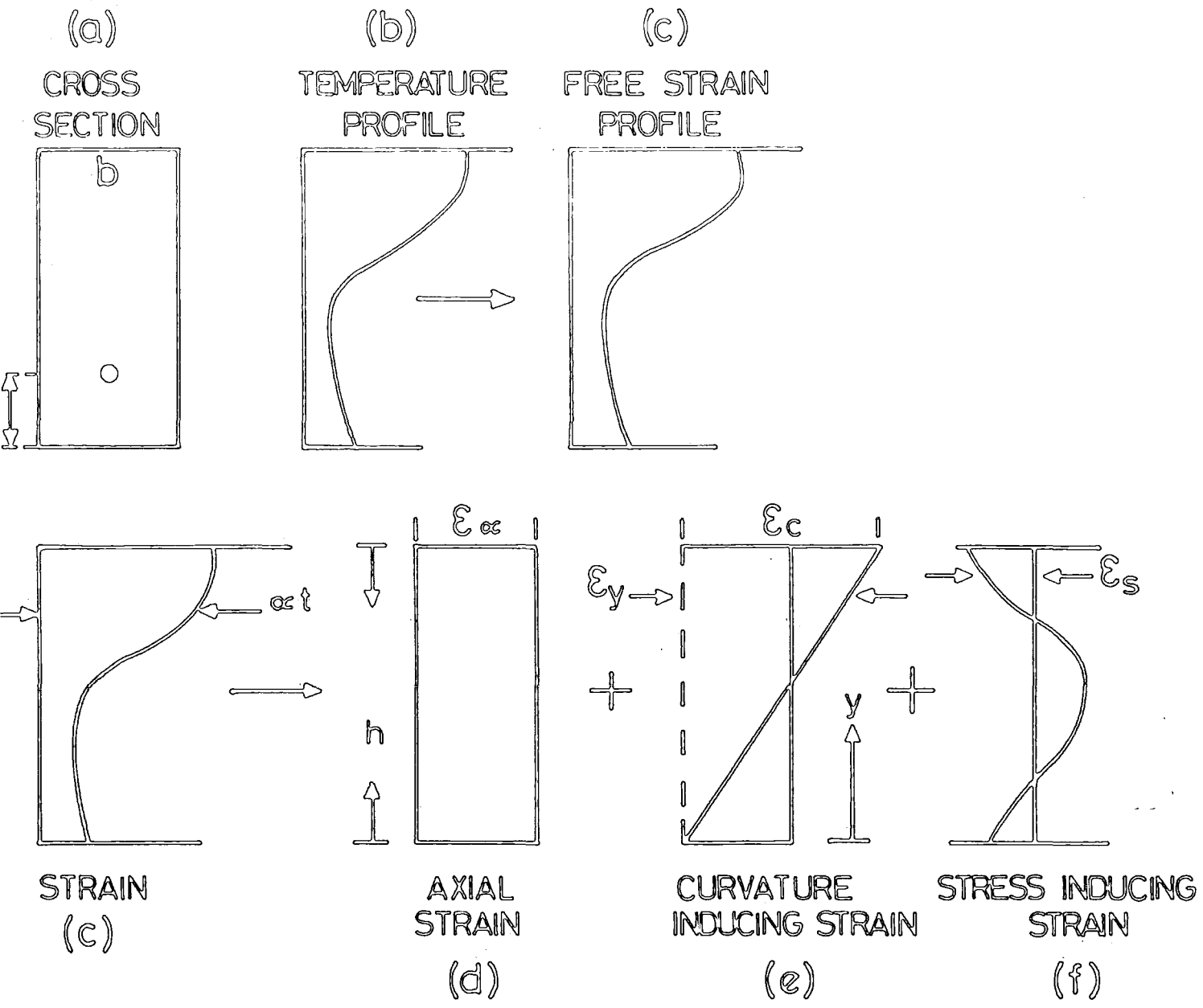

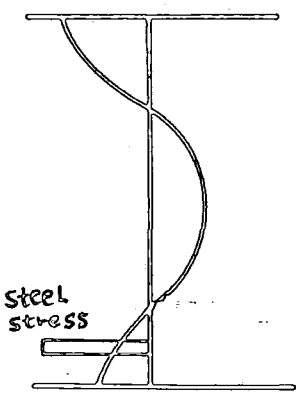

STRESS INDUCED BY STRAIN IN (F) PLUS STEEL STRESS.

(g)

FIG. 3-1

Applying the first condition for the force:-

$$\int_0^h s_y.b.dy + E_s\ (\varepsilon_a + y_s\ (\frac{\varepsilon_c}{h}) - \alpha_s t_s) A_s = 0$$

$\alpha_c, E_c, \alpha_s, E_s$ = The coefficient of thermal expansion and the elastic modulus of concrete and steel respectively.

h = depth of the section

b = width of the section

$\bar{y}$ = the vertical distance of the centroid from the origin

y_s = distance of the steel from the origin

t_s = temperature of the steel

S_y = stress at layer y from the origin

t_y = temperature at layer y from the origin

$$\therefore\ E_c \int_0^h (\varepsilon_a + y\ (\frac{\varepsilon_c}{h}) - \alpha_c t_y)\ b.dy + E_s\ (\varepsilon_a + y_s\ (\frac{\varepsilon_c}{h}) - \alpha_s t_s)\ A_s = 0$$

$$= \varepsilon_a \int_0^h b.dy + \frac{\varepsilon_c}{h} \int_0^h y.b.dy - \alpha_c \int_0^h b.t_y.dy + F_s = 0$$

where $$F_s = \frac{E_s}{E_c}\ (\varepsilon_a + y_s\ (\frac{\varepsilon_c}{h}) - \alpha_s.t_s)$$

But

$$\int_0^h b.dy = \text{area of the cross section} = A$$

$$\int_0^h y.b.dy = \text{moment of the area about the bottom} = \bar{y}\,A.$$

$$\therefore \quad \varepsilon_a + \frac{\varepsilon_c}{h}\,\bar{y} = \frac{1}{A}\left(\alpha_c \int_0^h b.t_y.dy - F_s\right) \qquad \ldots\ 3.1.2$$

Applying the second condition for moment equilibrium

$$\int_0^h S_y\,(y-\bar{y})\,b.dy + E_s\,(\varepsilon_a + y_s(\frac{\varepsilon_c}{h}) - \alpha_s t_s)\,(y_s-\bar{y})A_s = 0$$

substituting for S_y

$$\therefore \quad E_c = \int_o^h (\varepsilon_a + (\frac{\varepsilon_c}{h})y - \alpha_c t_y)\ (y - \bar{y})\ b.dy +$$

$$E_s\ (\varepsilon_a + y_s\ (\frac{\varepsilon_c}{h}) - \alpha_s t_s)(y_s - \bar{y})\ A_s = 0$$

$$\int_o^h (\varepsilon_a + y(\frac{\varepsilon_c}{h}) - \alpha_c t_y)\ (y - \bar{y})\ b.dy + M_s = 0$$

where $M_s = \dfrac{E_s}{E_c}\ (\varepsilon_a + y_s(\frac{\varepsilon_c}{h}) - \alpha_s t_s)\ (y_s - \bar{y})\ A_s$

$$\int_o^h \varepsilon_a(y - \bar{y})\ b.dy + (\frac{\varepsilon_c}{h}) \int_o^h y\ (y - \bar{y})\ b.dy - \alpha_c \int_o^h t_y\ (y - \bar{y})\ b.dy$$

$$+ M_s = 0$$

$$\varepsilon_a \int_o^h y.b.dy - \varepsilon_a \bar{y} \int_o^h b.dy + \frac{\varepsilon_c}{h} \left(\int_o^h y^2\ b.dy - \bar{y} \int_o^h y.b.dy \right)$$

$$- \alpha_c \int_o^h ty\ (y - \bar{y})\ b.dy + M_s = 0$$

But $\int_o^h y.b.dy = \bar{y} \int_o^h b.dy$ (first moment of area about the bottom)

$$\therefore \quad \frac{\varepsilon_c}{h} \int_o^h y^2.b.dy - \frac{\varepsilon_c}{h} \cdot \bar{y} \int_o^h y.b.dy$$

$$= \alpha_c \int_o^h t_y\ (y - \bar{y})\ b.dy - M_s$$

But $\int_o^h y^2.b.dy$ = second moment of area of the section about origin which equal to $I + \bar{y}^2 A$

I = second moment of area of the section about centroidal axis.

$$\therefore \quad \frac{\varepsilon_c}{h}(I + \bar{y}^2 A) - \left(\frac{\varepsilon_c}{h}\right)(\bar{y})(\bar{y}A) = = \alpha_c \int_o^h t_y (y - \bar{y})\, b.dy - M_s$$

$$\varepsilon_c = \frac{h}{I}\left(\alpha_c \int_o^h t_y (y - \bar{y})\, b.dy - M_s\right) \qquad \ldots 3.1.3$$

Substituting the value of ε_c in 3.1.3 into 3.1.2

$$\varepsilon_a + \frac{\bar{y}}{I}\left(\alpha_c \int_o^h t_y (y - \bar{y})\, b.dy - M_s\right) = \frac{1}{A}\left(\alpha_c \int_o^h b.ty.dy - F_s\right)$$

$$\varepsilon_a = \frac{1}{A}\left(\alpha_c \int_o^h b.t_y.dy - F_s\right) - \frac{\bar{y}}{I}\left(\alpha_c \int_o^h t_y (y - \bar{y})\, b.dy - M_s\right) \qquad \ldots 3.1.4$$

If we put the value of ε_a from 3.1.4 and ε_c from eq. 3.1.3 into eq. 3.1.1 we have

$$S_y = E_c \left[\frac{\alpha_c \int_o^h b.t_y.dy - F_s}{A} - \frac{\bar{y}\left(\alpha_c \int_o^h t_y (y-\bar{y})\, b.dy - M_s\right)}{I} \right.$$

$$\left. + \frac{y}{I}\left(\alpha_c \int_o^h t_y (y - \bar{y})\, b.dy - M_s - \alpha_c t\right) \right]$$

$$= E_c \left[\frac{\alpha_c \int_o^h bty.dy - F_s}{A} + \frac{(y-\bar{y})\left(\alpha_c \int_o^h t_y (y-\bar{y})\, b.dy + M_s\right)}{I} - \alpha_c t \right] \qquad \ldots 3.1.5$$

$$= E_c \left[\frac{F}{A} + \frac{(y-\bar{y})M}{I} - \alpha_c t \right]$$

where total $F = \dfrac{\int_o^h b.t_y.dy - F_s}{A}$

and $M = \dfrac{(y-\bar{y})\left(\alpha_c \int_o^h t_y (y-\bar{y})\, b.dy + M_s\right)}{I}$

These calculations are carried out by the computer program AZ (listed in the appendix).

In the computer program, the two integrals in eq.3.1.5 are solved numerically by sub-dividing the section into a finite number of layers. The temperature in each layer is found by linear interpolation between the temperature of the thermocouple above it and the thermocouple below it. Then each layer is allowed to expand freely by multiplying its calculated temperature by the coefficient of expansion. The strain obtained is converted into stress by multiplying it by elastic modulus of the concrete. Equilibrium is then enforced for both axial force and for moment. The resulting calculations yield actual strains and self-equilibrating stresses.

3.2 Long term analysis of creep curvature

In this section the rate of creep method with a step by step approach is applied in the prediction of long term creep curvature for simply supported, singly reinforced concrete beams, loaded in four point bending, and subjected to daily heating/cooling and humidity cycles.

Theory:-

Assumptions:-

(1) Plane sections remain plane.

(2) Creep both axially and flexurally is linearly proportional to stress and temperature in the range considered.

(3) Creep in tension is equal to creep in compression.

(4) Elastic modulus is independent of temperature and its value in compression is equal to its value in tension.

(5) Creep recovery due to reduction in magnitude of stress caused by stress redistribution is neglected.

(6) The contribution of the cracked parts of the section is ignored when balancing force and moment over the section. But the second moment of area of the section is calculated initially using the Branson (87) formula

$$I_{eff.} = \left(\frac{M_{cr}}{M^{max}}\right)^3 \cdot I_{\mathcal{U}} + \left[1 - \left(\frac{M_{cr}}{M^{max}}\right)^3\right] I_c$$

M_{cr} is the cracking moment = $I_{\mathcal{U}} f_{cm}/y$

$I_{\mathcal{U}}$ = second moment of area of the transformed uncracked section.

I_c = second moment of area of the cracked section.

y = Distance from centroid of the transformed section to the extreme tension fibre.

The rate of creep method as used for thermal-creep problems

$$\frac{d\epsilon}{dt} = \frac{1}{E} \cdot \frac{d\sigma}{dt} + \sigma \cdot \phi(T) \frac{dc}{dt}$$

..... 3.2.1

where ε is creep strain .

σ is stress

c is specific thermal creep (strain per unit stress per degree)

ϕ (T) a function that relates changes of specific creep with temperature

Thus the increment of creep that develops between t_0 and $t_0 + \Delta t$ during an assumed constant stress will be

$$\Delta\varepsilon = \sigma.\phi\ (T)\ .\ \Delta c \qquad \ldots\ 3.2.3$$

Further, if we assume that in the range of temperature considered, there is a direct proportionality between creep and temperature (assumption 2) then 3.2.3 becomes

$$\Delta\varepsilon = \sigma.T.\Delta c \qquad .....3.2.4$$

In the computer program CPCR (listed in the appendix), the section was subdivided into a finite number of layers. The temperature of each layer was found by linear interpolation between the thermocouple above it and the thermocouple below it. Then a weighted average for the temperature of the layer over the twenty four hours period was determined.

Since the temperature distribution is nonlinear. then free creep strain of each layer. assuming zero restraint. would take the profile shown in Figure 3.2.a which is the same shape as the time averaged temperature profile. However. because of the constraint of the section to a linear strain profile. it will take the shape shown in Figure 3.2.b with a residual strain inducing stress as shown in Figure 3.2.c. Stresses induced by these strains are usually called self-equilibrating stresses.

However because the cross section was cracked these stresses will take the shape shown in 3.2.f. The strains in 3.2.b are composed of an average axial shortening of 3.2.d and curvature inducing strain of 3.2.e. The strain inducing stress in 3.2.c. the axial strain in 3.2.d and the curvature in 3.2.e can be found from the two equilibrium conditions of force and moment. Since no external forces or moments are available to balance any thermally induced net forces or moments, the total axial force and moment change on the section must be zero. At the end of the time interval Δt, the quantity to be determined is

$$S_y = E\left(\sigma \cdot T \cdot \Delta C - \varepsilon a + y \left(\frac{\varepsilon_c}{h}\right)\right) \qquad \ldots 3.2.5$$

which is similar to equation 3.1.1.

The stresses found by eq. 3.2.5 are added to σ (applied moment stresses) at the end of the time interval Δt. and the two conditions of equilibrium are applied to force and moment over the section. The new determined stress σ is assumed to apply through the next time interval Δt and so on.

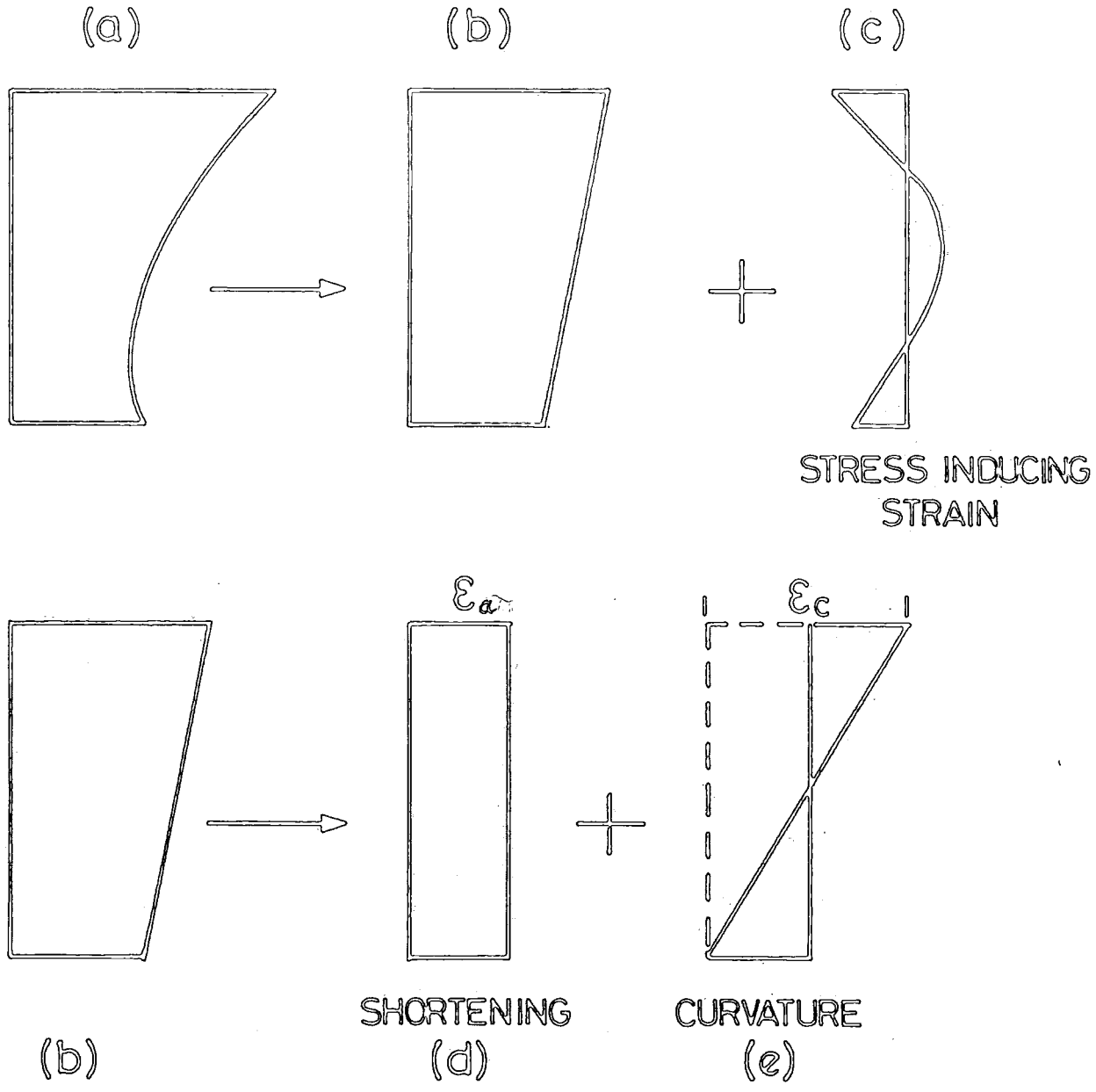

Because of cracking strain in c, will produce stress in (f)

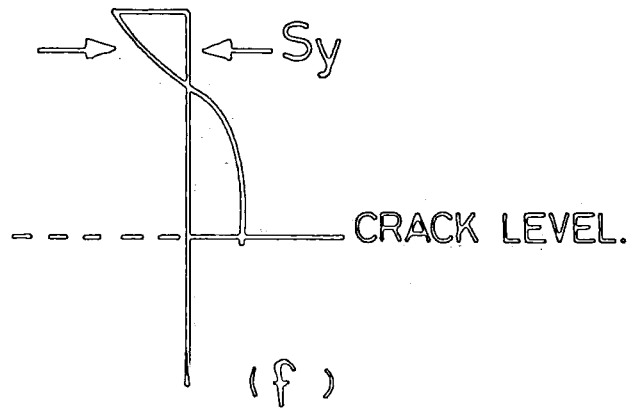

FIG. 3·2.

The following steps are followed:

1) At the start, the stress and displacement due to the applied physical loading are found for each layer.
2) Stresses found in (1) are sustained with the applied temperatue through time interval Δt while each layer is allowed to deform freely.
3) At the end of the interval, the strains and stresses of the layers are adjusted for strain compatibility, and force and moment equilibrium.
4) The integrated effects of these adjustments on the physical forces and displacements of the structure are determined, then superimposed onto those prevailing at the start of the interval.

The procedure is then taken through steps 2 to 4 for each successive time interval using the strsses determined at the end of the preceding interval, until the end of the period. The total creep at the end of the period is found by adding all the creep increments determined in each time interval.

The specific thermal creep used in the program was determined from tests on small unreinforced concrete cylinders (60mm ϕ and 200mm long) kept in an environment of relatively constant temperature and humidity (20°C and 50%R.H.)

3.3 Finite Element

3.3.1 Review of the finite Element formulation for transient Temperature distribution

The variation of temperature T over a beam cross section at any time t is governed by the parabolic partial differential equation (122,123).

$$\frac{\partial}{\partial X}\left(K\frac{\partial T}{\partial X}\right)+\frac{\partial}{\partial y}\left(K\frac{\partial T}{\partial y}\right)+Q=\rho.C\frac{\partial T}{\partial t} \qquad \ldots 3.3.1$$

where K is the thermal conductivity in W/m C°,

Q = rate of heat per unit volume generated within the body (e.g. by hydration of cement), W/m^3,

ρ = density Kg/m^3 and C = specific heat J/(Kg C°) if K is isotropic then eq. 3.3.1 becomes

$$K\left(\frac{\partial^2 T}{\partial X^2}+\frac{\partial^2 T}{\partial y^2}\right)+Q=\rho.C\frac{\partial T}{\partial t} \qquad \ldots 3.3.2$$

and the boundary condition associated with 3.3.2 can be expressed as

$$K\left(\frac{\partial T}{\partial X}\ell_x+\frac{\partial T}{\partial y}\ell_y\right)+q=0$$

where ℓ_x and ℓ_y are direction cosines of two unit outward normal to the boundary surface, and q is boundary heat input at or loss per unit area. W/m^2.

The rate of energy transfer q at the surface of the beam is the sum of solar radiation, convection and irradiation

$$q = q_s + q_c + q_r$$

The heat gain due to the sun's rays q_s is equal to $q_s = aI(s,t)$ in which $I(s,t)$ is the total solar radiation on surface s at time t. This depends upon the parameter s defining the position of the point considered and the angle of incidence of the sun's rays. a is a dimensionless coefficient and is the fraction of I absorbed by the surface.

The heat lost to or gained from the surrounding air by convection as a result of temperature differences between the concrete surface and the air is given by Newton's law of cooling as $q_c = h_c (T - T_a)$ in which h_c = convection heat transfer coefficient $W(m^2C°)$, T, T_a are temperatures of the surface and air respectively. h_c is a function of many variables such as wind speed. surface roughness. and geometric configuration of the exposed surface-structure.

The heat transfer between the concrete surface and the surrounding atmosphere due to long wave radiation. i.e. thermal irradiation. produces a nonlinear boundary condition which can be modelled by Stefan-Boltz man radiation law as

$$q_r = c_s \cdot e \left[(T + T^*)^4 - (T_a + T^*)^4 \right]$$

in which C_s = Stefan Boltzman constant = 5.677×10^{-8} $W/(m^2K^4)$.
e = emissivity coefficient relating the radiation of the bridge surface to that of an ideal black body and T* is a constant (273.15) used to convert temperature in degrees celsius °C. to degree Kelvin, K°.

Finite Element Formulation:-

The rectangular cross section is divided into a mesh of finite number of discrete elements with specified nodes. Two quadrilateral two-dimensional types of elements were used, an eight node interior element and a six node fictitious element to model the boundary heat transfer. The temperature within a finite element can be approximated by

$$T(x,y.t)^e = [\,N\,]\,\{\,T\,\}^e$$

in which [N] = linear shape functions and $\{T\}^e$ = column vector of eight or six nodal temperatures for interior and boundary elements respectively.

The finite element method uses the variation principle to obtain numerical solutions from the stationary conditions of a function (122). The functional is defined in terms of an unknown function that renders the functional stationary and is the solution to the differential equation.

At equilibrium, the functional is stationary and its first variation vanishes. The Euler-Lagrange equation must be satisfied. The functional, at stationary conditions, yields equations from which approximate solutions are obtained. These Euler-Lagrange equations are the equilibrium equations of the system which are described by the differential equation.

By applying the variational principle of the finite element method eq . 3.3.2 becomes (121,124).

$$[M]\{\dot{T}\} + [S]\{T\} = \{Q\}$$

in which [M] . [S] are respectively the square symmetric thermal mass and thermal conductivity matrices. {Q} is a vector of heat fluxes which enter the structure at the nodes. The thermal mass matrix for an element is given by (124)

$$[M]^e = \int_{V^e} \rho C [N]^T [N] \, dV$$

in which V^e indicates integration over the volume of the element. $[N]^T$ is the transpose matrix of [N]

The thermal conductivity matrix [S] is partitioned into $[S_a]^e$ and $[S_b]^e$ in which $[S_a]^e$ is for interior element and $[S_b]^e$ for boundary element. They are given by:-

$$[S_a]^e = K \int_{V^e} [B]^T [B] \, dV .$$

in which [B] = a matrix consisting of the first derivatives of the element shape functions with respect to x and y

$$[B] = \begin{bmatrix} \frac{\partial [N]}{\partial x} \\ \\ \frac{\partial [N]}{\partial y} \end{bmatrix}$$

The convection-radiation matrix $[S_b]^e$, of a boundary element e at time t can be expressed by:-

$$[S_b]^e = \int_{S_e} h\,[N]^T\,[N]\;dS$$

in which S^e = surface area of the element and h(s.t) = overall heat transfer coefficient which include both the effects of heat flow by convection and radiation ($h = h_c + h_r$).

The PAFEC (121) program, besides partitioning $[S]^e$, partitions also $[M]$ into $[M_a]$ and $[M_b]$, $\{T\}$ into $\{T_a\}$ and $\{\tilde{T}_b\}$, $\{Q\}$ into $\{\tilde{Q}_a\}$ and $\{Q_b\}$. where the tilde indicates a prescribed quantity, the program then solves the following equation.

$$[M_a]\{\dot{T}_a\} = \{\tilde{Q}_a\} - [S_a]\{T_a\} - [S_b]\{\tilde{T}_b\} - [M_b]\{\dot{\tilde{T}}_b\}$$

which if Ta and T_b are known at any one instant of time can be solved for the time derivative of the temperatures at the same instant of time. Thus for any node i

$$(T_i)_{t+\delta t} = (T_i)_t + (\dot{T}_i)_t \cdot \delta t$$

However because this marching process is slow. the Crank-Nicholson method is used where

$$\left([Sa] + \frac{2}{\delta t}[Ma]\right)\{Ta\}_{t+\delta t} = -\{\tilde{F}\} + [Ma]\left(\frac{2}{\delta t}\{Ta\}_t + \{\dot{T}\}_t\right)$$

where

$$\{\tilde{F}\} = [S_b]\{\tilde{T}_b\} + [M_b]\{\dot{\tilde{T}}_b\} - \{\tilde{Q}_a\}$$

The values of the time derivaties of temperatures at time $(t+\delta t)$ is obtained using

$$\{\dot{T}_a\}_{t+\delta t} = \frac{2}{\delta t}\left(\{T_a\}_{t+\delta t} - \{T_a\}_t\right) - \{\dot{T}_a\}_t$$

The stability of the solution is improved by taking $t = Z\ \delta t$. where Z is dependent upon the Fourier number

$$F = \delta t\ \Sigma\ (S_{ii}/M_{ii})$$

which is based upon the average value of the ratio between corresponding leading diagonal entries in the S_a and M_b, then Z is expressed empirically for a single degree of freedom by the formula.

$$Z = 0.55 + 1.093\ (F + 2.428) \qquad \ldots.3.3.3$$

Thus the program first finds F using the chosen value of time step δt, then Z is calculated from eq.3.3.3. The temperature distribution at $t = 0$ and $t = \delta t$ are then used in an interpolation process to find the temperatures at $t = Z\ \delta t$. The calculat ion of temperature then proceeds at increments of δt.

3.3.2 The Use of PAFEC -

Introduction

Here the finite element package programe PAFEC (125) is used to predict the transient temperature distribution inside a plain concrete beam of 0.2m thick subjected to climatical conditions similar to those of

Riyadh. However because of the lack of meteorological records of sufficient data necessary to calculate the various parameters used in the program and the experimental work, no exact correspondence between the few known climatical conditions prevelant in Riyadh and the ones used in the program and eventually in the experimental work was attempted. However, the few references available were used as a general guide for the data used.

3.3.2.1 Procedure:-

In the program the concrete cross section was divided into two interior elements and two fictitious boundary elements. Figure 3.3 shows the PAFEC node labelling system and the two types of elements used.

3.3.2.2.Shade temperature:-

Summer:

Reference (45)gave the highest temperature for Bahrain as 52°C with a return period of once in 100 years. But since it is known that the inland regions had a higher maximum temperature (126) than the coastal area. this maximum was increased to 56°C. The fourteen years meteorological record of (127) gave the minimum shade temperature during the summer as varying between 18°-26°C. the average value of 22°C was used as the mimimum. The average value rather than the lower value was taken. since it was felt unlikely that the lower value will occur at the same day with the highest value. This low value was assumed to occur just before sunrise at 05.00 hours Riyadh's time. The daily minimum

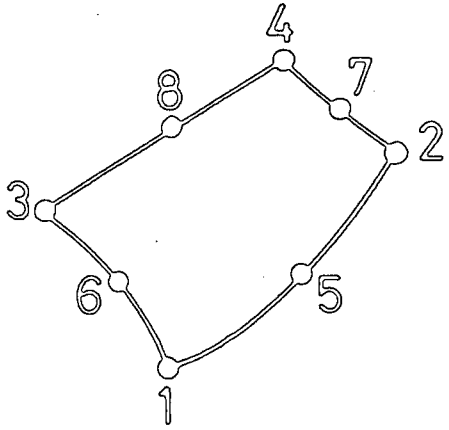

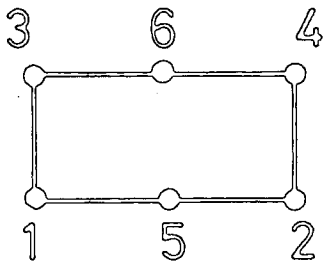

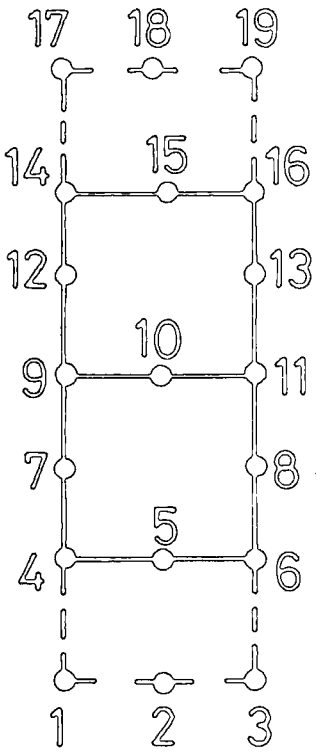

FIG. 3·3

effective temperature (that is when the gradient of the temperature through the depth of the beam is minimum) was assumed to occur at 08.00 Riyadh time (45).

Late Spring - Early Summer

The climatic condition necessary to produce a large positive temperature difference within the depth of the concrete beam is the coincidence of a high total of solar radiation, a large range of shade temperature, little wind and a low calculation starting temperature. Potocki (126) observed (from two years' of recording in Abu Dhabi) that this is more likely to happen in late spring-early summer rather than in any other season. The minimum temperature for the month of May (out of fourteen years metereological records) varied from 13° to 20°C. In the program the average temperature of 16.5°C was used.

The maximum shade temperature recorded for the month of May was 45°C. This was increased to 52°C in the program. Potocki also observed that the greatest rates of temperature change were recorded (over two years of recording) in the month of May. accordingly it was felt that the minimum effective temperature in Spring will occur earlier in the day than in the summer.

Emerson's (19) value for United Kingdom was 08.00± 1 hour. The value used in the program for late spring-early summer was 07.00 hours Riyadh time. That is the length of the cycle used in the program and the experimental work for late spring-early summer was taken as five hours rather than the value of four hours used for the summer.

3.3.2.3 Solar Radiation:-

The programe requires a value for nodal fluxes at nodes on the top surface. These fluxes were calculated using the equation for solar rays distribution suggested by Gloyne (128) and used by Emerson (19). Figure 3.4 shows the shape of the solar radiation curve. Emerson observed that a good agreement was obtained between measured and calculated values (eq.3.3.4) for the solar radiation distribution by increasing the solar day in the Gulf by two hours to 16 hours. She used a maximum total radiation of 9000 wh/m^2. These values were used in the program to model the solar radiation distribution for Riyadh in the summer and late spring-early summer.

Thus the values for the nodal fluxes is calculated as follows:

Summer:-

The calculation of the total radiation between two points in the solar day is represented by the following equation :-

$$\therefore I(t_o - t') = \int_{t_o}^{t'} \frac{2s}{T} \sin^2 \frac{\pi t}{T} \quad .... \quad 3.3.4$$

where t_o and t' are times from sunrise and S = Total radiation for the day

T = Length of solar day

for the summer equ.3.3.4 becomes

$$I(4\text{-}8) = \int_{t=4}^{t=8} \frac{2s}{T} \sin^2 \frac{\pi t}{T} \quad ..... \quad 3.3.5$$

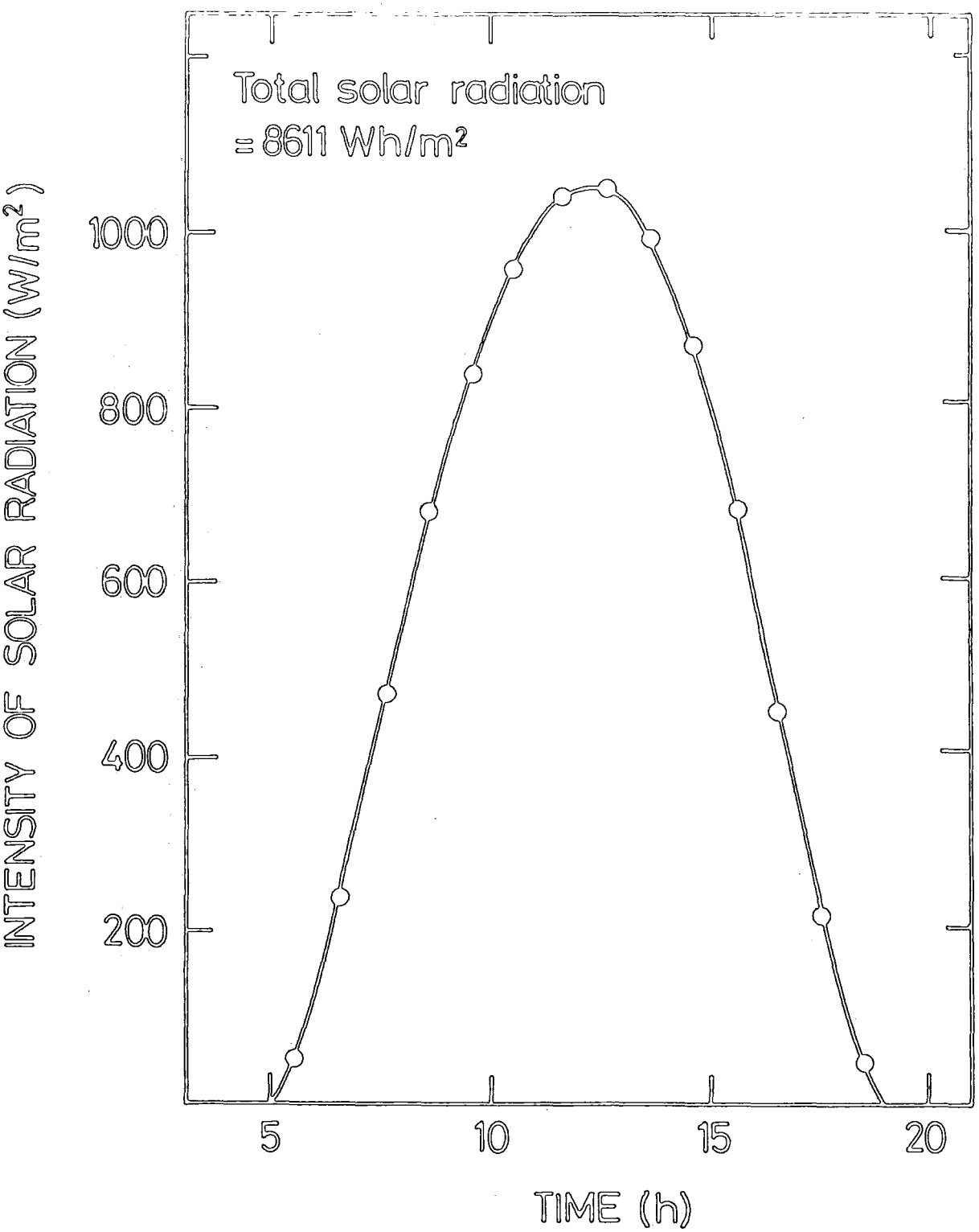

FIG. 3·4 MEASURED ARABIAN GULF SOLAR RADIATION. (From Ref. 45)

where S = 9000 Wh/m^2 and T = 16 hours

$\therefore$ $I(4\text{-}8) = 3682\ Wh/m^2$

$I(4) = 562.4$ and $I(8) = 1125\ Wh/m^2$

The correcting ratio = 1.09 so that $I(4) = 613$.
(for the correct integral by linear approximation.) $I(8) = 1226.3$

Because a consistent load vector apportions heat flux in the ratio 1:4:1 for corner to central nodes, the amount of radiation at nodes 14 and 16

At 08.00:-

$$= \frac{613}{6} = 102.2 \times 0.5 \times 0.1 = 5.1 \quad Wh/m^2$$

At 12.00:-

$$\frac{1226.3}{6} = 204.4 \times 0.5 \times 0.1 = 10.22 \quad Wh/m^2$$

The amount of radiation at node 15

At 08.00

$$= 5.1 \times 4 = 20.4 \quad Wh/m^2$$

At 12.00:- $= 10.22 \times 4 = 40.88 \quad Wh/m^2$

Note that the absorptivity used for plain concrete is 0.5 (Emerson).

The two numbers (4 and 8) used for the limit of the integral in eq.3.3.5 is the difference between sunrise (05.00 Riyadh time) after subtracting one hour as suggested by Emerson and the starting time of 08.00 and the end time of 12.00.

Late spring early summer:-

$$I(3\text{-}8) = \int_{t=3}^{t=8} \frac{2s}{T} \sin^2 \frac{\pi t}{T}$$

using this equation gives values of radiation fluxes at nodes 14 and 16 as follows:-

At 07.00

$$= 3.34 \quad Wh/m^2$$

At 12.00

$$= 10.78 \quad Wh/m^2$$

and at node 15

At 07.00

$$= 13.36 \quad Wh/m^2$$

At 12.00

$$= 43.13 \quad Wh/m^2$$

3.3.2.4 Other data used in the program (Emerson) :-

The program also requires the following data:-

Thermal conductivity K = 1.4W/m°C

Density. ρ = 2400 K9/m^3

specific heat. C = 960 J/gC°

Upper surface heat transfer coefficients = 23 W/m^2C°

Lower surface heat transfer coefficient = 9W/m^2C°

An example run for the program is listed in the appendix.

A comparison between predicted PAFEC values using the foregoing data and the measured experimental value for two typical days one modelling summer and the other modelling late spring-early summer is shown in Figures 3.5 and 3.6.

3.4 Statistics

3.4.1 Finding the confidence interval for curvature:-

We assume that all strain demec readings are independent. and that the depth of the strain demec buttons are fixed. Then if we take several strain readings over a particular depth, we will assume that these readings are randomly variable and that it is normally distributed.

The line connecting the means of these distributions is the population regression line:-

$$\eta(\dot{x}) = \alpha + \beta x$$

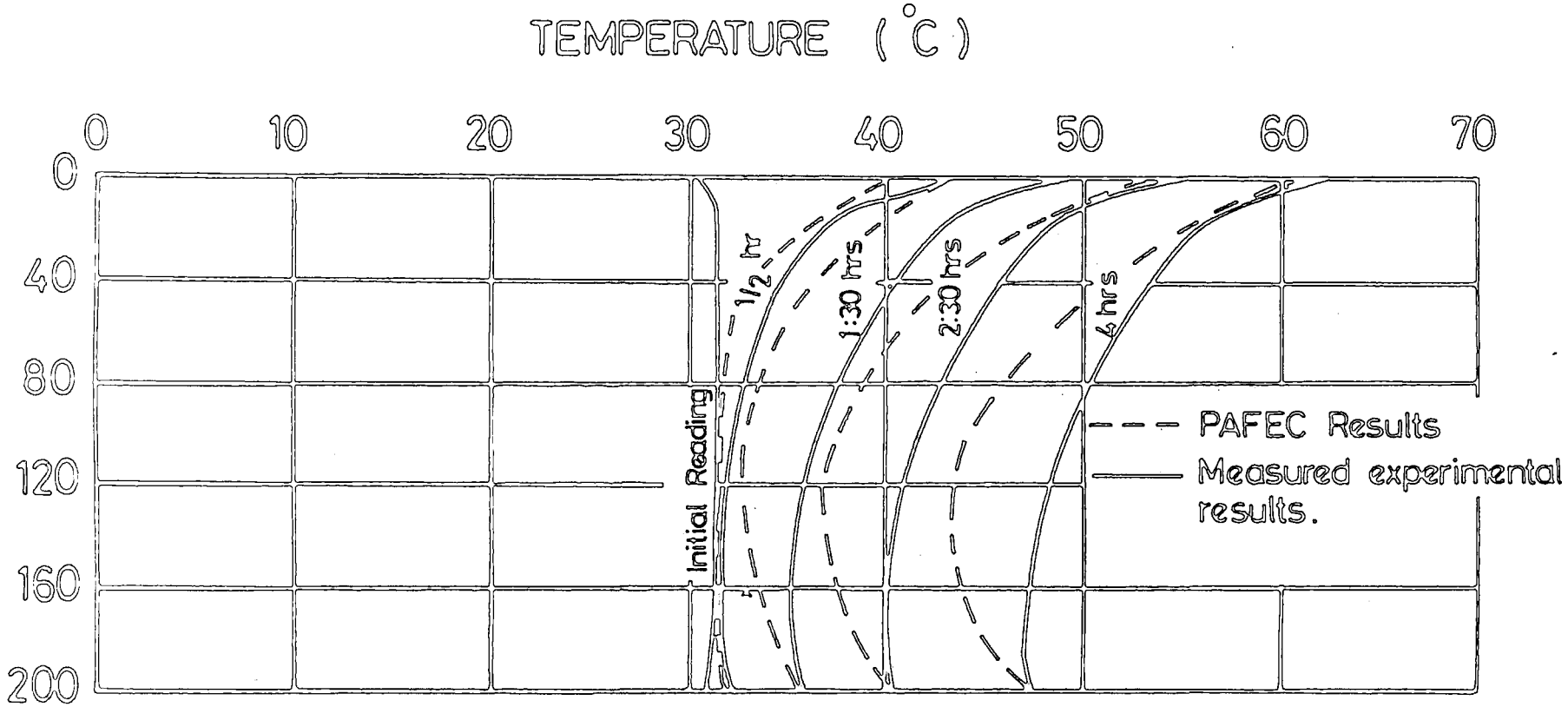

FIG.3.5 TEMPERATURE DISTRIBUTION THROUGH THE BEAM CROSS SECTION AT VARIOUS TIMES.

SUMMER CONDITIONS

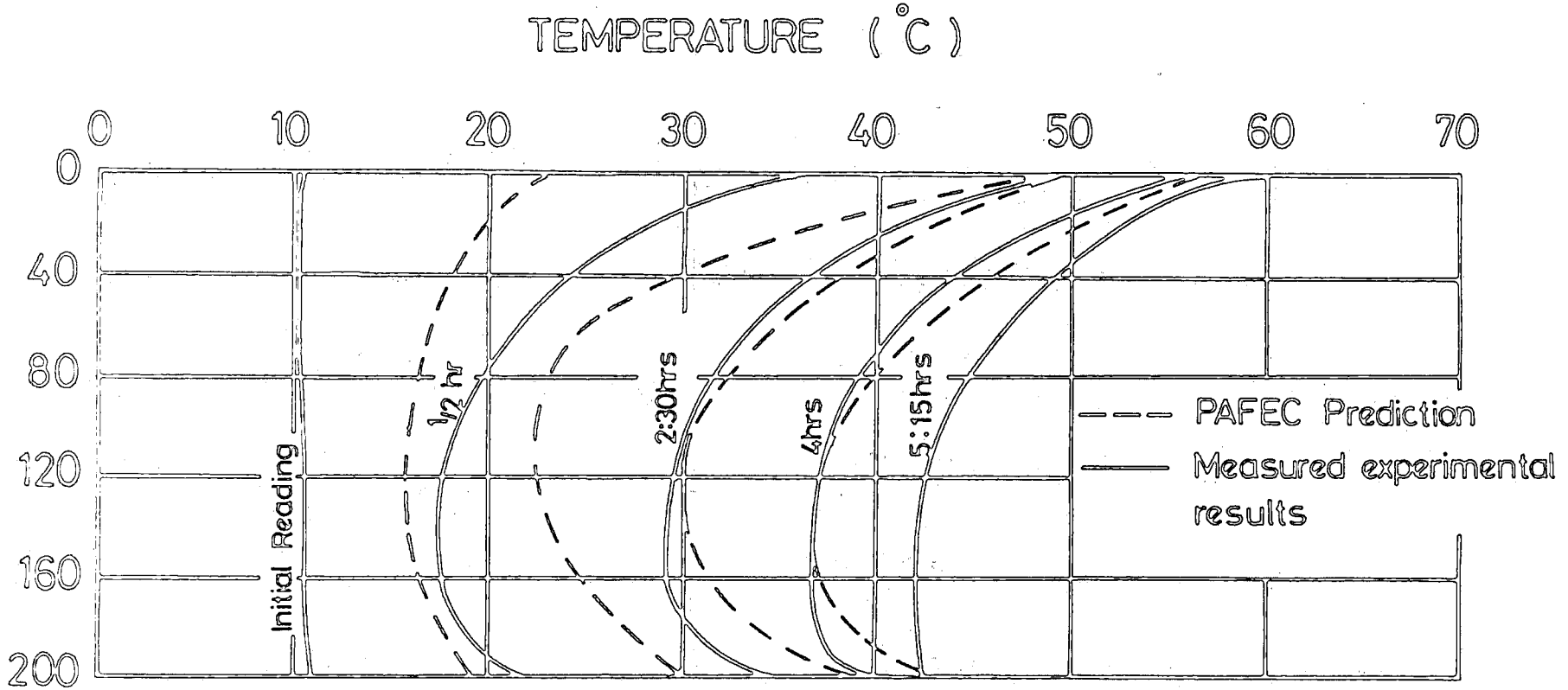

FIG. 3·6 TEMPERATURE DISTRIBUTION THROUGH THE BEAM CROSS SECTION AT VARIOUS TIMES.

SPRING CONDITIONS

if the estimates of the regression coefficients for strain at the soffit α and β (the curvature) are denoted by a and b respectively, then the estimate of $\eta(x)$ which is denoted by $\hat{y}$ is equal to

$$\hat{y} = a + b\,x$$

In figure 3.7 ϵ_i (error in the equation of the line) is a random error representing the vertical deviation of the point from the population regression line. and e_i is the vertical deviation of the point from the sample regression line

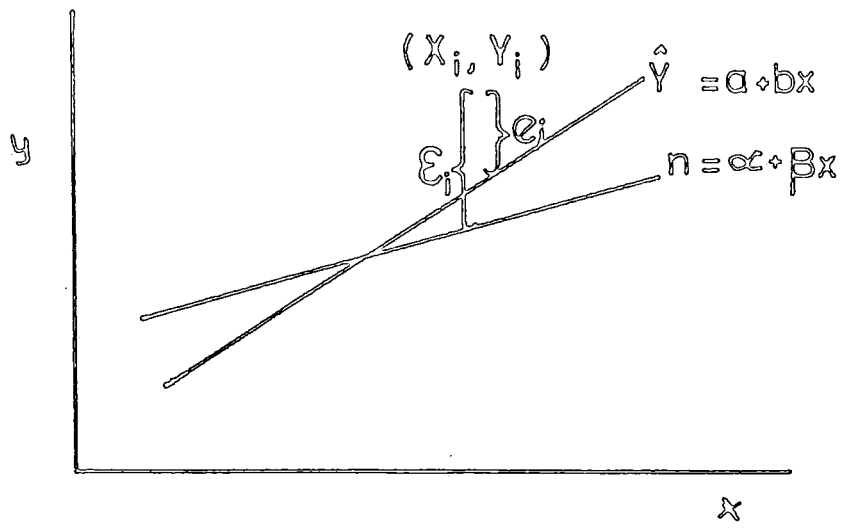

Figure 3.7

$$y_i = \hat{y}_i + e_i$$

where $\hat{y}_i$ is the predicted y value given by the sample regression line when $x = x_i$.

The variance of ϵ_i (which is normally distributed) is σ^2, and the unbiased estimate of σ^2 with n-2 degrees of freedom denoted by S^2_{ey} and equal to (129):-

$$S^2_{ey} = \frac{SSD}{n-2}$$

$$SSD = \sum_{i=1}^{n} (y_i - a - bx_i)^2$$

$$= \sum_{i=1}^{h} (y_i - \hat{y}_i)^2 \qquad \ldots\ 3.4.1$$

The variables a and b are only estimates of the true parameters α (y intersect) and β (curvature) based upon a given sample of n observations.

The different estimates of α and β that could be computed by drawing several samples of size n may be thought of as the values assumed by the random variable S and C (Soffit strain and curvature).

Since the values of x is fixed, the values of S and C depend on the variations in the values of strain readings, which were assumed to be independent and normally distributed, then it can be shown (129) that the random variables S and C are also normally distributed with mean

$$\mu_S = \alpha \qquad \mu_C = \beta$$

and variances

$$V(a) = \left[\frac{1}{n} + \frac{\bar{x}^2}{s(x^2)}\right] \sigma^2$$

where $S(x^2) = \sum_{i=1}^{n} (x_i - \bar{x})^2$

and

$$V(b) = \frac{\sigma^2}{S(x^2)}$$

and if σ is unknown, then it is replaced by its estimator S_{ey}

$$V(a) = \left[\frac{1}{n} + \frac{\bar{x}^2}{S(x^2)}\right] S_{ey}^2$$

and

$$V(b) = \frac{S_e^2}{s(x^2)}$$

and the standard normal distributions for S(y intercept) and C(curvature) are:

$$t_\nu = (S - a) / \left[\frac{S_{ey}^2}{S(x^2)}\right]^{\frac{1}{2}}$$

and

$$t_\nu = (C - B) / \left[\left(\frac{1}{n} + \frac{\bar{x}^2}{s(x^2)}\right) S_{ey}^2\right]^{\frac{1}{2}}$$

For S and C respectively, where t_ν is the standard t distribution and the $100(1-\gamma)\%$ confidence interval for S and C are

$$a \pm t_{n-2;\ \gamma/2} \left[\left(\frac{1}{n} + \frac{x^{-2}}{S(x^2)}\right) S_{ey}^2\right]^{\frac{1}{2}}$$

and $$C \pm t_{n-2;\ \gamma/2} \left[\frac{1}{S(x^2)} S_{ey}^2\right]^{\frac{1}{2}}$$

The computer program SA which calculates these confidence intervals, deflections, neutral position and strains in the top and at the steel level is listed in the appendix.

3.4.2 Curve Fitting Using Cubic Spline

Two programs written by Dr.M.G.Cox (130) from the National Physical Laboratory and included in the *NAG Library subroutine were used to fit a cubic spline through the set of data points using the least square approximation.

The program fits the cubic spline function S(x) through the points (X_r, Y_r) with weights Wr(r =1,2,....,m) and interior knots K_1, K_2,... K_{N-1}, interior to the data interval. These knots can be prescribed at the chosen points X_r. S(x) has the property that it minimises

$$\sigma = \sum_{r=1}^{m} \varepsilon_r^2$$

where $$\varepsilon_r = W_r \{S(X_r - Y_r\} \quad (r= 1,2, \ldots,m)$$

The procedure produces the minimising value and the coefficients Ci in the B-spline representation

$$S(x) = \sum_{i=1}^{N+3} C_i N_i (x)$$

where $N_i(x)$ denotes the normalised B-spline of degree 3 defined upon the knots K_{i-4}, K_{i-3}, K_{i-2}, K_{i-1}, and K_i. These knots has been represented by the ◦ symbol ▽ in the graphs throughout the theisis.

CHAPTER 4

DESIGN, INSTRUMENTATION AND TESTING PROCEDURE

Introduction

In this chapter the design of equipment for the experimental program on reinforced concrete beams is described. All the beams were tested in sustained four point bending, and subjected to daily cycled temperature and humidity. Seven tests were performed and they involved singly reinforced concrete unsealed, partly sealed and completely sealed.

The main technical requirements called for by the present investigation included:

Environmental chamber to maintain air temperature and relative Humidity

- Humidity reduction
- Transverse loading rig
- Temperature loading and measuring facilities, and
- Strain instrumentation

4.1 Cabin Design

Since controlling humidity was an essential parameter in this project a cabin 2340mm high 2260mm wide and up to 4850mm long was built for this purpose, where all tests were performed.

The floor of the cabin was covered with aluminium foil, on top of which lay 76mm thick fibreglass insulating material covered with sheets of plywood.

The walls and top of the cabin were made of 75m x 50mm red wood framework filled with fibreglass and covered with sheets of plywood joined together with red wood lathes.

The cabin was equipped with a Prestcold AS75H 3/4 horsepower compressor unit and C350 cooler capable of reducing the air temperature to the desired level of about 7°C from an initial ambient temperature of 50°C over a 16 hours period. The use of two electrical fan heaters of 2Kw each permitted cyclic chamber air-temperature variations within the range 7° to 50C, Figure (4.1) is an overview of the cabin. photo.6

The postions of the cooler element near the roof, and of the heaters at each end near the floor within the cabin were chosen so as to produce as uniform a temperature as possible, and in fact measurements of air temperature round the cabin showed variations to be less than 2°C, except very close to concrete surfaces, and near to the door immediately after access. lighting and power supplies were built in, and loosely-sealed access ducts were incorporated to introduce thermocouple wires and cooler supply pipes.

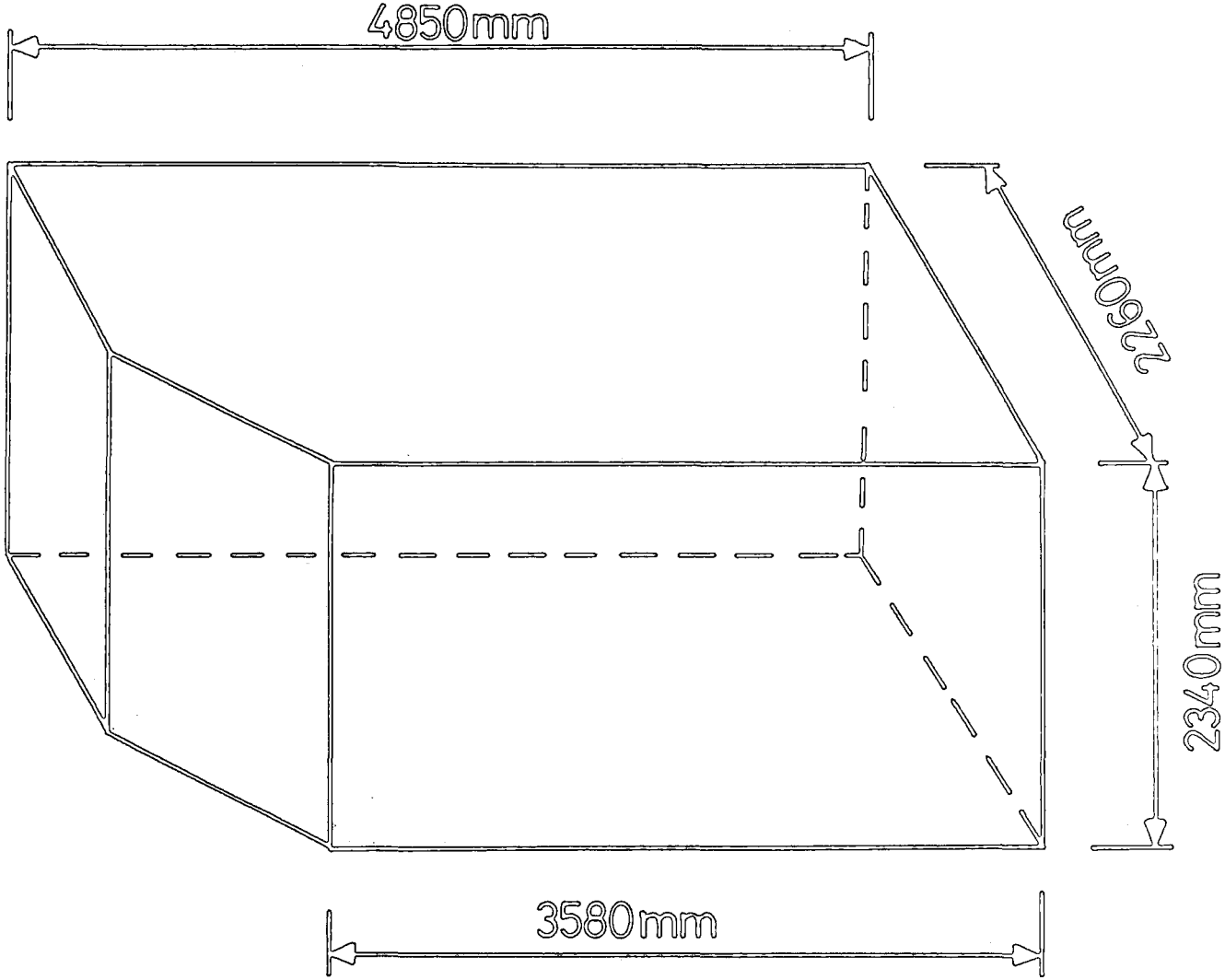

FIG. 4·1 AN OVERVIEW OF THE CABIN

4.2 Loading Rig

The loading rig used consisted of a weights and lever arrangement designed to provide stable long-term loads in four-point bending to a pair of beams Figure (4.2 and photo 1). This offers a reliable and stable long-term load system, fully tolerant of movements in short and long-term due to thermal curvature, cracking and creep.

The two loading arms were 2000mm long each and 500mm wide overall. They were fabricated of steel RSJ and of plate so as to fit outside of the end supports, and to bear onto steel outriggers fitted onto the concrete beams under test.

A steel bar passed through holes in the RSJS hole to support a load hangers near to the end of the loading aims. Each lever arm rested on two steel bolts passing through a fabricated steel outrigger resting on the bottom beam. The point of contact between two lever arms and the steel bolts was located at 150mm distance from the tip of each lever arm. The loading of the top beam was made through the top edge of the end plate of the lever arms initially. This was later modified into a portal frame and suspension system to ensure freedom of longitudinal movement. The two beams and the lever arms were supported on two end supports each with a wide base of 800mm square, in order to make a stable arrangement.

Sliding bearings of PTFE/stainless steel were incorporated at the end supports to allow unrestrained sliding. The end supports included adjustment to compensate for slight twist of the concrete beams during casting.

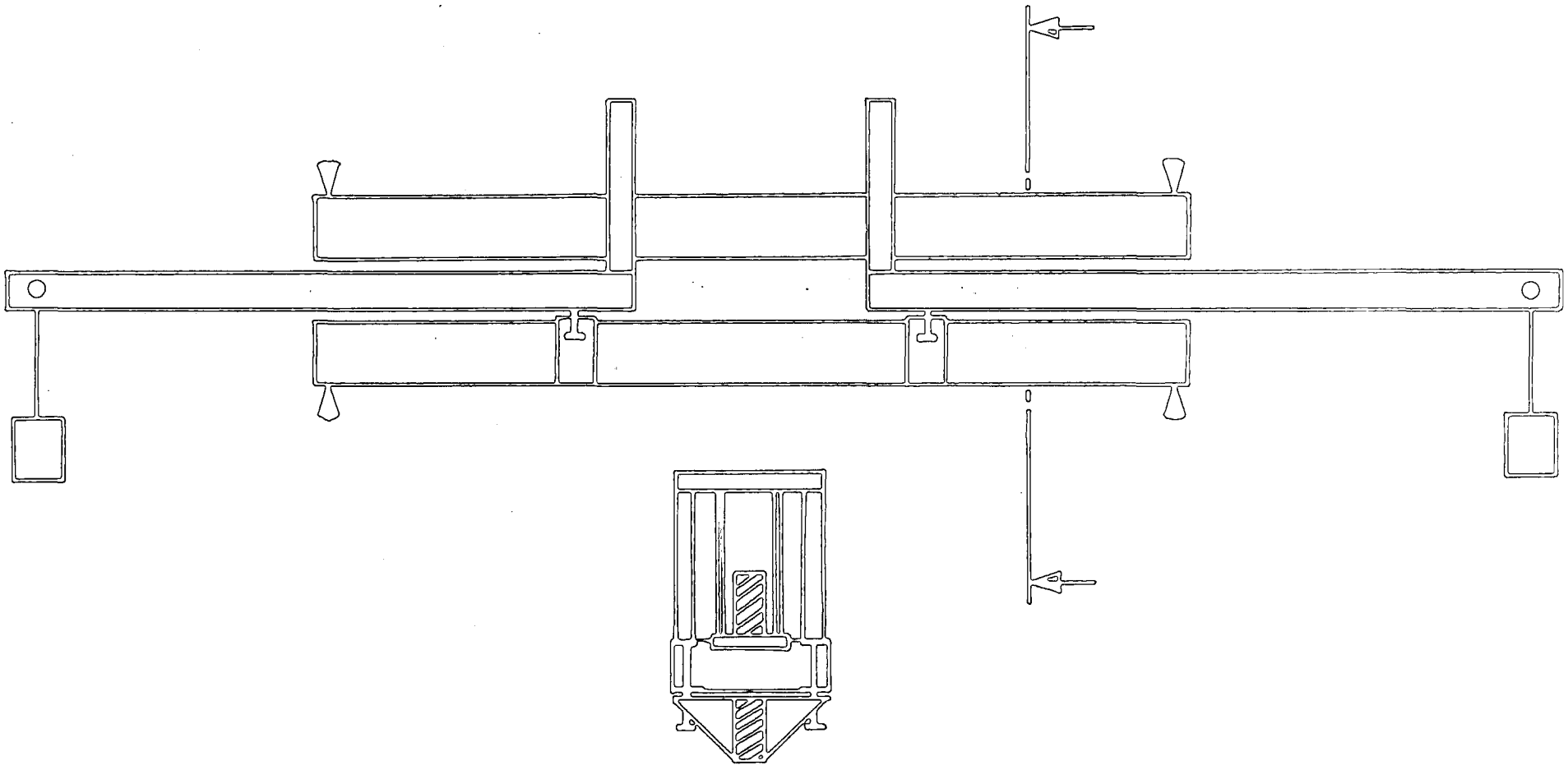

LOADING ARRANGEMENT

BEAMS : 2800 x 200 x 100

FIG. 4.2

Arrangement of the two concrete beams into the loading rig required considerable care in location of the various elements.

The end result was that a pair of concrete beams was loaded in four sustained point bending to the desired bending moment, although because of the geometry of the rig, the lower beam carried a slightly larger moment.

4.3 Temperature

4.3.1 Concrete surface heating

In order to model solar radiation gain, the top surfaces of the concrete beams were heated. Because the heating requirements of the various tests were variable, the aim was to use a mobile heating system capable of supplying the ranges of temperatures considered in these tests, and which was capable of supplying, power output which could be increased or decreased without impairment depending on the special requirements of the particular test. After considering various heating systems, it was decided to use a heating tape, 25mm wide, supplied by Electrothermo. The tape could be folded into any number of loops as desired, was easy to use and was capable of reaching its peak output quickly. It was made of a braided fine iron wire element surrounded by a glassfibre loose-knitted sleeve. Heat output was a simple function of the length of tape and of applied voltage. A 'Variac' variable transformer supplied the necessary voltage control.

4.3.2 Temperature measurement

For measurement of temperatures within the concrete beams copper-constantan thermocouples were used. They were carefully positioned in the concrete during casting. The thermocouples were connected to an automatically compensated cold junction and a millivoltmeter. After careful calibration, it was found that the reading given by the millivoltmeter divided by 4.0 gave temperature in degrees celsius.

The location of the thermocouples at the required positions in the concrete beam cross-section was of paramount importance, as the comparison of the results with the predictive analysis depended on the assumed distances used in analysis. Temperature variation with distance was very sensitive, particularly near the top surface where 5mm difference in distance could mean a difference of 3 to 4°C in temperature.

After several trials on one metre beams, the best method which evolved for the location of the thermocouples was to use a long slim stick of hardwood about 3mm square in section and 300mm long (photo 2). The stick was held in place by glueing it into a hole in a wooden bridge nailed to the top edges of the timber mould. The location of each thermocouple along the stick was measured carefully, and at every location, the stick was waisted slightly allowing the thermocouple to be tightened in its measured position; further a drop of glue was applied to the thermocouple. This procedure ensured that the system would withstand the ill-treatment associated with concrete casting, and that the locations of the thermocouples would not be disturbed.

4.4 Humidity

4.4.1 Humidity Control

Lowering the humidity of the air in the cabin was an important factor in the tests, and turned out to be a much more difficult task than controlling temperature. The humidity values required were cyclic and in the range between 5% and 35%. The meterological records of Riyadh show that the humidity can occasionally drop to zero. Achieving a zero humidity however in as large a volume as the testing chamber while large concrete specimens were present turned out to be an impossible task even for an elaborate and very expensive system. However lowering the humidity from midranges to a very low value might not have as great effect as lowering it from high to midrange values. This was shown in a carefully controlled experiment by de la Pena, where his tests had shown that although shrinkage values increased six times in lowering the humidity from 100 to 50%, it only increased by 1.23 times when the humidity was lowered from 50% to 10%.

After giving some consideration to the choice of the dehumidifying materials, it was decided to use silica gel, since it was considered to be the most appropriate for the present situation. This was due to its robustness through frequent handling, and the fact that it was possible to dry it by heating to moderate temperatures. Therefore twelve kilograms were put into a cylindrical pot 320mm in diameter and 400mm deep with a meshed base. The humidity in the cabin was lowered using a fan which forced air from the cabin through the cylindrical pot passing through the activated silica gel and back into the cabin. Photo 5. The system was switched on

daily at 5.00pm in the afternoon and switched off at 9.00am the next day. The pot was then taken outside and at about 2.00pm in the afternoon the fan was replaced by a pump with a heating element. It took approximately from two to three hours for the silica gel to dry and be reactivated, as was indicated by the change in its colour from sandy brown to clear blue.

The lowest measured humidity values using these arrangements were about 15% in summer condition and about 10% in spring conditions, and these both occurred, as expected, at the peak of the heating cycle.

4.4.2 Humidity measurement

The processes of altering and measuring humidty are interrelated since there are various instruments based on different principles for measuring humidity, and they all have relatively wide margin of error.

Measurement of humidity is subject to a wide error margin depending on the instrument used. There are available various instrumens which work on different principles such as Mechanical (change in some material length usually human hair), Psycrometer (temperature change due to evaporation), Dew point sensor (capacitance), Electrolytic, and Conductance (change in impendence of hygroscopic material). Measuring humidity was first tried by using thermohygrograph supplied by Casella. In this device, the element sensitive to the changes in relative humidity was made up of strands of human hair which shortened as relative humidity decreased and lengthened as it increased. The movement was made linear by a pair of curved cams between element and pen arm. The thermohygrograph continuously recorded both temperature and the relative humidity of the air, on a rectangular chart wrapped round a slowly rotating drum, giving values on a

weekly period. However it proved unreliable for low humiidites giving fluctuating and inconsistent values. Its values were compared to a wet and dry bulb whirling hygrometer and substantial random errors were found when measuring low values (below 30%).

Considerations were given to other measuring devices such as the Vaisalex digital indicator compacitance and a polymer element digital humidity indicator, based on wet and dry bulb principle but were ruled out on the basis of either a slow response or the range was not sufficient. A Dew point indicator was too expensive for this work.

Finally it was decided to use a wet and dry bulb hygrometer. There are a number of choices available in the market that work on the wet and dry bulb principle. Through investigating the available types, it was found that the whirling type was the most appropriate for our purpose. Two whirling wet and dry bulb hygrometers were used, one with a range of -5° to + 50°C which was used in the morning, and the other with a range of 10° to 65°C which was used at the peak of the heating cycle.

The manufacturer specification claimed accuracy to within + 2% relative humidity. This was considered sufficient for our purpose.

4.5 Strain measurements

The decision was taken, at the early stages of planning for the tests, not to use surface-mounted electrical resistance strain gauges for measurements of strain; because of the similarity of coefficients of

thermal expansion, the gauge would expand at a similar rate to the heated beam, so that the apparent signal would be very small indeed, and the majority of real strain would have to be obtained as the product of temperature change and thermal expansion. Tests performed in Durham prior to the present project had shown that even with the use of temperature compensated electrical strain gauges, the results obtained were not satisfactory. This unrealisticity would be exaggerated by the use of the electrical fan heaters as a heat source, leading to unstable air temperatures at the surfaces.

Accordingly the demountable type mechanical strain gauge appeared to be a convenient alternative. Hence a 200mm Demec gauge was chosen for the purpose (photo 3). The strain gauge dial was graduated in a unit of 0.81 x 10^{-5}; however the spacing between the marks was reasonably wide, so that by taking two successive readings, it was found possible to reproduce strains with this gauge to about 4.0 x 10^{-6}.

To provide measuring points in the beams for the concrete strains, a few possibilities were considered and tried on small blocks. One of these had proved to be promising and was thus tried in the first main test. This consisted of casting into the concrete brass bolts, drilled and tapped from the inside, properly located at the strain points. They were bolted direct to the inner face of the timber shutter using a matching bolt fitted through a hole in the wooden shutter. After demoulding, a glue was applied to the free bolts, and they were screwed back again into the concrete. Gauge buttons were glued onto the heads of the bolts, marking the contact points for the strain gauge at the chosen position.

However, this proved to be not completely satisfactory, where several of the locating bolts for the top beam were broken during beam production.

Accordingly this method was abandoned, and for the second test another method was chosen, which was both easier and proved to be much more reliable. This simply involved glueing the strain buttons directly on the surface of the concrete using Araldite adhesive after removing the paint off the concrete surface at these points. This method was used for all the tests after the first.

Due to the limited space in the cabin, strain measurements were made over only one sideface of the beam. Four demec buttons were located at 10mm, 35mm, 165mm and 190mm distance from the compression face, giving two gauge lengths at each level. In the first three tests a direct measurement for the strain of the reinforcing bar was also made. This involved welding two 25mm long 6mm ø steel studs onto the reinforcing rods at the centre line. Brass screws passing through holes drilled in th sides of the wooden mould were screwed into the studs in order to locate the rods accuractely near the centre of the mould. These studs served as strain measurement gauge points for the reinforcing steel. Each stud was covered with rubber tubing while casting so that the concrete did not bond on to it, the rubber tubing was later removed after demoulding.

4.6 Mix Design

The aim was to provide a concrete mix of adequate quality, both in terms of strength and workability. From a number of trials, a mix in the proportions 1:2:4 by weight and w/c ratio of 0.5 was finally adopted with coarse aggregate consisting of equal parts of 20mm and 10mm Scorton river gravel. This choice was made partly in consideration of the use of

nominated mixes in middle east countries. This easy and frequently used mix design had the added advantage of making the results obtained in the tests readily comparable with results obtained under temperature climate conditions using the same mix design. This mix gave a 28 days cube strength of about 45 N/mm^2. Details on the mix strength and elastic properties of the various test are given in the Appendices.

4.7 Dimension and reinforcements

In every test except those in which the beams were completely sealed, four beams were tested. The two beams to be loaded had dimensions of 2800mm x 200mm x 100mm. The other two shrinkage companion beams had dimensions of 1000mm x 200mm x 100mm.

Because temperature distribution inside the concrete was an important part of the investigation. It was felt preferable to limit as much as possible the amount of steel used in order not to intefere with the flow of temperature inside the concrete. Thus it was decided to use singly reinforced beams. Two 12mm diameter hot rolled high yield reinforcing bars were used in every beam. They were located at a distance 165mm from the compression surface, which was achieved during casting by the use of small precast mortar blocks resting on the floor of the mould. The mould used was a wooden framed plywood construction (photo 4).

4.8 Casting Procedure

The four beams, plus the control specimens were cast together. The materials were mixed in a pan mixer. Cement and fine aggregates were mixed dry for two minutes and after coarse aggregates were added they were mixed dry for an additional two minutes.

The volume of concrete normally necessitated three to four mixes. The beams were vibrated on a vibrating frame, while the control specimens were made on a vibrating table. The beams finally were smoothed off with a trowel.

4.9 Curing

After casting, the beams were left on the vibrating table in their moulds and covered with hessian sheets where they were kept wet by soaking the hessian sheets daily with water for seven days.

In cases where the beams were to be left unsealed, they were kept in their moulds without further curing for three more days until day 10 after casting where they were moved to the floor. The shutters of the moulds were stripped and the demec buttons were glued on the beam surfaces. The beams were then transferred to the cabin.

In the case of the partly and completely sealed beams, after they were cured for seven days, they were moved to the floor where the sides of the moulds were stripped, and only their bases were left in contact with the moulds. The top and side faces of the beams were then sealed, as described in 4.10

4.10 Sealing

Before commencing the tests, several types of sealants were tried on 100mm cubes, which were tested for weight loss by subjecting them to an oven temperature of 70°C over a twenty four hour period. The sealant which was clearly superior was found to be an epoxy resin coating system supplied by Colebrand of Lancashire with the brand name of CXL140, and a primer with the brand name of CXL121.

After demoulding, the beams were left for two hours to allow superficial surface drying then their surfaces were cleaned with a brush. The primer was applied to the beams using a paint brush by first mixing a sufficient quantity of its base and hardener in the proportions specified by the manufacturer. On the second day, the two-part resin was prepared and painted on top of the primer. Air bubbles which formed on the surface were pricked and filled, and those found later were scraped and filled with the resin. Sealing progressed from the upper to the lower surfaces through the sides and finally the ends of the beam. On the following day another coat of resin was applied to the beam by repeating the same procedure followed previously. In case of the completely sealed beams, it was turned on its side, and the same procedure was used to seal its base. When the paint was sufficiently dry, the strain points were marked on the surfaces of the beams, and the paint was removed at these points. Then the strain demec buttons were glued to the surface of the concrete. Finally the beams were transferred to the cabin on the following day.

4.11 Heating and loading application

After transferring the beams to the cabin, the top and sides of the surface to be heated beams were insulated using polystyrene sheets. The heating tapes were wrapped into sheets of aluminium foil and then laid on the top surfaces of the appropriate beams.

Temperature and humidity cyles were started on day 18, and on day 21 loading was applied. Fig. 4.3.

In the case where the beams were to be loaded before heating, loading was applied on day 21, and temperature and humidity cyles were started three days later.

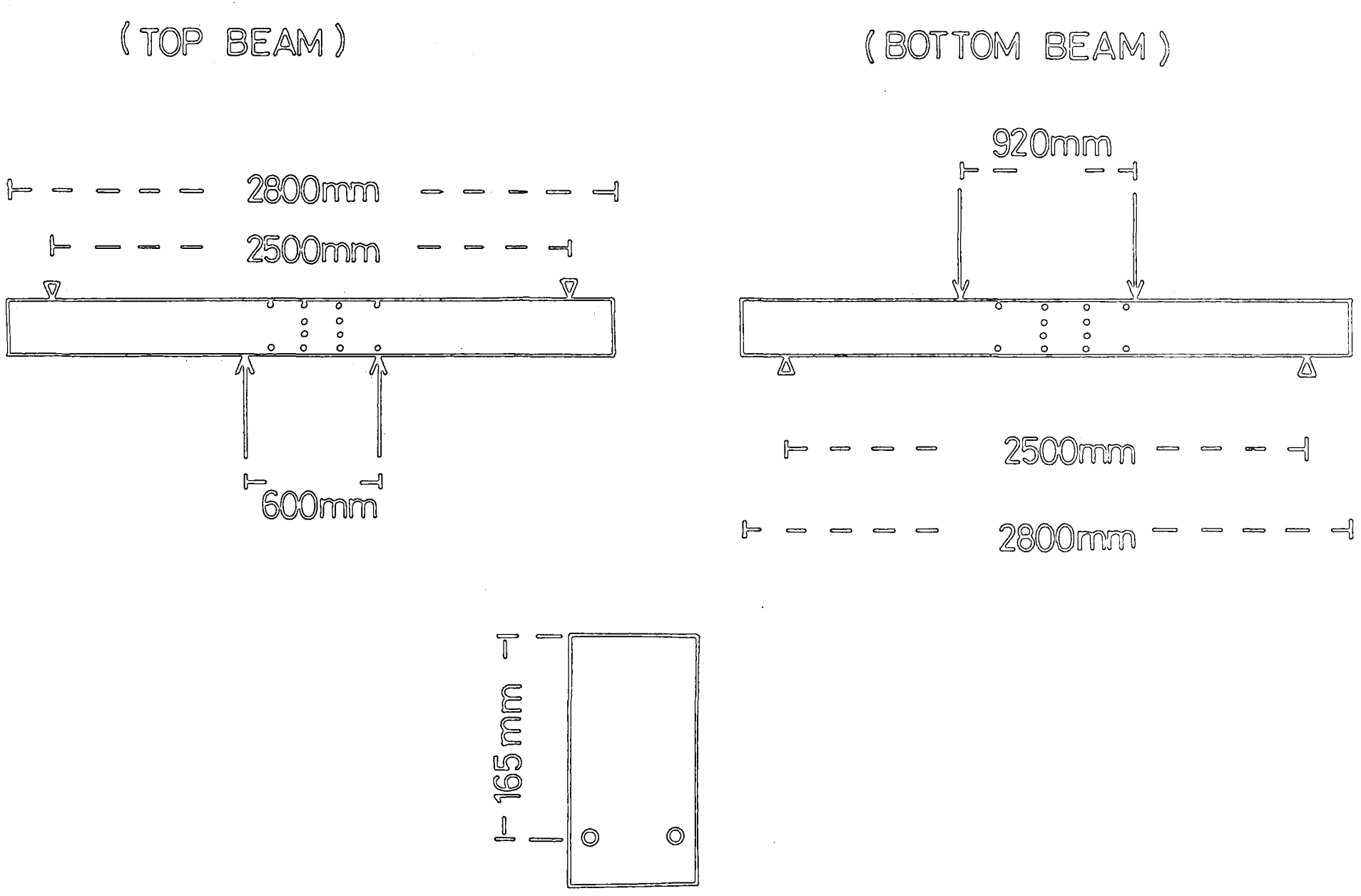
(TOP BEAM)
2800mm
2500mm
600mm
(BOTTOM BEAM)
920mm
2500mm
2800mm
165mm
CROSS SECTION

Fig. 4.3

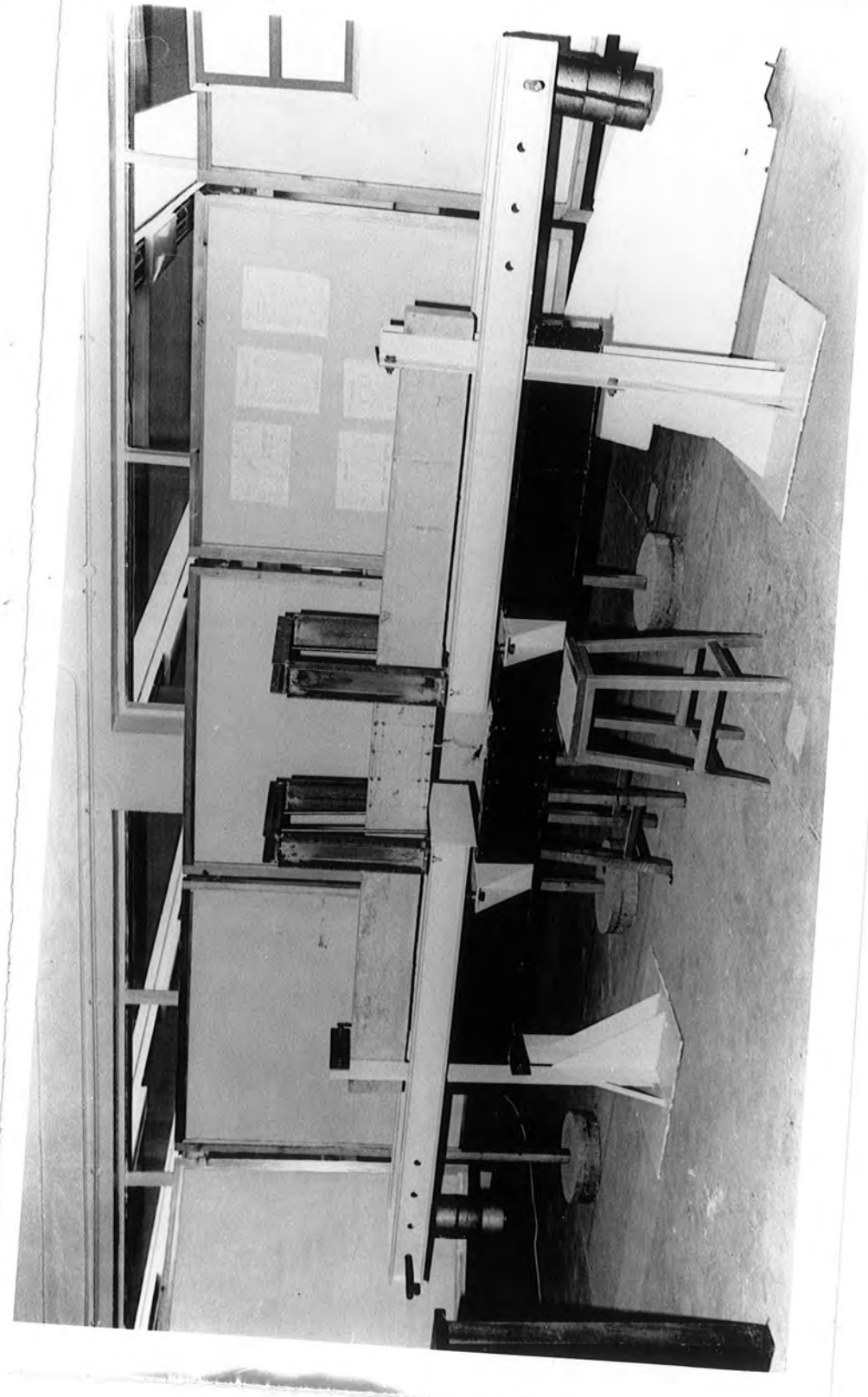

Photo 1

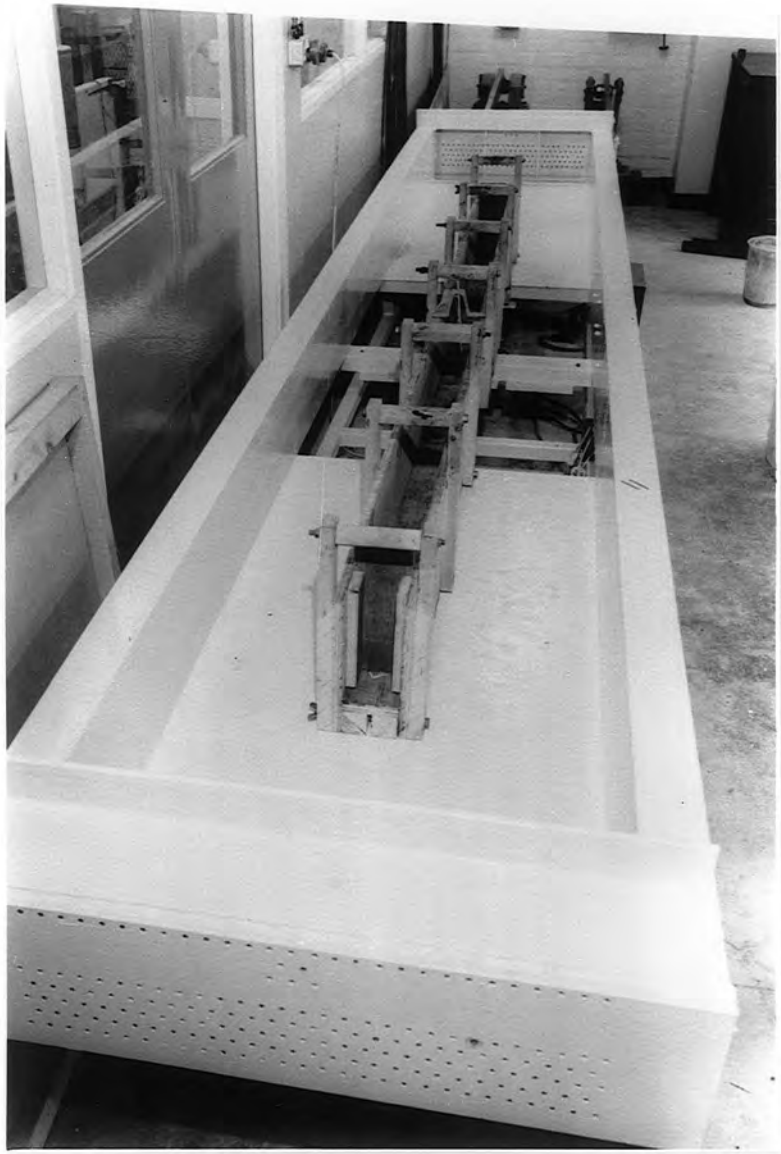

Photo 4

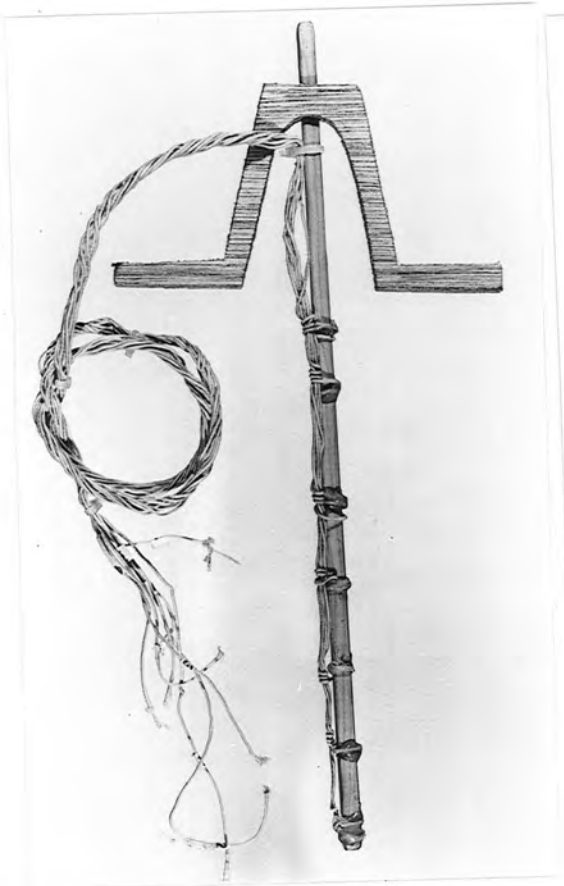

Photo 2

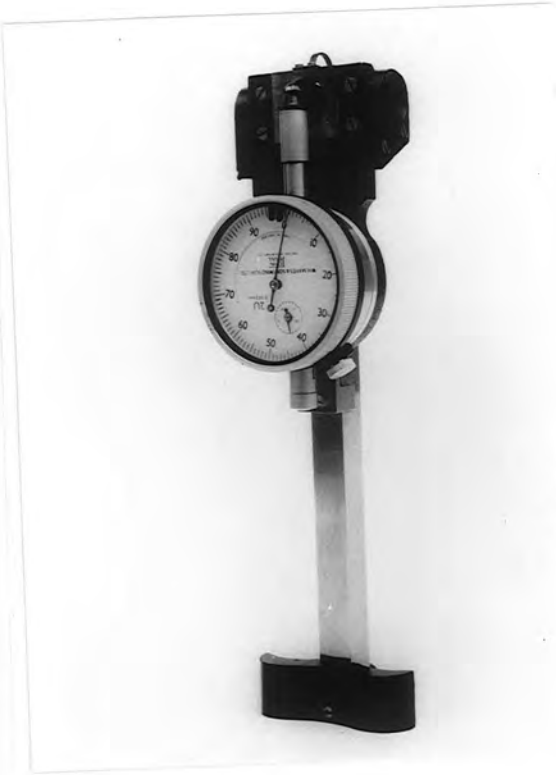

Photo 3

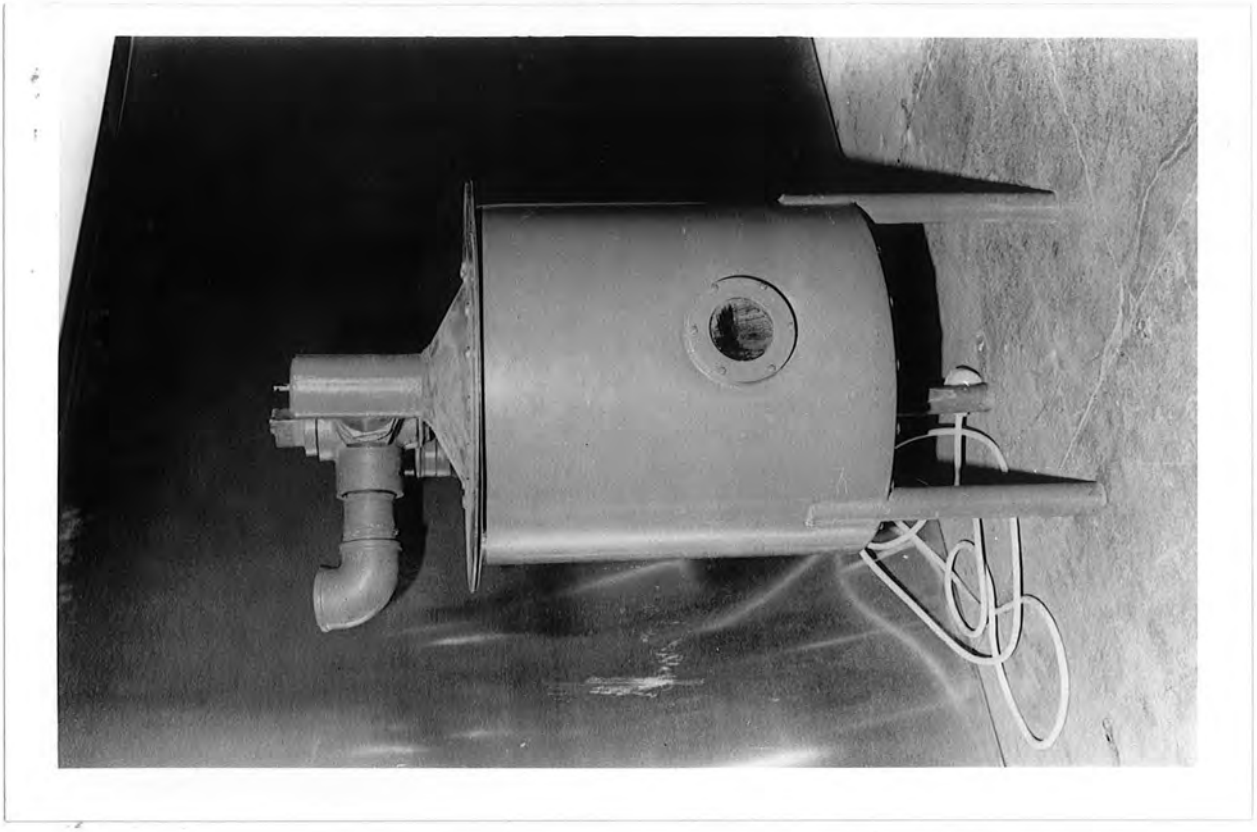

Photo 5

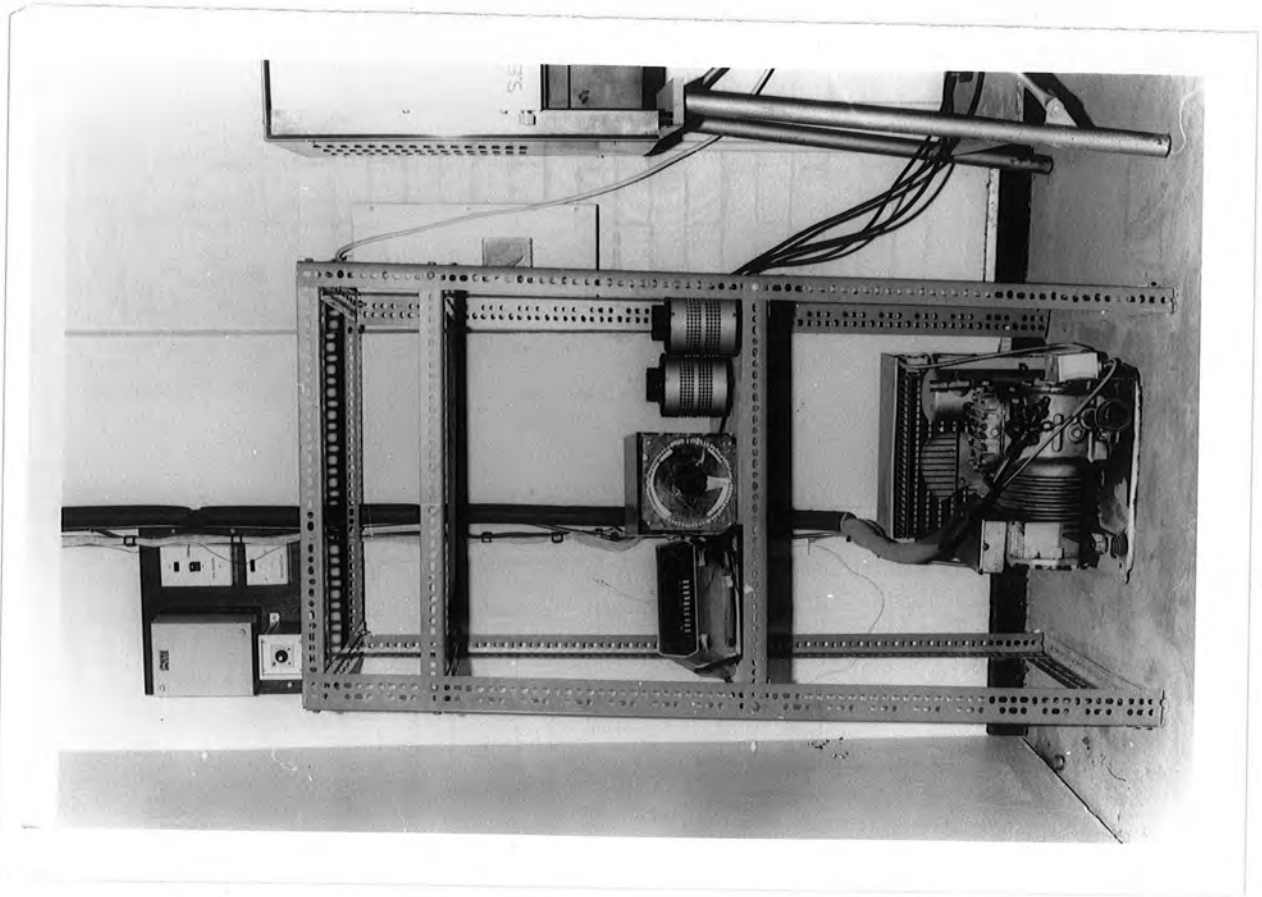

Photo 6

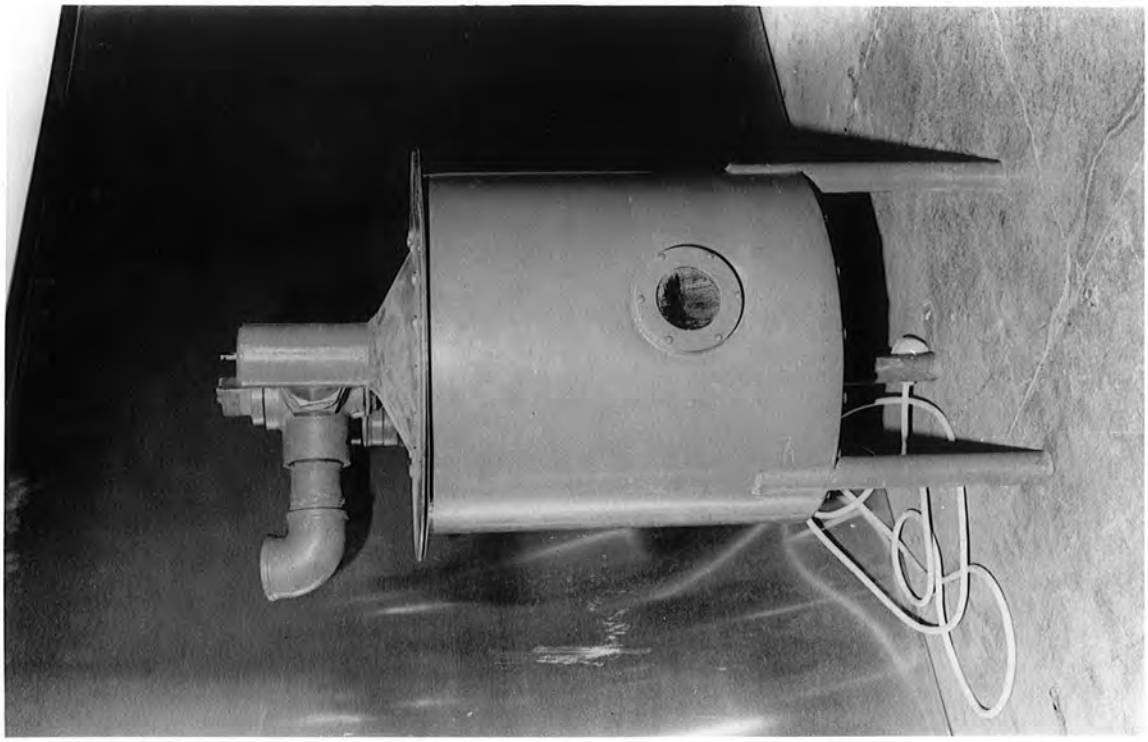

Photo 5

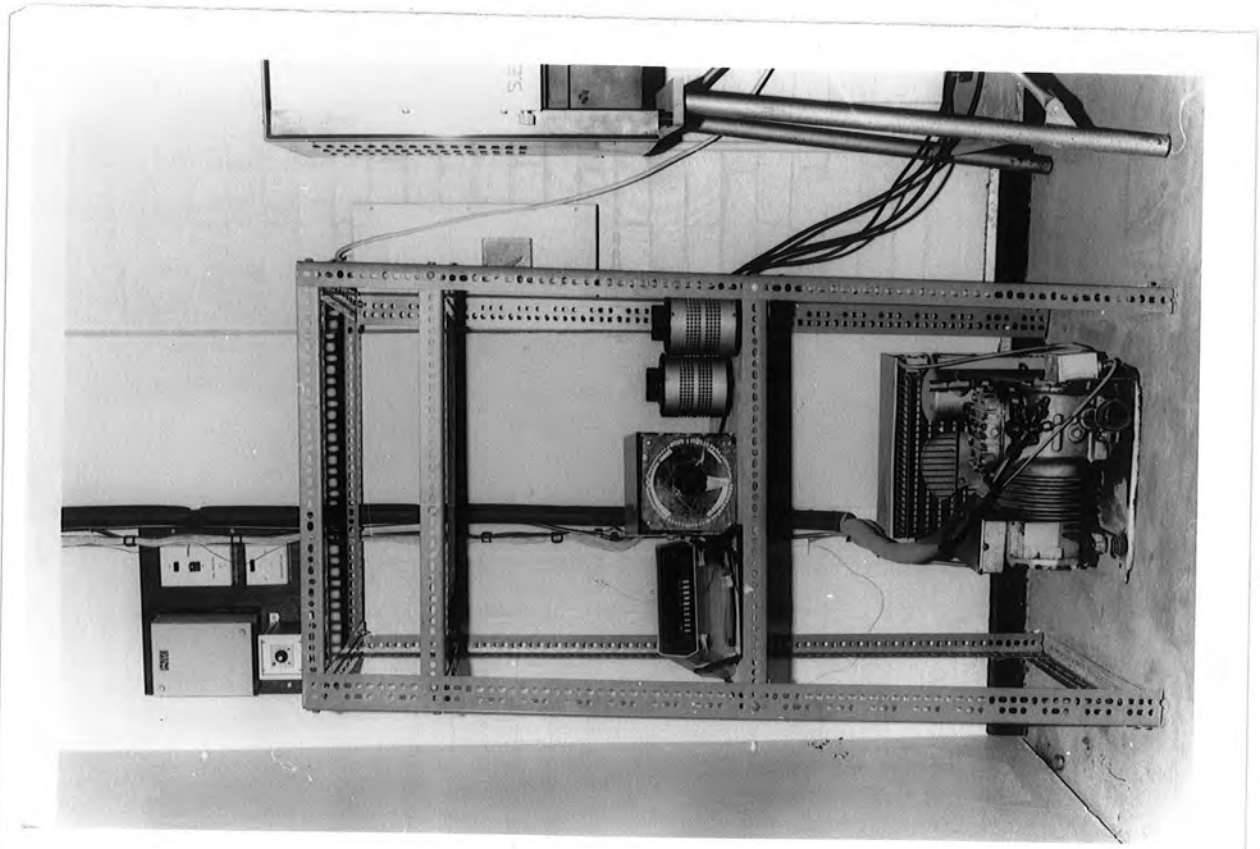

Photo 6

CHAPTER 5

TESTS UNDER CONDITIONS SIMILAR TO THE MID SUMMER CLIMATE IN CENTRAL SAUDI ARABIA

Synopsis

In this chapter the results of three tests are presented and analysed. The concrete beams were subjected to temperature and humidity regimes similar to the climatic conditions of midsummer in Riyadh, Saudi Arabia. In the first test the beams were partly sealed and were loaded before heating. In the second test the beams were partly sealed, and heat cycling commenced before loading. In the third test the beams were completely unsealed, and loaded before heating.

In each test the behaviour of four singly-reinforced simply supported beams was observed. Two beams were held under sustained load, one insulated and surface heated and one open to air temperatures. Two unloaded beams were exposed to similar thermal conditions so that shrinkage and creep behaviour could be separated.

It was found that heating three days before loading reduced creep by about 30% and that the consequence of sealing was to cause a significant reduction in elastic deflection and some modification to the creep deflections. No differences were found in the development of creep for the insulated, surface heated and the uninsulated beams.

Elastic and creep deflections as calculated using measured strain values were compared with predicted values in accordance with CP110:1972, ACI209 and the CEB-FIP 1978 model. Significant differences were found between calculated experimental values and values predicted by these codes.

Creep curvature values were also compared with predicted values from the rate of creep method based upon specific thermal creep values and a step by step approach. Correlation between measured and computed

curvature was acceptable, despite the inevitable slight differences between the conditions of the uniaxial creep specimens and the concrete beams under thermal and humidity cycling.

Behaviour of the beams during a daily thermal cycle was predicted using the simple iterative program described in 3.1. Computed values of self-equilibrating stresses were generally less than about 1.2 N/mm^2. Computed values of curvature were found to be within 20% of curvatures based upon measured strain readings. It was also found that correlation was highly dependent on the value of the coefficient of thermal expansion used in computation.

5.1 Introduction

The three tests discussed in this chapter are:-

I beams partly sealed, loaded before heating.

II beams partly sealed, heated before loading.

III beams unsealed, loaded before heating.

In each test singly reinforced beams were prepared (as described in §4) for testing under loading and heating. Beam codings, dimensions, and test conditions are summarised in Table 5.1.

Table 5.1 Beam Codings and Test Conditions

Beam	Beam Code Used in Test	Dimension	Cyclic Heating	Loading Condition
One	5.I.II.III/1	1.0 m	Heat tape + Air	No
Two	5.I.II.III/2	2.8 m	Heat tape + Air	Yes
Three	5.I.II.III/3	1.0 m	Air	No
Four	5.I.II.III/4	2.8 m	Air	Yes

Beams one and three were shrinkage companions for the loaded beams two and four, in that they were subjected to identical conditions, except that they were not mechanically loaded. Their primary purpose was to allow separation of creep and shrinkage in beams two and four.

5.2 Temperature State

5.2.1 Overall objectives

The meterological records for the period 1956-70 for the City of Riyadh, Saudi Arabia show the highest shade air temperature recorded was 49°C in the month of June. The meterological department keeps records only of maximum and minimum air temperature. Accordingly there is no record of temperature changes throughout the day. This being the case, it was not possible to reproduce exactly the 24 hour air temperature cycle. However the dominant part of the heat cycle was followed closely.

A second major factor was to model the solar radiation gain. Values quoted by Emerson (45) show radiation gain between 8.00am and 12.00noon of up to 3500wh/m^2, which will raise concrete surface temperature to about 62°C.

Finally records of relative humidity, again rather lacking in detail, show an average daily range of 10 to 25 per cent.

5.2.2 Results and discussions

At the start of the daily heating cycle, air and concrete temperatures throughout the tests were measured to be about 30°C except at the beginning of the week where they had fallen to about 21°C since the heating cycles were not run during Saturdays and Sundays. Daily variation of starting temperatures was within ± 1.4°C.

Temperature at the start of every day was found to be fairly uniform across the depth of the beam, with small variations of less than 1°C, similar to conditions at 08.00 hours as observed by Emerson (19). After

preliminary tests, it was found that a measured electrical input of 254 watts (equal to 907 w/m2) for beam two and 88 watts (equal to 880 w/m^2) for beam one was needed to raise the surface temperature of the concrete to 62.5°C in about four hours (during the week) or five hours (at the beginning of the week). This power was equivalent to about 3600 wh/m^2. It is of interest to note however that the highest measured total solar radiation (from three years of record,ref.126) between 8.00am and 12.00am at Bahrain on the Arabian Gulf with latitude of 26° 16'(Riyadh is at a latitude of 24° 42') was about 3500 wh/m^2.

The air temperature was raised to about 50°C by the fan heaters in the same period.

Throughout the daily cycle, temperature distributions in the beams surface-heated by the tape were found to be non-linear and in the transient state. Temperature increase was rapid at first. For example, for the particular day given in Fig 5.1, temperature of the thermocouple 5mm from the surface of the concrete beam increased in the first half hour by 10.6°C and only by 7.6°C in the last hour and a half. The largest temperature gradient through the beam depth occurred at the peak of the heating cycle when the difference between top surface temperature and bottom surface temperature was 15°C. Top surface temperature increased from 31.2° to 62.5°C in four hours of heating, an average increase of 7.8°C per hour. In the same time bottom surface temperature increased from 30.8°C to 47.5°C, an overall average increase of 4.8°C per hour.

At the beginning of the test, temperature was measured horizontally across both the top and bottom surfaces of beams one and two and variation of less than 1°C were observed. This demonstrated the effectiveness of the insulation system. Beams three and four were not insulated.

Slight adjustment of power input during the test was necessary due to fluctuations in the main laboratory temperature thus affecting the cabin air temperature to a small extent.

5.3 Humidity

Throughout the tests, relative humidity values varied from an average high value of 32% at the start of the daily cycle to an average low value of 15% at the peak of the heating cycle. These values were slightly higher than extreme values recorded in Riyadh, but were closer to typical daily values.

Figure 5.2 is a plot of humidity of air in the cabin at hourly intervals for a typical day during a heating cycle.

5.I. Partly sealed beams, loaded before heating

5.I.1 Introduction

In this test the beams were partly sealed, being painted with coats of epoxy resins on the top and side surfaces. They were subjected to the following conditions:-

Table 5.I.1

Beam	Sealing	Dimension	Cyclic heating	Applied Moment (KN-m
5.I/1	(Partly	1.0m	Heat tape + Air	0.0
5.I/2	(Sealed	2.8m	Heat tape + Air	4.03
5.I/3	(	1.0m	Air	0.0
5.I/4	(	2.8m	Air	3.30

Beam 5.I/2 was the bottom beam in the loading rig discussed at 4.2 , and beam 5.I/4 was the top beam.

5.I.2 Strain response of the beams

5.I.2.1 Introduction

In this section, the results of the strain responses of the four beams 5.I/1, 5.I/2, 5.I/3 and 5.I/4 are presented and analysed. Curvature was calculated as the slope of the least square best fit line of measured strain data across the depth of each beam. Deflection at midspan was calculated from curvature values by the use of the moment-area theorem.

In plotting variations of curvature, deflection and neutral axis position against time, use was made of the least square spline fit through the points (as described in 3.4.2).

5.I.2.2 Beam 5.I/1 - Shrinkage Companion to beam 5.I/2

Results

5.I/1 was the shrinkage companion to beam 5.I/2, in that it was subjected to identical conditions, except that it was not mechanically loaded. The beam was sealed and insulated on the top and side surfaces. The 1000 mm long beam was supported on two roller bearings, 250mm from each end. This configuration gave zero moment at midspan. The soffit of the beam was exposed to cyclic air temperature, and in addition the beam was heated on the top surface with electrical resistance heating tape, so as to model solar radiation gain.

Figure 5.I.1 is a plot of curvature changes with time. The datum was taken at 21 days after casting, coincident with the loading of beams 5.I/2 and /4.

Correlation between measured values of maximum curvature due to the daily temperature gradients which were imposed through the model of solar radiation and predicted values were within 12 per cent. The experimental values were computed from surface strains measured by demec gauge. The measured curvature values were small, varying in the range of 0.59×10^{-6} mm^{-1} to 0.72×10^{-6} $m\,m^{-1}$, with the variation being irregular. The predicted values were calculated using the computer program AZ (discussed in 3.1), with input of measured temperature profile from embedded thermocouple readings, and of coefficient of thermal expansion value of $10.88 \times 10^{-6}/C°$. Figure 5.3 is a temperature distribution for a typical day with the calculated stresses using the computer program AZ. Fig.5.4 gives comparison of measured curvature values due to the daily thermal cycle with predicted values.

Discussion

Figure 5.I.1. demonstrates that the beam initially showed upward shrinkage curvature reaching its peak of about $4.0 \times 10^{-7} mm^{-1}$ rapidly, only six days after the datum reading. Curvature then started to decrease.

It is believed that this behaviour was due to the interaction of the following concurrent factors:

a) Because the beam was sealed on all surfaces except the soffit, moisture was lost through the bottom surface only, causing shrinkage which initially occurred most rapidly in the lower part of the beam.

b) This shrinkage was partly restrained by the steel reinforcement and partly by the concrete in the upper part of the beam.

c) Moisture moved by diffusion from the top parts of the beam to the lower parts. However this process was slow causing the shrinkage in the lower parts to be the dominant factor at early stages. As the drying process extended upwards through the beam the shrinkage became more uniform. This together with the restraining effect of the reinforcement steel should result in the development of sag curvatures. However curvature was still hog after 44 days.

Steel stress was $-1.4\ N/mm^2$ three days from datum reading reaching a maximum of $-16.0\ N/mm^2$ fourteen days from datum reading. This decreased slightly to $-15.6\ N/mm^2$ forty days from the datum reading, due probably to the interaction between creep and shrinkage.

The correlation between measured values for the daily maximum curvature and predicted values using the computer program AZ (listed in the appendix) was found to be highly dependent on the value for the coefficient of thermal expansion used in the program. This is due to the

fact that the value of the coefficient of thermal expansion at any time is governed by many factors particularly the hygral state of the specimen at the time of investigation which is not expected to be represented exactly by the small cylinder used for finding the C.T.E.

There was slight variation in both measured and predicted values of curvature on different days because of slight differences in the initial and final temperature states. Initial temperature had a value of 32.4 $\pm$ 1.3°C during the week and 22 $\pm$ 1.2 for the beginning of the week. The peak top surface temperature had a value of 62.5 $\pm$ 1°C, and air temperature 48.5 $\pm$ 2. In the measurement of curvature, the demec gauge had a basic resolution of 0.81×10^{-5} thus introducing a potential error in curvature of about $\pm 0.25 \times 10^{-7}$ mm^{-1}. However, the repeatability of readings, which were each taken two or three times, showed good stability of the strain measurement process.

5.I.2.3 Beam 5.I/2, loaded and surface heated

Results

Beam 5.I.2 was loaded in four point bending, such that the central portion carried a sustained moment of 4.03 KN-m, at 21 days after casting. This moment corresponded to 31% of the ultimate moment of the beam as calculated in accordance with CP110, and as such was typical of the dead load moment in a beam spanning nearly 3m. The moment was about 1.24 times the theoretical crack moment based on modulus of rupture of 4.2 N/mm^2. However no cracks were observed.

The beam was sealed on top and side faces and insulated from the sides, so as to model the thermal behaviour of a bridge deck slab.

The soffit of the beam was exposed to cyclic air temperature, and in addition it was heated on the top surface with electrical resistance heating tape, so as to model solar radiation gain.

Figures 5.I.2-6 are plots against time of midspan deflection curvatures, top concrete strains, strains of steel and concrete at steel level and steel stress as calculated from steel strain. Curvatures and deflections values were corrected for shrinkage, and allowance for differences in the start of cycle temperatures from the datum temperature was made in calculation of top concrete strains, strains of steel and concrete at steel level, steel stress, and neutral axis position.

From statistical analysis two other curves were found for the upper and lower 95% confidence interval for curvature from the set of four demec readings. Figure 5.I.7 is a plot of change of neutral axis position with time.

Table 5.I.2 summarises values from the graphs on loading and after 39 days of sustained loading.

Table 5.I.2 Response of Beam 5.I/2 to sustained loading

Parameters	On Loading	After 39 days
Midspan curvature	-0.234×10^{-5} mm^{-1}	-0.491×10^{-5} mm^{-1}
Midspan deflection	-1.58 mm	3.33 mm
Extreme Concrete) Comp.Strain)	-0.190×10^{-3}	-0.673×10^{-3}
Steel Stress	34.83 N/mm^2	48.06 N/mm^2
Neutral axis	81.4 mm	134.7 mm

Discussion

Table 5.I.3 gives values for creep deflections at various dates.

Table 5.I.3

Time under load (days)	Deflection (mm)	Increase in Def. due to creep (mm)	Creep/ Elastic
0	1.58	0	0
6	2.34	0.76	0.48
28	3.02	1.44	0.91
39	3.32	1.74	1.10

Cyclic heating of the top surface will affect creep deflection in the following ways:

a) "Unrestrained" rate of creep of the top layers would be greater than in lower layers because of higher temperature (in addition to higher stress) leading to increased deflection.

b) It will accelerate drying of the top parts due to increase in rate of hydration of the cement paste and through movement of free moisture from the hotter to the cooler parts. This increases shrinkage at the top parts, but reduces later creep because of the increased strength and reduced moisture.

c) The nonlinearity of moisture and temperature distributions across the depth of the beam will create self-equilibrating stresses which will lead to redistribution of stresses with time, thus modifying creep deflection.

Table 5.I.4 gives values of the elastic and long-term deflections as compared to predictions by various codes.

Table 5.I.4 Comparison of values predicted by the Codes with test values

Method of Determination	Source of Materials Data	At Midspan	
		Elastic deflection (mm)	Increase in def. due to creep (mm)
CP110:1972 (131)	C & CA (132)	2.94	0.98
ACI-435 + (133)	*ACI-209(134)	2.48	1.89
Effective Modulus	CEB-FIP (135)	2.33	1.27
Test	-	1.58	1.74

+ The calculation of increase in deflection has been done by the use of the reduction factor method (see 2.5.4.3)

* Allowance for the contribution of tension stiffening has been incorporated here by the use of effective second moment of area, I_{eff}, as suggested by Branson (87). It is believed that the discrepancy between the measured and predicted values for the elastic deflection were due to the fact that cracks on the beam were not extensive. In fact they could not be seen by the naked eye. However by the use of the modulus of rupture predicted by the codes and the applied moment, ACI and CEB-FIP predict a fairly cracked beam.

As expected the increase in creep deflection as measured was higher than the predicted values by CP110, CEB-FIP, since there was no provision in these codes for elevated temperature. The higher value predicted by ACI is due to the use of the reduction factor method which is simply some factor multiplied by the elastic deflection multiplied by the predicted creep coefficient (2.5.4.3).

Figure 5.I.8 is a plot of changes of curvature with time as predicted by the rate of creep method with the use of specific thermal creep and step by step approach. For comparison purposes the two bounded curves of experimental curvature have been drawn.

The figure shows that the correlation between measured and predicted values is satisfactory, when consideration is taken of the differences between conditions of the uniaxial creep specimens and of the beam. However the discrepancy is believed to be due to the following reasons:

(i) The beams showed some drying creep which was accelerated by the heat, and low humidity, while the uniaxial creep sample gave only basic creep.

(ii) In the prediction, the temperature in each layer was taken as the average over the daily cycle. However it is suggested by other researchers (111) that when specimens undergo cyclic temperature, they respond as if they were heated to a higher temperature than the average.

(iii) Because of the nonlinearity of temperature, there is small redistribution of stresses during the daily cycle due to the existence of the self-equilibrating stresses.

(iv) The fact that creep is higher under flexure than under axial load.

Figure 5.I.3 shows that curvature had changed from a value of -0.234×10^{-5} on loading to a value of -0.49×10^{-5}. Its elastic recovery was -0.228×10^{-5}. This is about 97 per cent of its elastic value on loading. It changed from a value of -0.263×10^{-5} on unloading to a value of -0.184×10^{-5} ten days from unloading. That is about 0.3 of the creep curvature was recovered during this period.

After 39 days of sustained loading compressive top surface strain had increased to 0.00067 from its value on loading of 0.00019 giving a ratio of 3.54:1. This can be compared to the ratio of the curvature values (end to initial) which equals 2.1:1. Thus giving a reduction factor of 0.59 which is due to the lowering of the neutral axis.

Values in Figure 5.I.4 are the combined effects of creep and shrinkage. The figure shows the effect of heating on the fourth day, where there was a step rise in its value.

Figure 5.I.5 gives values for steel strain as measured from steel studs welded to the reinforcement and concrete strain at the level of the reinforcement. As the graph shows the average value of steel strain and of

concrete strain at the steel level were following similar trends. This indicates that there was negligible slip between the steel and concrete. The small discrepancy between the two values is believed due to the inaccuracy of the value of 10.88 x 10^{-6}/°C for the coefficient of thermal expansion used to correct for differences in the start-of-cycle temperatures from the datum temperature.

Figure 5.I.6 shows that steel stress on loading was 34.8N/mm^2. It reached its maximum value of 55.8 N/mm^2 on the tenth day. Then it decreased slightly and started to increase toward the end. After 39 days it was 48.1 N/mm^2. This is probably due to the fact that at early stages the rate of creep at the steel level was more than shrinkage. At later stages shrinkage was about equal to creep resulting in levelling out of the stress diagram.

The correlation between measured daily curvatures and predicted values were within 15 per cent (except for the first few days because of rapid primary creep). The measured curvature values were small and in the range of 0.62 x 10^{-6} to 0.79 x 10^{-6}. The ratios of predicted to measured values were almost always higher than one, and decreased with time. This is due to the decrease in the rate of creep with time and a possible increasein the coefficient of thermal expansion as the concrete dried out with age. A calculated deflection for a typical value due to the daily thermal cycle was 0.5mm. Curvature values obtained for this beam were very close to similar values obtained for the uncracked companion beam 5.I/1 indicating that cracking had only very slight influence on the behaviour of the beam during a daily thermal cycle.

Self equilibrating stresses in general were very small. For the first heating cycle,the largest compressive stress at the top layer was only 0.9 N/mm^2 that is about 16% of the applied moment stress.

5.I.2.4 Beam 5.I/3 Shrinkage companion to beam 5.I/4

Results

Beam 5.I/3 was a shrinkage companion to the top beam 5.I/4, The 1000mm long beam was supported on two roller bearings, 250mm from each end. The beam was subjected to air temperature cycles only, and was not insulated.

Figure 5.I.9 is a plot of curvature with time due to shrinkage only. The datum was taken at 21 days after casting (i.e. the date of loading of beam 5.I/4).

Steel stress changed from a tensile stress of 1 N/mm^2 three days from datum to a compressive stress of -7.6 N/mm^2 thirty nine days from datum.

Discussion

Initial shrinkage curvature was broadly similar to that for beam 5.I/1 with slightly less positive peak of $3 \times 10^{-7} mm^{-1}$ which it reached after about six days from datum reading. Curvature then started to decrease and changed from positive to negative after 31 days. After 49 days curvature was continuing to increase in sag at an appreciable rate. Its reversal toward sag curvature was quicker than in beam 5.I/1.

The likely reason for this is that beam 5.I/3 was not insulated, causing it to heat up more rapidly around its open faces, with consequent more rapid moisture loss, than beam 5.I/1.

The positive value for the stress in the reinforcement three days from datum which was before the heating cycle is surprising, but is so small that it could be due to a minor error in strain reading.

The ultimate sag curvature of this specimen cannot be predicted from this information, but the primary purpose of this test was to allow separation of creep and shrinkage effects in the beam 5.I.4. This has been achieved.

5.I.2.5 Beam 5.I/4 loaded and air heated only

Results

Beam 5.I/4 was loaded, in four-point bending such that the central section carried a sustained moment of 3.3 KN-m at 21 days after casting. This moment corresponded to 25% of the ultimate moment of the beam, just about equal to the crack moment based on a modulus of rupture of 4.2 N/mm^2. However no cracks were observed.

The beam was sealed on the compression face and sides but not insulated. It was subjected to cyclic air temperature only, with no "solar" surface heating.

Figures 5.I.10 - 14 are plots against time of midspan deflection, curavture, extreme compressive concrete strains, steel strain and concrete strain at the steel level and steel stress. From statistical analysis (described in 3.4.1) two other curves were found for the upper and lower 95% confidence interval for curvature from the set of four demec readings.

Figure 5.I.15 is a plot of change of neutral axis with time.

Table 5.I.5 summarises values from the graphs on loading and after 39 days of sustained loading for curvature and deflection values which were adjusted to remove shrinkage strain (from 5.I/3), so that effects shown were due to creep alone. Allowance for differences in the start-of-cycle temperature from datum temperature was made in calculating top concrete strains, steel and concrete strain at steel level, steel stress and neutral axis position.

Table 5.I.5 Response of Beam 5.I/4 to sustained loading

Parameter	On Loading	After 39 days
Midspan Curvature	$-0.19 \times 10^{-5} mm^{-1}$	$-0.365 \times 10^{-5} mm^{-1}$
Midspan Deflection	1.2 mm	2.53 mm
Extreme concrete compression strain	-0.179×10^{-3}	-0.474×10^{-3}
Neutral axis	94.4 mm	127.7 mm
Steel stress	$17.8 N/mm^2$	$37.7 N/mm^2$

Discussion

Table 5.I.6 lists values of deflection at various dates

Table 5.I.6

Time after loading (days)	Deflection (mm)	Increase in Deflection due to creep	Ratio of increase to elastic
0	1.2	o.0	0.0
6	1.80	0.6	0.5
28	2.31	1.11	0.93
39	2.53	1.33	1.11

Results in this table show, as expected, that creep was rapid in the first few days after loading, but that after four weeks of increasing deflection due to creep, the rate slowed considerably. In the last 11 days this increase was only 0.08 mm which was less than 12 per cent of its value after the first six days. However after 39 days of sustained loading creep deflection was continuing at a slow rate, so that ultimate creep deflection could not be estimated.

Table 5.I.7 gives values of the elastic and long term deflections as compared to predictions by various codes without allowing for temperature.

Table 5.I.7

Method of Determination	Source of Material Data	At Midspan	
		Elastic Deflection	Increase in Deflection due to creep
CP110:1972 (131)	C & CA(132)	2.09	0.78
ACI-435 (133)	ACI209(134)	1.46	1.12
Effective Modulus	CEB-FIP(135)	1.34	0.96
Test	-	1.2	1.33

For explanation of this table, the same comments and reasoning as were presented for beam 5I./2 apply here.

After 39 days of sustained loading, extreme concrete compression strain (Figure 5.I.11) had changed to -0.00047 from its initial value of -0.00018 giving a ratio of 2.64:1, which is less than the similar results obtained for beam 5.I.2. This is due to the difference in the applied moment and probably to the increase in creep of the top parts of beam 5.I/2 caused by the suface heating.

The beam showed a clear increase in creep strains at the start of the air temperature cycling on the fourth day, which was a response similar to that of beam 5.I/2 at the start of its heating regime.

Using a modulus of 210 KN/mm^2, and the measured steel strain values, steel stress was calculated to have changed from a value of 17.8 N/mm^2 on loading to 37.7 N/mm^2 after 39 days. It reached its maximum value of 41.8 N/mm^2 after ten days of loading, then decreasing slightly toward the end. This behaviour was caused by the interaction between creep and shrinkage at the steel level. At the steel level, creep resulted in an increase in tension in the steel, while shrinkage resulted in compression. In the first ten days of loading, the effect of primary creep and transitional thermal creep was more than the effect of shrinkage, thus initially increasing the tension stress in the steel.

Figure 5.I.13 gives values for steel strain as measured from steel studs welded to the reinforcement and concrete strain at the level of the reinforcement. As the graph shows the average value of steel strain and concrete at the same level were similar, which indicates as has been mentioned for beam 5.I/1 that there was negligible slip between the steel and concrete.

5.I.3 Comparisons between beam 5.I/2 and beam 5.I/4

The total moment on beam 5.I/2 is 4.03 KN-m and that of beam 5.I/4 is 3.30 KN-m, giving a ratio of 1.22. This compares with the ratio of curvature on loading for the two beams of 1.23.

Table 5.I.8 below gives a comparison of the ratio of creep plus elastic curvature to elastic curvature of the two beams

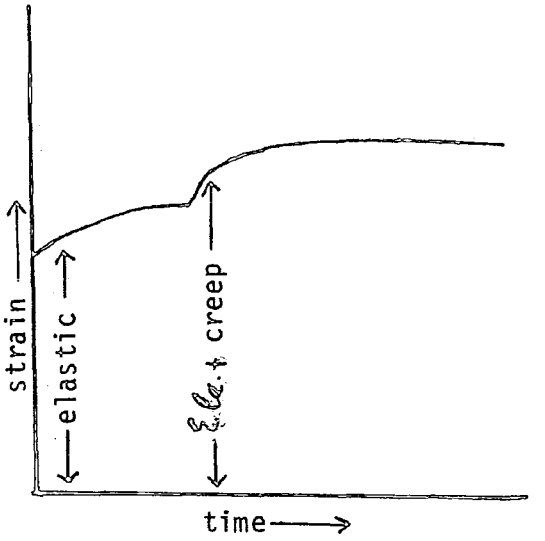

Table 5.I.8

Time under load (days)	Beam 5.1/2 Total Curvature / Elastic Curvature	Beam 5.1/4 Total curvature / elastic	Ratio
6	1.48	1.5	0.99
13	1.66	1.70	0.98
22	1.79	1.81	0.99
28	1.91	1.93	0.99
39	2.1	2.12	0.99
(6/Total)	0.43	0.45	

The table shows that there was generally no difference in the chronological development of creep between the two beams, even though beam 5.I/2 was surface heated and insulated while beam 5.I/4 was not.

5.II Partly sealed beams, heated before loading

5.II.1 Introduction

Unfortunately two of the brass bolts that were cast into the concrete (discussed in 4.5) on beam 5.II/4 were broken during transporting of the beam from casting area to the cabin. This made the datum reading erroneous. Accordingly we had to abandon analysis of the beam since no useful information could be extracted from collected data. This being the case the only beams that will be discussed in this section are 5.II/1 and 5.II/2. These two beams were partly sealed and were subjected to the following conditions:

Table 5.II.1

Beam	Sealing	Dimensions	Cyclic Heating	Applied Moment(KN-m)
5.II.1	Partly	1.0 m	Heat tape + Air	0.0
5.II.2	sealed	2.8 m	Heat tape + Air	4.03

both of the beams 5.II/1 and /2 were insulated from top and sides using polystyrene sheets.

5.II.2 Beam 5.II/1 - Shrinkage companion to beam 5.II/2

Results and Discussion

Beams 5.II/1 was the shrinkage companion to beam 5.II/2, in that it was subjected to identical conditions, except that it was not mechanically loaded. The beam was partly sealed, but was insulated from the top and sides.

Figure 5.II.1 is a plot of curvature changes with time due to shrinkage. The datum was taken at 21 days after casting, coincident with the loading of beam 5.II/2.

The correlation between measured values of maximum daily curvatures due to thermal gradients and predicted values, were within 13 per cent. Predicted values were obtained using the computer program AZ (listed in the appendix).

Figure 5.II.1 demonstrates that the beam initially showed upward shrinkage curvature reaching its peak of about 3.5×10^{-7} mm^{-1} in about five days from datum, then started to decrease. This behaviour can be explained by the same reasons that were discussed in 5.I.2.2 namely the interaction between differential movement of moisture in the heated top parts of the beam and the exposed soffit with the restraining reinforcement.

5.II.3 Beam 5.II/2, loaded and surface heated

Results

Beam 5.II/2 was loaded in four point bending at 21 days after casting such that the central portion carried a sustained moment of 4.03 KN-m. This moment corresponded to about 1.24 of the theoretical cracking moment using a modulus of rupture of 4.2 N/mm^2. However the beam showed no visible cracks on loading.

Figures 5.II.2-5 are plots against time of midspan deflections, curvatures, top concrete strains, strains of concrete at steel level. Curvatures and deflections values were corrected for shrinkage, and allowances in the start-of-cycle temperatures from the temperature were made in calculation of top concrete strains, strains of steel and concrete at steel level, steel stress and neutral axis position.

Figure 5.II.6 is a plot of change of neutral axis position with time.

Table 5.II.2 summarises values from the graphs on loading and after 29 days of sustained loading.

Table 5.II.2

Parameters	On loading	After 29 days
Curvature	$-0.196 \times 10^{-5} mm^{-1}$	$-0.36 \times 10^{-5} mm^{-1}$
Deflection	1.33 mm	2.44 mm
Top Strain	-0.2×10^{-3}	-0.47×10^{-3}
Steel Stress	25.8 N/mm^2	47.7 N/mm^2
Neutral Axis	93 mm	119 mm

Discussion

Table 5.II.3 gives values for creep deflections at various dates.

Table 4.II.3

Time under load (days)	Deflection (mm)	Increase in deflection due to creep (mm)	Creep elastic
0	1.33	0	0
6	2.01	0.68	0.52
13	2.07	0.74	0.56
22	2.16	0.83	0.63
28	2.33	1.0	0.75

The difference in deflection from day six to day thirteen was only 0.06mm. However the difference from day 22 to 28 was 0.17mm. This cannot be readily explained, bearing in mind that shrinkage values were deducted from deflection. This relatively big increase of strain values toward the end can only be attributed to one of two things. It is either that some micro-cracks had developed on the beam that were not visible to the naked eye, or that the bolts that were used to locate strain studs had started to loosen up giving erroneous readings toward the end.

Table 5.II4 gives values of the elastic and long term deflections as compared to predictions by various codes.

Table 5.II.4

Method of determination	Source of Materials data	At midspan	
		Deflection on Loading (mm)	Increase in def. due to creep (mm)
CP110:1972(131)	C & CA (132)	2.94	0.98
ACI-435 + (133)	*ACI-209(134)	2.64	1.80
Effective Modulus	*CEB-FIP (135)	2.42	1.07
Test	-	1.33	1.11

+ The calculation of increase in deflection was by the use of a reduction factor.

* Allowance for the contribution of tension stiffening was incorporated here by the use of I_{eff} as suggested by Branson (87).

The low value for the measured immediate deflection was due to the fact that the beam was subjected to heating cycles three days before loading. This of course increased its maturity and accordingly its stiffness.

The test creep values were as expected higher than predicted values by CP110 and the CEB-FIP. but surprisingly lower than value predicted by ACI. This again, as has been explained in 5.I.3.2, is due to the use by the ACI of the reduction factor with the elastic deflection in relation to creep deflection prediction.

Figure 5.II.7 shows that the predicted curve using the rate of creep method lies inside the 95% confidence limit calculated statistically. The range however between the two limits of curvature is relatively wide. Nevertheless the correlation between measured and predicted values seems to be satisfactory. Here the contribution of humidity is small since only the soffit of the beam was exposed to the outside environment. However the small variation is due to the same reasons that were discussed in 5.I.3.2.

After 29 days of sustained loading compressive top surface strain had become 2.35 times its value on loading as shown in Figure 5.II.4. Values in the figure are the combined effects of creep and shrinkage. The ratio of the curvature values (on loading to end value) is 1.84, giving a reduction factor of 0.78 (which is due to the lowering of the neutral axis). This compares to 0.59 for beam 5.I/1 which was loaded before heating and sustained under load for a longer period of time.

Figure 5.II.5 gives values for concrete strain at steel level. Values in the figure include creep and shrinkage effects, but are corrected for differences in the start-of-cycle temperatures from datum temperature. The figure shows that the values increased fairly rapidly from a value of 0.00012 on load to a value of 0.0002 five days after loading. It decreased slightly until toward the end where it picked up again increasing to a value of 0.00023. This is due to the interaction between creep and shrinkage at the level, which is relatively close to the neutral axis.

The correlation between measured values of maximum daily curvatures, and predicted values were within 17 per cent, except for the first few days, because of rapid primary creep, the first few measured values were very small compared to the predicted values. A typical measured curvature value was $0.75 \times 10^{-6} mm^{-1}$. The measured curvature values for this beam were close to the measured curvature values for the uncracked companion beam 5.II/1, indicating that cracking of beam 5.II/2 did not alter its behaviour markedly during the daily thermal cycle.

5.III Unsealed beams loaded before heating

5.III.1 Introduction

In this test the beams were unsealed. and were subjected to the following conditions:-

Table 5.III.1

Beam	Sealing	Dimension(m)	Cyclic Heating	Applied Moment (KN-m)
5.III/1)		1.0m	Heat Tape + Air	0.00
5.III/2)	Unsealed	2.8m	Heat Tape + Air	6.1
5.III/3)		1.0m	Air	0.0
5.III/4)		2.8m	Air	5.53

5.III/2 was the bottom beam in the loading rig discussed at 4.2. and 5.III/4 was the top beam.

Beams 5.III/1 and /2 were insulated from the top and sides using polystrene sheets. Beams 5.III/3 and /4 were not insulated.

5.III.2 Strain response of the beams

5.III.2.1 Introduction

In this section the results of the strain responses of the four beams 5.III/1, 5.III/2, 5.III/3 and 5.III/4 are presented and analysed. Curvatures. deflections and strain parameters were calculated and plotted using the techniques employed in test 5.I and described in 3.4.2.

5.III.2.2 Beam 5.III/1 - Shrinkage companion to beam 5.III/2

Results and discussion

Beam 5.III/1 was the shrinkage companion to beam .III/2, in that it was subjected to identical conditions, except that it was not mechanically loaded. The beam was not sealed, but was insulated from the top and sides.

Figure 5.III.1 is a plot of curvature changes with time due to shrinkage. The datum was taken at 21 days after casting, coincident with the loading of beams 5.III/2 and 4.

Correlation between measured values of maximum daily curvatures, due to thermal gradients and predicted values were within 19 per cent. Predicted values were obtained using the computer program AZ (listed in the Appendix).

Shrinkage curvature was, as expected, sagging at all times due to the restraining effect of the reinforcement. Its value 56 days from datum was 0.157×10^{-5}. This corresponds to a deflection of 0.2mm, and for a 4m beam a deflection of 3.2m. This curvature value corresponds to 68% of the 30 years curvature value as calculated using the equivalent tensile force with data supplied by Hobbs (86).

Steel stress was 2.42 N/mm^2 two days after datum, and increasing to a value of 27.6 N/mm^2 fifty six days from datum. This was only 6.5% of the yield stress of the steel, clearly a very small value.

5.III.2.3. Beam 5.III/2, loaded and surface heated

Results

Beam 5.III/2 was loaded in four point bending (at 21 days after casting) such that the central portion carried a sustained moment of 6.1 Kn-m. This moment corresponded to 48% of the ultimate moment of the beam as calculated in accordance with CP110, and about 1.88 of the theoretical cracking moment using a modulus of rupture of 4.2 N/mm^2. The beam cracked during loading, as was anticipated.

Figures 5.III.2-5 are plots against time of midspan deflections curvatures, top concrete strain, strains of steel and concrete at steel level. Curvatures and deflections values were corrected for shrinkage, and allowances in the start-of-cycle temperatures from the datum temperature were made in calculation of top concrete strains, strains of steel and concrete at steel level, steel stress and neutral axis position.

Figure 5.III.6 is a plot of change of neutral axis position with time.

Table 5.III.3 summarises values from the graphs on loading and after 44 days of sustained loading.

Table 5.III.2

Parameters	On Loading	After 44 days
Curvature	-0.74×10^{-5} mm^{-1}	$-0.14 \times 10^{-4} mm^{-1}$
Deflection	4.98	9.48 mm
Top Strain	-0.54×10^{-3}	-0.164×10^{-2}
Steel Stress	131.8 N/mm^2	141.1 $/mm^2$
Neutral axis	73.4 mm	106.3 mm

Table 5.III.3

Time under load (days)	Deflection (mm)	Increase in Deflection due to creep (mm)	Creep / elastic
0	4.98	0	0
6	6.91	1.9	0.38
13	8.33	3.32	0.67
28	9.11	4.1	0.83
38	9.36	4.35	0.88
44	9.50	4.52	0.91

As in test 5.I, the effect of the start of temperature and humidity cycling was to produce a step rise in the curve. This was due to the increase in the rate of creep and probably to the reduction in the elastic modulus upon heating. It may also be attributed to a change in the structure of the cement gel caused by heating and the presence of transitional thermal creep.

After forty four days of sustained loading, the span/deflection ratio was reduced from 502 to 263 under the effects of creep and shrinkage. This last value is clearly low. This is even though the span/depth ratio is only 12.5. For a larger span/depth ratio and under the effects of reversed temperature, the span/deflection ratio will be even quite lower than 263, thus presenting an obvious serviceability problem.

Table 5.III.4 gives values of the elastic and long term deflections as compared to predictions by various codes.

Table 5.III.4

Method of Determination	Source of Materials data	At Midspan	
		Deflection on loading (mm)	Increase in Def. due to creep(mm)
CP110 : 1972(131)	C & CA (132)	4.89	1.42
ACI-435(133)	ACI-209(134)	5.82	3.82
Effective Modulus	CEB-FIP(135)	4.82	2.29
Test	-	4.98	4.52

The measured and predicted values for the elastic deflection are reasonably close for all the codes.

However as expected the deflection due to creep as measured in the test was much larger than the values predicted by CEB-FIP (using an effective modulus approach) and CP110. The measured value was about two times its predicted value using CEB-FIP and more than three times its predicted values using CP110. The ACI value predicted for creep was large, and suggested that the creep analysis by this approach might give too high a value for prediction of deflection under normal ambient conditions.

Figue 5.III.7 is a plot of changes of curvature with time as predicted by the rate of creep method.

The graph shows that the rate of creep analysis correlated well at early stages but predicted lower values than obtained by the test at later stages. This can be explained by the following reasoning:

At early stages the small size of the cylinder and its high rate of moisture loss lead to a high rate of drying creep. However this was balanced in the beam by the higher value of creep in flexure, but as the cylinder dried out it lost its potential to creep, leading to the higher values obtained for the beam at later stages.

Figure 5.III.3 is a lot of changes of curvature with time. It changed from a value of -0.736×10^{-5} on loading to a value of -0.14×10^{-4}. Its elastic recovery was about 82 per cent of its elastic value on loading. It changed from a value of -0.8×10^{-5} on unloading to a value of -0.678×10^{-5} twelve days from unloading. That is only about 18 per cent was recovered during this period.

Compressive top surface strain had increased from 0.00054 on loading to 0.0016 forty four days after loading, as is shown in Figue 5.III.4. This last value was 45% of the ultimate compressive strain of the concrete. The ratio of top surface strain on loading to its value at 44 days was 1:2.96.

Figure 5.III.5 gives values for steel strain as measured from steel studs welded to the reinforcement and values of surface concree strain at the level of the reinforcement. The average values of steel strain and concrete strain at the same level were slightly different, which indicated that there was little slip betwen the steel and concrte. Another contributing factor to the differences was the inexactness of the value of coefficient of thermal expansion used to correct for differences in the start of cycle temperatures from the datum temperature.

The steel stress which was obtained from the steel strain and a modulus of 210 KN/mm^{-1} changed from 124 KN/mm^2 upon loading to 150 KN/mm^2, forty-four days from loading. This last value is 35% of the yield strength of the reinforcement, which is relatively a high value.

The correlation between measured values of maximum daily curvatures, due to daily thermal gradients and predicted values were within 21 per cent. Measured curvature values were very small within the range 0.57×10^{-6} mm^{-1} and $0.73 \times 10^{-6} mm^{-1}$ and were close to the similar values obtained for beam 5.III/1. Maximum predicted compressive stresses were less than 1.2 N/mm^2. The discrepancy between computed and measured values can be attributed (as was discussed previously) to the coefficient of thermal expansion used in the prediction.

5.III.2.4 Beam 5.III/3 Shrinkage companion to Beam 5.III/4

Results and Discussion

Beam 5.III/3 was a shrinkage companion to the top beam. It was unsealed and uninsulated.

Figure 5.III.8 is a plot of curvature with time due to shrinkage only. The datum was taken at 21 days after casting (i.e. the date of loading of beam 5.III/4).

Steel stress changed from 6.9 N/mm^2 two days from datum to 44.1 N/mm^2 fifty four days from datum. This was about 10% of the yield stress of the reinforcement and much larger than the similar value obtained for beam 5.III/1.

Figure 5.III.8 shows that the curvature was similar to that of 5.III/1 with higher values. Fifty four days from datum its value was 0.28×10^{-5} mm^{-1}, and was starting to level out. The comparable value of maximum shrinkage curvature in beam 5.III/1 was $.157 \times 10^{-5} mm^{-1}$ The reason for the high value of shrinkage curvature for Beam 5.III/3 relative to beam 5.III/1, was that beam 5.III/3 was not insulated, thus reached a higher average temperature earlier than beam 5.III/1, leading to a more accelerated loss of moisture.

The value of 0.28×10^{-5} mm^{-1} is more than the thirty years estimated value using expression and data given by reference (86) for a small unsealed specimen under internal exposure. The reason for this high value is possibly the fact that since moisture movement is relatively slow, then because of low humidities and high temperatures the exposed surfaces of the specimen will undergo rapid drying as compared to the interior, this increasing the non-linearity of distribution of moisture, and leading to an increase in curvature values.

5.III.2.5. Beam 5.III/4 loaded and air heated only

Results

Beam 5.III/4 was loaded in four point bending such that the central section carried a sustained moment of 5.53 KN-m. This moment corresponds to 43% of the ultimate as calculated in accordance with CP110, and about 1.7 times the theoretical cracking moment using a modulus of rupture of 4.2 N/mm^2. The beam showed visible cracks on loading.

Figures 5.III/9-12 are plots against time of midspan curvature, deflection, top concrete strains, steel strain and concrete strain at the steel level and steel stress. The two bounded curves in Figure 5.III/10 are the 95% confidence interval for curvature.

Figure 5.III.13 is a plot of change of neutral axis position with time.

Table 5.III.5 summarises values from the graphs on loading and after 39 days of sustained loading for curvature, extreme concrete strain neutral axis position and deflection values. Curvature and deflection values were adjusted to remove shrinkage strain (from 5.III/8), so that effects shown were due to creep alone. Allowance for differences in the start-of-cycle temperature from datum temperature was made in calculating top concrete strains. steel and concrete strain at steel level, steel stress and neutral axis position.

Table 5.III.5

Parameter	On loading	After 56 days
Midspan curvature	-0.607×10^{-5} mm^{-1}	-0.991×10^{-5} mm^{-1}
Midspan deflection	3.83 mm	6.25 mm
Extreme concrete compression strain	-0.461×10^{-3}	-0.12×10^{-2}
Neutral axis position	76 mm	99 mm

Discussion

Table 5.III.6 lists values of deflection at various dates.

Table 5.III.6

Time after loading (days)	Deflection (mm)	Increase in Deflection due to creep (mm)	Ratio to elastic
0	3.83	0	0
6	4.71	0.88	0.23
28	6.24	2.41	0.63
44	6.25	2.42	0.63

Results in this table show that after twenty eight days of sustained loading creep had practically stopped. This is of course due to the fact that the beam was nearly desiccated.

The span/deflection ratio changed from 653 on loading to 400 after forty four days of sustained loading.

Table 5.III.7 gives values of the elastic and long term deflections as compared to predictions by various codes.

Table 5.III.7

Method of determination	Source of Material data	at Midspan	
		Elastic Deflection (mm)	Increase in Def. due to creep
CP110:1972 (131)	C & CA (132)	4.06	1.21
ACI-435 (133)	ACI 209 (134)	3.86	3.06
Effective Modulus	CEB-FIP (135)	3.86	2.0
Test	-	3.83	2.42

Extreme concrete compression strain changed from a value of 0.00046 on loading to a value of 0.00124 forty four days after loading giving a ratio of 2.7 : 1.

The beam showed a clear increase in creep strains at the start of the air temperature and humidity cycling, which was a response similar to that of beam 5.III/2 at the start of its cycles.

5.III.3 Comparison between Beam 5.III/2 and Beam 5.III/4

The ratio of curvature on loading of beam 5.III/2 to curvature of beam 5.III/4 was 1.2. But the ratio between the applied two moments was 1.1. However, the two beams were extensively cracked and accordingly the moment-curvature relation was non-linear.

In table 5.III.8 a comparison of the ratio of creep plus elastic curvature to elastic curvature of the two beams is given at various dates of the test.

Table 5.III.8 Comparison between elastic plus creep curvature of beam 5.III/2 to beam 5.III/4

Time under load	Beam 5.III/2 Creep plus elastic / elastic	Beam 5.III/4 Creep plus elastic / elastic	Ratio
6	1.39	1.23	1.13
13	1.67	1.52	1.10
22	1.79	1.61	1.11
28	1.83	1.63	1.12
44	1.91	1.63	1.17

The table shows that there was generally no difference in the chronological development of creep between the two beams, except that after 28 days beam 5.III/4 was nearly dessicated and lost its potential to creep. Its increased moisture loss relative to beam 5.III/2 was due to the fact that it was uninsulated.

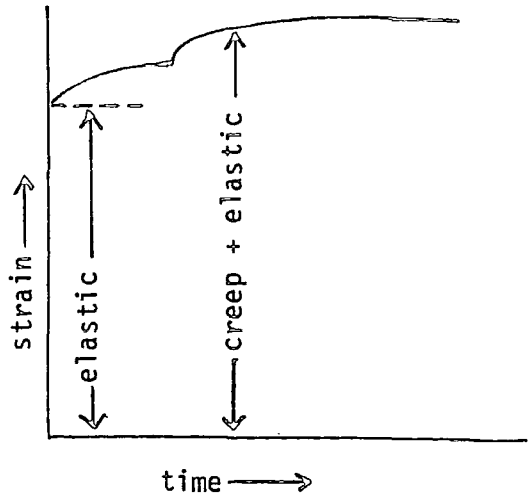

5.4 Comparison and Conclusion

5.4.1 Comparison between beam 5.I/2 and 5.II/2

The two beams were partly sealed. Beam 5.I/2 was loaded at the age of 21 days. Cyclic heat and humidity was applied five days after loading (at age 26 days).

Cyclic heat and humidity was applied to beam 5.II/2 at the age of 18 days, and at the age of 21 days it was loaded.

Prior to heating or loading they were both treated similarly, the length of the curing period was the same, and they were both partly sealed at the same age. The total moment on each beam was 4.03 KN-m.

Using the expression

$$t = \frac{1}{30} (T + 10) \Delta t$$ (where T is the temperature of the concrete during a period Δt days)

to calculate the increase in maturity of beam 5.II/2 due to the applied heat cycles prior to loading increases the age of loading by less than

three days which is clearly not significant.

In table 5.4.1 a comparison is made between the ratios (for the two beams) of creep deflection to elastic, for the first six days, and for the increase in creep between day six to day 28.

Table 5.4.1

Time under load (days)	Creep Deflection Beam 5.I/2 (mm)	Creep Deflection Beam 5.II/2 (mm)
6	0.76	0.68
28	1.44	1.0
Elastic deflection	1.58	1.33
Total deflection (at 28 days)	3.02	2.33
6/elastic	0.48	0.51
(6→28)/elastic	0.43	0.24

Comparing the ratios of the six days creep deflection to elastic deflection for the two beams, the table shows that heating beam 5.II/2 only increased the ratio slightly, 0.51 as compared to 0.48 for the non-heated beam (5.I/2). However when heat was applied to beam 5.I/2 on day six (from loading), the ratio of the increase in creep deflection from day 6 to day 28was 0.43 of the elastic as compared to only 0.24 of the elastic for beam 5.II/2. The ratio of the total deflection after 28 days of sustained loading is 1.30 to 1. This demonstrates clearly the reduction that heat prior to loading made on deflection. (For the period considered in these tests.)

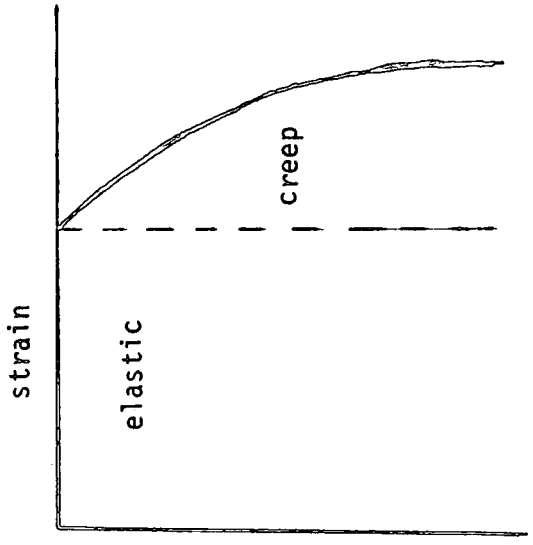

5.4.2 Comparison between beam 5.I/2 and 5.III/2

Beam 5.I/2 was partly sealed and beam 5.III/2 was completely unsealed. After casting they were both left in the moulds for a week and covered by wet hessian and plastic sheets. A week after casting beam 5.I/2 was transferred to the floor and sealed using the procedure described in 4.10 The two beams were loaded at an age of 21 days. The total moment on beam 5.I/2 was 4.03 KN.m, and the total moment on beam 5.III/2 was 6.1 KN-m. There were no noticeable cracks on beam 5.I/2 on loading, while beam 5.III/2 was cracked on loading.

Cyclic heat and humidity was applied to each beam at the age of 26 days from casting (five days after loading).

Table 5.4.2 gives the ratio of the total curvature to elastic (for the two beams) at various dates and the ratio of the two ratios.

Table 5.4.2

Time under load (days)	$\left[\frac{\text{Total curvature}}{\text{elastic (Beam 5.III/2)}}\right]$	$\left[\frac{\text{Total curvature}}{\text{elastic (Beam 5.I/2)}}\right]$	Ratio
6	1.39	1.48	0.94
13	1.67	1.66	1.01
22	1.79	1.79	1.0
28	1.83	1.91	0.96
34	1.85	1.99	0.93
38	1.88	2.08	0.90
$\left[\frac{6}{\text{Total}}\right]$	0.44	0.43	
$\left[\frac{\text{Total C.}}{\text{Elastic}}\right]$ =	0.9	1.0	

After applying heat, the ratio of the two ratios (the ratio of total curvature/elastic for the two beams)) increased due to the influence of drying creep on the unsealed beam (5.III/2) from 0.94 to 1.01, then it started to decrease afterwards. It became 0.90, thirty eight days from loading.

Table 5.4.2 also shows that creep chronological development for the two beams were different. Seven days from the start of heat, the increase in the ratio of creep curvature to elastic curvature was 0.28 for the unsealed beam (5.III/2), while it was 0.18 for the partly sealed beam (5.I/2). However this ratio changed for the period from 13 to 38 days to become 0.21 for beam 5.III/2 and 0.42 for beam 5.I/2.

5.5 Conclusions

From these limited tests, we can conclude the following:

That heating before loading reduces creep. The three days prior heating reduced creep by as much as 30%. It can be argued that the heat before loading will increase maturity, and accordingly the beam will behave as it had been loaded at a later age than 21 days. However the three days heat makes only small change, certainly not accounting for the 30% difference.

The rate of creep method using a specific thermal creep measured on small unreinforced cylinders gave generally a satisfactory prediction. However as chapter 7 will later show, the assumption that creep increases with an increase in temperature and lowering of humidity is not valid at all times for different sealing conditions.

Prediction by codes CP110 and CEB-FIP underestimated deflections in varying ratios, while the use of the reduction factor method of the ACI gave, in general, higher values.

Computed values of self-equilibrating stresses due to the daily thermal cycle were generally less than about 1.2 N/mm^2. Measured curvature values were small, less than 0.8×10^{-6} mm^{-1}

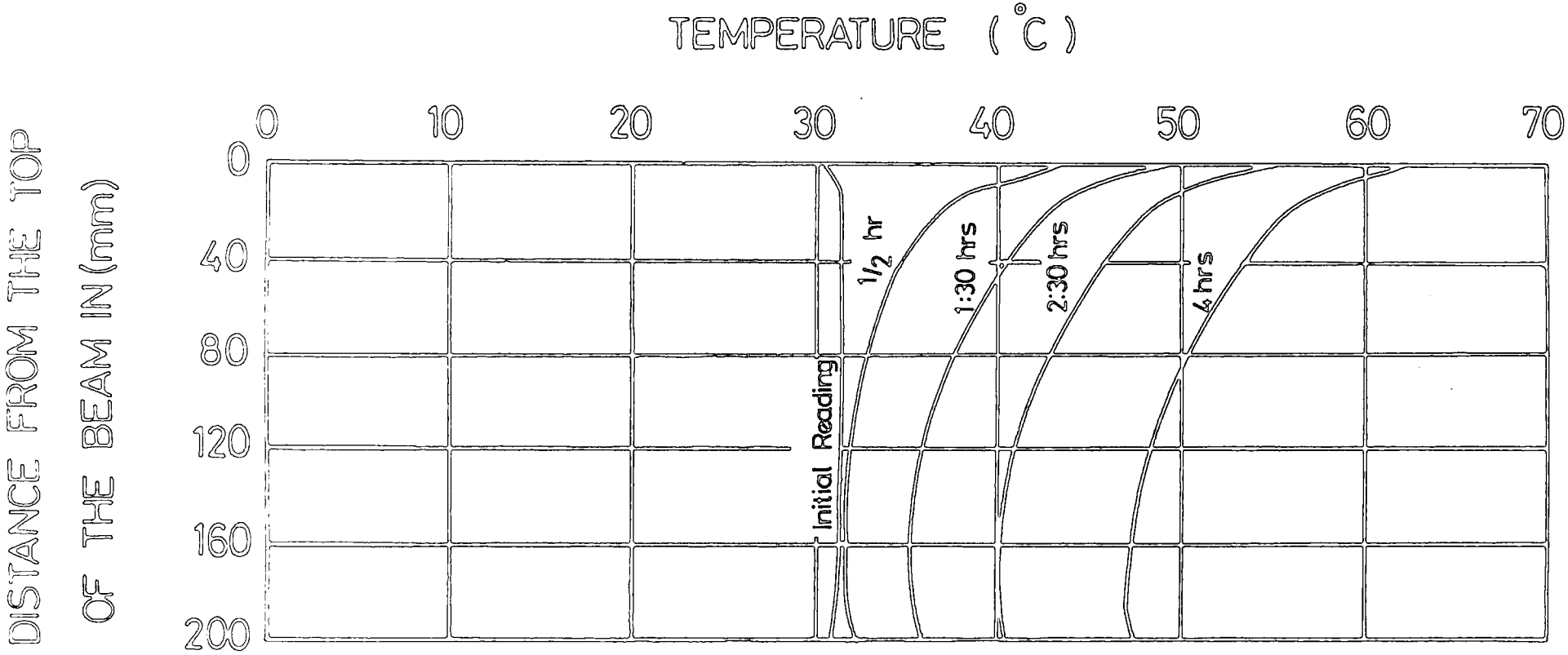

FIG. 5·1 TEMPERATURE DISTRIBUTION THROUGH THE BEAM CROSS SECTION AT VARIOUS TIMES.

SUMMER CONDITIONS

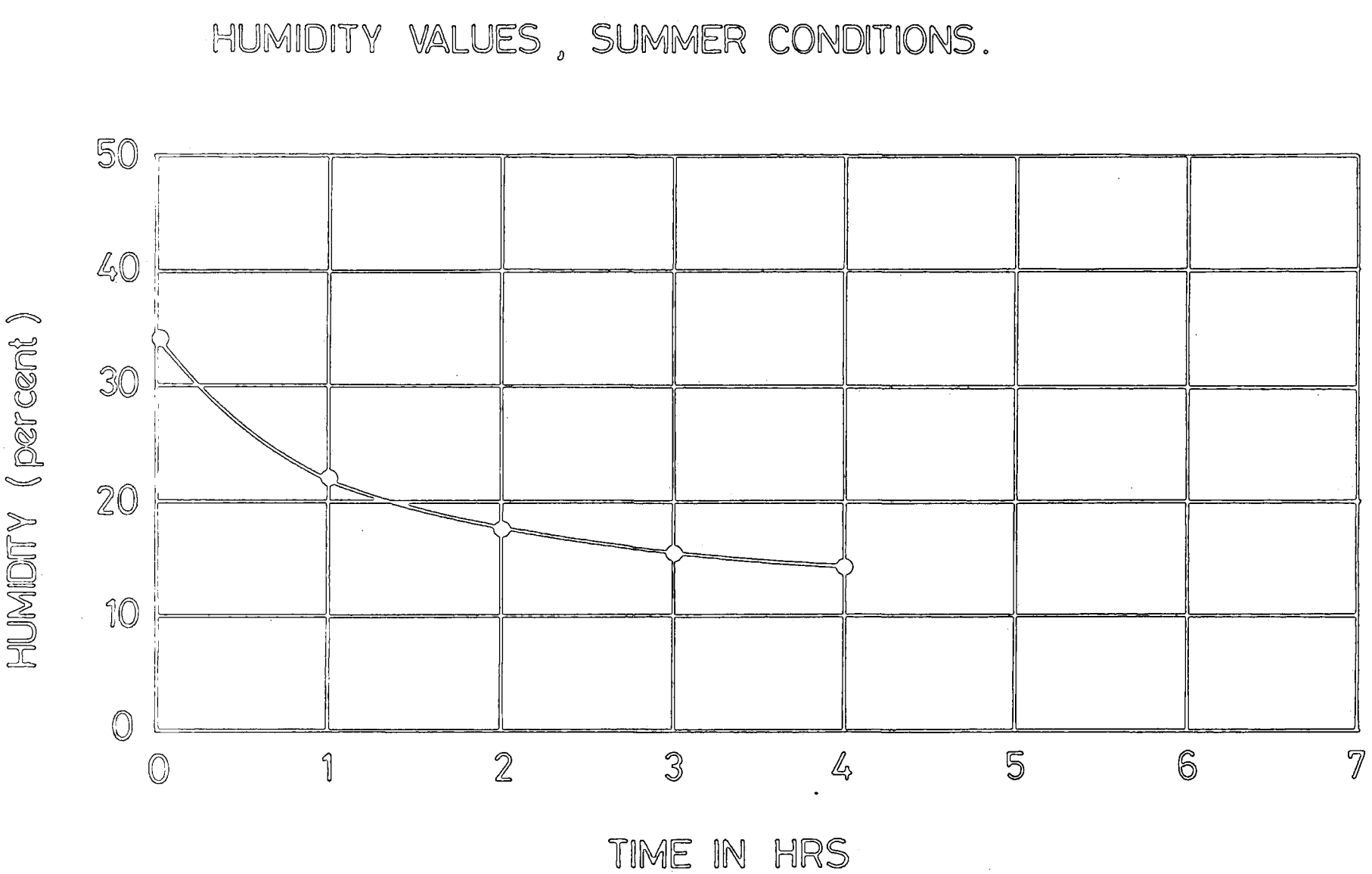
HUMIDITY VALUES, SUMMER CONDITIONS.
HUMIDITY (percent)
50
40
30
20
10
0
0
1
2
3
4
5
6
7
TIME IN HRS

FIG.5·2.

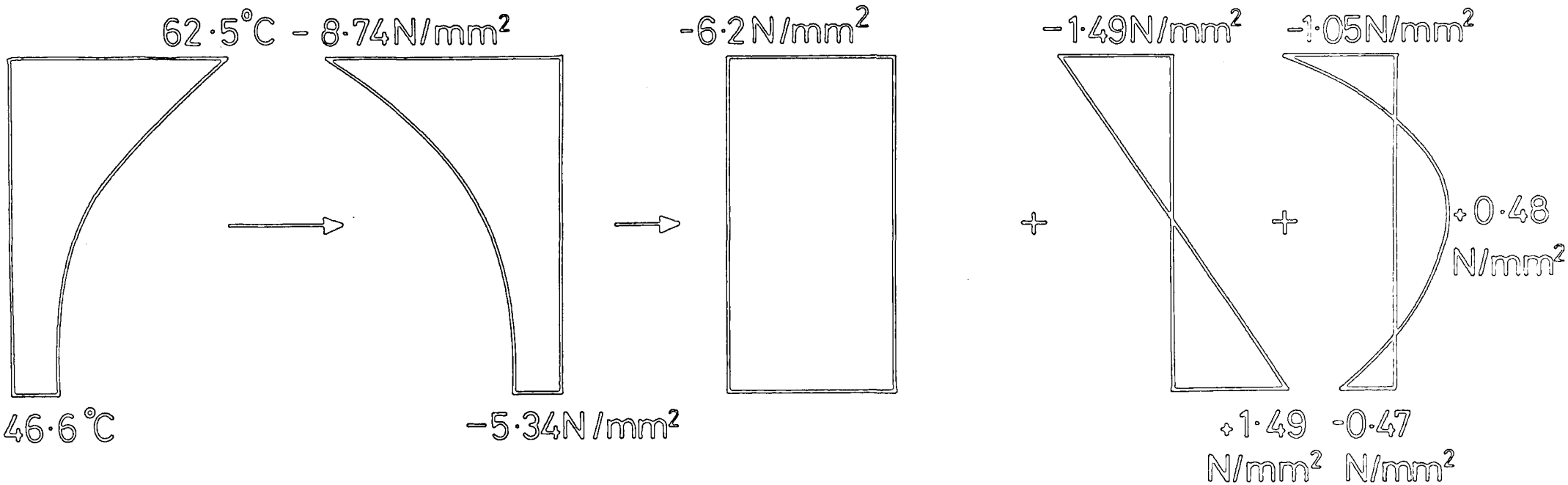
62·5°C
- 8·74N/mm²
-6·2N/mm²
46·6°C
-5·34N/mm²
-1·49N/mm²
-1·05N/mm²
+0·48 N/mm²
+1·49 N/mm²
-0·47 N/mm²

FIG. 5.3

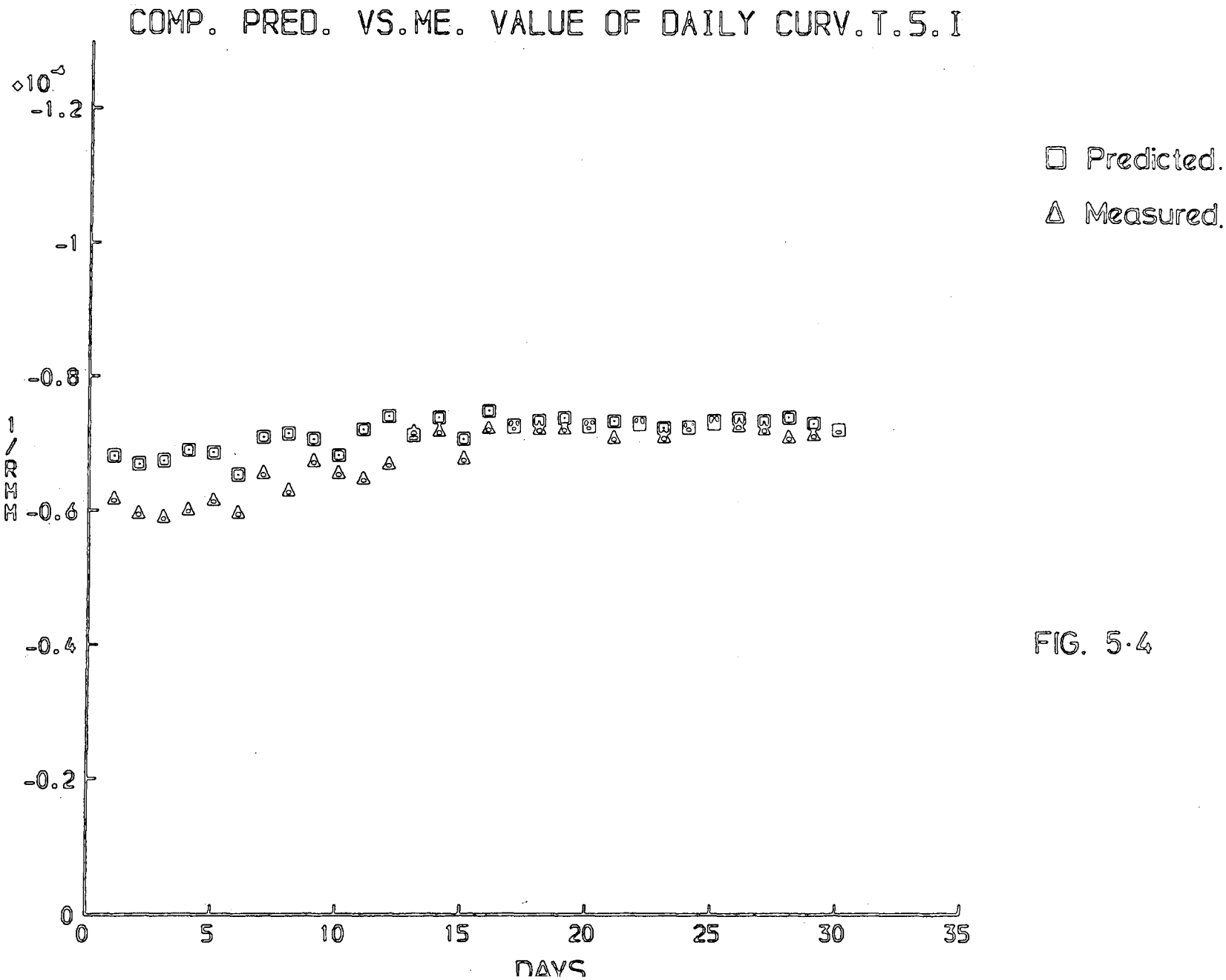
COMP. PRED. VS.ME. VALUE OF DAILY CURV.T.5.I
◇10^-5
-1.2
-1
-0.8
-0.6
-0.4
-0.2
0
1/RMM
0
5
10
15
20
25
30
35
DAYS
Predicted.
Measured.

FIG. 5·4

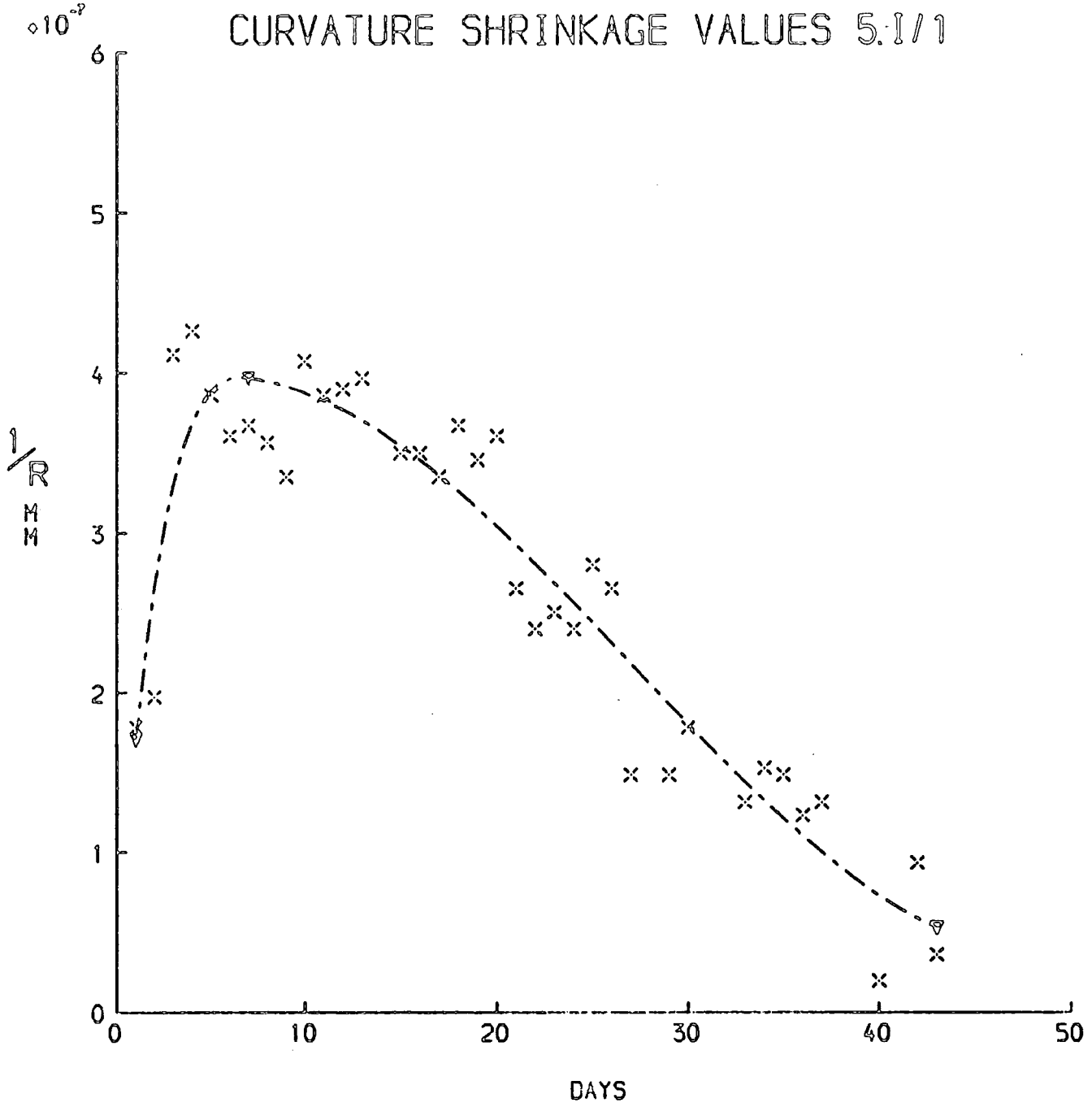
CURVATURE SHRINKAGE VALUES 5.I/1
$\circ 10^{-6}$
1/R
M
M
0
1
2
3
4
5
6
0
10
20
30
40
50
DAYS

FIG. 5.1.1.

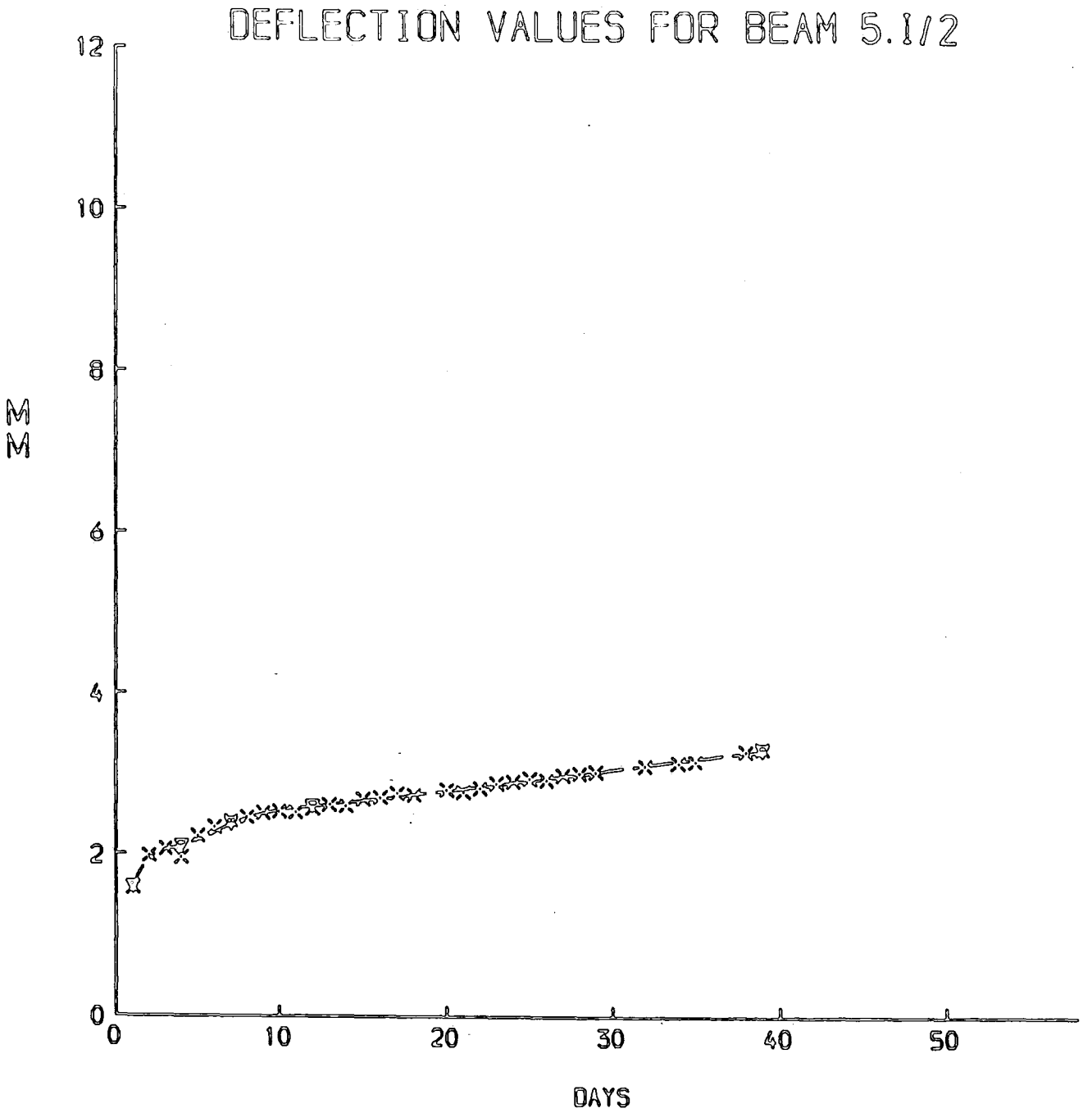
DEFLECTION VALUES FOR BEAM 5.1/2
MM
12
10
8
6
4
2
0
0
10
20
30
40
50
DAYS

FIG. 5.1.2

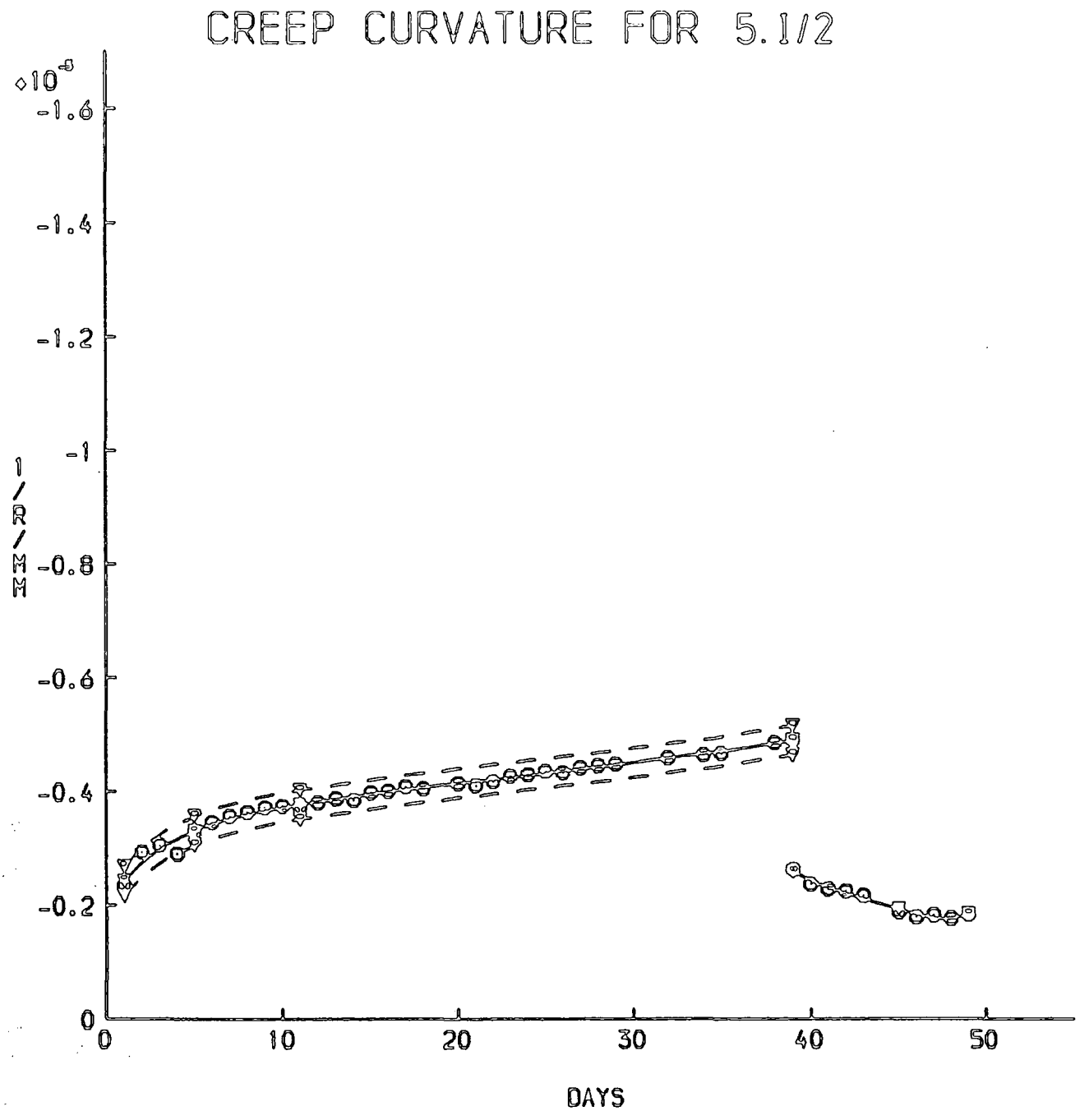
CREEP CURVATURE FOR 5.1/2
◇10⁻⁵
-1.6
-1.4
-1.2
-1
-0.8
-0.6
-0.4
-0.2
0
1/R/MM
0
10
20
30
40
50
DAYS

FIG. 5.1.3.

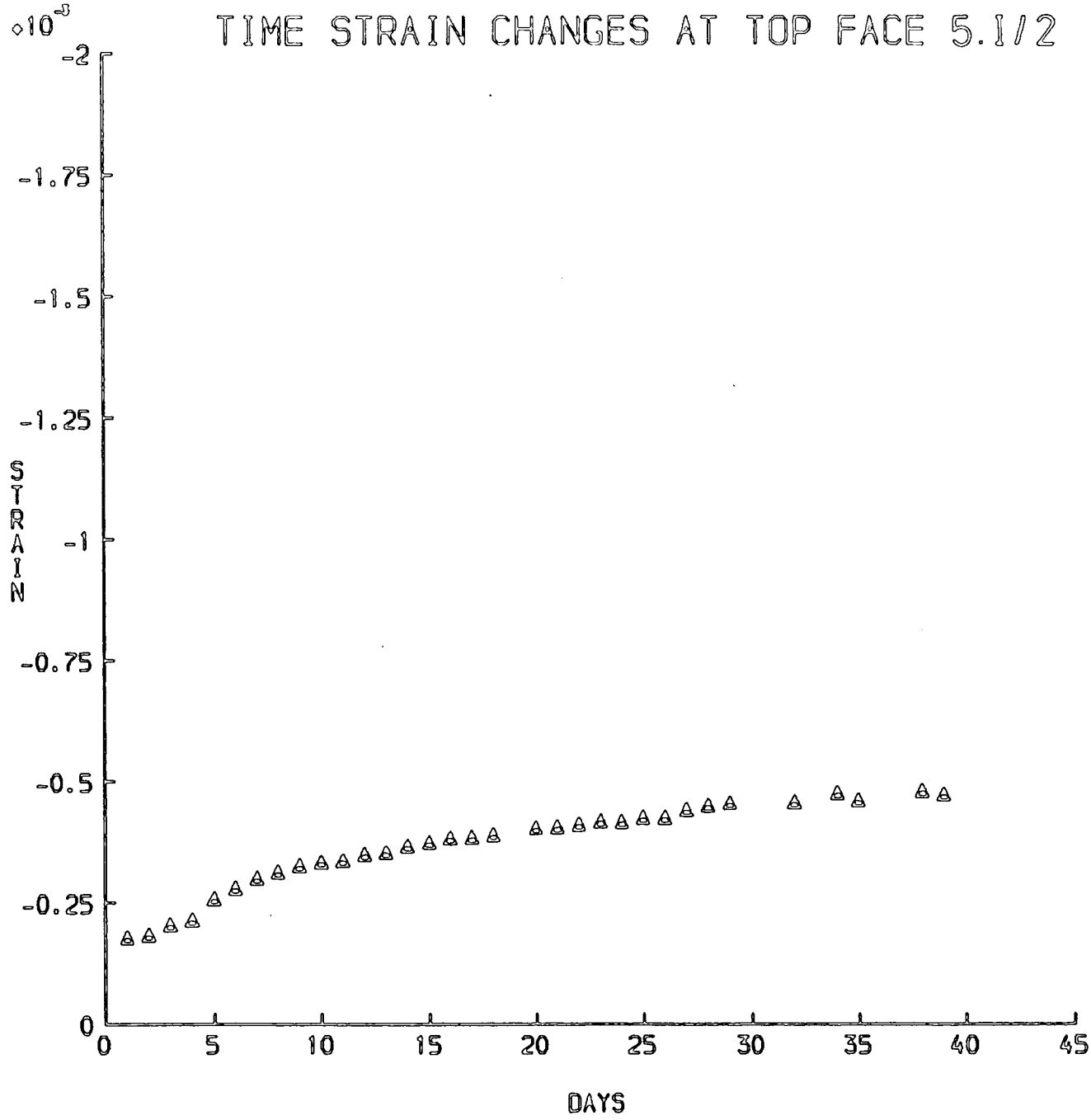
TIME STRAIN CHANGES AT TOP FACE 5.1/2
$\diamond 10^{-3}$
-2
-1.75
-1.5
-1.25
-1
-0.75
-0.5
-0.25
0
STRAIN
0
5
10
15
20
25
30
35
40
45
DAYS

FIG. 5.1.4.

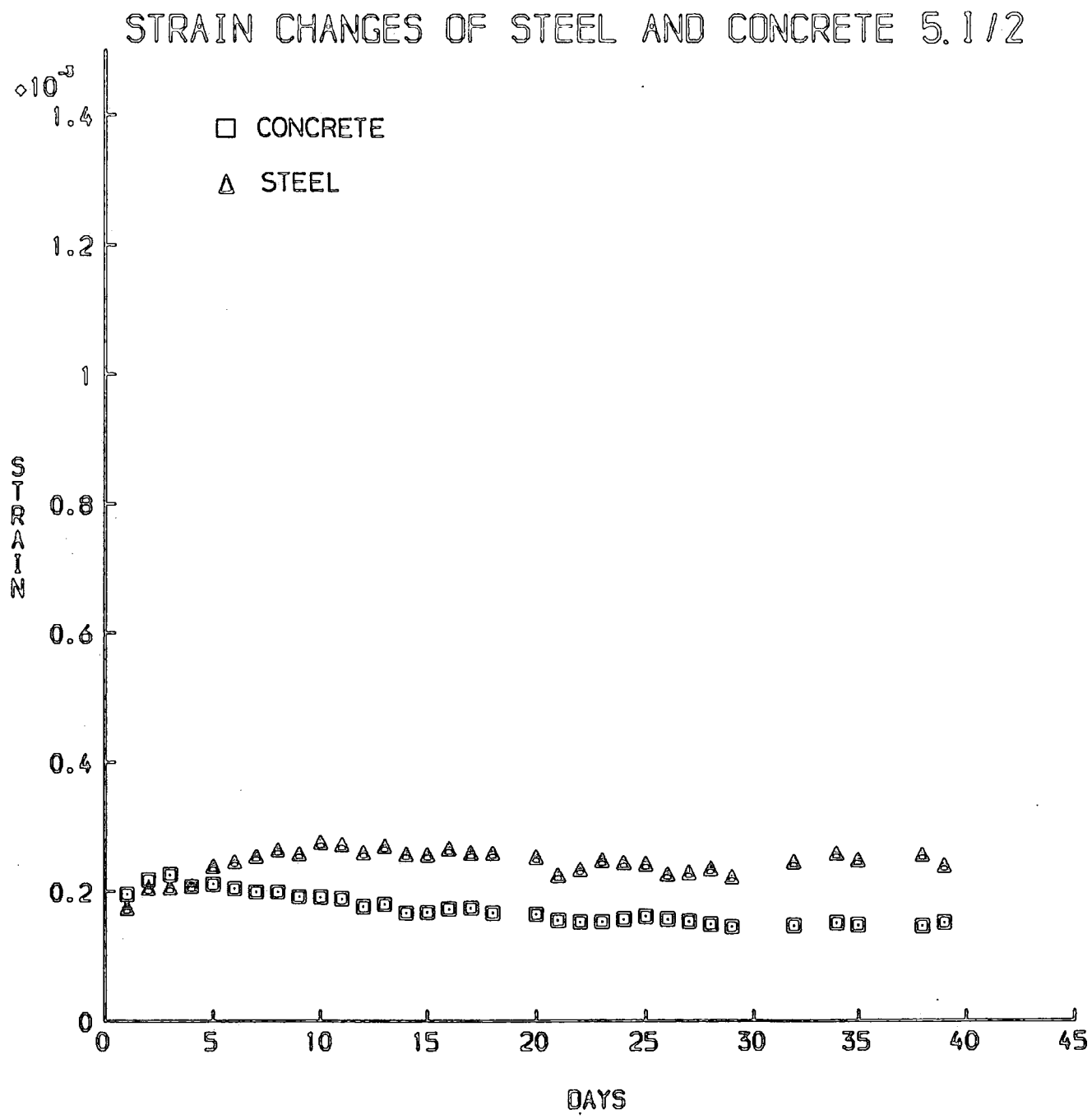
STRAIN CHANGES OF STEEL AND CONCRETE 5.1/2
◇10⁻³
1.4
1.2
1
0.8
0.6
0.4
0.2
0
STRAIN
□ CONCRETE
Δ STEEL
0
5
10
15
20
25
30
35
40
45
DAYS

FIG. 5.1.5.

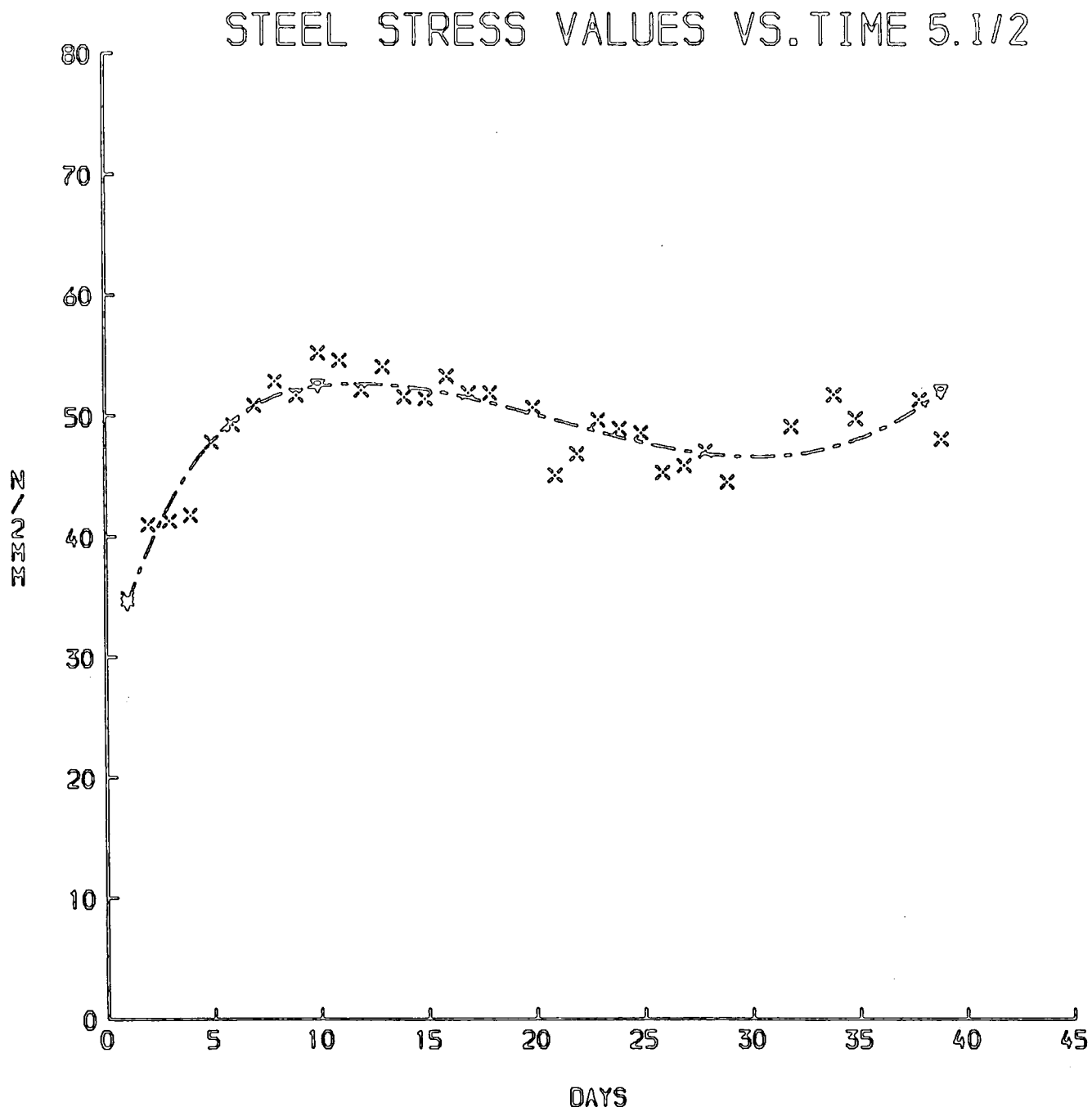
STEEL STRESS VALUES VS. TIME 5.1/2
N/2MM
80
70
60
50
40
30
20
10
0
0
5
10
15
20
25
30
35
40
45
DAYS

FIG. 5. 1. 6.

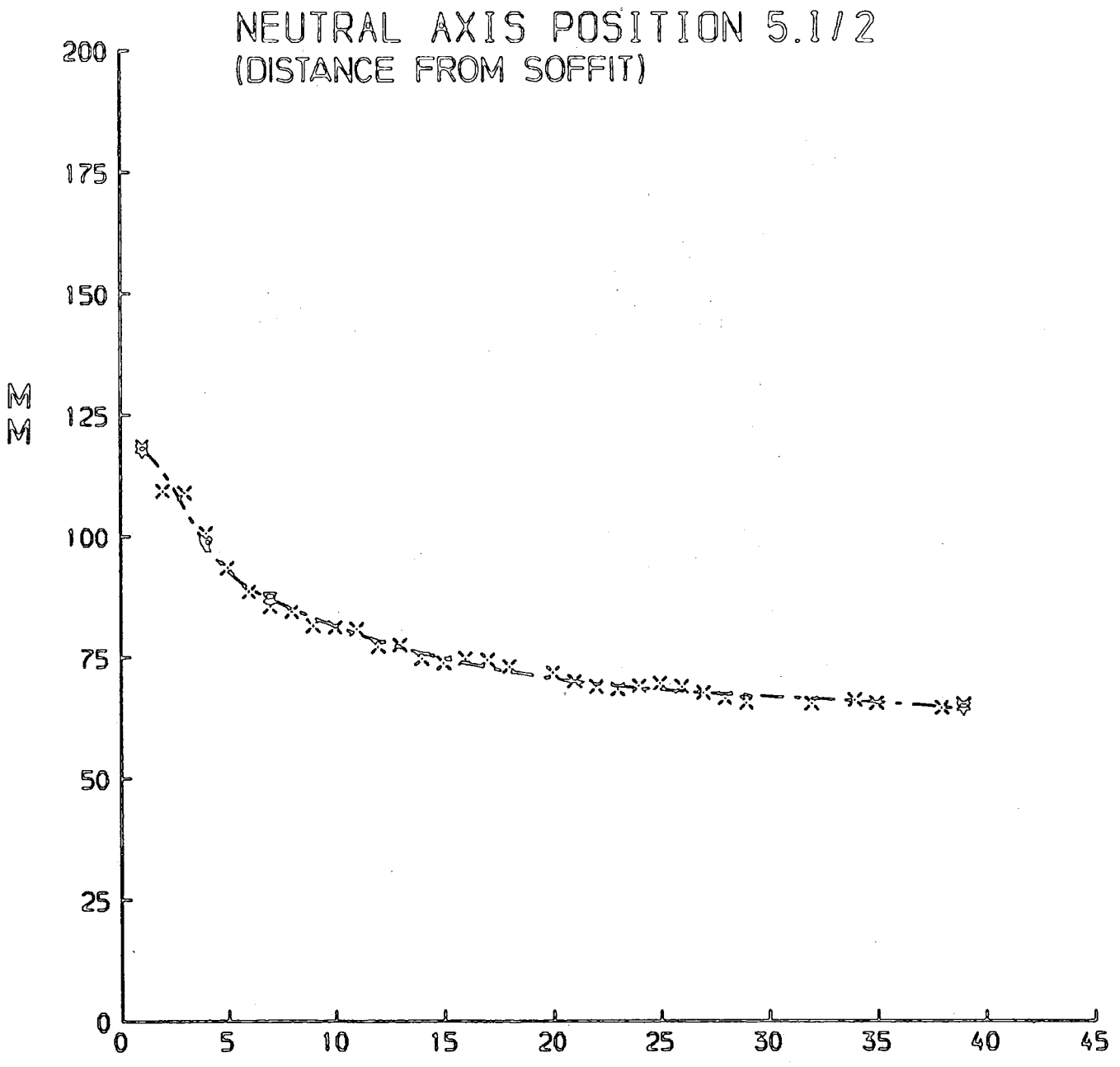
NEUTRAL AXIS POSITION 5.1/2
(DISTANCE FROM SOFFIT)
MM
200
175
150
125
100
75
50
25
0
0
5
10
15
20
25
30
35
40
45

FIG. 5. 1. 7.

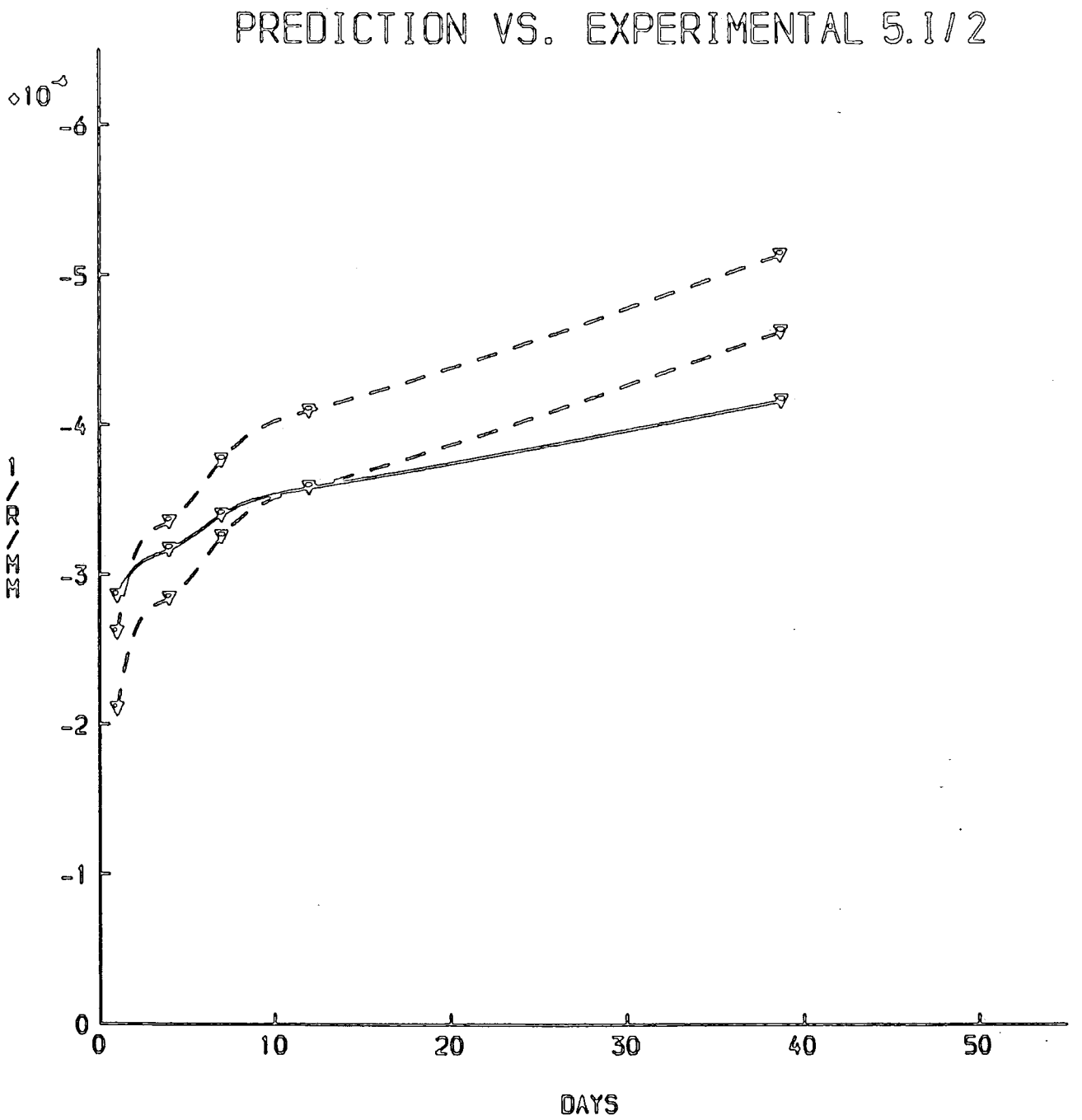
PREDICTION VS. EXPERIMENTAL 5.1/2
◇10⁻⁶
-6
-5
-4
-3
-2
-1
0
1/R/MM
0
10
20
30
40
50
DAYS

FIG. 5.1.8.

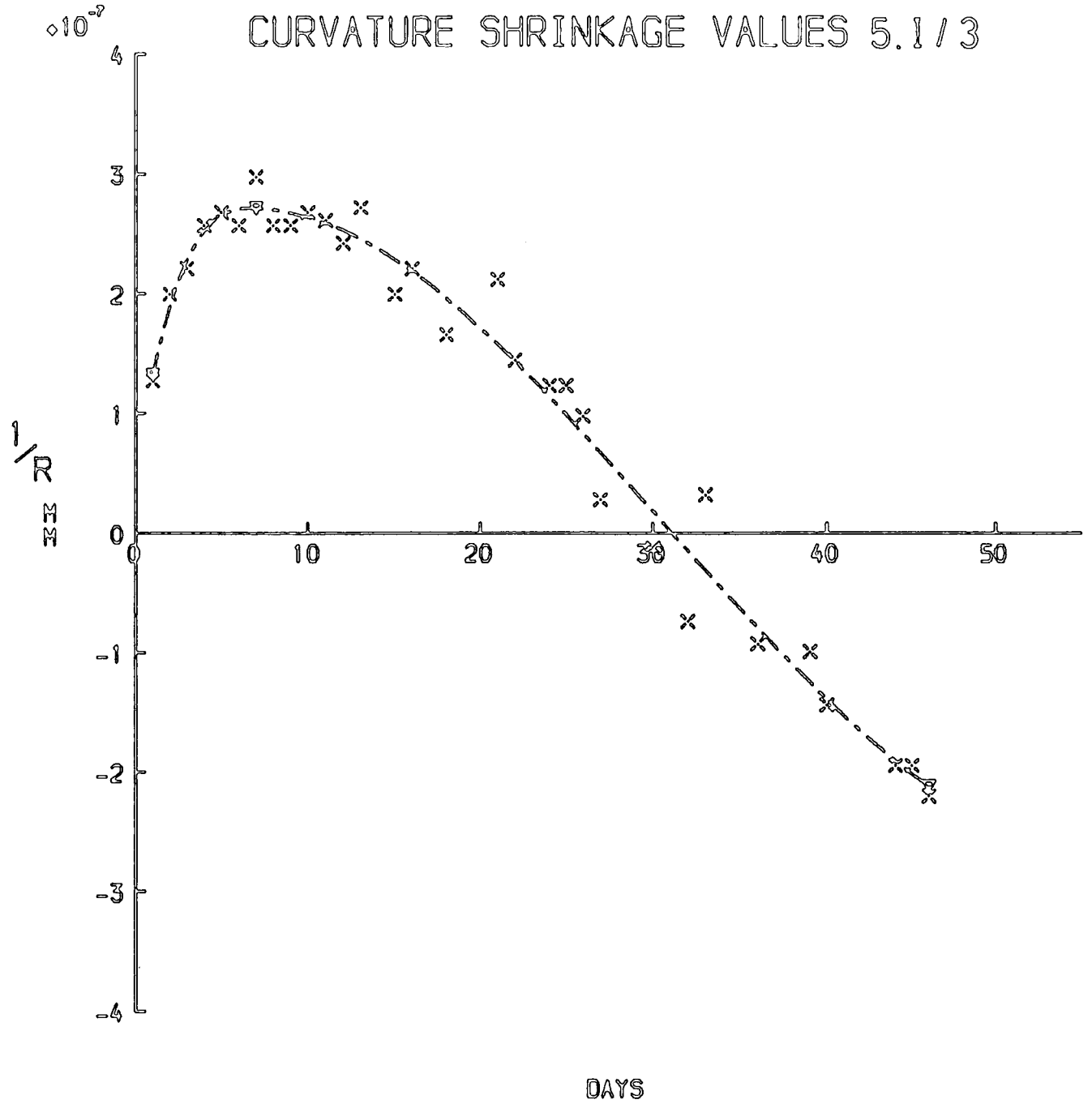
CURVATURE SHRINKAGE VALUES 5.1/3
◇10⁻⁷
4
3
2
1
0
-1
-2
-3
-4
1/R
MM
0
10
20
30
40
50
DAYS

FIG. 5.1.9

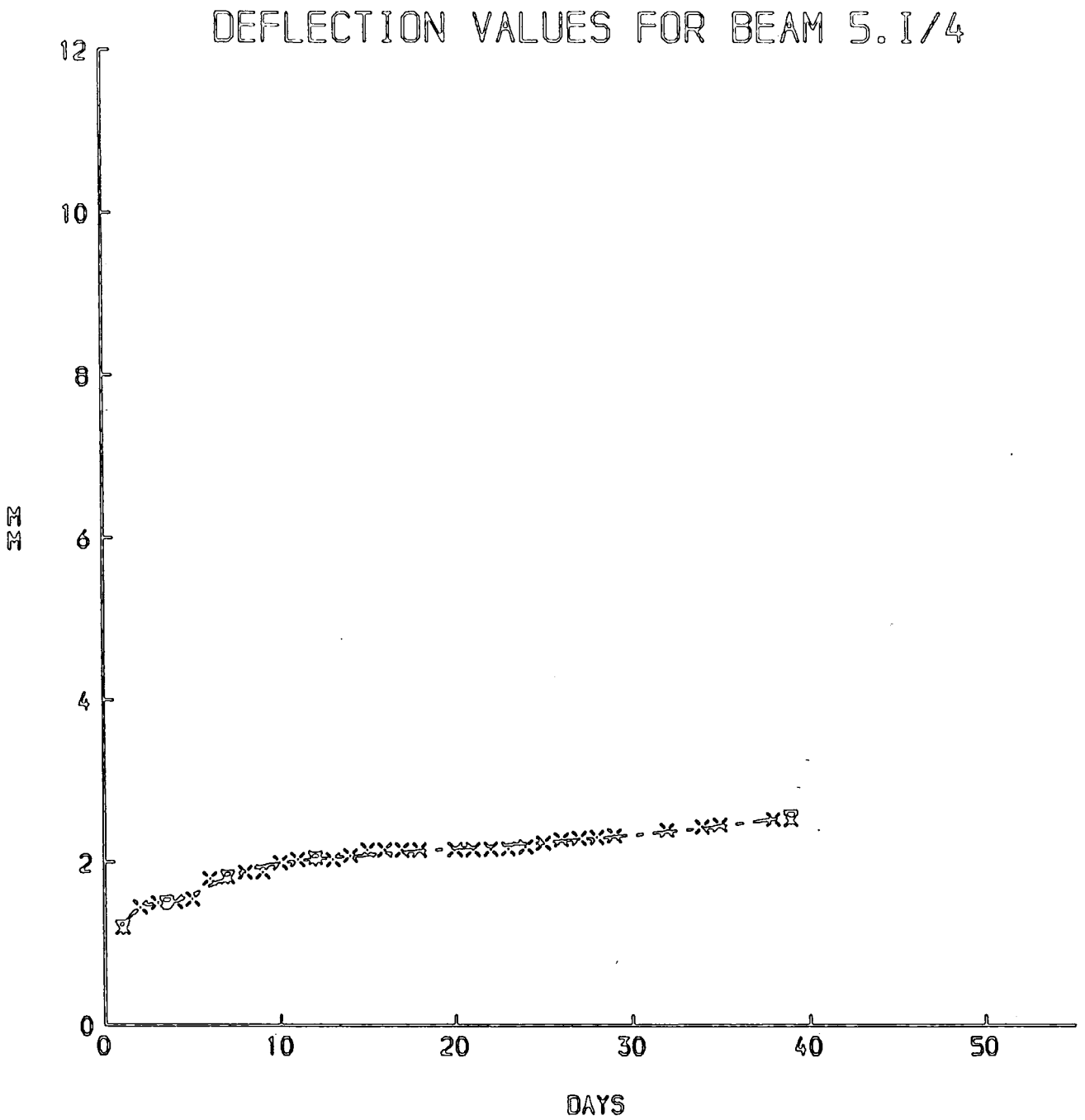
DEFLECTION VALUES FOR BEAM 5.I/4
MM
12
10
8
6
4
2
0
0
10
20
30
40
50
DAYS

FIG. 5·I .10.

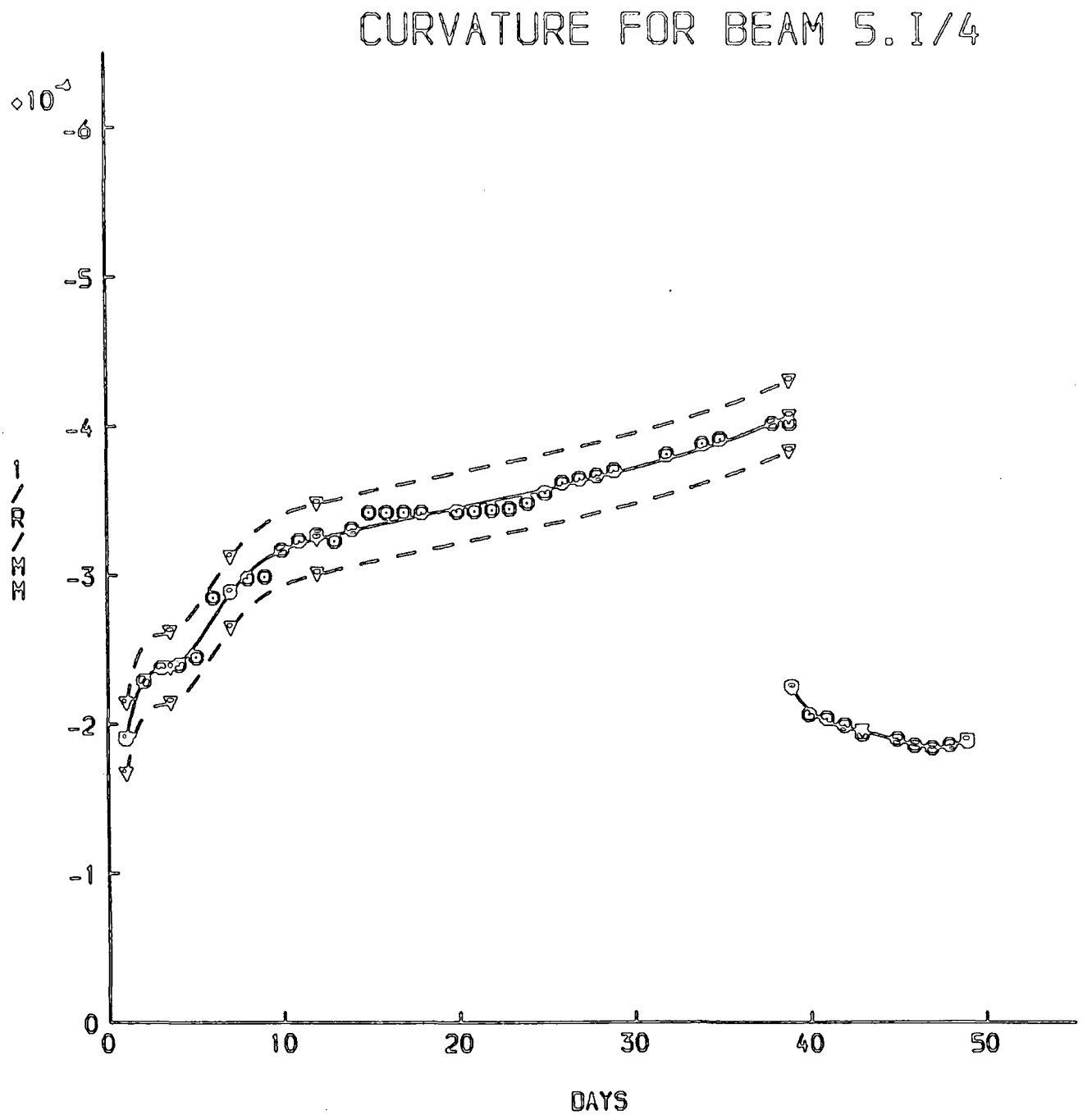

FIG. 5.I.11.

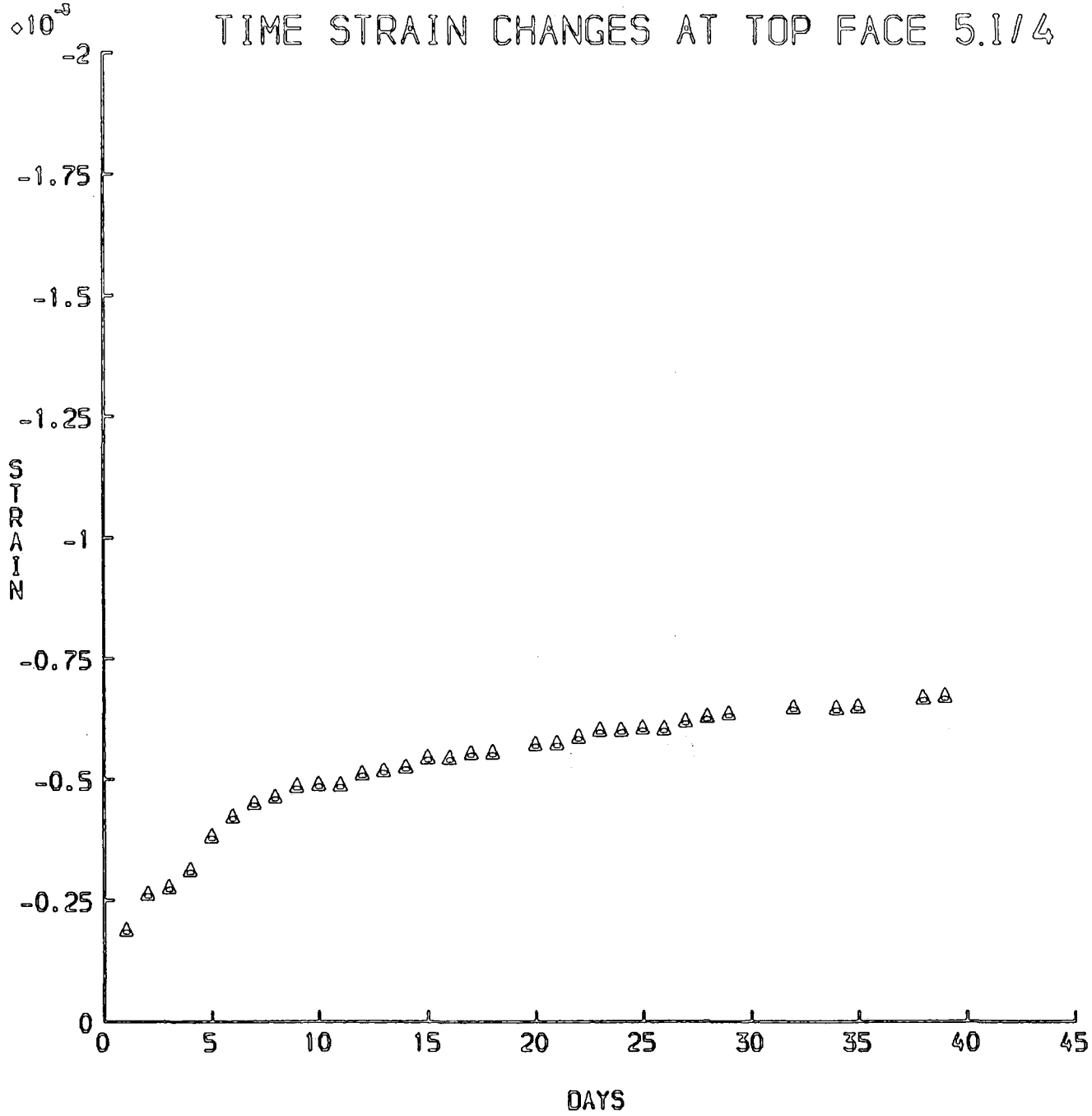
TIME STRAIN CHANGES AT TOP FACE 5.1/4
$\diamond 10^{-3}$
-2
-1.75
-1.5
-1.25
-1
-0.75
-0.5
-0.25
0
STRAIN
0
5
10
15
20
25
30
35
40
45
DAYS

FIG. 5.1.12.

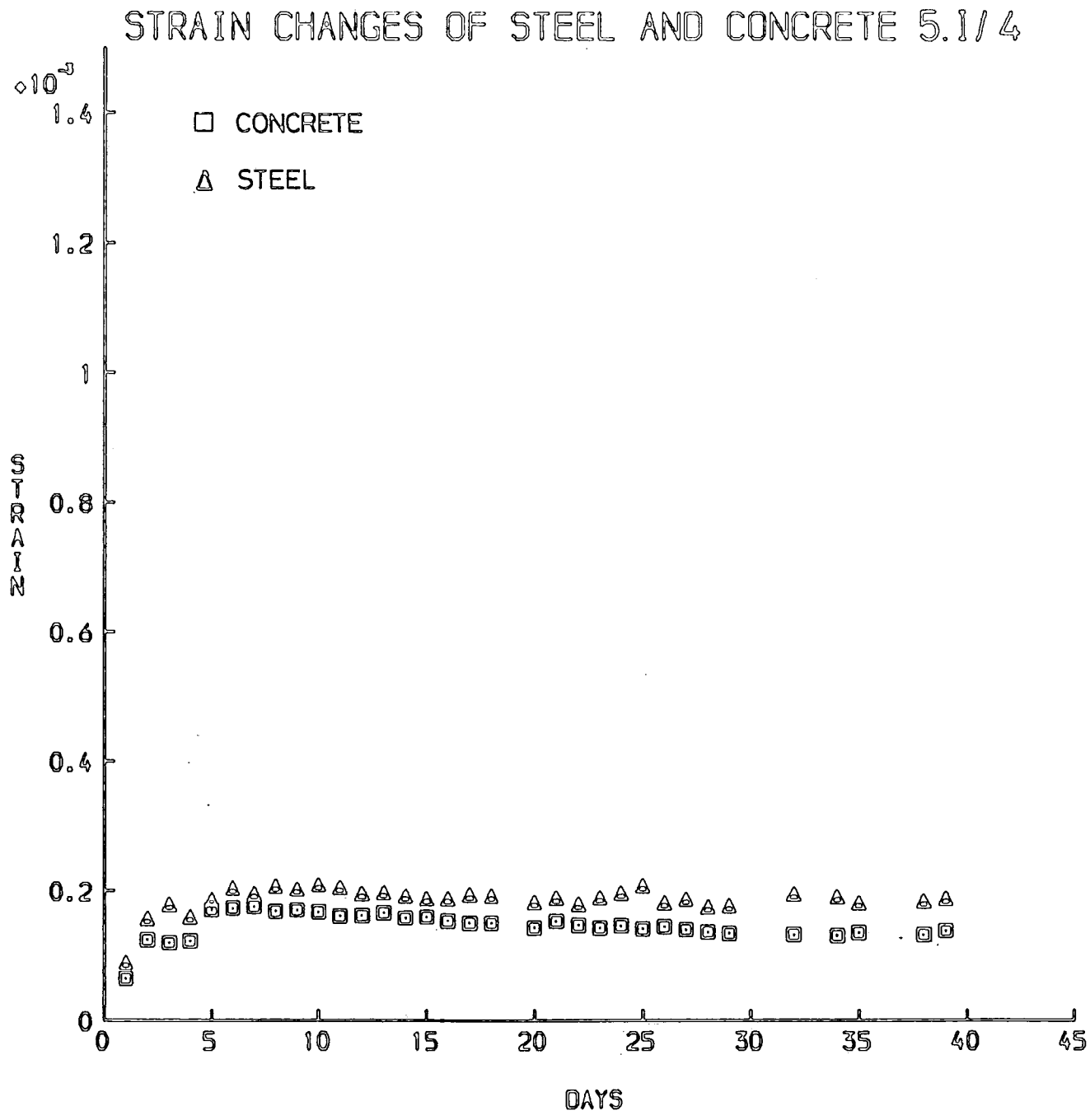
STRAIN CHANGES OF STEEL AND CONCRETE 5.1/4
◇10⁻³
1.4
1.2
1
0.8
0.6
0.4
0.2
0
STRAIN
□ CONCRETE
△ STEEL
0
5
10
15
20
25
30
35
40
45
DAYS

FIG. 5.1.13

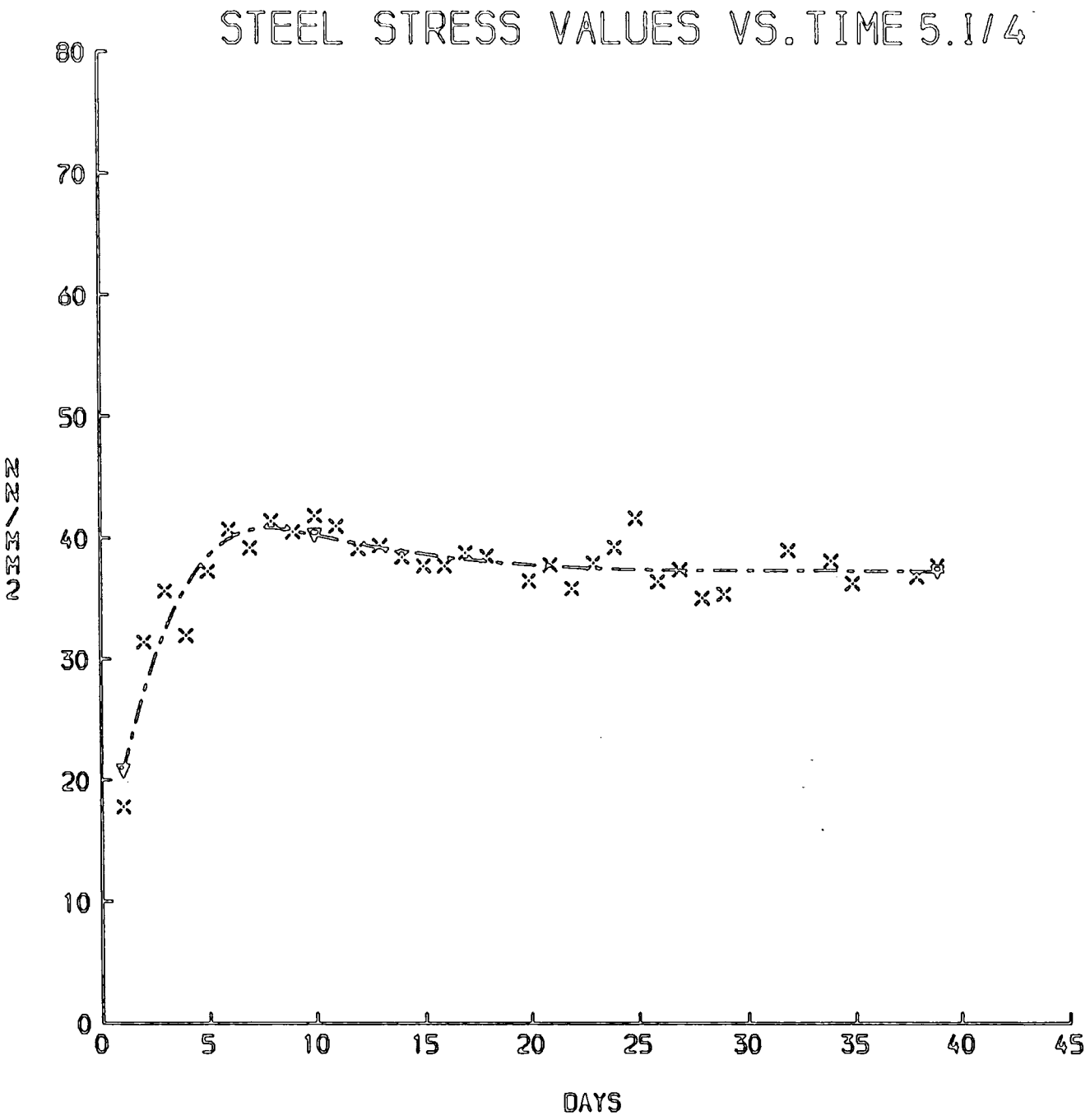
STEEL STRESS VALUES VS. TIME 5.1/4
80
70
60
50
40
30
20
10
0
0
5
10
15
20
25
30
35
40
45
DAYS
N/MM2

FIG. 5.1.14

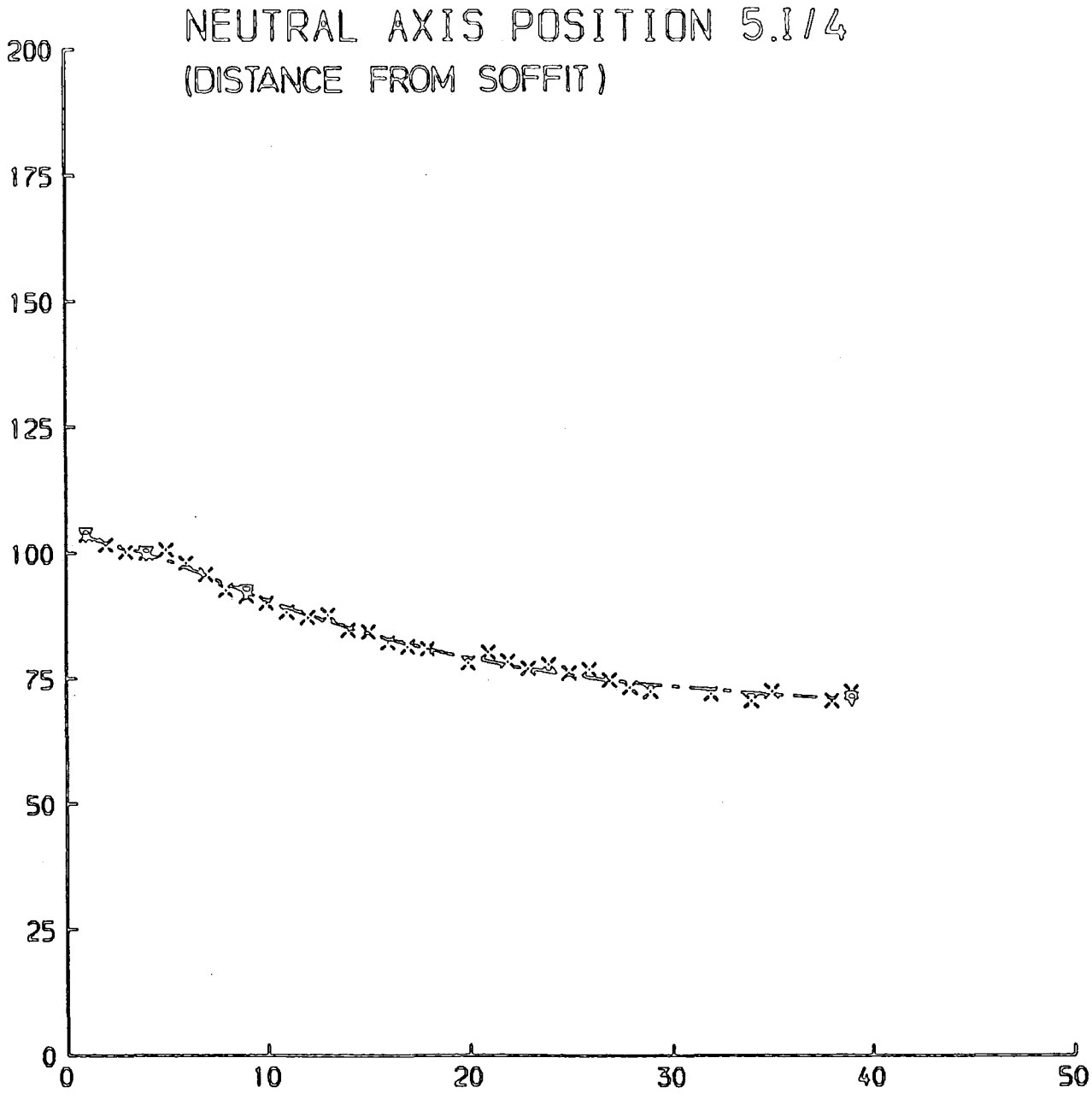
NEUTRAL AXIS POSITION 5.1/4
(DISTANCE FROM SOFFIT)
200
175
150
125
100
75
50
25
0
0
10
20
30
40
50

FIG. 5.1.15.

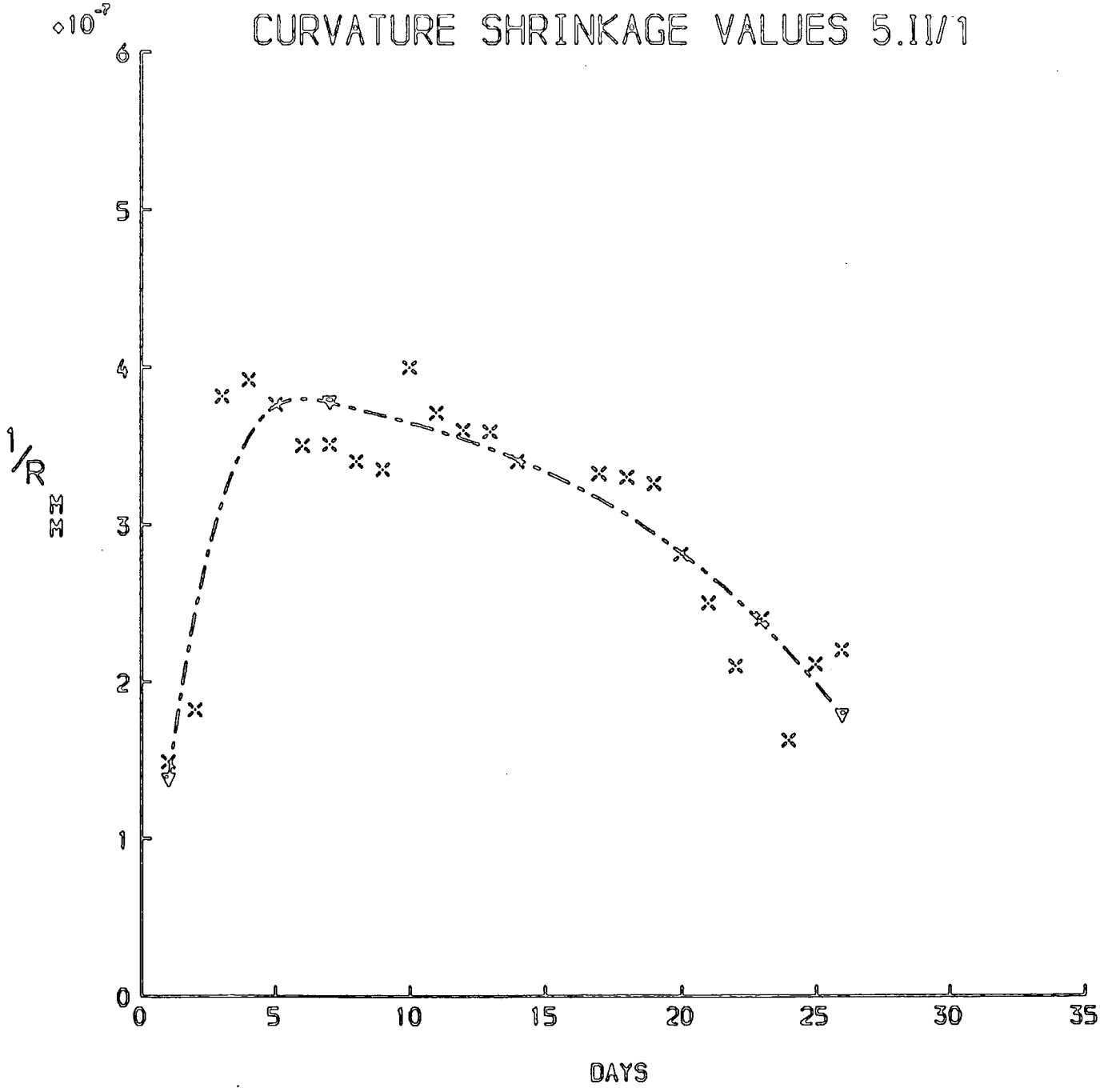
CURVATURE SHRINKAGE VALUES 5.II/1
$\diamond 10^{-7}$
6
5
4
3
2
1
0
$\frac{1}{R}$ MM
0
5
10
15
20
25
30
35
DAYS

FIG. 5.II.1

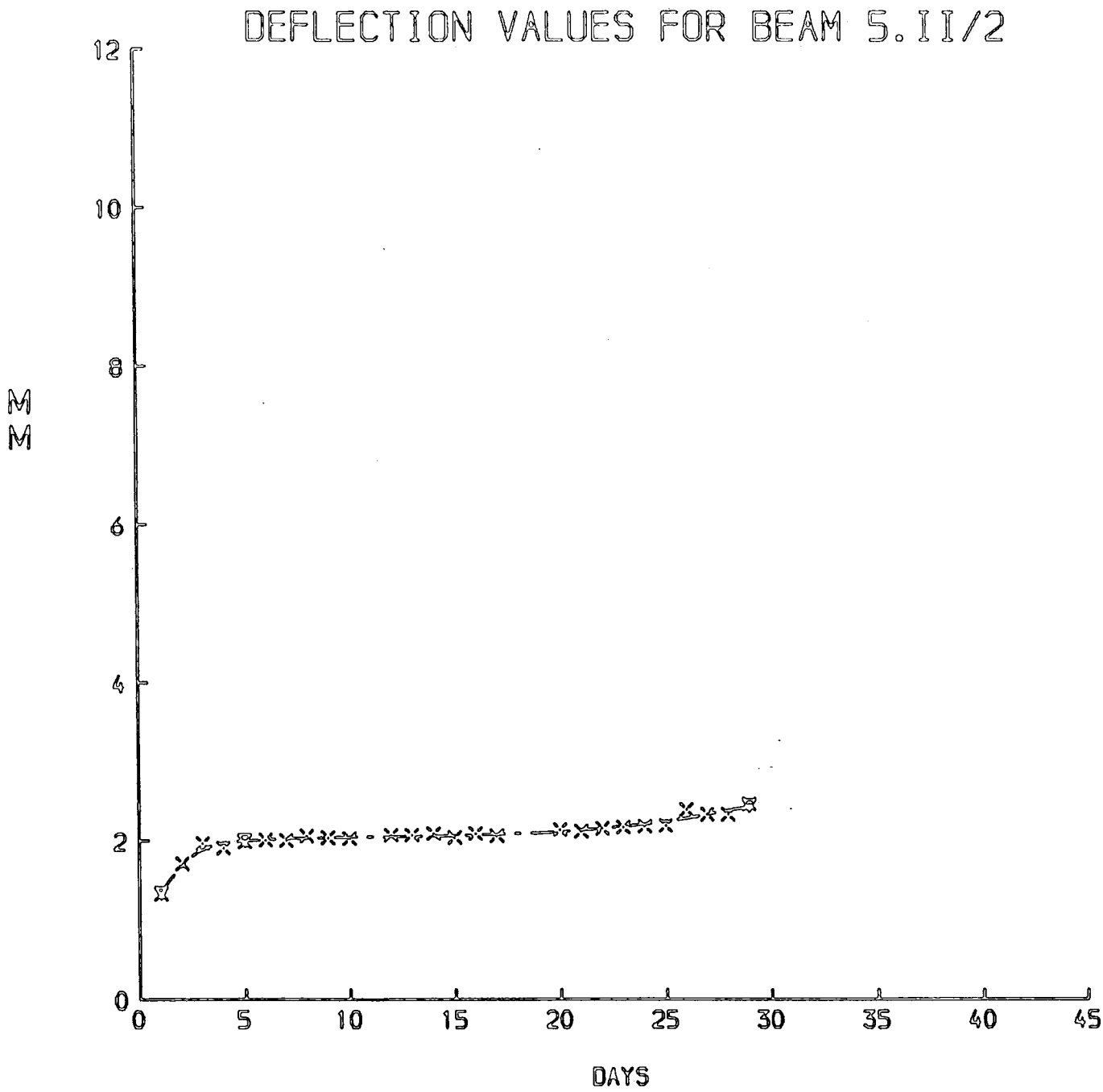
DEFLECTION VALUES FOR BEAM 5.II/2
12
10
8
6
4
2
0
M
M
0
5
10
15
20
25
30
35
40
45
DAYS

FIG. 5.II.2.

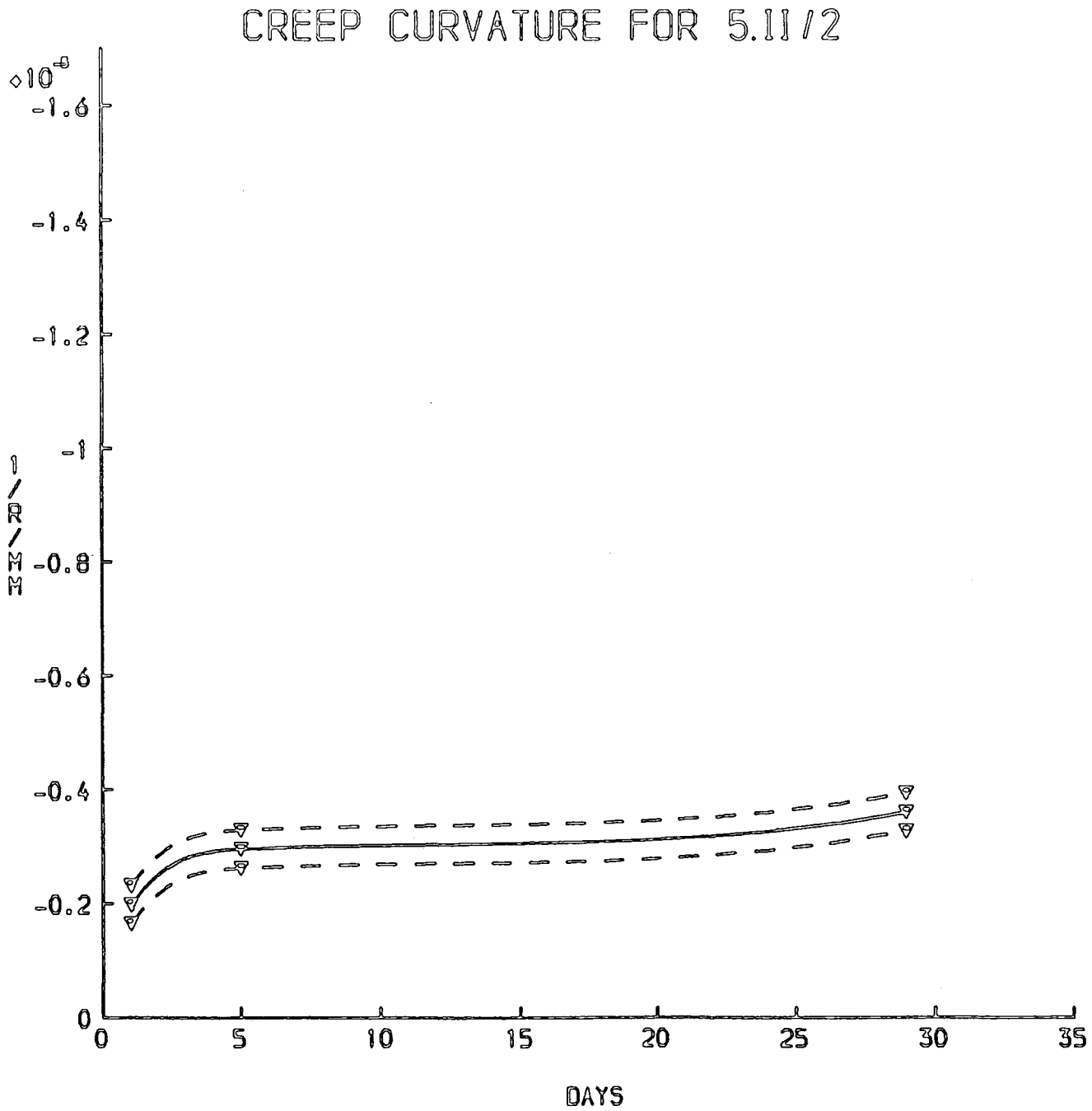
CREEP CURVATURE FOR 5.II/2
◇10⁻⁵
-1.6
-1.4
-1.2
-1
-0.8
-0.6
-0.4
-0.2
0
1/R/M/M
0
5
10
15
20
25
30
35
DAYS

FIG.5.II.3

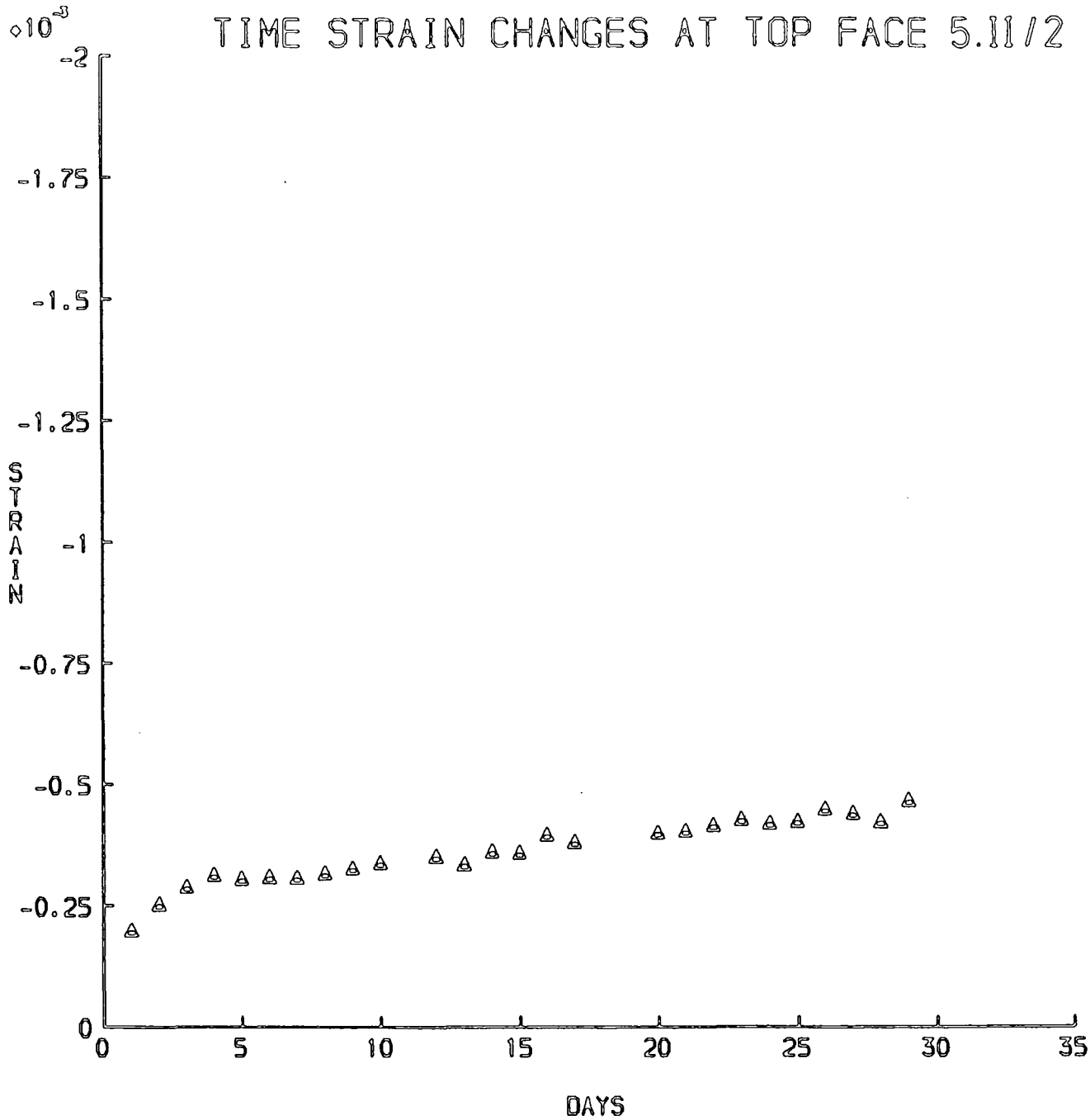
TIME STRAIN CHANGES AT TOP FACE 5.II/2
$\diamond 10^{-3}$
-2
-1.75
-1.5
-1.25
-1
-0.75
-0.5
-0.25
0
STRAIN
0
5
10
15
20
25
30
35
DAYS

FIG. 5.II.4.

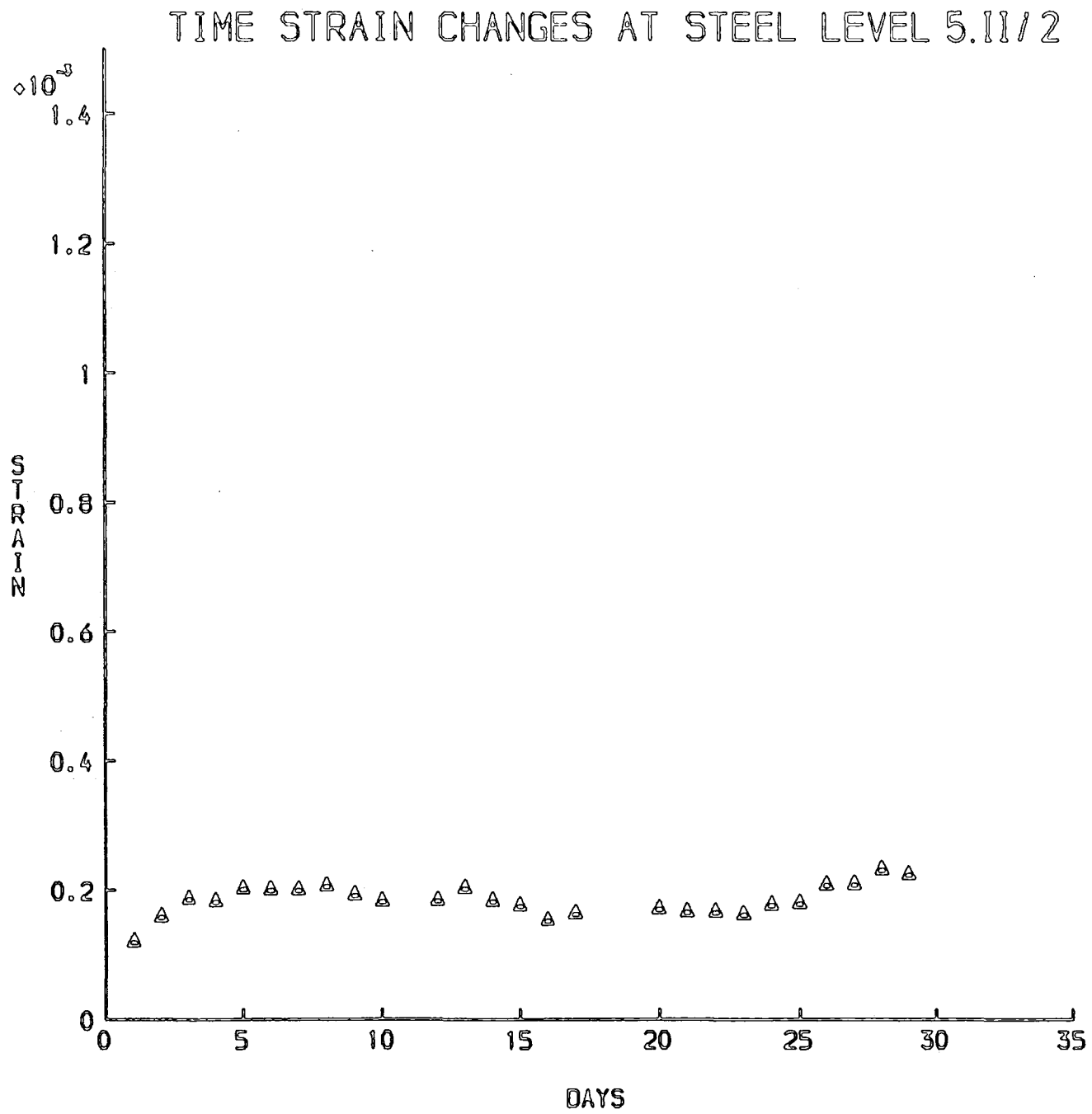
TIME STRAIN CHANGES AT STEEL LEVEL 5.11/2
◇10⁻³
1.4
1.2
1
0.8
0.6
0.4
0.2
0
STRAIN
0
5
10
15
20
25
30
35
DAYS

FIG. 5.11.5.

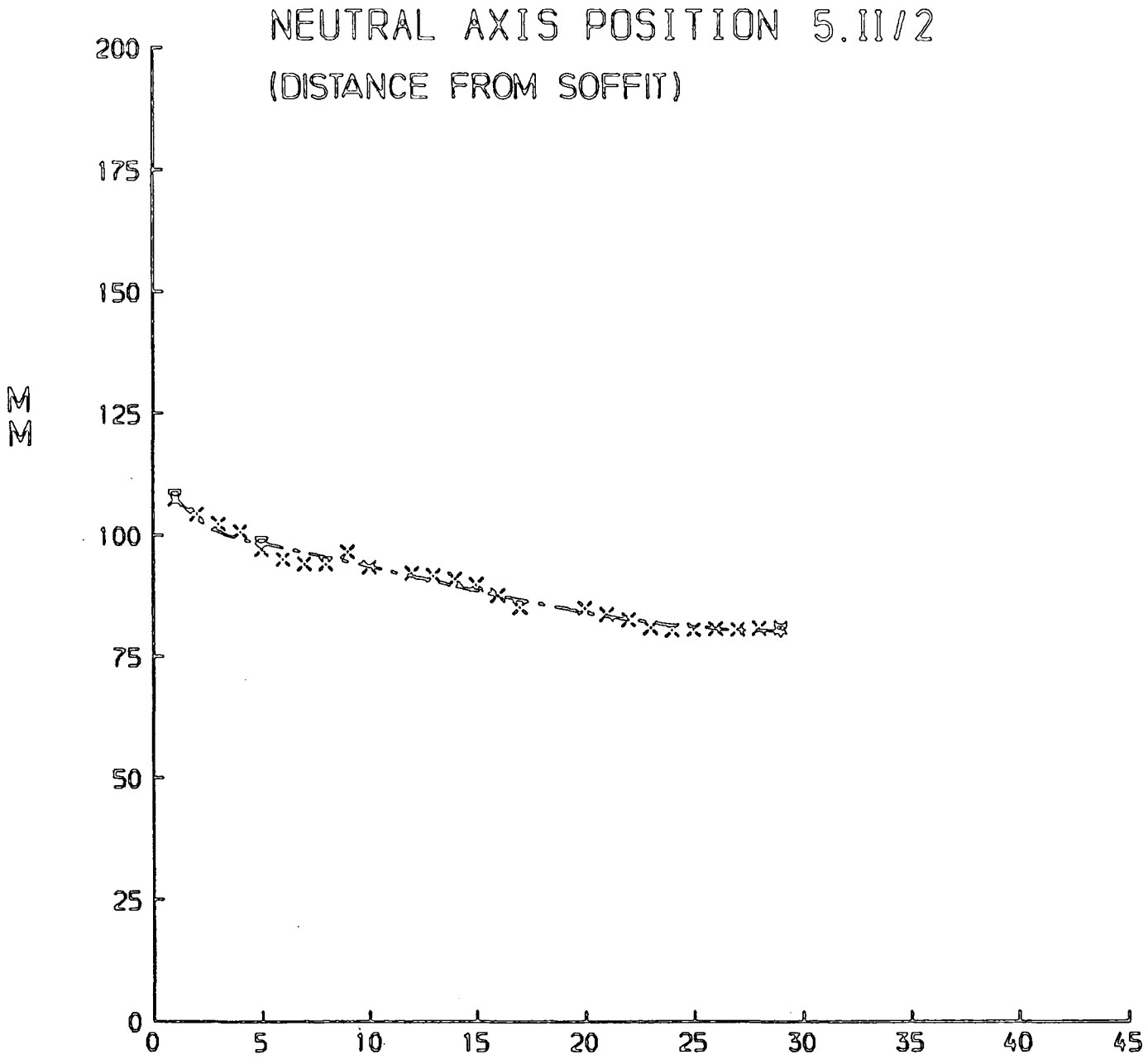
NEUTRAL AXIS POSITION 5.11/2
(DISTANCE FROM SOFFIT)
MM
200
175
150
125
100
75
50
25
0
0
5
10
15
20
25
30
35
40
45

FIG. 5.11.6.

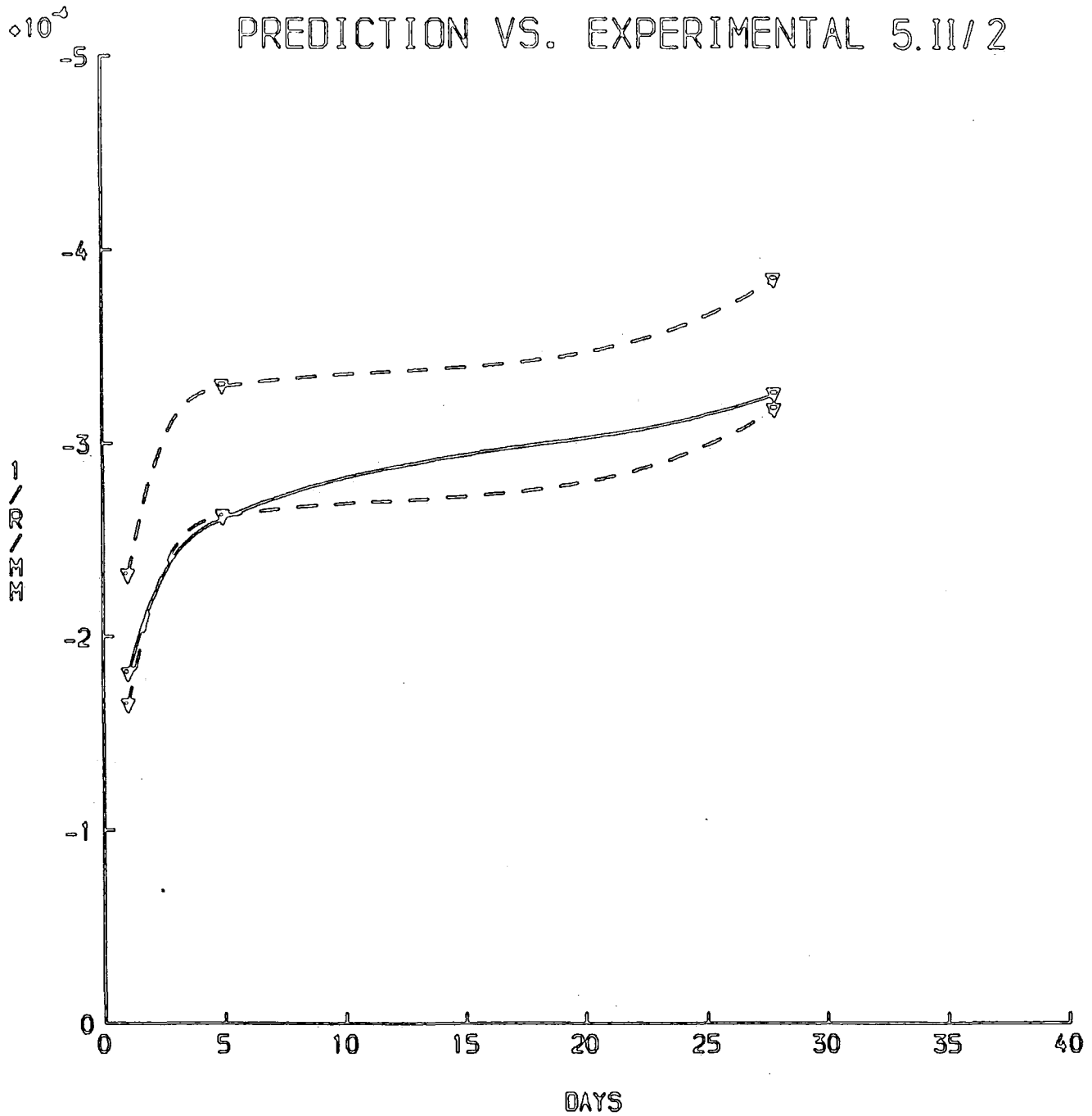
PREDICTION VS. EXPERIMENTAL 5.11/2
◇10⁻⁵
-5
-4
-3
-2
-1
0
1/RMM
0
5
10
15
20
25
30
35
40
DAYS

FIG. 5.11.7

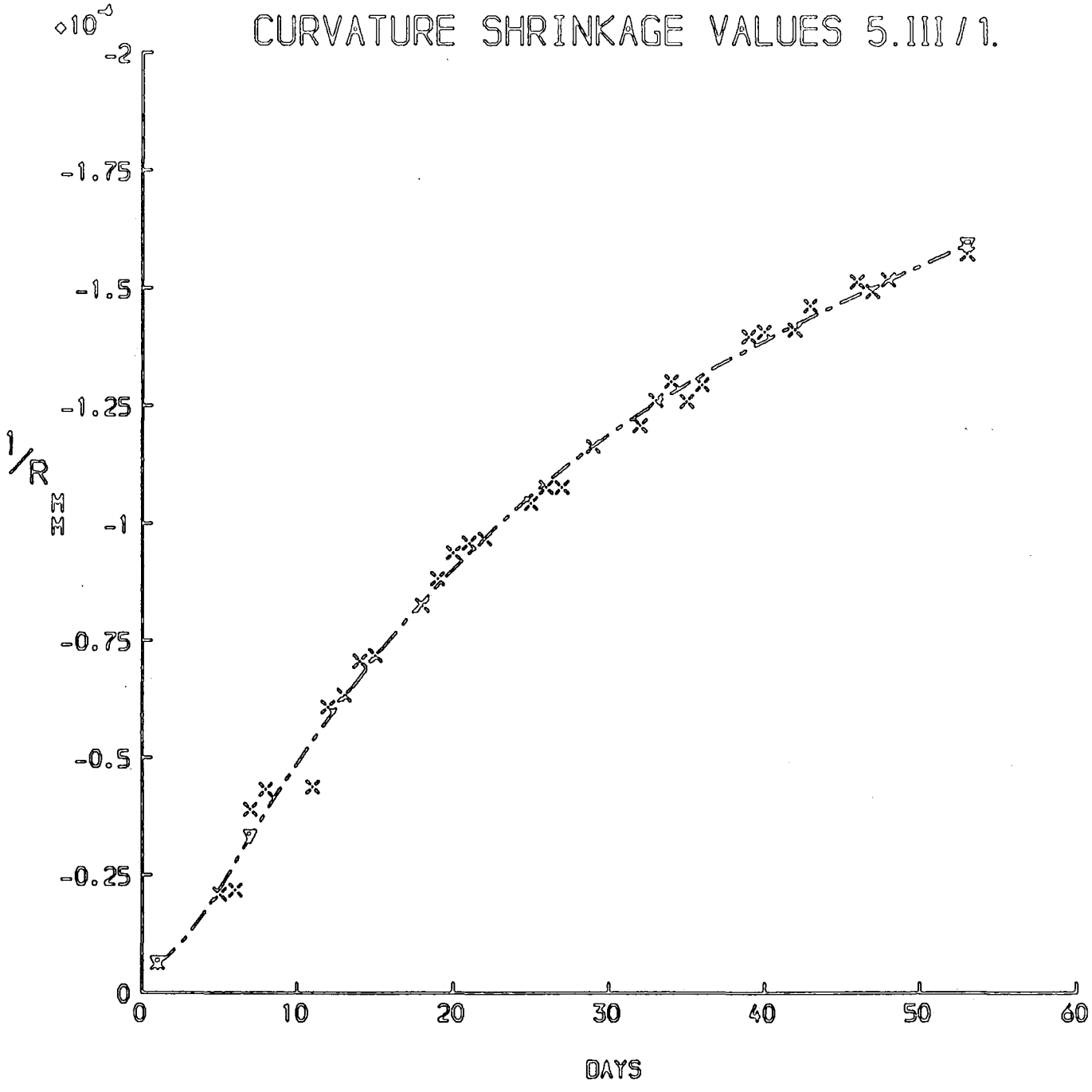
CURVATURE SHRINKAGE VALUES 5.III/1.
$\circ 10^{-5}$
-2
-1.75
-1.5
-1.25
-1
-0.75
-0.5
-0.25
0
$1/R_{MM}$
0
10
20
30
40
50
60
DAYS

FIG. 5.III.1

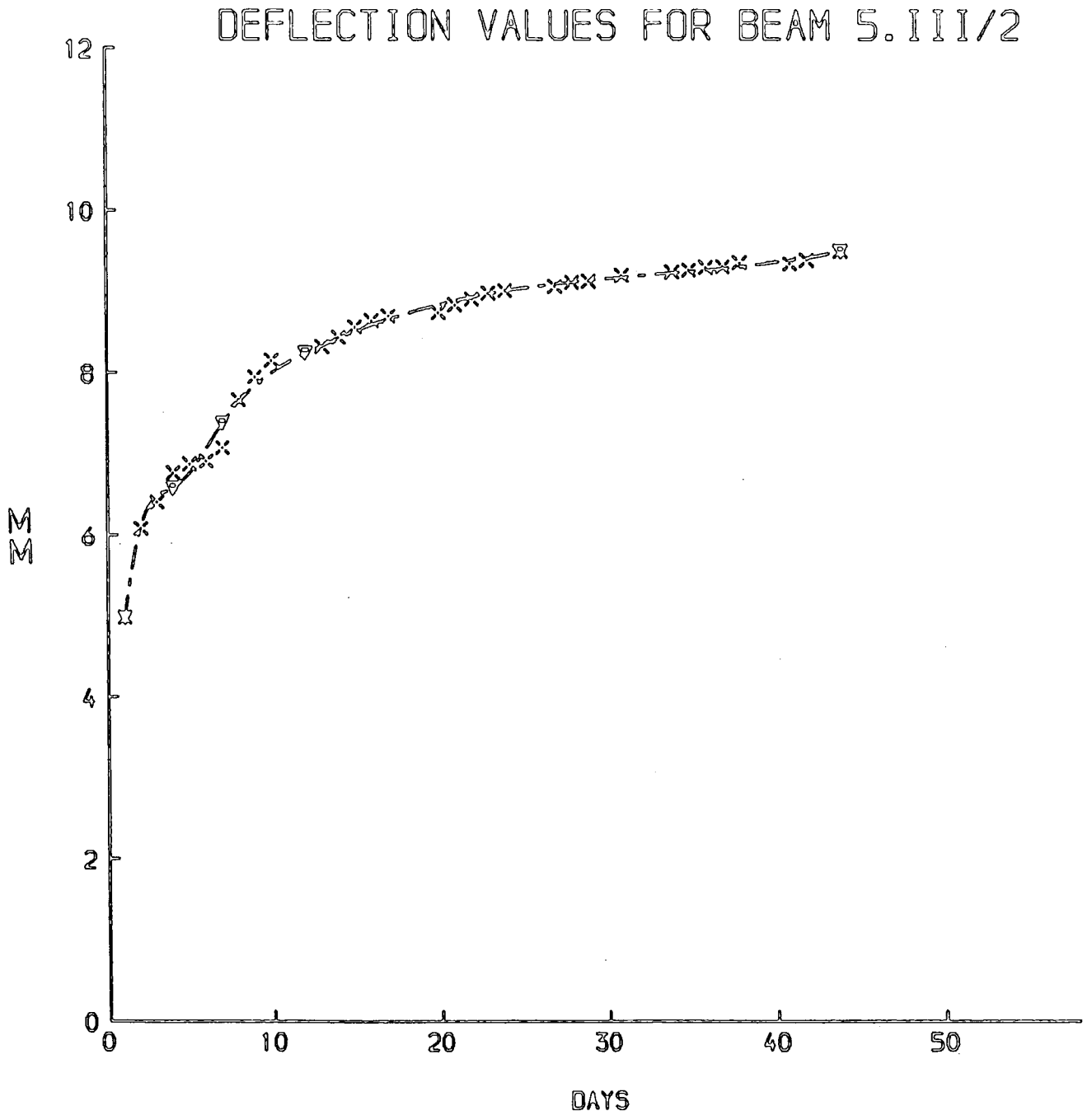
DEFLECTION VALUES FOR BEAM 5.III/2
12
10
8
6
4
2
0
MM
0
10
20
30
40
50
DAYS

FIG. 5.III .2

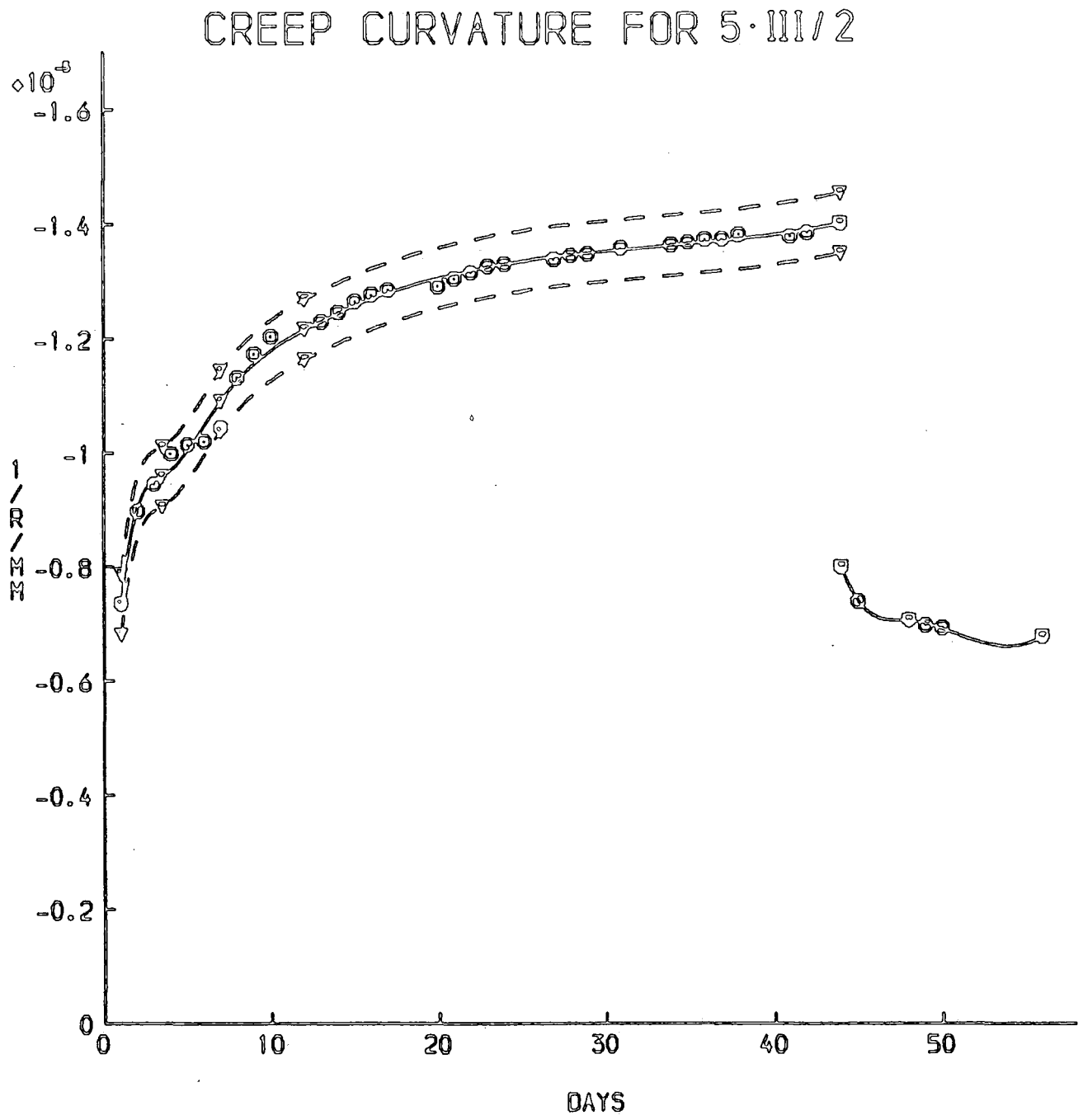
CREEP CURVATURE FOR 5·III/2
◇10⁻³
-1.6
-1.4
-1.2
-1
-0.8
-0.6
-0.4
-0.2
0
1/R/MM
0
10
20
30
40
50
DAYS

FIG. 5.III.3

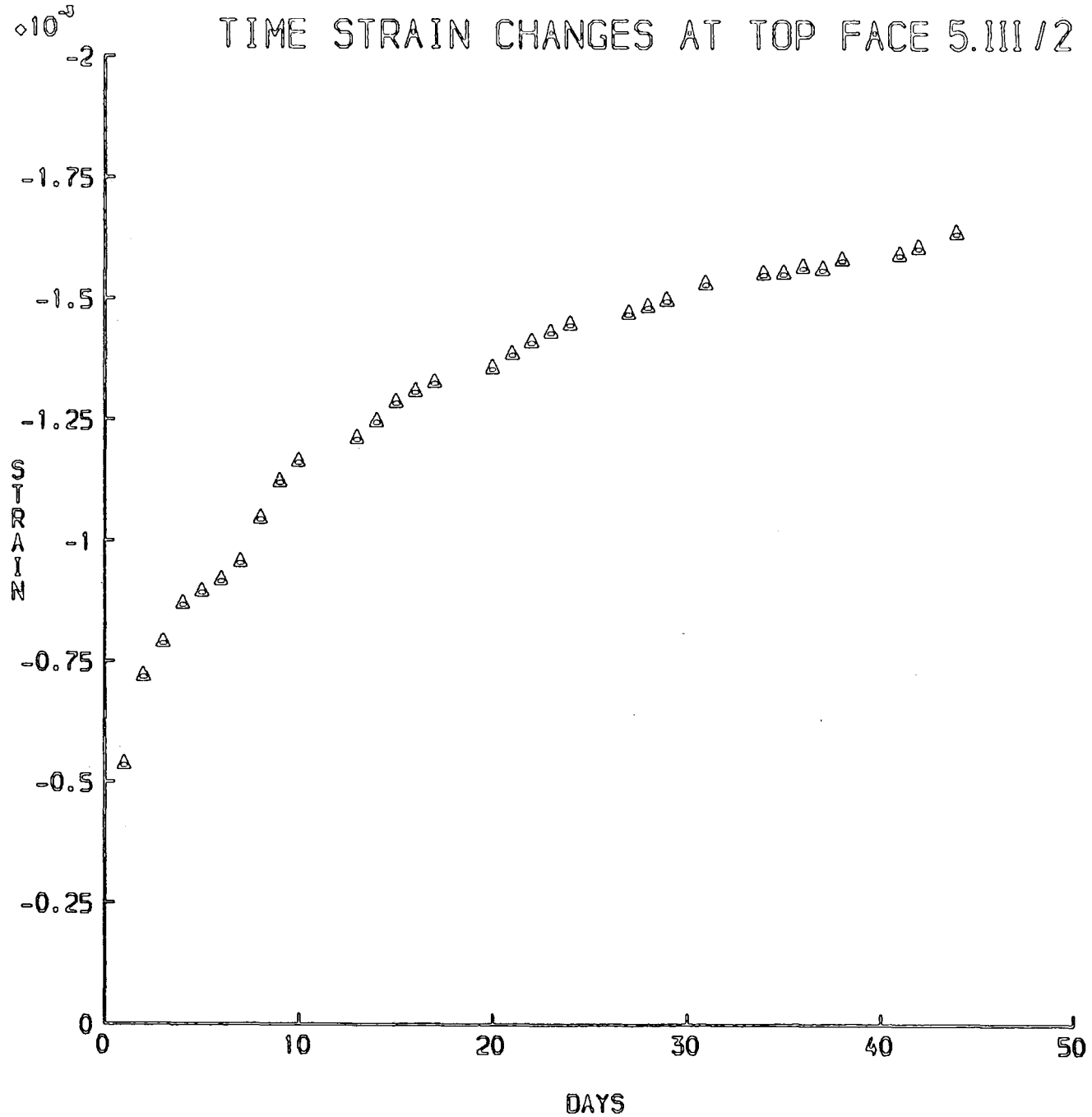
TIME STRAIN CHANGES AT TOP FACE 5.III/2
◇10⁻³
-2
-1.75
-1.5
-1.25
-1
-0.75
-0.5
-0.25
0
STRAIN
0
10
20
30
40
50
DAYS

FIG. 5.III.4.

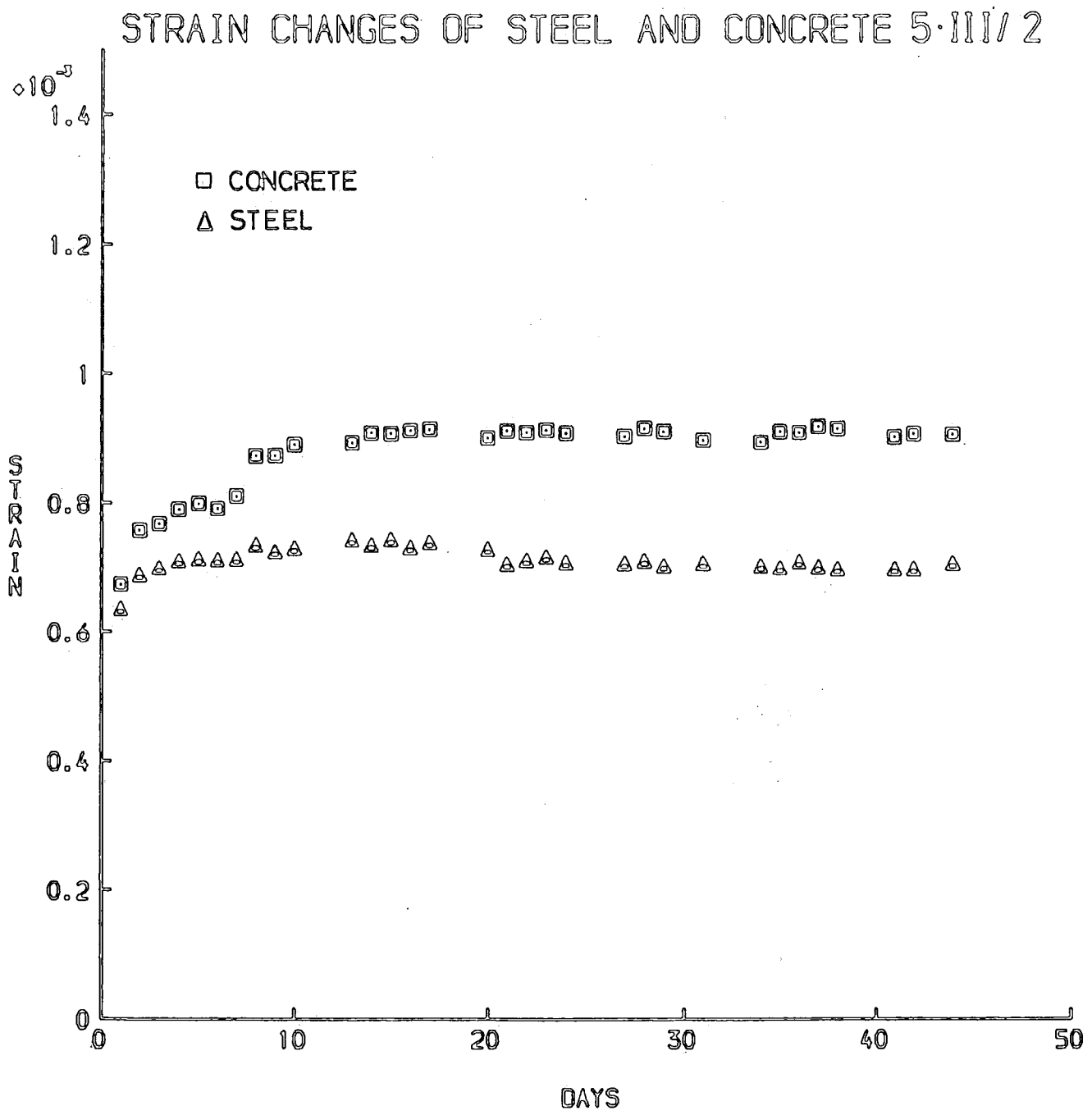
STRAIN CHANGES OF STEEL AND CONCRETE 5·III/2
◇10⁻³
1.4
1.2
1
0.8
0.6
0.4
0.2
0
STRAIN
□ CONCRETE
Δ STEEL
0
10
20
30
40
50
DAYS

FIG. 5.III.5

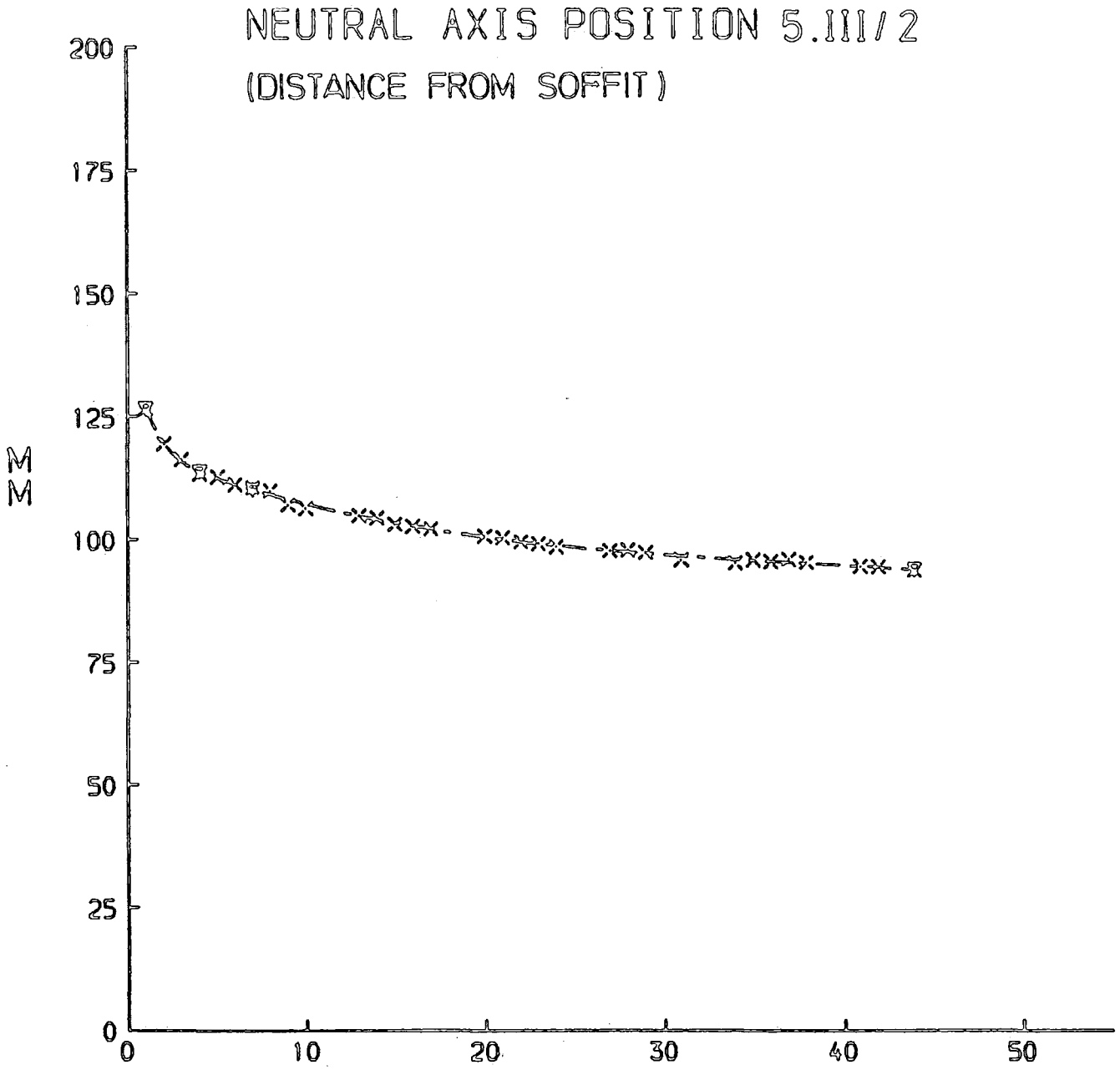
NEUTRAL AXIS POSITION 5.III/2
(DISTANCE FROM SOFFIT)
200
175
150
125
100
75
50
25
0
MM
0
10
20
30
40
50

FIG. 5.III.6

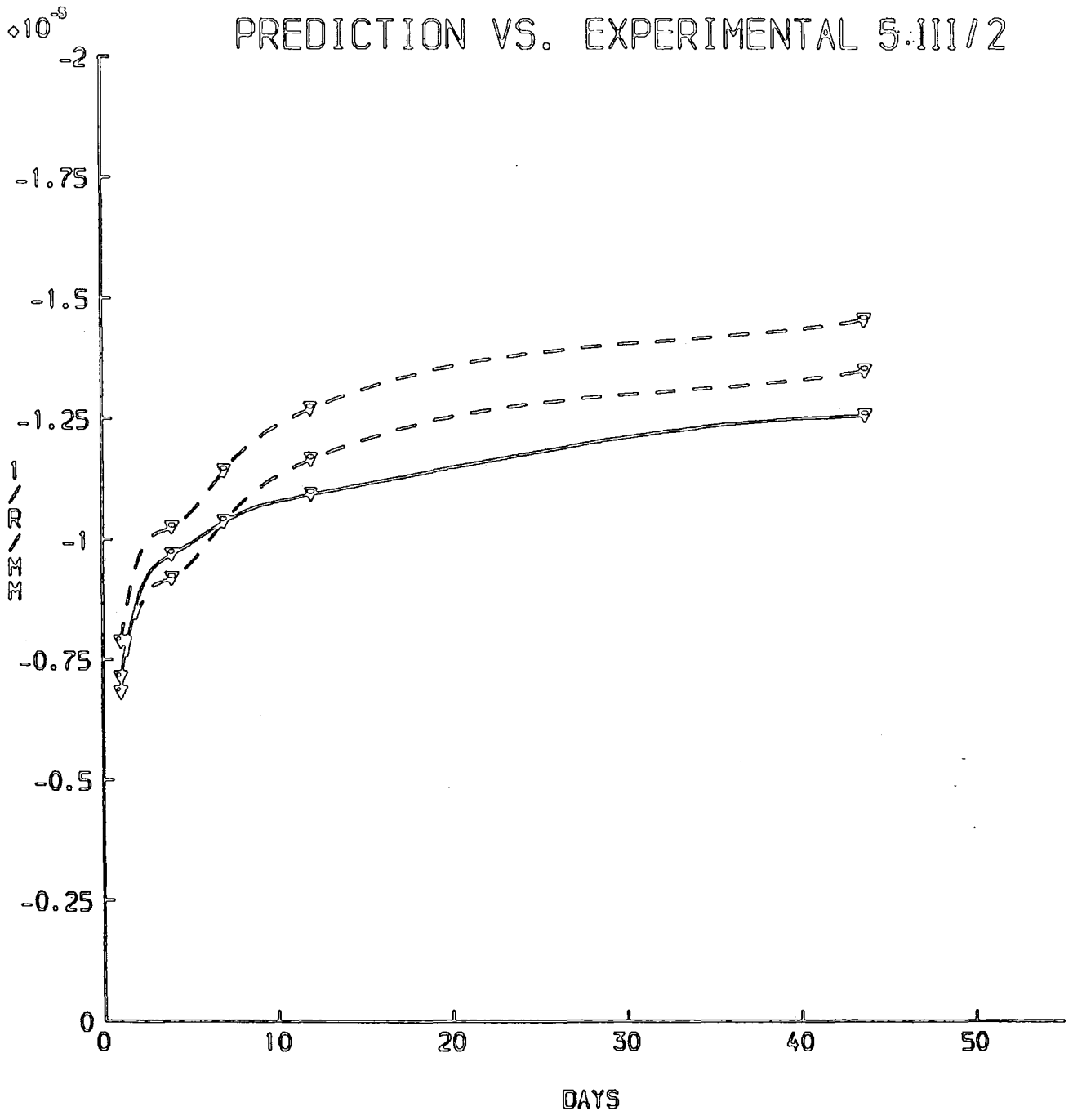
PREDICTION VS. EXPERIMENTAL 5:III/2
◇10⁻⁵
-2
-1.75
-1.5
-1.25
-1
-0.75
-0.5
-0.25
0
1/R MM
0
10
20
30
40
50
DAYS

FIG. 5.III.7.

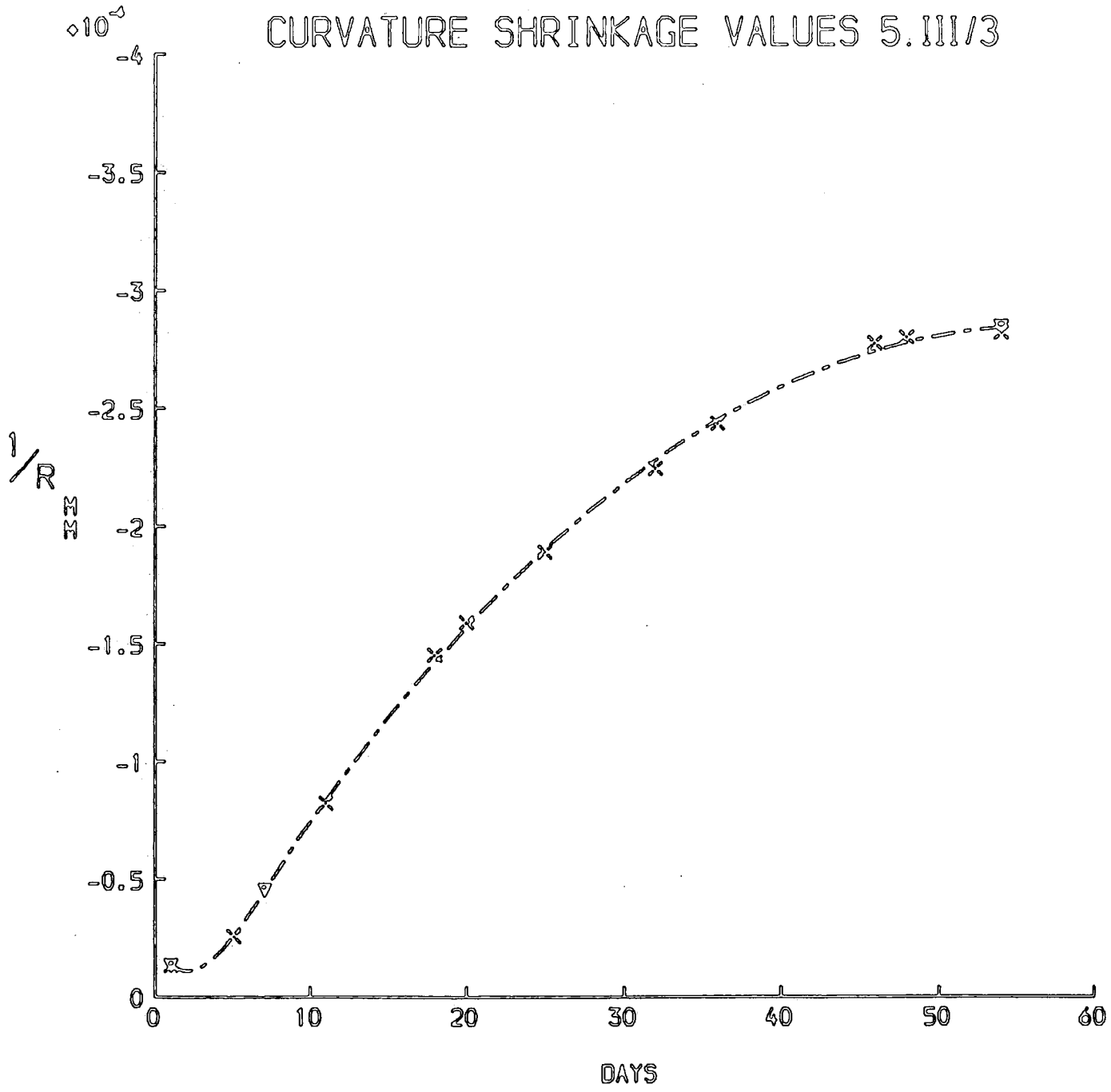
CURVATURE SHRINKAGE VALUES 5.III/3
$\circ 10^{-4}$
-4
-3.5
-3
-2.5
-2
-1.5
-1
-0.5
0
1/R
MM
0
10
20
30
40
50
60
DAYS

FIG. 5.III.8.

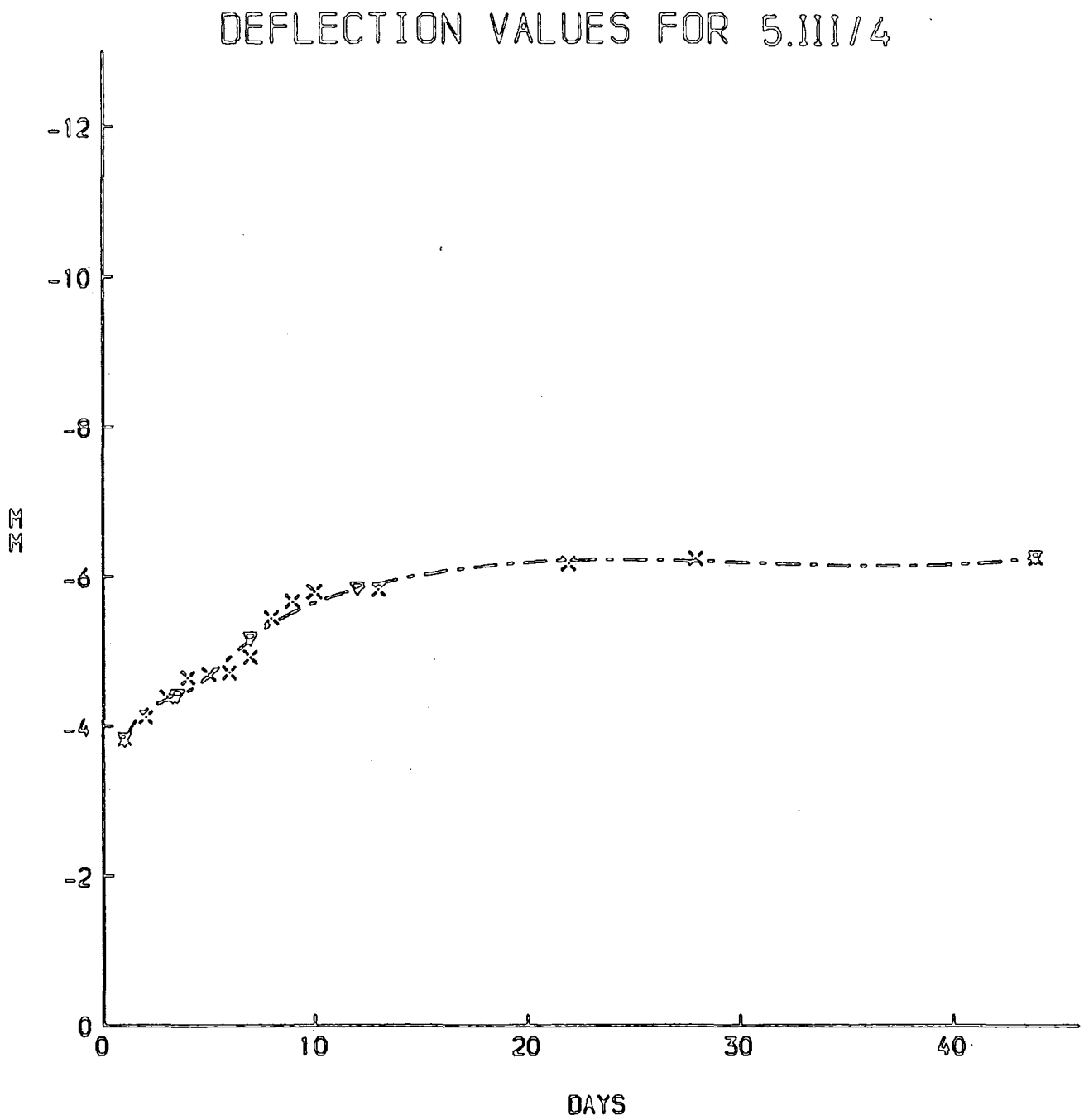

FIG.5.III.9

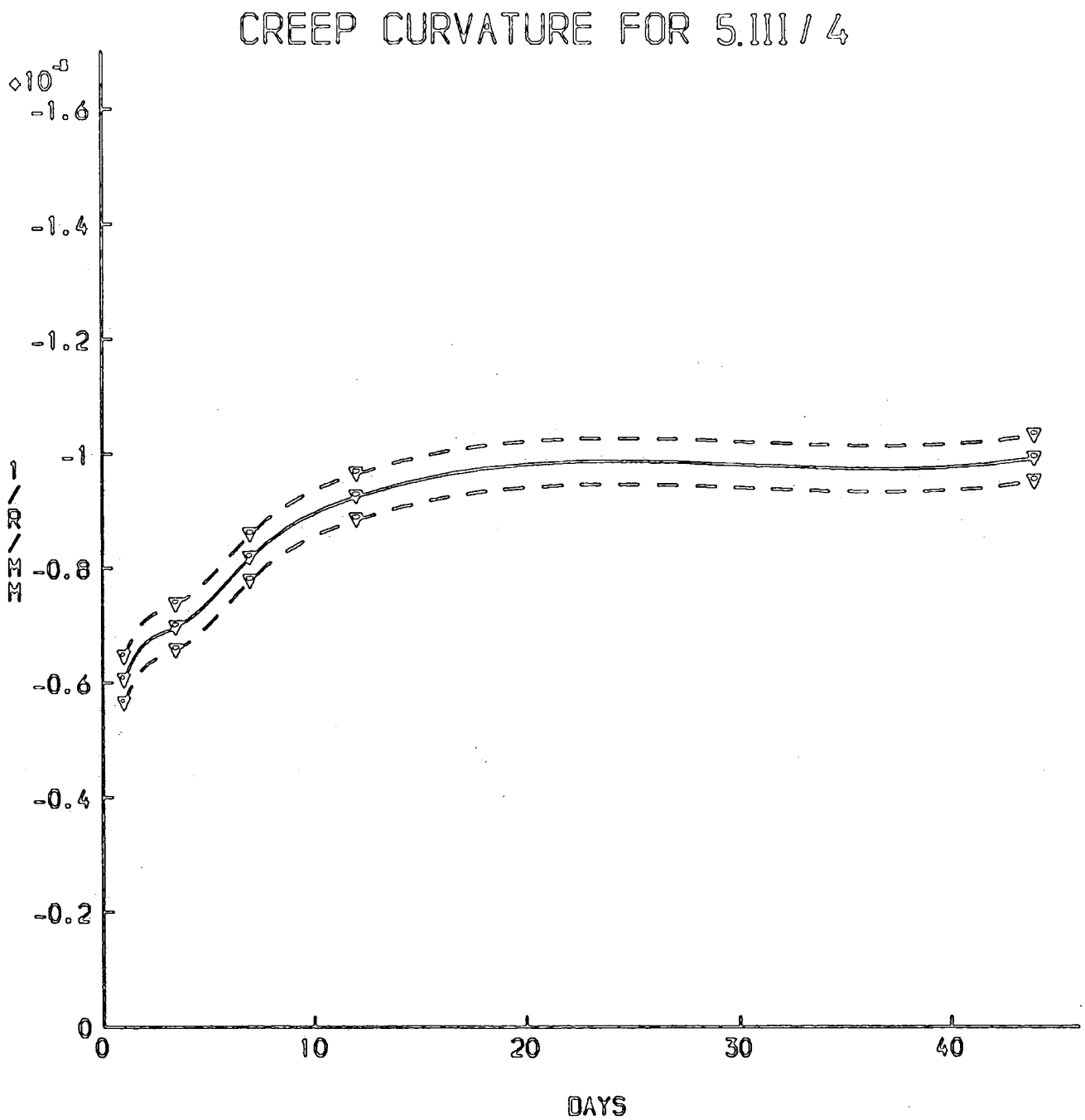
CREEP CURVATURE FOR 5.III / 4
◇10⁻³
-1.6
-1.4
-1.2
-1
-0.8
-0.6
-0.4
-0.2
0
1/R/MM
0
10
20
30
40
DAYS

FIG. 5.III.10.

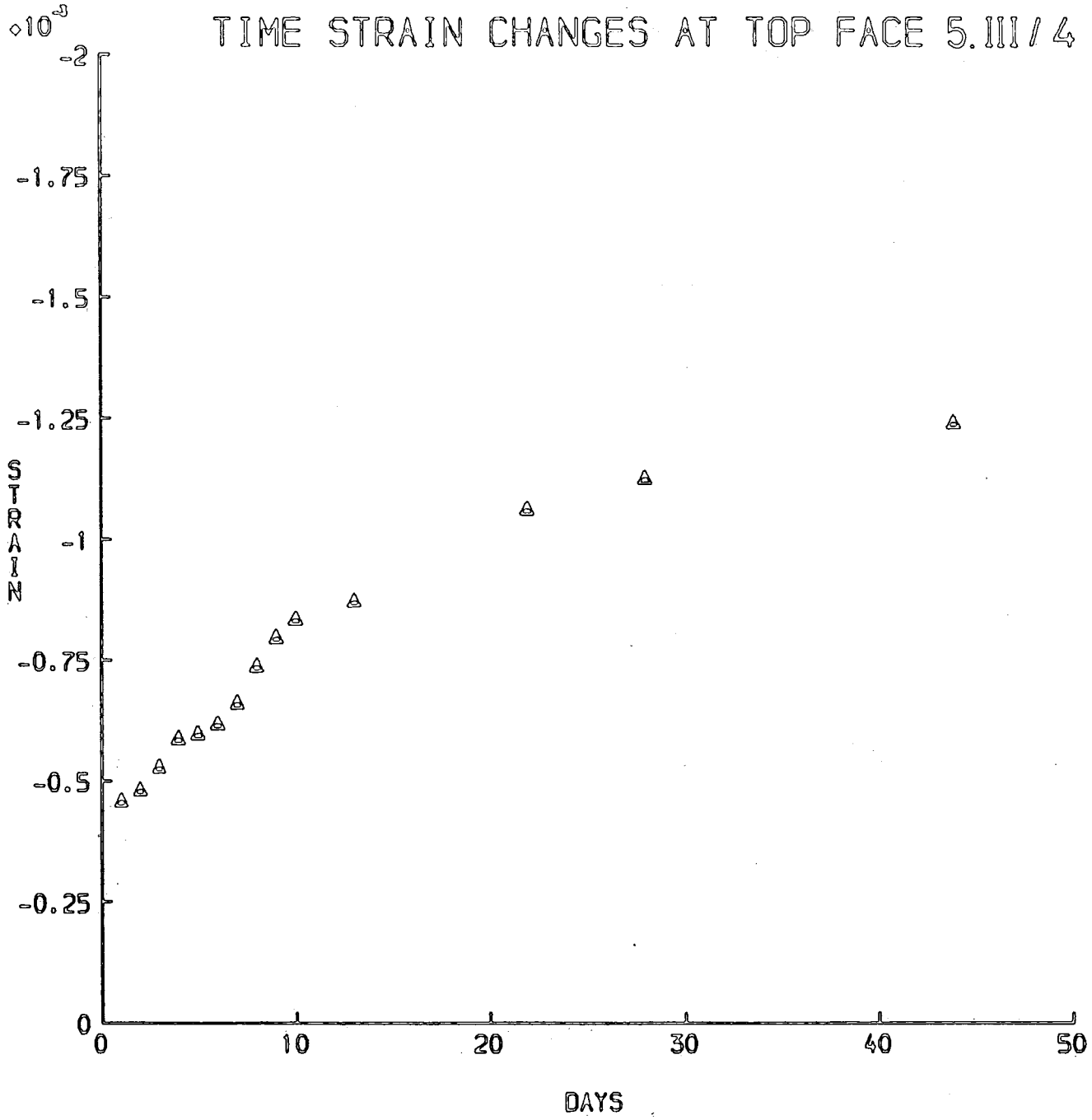
TIME STRAIN CHANGES AT TOP FACE 5.III/4
◇10⁻³
-2
-1.75
-1.5
-1.25
-1
-0.75
-0.5
-0.25
0
STRAIN
0
10
20
30
40
50
DAYS

FIG. 5.III.11

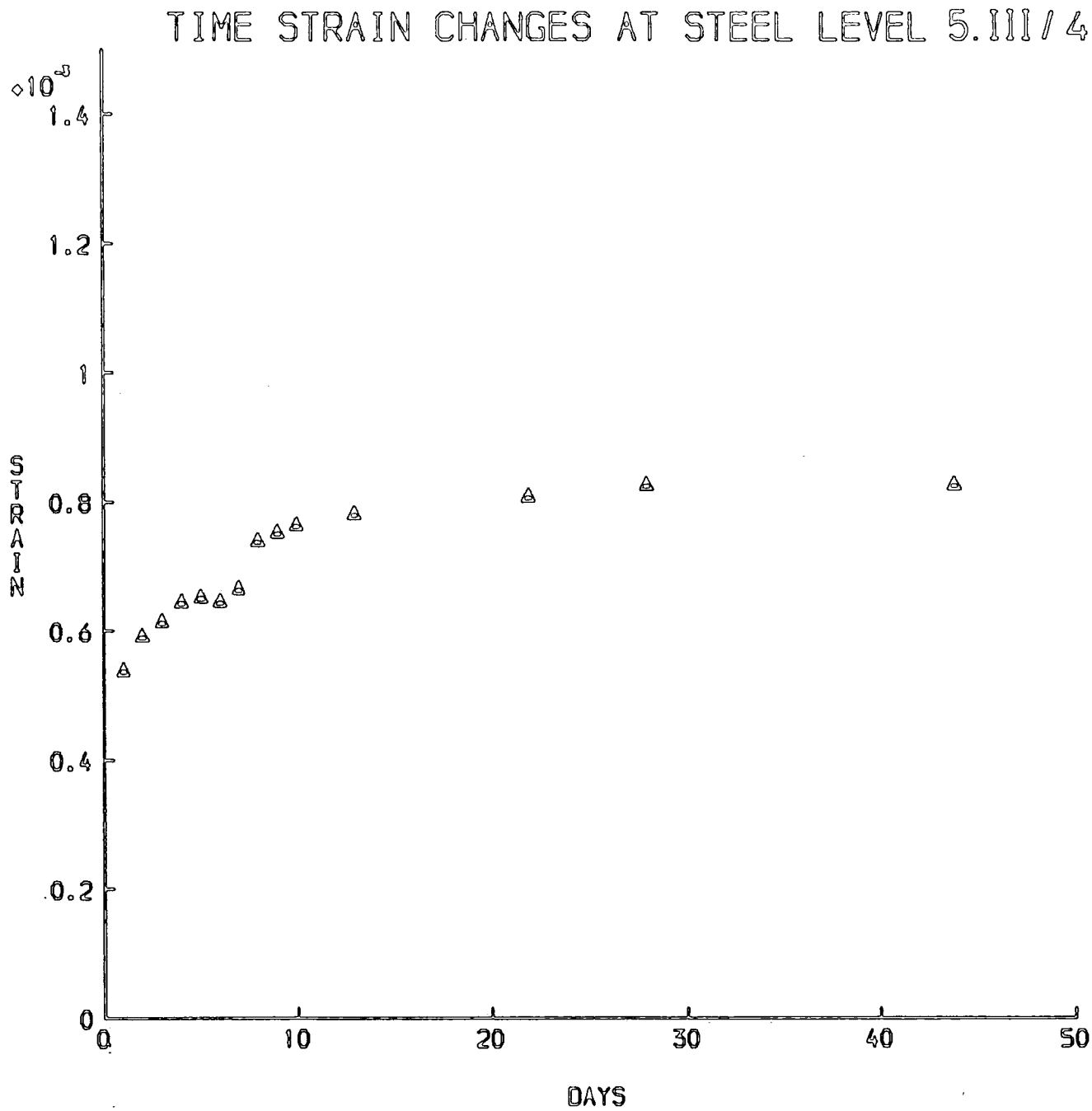
TIME STRAIN CHANGES AT STEEL LEVEL 5.III/4
◇10⁻³
1.4
1.2
1
0.8
0.6
0.4
0.2
0
STRAIN
0
10
20
30
40
50
DAYS

FIG. 5.III.12

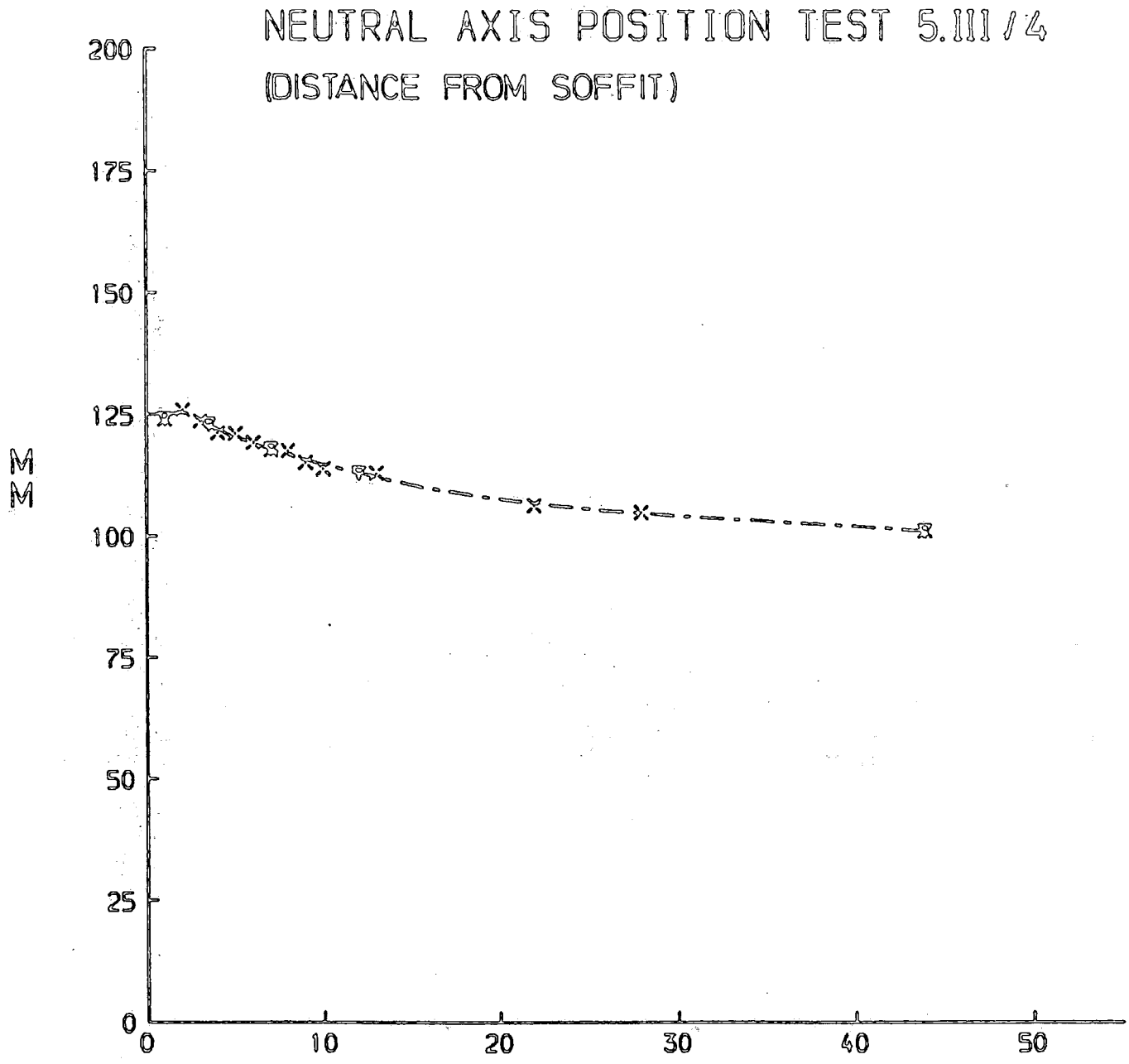
NEUTRAL AXIS POSITION TEST 5.III/4
(DISTANCE FROM SOFFIT)
200
175
150
125
100
75
50
25
0
MM
0
10
20
30
40
50

FIG. 5.III.13

CHAPTER 6

TESTS UNDER CONDITIONS SIMILAR TO LATE SPRING AND EARLY SUMMER CLIMATE IN CENTRAL SAUDI ARABIA

Synopsis

In this chapter the results of three tests are presented and analysed. Concrete beams were subjected to temperature and humidity regimes similar to the climatic conditions of late spring in Riyadh, Saudi Arabia.

In all three tests beams were subjected to cyclic heating/cooling and humidity three days before loading. In the first test the concrete beams were completely unsealed. In the second test they were partly sealed, and in the third test they were completely sealed.

In each test the behaviour of four singly-reinforced, simply supported beams was observed. Two beams were held under sustained load, one insulated and surface heated and one open to air temperatures. Two unloaded beams were subjected to similar cyclic humidity and temperature conditions so that shrinkage and creep behaviour could be separated.

It was found that the sealing conditions had a marked influence not only on the elastic and creep deflection values, but also on the chronological development of creep.

Elastic and creep deflections as calculated using measured strain values were compared with predicted values in accordance with CP110:72, ACI 209 and the CEB-FIP 1978 model. Significant differences were found between calculated experimental values and values predicted by the codes.

Creep curvature values were also compared with predicted values from the rate of creep method based upon specific thermal creep values and a step by step approach. Correlation between measured and computed

curvature was acceptable, even though that comparison between the various beams showed that the relation between temperature, humidity and creep is more complex than the simple assumptions upon which this method is based.

Behaviour of the beams during a daily thermal cycle was predicted using the simple iterative program with uncracked section described in 3.1 Computed values of curvature were found to be within 24% of curvatures based upon measured strain readings after allowing for creep, which was only dominant in the first few days.

It was also found that correlation was highly dependent on the value of coefficient of thermal expansion used in computation.

6.1 Introduction

The three tests discussed in this chapter were:-

6. I Beams were unsealed.

6.II Beams were partly sealed.

6.III Beams were completely sealed.

In all of the three tests the beams were heated before loading. In each test the singly reinforced beams were prepared (as described in 4) for testing under loading and cyclic temperature and humidity. Beam codings, dimensions, and test conditions are summarised in table 6.1.

Table 6.1 Beam Codings and test conditions

Beam	Beam Code used in Test	Dimension	Cyclic Heating	Loading
One	6.I,II/1	1.0m	Heat tape + air	No
	6.III/1	2.8 m	Heat tape + air	Yes
Two	6.I,II/2	2.8m	//	Yes
	6.III/2	2.8m	Air	Yes
Three	6.I,II/3	1.0m	Air	No
Four	6.I,II/4	2.8m	Air	Yes

Beams one and three were shrinkage companions for the loaded beams two and four, in that they were subjected to identical conditions, except that they were not mechanically loaded. Their primary purpose was to allow separation of creep and shrinkage effects in beams two and four.

6.2 Temperature State

6.2.1 Overall objectives

The meteorological records for the perid 1956-70 for the City of Riyadh, Saudia Arabia, show the highest shade air temperature recorded in late spring was 45°C in the month of May and the minimum recorded was 13°C.

According to Potocki (126)from the TRRL, the highest radiation recorded (over a period of one year) in May was 8610 Wh/m^2 for Abu Dabi with a latitude of 24°27' (Riyadh latitude is 24°42').

To simulate this, heat tape on the beam surface was switched on for five and a half hours daily, then two hours after switching it off, the cooling system was switched on overnight for sixteen hours. The cycle was then repeated.

6.2.2 Results and discussions

At the start of the daily heating cycle, air and concrete temperatures throughout the three tests were measured to be about 11°C except at the beginning of the week where they had risen to about 21°C since heating and cooling cycles were not run during Saturdays and Sundays. Daily variations of starting temperature were within ± 2°C during the week and ± 1°C on Mondays.

Temperature at the start of every day was found to be fairly uniform across the depth of the beam, with small variations of less than 1°C. It was found that an electrical input of 271.7 watts (equal to 970 W/m^2) for beam two and 95.6 watts (equal to 955 W/m^2) for beam one was needed to raise the surface temperature of the concrete to 62.5°C in about five and a half hours (during the week) and four and a half hours (at the beginning of the week).
This power is equivalent to about 5300Wh/m^2. The total measured value for the highest radiation recorded in 5.5 hours (under a sin curve) is about 5100 Wh/m^2.

The air temperature was raised to about 45°C by the two fan heaters in the same period.

The largest temperature gradient through the beam depth occurred at the peak of the heating cycle when the difference between top surface temperature and bottom surface temperature was 19°C for a typical day (Figure 6.1). Top surface temperature increased from 9.25°C to 63.5°C in five hours and fifteen minutes of heating, an average increase of 10.3°C per hour. In the same time bottom surface temperature increased from 9.5°C to 44.5°C an overall average increase of 6.67°C per hour.

At the beginning of the test, temperature was measured horizontally across both the top and bottom surfaces of beams one and two and variation of less than 1°C was observed. This demonstrated the effectiveness of the insulation system. Beams three and four were not insulated.

Slight adjustment of power input during the test was necessary due to fluctuations in the main laboratory temperature thus affecting the cabin air temperature to a small extent.

The diurnal change for the top surface temperature was about 54°C.

6.3 Humidity

Throughout the three tests, relative humidity values varied from an average high value of 36 per cent at the start of the daily cycle to an average low value of 10 per cent at the peak of the heating cycle. These values were higher than extreme values recorded in Riyadh, but were closer to typical daily values.

Figure 6.2 is a plot for humidity at an hourly interval for a typical day during a heating cycle.

6.I. Unsealed Beams

6.I.1 Introduction

In this test the beams were completely unsealed, and subjected to cyclic temperatures and humnidities three days before loading. They were subjected to the following conditions:-

Table 6.I.1

Beam	Sealing	Dimensions	Cyclic Heating	Applied moment (KN-m)
6.I/1	Unsealed	1.0m	Heat tape + air	0.0
6.I/2	Unsealed	2.8m	Heat tape + air	6.10
6.I/3	Unsealed	1.0m	Air	0.0
6.I/4	Unsealed	2.8m	Air	5.53

Beam 6.I/2 was the bottom beam in the loading rig discussed at 4.2 and beam 6.I/4 was the top beam. Beams 6.I/1 and /2 were insulated with polystyrene sheets from top and sides.

6.I.2 Strain response of the beams

6.I.2.1 Introduction

In this section, the results of the strain responses of the four beams 6.I./1, 6.I/2, 6.I/3 and 6.I/4 are presented and analysed.

Deflections, curvatures and strain parameters were calculated and plotted using the techniques employed in test 5.I and described in 3.4.2.

6.I.2.2 Beam 6.I/1 - Shrinkage companion to beam 6.I/2

Results and Discussion

Beam 6.I/1 was the shrinkage companion to beam 6.I/2, in that it was subjected to identical condtions, except that it was not mechanically loaded. The beam was not sealed, but was insulated from the top and sides.

Figure 6.I.1 is a plot of curvature changes with time due to shrinkage. The datum was taken at 21 days after casting, coincident with the loading of beams 6.I/1 and /4.

Correlation between measured values of maximum daily curvature due to the thermal gradients and predicted values was within 24 per cent. The correlation was found (as has been discussed ealier) to be highly dependent on the coefficient of thermal expansion used in the prediction. Figure 6.3 gives a temperature distribution at the end of the heating cycle for a typical day and the calculated stresses using the computer program AZ.

Shrinkage curvature was, as expected, sagging at all times due to the restraining effect of the reinforcement. Its value 36 days from datum was $0.1 \times 10^{-5}mm^{-1}$. This corresponds to a deflection of 0.13mm, and for the 2500mm beam a deflection of 0.78mm.

Using a modulus of 210 KN/mm^2, steel stress as measured from strain of concrete at the same level changed from $1.47N/mm^2$ two days after datum to $12.4N/mm^2$ thirty six days after datum.

6.I.2.3 Beam 6.I/2 Loaded and Surface heated

Results

Beam 6.I/2 was loaded in four point bending at 21 days after casting, such that the central portion carried a sustained moment of 6.1 KN-m This moment was about 1.88 of the theoretical cracking moment using a modulus of rupture of $4.2N/mm^2$. The beam was visibly cracked on loading.

Figure 6.I.2-5 are plots against time of midspan deflections, curvature, top concrete strains, strains of concrete at steel level.

Curvatures and deflection values were corrected for shrinkage, and allowances in the start-of-cycle temperatures from the datum temperature was made in calculation of top concrete strains, strains of concrete at steel level and neutral axis position.

Figure 6.I.6 is a plot of change of neutral axis position with time.

Table 6.I.2 summarises values from the graphs on loading and after 36 days of sustained loading.

Table 6.I.2

Parameters	On loading	After 36 days
Curvature	$-0.86 \times 10^{-5} mm^{-1}$	$-1.38 \times 10^{-5} mm^{-1}$
Deflection	5.85mm	9.35mm
Top Strain	-0.63×10^{-3}	0.129×10^{-2}
Steel Stress	$148 N/mm^2$	$191.2 N/mm^2$
Neutral axis	79mm	100mm

Discussion

Table 6.I.3 gives values for creep deflections at various dates.

Table 6.I.3.

Time under load (days)	Deflection (mm)	Increase in def. due to creep (mm)	Creep def. / elastic
0	5.82	0	0
6	7.93	2.11	0.36
11	8.35	2.53	0.43
28	9.25	3.43	0.58
32	9.31	3.49	0.60

This table shows that 60% of the 32 days creep had occurred in the first six days.

After 32 days of sustained loading, the span/deflection ratio was reduced from 430 to 268, which is a low value, if we take into consideration that the span /depth ratio was only 12.5 For a larger span/depth ratio and under the effects of reversed temperature, the span/deflection ratio would be expected to be reduced below the 250 ratio, which is acceptable according to CP110.

Table 6.I4 gives values of the elastic and long term deflections as compared to predictions by various codes.

Table 6.I.4

Method of determination	Scource of Material data	At Midspan	
		Deflection on loading (mm)	Increase in def. due to creep(mm)
CP110:1972 (131)	C & CA (132)	4.89	1.42
ACI-435 (133)	ACI-209 (134)	5.09	3.73
Effective Modulus	CEB-FIP (135)	4.9	1.98
Test		5.82	3.52

The elastic deflections prediction by the codes underestimated the deflection slightly. The beam was subjected to heating-cooling and humidity cycles three days before loading. It was also unsealed. Its deflection was about 17 per cent higher than the deflection of beam 5.III/2 which was similar to this beam except that it was not subjected to cyclic heating-cooling and humidity before loading.

The creep prediction by CP110 and CEB-FIP as expected, underestimated creep deflection. However the ACI recommended use of the reduction factor method slightly overestimated the creep deflection.

Figure 6.I.7 is a plot of changes of curvature with time as predicted by the rate of creep method - with the two bounded curves for the 95% confidence limit interval of curavature. The correlation seems to be good at all times. However, it is believed (based on the results of the other tests) that the correspondence is probably due to the interactions of various factors rather than an exact prediction.

Figure 6.I.3 is a plot of changes of curvature with time. It changed from a value of - 0.864 x 10^{-5} on loading to a value of -0.138 x 10^{-4} thirty two days after loading. Its elastic recovery was -0.77 x 10^{-5}. This was about 89 per cent of its value on loading. After one week a value of 0.22 of the total creep deflection was recovered.

Top surface strain value on loading was 0.68 x 10^{-3}. It had increased to 0.147 x 10^{-2} after 32 days of sustained loading. This is 42% of the ultimate concrete strain value of 0.0035 according to CP110.

The use of Ross's hyperbola gives an estimate of a limiting creep value of 0.164 x 10^{-2}. This approximate law (see 2.5.4.1) is usually used to predict uniaxial creep where the assumption of constant stress applies. This, strictly speaking, does not apply here, since the beam will undergo some stress redistribution due to creep which will lead with time to stress relaxation of the top fibre stress of the beam. However in simply supported beam, the stress redistribution is not expected to be large.

Figure 6.I.5 gives changes with respect to time of concrete strain at steel level. Values in the figure include creep and shrinkage effects, but are corrected for differences in the start-of-cycle temperatures from datum temperature.

The figure show that the strain values increased fairly rapidly from a value of 0.743 x 10^{-3} on loading to a value of 0.928 x 10^{-3} seven days after loading. (primary creep). Then they increased only slowly to a value of 0.956 x 10^{-3} thirty two days after loading. The relatively small increase of strain after the first seven days is believed to be partly due to the fact that the position is relatively close to the neutral axis position and partly to the cancelling effect of shrinkage. For even though the shrinkage curvature is additive to the creep curvature, the effect of shrinkage on the beam is shortening, thus reducing the tensile effect of creep. Strain values of beam 6.I/1 show that concrete strain at steel level had reduced by 56uε in thirty two days.

The correlation between measured values of maximum daily curvatures and predicted values was within 21 per cent. However Because of the rapid primary creep, the first few measured values were very small compared to the predicted values. Measured curvature values were very close to the measured curvature values for the uncracked companion beam 6.I/1, indicating that cracking influenced the daily curvature values only slightly.

6.I.2.4 Beam 6.I/3 shrinkage companion to beam 6.I/4

Beam 6.I/3 was a shrinkage companion to the top beam 6.I/4, in that it was subjected to identical conditions except that it was not mechanically loaded. It was unsealed and uninsulated.

Figure 6.I.8 is a plot of curvature with time due to shrinkage only. The datum was taken at 21 days after casting (i.e. the date of loading of beam 6.I/4). It reached a maximum of about 0.123×10^{-5} thirty two days from datum. This is slightly more than value obtained for beam 6.I/1, and is probably due to the fact that beam 6.I/1 was insulated from the top and sides thus hindering the movement of moisture.

Steel stress, as estimated from concrete strain at the steel level (assuming no slip) and the use of an elastic modulus value of $2.1 \times 10^{+5}$ N/mm^2 was 25 N/mm^2 thirty two days from datum.

6.I.2.5 Beam 6.I/4, loaded and air heated only

Results

Beam 6.I/4 was loaded in four point bending at 21 days after casting, such that the central portion carried a sustained moment of 5.53 KN-m. This moment corresponds to 43% of the ultimate as calculated in

accordance with CP110, and about 1.7 times the theoretical cracking moment using a modulus of rupture of 4.2 N/mm^2. The beam was visibly cracked on loading.

Figs. 6.I.9 - 12 are plots against time of midsdpan deflections, curvatures, top concrete strains and strains of concrete at steel level. Curvature and deflections values were corrected for shrinkage, and allowance for the start-of-cycle temperatures relative to the datum temperature was made in calculation of top concrete strains, strains of concrete at steel level and neutral axis position.

Figure 6.I.13 is a plot of change in neutral axis position with time.

Table 6.I.5 summarises values from the graphs on loading and after 32 days of sustained loading.

Table 6.I.5

Parameters	On Loading	After 32 days
Curvature	$-0.82 \times 10^{-5} mm^{-1}$	$-0.121 \times 10^{-4} mm^{-1}$
Deflection	5.20mm	7.63mm
Top Strain	-0.63×10^{-3}	-0.129×10^{-2}
Steel Stress	$153.3\ N/mm^2$	$186.4\ N/mm^2$
Neutral Axis	76.2mm	97.8 mm

Discussion

Table 6.I.6 lists values of deflection at various dates.

Table 6.I.6

Time under load (days)	Deflection (mm)	Increase in def. due to creep (mm)	Ratio of increase
0	5.2	0	0
6	6.69	1.49	0.29
11	7.03	1.83	0.35
28	7.56	2.36	0.45
32	7.63	2.43	0.47

Results in this table show that more than sixty per cent of the 32 days creep occurred in the first six days. The rate of creep deflection in the last four days was only .018mm a day, suggesting that the beam is close to being dessicated.

The span/deflection ratio changed from 481 on loading to 291 thirty two days after loading.

Table 6.I.7 gives values of the elastic and long term deflections as compared to predictions by various codes.

Table 6.I.7

Method of determination	Source of material data	At midspan	
		Elastic deflection (mm)	Increase in def. due to creep
CP 110:1972 (131)	C + CA (132)	4.06	1.21
ACI - 435 (133)	ACI - 209 (134)	4.12	3.02
Effective Modulus	CEB-FIP (135)	3.92	1.74
Test	-	5.2	2.43

Figure 6.I.10 is a plot change of creep curvature with time. It changed from a value of -0.824×10^{-5} on loading to a value of -0.121×10^{-4} thirty two days after loading. Its value on unloading was -0.666×10^{-5} giving an elastic recovery of -0.54×10^{-5}. This is about 66 per cent of its elastic value on loading. After a week a value of 0.26 of the total creep deflection was recovered.

After 32 days of sustained loading, extreme compression strain became 0.129×10^{-2}, more than two times its value on loading. This included the effects of both creep and shrinkage. Its value was still increasing after 32 days of loading.

If we assume that the stress in the extreme compression face to undergo no redistribution and use and Brook's approach (136) to predict the ten years value out of 28 day value, we obtain a value of 0.282×10^{-2}.

The expression however was deduced empirically from creep data under normal ambient conditions, and could not be expected to predict values under higher than normal temperatures.

Ross's hyperbola gives an estimate for final creep a value of 0.146×10^{-2}. (However this has to be viewed with the same limitations discussed in 6.I/2).

6.II Partly Sealed Beams

6.II.1 Introduction

In this test the beams were partly sealed, heated before loading and they were subjected to the following conditions:

Table 6.II.1

Beam.	Sealing	Dimension	Cyclic heating	Applied moment (KN-m)
6.II/1)	All	1.0m	Heat tape + air	0.0
6.II/2)	surfaces	2.8m	Heat tape + air	6.10
6.II/3)	except	1.0m	Air	0.0
6.II/4)	Soffit	2.8m	Air	5.53

Beam 6.II/1 was the bottom beam in the loading rig discussed at §4.2 and beam 6.II/4 was the top beam.

Beams 6.II/1 and /2 were both insulated from the top and sides. Beams 6.II/3 and /4 were uninsulated and open to the hot air from the fans.

6.II.2 Strain response of the beams

6.II.2.1 Introduction

In this section, the results of the strain responses of the four beams 6.II/1, 6.II/2, 6.II/3, 6.II/4 are presented and analysed.

Deflections, curvatures and strain parameters were calculated and plotted using the techniques described in 3.4.2.

6.II.2.2 Beam 6.II/1 shrinkage companion to beam 6.II/2

Results and discussion

Beam 6.II/1 was the shrinkage companion to beam 6.II/2, in that it

was subjected to identical conditions, except that it was not mechanically loaded. The beam was partly sealed, and insulated from the top and sides.

Figure 6.II.1 is a plot of curvature changes with time due to shrinkage. The datum was taken at 21 days after casting, coincident with the loading of beams 6.II/2 and /4.

Figure 6.II.1 demonstrates that the beam initially showed an upward shrinkage curvature reaching its peak of about 4×10^{-7} in approximately five days from datum. Curvature then started to decrease. This behaviour can be explained by the same reasons that were discussed in 5.I.2.2 namely the interaction between differential movement of moisture in the heated top parts of the beam and the exposed soffit with the restraining reinforcement.

The use of the computer program AZ (listed in the appendix) gave values for curvature due to the daily thermal cycle that correlated to within 18 per cent of measured curvature values. Again as had been discussed previously the correlation was highly dependent on the coefficient of thermal expansion used in the analysis. Measured curvature values were small. A typical value is 0.9×10^{-6} mm^{-1}.

6.II.2.3 Beams 6.II/2, loaded and surface heated

Results

Beam 6.II/2 was loaded in four points bending, at 21 days after casting, such that the central portion carried a sustained moment of 6.1 KN.m. This moment corresponded to about 1.88 of the theoretical cracking moment, on the assumption of a modulus of rupture of $4.2 N/mm^2$. The beam, as expected, was cracked on loading.

Figures 6.II .2-5 are plots against time of midspan deflections, curvatures, top concrete strains, and strains of concrete at steel level. Deflection and curvature values were corrected for shrinkage, and allowance in the start-of-cycle temperatures from the datum temperature was made in calculation of top concrete strains, strains of concrete at steel level and neutral axis position.

Figure 6.II.6 is a plot of changes of neutral axis position with time.

Table 6.II.2 summarises values from the graphs on loading and after 36 days of sustained loading.

Table 6.II.2

Parameters	On loading	After 36 days
Curvatures	$-0.57 \times 10^{-5}mm^{-1}$	$-0.929 \times 10^{-5}mm^{-1}$
Deflection	3.86mm	6.29mm
Top Strain	-0.34×10^{-3}	-0.7×10^{-3}
Neutral Axis	60mm	73.2mm

Discussion

Table 6.II.3 gives values for creep deflections at various dates.

Table 6.II.3

Time under load (days)	Deflection (mm)	Increase in Deflection due to creep (mm)	Creep/ Elastic
0	3.86	0	0
6	5.57	1.71	0.44
13	5.77	1.91	0.49
22	6.03	2.17	0.56
28	6.11	2.25	0.58
36	6.29	2.43	0.63

The rate of creep between day six and day thirteen was 0.029mm a day and from 28 and 36 was 0.022mm a day. This suggests that the rate of creep had not decreased considerably. The difference in shrinkage curvature from approximately day five was negative,(Fig. 6.II.1) thus being additive to the difference in creep. The shrinkage curvature rate of sagging was almost constant, and its value was very small.

The six days creep was 70% of the 36 days creep.

Table 6.II4 gives values of the elastic and long term deflections as compared to predictions by various codes.

Table 6.II4

Method of determination	Source of Materials data	At Midspan	
		On loading (mm)	Increase in Def. due to creep(mm)
CP110:1972	C & CA (132)	4.89	1.42
ACI-435 +	*ACI-209 (134)	4.98	3.65
Effective Modulus	*CEB-FIP (135)	4.78	1.55
Test	———	3.86	2.43

+ The calculation of increase in deflection has been done by the use of the reduction factor method (see 2.5.4.3).

* Allowance for the contribution of tension stiffening has been incorporated here by the use of I_{eff} as suggested by Branson (87).

Figure 6.II.7 is a plot of changes of curvature with time as predicted by the rate of creep method. Results show that the method underestimated creep values for the first few days, then from about day six, the slopes of the curves were almost equal. This can be explained by the following reasoning: since the beam was not sealed from the soffit, and was heated three days prior to loading, it would have some microcracking as a result of shrinkage, this will lead to a higher early creep on loading compared to the cylinder, this coupled with the fact mentioned previously of expected higher value of flexure compared to axial creep.

Figure6II.3 shows that curvature value had changed from a value of -0.57×10^{-5} on loading to a value of -0.929×10^{-5} thirty six days after loading. Its elastic recovery was -0.5×10^{-5}. This is about 88 per cent of its elastic value on loading. It changed from a value of -0.427×10^{-5} on unloading to a value of -0.344×10^{-5} seven days after unloading. That is only 0.23 of creep was recovered in this period. It is of interest to note that CEB-FIP gives a maximum of 0.4 at ultimate for the recoverable creep.

Compressive top surface strain had increased from 0.00034 on loading to 0.0007 thirty six days from loading, giving a ratio of 1 : 2.1 (Figure 6.II.4). Values in the figure include both creep and shrinkage.

The estimated value of limiting creep obtained by the use of Ross's hyperbola is 0.726×10^{-3}. This value is clearly very small and has to be looked at with caution.

Concrete strain at steel level had changed from a value of 0.6×10^{-3} on loading to a value of 0.876×10^{-3} after thirty six days of sustained loading. The effect of shrinkage at the steel level is in opposite direction to creep. It was estimated from Beam 6.II/1 that at steel level a shortening of approximately 200 uϵ did occur after 36 days from datum.

Measured curvature values due to the daily thermal cycle were very small and ranged between $0.79 \times 10^{-6} mm^{-1}$ and $0.98 \times 10^{-6} mm^{-1}$. Their correlations with the predicted values using programe AZ described in Appendix were within 22 per cent. The measured curvature values were very close to the measured curvature values for the uncracked companion beam 6.II/1, indicating again that cracking did not influence greatly the values of curvature due to the daily thermal cycle.

6.II.2.4 Beam 6.II/3 shrinkage companion to beam 6.II/4

Results and Discussion

This beam was a shrinkage companion to the top beam 6.II/4. It was partly sealed and uninsulated.

Figure 6.II.8 is a plot of curvature with time due to shrinkage only. The datum was taken at 21 days after casting (i.e. the date of loading of beam 6.II/4).

Steel stress was estimated from concrete strain at steel level and using steel modulus of $2.1 \times 10^5 N/mm^2$ to be $-27\ N/mm^2$ thirty nine days from datum.

Figure 6.II.8 shows scattered and very small values of hogging curvature. The beam was under heating and cooling cycles, so it is possible that moisture movement occurred in both directions due to the condensation of moisture (because of cooling) on the unsealed (soffit) side of the beam, thus contributing to the scattered values obtained for curvature.

6.II.2.5 Beam 6.II/4 loaded and air heated only

Results

Beam 6.II/4 was loaded in four point bending such that the central section carried a sustained moment of 5.53 KN-m at 21 days after casting. This moment corresponded to 43% of the ultimate moment of the beam, and about 1.7 times the theoretical cracking moment using a modulus of rupture of $4.2\ N/mm^2$.

The beam was sealed on the compression face and sides but not insulated. It was subjected to cyclic air temperature (heating and cooling) and humidity with no surface heating.

Figures 6.II.9-12 are plots against time of midspan deflections, curvature, top concrete strains, and strain of concrete at the steel level. The two other curves for curvature are the 95% confidence limit.

Figure 6.II.13 is a plot of changes of neutral axis with time.

Table 6.II.5 summarises values from the graphs on loading and after 36 days of sustained loading for curvature and deflection values which were adjusted to remove shrinkage strain (from 6.II/3), so that effects shown were due to creep alone. Allowance for differences in the start-of-cycle temperature from datum temerature was made in calculating top concrete strains, concrete strain at steel level and neutral axis position.

Table 6.II.5

Parameter	On loading	After 36 days
Midspan curvature	$-0.295 \times 10^{-5} mm^{-1}$	$-0.56 \times 10^{-5} mm^{-1}$
Midspan deflection	1.86mm	3.54mm
Extreme concrete compression strain)	-0.249×10^{-3}	-0.57×10^{-3}
Neutral axis	69.1 mm	97.3 mm

Discussion

Table 6.II.6 lists values of deflection at various dates.

Table 6.II.6

Time after loading	Deflection (mm)	Increase in deflection due to creep (mm)	Ratio of increase
0	1.86	0	0
6	3.08	1.22	0.66
13	3.28	1.42	0.76
28	3.44	1.58	0.85
36	3.54	1.68	0.90

The six days creep was about 72% of the 36 days creep. This is very similar to the ratio obtained for beam 6.II/2 (70%), thus indicating that the surface heating did not have any influence on the chronological development of creep.

Table 6.II.7 gives values of the elastic and long-term deflections as compared to predictions by various codes without allowing for temperature.

Table 6.II.7

Method of determination	Source of Material data	At Midspan	
		Elastic Deflection	Increase in creep def.due to creep
CP110:1972 (131)	C & CA (132)	4.05	1.21
ACI-435 (133)	ACI-209 (134)	4.02	2.95
Effective modulus	CEB-FIP(135)	3.81	1.37
Test	--	1.86	1.68

The difference between the elastic prediction of the codes and the measured prediction was due to the degree of cracking as the test beam did not show any visible cracks ,while the codes predict, with a moment of 1.7 of the theoretical cracking moment beam with extensive cracks. The $I_{.eff.}$ used in the ACI and CEB-FIP calculation was very close to $I_{cracked}$ value.

Figure 6.II.10 is a plot of changes of curvature with time. On loading its value was $-0.295 \times 10^{-5} mm^{-1}$. It changed to $-0.56 \times 10^{-5} mm^{-1}$ thirty six days after loading.. Its value on unloading was -0.288×10^{-5}, giving an elastic recovery of -0.272×10^{-5}, which was about 92 per cent of its elastic value on loading. The reason for this high value of elastic recovery was that the value included some delayed elastic recovery because in this test it took some time to dismantle the rig and take a set of readings after unloading. Seven days after unloading the sagging curvature value dropped by about 0.74×10^{-6}. That is about 0.28 times the total creep deflection was recovered. This is slightly more than the recovered value for th surface heated beam 6.II/2.

After thirty six days of sustained loading extreme compression strain changed from 0.249×10^{-3} on loading to 0.57×10^{-3}, givinga ratio of 1:2.29. which is close to the value obtained for beam 6.II/2.

6.III Completely Sealed Beams

6.III.1 Introduction

In this test two beams are discussed, they were both completely sealed and heated before loading. In addition they were subjected to the following conditions:

Table 6.III.1

Beam	Sealing	Dimension	Cyclic Heating	Applied Moment
6.III/1	Completely	2.8 m	Heat tape + Air	6.1 KN-m
6.III/2	Sealed	2.8 m	Air	5.53 KN-m

Beam 6.III/1 was the bottom beam in the loading rig (discussed in 4.2) and beam 6.III/2 was the top beam.

6.III.2 Strain response of the beams

6.III.2.1 Introduction

In this section, the results of the strain responses of the two beams 6.III/1 and /2 are presented and analysed.

Deflections, curvatures and strain parameters were calculated and plotted using the technique described in 3.4.2.

6.III.2.2 Beam 6.III/1, loaded and surface heated

Results

Beam 6.III/1 was loaded in four point bending at 21 days after casting, such that the central portion carried a sustained moment of 6.1 KN-m. This moment corresponded to 48% of the ultimate moment of the beam as calculated in accordance with CP110, and about 1.88 of the theoretical cracking moment using a modulus of rupture of 4.2 N/mm^2. The beam was cracked on loading.

Figures 6.III.1-4 are plots against time of midspan deflections, curvatures, top concrete strains and strains of concrete at steel level. Curvatures and deflections values were corrected for shrinkage, and allowances in the start-of-cycle temperatures from the datum temperature were made in calculation of top concrete strains, strains of concrete at steel level and neutral axis position.

Figure 6.III.5 is a plot of changes of neutral axis position with time.

Table 6.III.2 summarises values from the graphs on loading and after thirty three days of sustained loading.

Table 6.III.2

Parameters	On loading	After 33 days
Curvatures	-0.54×10^{-5} mm^{-1}	-0.88×10^{-5} mm^{-1}
Deflection	3.69 mm	5.94 mm
Top strain	-0.439×10^{-3}	-0.846×10^{-3}
Neutral axis	76.2 mm	97.8 mm

Discussion

Table 6.III.3 lists values (from graph) for creep deflections at various dates.

Table 6.III.3

Time under load (days)	Deflection (mm)	Increase in Def. due to creep	Creep/ Elastic
0	3.69	0	0
6	4.96	1.28	0.34
13	5.35	1.66	0.45
22	5.67	1.98	0.54
28	5.78	2.09	0.57
33	5.94	2.25	0.61

The first six days creep is about 56 per cent of the 33 days value. The rate of creep for the last five days was 0.03 mm/day, indicating that the beam was still creeping appreciably.

Figure 6.III.6 is a plot of changes of curvature with time as predicted by the rate of creep method.

The graph shows that the correlation between predicted and measured value was good, at early stages, but underestimated creep curvature at later stages.

Figure 6.III.2 is a plot of curvature changes with time. The elastic recovery on unloading was -0.425×10^{-5} mm.$^{-1}$ This was about 78% of the value of the elastic curvature on loading. After seven days the curvature recovered to -0.343×10^{-5}. That is about 0.24 of the creep deflection was recovered in this period.

Compression top surface strain had changed from a value of -0.439×10^{-3} on loading to a value of -0.846×10^{-3} after thirty three days of sustained loading, giving a ratio of 1:1.93. This is less than the similar ratio for the partly sealed beam (6.II/2).

Ross's hyperbola gave an estimate for the limiting elastic plus creep strain of 0.869×10^{-3}; again this is an underestimate. Brook's power law gives the value for the ten years elastic plus creep strain as 0.13×10^{-2}. This predictive law is used for uniaxial creep where stress is assumed to be constant and under normal amient conditions.

Figure 6.III.4 gives values for concrete strain at the steel level. On loading its value was 0.459×10^{-3}. Then it increased rapidly, reaching its maximum value of about 0.6×10^{-3} on the tenth day. It levelled out after this, and after 33 days its value was unchanged at 0.6×10^{-3}. This was probably due to two things. First was the lowering of the neutral axis with time thus reducing the lever arm. Secondly, there probably was some slight slipping between concrete and steel.

The correlation between measured values for maximum curvature, due to the daily thermal cycle and predicted values were within 16 per cent (except

for the first few days due to creep). Measured curvature values were small, less than 1.0×10^{-5}.

6.III.2.3 Beam 6.III/2 loaded and air heated only

Results

Beam 6.III/2 was loaded in four point bending, at 21 days after casting such that the central section carried a sustained moment of 5.53 KN-m. This moment corresponds to 43% of the ultimate as calculated in accordance with CP110, and about 1.7 of the theoretical cracking moment, using a modulus of rupture of 4.2 N/mm^2.

Figures 6.III.7-10 are plots against time of midspan deflection, curvature, top concrete strains, and concrete strains at steel level. The two bounded curves are the 95% confidence interval for curvature.

Figure 6.III.11 is a plot of change of neutral axis position with time.

Table 6.III.4 summarises values from the graphs on loading and after 33 days of sustained loading for curvature, deflection, extreme concrete compression strain and neutral axis position. Allowance for differences in the start-of-cycle temperature from datum temperature was made in calculating extreme concrete compression strain, concrete strain at steel level, and neutral axis position.

Table 6.III.4 Response of beam 6.III/2 to sustained loading

Parameter	On loading	33 days after loading
Midspan curvature	-0.45×10^{-5} mm^{-1}	-0.69×10^{-5} mm^{-1}
Midspan deflection	2.82 mm	4.38 mm
Extreme concrete compression strain	-0.44×10^{-3}	-0.78×10^{-3}
Neutral axis position	99.2 mm	111.6 mm

Discussion

Table 6.III.5 lists values of deflection at various dates

Table 6.III.5

Time after loading	Deflection (mm)	Increase in Def. due to creep	Ratio of increase to elastic
0	2.82	0	0
6	3.66	0.84	0.30
13	3.97	1.15	0.41
22	4.20	1.38	0.49
28	4.29	1.47	0.52
33	4.38	1.56	0.55

In the first six days creep deflection reached about 53 per cent of the 33 days value. In the last five days creep deflection rate value was about 0.018 mm/day.

On loading the value of curvature was -0.447×10^{-5}. Its value after 33 days of loading was -0.695×10^{-5}. On unloading its value became 0.408×10^{-5}, giving an elastic recovery of -0.287×10^{-5}, which was about 64 per cent of its value on loading. Seven days after unloading, its value became -0.337×10^{-5}, thus a recovery (delayed elastic) of -0.708×10^{-6}. This is about 0.29 of the total creep deflection.

Extreme concrete strain had changed from a value of -0.44×10^{-3} on loading to a value of -0.78×10^{-3} after thirty three days of sustained loading, giving a ratio of 1:1.77.

Concrete strain had changed from a value of 0.29×10^{-3} on loading to 0.37×10^{-3} after 33 days of sustained loading. It reached its maximum value of 0.37×10^{-3} ten days after loading, where it did not increase after this. This was again due to the reduction of the lever arm and possibly small slipping between the steel and concrete.

6.4 Comparison of tests 6.I and 6.II with 6.III

A comparison is made here of the development of creep through time and its various ratios at different dates including its ratio to the elastic for the loaded beams in these three tests.

Test 6.I was completely unsealed, test 6.II was partly sealed, test 6.III was completely sealed.

6.4.1 Curing conditions

After casting, the beams were left on the vibrating table on their moulds and covered with hessian sheets where they were kept wet by soaking the hessian sheets daily. Then after seven days of curing in this way, they were moved to the floor, where the sides of the moulds were stripped, and only their bases were left. Then after two hours, the primer was applied to the beams. On day 8, one coat of paint was applied to them, and on day 9 another coat of paint was applied to them. On day 10 the demec buttons were glued to the surfaces, and in the case of the partly sealed they were moved to the cabin on day 11. In the case of the completely sealed, after painting their sides on day 9, they were turned on their sides on day 10 and their bases were sealed. They were moved to the cabin on day 13.

In the case of the completely unsealed (test 6.I) after curing the beams for seven days, they were left in their moulds (without curing) until day 10, where they were moved to the floor. The shutters of the moulds were then taken out and the demec buttons were glued on their surfaces.

On day 15, insulations (polystyrene sheetings) were put on beams 6.I/2, 6.II /2 and 6.III/1, and heating tapes were laid on their surfaces.

On day 18, the heating-cooling and humidity cycles were started for all the beams, and on day 21, they were all loaded.

6.4.2 Basis of Comparison

Tables 6.4.1 and 6.4.2 compare creep deflection for beams in tests 6.I (unsealed) and 6.II (partly sealed), with creep deflection in test 6.III (completely sealed). The comparison highlights the effects of humidity and the influence of drying creep under different sealing conditions.

The comparison is made of the first six days creep deflection for the beams in the three tests. The six days creep deflection was chosen, since it was believed, that all of the primary creep will occur during this period.

The increase in creep deflection from day six to day 32, and the total 32 creep was also compared for the three tests.

Finally the elastic and other various ratios are presented in the two tables.

Figure 6.4.1 gives a comparison of deflections for beams 6.I/2, 6.II/2, with 6.III/2.

Table 6.4.1 Comparison of beam 6.I/2 deflection, 6.II/2 with 6.III/1 deflection

Time under load (days)	Beam 6.III/1 (Deflection) (mm)	Beam 6.I/2		Beam 6.II/2	
		Value (mm)	Ratio to 6.III/1	Value (mm)	Ratio to 6.III/1
6	1.28	2.11	1.65	1.71	1.34
6-32	0.97	1.38	1.42	0.65	0.67
32	2.24	3.49	1.56	2.35	1.05
Elastic	3.69	5.82	1.58	3.86	1.05
Ratio of 32 day creep to elastic	0.61	0.60		0.61	
Ratio of 6 days creep to 32 days creep	0.57	0.6		0.72	

All the three beams were insulated and surface heated. They had an applied moment of 6.1 KN-m, and they all cracked on loading.

Results in this table show the following points:-

a) That temperature and humidity cycling affect the development of creep in different ways, depending on the sealing conditions of the beams. For example, the first six days creep of beam 6.II/2 (P.S) was more than thirty per cent of the first six days for beam 6.III/1 (C.S), while the increase in creep deflection from day 6 to day 32 for beam 6.II/2 (P.S) was only sixty seven per cent of beam 6.III/1 (C.S).

b) The importance of the first six days creep, in the case of beam 6.II/2 more than seventy per cent of the 32 day creep occurred during the first six days.

c) The ratio of the thirty two days creep deflection to elastic deflection was approximately the same for the three beams. This indicates that the factors influencing the elastic deflection might influence creep in the same manner. Clearly a conclusion cannot be drawn from these limited results, but if it is true, it is significant, and suggests that creep values might be obtained from simple mathematical expressions involving elastic values.

d) The importance of sealing (i.e. curing) on the value of the elastic deflection, an increase of almost sixty per cent, was observed in the value of the elastic deflection of the unsealed beam over the value for the completely sealed. It is of interest to note that the value of the elastic deflection for beam 5.III/2, which was completely similar to beam 6.I/2, except that it was loaded before heating, was 4.98 mm. That is 85 per cent of the elastic deflection for beam 6.I/2. This indicates that the three days temperature and humidity cycling actually increased the elastic deflection for the unsealed beams.

e) The table shows also the similarity of the various ratios for the completely sealed and the completely unsealed. This coupled with the

fact that the increase in creep from day six to day 32 for the open faced beam 6.II/2 was only 67 per cent of the increase in creep deflection for beam 6.III/3 (C.S.) demonstrates that it is not only the open surface to volume ratio which influences creep deflection, but that the position of the open face in a partly sealed beam is also significant in the rate of creep development. It is also likely to affect the value of final creep deflection.

f) The 32 elastic plus creep deflection for the unsealed beam (6.I/2) is 2.52 times the elastic deflection of beam 6.III/1. This is significant, since if as has been suggested by other researchers (137) that ultimate creep coefficient ϕ_∞ is between 2 and 4 for 80 per cent of structural concrete applications and for all exposure conditions, then if the average value of 3 is used with the ACI reduction factor method, we obtain an ultimate creep plus elastic deflection of 13.1mm, and if a creep coefficient value of 2.5 was used, then we get 11.52 mm. The total 32 days elastic plus creep deflection for beam 6.I/2 was 9.31 mm, which is more than 80% of the ultimate deflection based on a creep coefficient value of 2.5.

Table 6.4.2 and figure 6.4.2 give comparison of elastic and creep deflection values of beams 6.I/4 and 6.II/4 with 6.III/2.

Table 6.4.2 Comparison of beams 6.I/4 and 6.II/4 with 6.III/2

Time under load (days)	Beam 6.III/2 (sealed)	Beam 6.I/4 (unsealed)		Beam 6.II/4 (partly sealed)	
		Value (mm)	Ratio to 6.III/2	Value (mm)	Ratio to 6.III/2
6	0.84	1.49	1.77	1.22	1.45
6-32	0.71	0.94	1.32	0.42	0.59
32	1.55	2.43	1.57	1.64	1.06
Elastic	2.82	5.2	1.84	1.86	0.66
Ratio of 32 creep to elastic	0.55	0.47		0.88	
Ratio of 6 days creep to 32	0.54	0.61		0.74	

All the three beams were uninsulated. They all had an applied moment of 5.53 KN-m. Beams 6.I/4 and 6.III/2 were cracked on loading, but beam 6.II/4 was not cracked.

Results in this table show that the uninsulated beams had similar ratios to those of the insulated, surface heated beams, except in the case of beam 6.II/2, it had a low elastic deflection value because it was not cracked.

6.5 Conclusion

From the tests presented in this chapter we can conclude the following:

- That the sealing conditions had a marked influence not only on the elastic and creep values but also on the rate of chronological development of creep.
- The importance of early creep. For example, the first six days creep deflection for the partly sealed was more than seventy per cent of the thirty two days creep deflection.
- Again, as was found in chapter five, the use of the rate of creep method based upon specific thermal creep (measured from small unreinforced concrete cylinders) and a step by step approach gave satisfactory results for the unsealed for the period investigated in this test, but was less satisfactory for the partly and completely sealed beams. However the tests show that the assumption that creep increases with temperature at all times is not correct.
- That the use of uncracked section in the predictive computer program for the curvature due to daily thermal cycle leads to good correlation with measured curvature of cracked beams.
- The value of measured curvature due to a daily thermal cycle was less than $1 \times 10^{-5} mm^{-1}$ and self equilibrating stress for the uncracked beams

was less than 1.7 N/mm^2 in the top fibre and less than 1.0 N/mm^2 in the bottom fibre. However these values are expected to be more severe for deeper beams.

- That shrinkage curvature was hogging for the partly sealed beams for the period of the test, but was decreasing in magnitude, and was expected to change to sagging at later times.
- That the values for creep deflection predicted by the codes CP110 and CEB-FIP underestimaated measured deflection, but ACI-209 tended to overestimate creep deflection values.
- The surface heating did not have any marked influence on the chronological development of creep.
- The elastic recovery varied between 66 and 92 per cent, and the recoverable creep after one week varied between 22 and 29 per cent, with the high values being for the air heated beams.

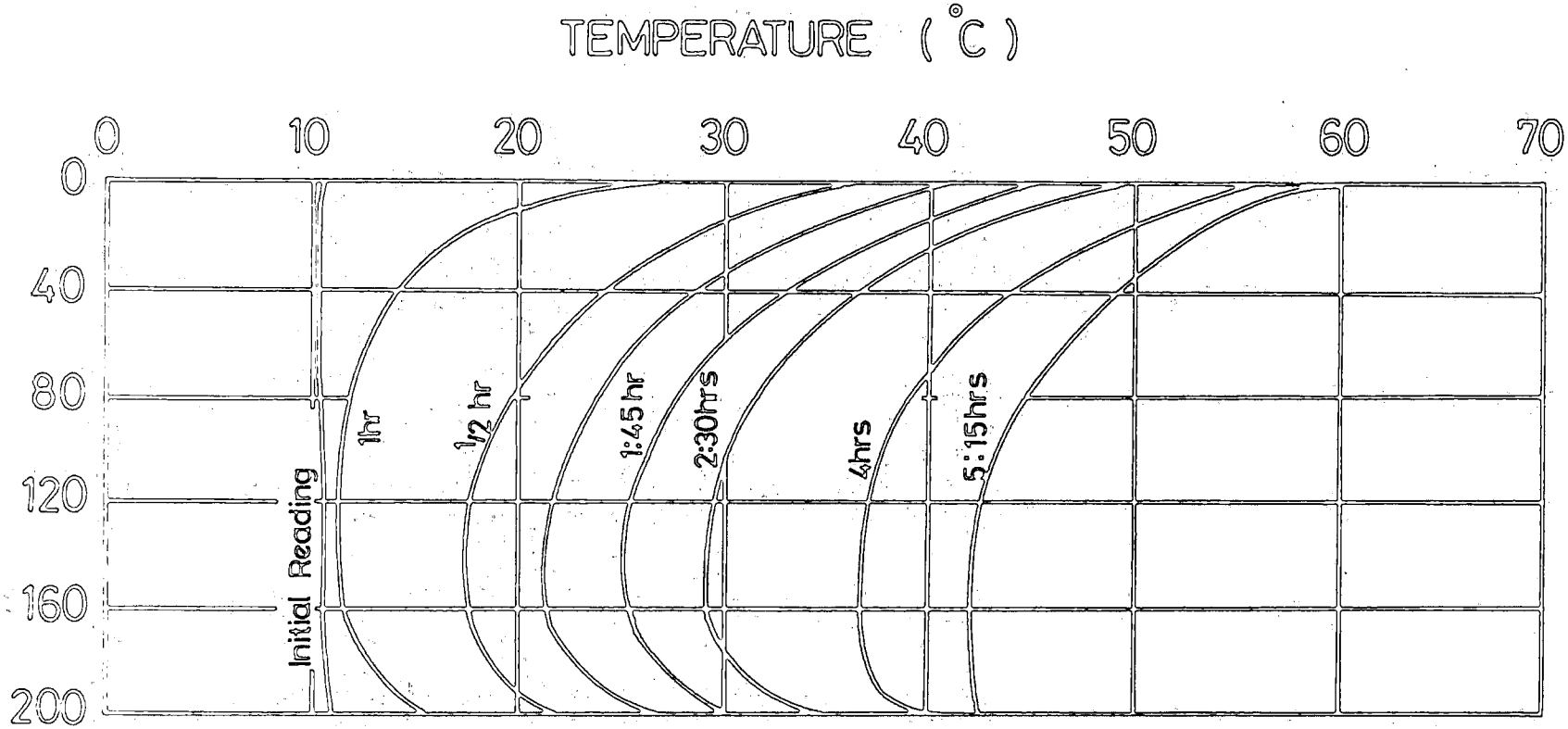

FIG. 6·1 TEMPERATURE DISTRIBUTION THROUGH THE BEAM CROSS SECTION AT VARIOUS TIMES.

SPRING CONDITIONS

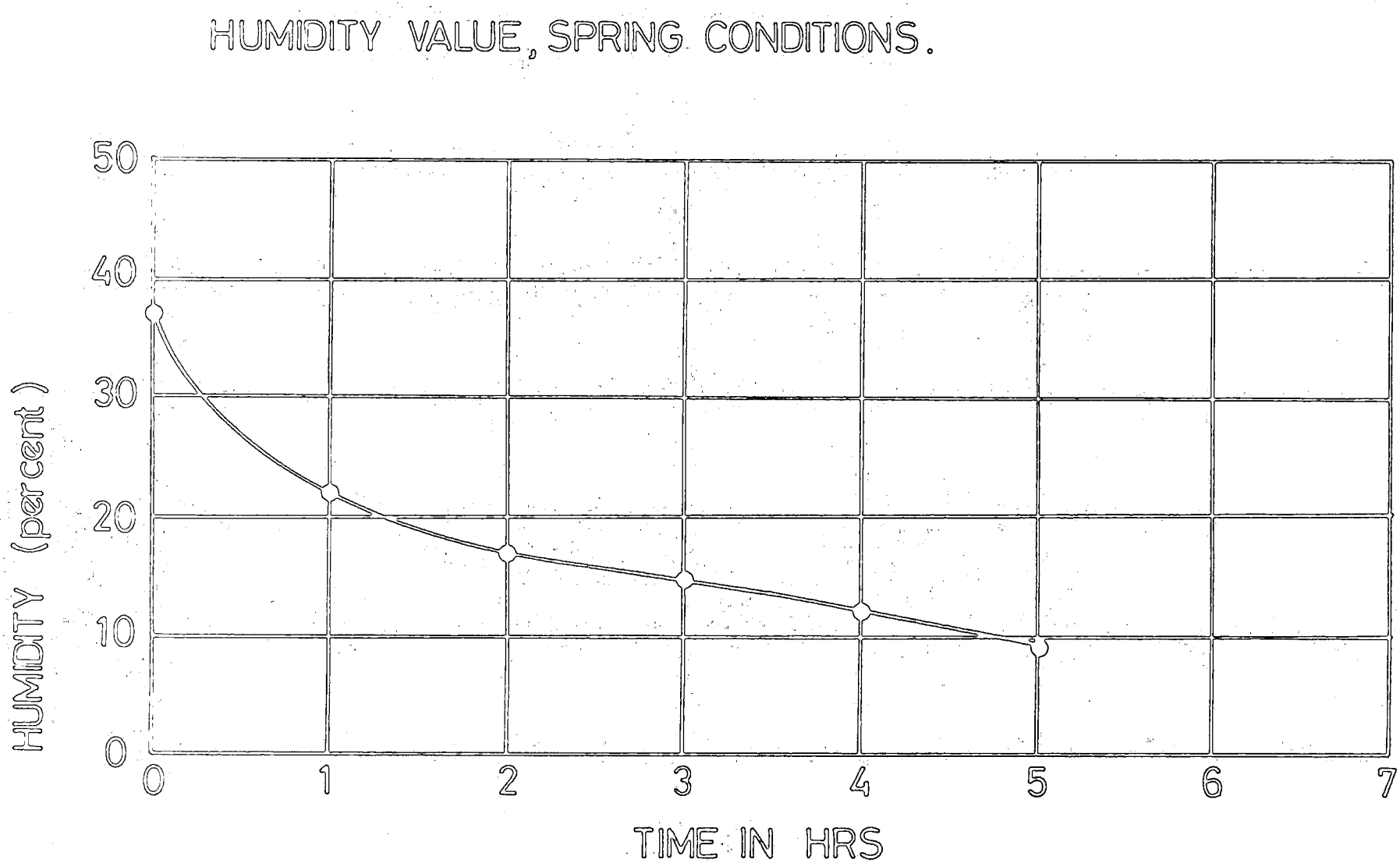
HUMIDITY VALUE, SPRING CONDITIONS.
HUMIDITY (percent)
50
40
30
20
10
0
0
1
2
3
4
5
6
7
TIME IN HRS

FIG. 6·2

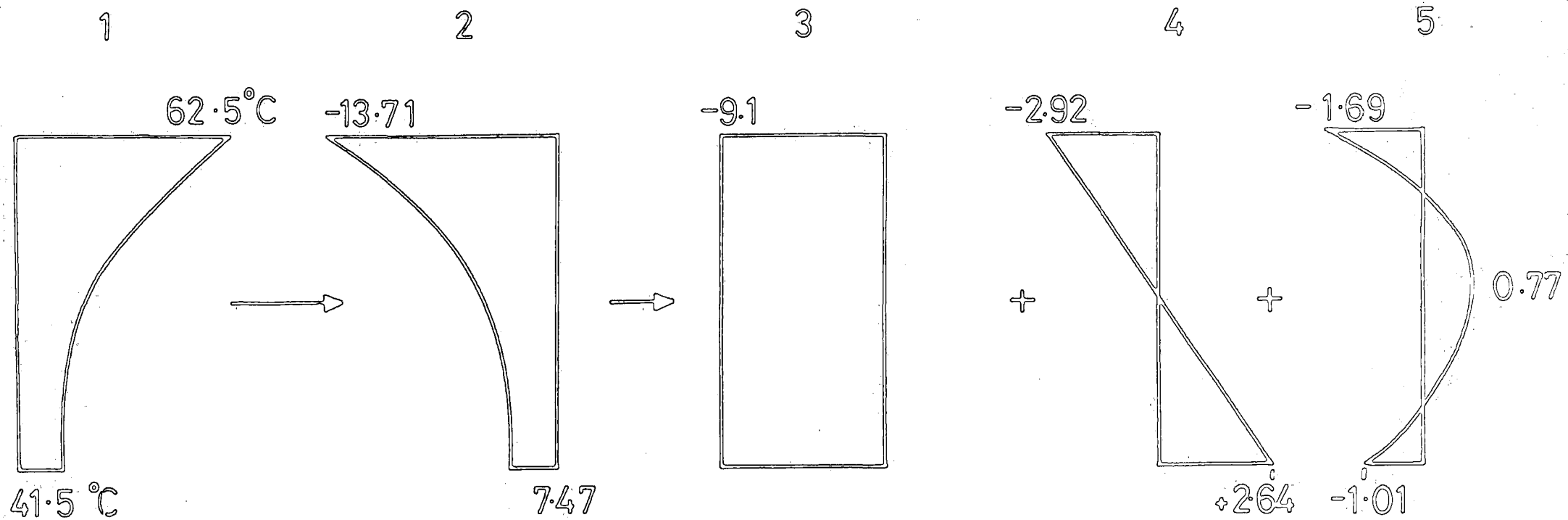

FIG. 6.3

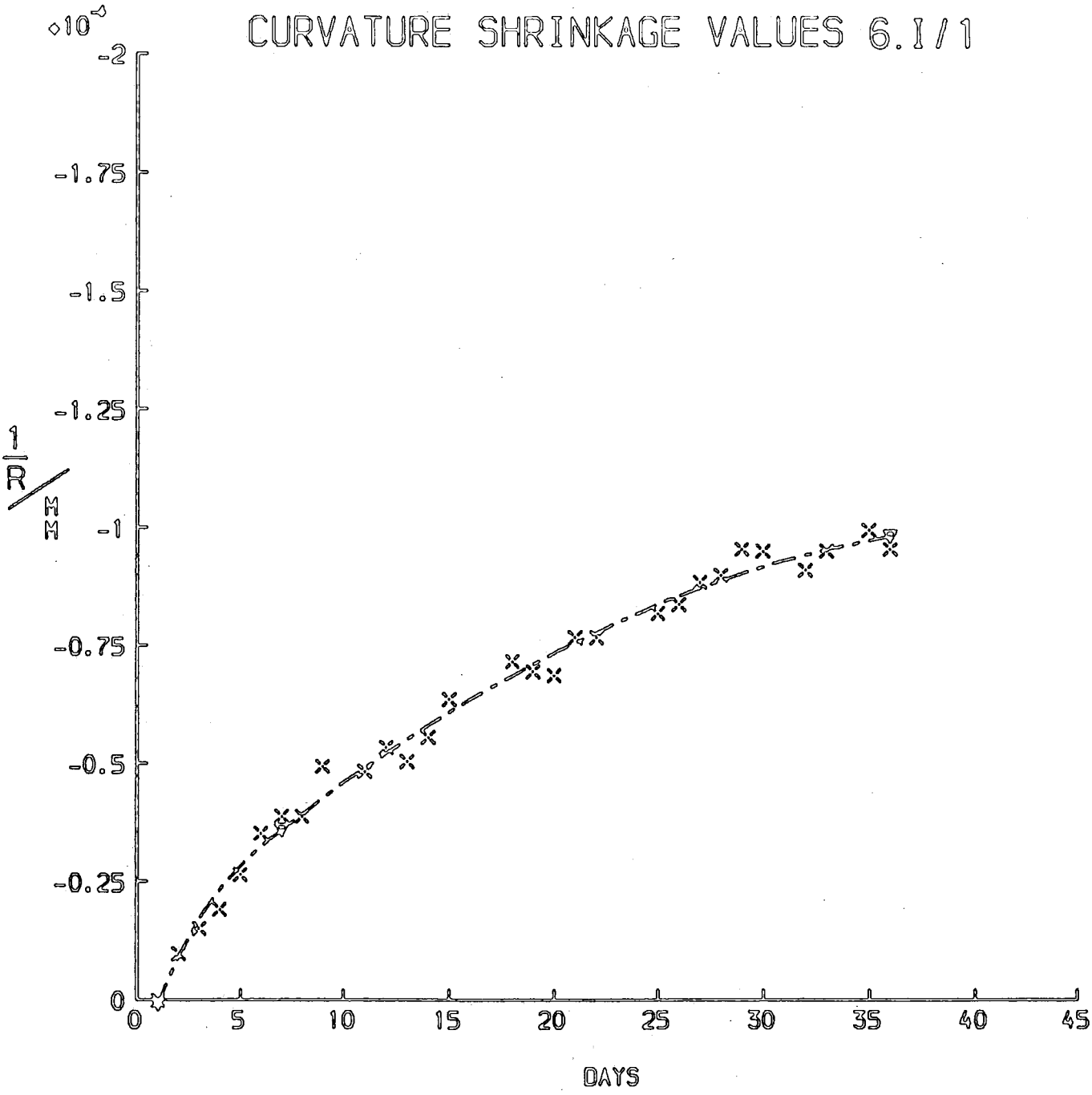
CURVATURE SHRINKAGE VALUES 6.I/1
$\diamond 10^{-3}$
-2
-1.75
-1.5
-1.25
-1
-0.75
-0.5
-0.25
0
$\frac{1}{R}_{MM}$
0
5
10
15
20
25
30
35
40
45
DAYS

FIG. 6.I.1.

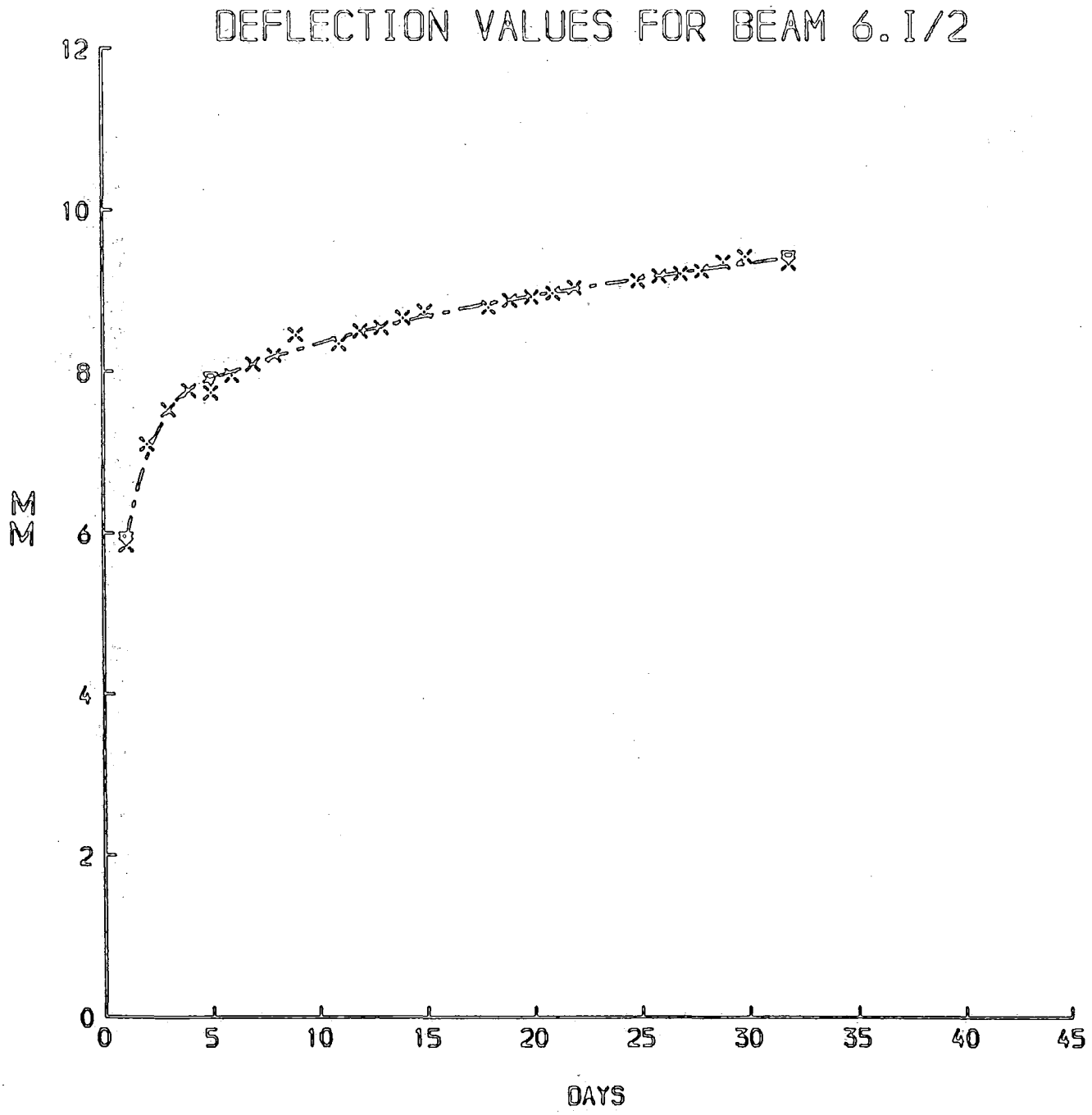
DEFLECTION VALUES FOR BEAM 6.I/2
12
10
8
6
4
2
0
MM
0
5
10
15
20
25
30
35
40
45
DAYS

FIG. 6.1.2.

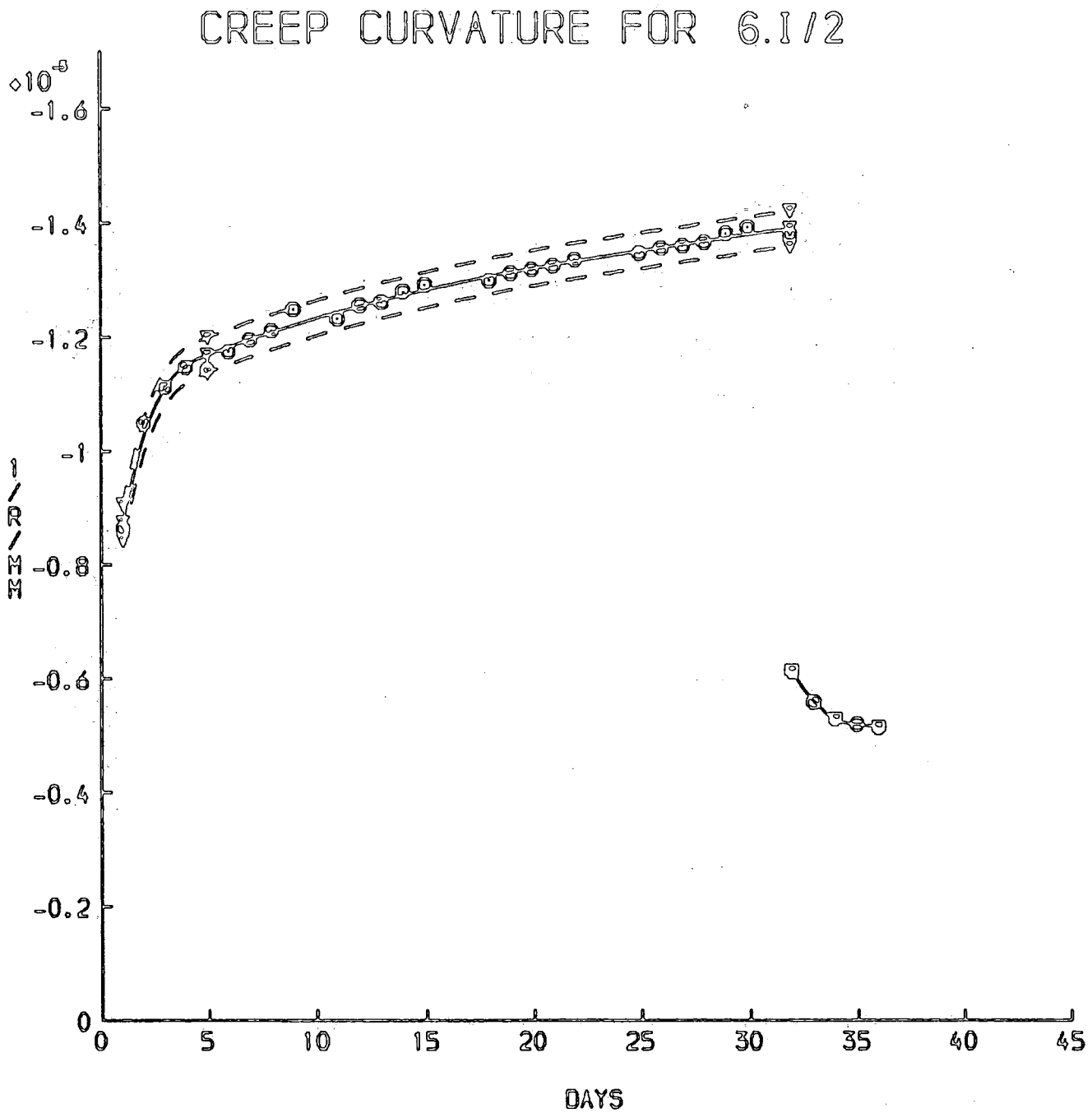
CREEP CURVATURE FOR 6.1/2
◇10⁻⁵
-1.6
-1.4
-1.2
-1
-0.8
-0.6
-0.4
-0.2
0
1/R/MM
0
5
10
15
20
25
30
35
40
45
DAYS

FIG.6.1.3

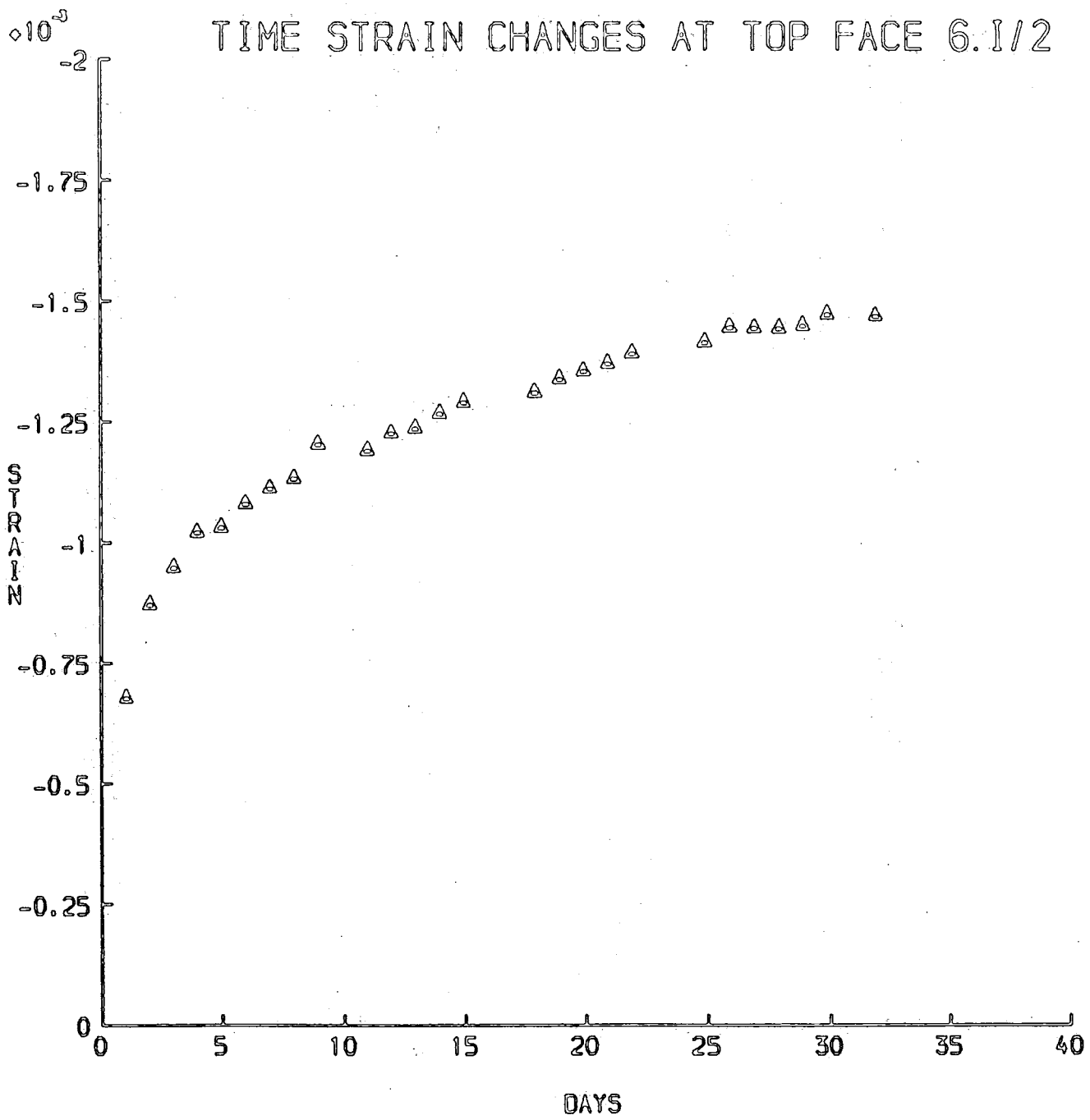
TIME STRAIN CHANGES AT TOP FACE 6.I/2
◇10⁻²
-2
-1.75
-1.5
-1.25
-1
-0.75
-0.5
-0.25
0
STRAIN
0
5
10
15
20
25
30
35
40
DAYS

FIG. 6.I.4

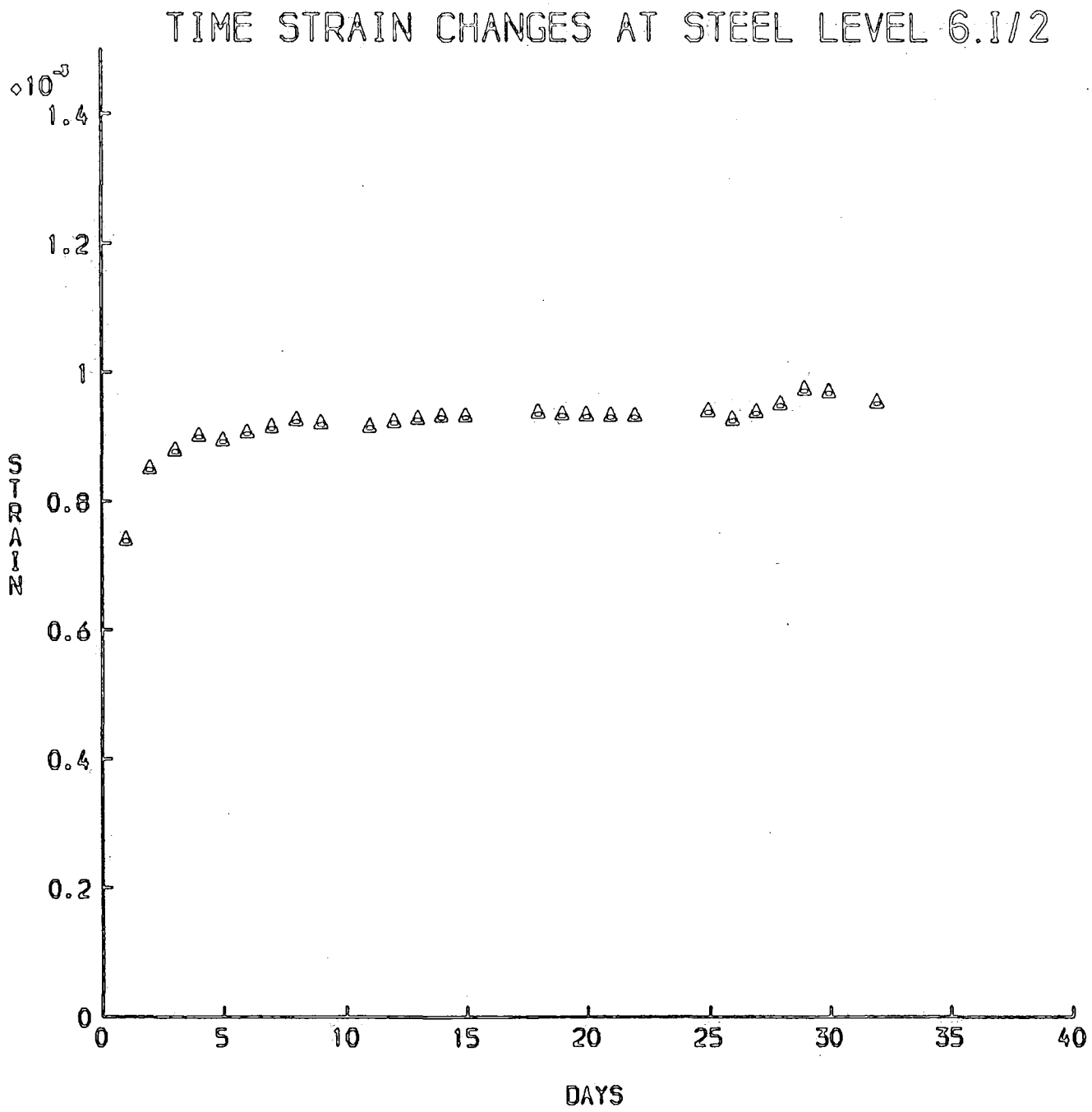
TIME STRAIN CHANGES AT STEEL LEVEL 6.1/2
$\diamond 10^{-3}$
1.4
1.2
1
0.8
0.6
0.4
0.2
0
STRAIN
0
5
10
15
20
25
30
35
40
DAYS

FIG. 6.1.5.

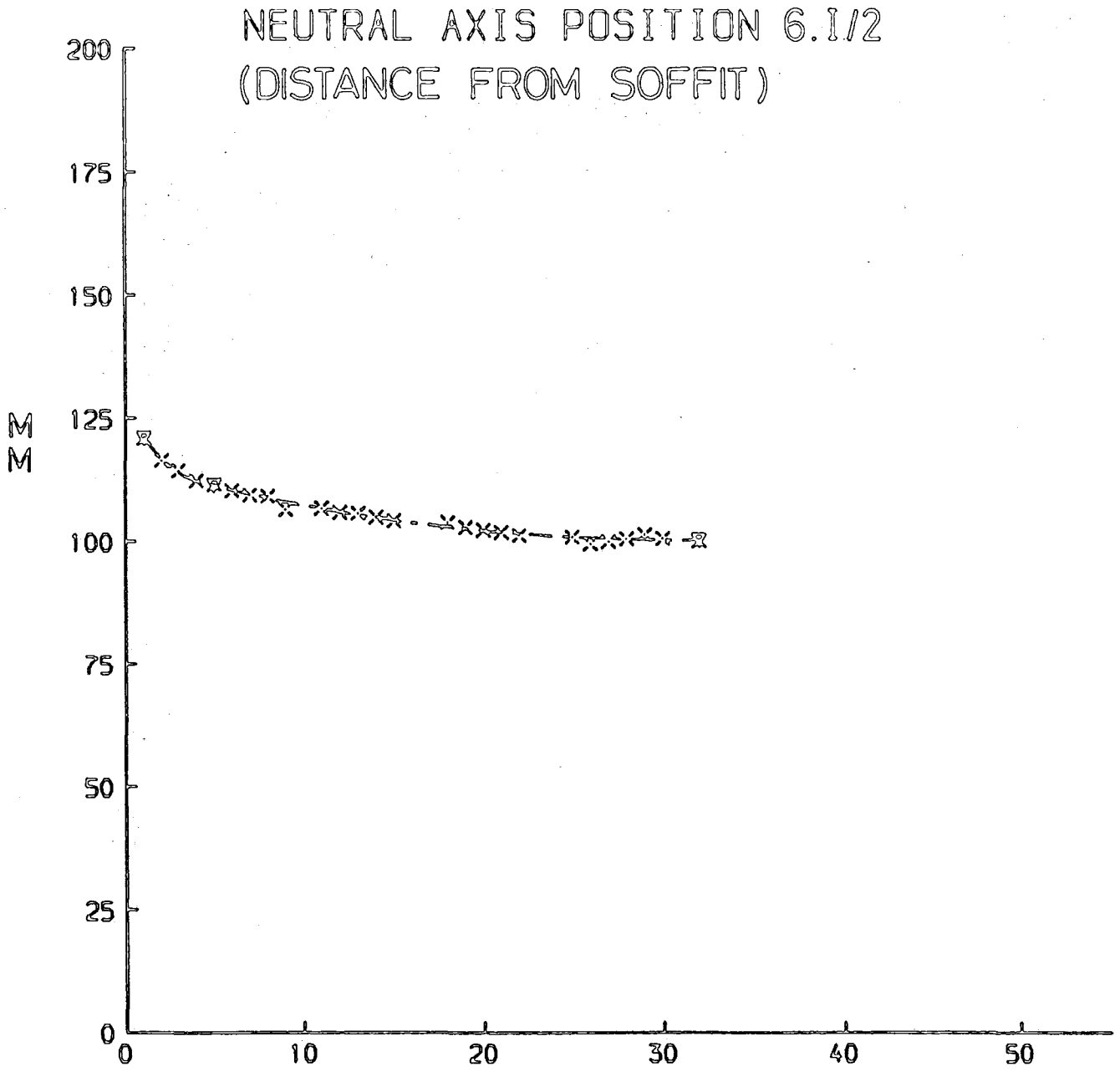
NEUTRAL AXIS POSITION 6.1/2
(DISTANCE FROM SOFFIT)
M
M
200
175
150
125
100
75
50
25
0
0
10
20
30
40
50

FIG. 6.1.6

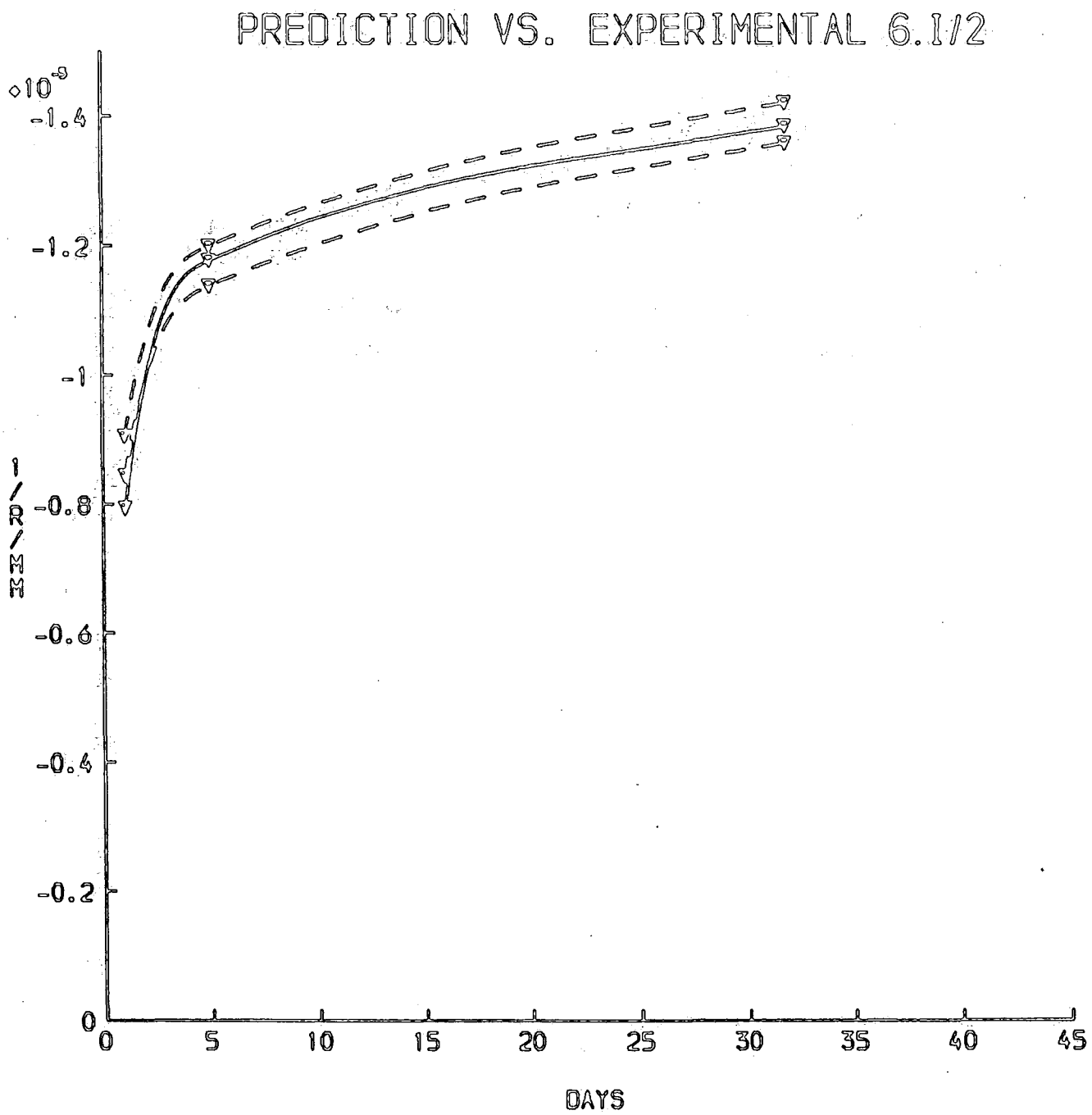
PREDICTION VS. EXPERIMENTAL 6.I/2
◇10⁻³
-1.4
-1.2
-1
-0.8
-0.6
-0.4
-0.2
0
1/R/MM
0
5
10
15
20
25
30
35
40
45
DAYS

FIG. 6.I.7.

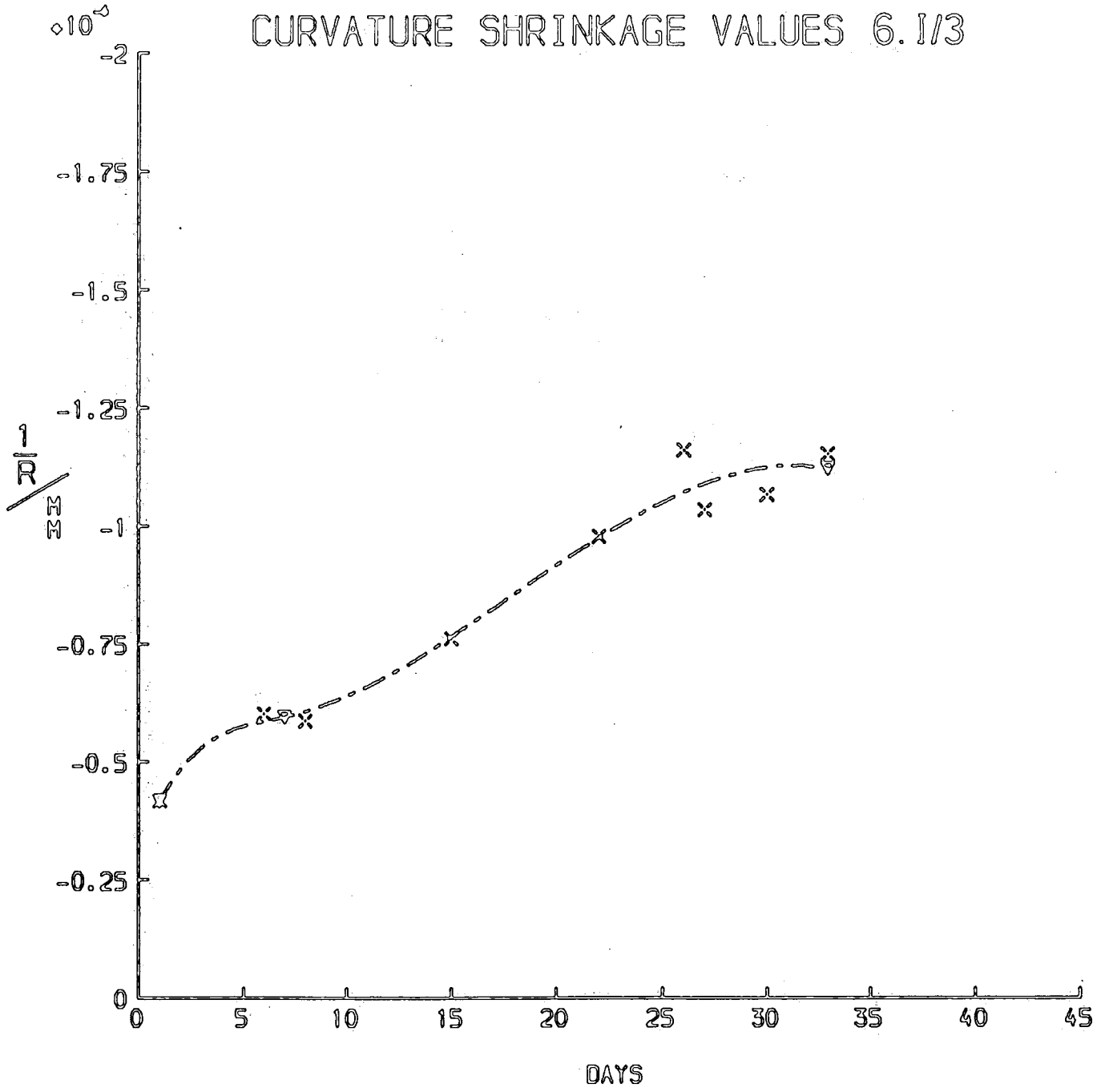
CURVATURE SHRINKAGE VALUES 6.I/3
$\circ 10^{-5}$
-2
-1.75
-1.5
-1.25
-1
-0.75
-0.5
-0.25
0
$\frac{1}{R}_{MM}$
0
5
10
15
20
25
30
35
40
45
DAYS

FIG. 6.I.8.

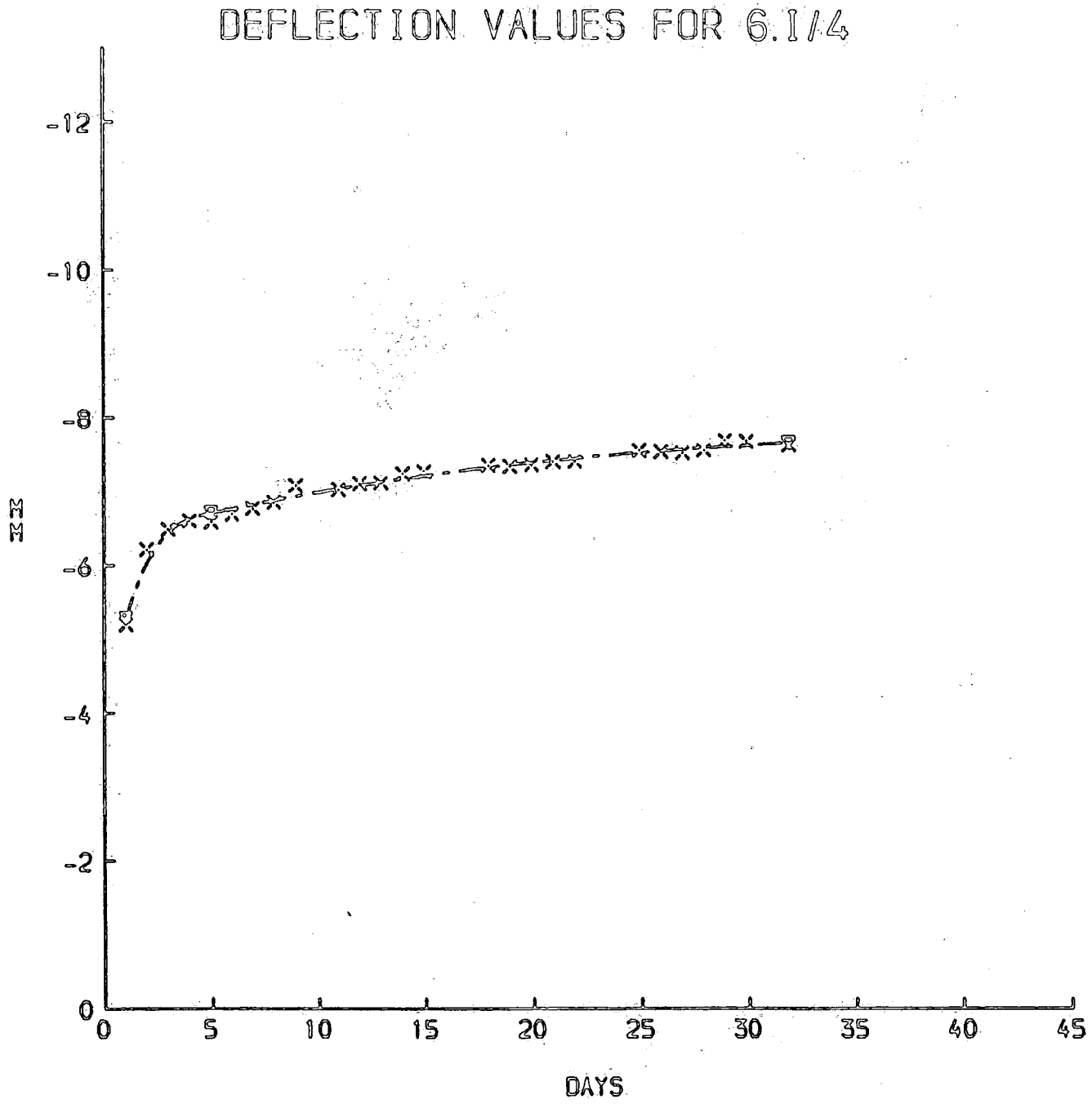
DEFLECTION VALUES FOR 6.I/4
-12
-10
-8
-6
-4
-2
0
MM
0
5
10
15
20
25
30
35
40
45
DAYS

FIG. 6.I.9

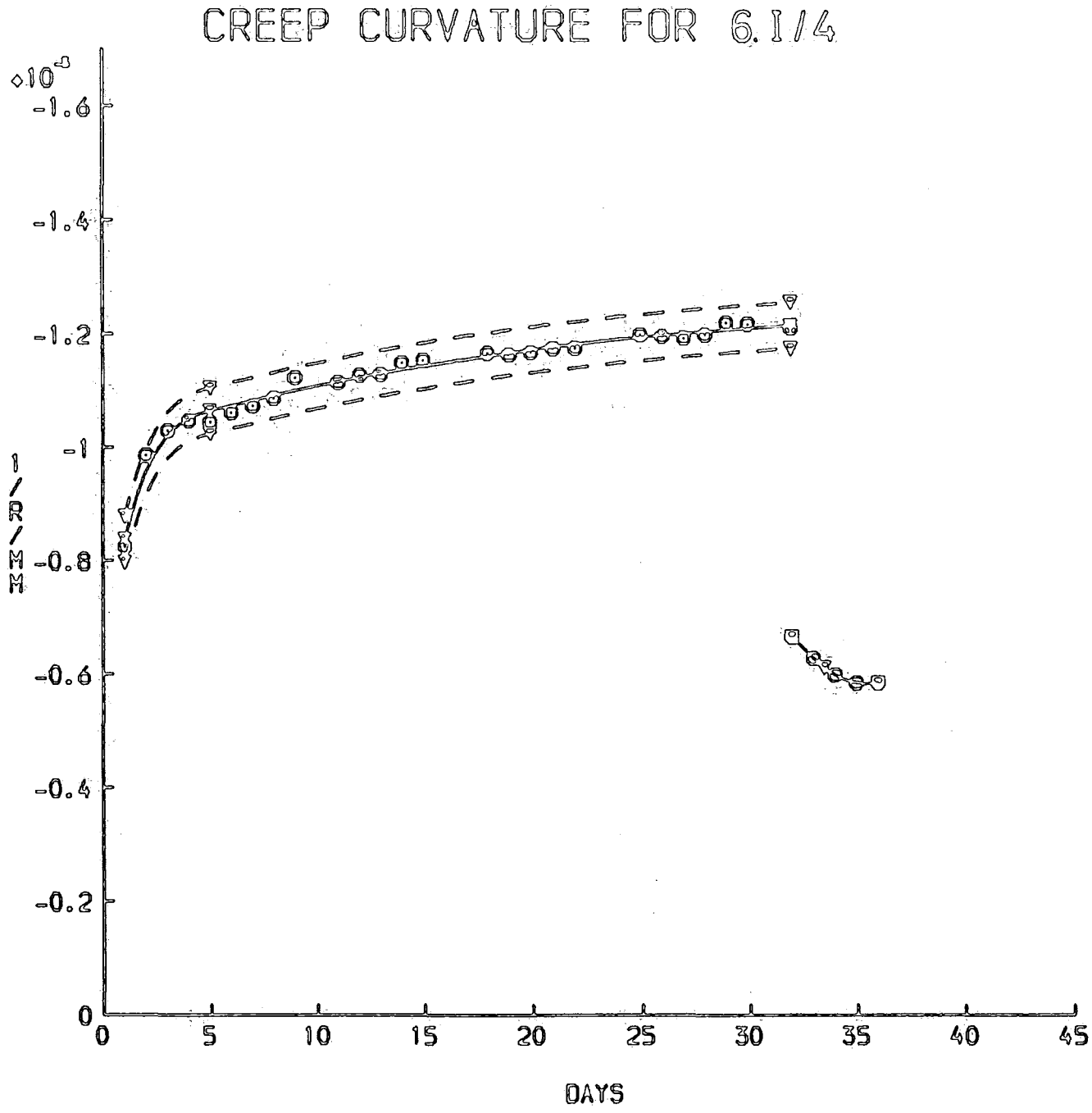
CREEP CURVATURE FOR 6.1/4
◇10⁻³
-1.6
-1.4
-1.2
-1
-0.8
-0.6
-0.4
-0.2
0
1/R/MM
0
5
10
15
20
25
30
35
40
45
DAYS

FIG. 6.1.10.

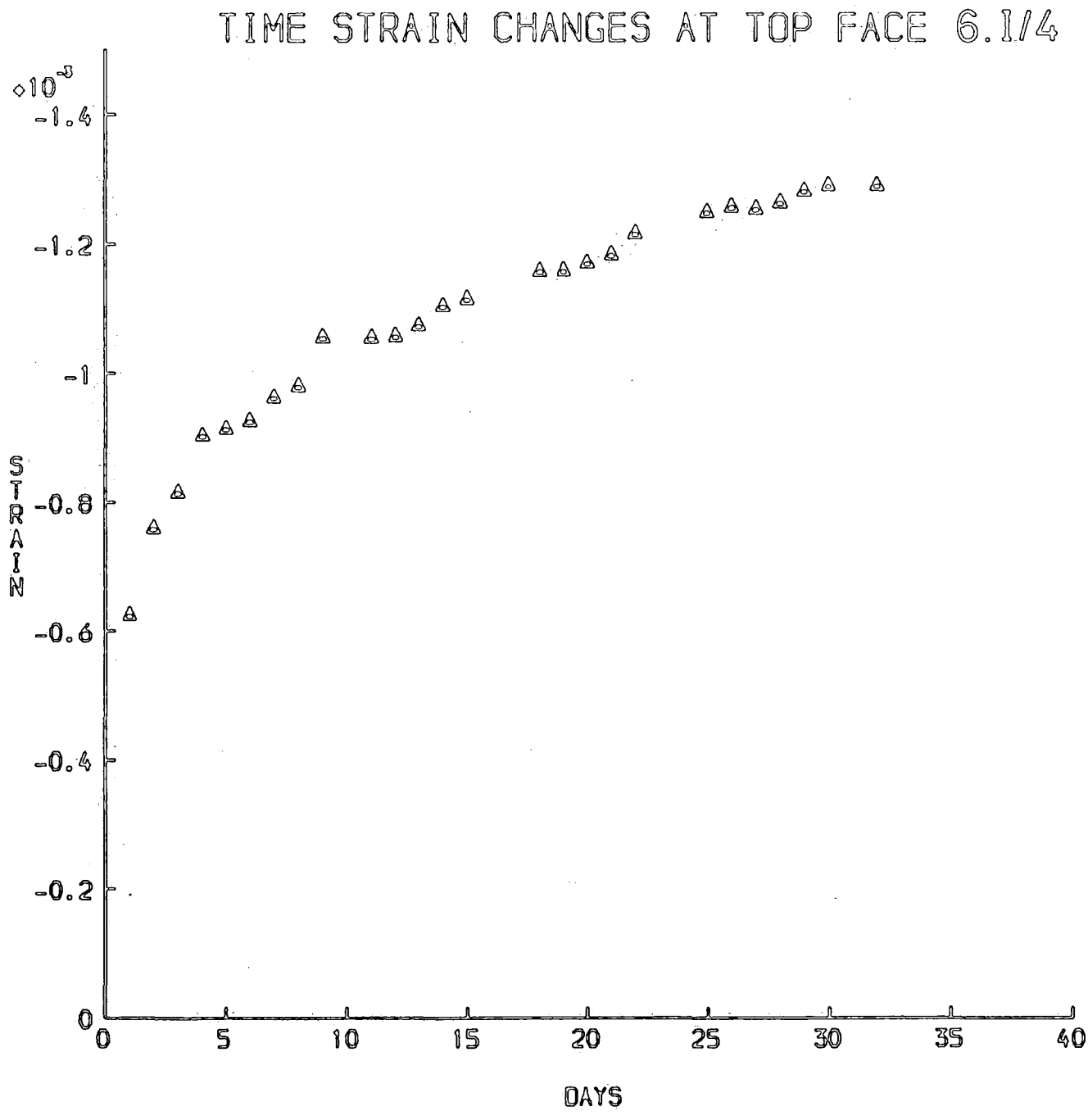
TIME STRAIN CHANGES AT TOP FACE 6.1/4
$\diamond 10^{-3}$
-1.4
-1.2
-1
-0.8
-0.6
-0.4
-0.2
0
STRAIN
0
5
10
15
20
25
30
35
40
DAYS

FIG 6.1 .11

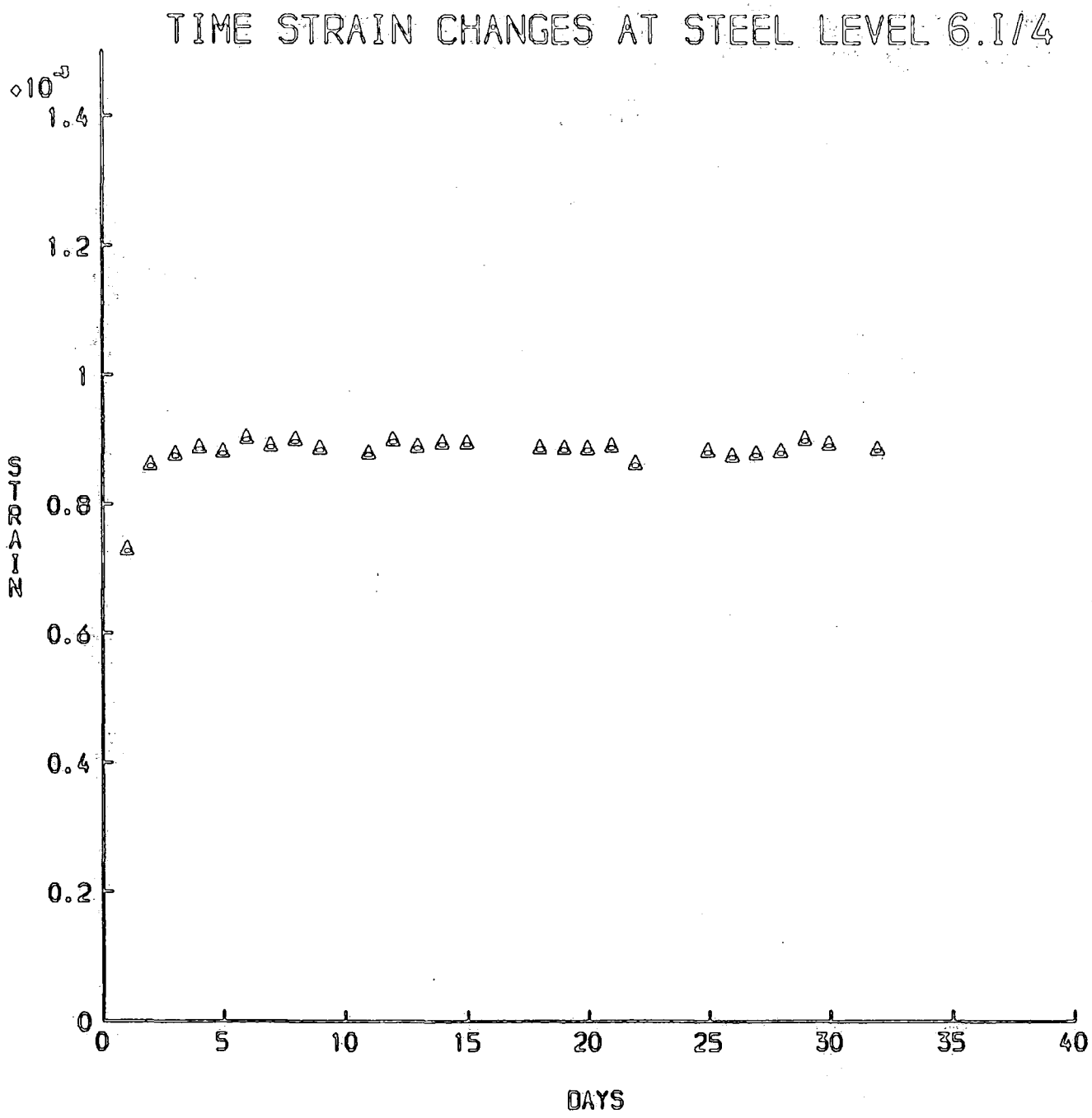
TIME STRAIN CHANGES AT STEEL LEVEL 6.I/4
$\diamond 10^{-3}$
1.4
1.2
1
0.8
0.6
0.4
0.2
0
STRAIN
0
5
10
15
20
25
30
35
40
DAYS

FIG. 6.1.12.

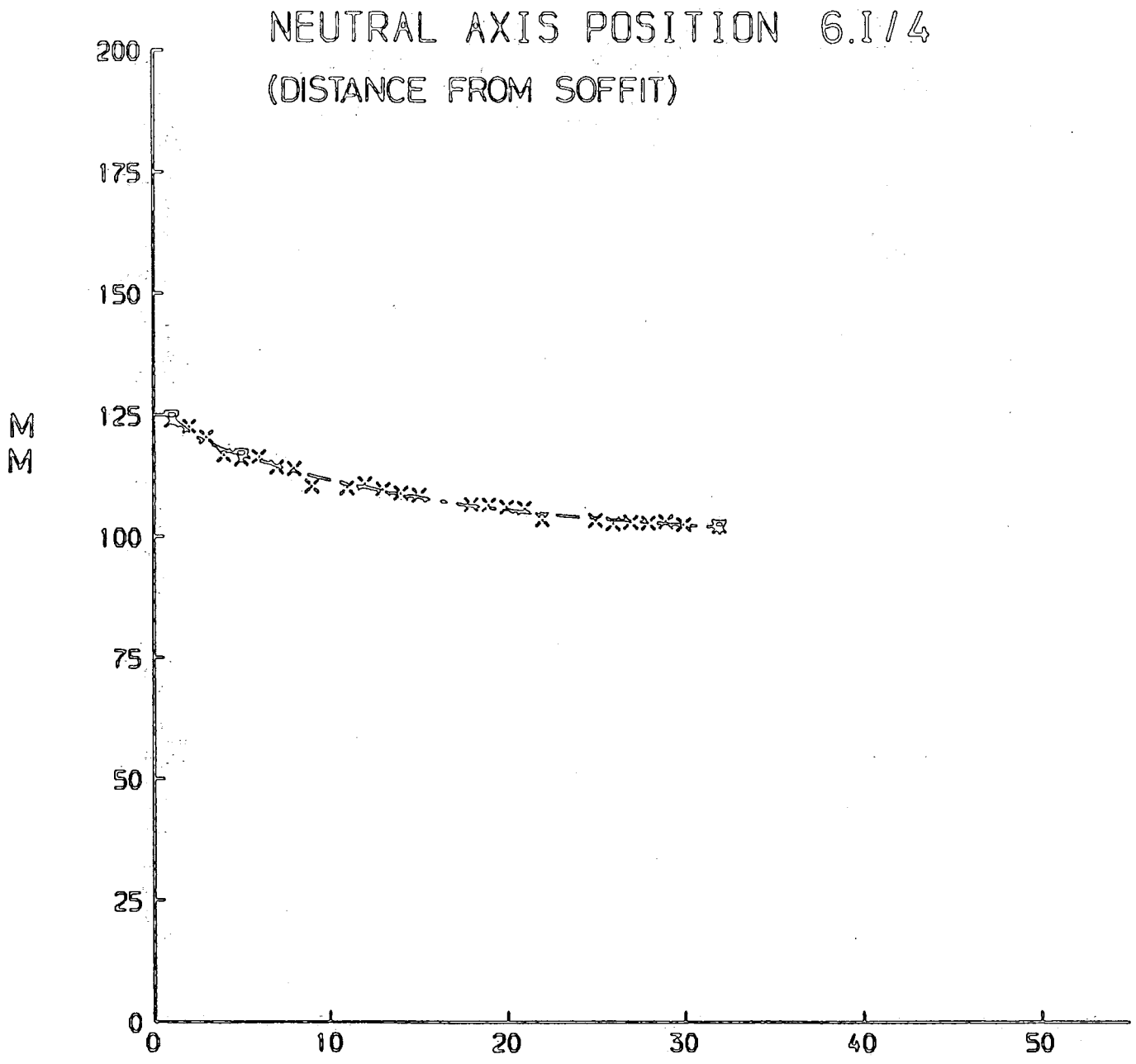
NEUTRAL AXIS POSITION 6.I/4
(DISTANCE FROM SOFFIT)
200
175
150
125
100
75
50
25
0
M
M
0
10
20
30
40
50

FIG. 6.I.13.

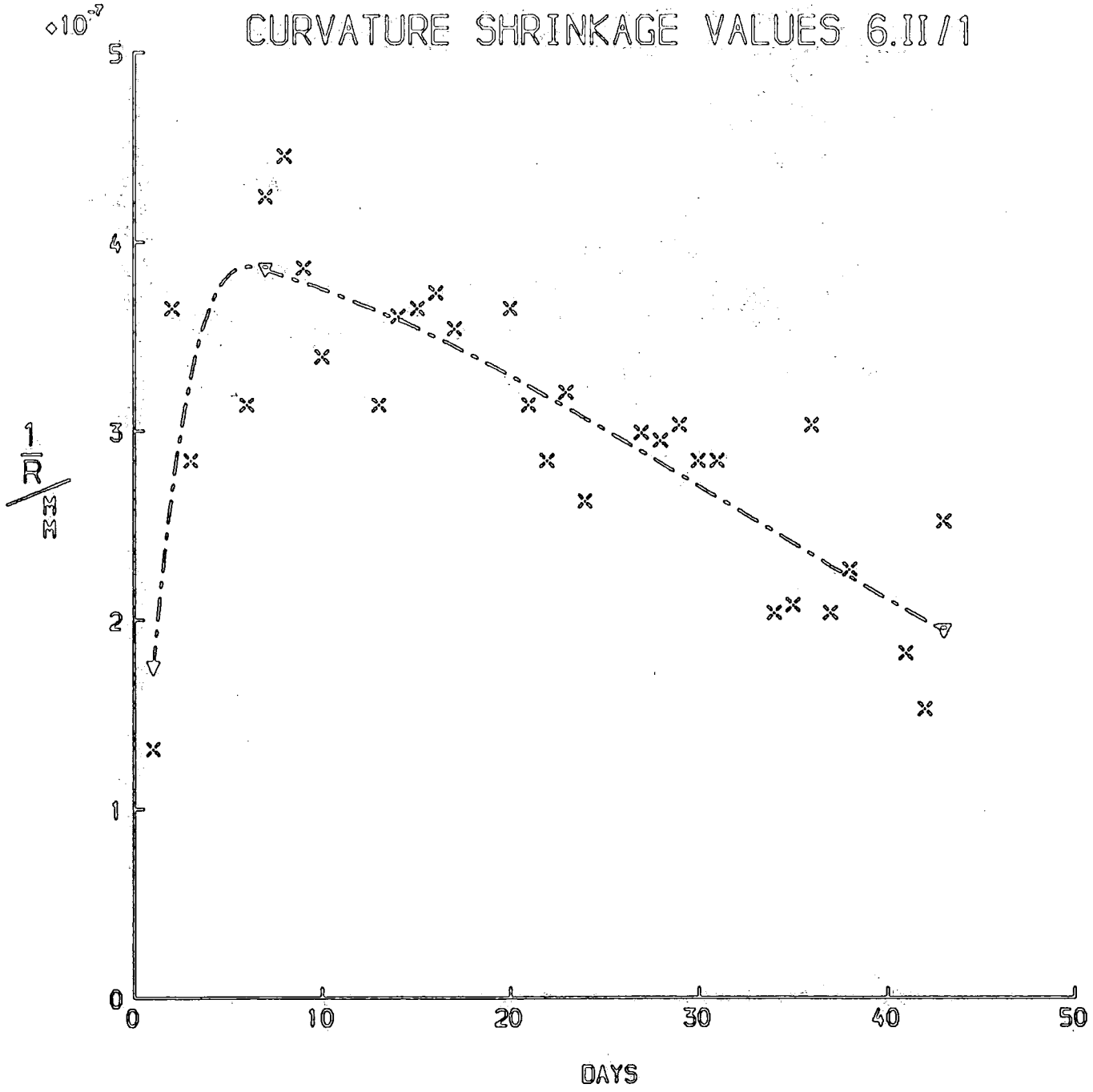
CURVATURE SHRINKAGE VALUES 6.II/1
$\circ 10^{-7}$
$\frac{1}{\bar{R}}$ / MM
0
1
2
3
4
5
0
10
20
30
40
50
DAYS

FIG. 6.II.1.

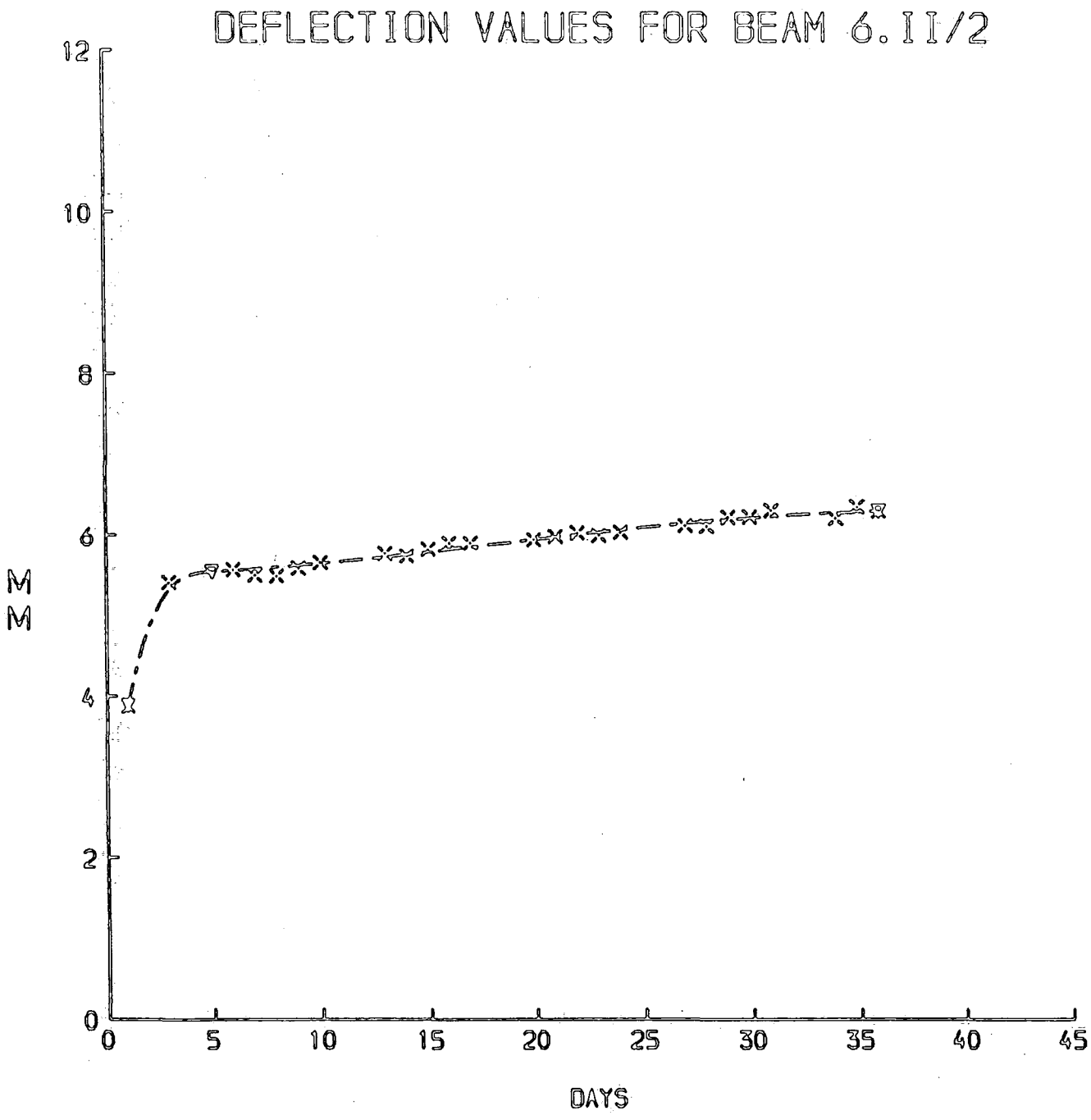
DEFLECTION VALUES FOR BEAM 6.II/2
12
10
8
6
4
2
0
M
M
0
5
10
15
20
25
30
35
40
45
DAYS

FIG. 6.II.2

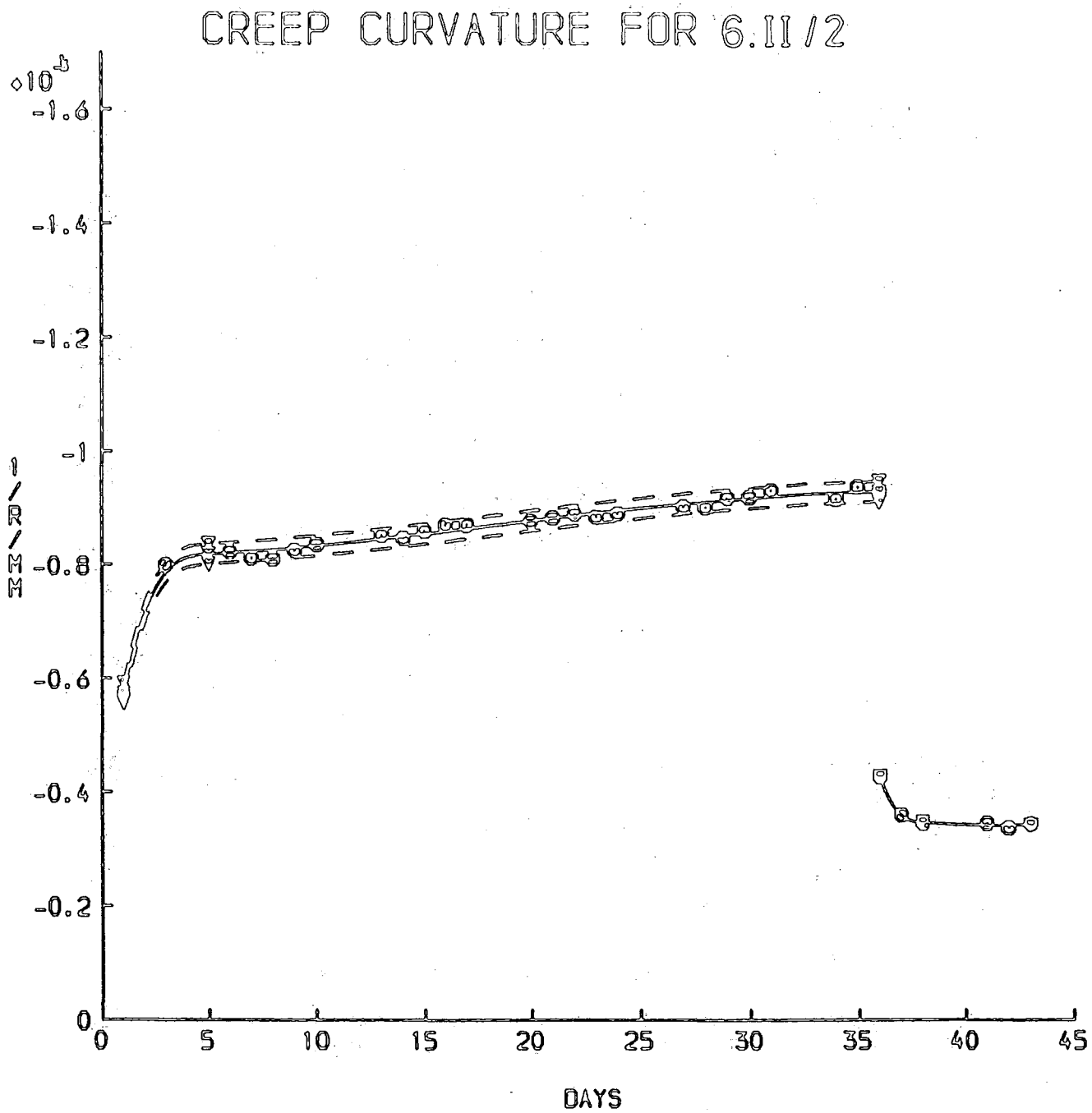
CREEP CURVATURE FOR 6.II/2
◇10⁻³
-1.6
-1.4
-1.2
-1
-0.8
-0.6
-0.4
-0.2
0
1/R/MM
0
5
10
15
20
25
30
35
40
45
DAYS

FIG. 6.II.3

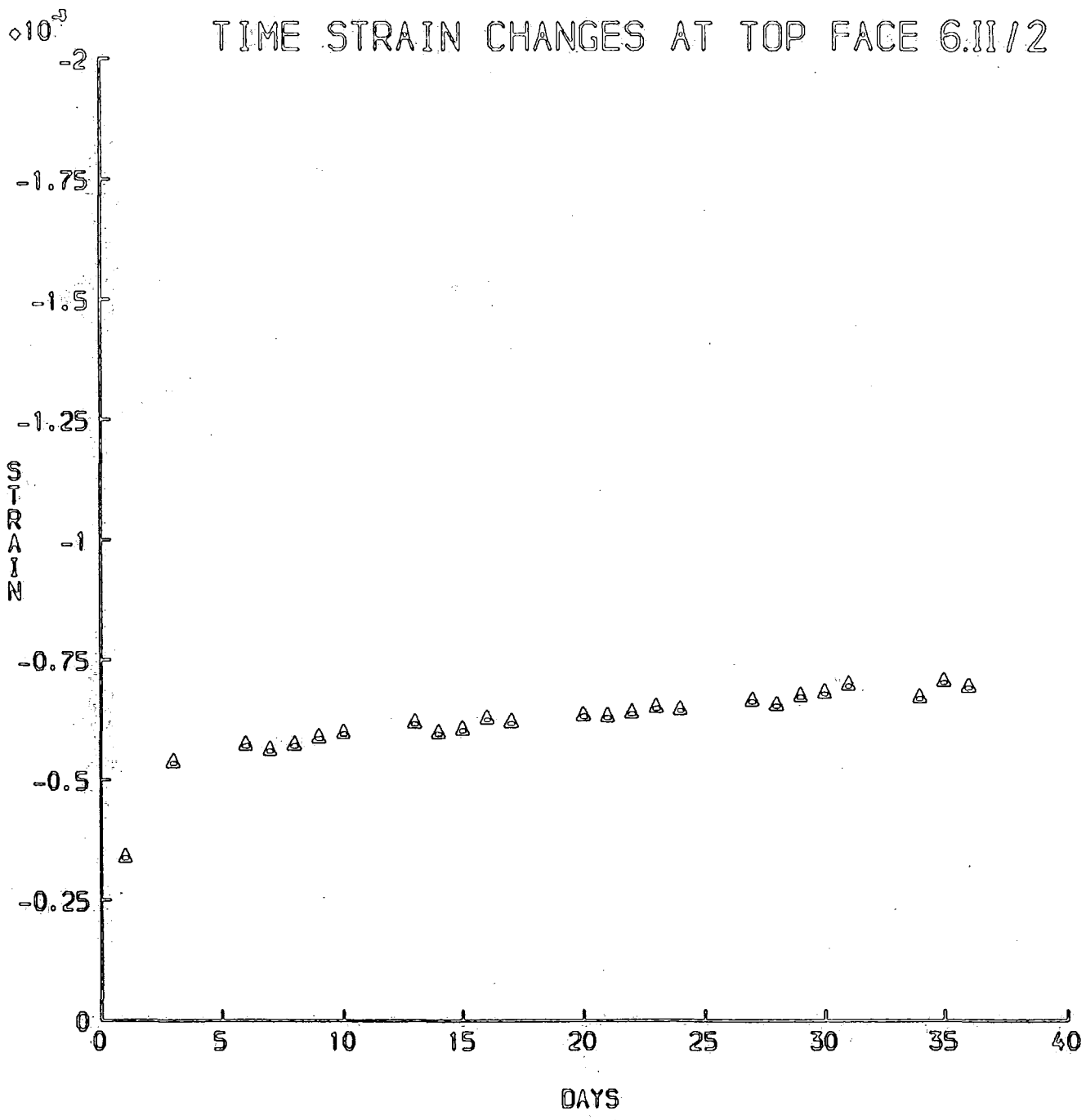
TIME STRAIN CHANGES AT TOP FACE 6.II/2
◇10⁻³
-2
-1.75
-1.5
-1.25
-1
-0.75
-0.5
-0.25
0
STRAIN
0
5
10
15
20
25
30
35
40
DAYS

FIG.6.II.4

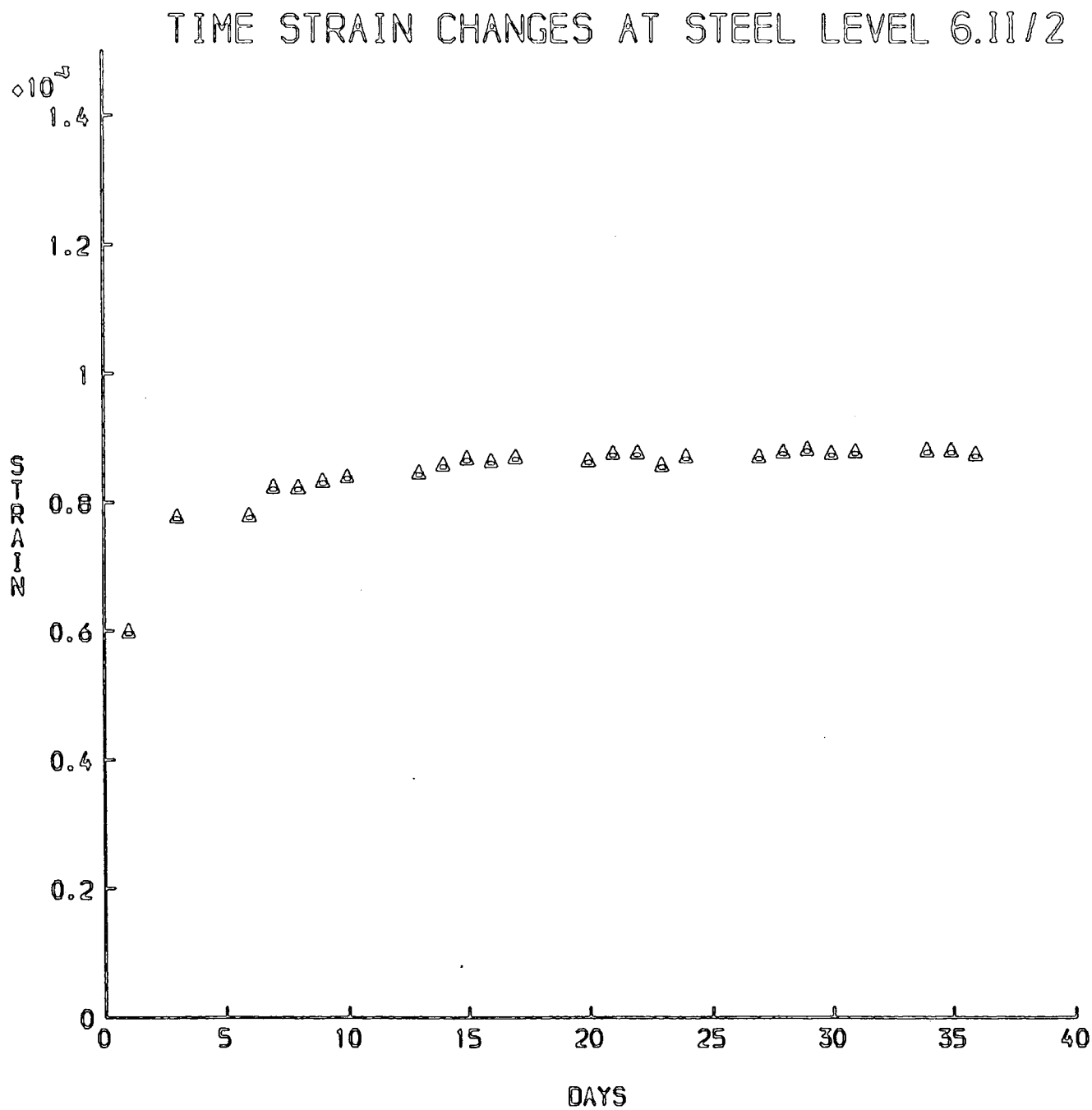
TIME STRAIN CHANGES AT STEEL LEVEL 6.11/2
$\diamond 10^{-3}$
1.4
1.2
1
0.8
0.6
0.4
0.2
0
STRAIN
0
5
10
15
20
25
30
35
40
DAYS

FIG. 6.11.5.

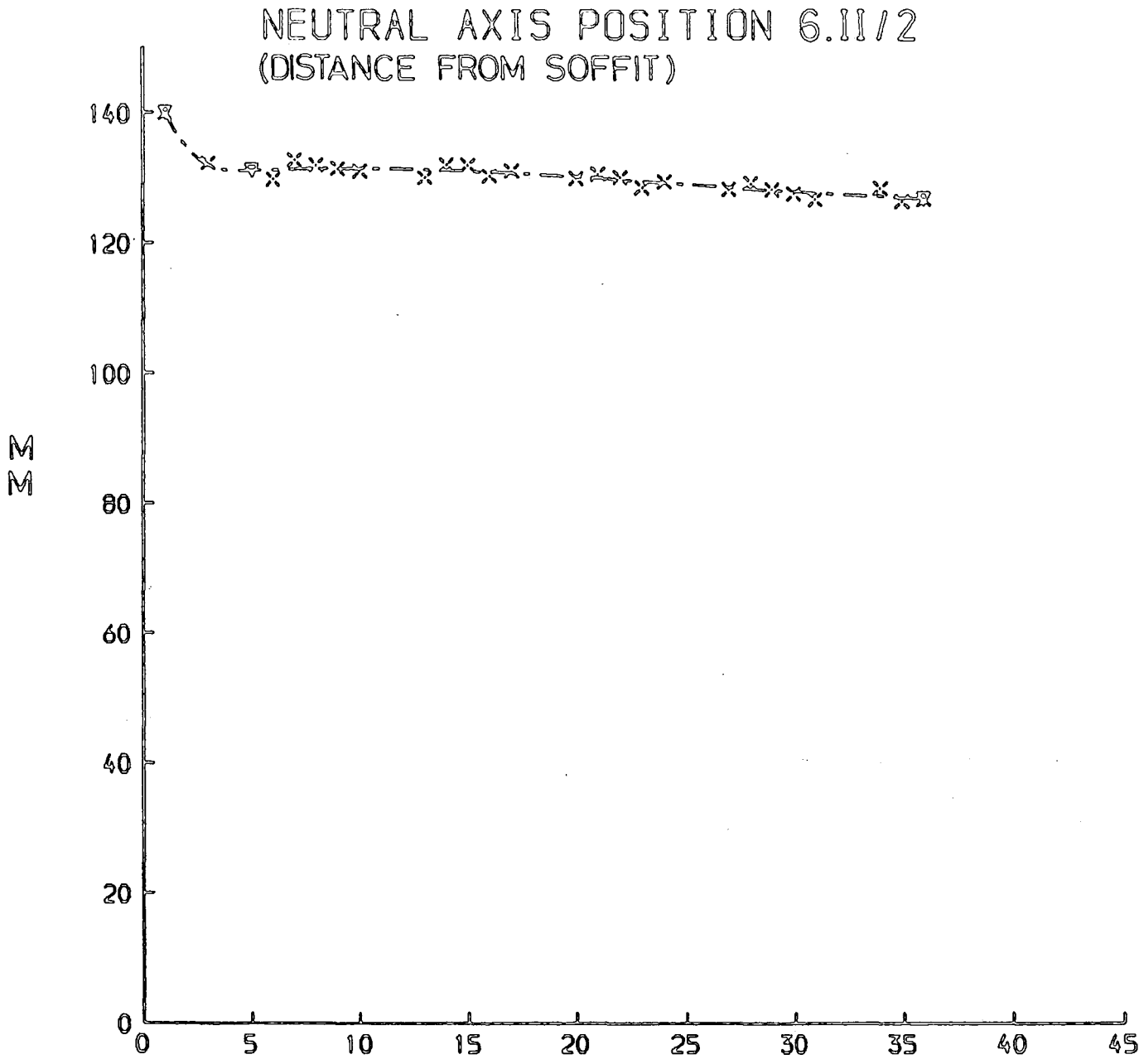
NEUTRAL AXIS POSITION 6.11/2
(DISTANCE FROM SOFFIT)
M
M
140
120
100
80
60
40
20
0
0
5
10
15
20
25
30
35
40
45

FIG. 6.11.6.

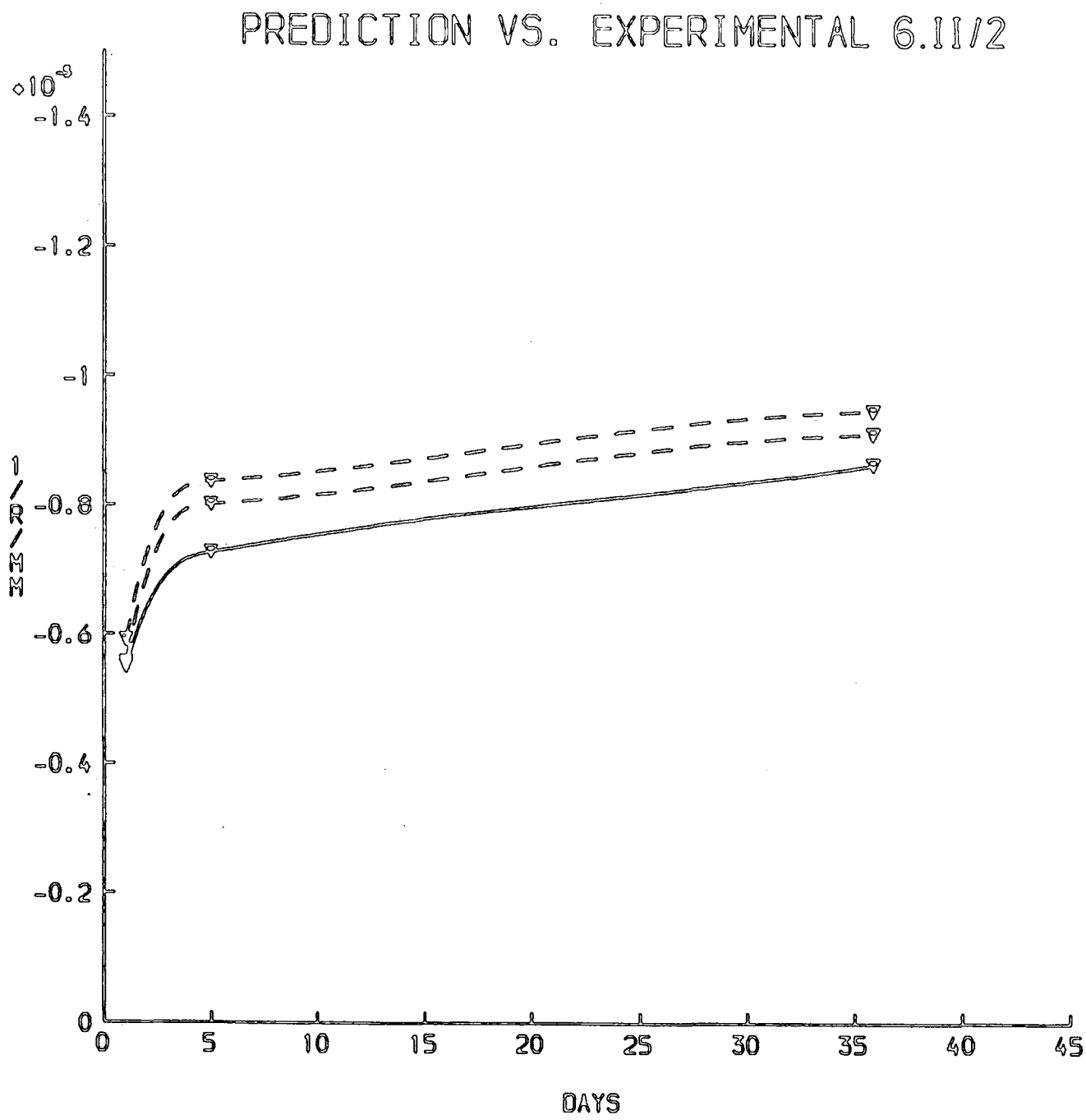
PREDICTION VS. EXPERIMENTAL 6.II/2
$\diamond 10^{-3}$
-1.4
-1.2
-1
-0.8
-0.6
-0.4
-0.2
0
1/R/MM
0
5
10
15
20
25
30
35
40
45
DAYS

FIG. 6.II.7

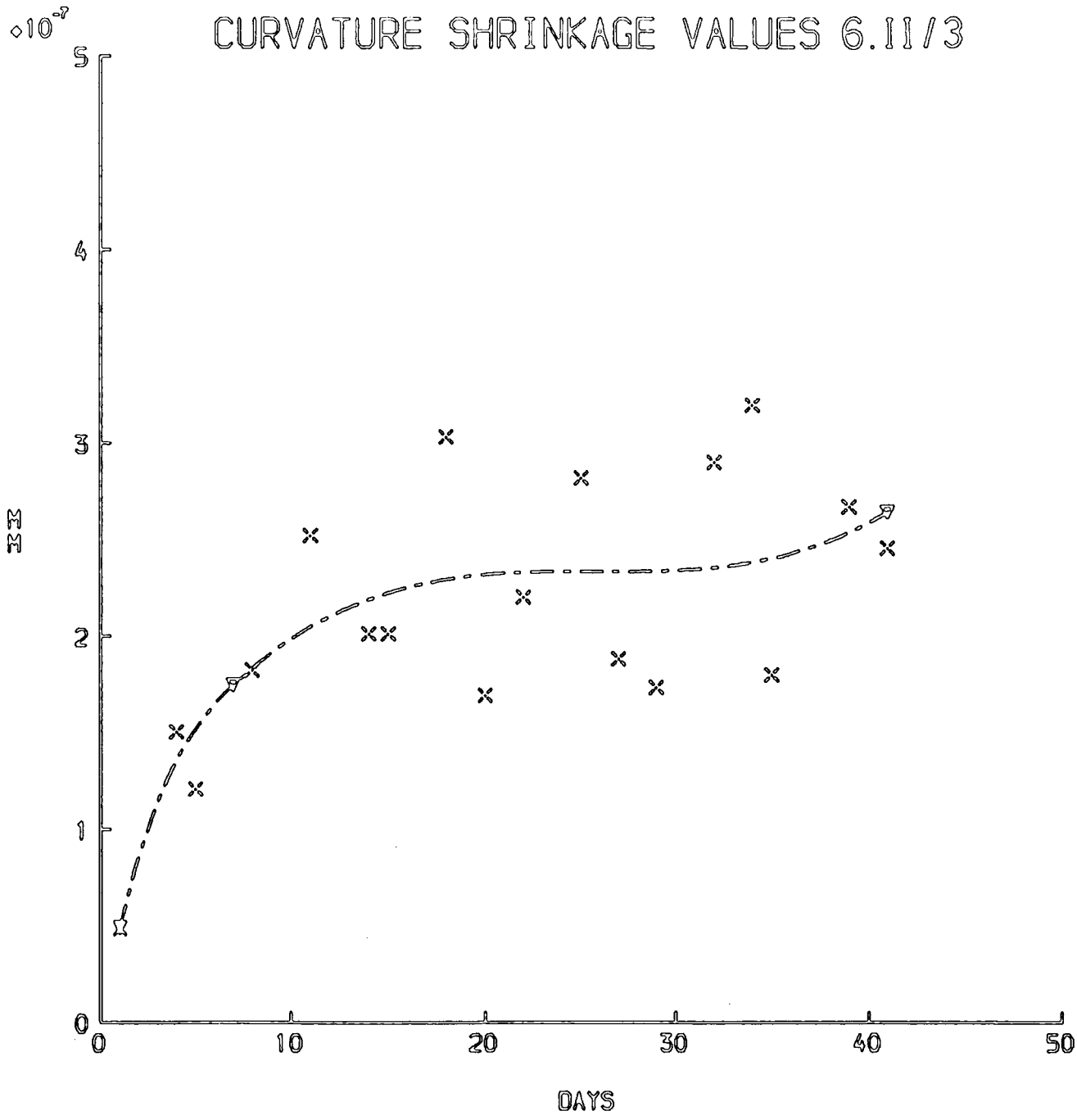
CURVATURE SHRINKAGE VALUES 6.11/3
◇10⁻⁷
5
4
3
2
1
0
MM
0
10
20
30
40
50
DAYS

FIG. 6.11.8.

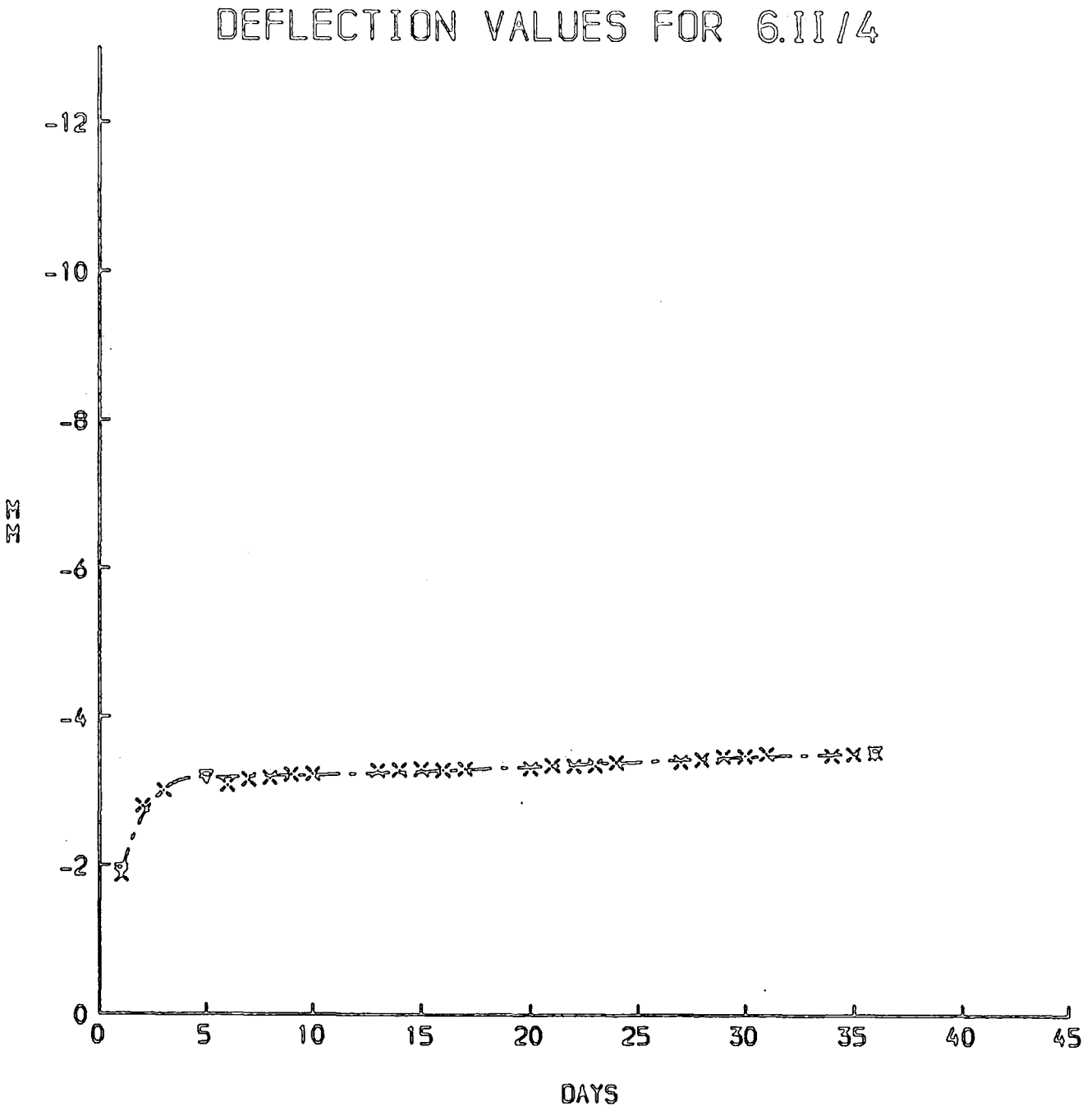
DEFLECTION VALUES FOR 6.II/4
-12
-10
-8
-6
-4
-2
0
MM
0
5
10
15
20
25
30
35
40
45
DAYS

FIG. 6.II.9.

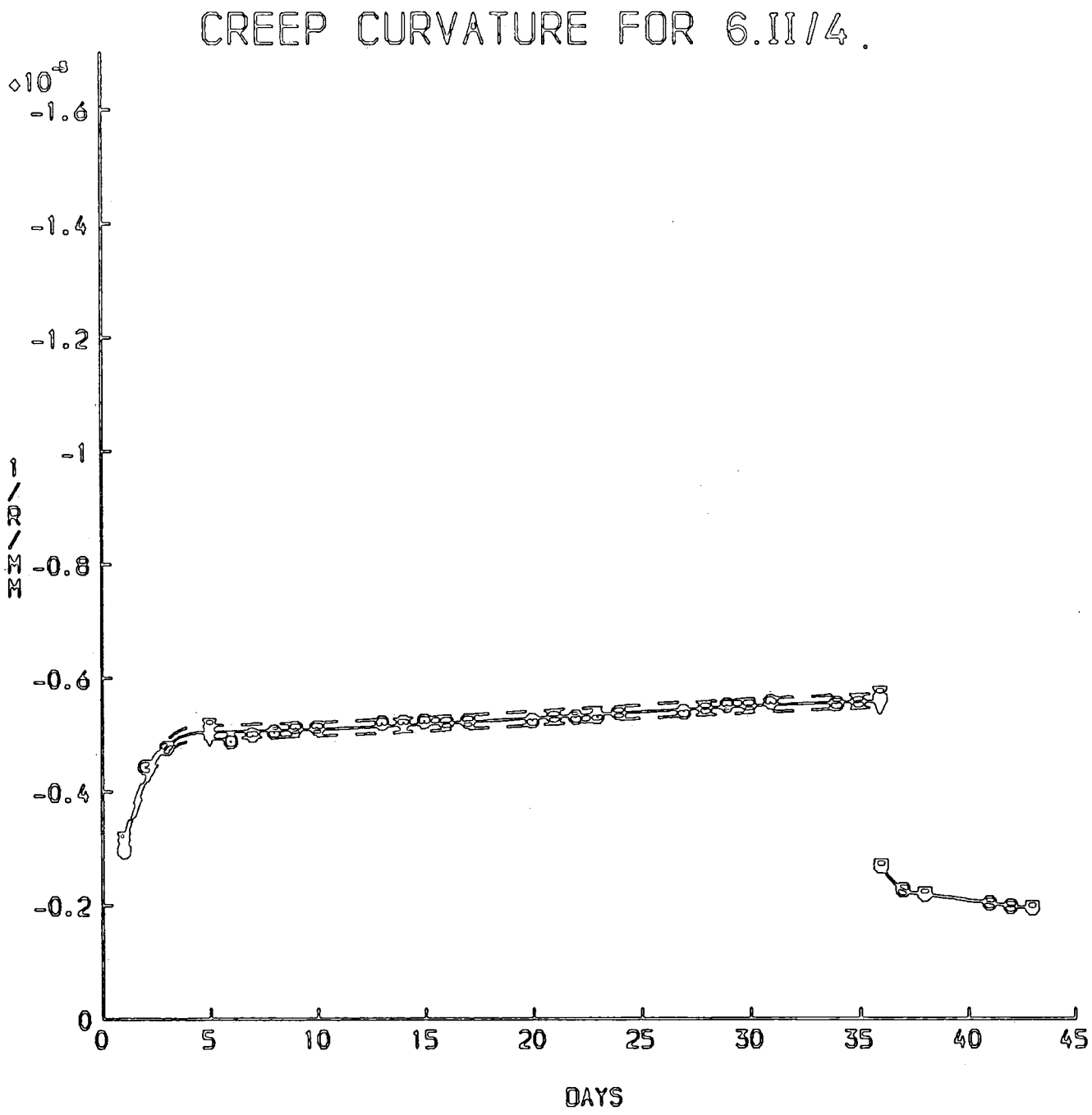
CREEP CURVATURE FOR 6.II/4.
◇10⁻⁵
-1.6
-1.4
-1.2
-1
-0.8
-0.6
-0.4
-0.2
0
1/R/MM
0
5
10
15
20
25
30
35
40
45
DAYS

FIG. 6.11.10.

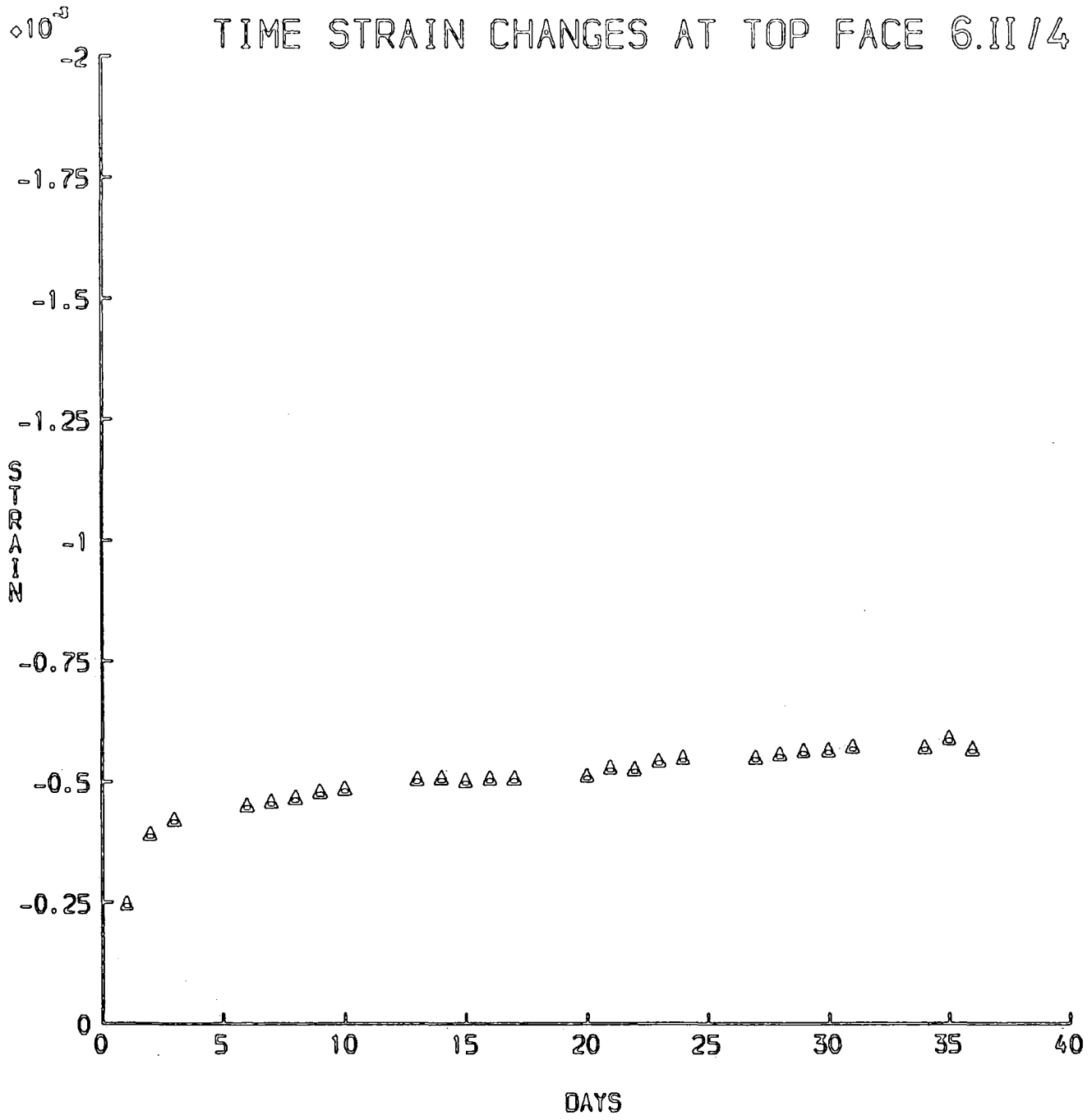
TIME STRAIN CHANGES AT TOP FACE 6.II/4
◇10⁻³
-2
-1.75
-1.5
-1.25
-1
-0.75
-0.5
-0.25
0
STRAIN
0
5
10
15
20
25
30
35
40
DAYS

FIG. 6.II.11.

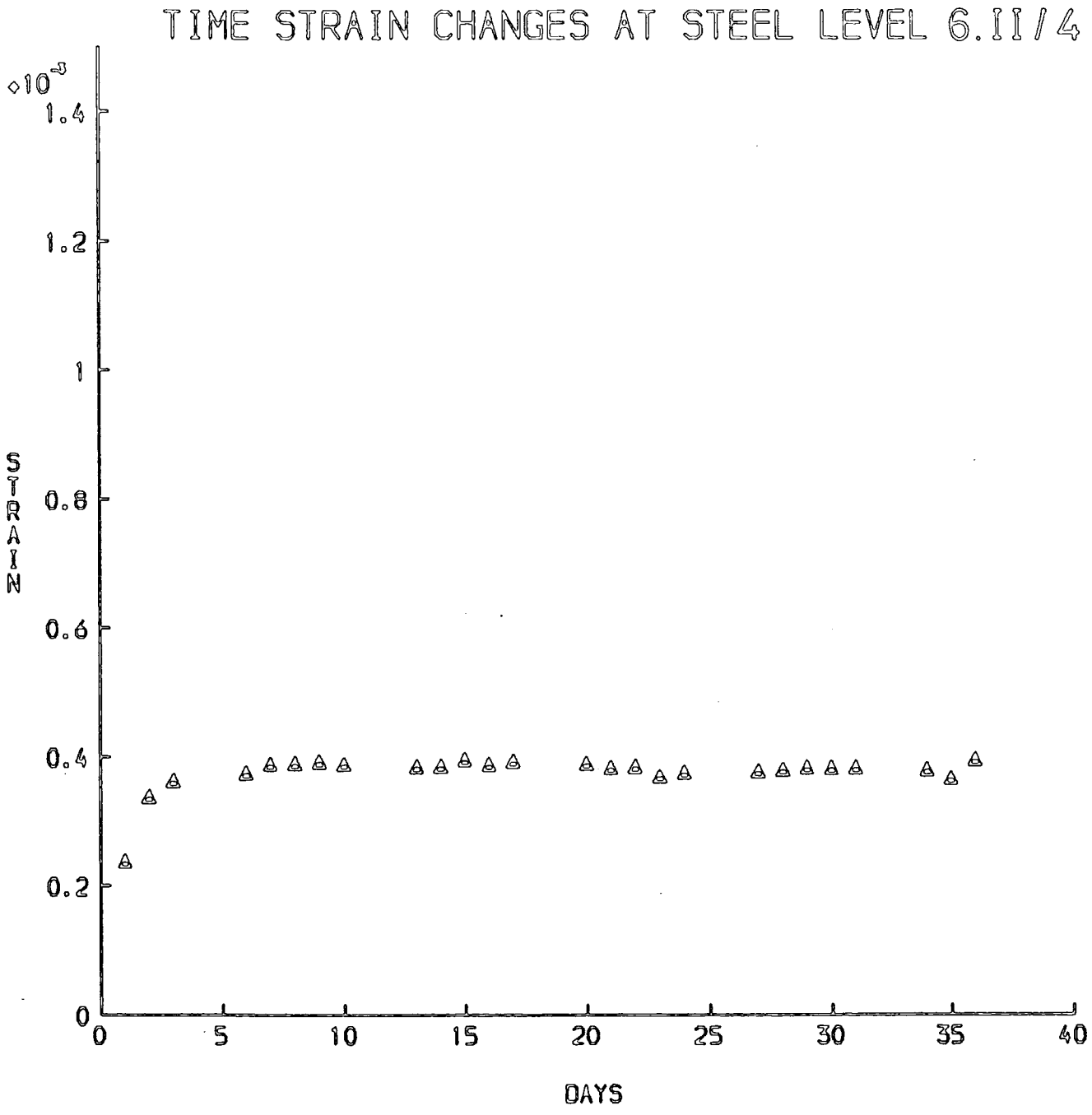
TIME STRAIN CHANGES AT STEEL LEVEL 6.II/4
◇10⁻³
1.4
1.2
1
0.8
0.6
0.4
0.2
0
STRAIN
0
5
10
15
20
25
30
35
40
DAYS

FIG. 6.11.12

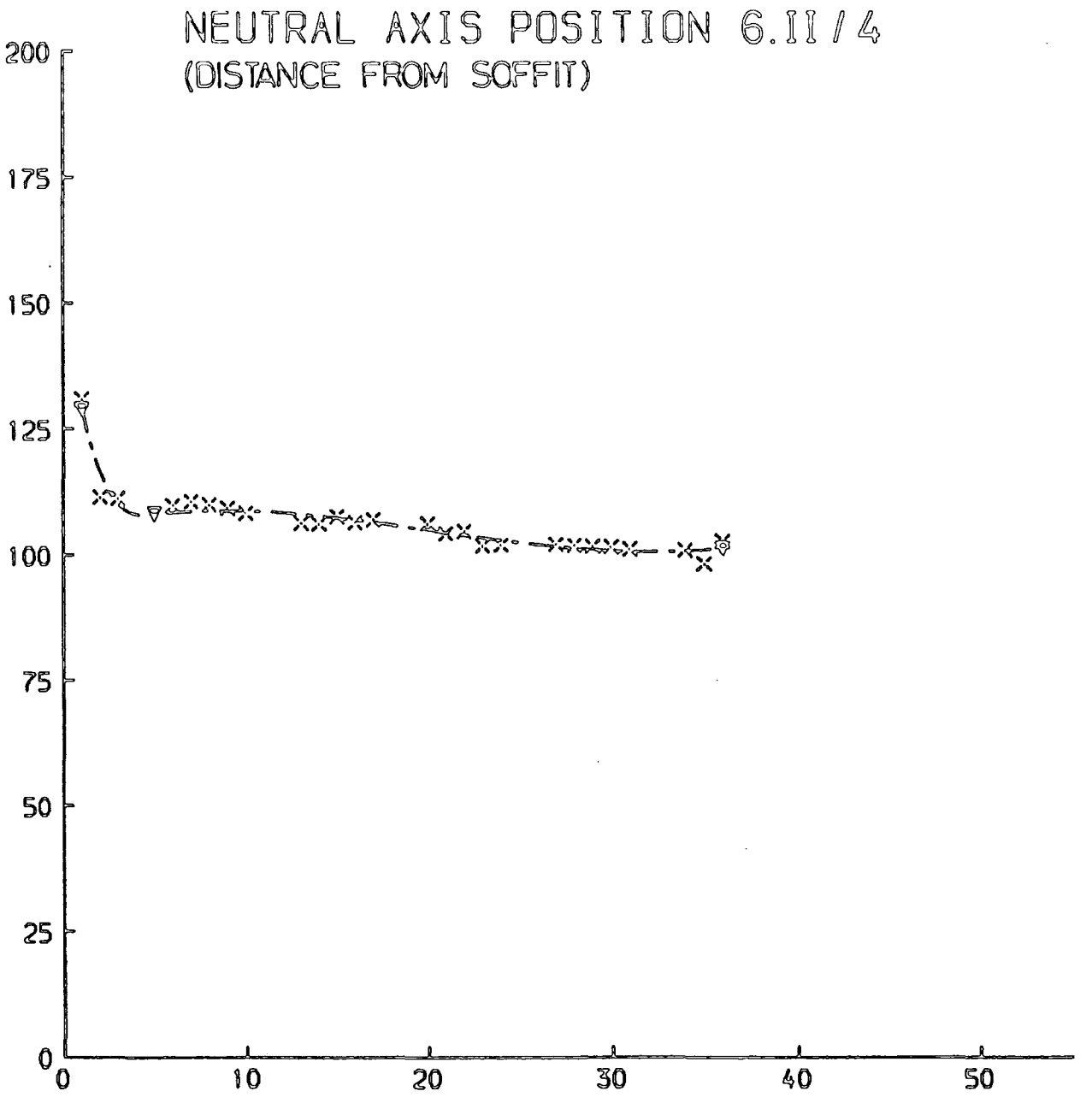
NEUTRAL AXIS POSITION 6.11/4
(DISTANCE FROM SOFFIT)
200
175
150
125
100
75
50
25
0
0
10
20
30
40
50

FIG. 6.11.13.

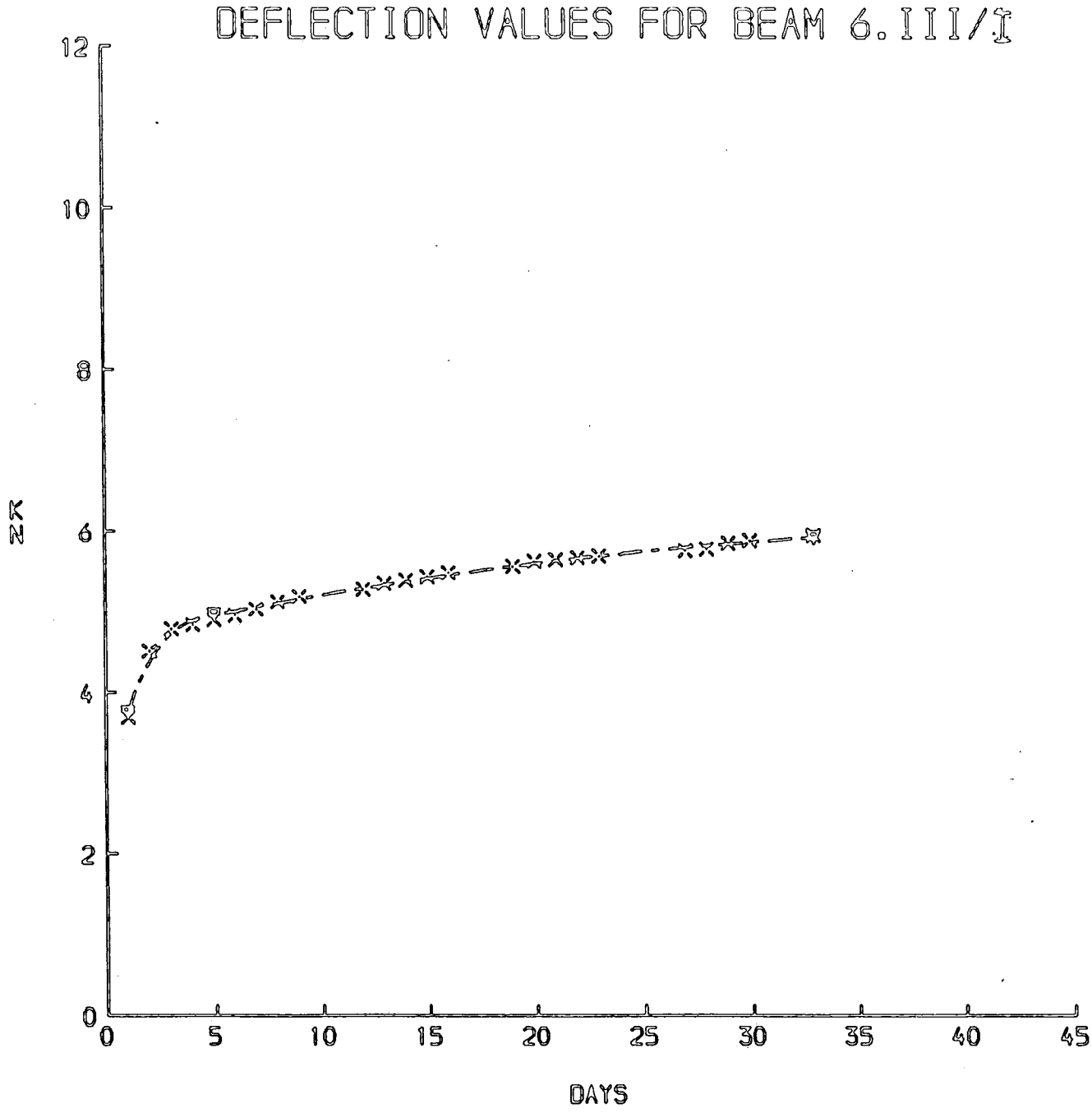
DEFLECTION VALUES FOR BEAM 6.III/I
12
10
8
6
4
2
0
ZK
0
5
10
15
20
25
30
35
40
45
DAYS

FIG. 6.III.1.

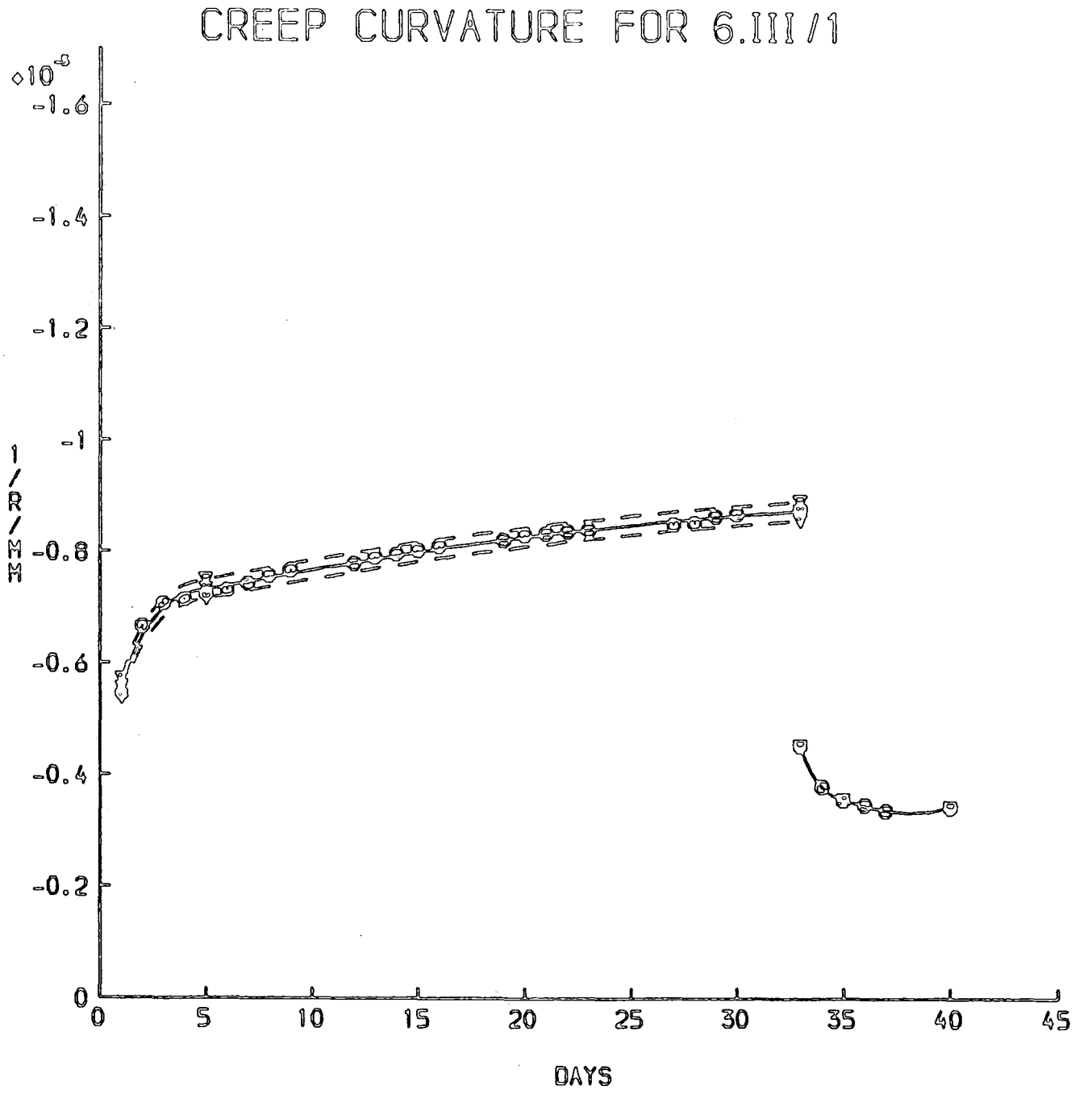
CREEP CURVATURE FOR 6.III/1
◇10⁻³
-1.6
-1.4
-1.2
-1
-0.8
-0.6
-0.4
-0.2
0
1/R/MM
0
5
10
15
20
25
30
35
40
45
DAYS

FIG. 6.III.2.

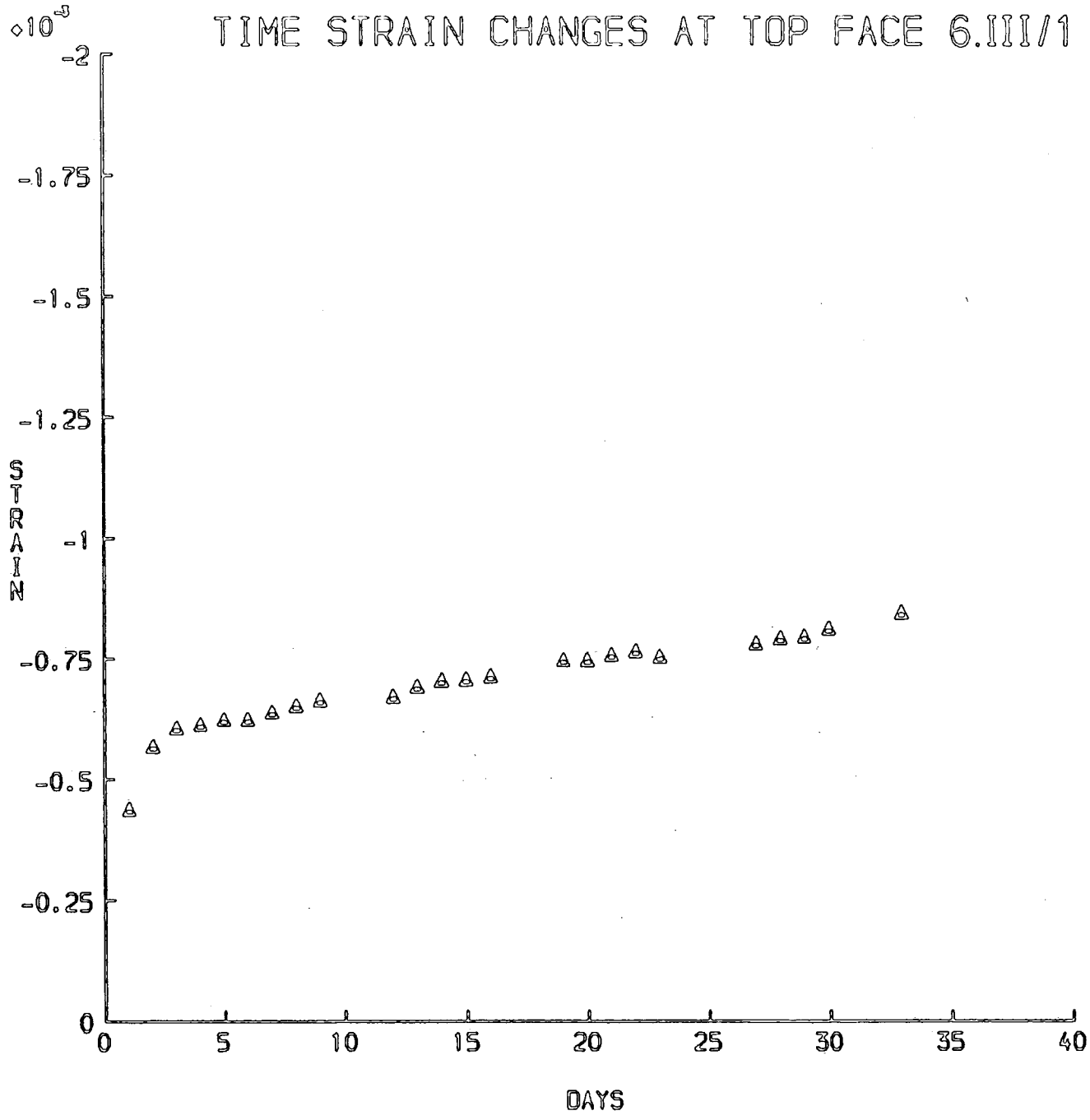
TIME STRAIN CHANGES AT TOP FACE 6.III/1
◇10⁻³
-2
-1.75
-1.5
-1.25
-1
-0.75
-0.5
-0.25
0
STRAIN
0
5
10
15
20
25
30
35
40
DAYS

FIG. 6.III.3.

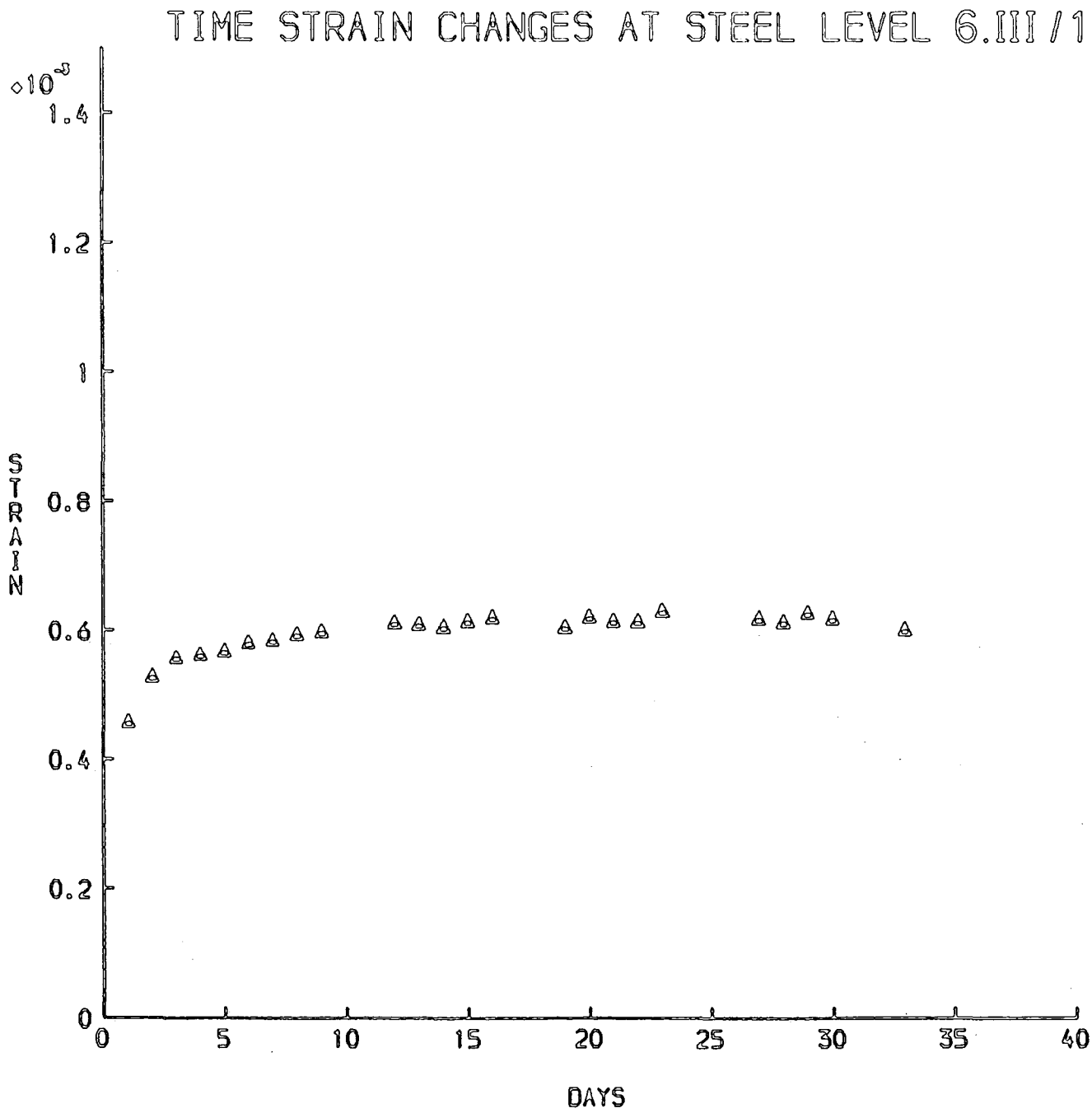
TIME STRAIN CHANGES AT STEEL LEVEL 6.III/1
◇10⁻³
1.4
1.2
1
0.8
0.6
0.4
0.2
0
STRAIN
0
5
10
15
20
25
30
35
40
DAYS

FIG. 6.III.4.

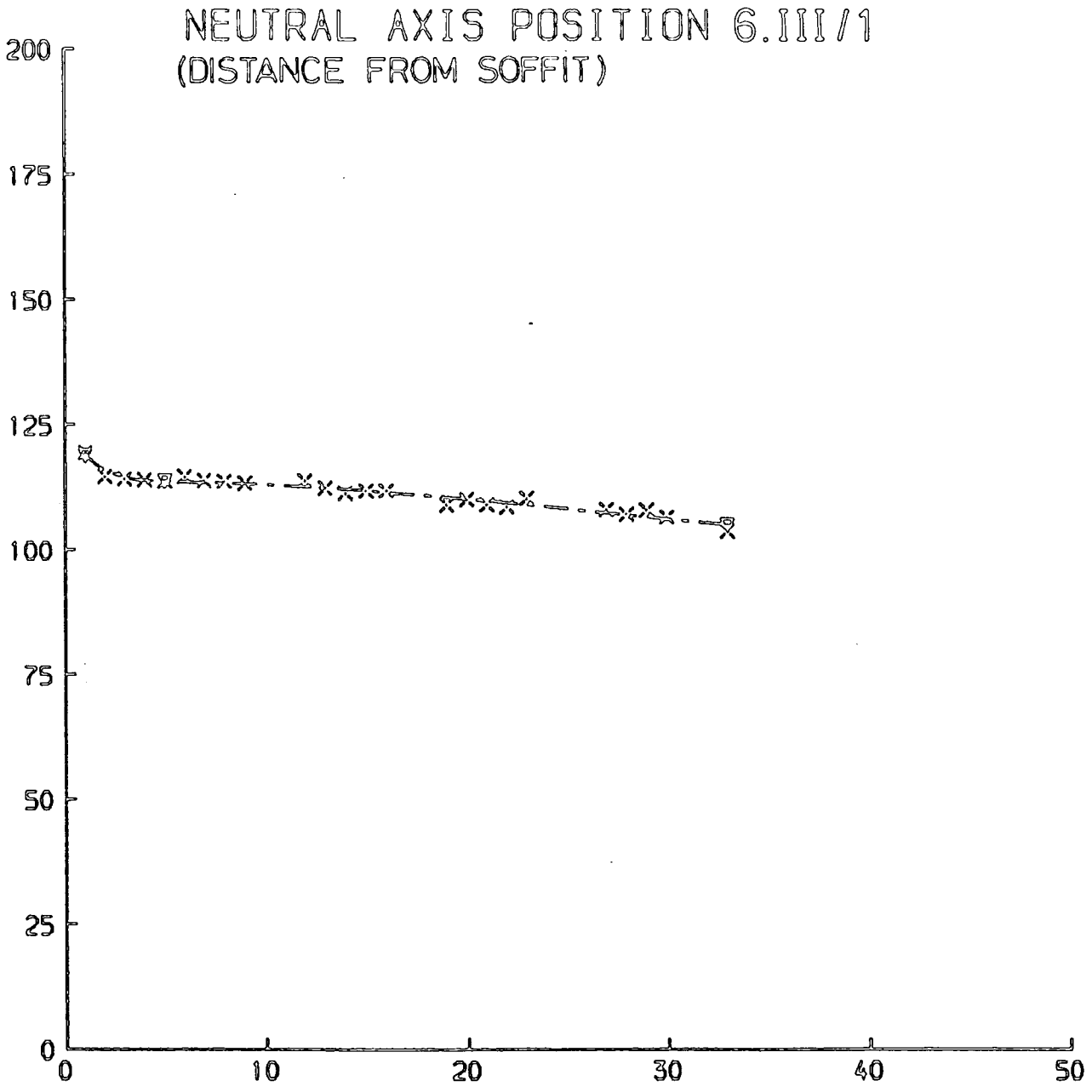
NEUTRAL AXIS POSITION 6.III/1
(DISTANCE FROM SOFFIT)
200
175
150
125
100
75
50
25
0
0
10
20
30
40
50

FIG. 6.III. 5

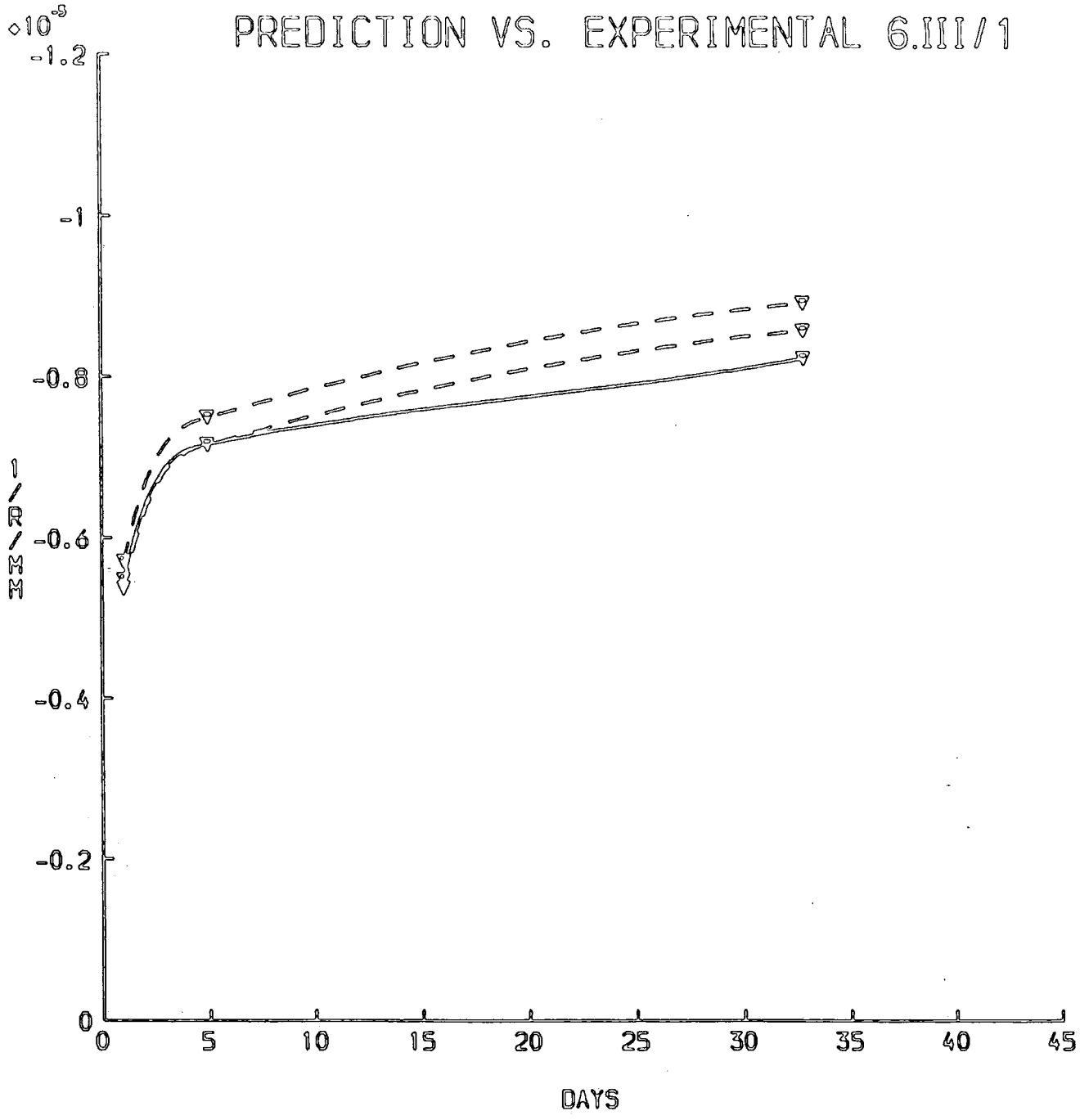
PREDICTION VS. EXPERIMENTAL 6.III/1
◇10⁻³
-1.2
-1
-0.8
-0.6
-0.4
-0.2
0
1/R/MM
0
5
10
15
20
25
30
35
40
45
DAYS

FIG. 6.III.6

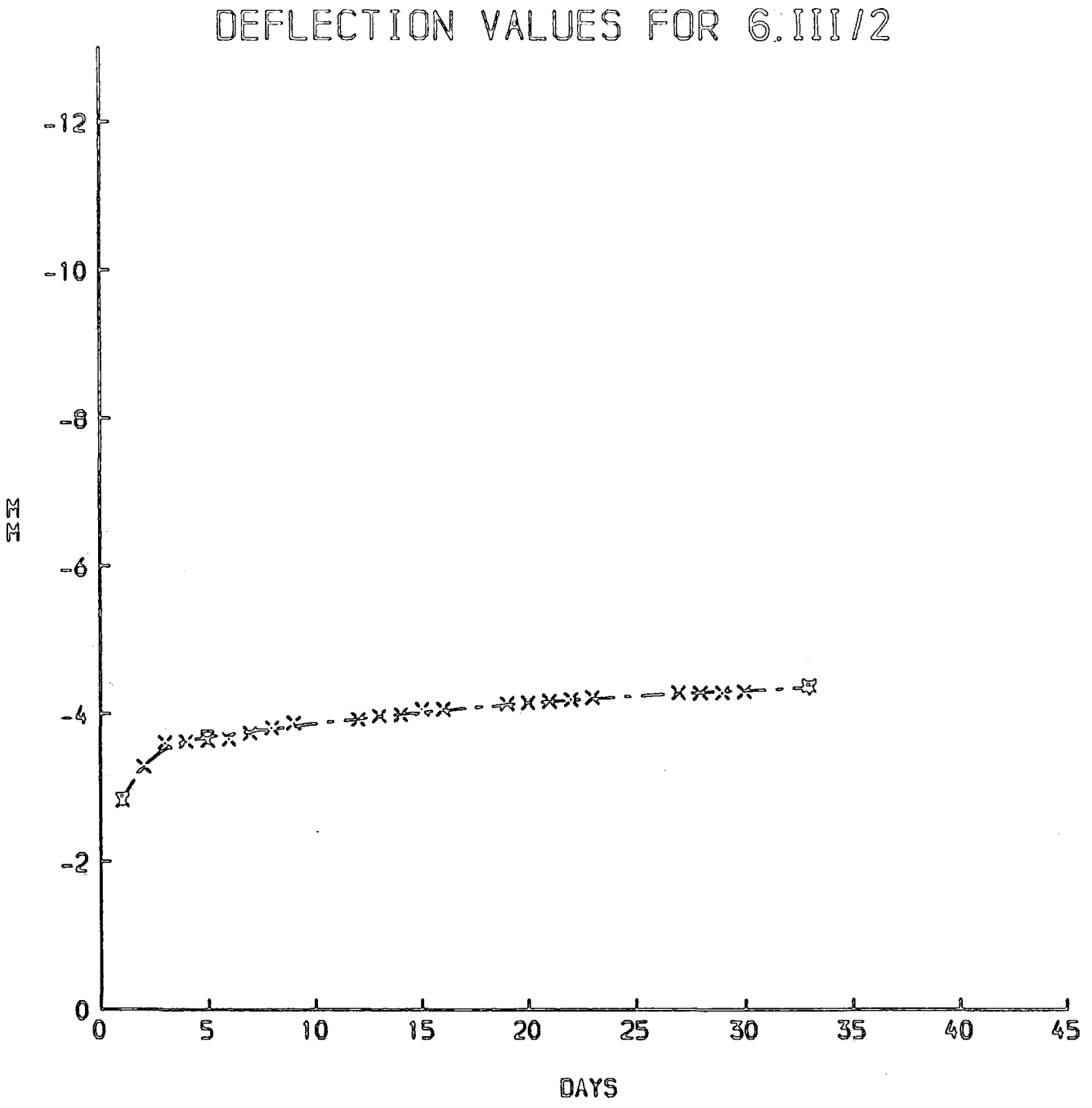
DEFLECTION VALUES FOR 6.III/2
-12
-10
-8
-6
-4
-2
0
MM
0
5
10
15
20
25
30
35
40
45
DAYS

FIG. 6.III. 7.

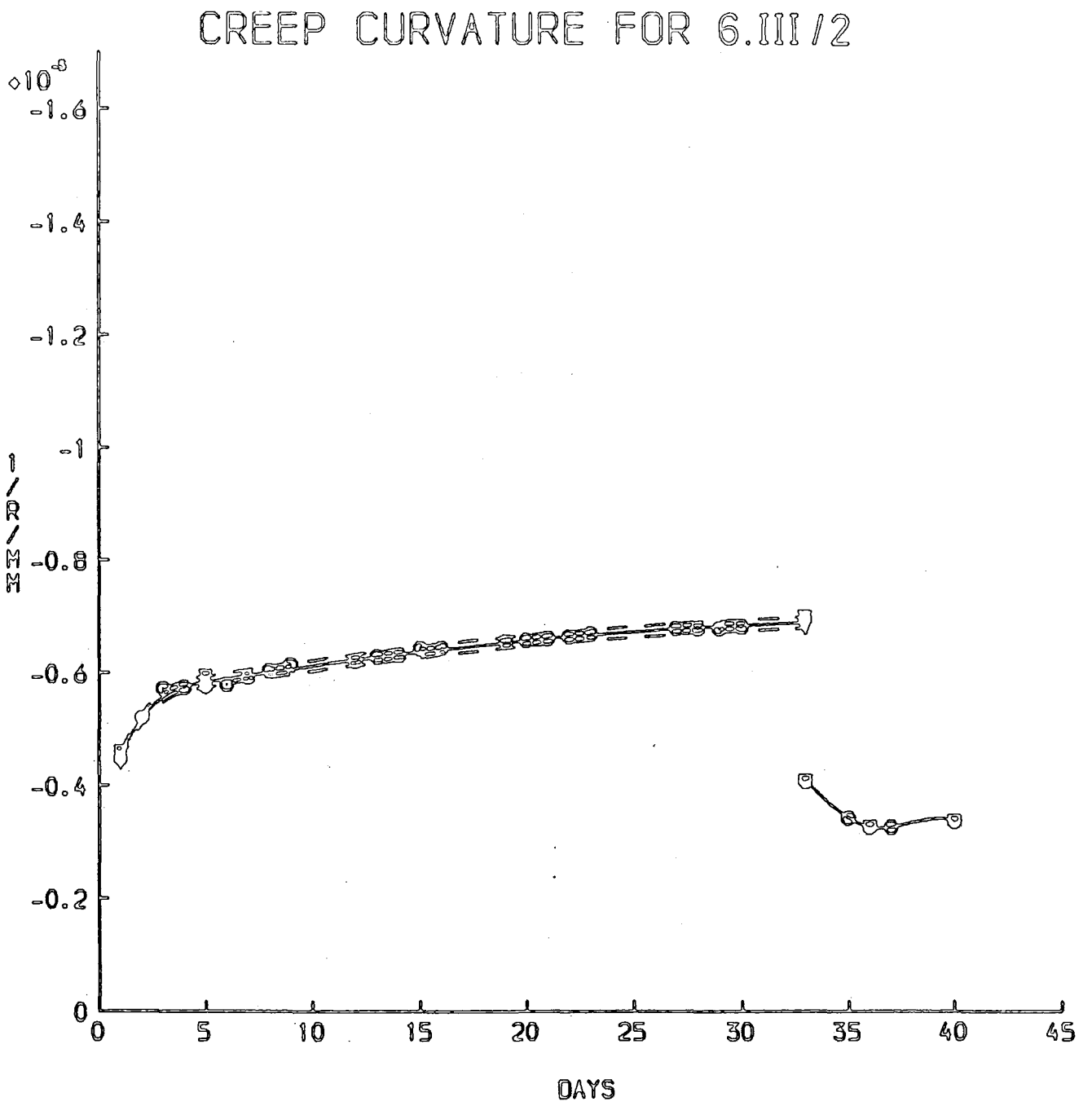
CREEP CURVATURE FOR 6.III/2
◇10⁻⁵
-1.6
-1.4
-1.2
-1
-0.8
-0.6
-0.4
-0.2
0
1/R/MM
0
5
10
15
20
25
30
35
40
45
DAYS

FIG. 6.III.8.

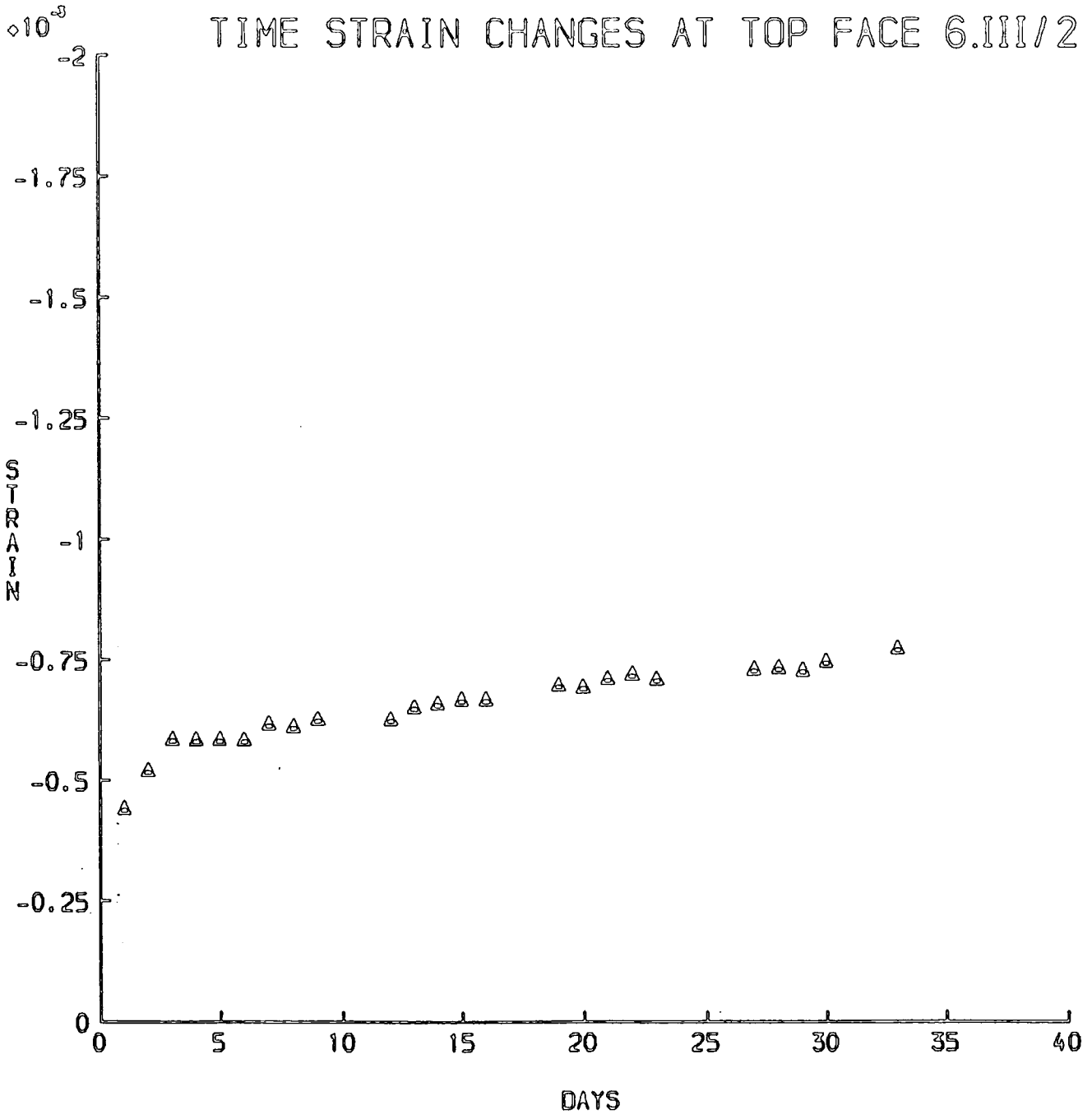
TIME STRAIN CHANGES AT TOP FACE 6.III/2
$\diamond 10^{-3}$
-2
-1.75
-1.5
-1.25
-1
-0.75
-0.5
-0.25
0
STRAIN
0
5
10
15
20
25
30
35
40
DAYS

FIG. 6.III.9.

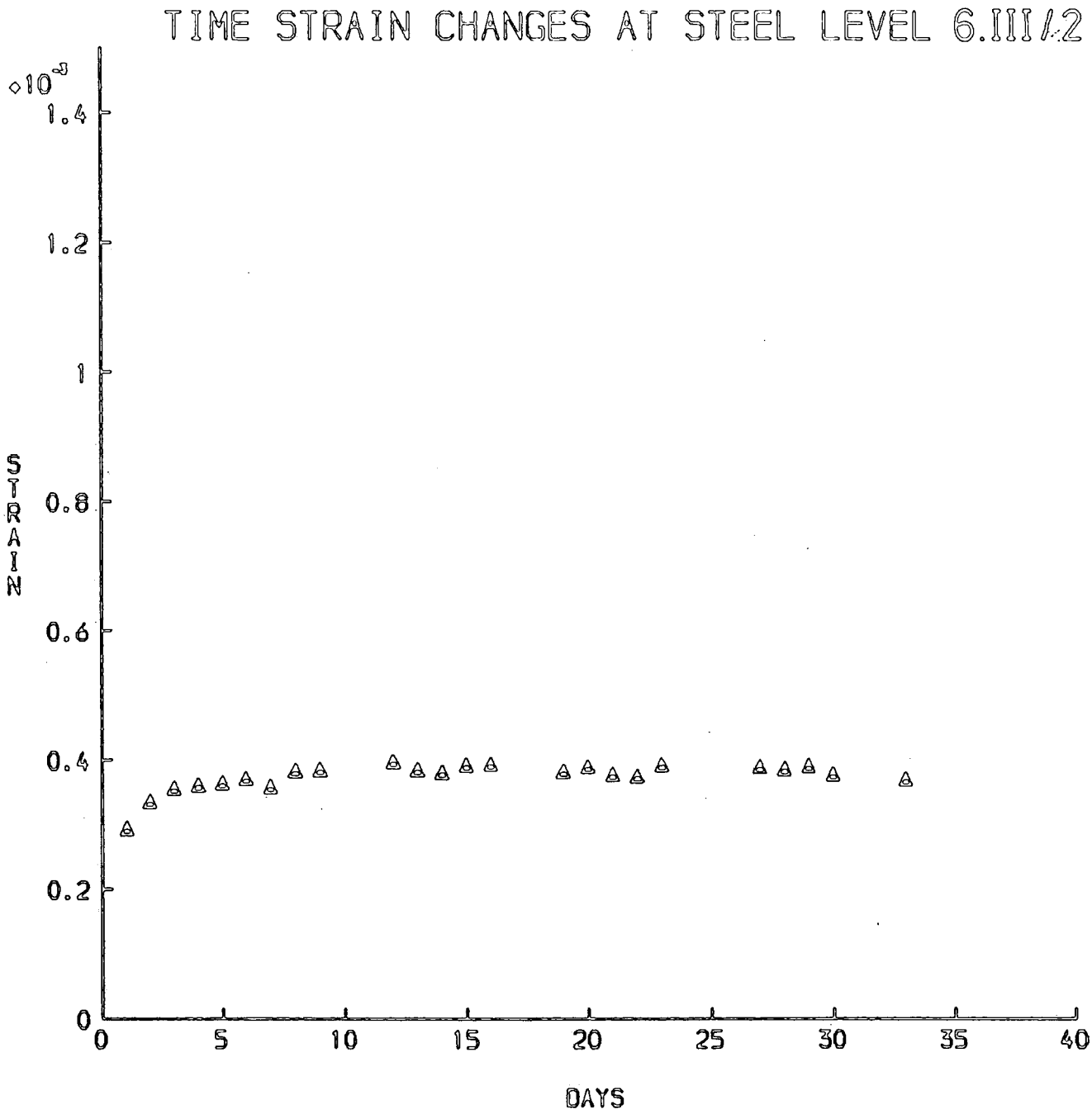
TIME STRAIN CHANGES AT STEEL LEVEL 6.III/2
◇10⁻³
1.4
1.2
1
0.8
0.6
0.4
0.2
0
STRAIN
0
5
10
15
20
25
30
35
40
DAYS

FIG. 6.III.10

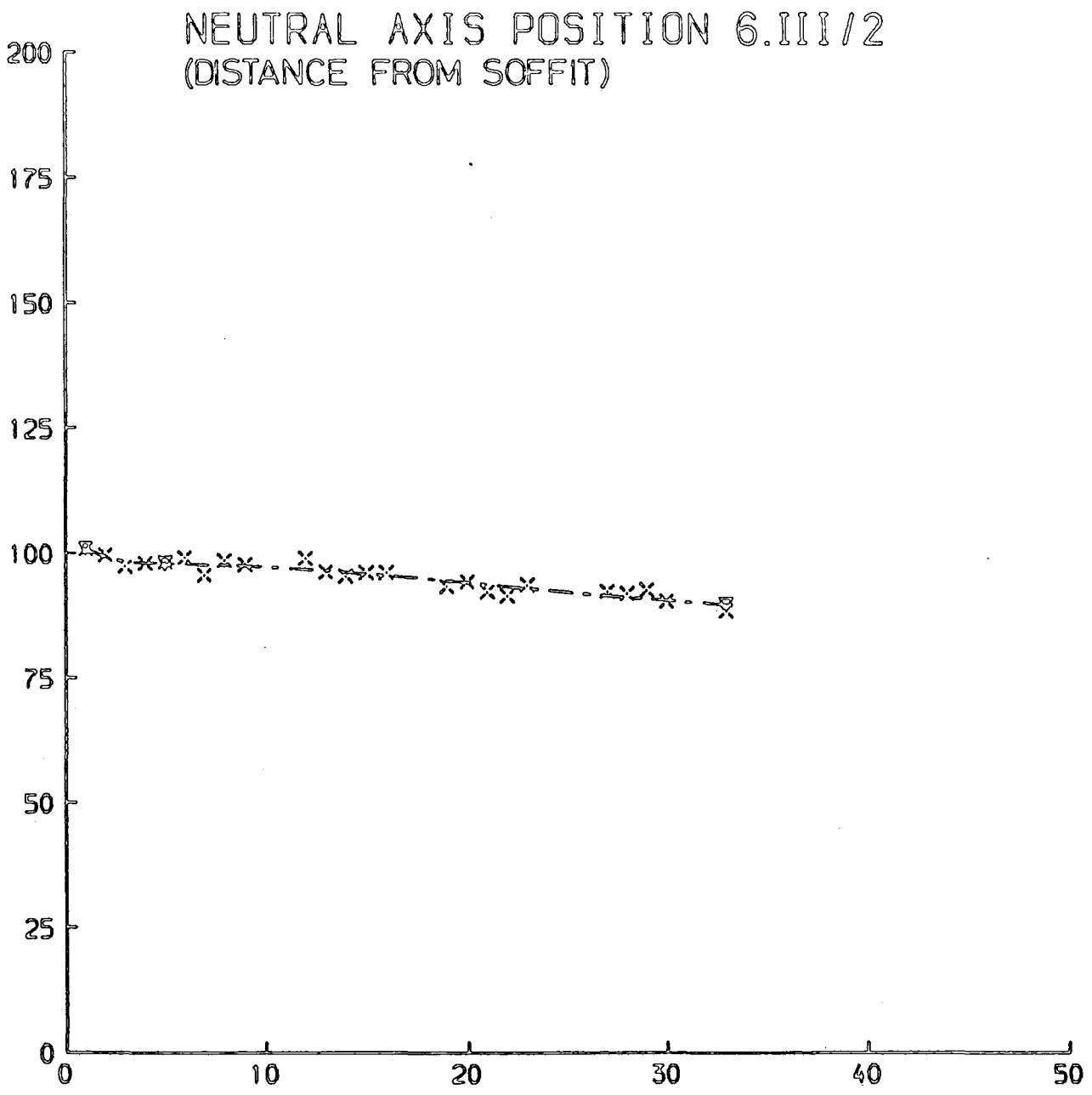
NEUTRAL AXIS POSITION 6.III/2
(DISTANCE FROM SOFFIT)
200
175
150
125
100
75
50
25
0
0
10
20
30
40
50

FIG. 6.III. 11.

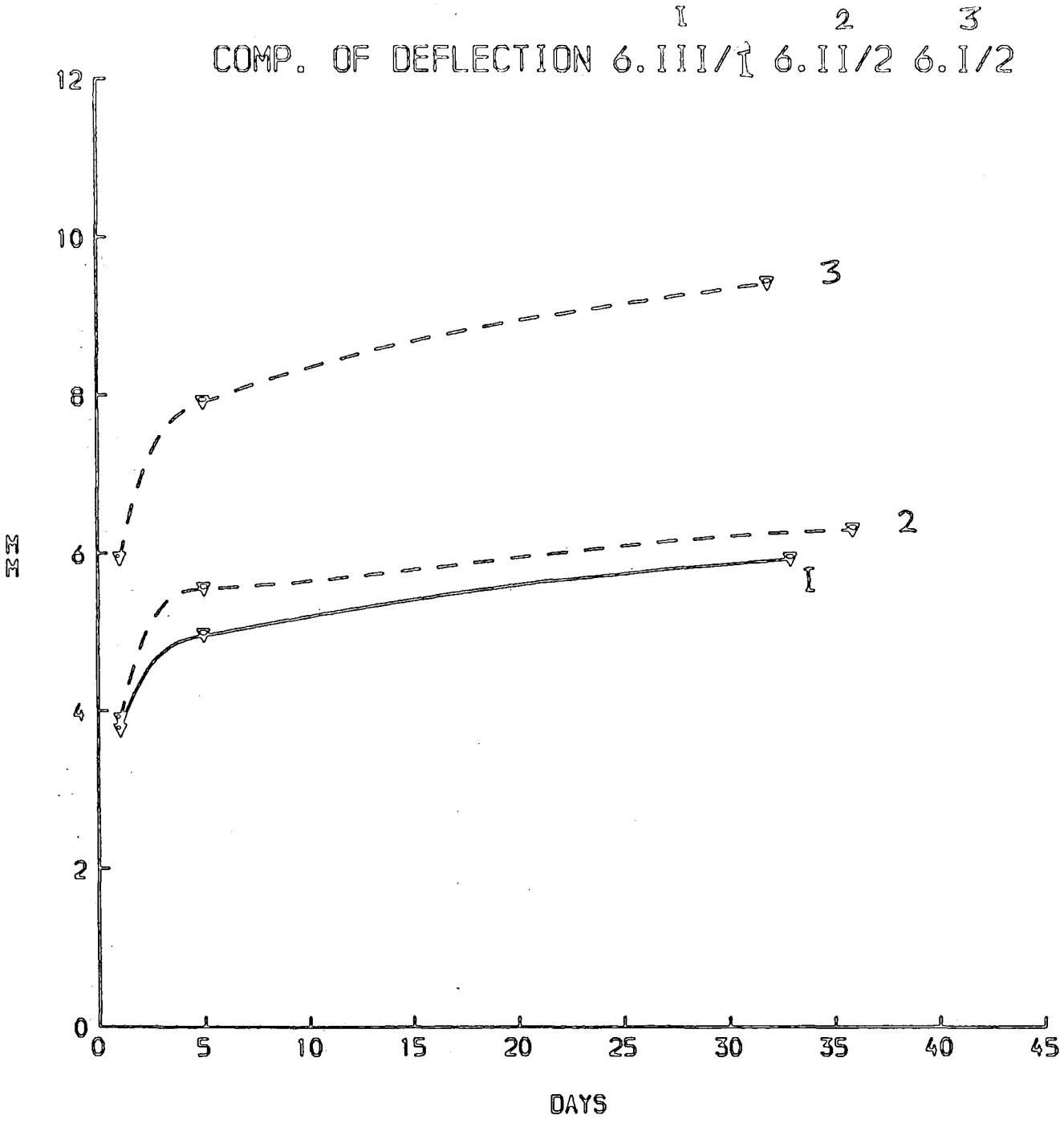
COMP. OF DEFLECTION 6.III/1 6.II/2 6.I/2
1
2
3
12
10
8
6
4
2
0
MM
0
5
10
15
20
25
30
35
40
45
DAYS

FIG. 6.4.1.

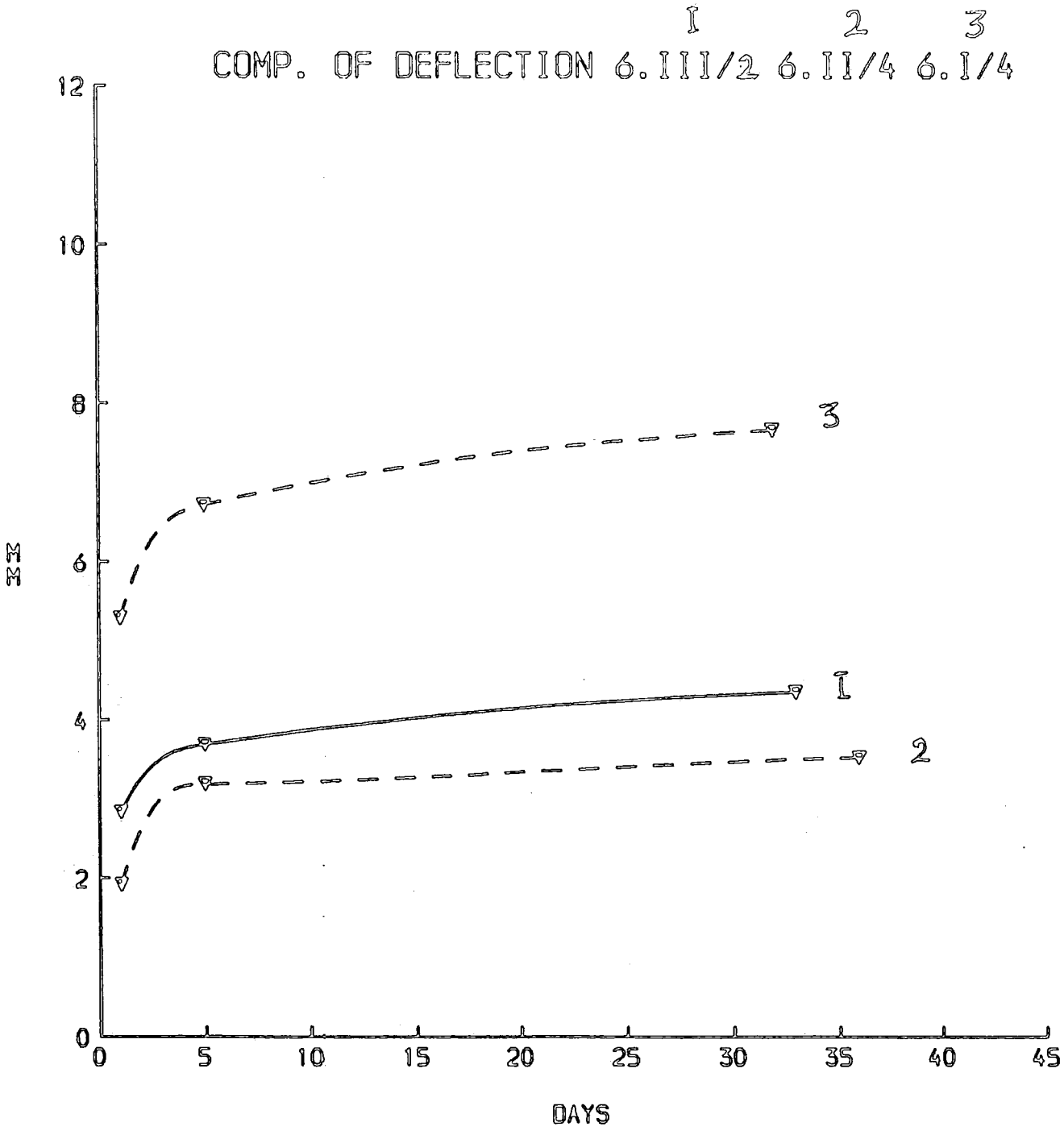
COMP. OF DEFLECTION 6.III/2 6.II/4 6.I/4
1
2
3
MM
12
10
8
6
4
2
0
0
5
10
15
20
25
30
35
40
45
DAYS

FIG. 6.4.2.

CHAPTER 7

RESULTS OF TEST UNDER ORDINARY LABORATORY ENVIRONMENTAL CONDITIONS AND COMPARISON WITH TESTS 6.I, 6.II and 6.III

7.I. Results of test under ordinary laboratory environmental conditions

7.I.1 Introduction

In this test four beams are discussed. Two were partly sealed, and two were unsealed. All four beams were tested in the laboratory under normal ambient conditons (20 + 1.5°C and 50% ± 5R.H). They were subjected to the following conditions.

Table 7.I.1

Beam	Sealing	Dimension	Heat Conditions	Applied Moment KN-m
7.I/1	Partly Sealed	1.0m	Under ordinary	0.0
7.I/2		2.8m	environmental	6.1 KN-m
7.I/3	Unsealed	1.0m	conditions	0.0
7.1/4	Unsealed	2.8m		5.53 KN-m

Beam 7.I/2 was the bottom beam on the loading rig (discussed in 4.2) and beam 7.I/4 was the top beam.

The object of this test was to compare results obtained with the previous tests, in order to obtain more insight into the effects of humidity and temperature values used in the previous tests.

7.I.2 Strain response of the beams

7.I.2.1 Introduction

In this section, the results of the strain responses of the four beams 7.I/1, /2, /3 and /4 are presented and analysed.

Curvatures, deflections and strain parameters were calculated and plotted using the techniques described in 3.4.2.

7.I.2.2 Beam 7.I/1 shrinkage companion to beam 7.I/2

Results and discussion

Beam 7.I/1 was the shrinkage companion to beam 7.I/2, in that it was subjected to identical conditions, except that it was not mechanically loaded. The beam was partly sealed.

Figure 7.I.1 is a plot of curvature changes with time due to shrinkage. The datum was taken at 21 days after casting, coincident with the loading of beam 7.I/1 and /4.

Shrinkage curvature reached a maximum of approximately 0.45×10^{-6} in 22 days then it started to decrease to reach a value of about 0.38×10^{-6} thirty six days from datum. This behaviour can be explained by the same reasons discussed in 5.I.2.2. except that the beam took longer time to reach its maximum hogging curvature, about twenty days as compared to about 6 days in test 5.I.

Steel stress as estimated from concrete strain at steel level, and using an elastic modulus value of $2.1 \times 10^5 N/mm^2$ was about 20.4 N/mm^2 thirty six days from datum.

Top face concrete had shortened by approximately 40 microstrain in thirty six days, while bottom fibres had shortened by approximately 100 microstrain during the same period.

7.I.2.3 Beam 7.I/2, loaded and partly sealed

Results

Beam 7.I/2 was loaded in four point bending at 21 days after casting, such that the central portion carried a sustained moment of 6.1KN-m. This moment corresponded to 48% of the ultimate moment of the beam as calculated in accordance with CP110, and about 1.88 of the theoretical cracking moment using a modulus of rupture of 4.2 N/mm^2. The beam showed visible cracks on loading.

Figure 7.I.2-5 are plots against time of midspan deflections, curvatures, top concrete strains, and concrete strains at steel level.

Figure 7.I.6 is a plot of change of neutral axis position with time.

Curvatures and deflection values were corrected for shrinkage, and allowances in the start-of-cycle temperatures from datum temperature was made in calculation of top concrete strains, strains of concrete at steel level and neutral axis position.

Table 7.I.2 summarises values from the graphs on loading and after 36 days of sustained loading.

Table 7.I.2

Parameter	On loading	After 36 days
Curvature	$-0.7 \times 10^{-5} mm^{-1}$	-0.92×10^{-5} mm^{-1}
Deflection	4.78 mm	6.26 mm
Top Strain	-0.61×10^{-3}	-0.94×10^{-3}
Neutral Axis	87mm	97.1 mm

Discussion

Table 7.I.3 gives values for creep deflections at various dates.

Table 7.I.3

Time under load (days)	Deflection (mm)	Increase in Def. due to creep	Creep/ Elastic
0	4.78	0	0
5	5.63	0.85	0.18
15	5.90	1.13	0.24
29	6.18	1.41	0.30
36	6.26	1.48	0.31

After 36 days of sustained loading, the span/deflection ratio was reduced from 523 on loading to 399. After five days creep deflection was about 58 per cent of its value after 36 days of sustained loading.

Table 7.I.4 gives values of the elastic and long-term deflections as compared to predictions by various codes.

Table 7.I.4

Method of determination	Source of Materials data	At midspan	
		Deflection on loading (mm)	Increase in Def. due to creep (mm)
CP110 : 1972(131)	C & CA (132)	4.89	1.42
ACI-435 (133) Effective Modulus	ACI-209 (134)	5.04	3.07
CEB-FIP	CEB-FIP (135)	4.84	1.47
Test		4.78	1.48

The measured elastic deflection was predicted reasonably closely by all the codes. Predicted value of creep deflection using CP110 underestimated creep by about 5%. However ACI overestimated the value considerably.

Figure 7.I.3 is a plot of changes of curvature with time. Its value on loading was -0.705×10^{-5}, and after 36 days of sustained loading it reached a value of -0.925×10^{-5}. Its value on unloading was -0.342×10^{-5}, giving an elastic recovery of -0.582×10^{-5}. This was about 83 per cent of its elastic value on loading. It decreased to a value of -0.277×10^{-5} fourteen days after unloading, which was a recovery of -0.65×10^{-6}. That is about 0.3 of the creep deflection was recovered in this period

Figure 7.I.7 is a plot of changes of curvature with time as predicted by the rate of creep method. The figure shows also the two bounded curves of measured experimental curvature. Results indicate that the prediction method underestimated creep for the first few days, but at later stages the slopes of the curvature curves were about equal. This can be explained by the same reasoning presented for beam 6.II/2, namely the effect of microcracking resulting from shrinkage prior to loading, and the increase of creep in flexure compared to uniaxial.

Top surface strain had changed from a value of -0.61×10^{-3} on loading to a value of $-.94 \times 10^{-3}$ thirty six days after loading, giving a ratio of 1:1.54.

Ross's hyperbola gives an estimate of limiting creep plus elastic strain value of -0.99×10^{-3}, clearly an underestimate. The ten years value as predicted by Brook's (136) expression is -0.139×10^{-2}.

Strain of concrete at steel level had changed from a value of 0.55×10^{-3} on loading to a value of 0.66×10^{-3} thirty six days after loading. Changes of strain at steel level was very small except in the first few days of loading. At this level creep was offset by the following factors. First the reduction of the lever arm due to the lowering of the neutral axis thus reducing creep. Secondly, shrinkage curvature was hogging upward particularly for the first 25 days. This curvature was opposite to creep curvature. Thirdly, there was a shortening of the beam due to shrinkage with hydration and moisture loss.

7.I.2.4 Beam 7.I/3 shrinkage companion to beam 7.I/4

Results and discussions

Beam 7.I/3 was a shrinkage companion to the top beam. It was unsealed.

Figure 7.I.8 is a plot of curvature with time due to shrinkage only. The datum was taken at 21 days after casting (i.e. the date of loading of beam 7.I/4).

Shrinkage curvature reached a maximum of 0.9×10^{-6}. This corresponds to 39% of the 30 years curvature value predicted by the equivalent tensile force, and data supplied by reference (86).

Steel stress as estimated from strain of concrete at steel level and using an elastic modulus of 2.1×10^{-5} N/mm^2 was about 40.8 N/mm^2 thirty six days from datum. Top fibre concrete had shortened by approximately 340 microstrain in thirty six days, while the bottom fibre had shortened by approximately 180 microstrain during the same period.

7.I.2.5 Beam 7.I/4 loaded and unsealed

Results

Beam 7.I/4 was loaded in four point bending, at 21 days after casting, such that the central portion carried a sustained moment of 5.53 KN-m. This moment corresponded to 43% of the ultimate moment of the beam as calculated in accordance with CP110, and about 1.7 of the theoretical cracking moment using a modulus of rupture of 4.2N/mm^2. The beam was cracked on loading.

Figures 7.I.9-12 are plots against time of midspan deflections, curvature, top concrete strains and concrete strain at steel level. The two bounded curves are the 95% confidence interval for curvature.

Figure 7.I.13 is a plot of change of neutral axis position with time.

Table 7.I.5 summarises values from the graph on loading and after 36 days of sustained loading for curvature, deflection, extreme concrete compression strain, and neutral axis position. Curvature and deflection values were adjusted to remove shrinkage strain (from 7.I/3), so that effects shown were due to creep alone. Allowance for differences in the start-of-cycle temperature from datum temperature was made in calculating extreme concrete compression strain, concrete strain at steel level and neutral axis position.

Table 7.I.5 response of beam 7.I/4 to sustained loading.

Parameter	On loading	After 36 days
Midspan curvature	-0.65×10^{-5}mm^{-1}	0.10×10^{-4}mm^{-1}
Midspan deflection	4.09mm	6.6 mm
Extreme concrete compression strain	-0.64×10^{-3}	-0.13×10^{-2}
Neutral axis position	98.6mm	125.7mm

B. Discussion

Table 7.I 6 lists values of deflection at various dates.

Table 7.I.6

Time after loading (days)	Deflection (mm)	Increase in Def. due to creep	Ratio of increase
0	4.09	0	0
5	5.10	1.01	0.25
15	5.87	1.78	0.44
29	6.47	2.38	0.58
36	6.60	2.51	0.61

Creep deflection for the first five days was abut 40 per cent of its value after 36 days of sustained loading. Its rate of increase in the last seven days was 0.019 mm/day. This is almost equal to the rate at similar period for the heated beam 6.I/4.

Table 7.I.7 gives values of the elastic and long term deflections as compared to predictions by various codes.

Table 7.I.7

Method of determination	Source of Material data	At midspan	
		Elastic Deflection	Increase in Def. due to creep
CP110:1972 (131)	C & CA (132)	4.06	1.21
ACI-435 (133)	ACI-209 (134)	4.07	2.48
Effective modulus	CEB-FIP (135)	3.88	1.36
Test	-	4.09	2.51

All the codes gave good prediction of the immediate deflection measured in the beam.

Figure 7.I.10 is a plot of changes of curvature with time. Its value on loading was -0.648×10^{-6}. It reached a value of -0.105×10^{-4} thirty six days after loading. Its value on unloading was -0.582×10^{-5}, giving an elastic recovery of -0.464×10^{-5}. This was about 72 per cent of its elastic value on loading. The residual curvature one week after unloading had decreased to a value of -0.505×10^{-5}, corresponding to a recovery of -0.77×10^{-6}. That is about 0.19 times of creep deflection was recovered in this period. This is a lot less than the similar value obtained for the partly sealed beam 7.I/2

Figure 7.I.14 is a plot of changes of curvature with time as predicted by the rate of creep method. Results in the figure indicate that the method underestimated measured experimental creep at all times. However the correlation was better at early stages, with the gap widening up with time. This can be explained by the following reasons: creep in flexure is larger than uniaxial creep, at all times, however at early stages because of the high surface to volume ratio for the cylinder its drying creep was high at early stages thus reducing the gap between its value and the beam. At later

stages the cylinder started to desiccate faster than the beam thus reducing its drying creep and widening the gap between its creep values and the measured creep values for the beam.

Extreme compression strain had changed from a value of -0.64×10^{-3} on loading to a value of 0.13×10^{-2} after 36 days of sustained loading, giving a ratio of 1:2.03. This is a lot higher than the similar value for the partly sealed beam 7.I/2 even though the applied moment of this beam is lower than that of beam 7.I/2. This is due to the effect of shrinkage.

Concrete strain at steel level had changed from a value of 0.43×10^{-3} on loading to a value 0.41×10^{-3} 36 days after loading. It reached its maximum value 0.46×10^{-3} on the second day after loading, decreasing afterwards.

This again was due to the lowering of the neutral axis and the shrinkage in the beam.

7.II Comparison of tests 6.I, 6.II and 6.III with 7.I

7.II.1 Introduction

Here a comparison is made of deflections (creep and elastic) of tests exposed to cyclic heating-cooling and humidity conditions (tests 6.I, 6.II and 6.III) with deflection of test exposed to normal (laboratory) ambient conditions (test 7.I) of constant temperature 20° ± 1.5°C and a relative humidity of 50% ± 5.

Beams were cured as described in 6.4.1. Also the bases of comparison were the same as was discussed in 6.4.2.

Test 6.I is unsealed, test 6.II/2 is partly sealed, test 6.III is completely sealed, beam 7.1/2 (bottom beam in the rig) is partly sealed, and beam 7.1/4 (top beam in the rig) is unsealed.

7.II.2 Comparison of beams 6.I/2, 6.II/2 and 6.III/1 with 7.I/2

Fig. 7.II.1 gives comparison of deflections for the four beams, while table 7.II.1 gives comparison of the chronological development of creep for the four beams.

Table 7.II.1 Comparison of beams 6.I/2, 6.II/2 and 6.III/1 with 7.I/2

Time under load (days)	Beam 7.I/2 Partly sealed value (mm)	Beam 6.I/2 (unsealed) Value (mm)	Ratio to 7.I/2	Beam 6.II/2 (partly sealed) Value (mm)	Ratio to B.7.I/2	Beam 6.III/1 (completely sealed) Value (mm)	Ratio to 7.I/2
1 - 6	0.88	2.11	2.40	1.71	1.94	1.28	1.45
6 - 32	0.56	1.38	2.46	0.65	1.16	0.97	1.73
1 - 32	1.43	3.49	2.43	2.35	1.64	2.24	1.57
Elastic	4.78	5.82	1.22	3.86	0.81	3.69	0.77
Ratio of 32 creep to elastic	0.30	0.60		0.61		0.61	
Ratio of 6 days to 32	0.61	0.6		0.72		0.57	

Beams 6.I/2, 6.II/2 and 6.III/1 were insulated from the sides and top. All the four beams had an applied moment of 6.1KN-m. They all had noticeable cracks on loading.

Results in table 7.II.1 show that although the total creep of beams 6.I/2, 6.II/2 and 6.III/1 were each larger than 7.I/2 there were differences in the ratios of early creep and of later creep. For example in beam 6.II/2 which was similar to beam 7.I/2, in that it was partly sealed, results show that the ratio of the six days creep was 1.94, but it dropped to 1.16 for later creep. In fact the graph shows that the two plots of curvature (Figure 7.II.1) almost coincide with each other after early creep stage. In the case of beam 6.III/1 (which is completely sealed) the ratio actually increased from 1.45 to 1.73, and in the case of beam 6.I/2 (which was unsealed), the ratio varied very little. This again (as had been discussed in 6.4) demonstrates the complex nature of the influence of temperature and humidity on flextural creep with various sealing conditions.

Comparing the elastic deflection of beam 7.I/2 to that of beam 6.II/2, the results show that the three days of cyclic heating before loading had reduced the elastic deflection by about 20%. This is in contrast to the effect of early cyclic heating on the unsealed beams (beams 6.I/2 and 5.III/2), where the three days preloading cyclic heating had increased the elastic deflection by about 18%.

The table shows that the effect of temperature on the partly sealed is two fold, it decreased the elastic deflection, but it also increased creep deflection. The total deflection of beam 7.I/2 after 32 days of sustained loading was 7.49mm as compared with 7.50mm for beam 6.II/2. The near equality here for the deflections of the two beams is not significant, since they are expected to be different at later times.

Ratios of the thirty two days creep deflection to elastic deflection for the three heated beams were approximately the same, and different from that of beam 7.I/2. This difference is expected, since, although all the beams were cured in a similar way, except for the three days prior to loading, heating/cooling and humidity cycles the creep of beam 7.I/2 had developed under a different environmental condition than those of beams 6.I/2, 6.II/2 and 6.III/2.

7.II .3 Comparison of beams 6.I/4, 6.II/4, and 6.III/2 with 7.I/4.

Fig. 7.II.2 gives a comparison of deflection for the four beams, while table 7.II.2 gives comparison of the chronological development of creep.

Table 7.II2 Comparison of beams 6.I/4, 6.II/4, 6.III/2 with 7.I/4

Time under load	Beam 7.I/4 (unsealed) Value (mm)	Beam 6.I/4 (unsealed) Deflection	Ratio	Beam 6.II/4 (partly sealed) Deflection	Ratio	Beam 6.III/2 (completely sealed) Deflection	Ratio
1 - 6	1.15	1.49	1.3	1.22	1.06	0.84	0.73
6 - 32	1.38	0.94	0.68	0.42	0.30	0.71	0.51
1 - 32	2.44	2.43	1.	1.64	0.67	1.55	0.64
Elastic	4.09	5.20	1.27	1.86	0.45	2.82	0.69
Ratio of 6 days to total creep	0.47	0.61		0.74		0.54	
Ratio of 32 days to elastic	0.60	0.47		0.88		0.55	

All the beams here are uninsulated, and not surface-heated. Beams 6.I/4, 6.II/4 and 6.III/2 are compared to beam 7.I/4. Beams 6.I/4, 6.II/4 and 6.III/2 were exposed to heating cooling and humidity cycles, while beam 7.I/4 was exposed to normal (laboratory) ambient conditions of 20°+ 1.5° temperature and 50% ± 5 relative humidity.

All the beams had an applied moment of 5.53 KN-m, and they all were cracked on loading except beam 6.II/4.

Results in the table shows that the ratio of the six days creep for the two unsealed beams was 1.3. This value dropped to 0.68 for later creep. This is interesting and shows that the effect of drying creep was only pronounced at early stages. At later stages, beam 6.I/4 was desiccated under the effect of high temperature and low humidity, and lost some of its potential to creep. Their total 32 days creep were about equal. The three days preloading cyclic heating-cooling and humidity conditions had increased the elastic deflection of beam 6.I/4 by 27% over that of beam 7.I/4. This is significant and highlights the importance of curing in the hot and dry climate.

The ratio of 6 days creep deflection of beams 6.II/4 (partly sealed) and 6.III/2 (completely sealed) to beam 7.I/4 were 1.06 and 0.84 respectively. It dropped considerably for later creep in beam 6.II/4 to only 0.3, and only dropped slightly in beam 6.III/2 to 0.71. Their 32 days creep deflection was less than that of beam 7.I/4, even though beam 7.I/4 was exposed to normal ambient conditions.

The ratio of the six days creep deflection to elastic deflection is about the same for all the beams except for the uncracked beam 6.II/4.

The ratios of the six days creep deflection to the 32 days creep deflection are similar to values in table 7.II.1 except that beam 7.I/4 had a smaller ratio than the partly sealed beam 7.I/2. Also the six to 32 days creep deflection ratios for beam 6.II/2 and 6.II/4 is similar even though that beam 6.II/2 was cracked and beam 6.II/4 was not.

The ratio of the thirty two days creep to elastic of beams 6.I/4, 6.III/4 and beam 7.I/4 were close to each other and different than that of beam 6.II/4, since it was uncracked on loading. The similarity of the ratio for beam 7.I/4 to those of beams 6.I/4 and 6.III/4 is probably accidental, and is expected to be different for different shapes of beams. This is so since beam 7.I/4 was not sealed and lost as much moisture as the heated beams as its comparison with beam 6.I/4 shows.

These results demonstrate the complex nature of the effect of temperature and humidity and the major effect of sealing (or lack of it) on the chronological development of creep. Also the results demonstrate the importance of the early creep particularly for the heated beams.

7.II.4 Conclusions

First conclusions drawn from the comparisons of beams 6.I/2, 6.II/2 and 6.III/1 (exposed to heating-cooling and humidity cycles) with the partly sealed beam exposed to normal ambient conditions.(beam 7.I/2)

The ratios of the thirty two days creep deflections of the different beams under temperature and humidity cycling to the partly sealed beam exposed to normal ambient conditions were 1.56, 1.67 and 2.43 for the completely sealed, partly sealed and unsealed respectively. However, the ratios were not constant throughout the time of the test and the ratio for the partly sealed beam in particular varied during the test.

The ratios of the six days creep deflection to the thirty two days creep deflection for the various beams were close to each other except for the partly sealed, where the ratio was considerably higher.

The ratios of the thirty two days creep to elastic for the surface heated and insulated beams were about equal.

Second, comparison with the unsealed beam under normal ambient conditions.

The ratios of the thirty two days creep deflection of the different beams to the value of the unsealed beam exposed to normal ambient conditions were 0.64, 0.67 and 1.0 for the comletely sealed, partly sealed and unsealed beams. That is, the partly sealed and completely sealed had actually lower creep deflection values even though they were exposed to heating-cooling and humidity cycles.

The behaviour of the unsealed beam under heating-cooling and humidity cycles showed that the creep deflection for this beam for the first six days of loading was 1.30 times the creep deflection for the first six days of loading of the unsealed beam under normal ambient conditions. However, after the first six days, the rate of creep for the beam under heating-cooling and humidity cycles was much lower than the rate of creep for the unsealed beam under normal ambient conditions. This indicates that the ultimate creep for unsealed beam under heating-cooling cycles would be less than the limiting creep deflection for the unsealed beam under normal ambient conditions. The effect of the three days preloading heating-cooling and humidity cycles were to increase elastic deflection for the unsealed beam by about 27%. This is in contrast to its effects on the elastic deflection of the completely sealed and partly sealed, where the

three days preloading heating-cooling and humidity cycles had reduced the elastic deflection by about 19% and 23% for the partly sealed and completely sealed respectively. This demonstrates the crucial importance of curing in the hot and dry climate particularly for small members.

The ratio of the first six days creep deflection to the thirty two days creep deflection for the unsealed beam under normal ambient conditions was considerably less than the comparable ratio for the partly sealed beam under normal ambient conditions and close to the comparable ratio of the completely sealed beam. This might be attributable to the symmetry of sealing.

Third: The value of the peak hogging shrinkage curvature for the partly sealed beams was approximately equal for both beams under heating cooling and humidity cycles and the beam under normal ambient conditions, although the latter value developed more slowly. This however was completely different for the unsealed beams where although the shape of the sagging shrinkage curvature with time was similar for the unsealed beams of tests exposed to heating and cooling and humidity cycles and the unsealed beams exposed to normal ambient temperature, the value of the maximum measured shrinkage curvature for tests under H/C and humidity cycle was as much as three times the shrinkage curvature for the beam under normal ambient conditions.

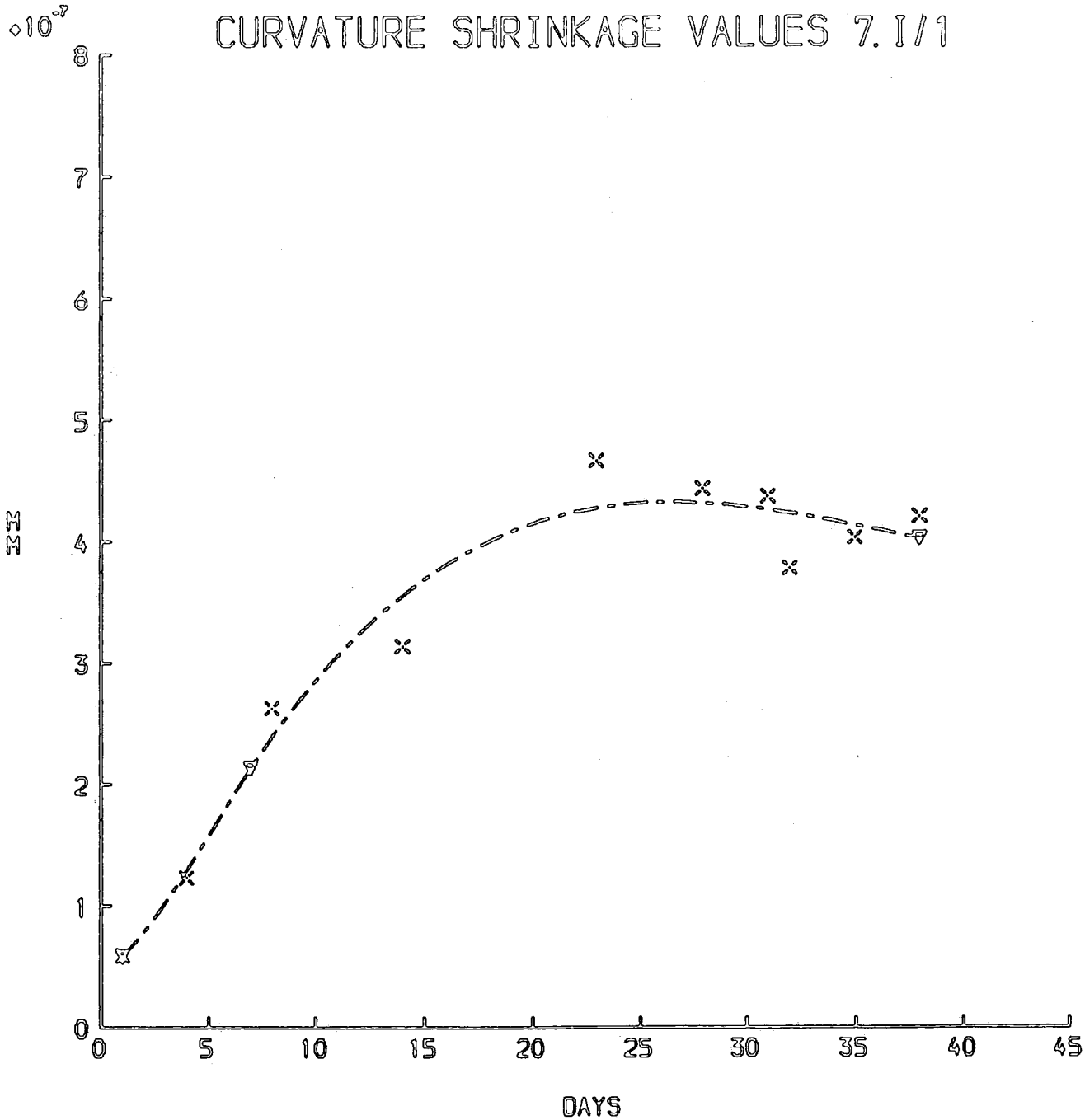
CURVATURE SHRINKAGE VALUES 7.I/1
◇10⁻⁷
8
7
6
5
4
3
2
1
0
MM
0
5
10
15
20
25
30
35
40
45
DAYS

FIG. 7. I. 1.

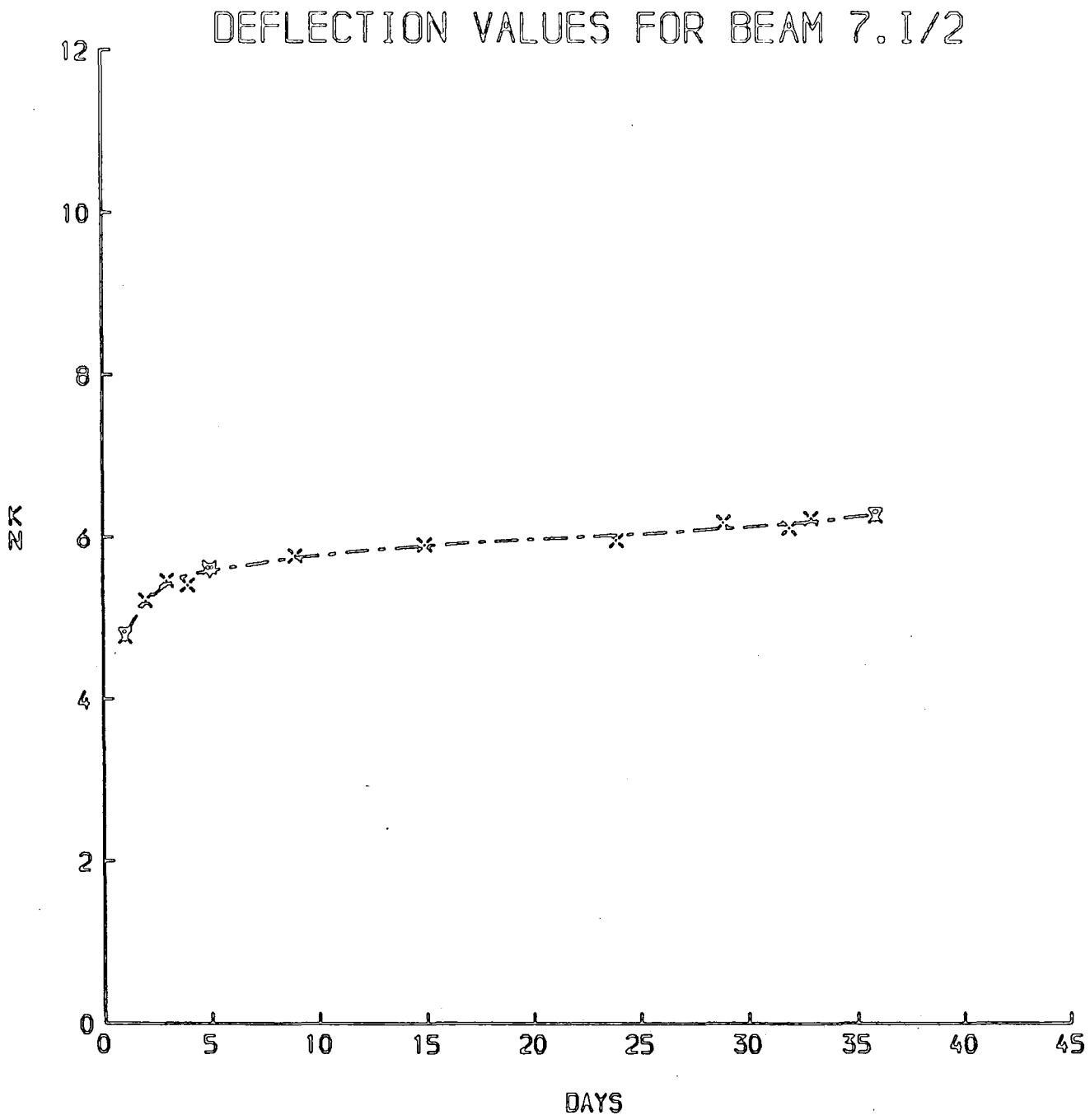
DEFLECTION VALUES FOR BEAM 7.I/2
12
10
8
6
4
2
0
ZK
0
5
10
15
20
25
30
35
40
45
DAYS

FIG. 7. I. 2.

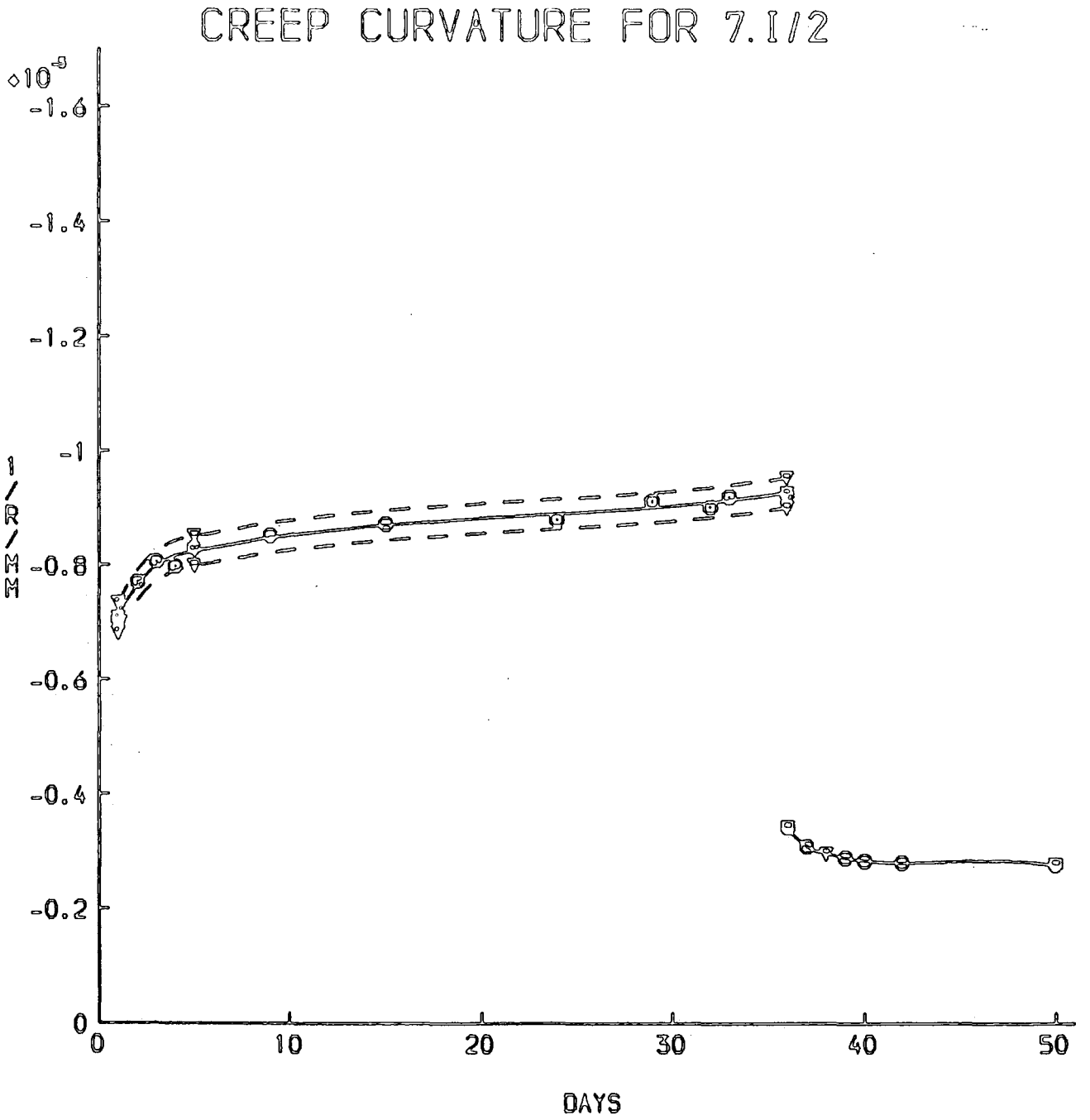
CREEP CURVATURE FOR 7.1/2
◇10⁻³
-1.6
-1.4
-1.2
-1
-0.8
-0.6
-0.4
-0.2
0
1/R/MM
0
10
20
30
40
50
DAYS

FIG. 7.1.3.

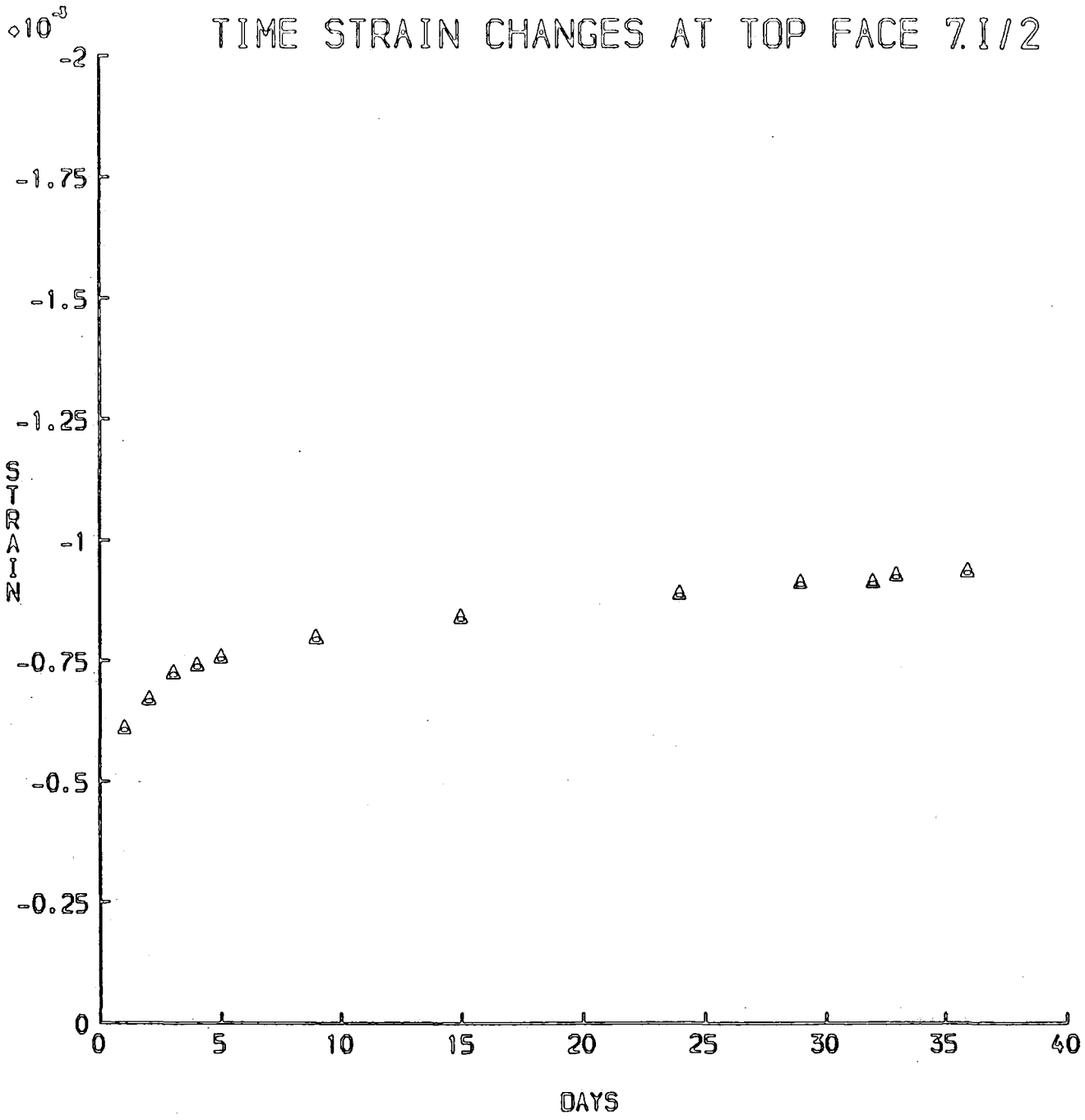
TIME STRAIN CHANGES AT TOP FACE 7.1/2
$\diamond 10^{-3}$
-2
-1.75
-1.5
-1.25
-1
-0.75
-0.5
-0.25
0
STRAIN
0
5
10
15
20
25
30
35
40
DAYS

FIG. 7.1.4.

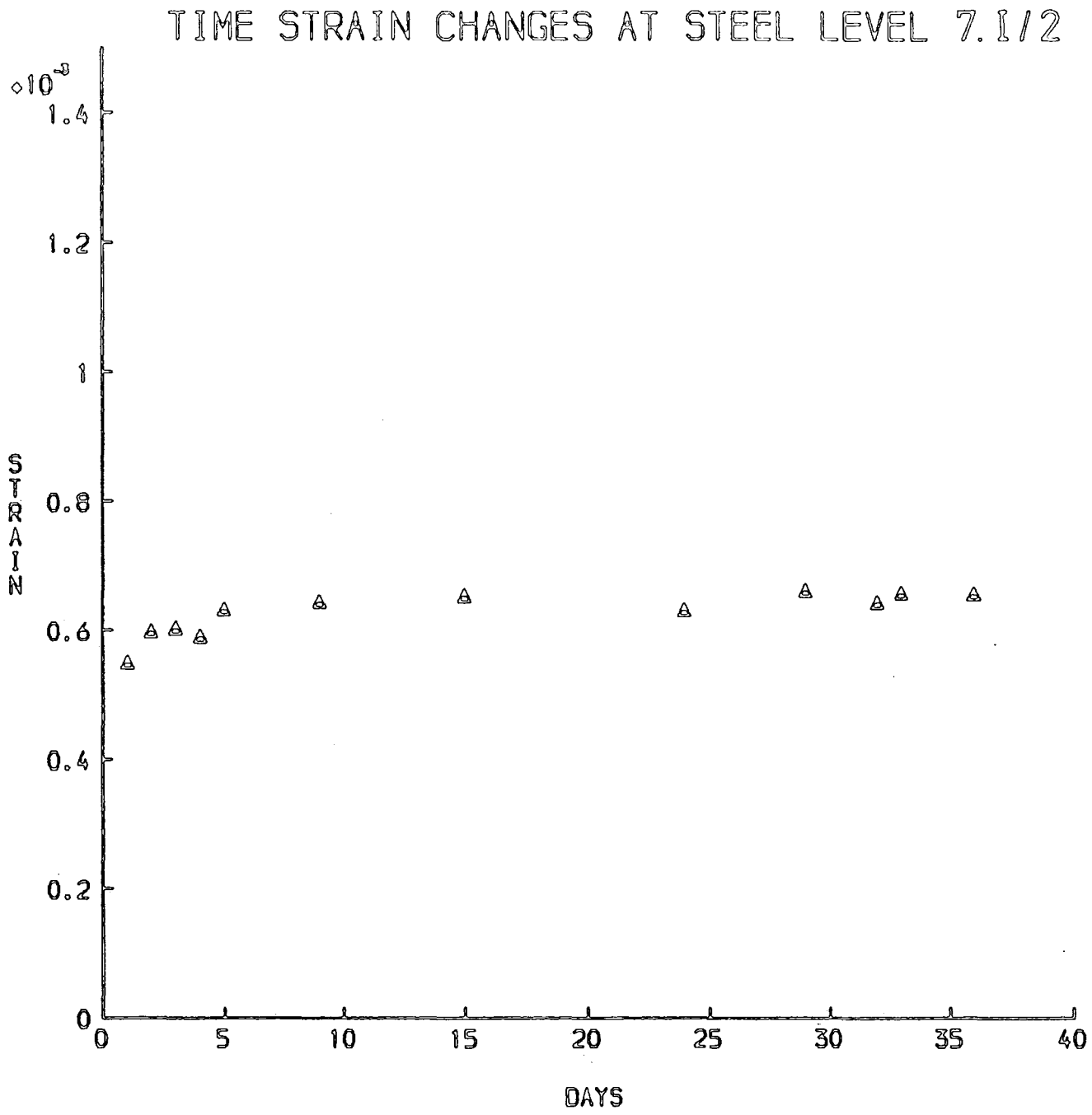
TIME STRAIN CHANGES AT STEEL LEVEL 7.1/2
$\diamond 10^{-3}$
1.4
1.2
1
0.8
0.6
0.4
0.2
0
STRAIN
0
5
10
15
20
25
30
35
40
DAYS

FIG. 7.1.5.

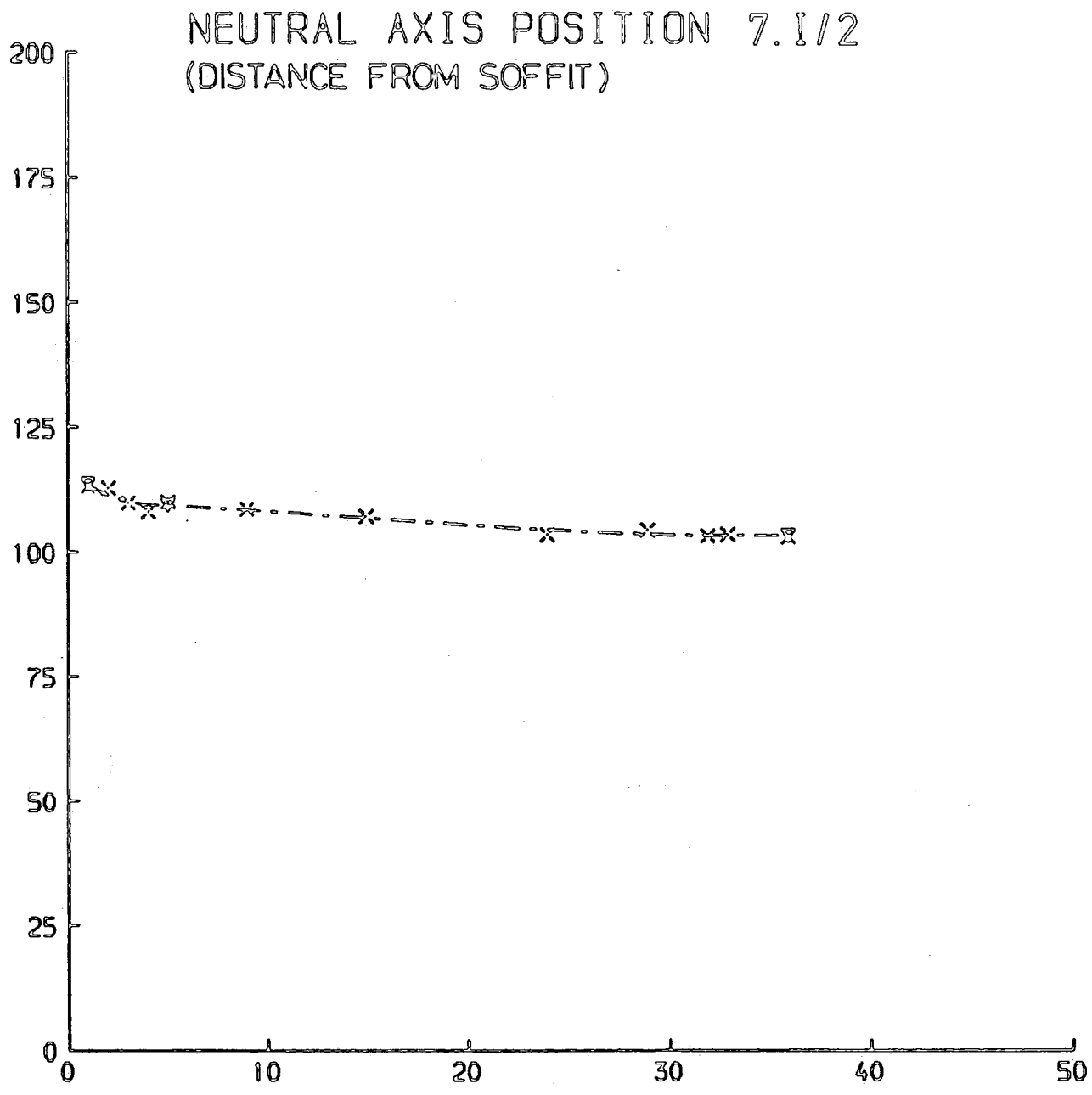
NEUTRAL AXIS POSITION 7.1/2
(DISTANCE FROM SOFFIT)
200
175
150
125
100
75
50
25
0
0
10
20
30
40
50

FIG. 7.1.6.

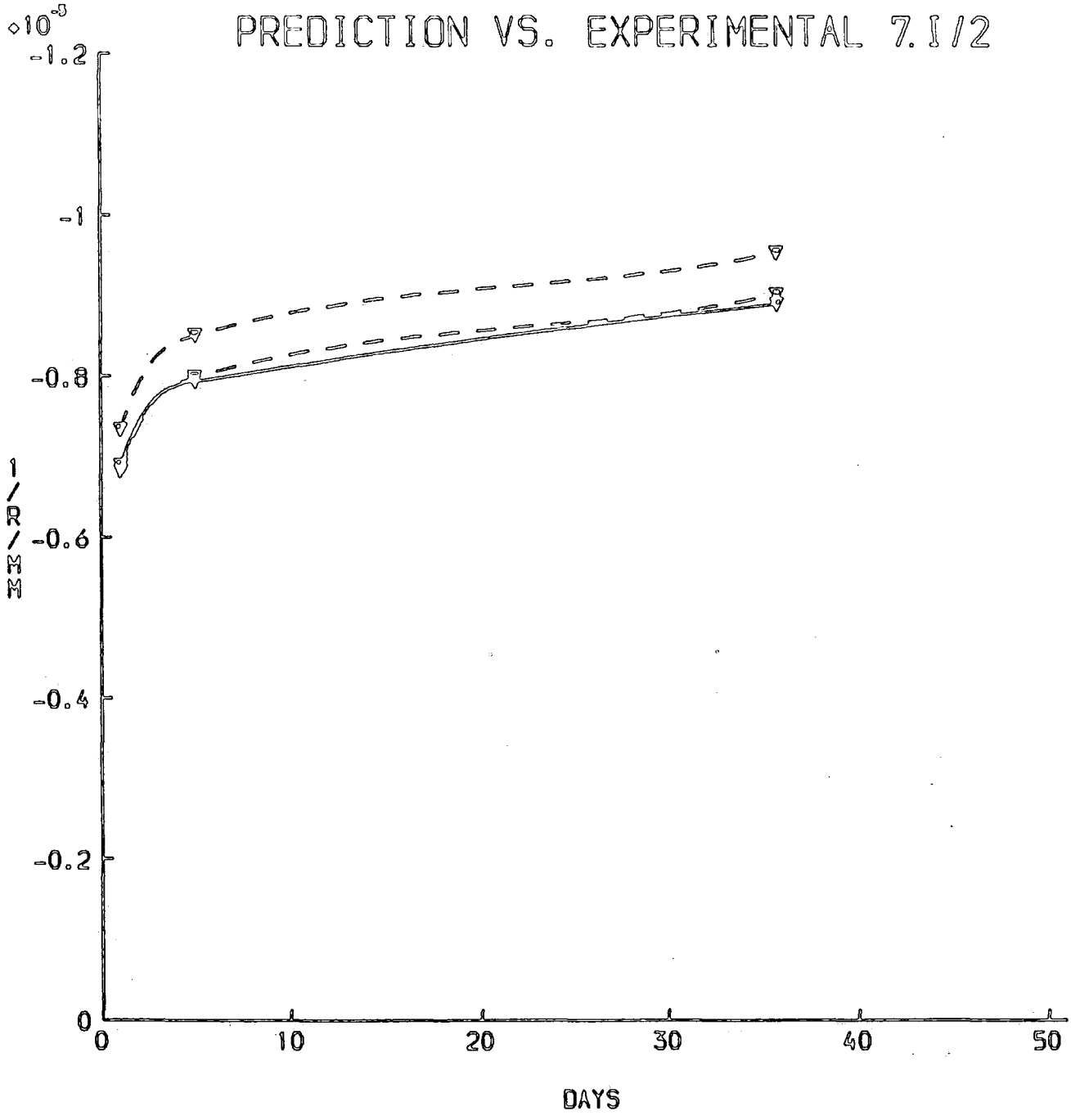
PREDICTION VS. EXPERIMENTAL 7.1/2
◇10⁻³
-1.2
-1
-0.8
-0.6
-0.4
-0.2
0
1/R/MM
0
10
20
30
40
50
DAYS

FIG. 7.1.7

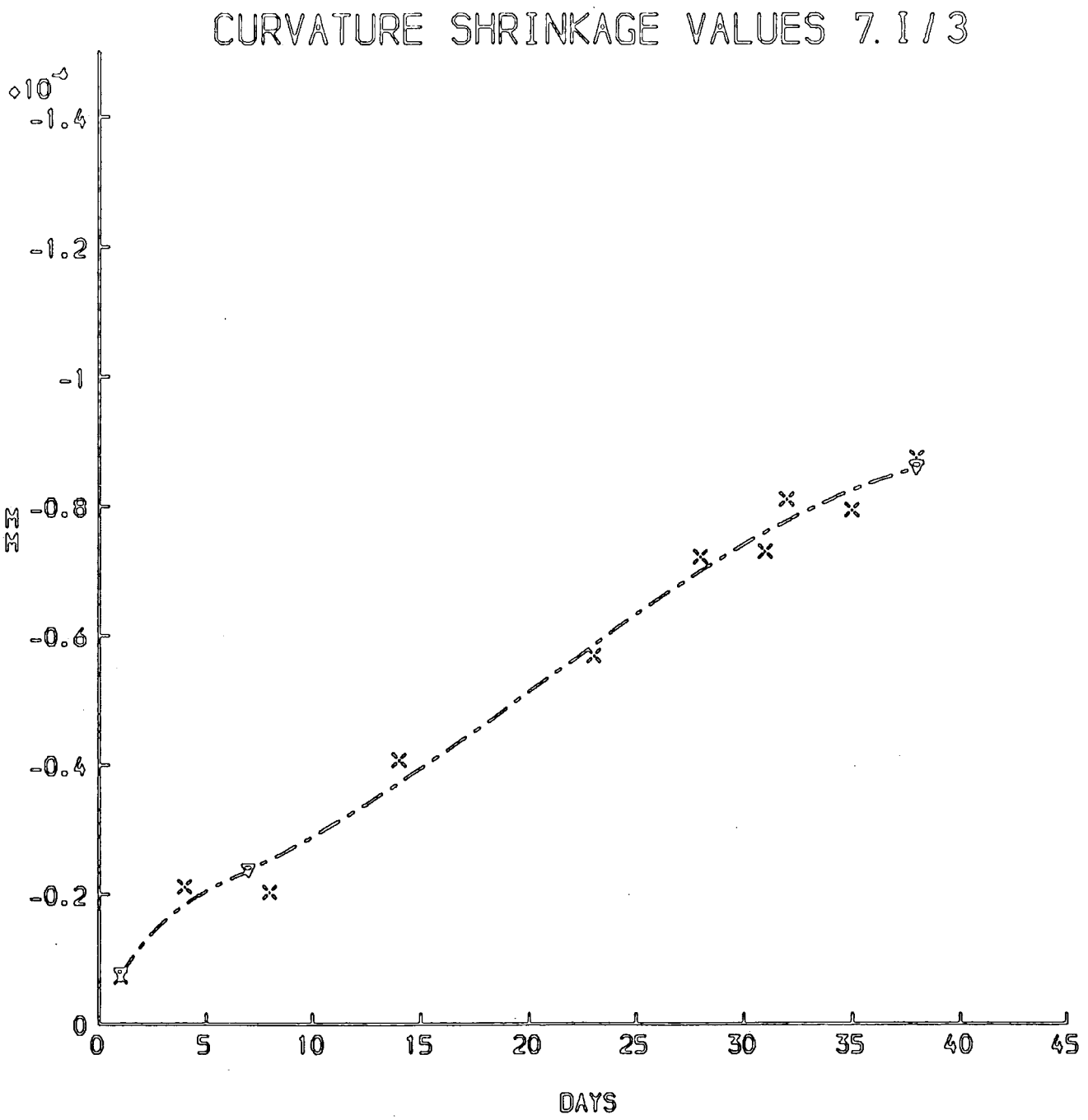
CURVATURE SHRINKAGE VALUES 7.1/3
◇10⁻⁵
-1.4
-1.2
-1
-0.8
-0.6
-0.4
-0.2
0
1/M
0
5
10
15
20
25
30
35
40
45
DAYS

FIG. 7.1.8

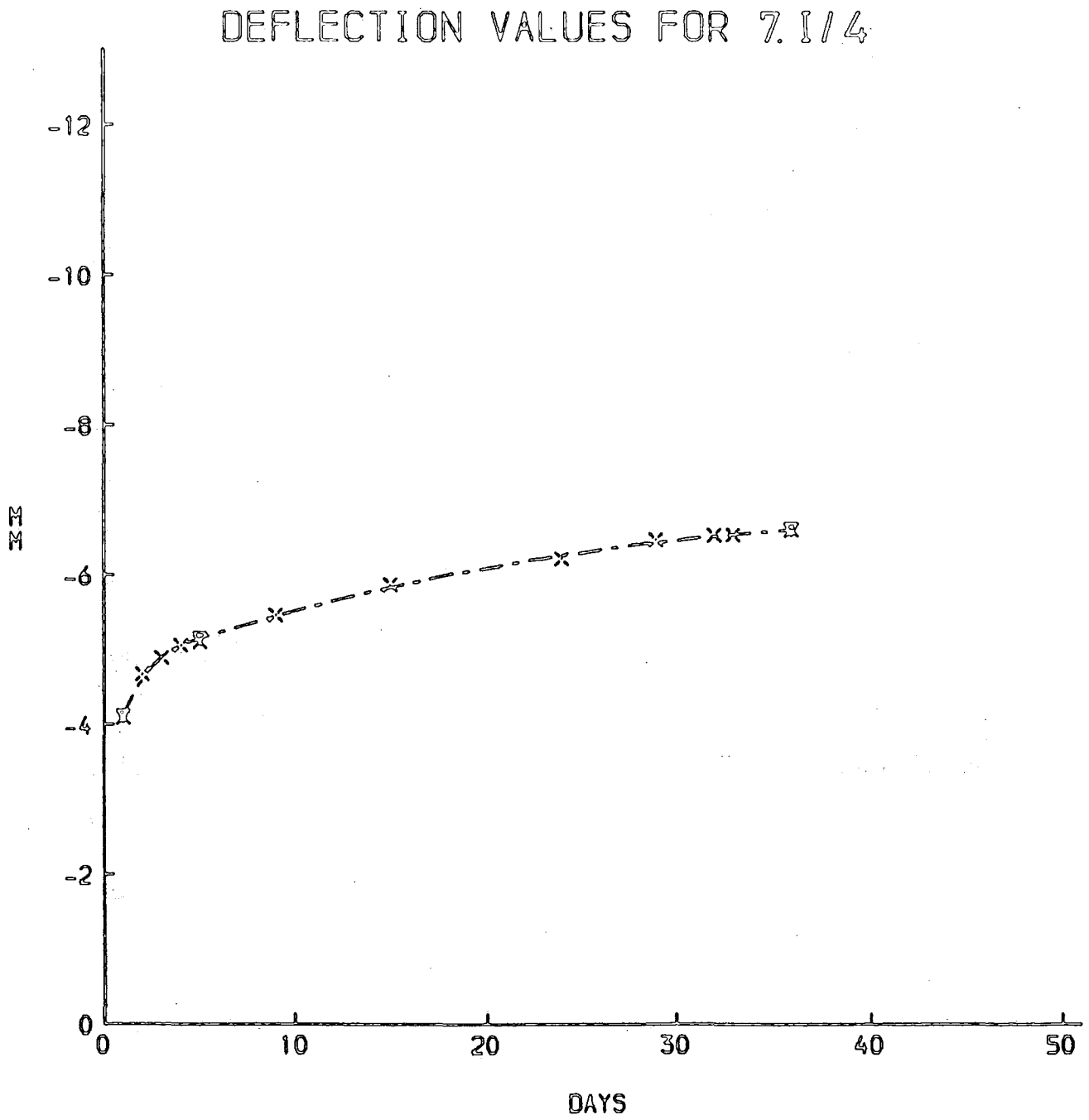

FIG. 7.1.9.

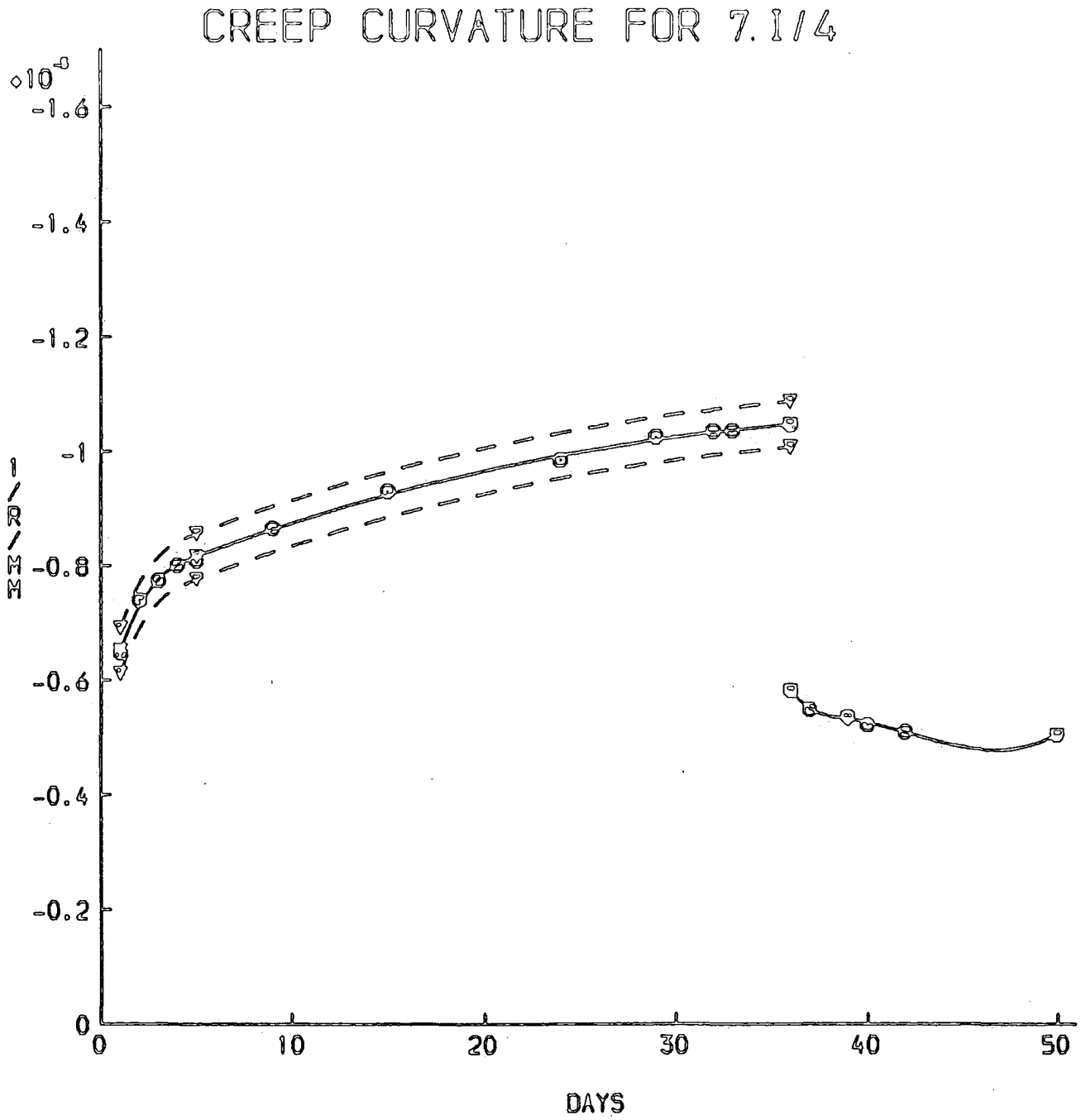
CREEP CURVATURE FOR 7.1/4
◇10⁻³
-1.6
-1.4
-1.2
-1
-0.8
-0.6
-0.4
-0.2
0
1/R/M/M
0
10
20
30
40
50
DAYS

FIG. 7.1.10

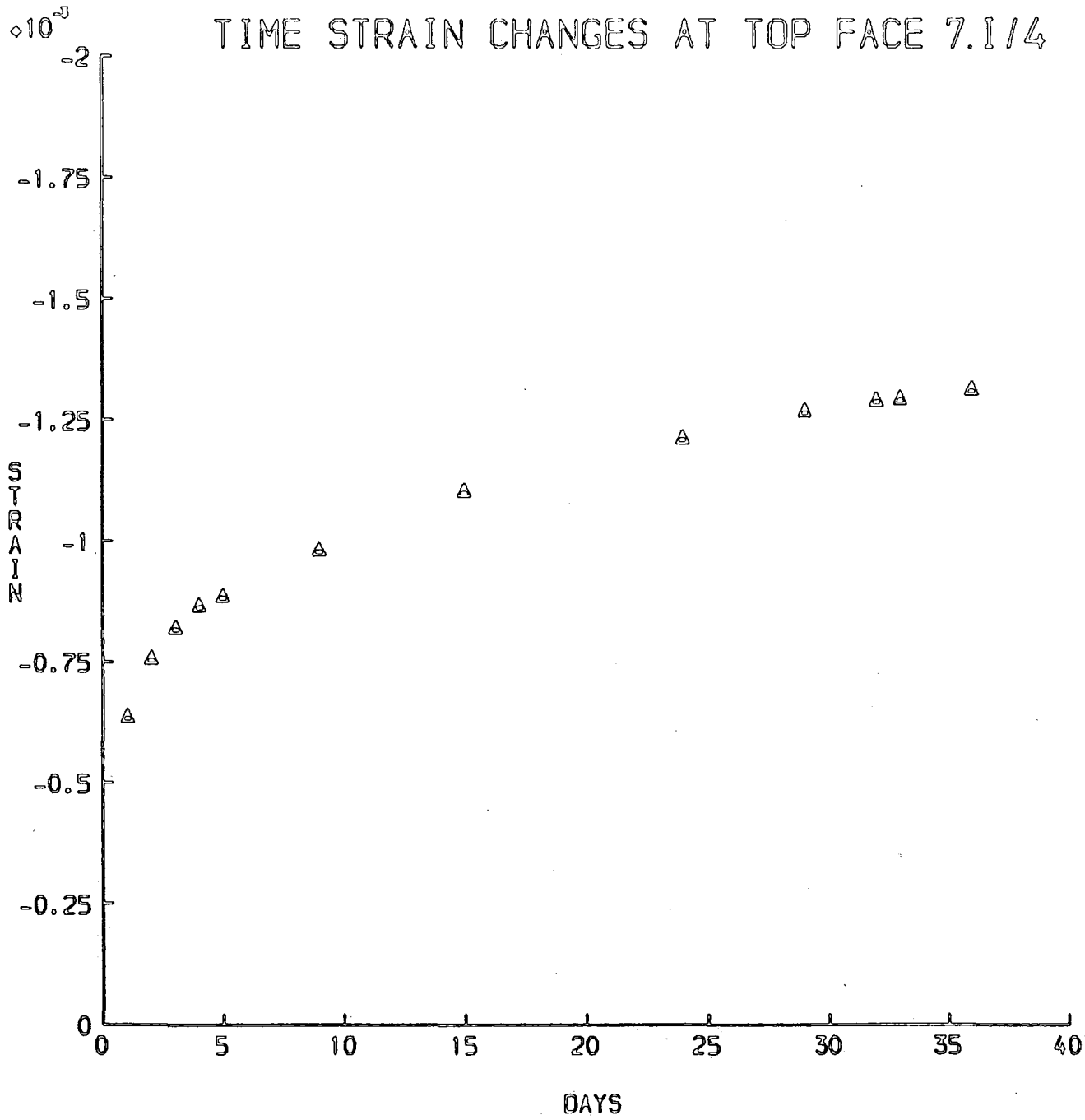
TIME STRAIN CHANGES AT TOP FACE 7.1/4
◇10⁻³
-2
-1.75
-1.5
-1.25
-1
-0.75
-0.5
-0.25
0
STRAIN
0
5
10
15
20
25
30
35
40
DAYS

FIG. 7.1. 11.

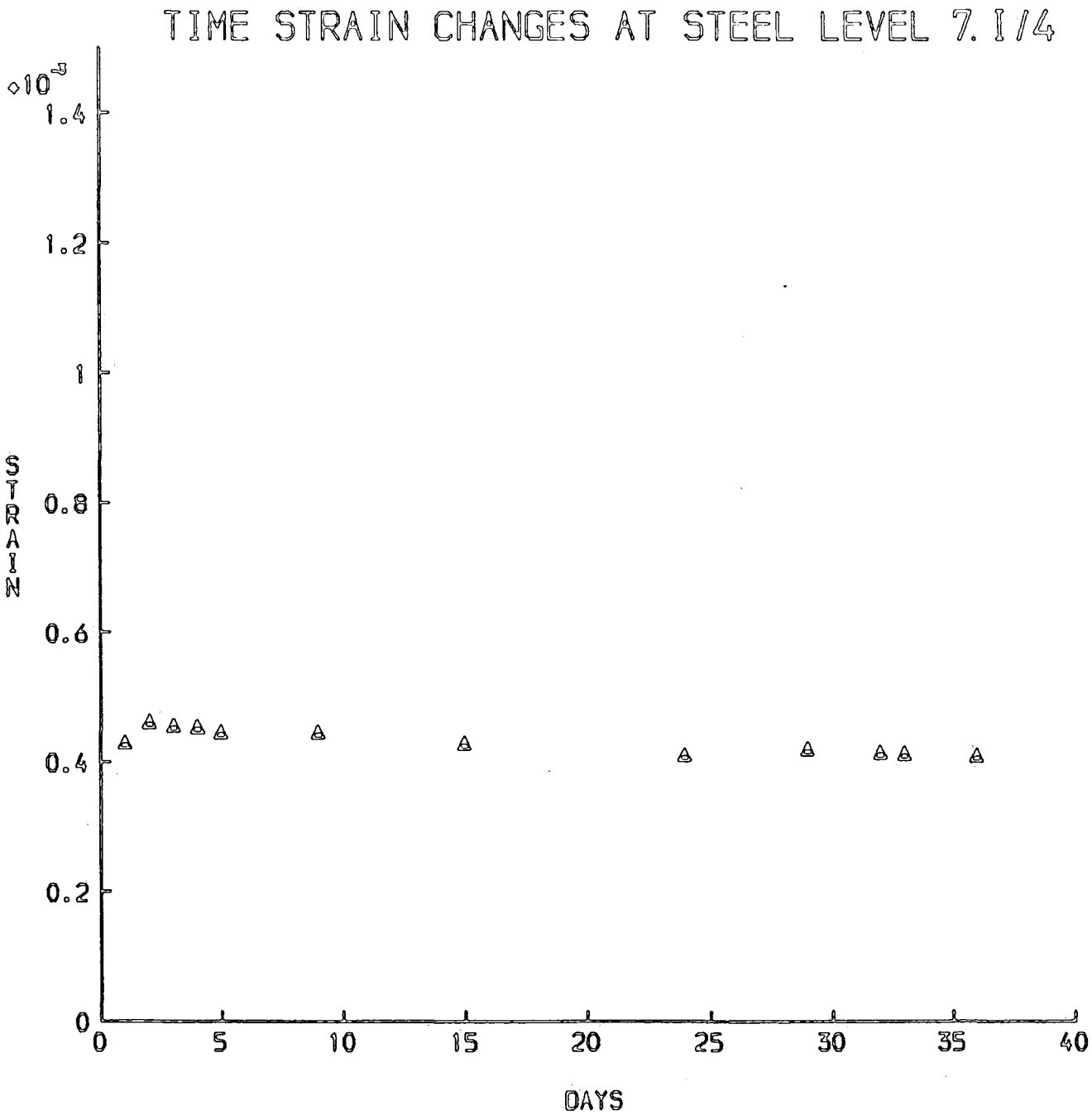
TIME STRAIN CHANGES AT STEEL LEVEL 7.1/4
$\diamond 10^{-3}$
1.4
1.2
1
0.8
0.6
0.4
0.2
0
STRAIN
0
5
10
15
20
25
30
35
40
DAYS

FIG. 7.1.12.

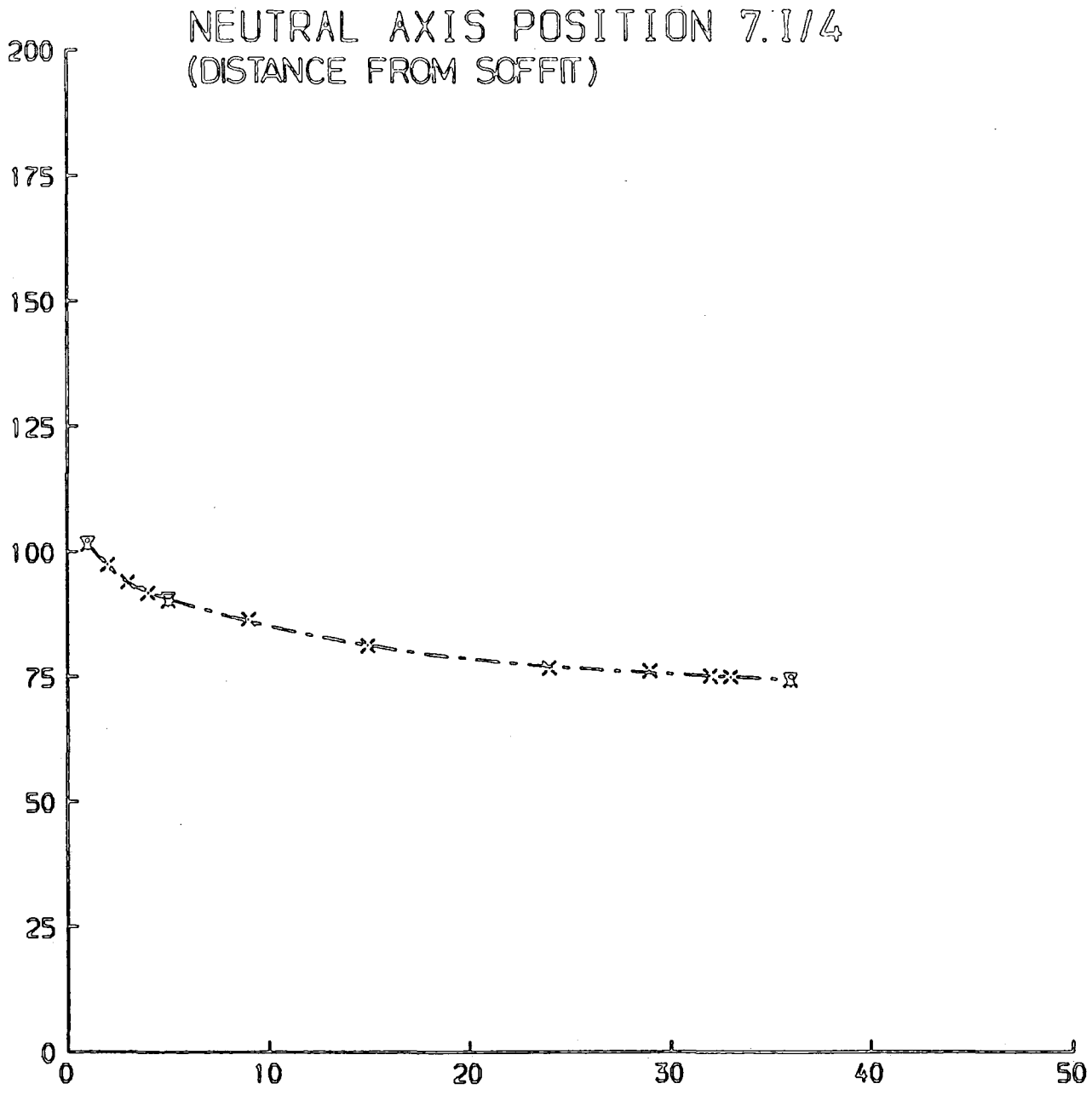
NEUTRAL AXIS POSITION 7.1/4
(DISTANCE FROM SOFFIT)
200
175
150
125
100
75
50
25
0
0
10
20
30
40
50

FIG. 7.1.13.

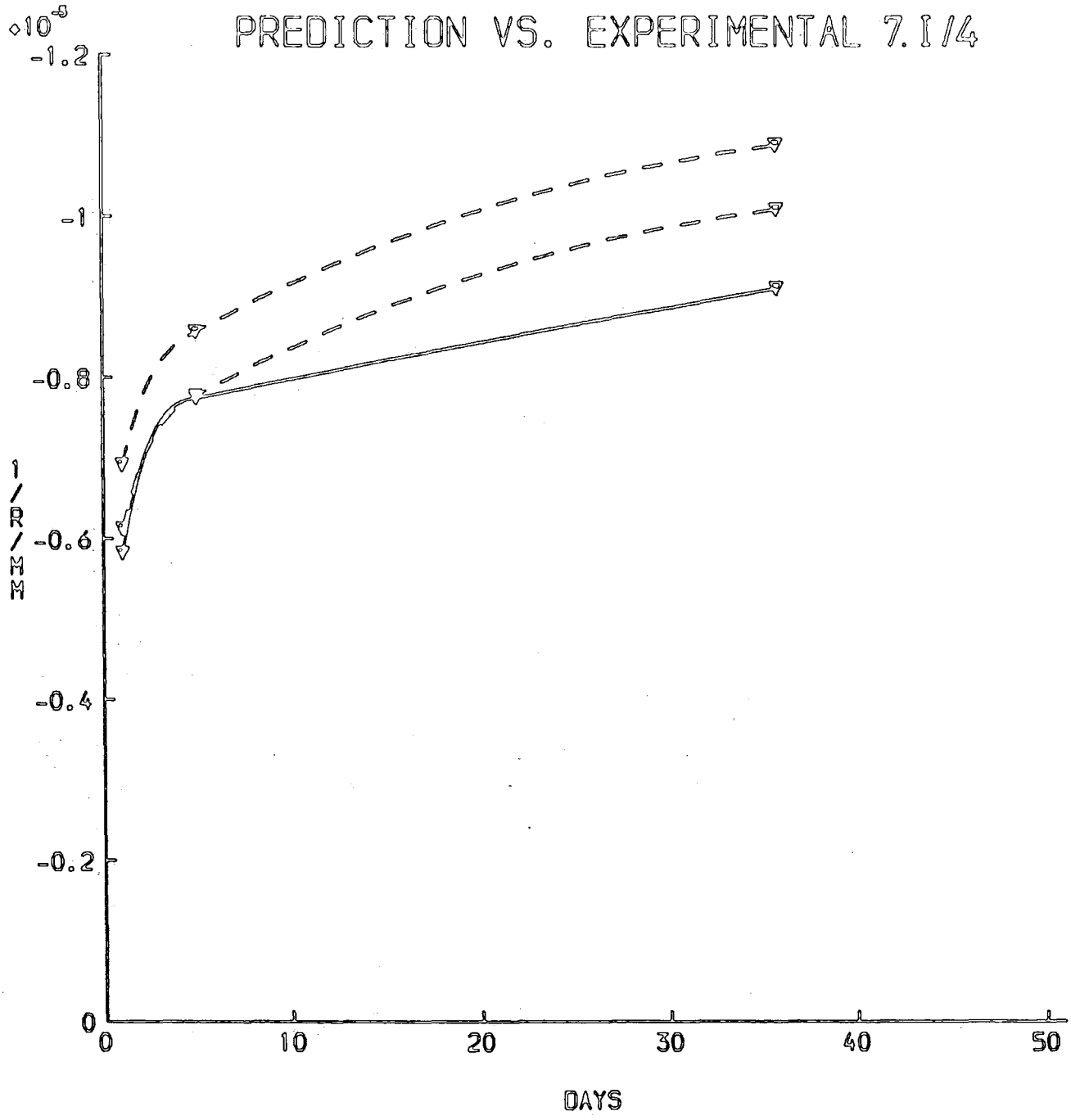
PREDICTION VS. EXPERIMENTAL 7.I/4
◇10⁻³
-1.2
-1
-0.8
-0.6
-0.4
-0.2
0
1/R/MM
0
10
20
30
40
50
DAYS

FIG. 7.1.14.

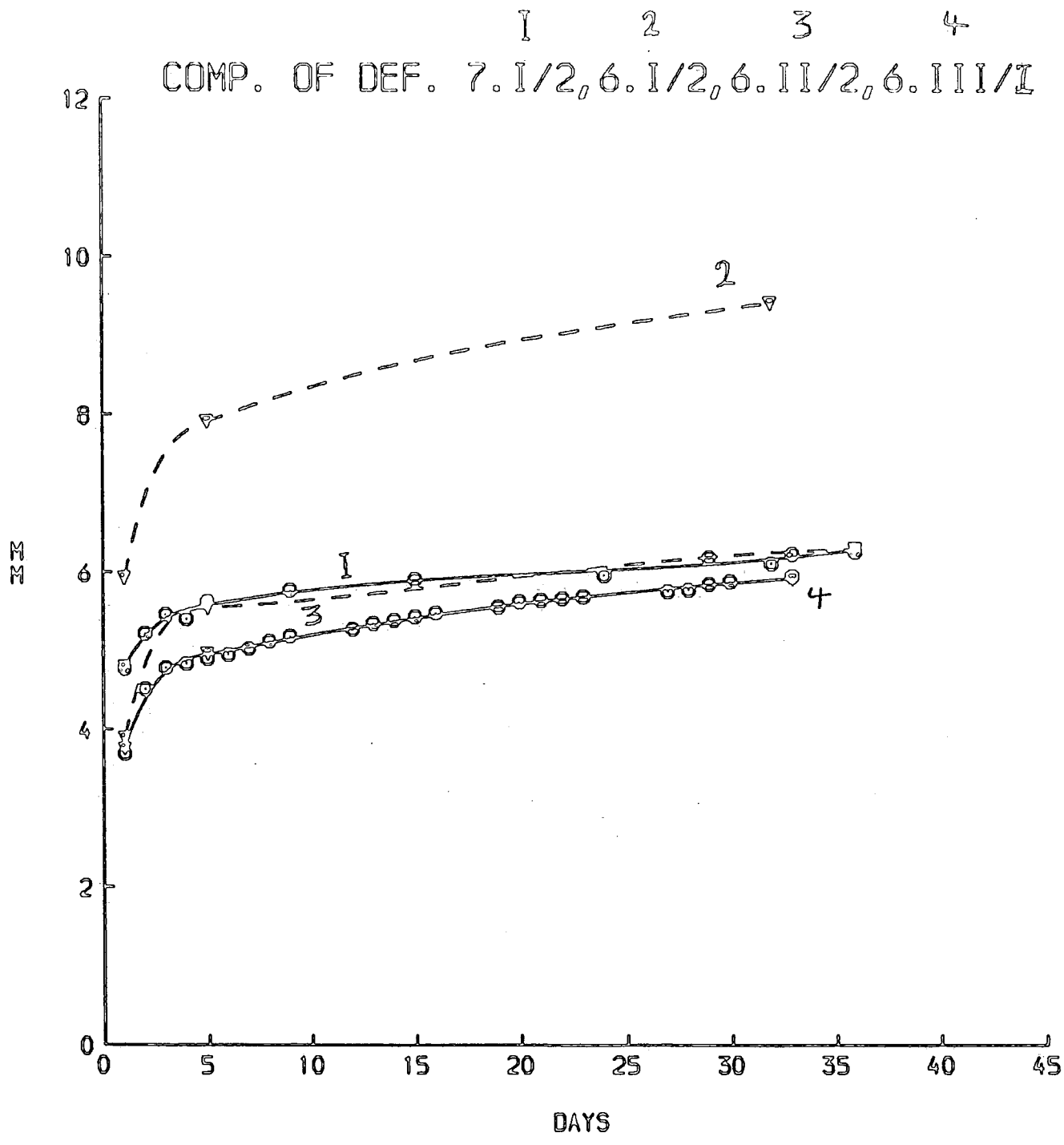
1 2 3 4
COMP. OF DEF. 7.I/2,6.I/2,6.II/2,6.III/I
12
10
8
6
4
2
0
MM
0
5
10
15
20
25
30
35
40
45
DAYS
1
2
3
4

FIG. 7.11.1

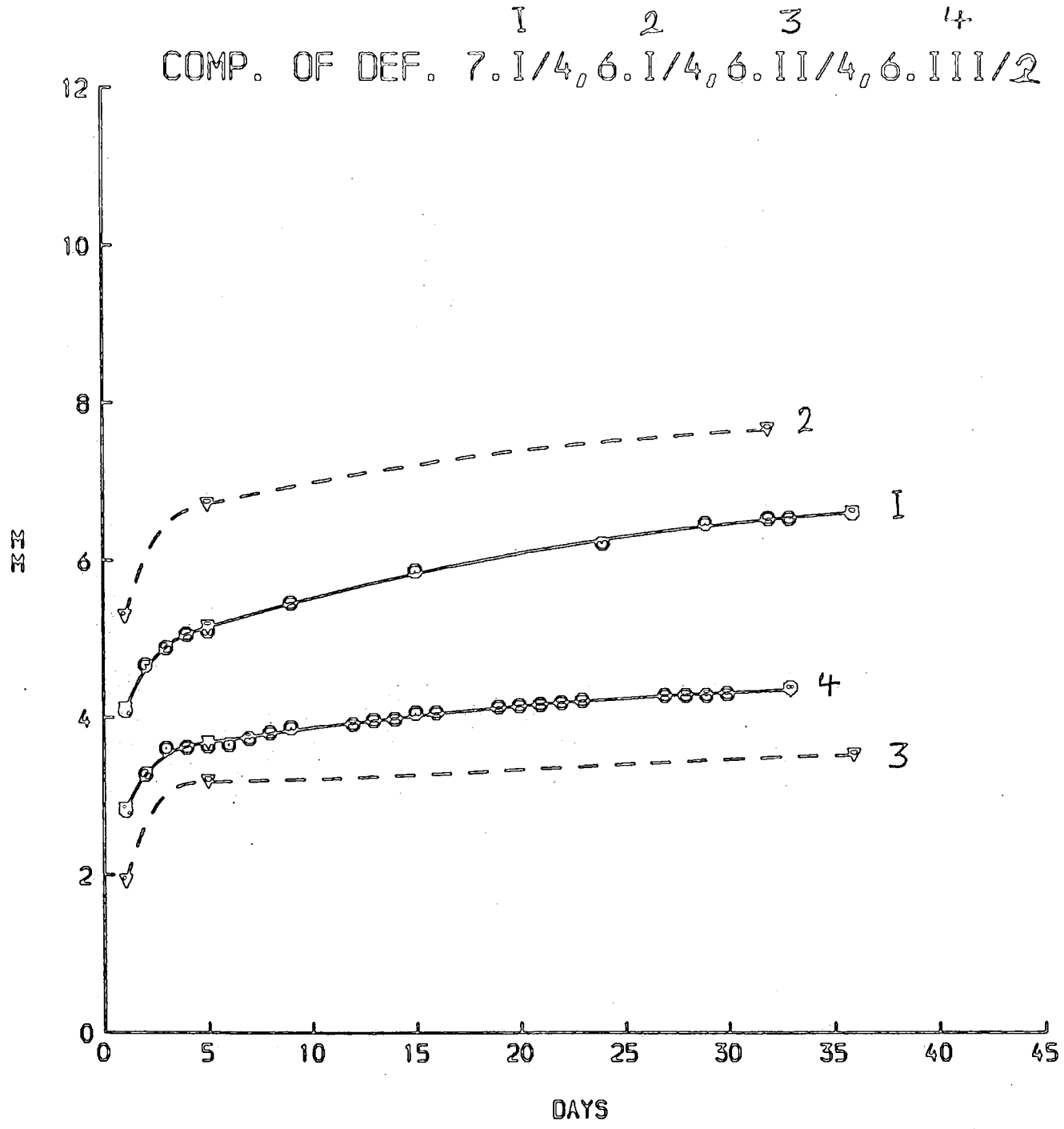
1 2 3 4
COMP. OF DEF. 7.I/4, 6.I/4, 6.II/4, 6.III/2
12
10
8
6
4
2
0
MM
0
5
10
15
20
25
30
35
40
45
DAYS
1
2
3
4

FIG. 7.11.2.

CHAPTER 8

PRESTRESSED BEAMS

8. PRESTRESSED BEAMS

Synopsis

In broad terms, the trends of creep and thermal strains for the prestressed beams were similar to those observed in the reinforced concrete beams. However because the prestressed beams were tested at a much earlier age than the reinforced beams, they underwent negligible shrinkage only during the first eight days, indicating that the water lost from these beams to the environment during this period was water held in the capillary pores. This led to a low value for the primary creep as compared with the reinforced beams.

The use of the program AZ to predict curvature gave a better agreement with the measured values than in the case of the reinforced beams, possibly because of absence of cracking.

8.1 Introduction

In this chapter the results of two tests on prestressed beams are presented and analysed. In the first test the beams were partly sealed, and in the second test the beams were unsealed.

In each test strains were recorded on two prestressed concrete beams, each 2000 x 200 x 100mm, and on two plain blocks 300 x 200 x 100mm blocks which acted as shrinkage companions in that they were treated similarly to the beams.

In each test one beam and one block was exposed to daily heating-cooling cycles similar to the climatic conditions of late spring in Riyadh, Saudi Arabia. The other beam and its shrinkage companion block were exposed to normal laboratory ambient conditions. Details of the temperature and humidity are given in §6.2 and §6.3.

The objectives of the tests on the prestressed beams were as follows:-

- To measure the loss of the prestressed force for the beams exposed to heating-cooling and humidity cycles, and to compare that with the loss of prestressing force for beams exposed to normal laboratory ambient conditions.
- To measure response to the daily temperature gradient.
- To compare the chronological development of axial creep for beams exposed to heating-cooling and humidity cycles and beams exposed to normal laboratory ambient conditions.
- To compare the behaviour of the partly sealed beams with the behaviour of the unsealed beams.

8.2 Specimen

The prestress force was applied by a Macalloy bar of 20mm diameter, inside a centrally located duct. A steel tube of square box section 300mm long, 66mm inside dimension and 6mm thickness, was stressed in series with the concrete beam to act as a load cell. It had four demec gauge lengths spaced at 200mm along its facets and was previously calibrated so that the load could be obtained from the measured strain.

The load cell was located between end-plates 200 x 100 x 25mm thick, with the prestressing bar running centrally through the assembly (Figure 8.1).

Two drilled wooden blocks were fitted into the tube ends to locate the Macalloy bar centrally.

The calibration of the load cell was carried out at known temperature. Allowance for thermal strains was made from knowledge of the coefficient of thermal expansion and from tube temperature measured from the averaged readingsof the thermocouples attached to the tube.

8.3 Mix

The same mix that was used for the reinforced concrete was used here namely a 1:2:4 mix by weight with equal amounts of coarse aggregates of sizes 10mm and 20mm and water cement ratio of 0.5 by weight.

8.4 Test Preparation

8.4.1 Mould

The moulds used here were of wooden framed plywood construction. A duct was provided for the prestressing rod consisting of a plastic tube 25mm in diameter. The tube was passed through holes cut in the end shutters.

The thermocouples could not be located at the centre line of the beam's cross section because of the prestressing sheathing and were placed 17mm from the vertical central axis.

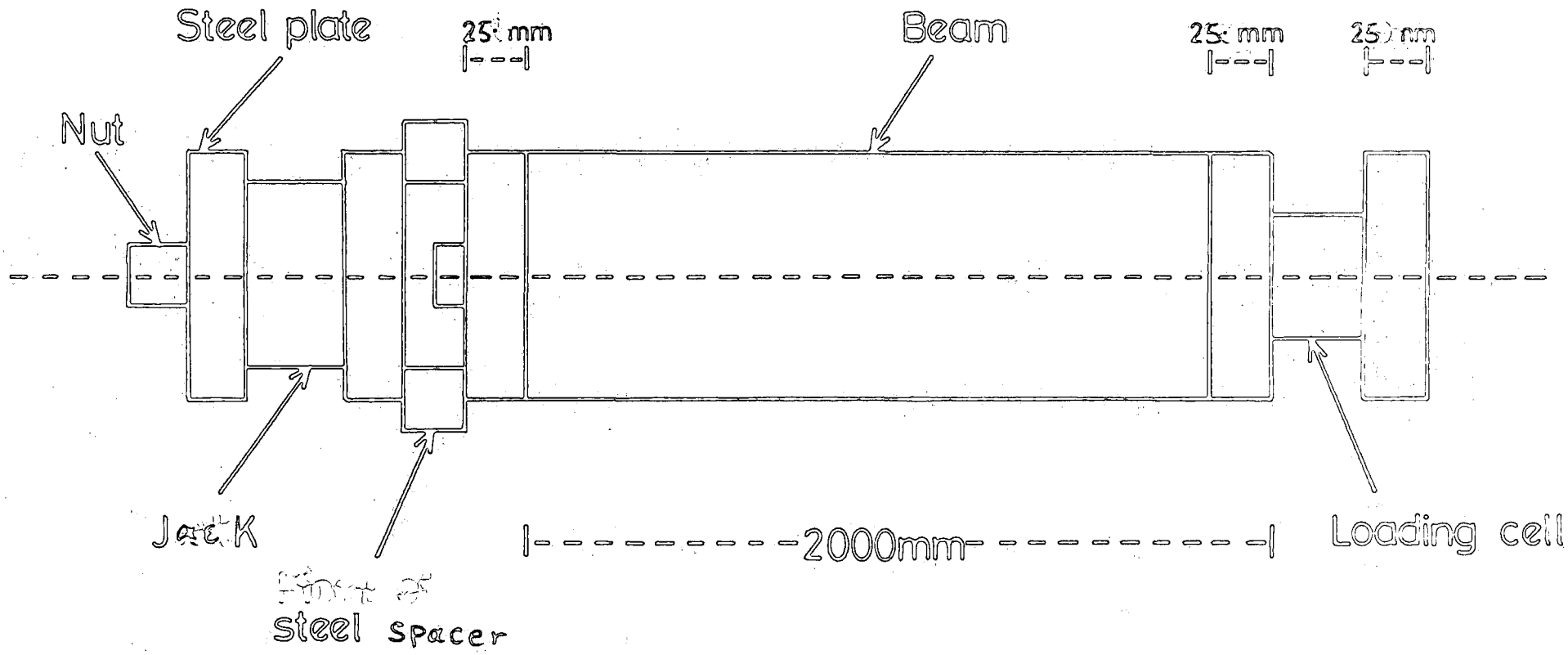
Steel plate
25 mm
Beam
25 mm
25 mm
Nut
Jack
2000mm
Loading cell
steel spacer

FIG. 8.1

8.4.2 Casting procedure

The method of casting was the same as for reinforced concrete beams of chapter 5.

8.5 Preparation

The beams were left in their moulds on the vibrating table for six days, where they were covered with hessian and polystyrene sheets. The hessian sheets were kept wet by soaking them with water daily. After six days, in case of the partly sealed beams they were taken to the floor where the shutters of the moulds were stripped, and the beams were left for two hours to surface dry. Then they were painted with a primer. On day seven, they were given one coat of epoxy paint, and on day eight they were given a second coat of epoxy paint. On day ten they were prestressed and then they were moved to the testing areas. In case of the unsealed beams, they were left in their moulds until day ten where they were prestressed and then moved to the testing areas.

Sheets of polystyrene were used to insulate the sides and top of the cyclically heated beams.

8.6 Strain measurement

The demec gauge lengths on the side faces of the concrete were located at midspan.

The depths of the gauge lengths were 10, 35, 165 and 190mm from the top. This was repeated on the opposite face so that the strain obtained at any level was the average of two strain measurements.

8.7 Prestressing procedure

The prestressing force was applied to the beams using a calibrated hydraulic centre pull jack. The threaded length of prestressing bar was passed through the jack and restrained by a temporary bolt. The jack acted against a steel bridge, allowing stressing to the desired load followed by lock off by means of a front end nut, see Figure 8.1.

The jack was loaded to 10% of the required force, after careful centring, and reference for extension was taken. The jack was then pumped up to the desired load , and bar extension was measured. The bar was then locked off using a long spanner on the front end nut.

8.8 Stress Levels

The average 28 days cube strength of all the previous reinforced concrete mixes was about 44 N/mm^2. For direct compression the CP110 limit on stress is 0.25 f_{cu}, that is a stress of 11 N/mm^2.

In the realistic prestress design, a typical stress situation could be as shown in Figure 8.2.
Consequently, for the long term loading condition, a stress state of a uniform compressive stress of 9.5N/mm^2 was chosen. This incorporated a loss of 1N/mm^2 or 10.5% for transfer effects. The stress field was achieved by prestressing a bar at midheight of the beam to an initial force of 188KN. This force was easily carried by the 20mm Macalloy bar, as 188.0KN corresponded to 58% of c.u.t.s of the bar, whereas typical site practice would be to use 70% c.u.t.s.

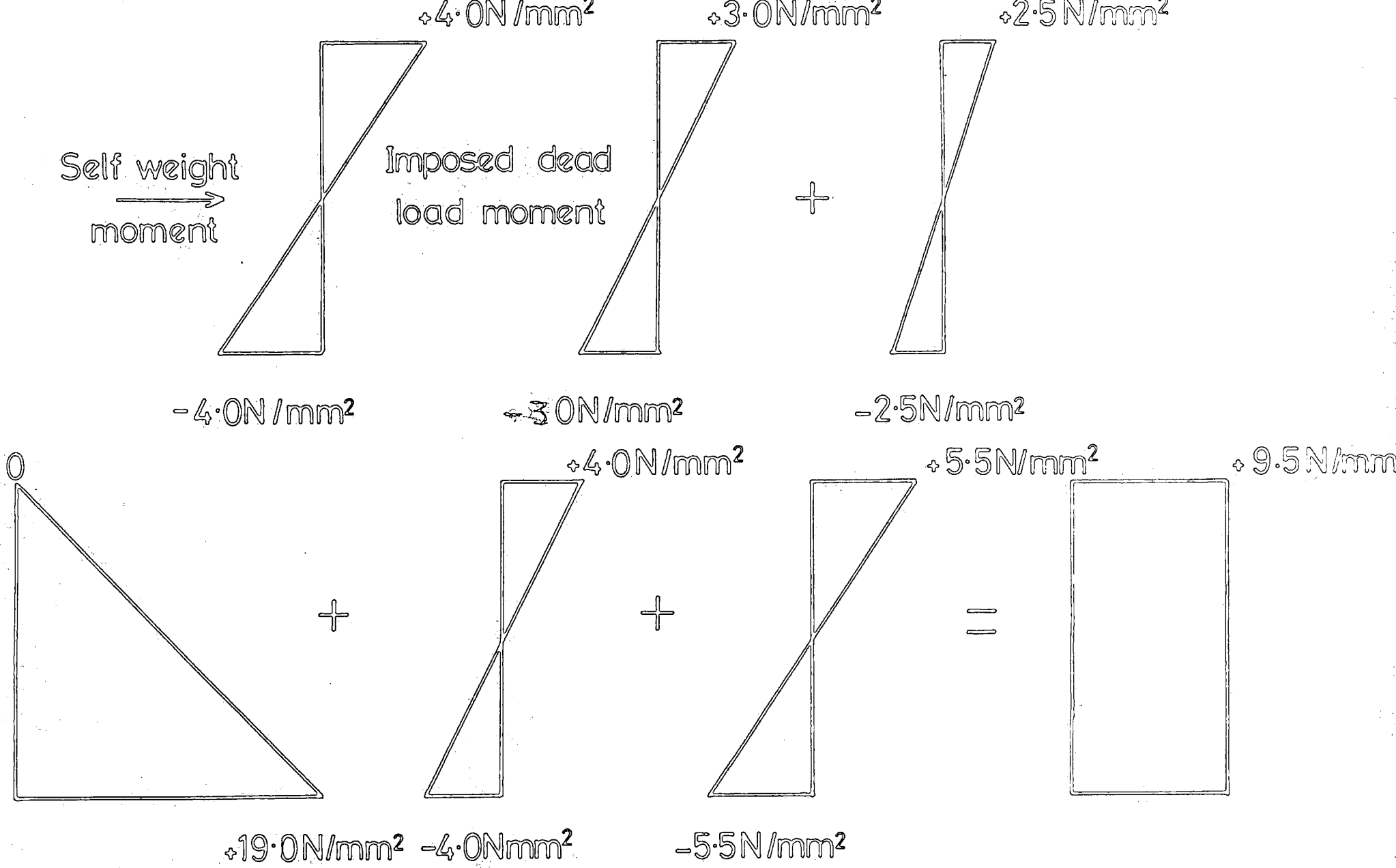
+4·0N/mm²
+3·0N/mm²
+2·5N/mm²
Self weight moment
Imposed dead load moment
-4·0N/mm²
+3·0N/mm²
-2·5N/mm²
0
+4·0N/mm²
+5·5N/mm²
+9·5N/mm
+19·0N/mm²
-4·0Nmm²
-5·5N/mm²

FIG. 8.2

8.9 Test procedure

Because the prestress technique provided prestress plus dead load - the beams were not physically loaded, but were supported at their 1/4 length points.

8.I PRESTRESSED BEAM, PARTLY SEALED

8.I.1 Prestressing the beams

The prestressing force at transfer was determined from the strain readings of the steel tubes to be 174.4KN and 159.9KN for beams one and two respectively.

The concrete strain readings showed that the Macalloy bar was displaced from the centre position. The eccentricity of the bar was calculated from the initial strain readings of the concrete. Its values were 5.75mm for beam one and 6.4mm for beam two.

At transfer, the stresses at the top and at the bottom were calculated to be $10.3N/mm^2$ and $7.2N/mm^2$ respectively for beam one, $9.6N/mm^2$ and $6.5N/mm^2$ for the top and bottom of beam two, from a value of elastic modulus at transfer of $18.8KN/mm^2$.

At transfer beam one had a sagging curvature of $-0.86 \times 10^{-6}mm^{-1}$, and beam two had a sagging curvature of $-0.9 \times 10^{-6}mm^{-1}$.

The beams were placed on supports with a configuration that yielded zero moment at the point of measurement of Strain.

8.I.2 Beam one

Long term results:

Figure 8.I.1 shows changes of axial strain with respect to time. The strains were the total effect of creep and shrinkage. Cyclic heating/cooling and humidity was applied nine days after prestressing. Axial shrinkage effects were very small, although shrinkage curvature was more pronounced.

The total creep and shrinkage value after thirty six days from prestressing was 0.45×10^{-3}. The use of the hyperbolic law predicts an ultimate value of 0.77×10^{-3}.

Figure 8.I.1 shows similar response to heat as was evidenced in the reinforced beams, where there was a step rise in value of strain after the start of heat. Initially the beam had a sagging curvature of 0.86×10^{-6}, it reduced to 0.2×10^{-6} thirty six days after prestressing.

After twenty eight days of cyclic heating-cooling and humidity, and thirty six days from start of prestressing, the initial prestressing force was reduced by 17.75KN, that is about 10 per cent of its initial value.

Figure 8.I.2 gives changes of force with respect to time as compared with predicted results using creep values measured in a small unreinforced concrete cylinder.

Shrinkage

Figure 8.I.3 gives values of changes of shrinkage curvature with time. After 32 days from datum, it had a hogging value of $0.8 \times 10^{-6} mm^{-1}$.

Daily cycle:

Predicted curvature varied from 0.8 x $10^{-6}mm^{-1}$ to 0.9 x $10^{-6}mm^{-1}$ and was within 10% of the measured value. Predicted stresses at the top varied throughout the test from a compressive value $1.72N/mm^2$ to a compressive value of $1.1N/mm^2$, and at the soffit from a compressive value of $1.1N/mm^2$ to a compressive value of $0.62N/mm^2$. The highest predicted tension stresses at the middle parts of the beam was $-0.74N/mm^2$.

8.I.3 Beam Two

Figure 8.I.4 shows changes of total axial strain (creep and shrinkage) with respect to time. The total creep and shrinkage value 36 days after prestressing was 0.35 x 10^{-3}. The hyperbolic law predicts an ultimate value of 0.47 x 10^{-3}. Initially the beam had a sagging curvature of -0.9 x $10^{-6}mm^{-1}$ which changed to a hogging curvature of 0.5 x $10^{-6}mm^{-1}$ thirty six days after prestressing from the combined effects of both creep and shrinkage.

Prestressing force was reduced (due to creep and shrinkage) by 18.6KN thirty six days after prestressing.

Figure 8.I.5 gives changes of prestressing force as compared to predicted value using measured creep values on small (60mm Ø 200 long) unreinforced concrete cylinders.

Shrinkage

Figure 8.I.6 gives changes in shrinkage curvature with time. It had a hogging value of 0.76×10^{-6} thirty six days after prestressing.

8.I.4 Comparison between beam one and beam two

Both beams one and two were cast, cured and sealed in the same way. They were prestressed at the same time. Beam one prestressing force at transfer was 174.4KN and beam two prestressing force at transfer was 160.0KN. Immediately after transfer beam one was moved to the cabin, and beam two to the outside laboratory. Beam one was insulated with polystyrene sheets from top and sides. The detailed description of the curing and prestressing process was discussed at the beginning of the chapter. Cyclic heat-cooling and humidity was applied to beam one nine days after prestressing.

Here a comparison is made of the chronological development of creep and shrinkage. Table 8.I.4.1 gives ratios of creep plus shrinkage for the two beams at different periods. Shrinkage values were small as compared to creep.

Figure 8.I.7 gives comparison of changes of strain for the beams with time.

Test - 1

Table 8.I.4.1

Comparison between beam one and two

(creep and shrinkage)

Period (days)	Creep and Shrinkage Strain *Strain on prestressing Beam 1	Creep and Shrinkage Strain *Strain on prestressing Beam 2
1-5	0.28	0.30
1-9	0.40	0.41
9-17	0.37	0.13
17-27	0.12	0.14
27-36	0.08	0.12
1-36	0.97	0.80

* Strain on prestressing was used as opposed to elastic strain, as it took sometime to record the readings, so that some primary creep must have been included.

Results in the table show that before applying heating-cooling and humidity cycling to beam one, the two beams had a similar rate of axial creep and shrinkage. After applying heating-cooling and humidity cycles to beam one its creep and shrinkage in the first eight days (9-17) was almost three times as much as that of the unheated beam. However at later periods, creep and shrinkage for the heated beam were less than that of the unheated beam. This result is similar to the behaviour of the reinforced beams, that is creep increased with temperature only during the first few days of cyclic heating, while at later stages temperature had a reduced effect on creep due to increased maturity and to lower moisture content.

Table 8.I.4.2:Comparison of beam one and two for creep only

Period (days)	(Average Force) KN		Ratio of forces	(Average Stress) N/mm^2		(*Average specific) creep x 10^6	
	B1	B2		B1	B2	B1	B2
1-8	173.5	156.1	1.11	8.81	7.93	16.1	18.8
8-17	167.5	149.2	1.12	8.51	7.58	19.3	7.2
17-27	159.3	145.0	1.099	8.09	7.36	6.2	7.3
27-36	156.5	142.6	1.097	7.95	7.24	4.4	7.0

* Specific creep is creep per unit stress (N/mm^2).

Table 8.I.4.2 gives a comparison between creep of beam one the heated beam and beam 2 the unheated beam. It gives the average force as measured from the load cell strain in the time period indicated. The ratio between the average force on beam one to that on beam two in the first period was 1.11. It changed to 1.12 in the second period when beam one was first heated. The ratio then decreased to 1.099 and 1.097 for the last two periods. This indicates that even though creep of the two beams were markedly different through the time of the test, the longer term force ratio changed only slightly for the two beams.

8.II PRESTRESSED BEAMS,UNSEALED

8.II.1 Prestressing the beams

The prestressing forces at transfer as determined from the strain readings of the load cell were 185.4 KN and 186.1 KN for beams one and two respectively.

The concrete strain readings showed that the Macalloy bars were displaced from the centre postion. Their eccentricities were 2.66mm and 6.14mm for beams one and two respectively.

At transfer, stresses at the top and bottom for beam one were 9.72 N/mm^2 and 8.24 N/mm^2 for beam two the stresses were 10.28 and 6.85 for top and bottom of the beam respectively based on an elastic modulus value of $18.8KN/mm^2$.

At transfer beam one had a sagging curvature of -0.44×10^{-6} mm^{-1}, and beam two had a sagging curvature -0.1×10^{-6} mm^{-1}.

8.II.2 Beam one

Long term results:

Figure 8.II.1 shows changes of total (creep and shrinkage) strain with respect to time. The figure shows steep rise in strain as the beam was first heated. Thirty eight days after prestressing, the beam had a creep and shrinkage value of 0.71×10^{-3}. The hyperbolic law predicts an ultimate value of 0.14×10^{-2}.

Initially the beam had a sagging curvature of 0.44×10^{-6}, this increased to 0.17×10^{-5} at the end of the test.

Thirty eight days after prestressing (thirty days of cyclic heating), the initial prestressing force was reduced (Figure 8.II.2) by 40.5 KN, that is about 22 per cent of its initial value.

Shrinkage

Figure 8.II.3 gives values of changes in axial shrinkage strain with time. After 32 days from datum it was 225×10^{-6}. CP110 predicts an ultimate shrinkage of 200×10^{-6} for normal exposure.

Daily thermal cycle:

Predicted curvature values were between 0.62 x $10^{-6}mm^{-1}$ and 0.83 x 10^{-6} mm^{-1} and were within 13% of measured values. Predicted stresses at the top and bottom were about -1.5 ± 0.2 N/mm^2. The highest predicted tensile stress at the middle parts of the beam was $+0.62$ N/mm^2.

8.II.3 Beam Two

Figure 8.II.4 shows changes of strain with respect to time. The figure shows combined creep and shrinkage. Thirty eight days after prestressing, the creep and shrinkage value was 0.65 x 10^{-3}. The hyperbolic law predicts an ultimate value of 0.12 x 10^{-2}.

Figure 8.II.5 gives changes of prestressing force with time. Thirty eight days after the start of prestressing, the initial prestressing force was reduced by 29.3KN, that is about 16 per cent of its initial value.

The initial sagging curvature of 0.1 x 10^{-5} had increased to 0.19 x 10^{-5} thirty eight days after prestressing.

Shrinkage

Figure 8.II.6 gives changes in shrinkage strain with respect to time. Its value after thirty eight days from datum was 122 x 10^{-6}.

8.II.4 Comparison between beam one and beam two

Both beams one and two were cast and cured in the same way. They were prestressed at the same time to initial prestressing forces of 185.KN and 186 KN for beam one and two respectively. Cyclic heat-cooling and humidity was applied to beam one eight days after prestressing.

Figure 8.II.7 gives comparison of changes with respect to time of strain (due to creep and shinkage) for the two beams.

Table 8.II.4.1 gives a comparison of the chronological development of creep and shrinkage at different periods of the test for the two beams.

Table 8.II.4.1 Comparison of beams one and two for creep and shrinkage

Period (days)	Creep and shrinkage strain / Strain on prestressing	Creep and shrinkage strain / Strain on prestressing
	Beam 1	Beam 2
1 - 8	0.3	0.33
8 - 17	0.77	0.56
17 - 27	0.27	0.24
27 - 38	0.14	0.27
1 - 38	1.48	1.40

During the first eight days, strain readings for the two companion shrinkage blocks did not show any shrinkage. The reason for this was possibly the fact that during this time the water lost to the environment was water held in the capillary pores, which did not lead to shortening of the specimen, and it was only when the gel pores started to lose some water that the specimen underwent shrinkage.

The first eight days creep and shrinkage ratio to elastic was only 0.3 and 0.33 for beams one and two respectively. This ratio changed considerably at the later stage (8-17) not only for the heated beam, but also for the non-heated beam, where it was 1.7 times its

value for the first eight days where primary creep is expected to occur. This was because the beam had negligible shrinkage during the first eight days.

At the first nine days of heating beam one had considerably more creep and shrinkage than the unheated beam. However, in the last period of the test the unheated beam had more creep and shrinkage.

Table 8.II.4.2 gives comparison of the two beams for specific creep and average forces at different periods of the test.

Results in the table show that the specific creep was as expected, about the same for the two beams at the first period (before the start of the heating cooling cycle). The average specific creep for beam one for the first nine days of heating was 44 per cent more than that of the unheated beam. However, for later stages the specific creep for the heated beam was much less than that of the unheated beam, indicating that the heated beam was nearly dessicated and lost its potential to creep.

Also the table shows, as has been found in test 8.I .4.2 that the ratio of the two forces had not changed markedly through time.

Table 8.II.4.2 Comparison of beams one and two for creep only

Period (days)	Average Force KN		Ratio of Forces	Average Stress N/mm^2		Average Creep per Unit stress x 10^6	
	B1	B2		B1	B2	B1	B2
1 - 8	183.3	184.5	1.008	9.31	9.37	15.1	15.8
8 - 17	170.6	173.7	1.018	8.67	8.82	32.5	22.5
17 - 27	157.3	161.9	1.029	7.99	8.22	3.2	11.2
27 - 38	149.7	158.1	1.056	7.60	8.03	4.5	8.6

8.10 Comparison between the two tests

Results in tables 8.I.4.2 and 8.II.4.2 show that during the first eight days after prestressing the partly sealed beams had more average specific creep than the unsealed beams. This was because during this period, the two unsealed beams did not undergo any shrinkage as was indicated from strain readings on their companion shrinkage blocks.

The specific creep for the first nine days of heating was as expected considerably more for the unsealed beam than that of the partly sealed beam, since the unsealed beam underwent more drying creep than the partly sealed. Their ratio during this period was 1.69 to 1. During the same period (day 8 to 17), the average specific creep ratio of the unsealed unheated beam to the partly sealed unheated beam was 3.13 to 1. The difference of the two ratios was due to the fact that the heated beam lost its moisture quickly. In fact if we compare the average specific creep of the two heated beams for the first three days of heating, the ratio becomes 3.85 to 1 for the unsealed and partly sealed respectively as compared with 1.69 to 1 for the nine days period.

At later stages, the heated unsealed beam had less average specific creep than the partly sealed beam, while the unheated unsealed beam had more average specific creep than the unheated partly sealed beam.

8.11 Conclusions

Results obtained in this chapter for axial creep in prestressed beams are similar to results of the previous chapters for flexural creep in reinforced beams. The effects of the heating-cooling and humidity cycles were to increase axial creep significantly during the first few days of heating, but its effects at later stages were to reduce rather than to

increase creep for both the partly sealed and the unsealed beams. The first eight days of heating-cooling and humidity cycles increased creep for the partly sealed to almost three times its value for the unheated beam. However for the unsealed beams the ratio was much less (about 1.6 to 1).

The partly sealed beam experienced no increased loss in the prestressing force due to the applied heating-cooling and humidity cycles as compared to the beam exposed to laboratory ambient conditions, while the unsealed beam experienced slight reduction in force as a result of heating-cooling and humidity cycling. The difference was about 6 per cent.

In the daily cycles, values for self equilibrating stresses as predicted by the computer program were generally small, less than 1.72 N/mm^2 (compression) for both top and bottom fibres and less than 1.1 N/mm^2 (tension) in the middle parts of the beams. Predicted curvature values were within 13% of the measured values, and their variation depends on the thermal coefficient of expansion used in the analysis.

Hogging shrinkage curvature was approximately equal for both the partly sealed block under heating/cooling and humidity cycle and the block under normal laboratory conditions. The axial shrinkage strain for the unsealed block under H/C and humidity cycle was almost two times that of the value for the block under normal laboratory conditions.

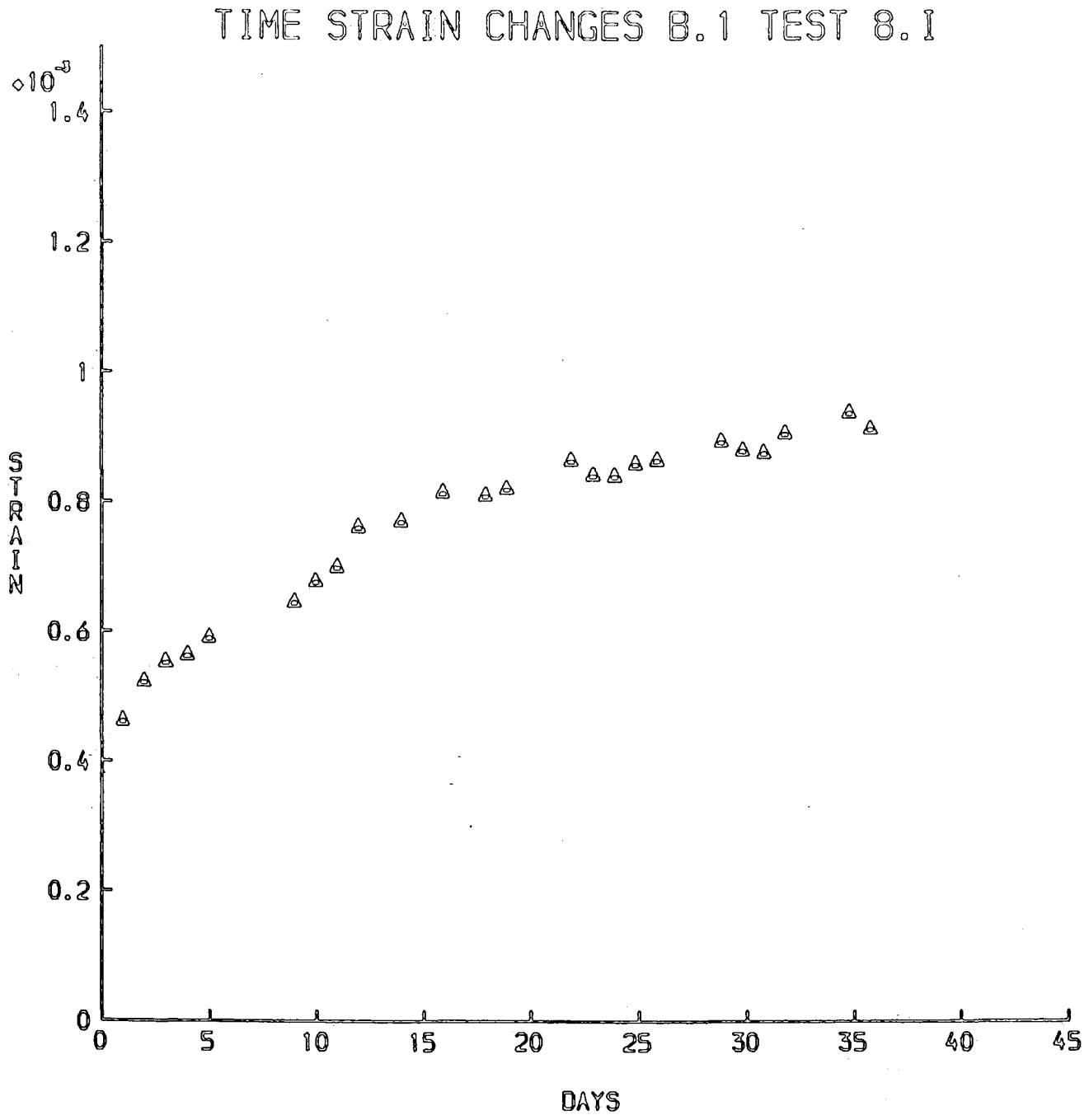
TIME STRAIN CHANGES B.1 TEST 8.I
$\diamond 10^{-3}$
1.4
1.2
1
0.8
0.6
0.4
0.2
0
STRAIN
0
5
10
15
20
25
30
35
40
45
DAYS

FIG. 8.I.1

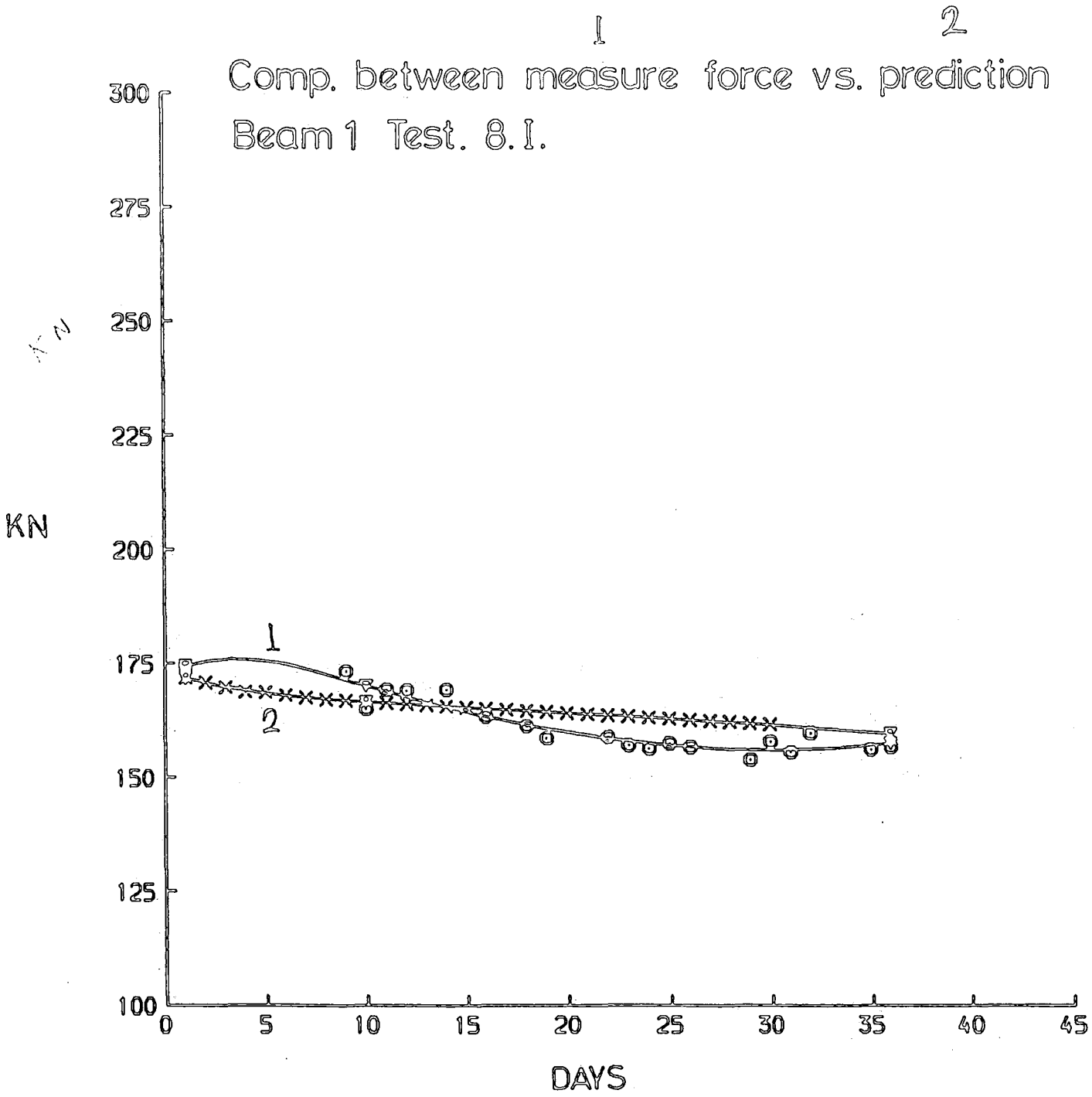
1
2
Comp. between measure force vs. prediction
Beam 1 Test. 8.1.
300
275
250
225
200
175
150
125
100
KN
1
2
0
5
10
15
20
25
30
35
40
45
DAYS

FIG. 8.1.2.

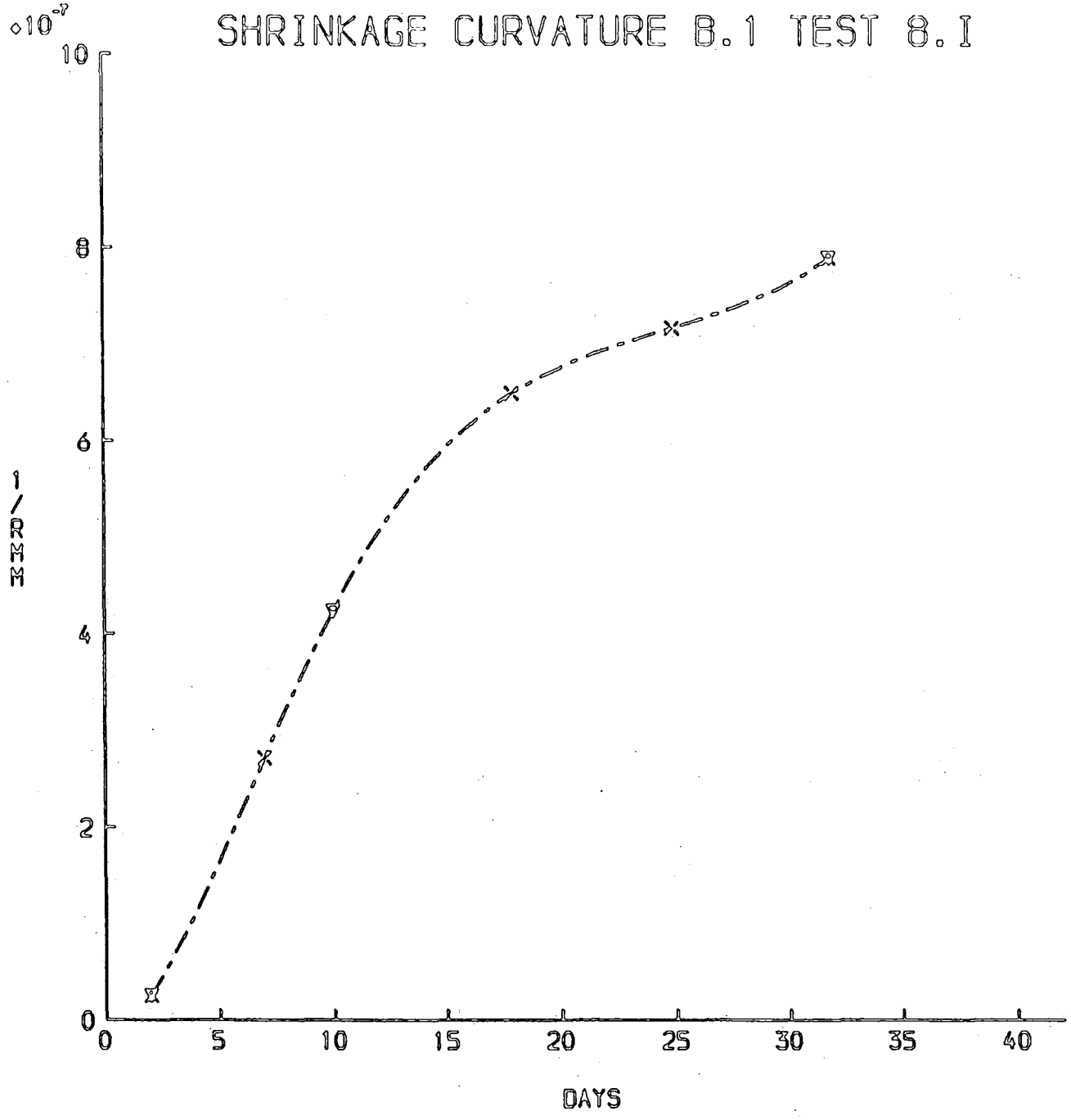
SHRINKAGE CURVATURE 8.1 TEST 8.I
◇10⁻⁷
10
8
6
4
2
0
1/RMM
0
5
10
15
20
25
30
35
40
DAYS

FIG. 8.1.3.

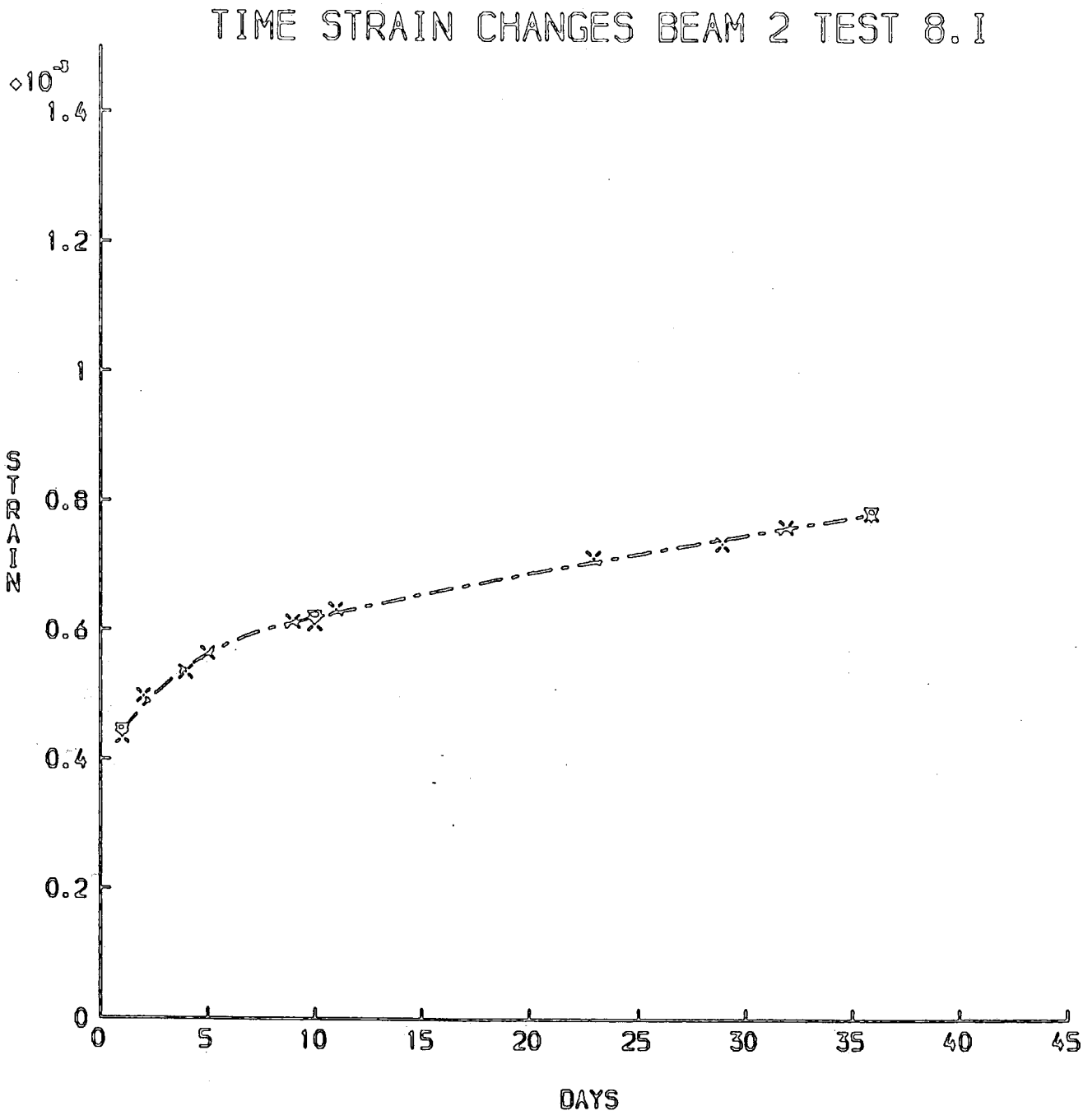
TIME STRAIN CHANGES BEAM 2 TEST 8.1
$\diamond 10^{-3}$
1.4
1.2
1
0.8
0.6
0.4
0.2
0
STRAIN
0
5
10
15
20
25
30
35
40
45
DAYS

FIG. 8.1.4.

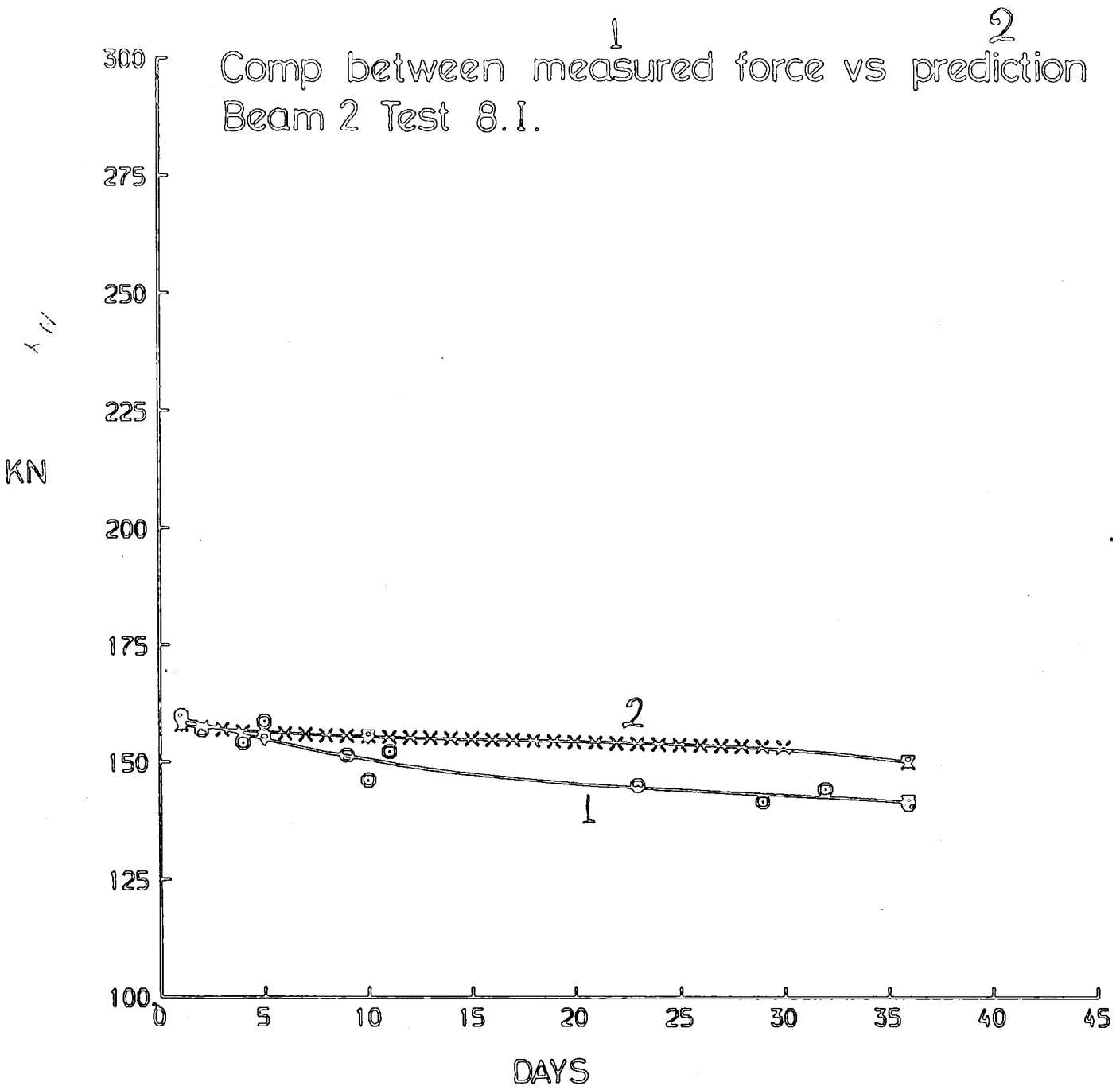
1
2
Comp between measured force vs prediction
Beam 2 Test 8.I.
300
275
250
225
200
175
150
125
100
KN
0
5
10
15
20
25
30
35
40
45
DAYS
2
1

FIG. 8. I. 5.

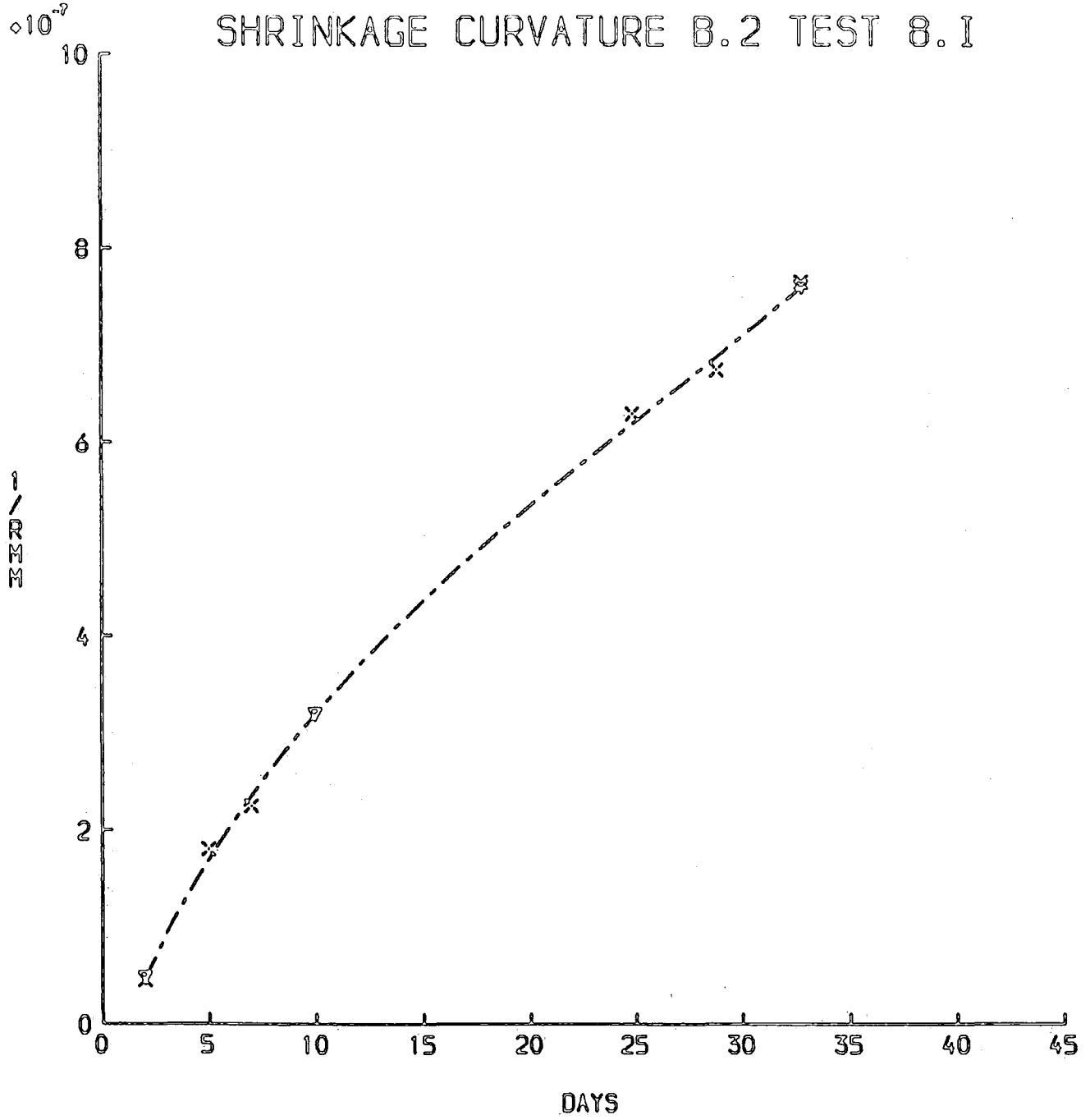
SHRINKAGE CURVATURE B.2 TEST 8.1
◇10⁻⁷
10
8
6
4
2
0
1/RMM
0
5
10
15
20
25
30
35
40
45
DAYS

FIG. 8.1.6.

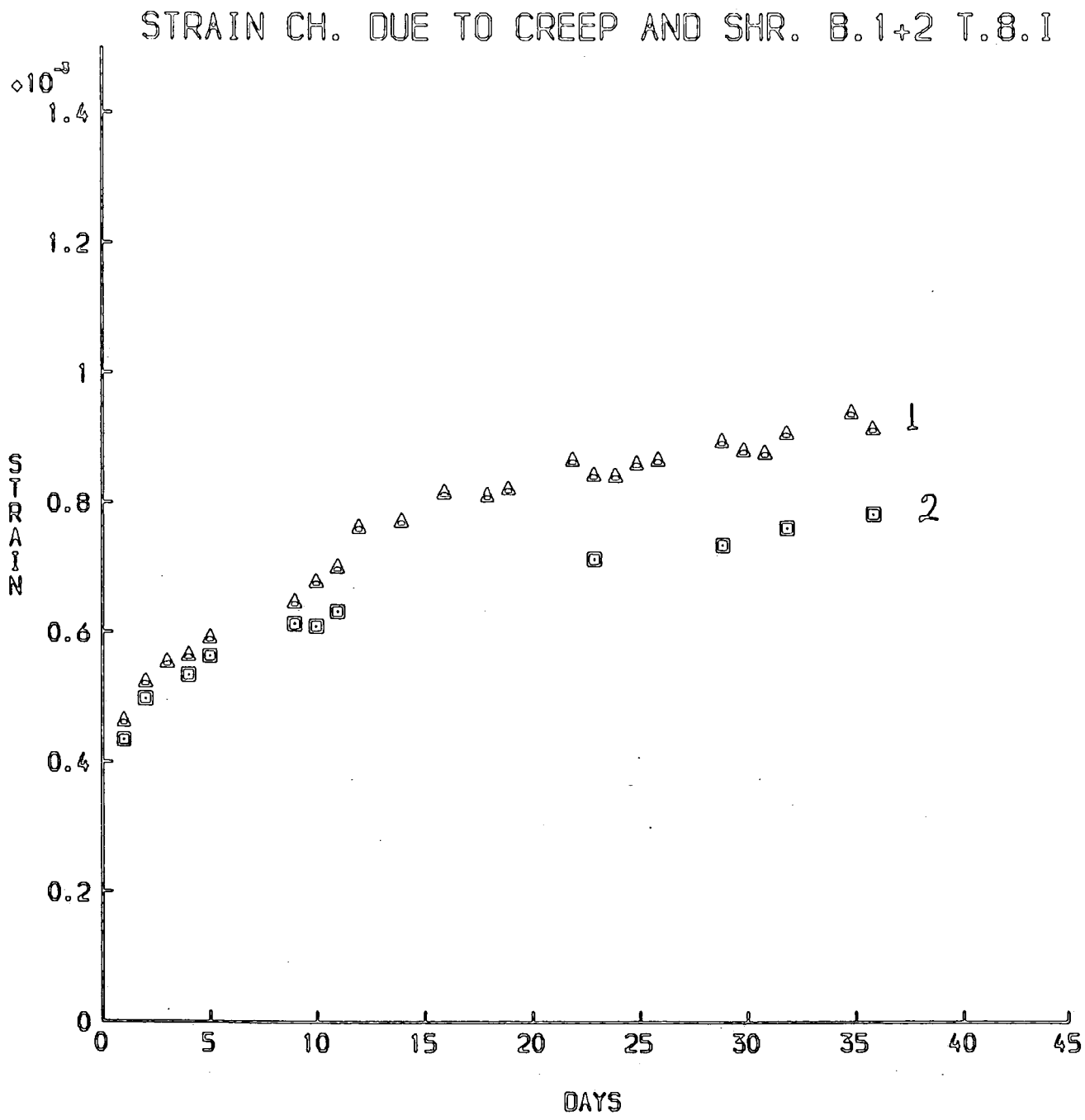
STRAIN CH. DUE TO CREEP AND SHR. B.1+2 T.8.1
◇10⁻⁵
1.4
1.2
1
0.8
0.6
0.4
0.2
0
STRAIN
0
5
10
15
20
25
30
35
40
45
DAYS
1
2

FIG. 8.1.7

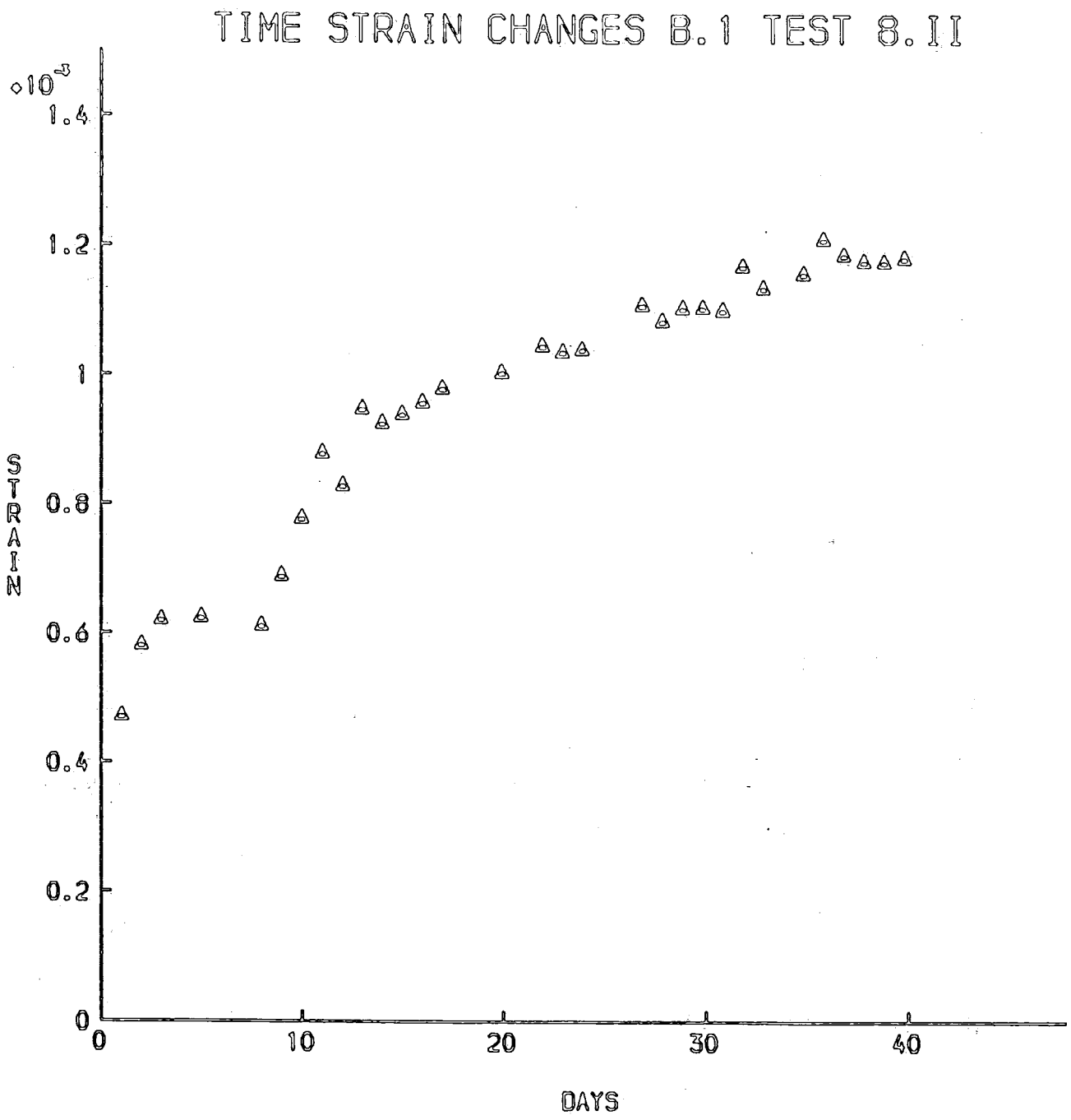
TIME STRAIN CHANGES B.1 TEST 8.II
$\diamond 10^{-3}$
1.4
1.2
1
0.8
0.6
0.4
0.2
0
STRAIN
0
10
20
30
40
DAYS

FIG. 8.II.1

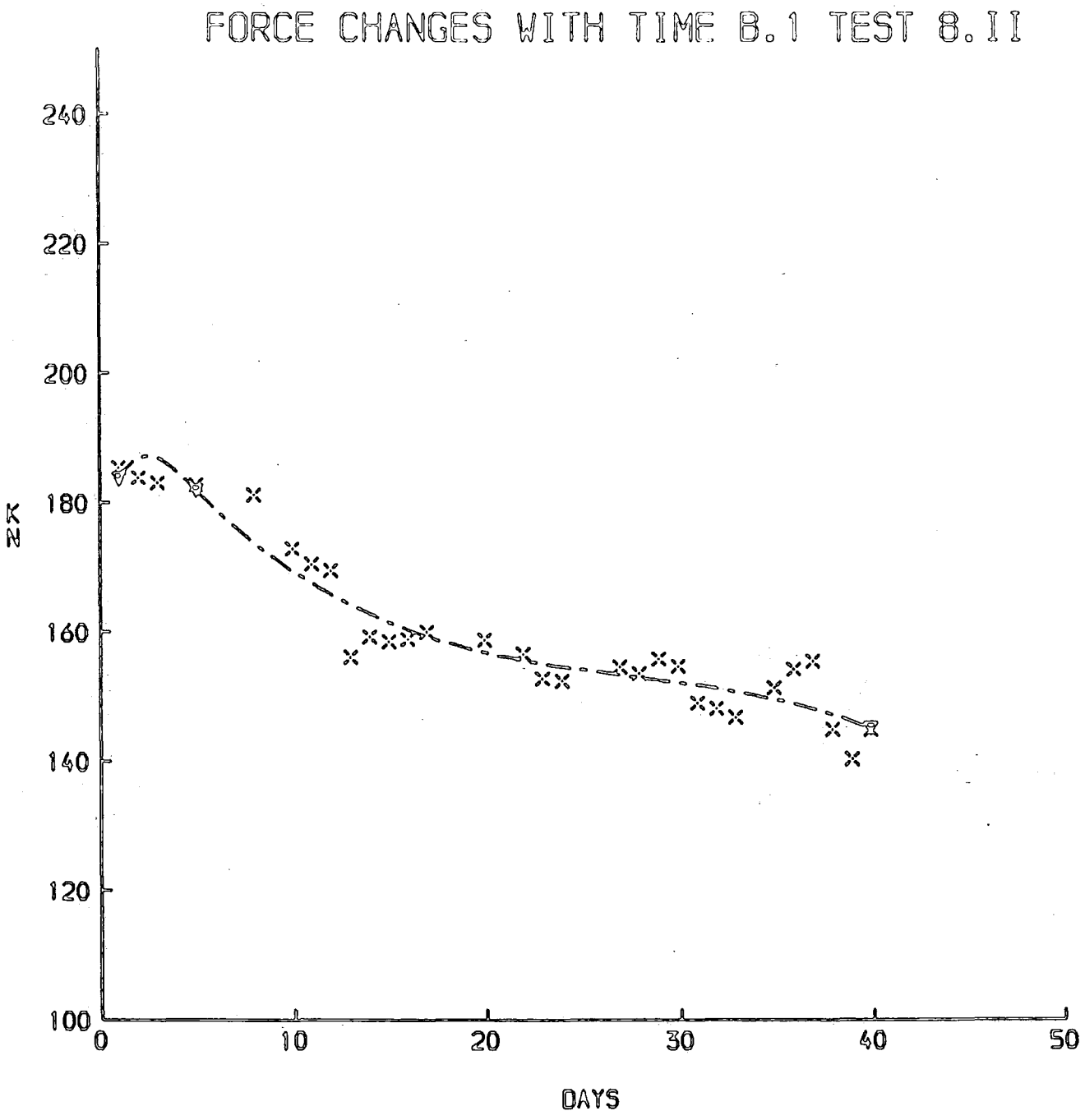
FORCE CHANGES WITH TIME B.1 TEST 8.II
240
220
200
180
160
140
120
100
KN
0
10
20
30
40
50
DAYS

FIG. 8.II.2

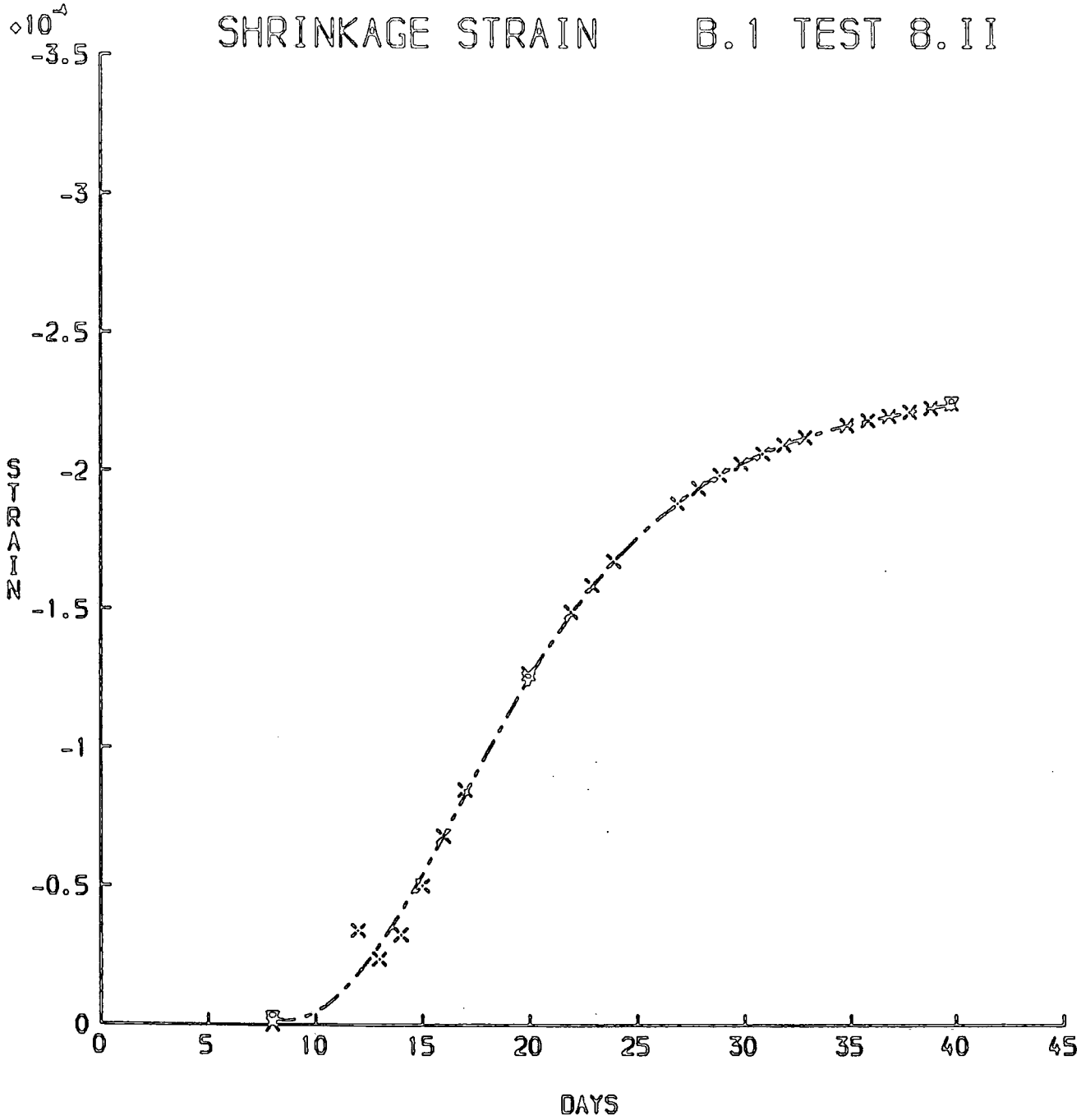
SHRINKAGE STRAIN B.1 TEST 8.II
◇10⁻⁴
-3.5
-3
-2.5
-2
-1.5
-1
-0.5
0
STRAIN
0
5
10
15
20
25
30
35
40
45
DAYS

FIG. 8.11.3

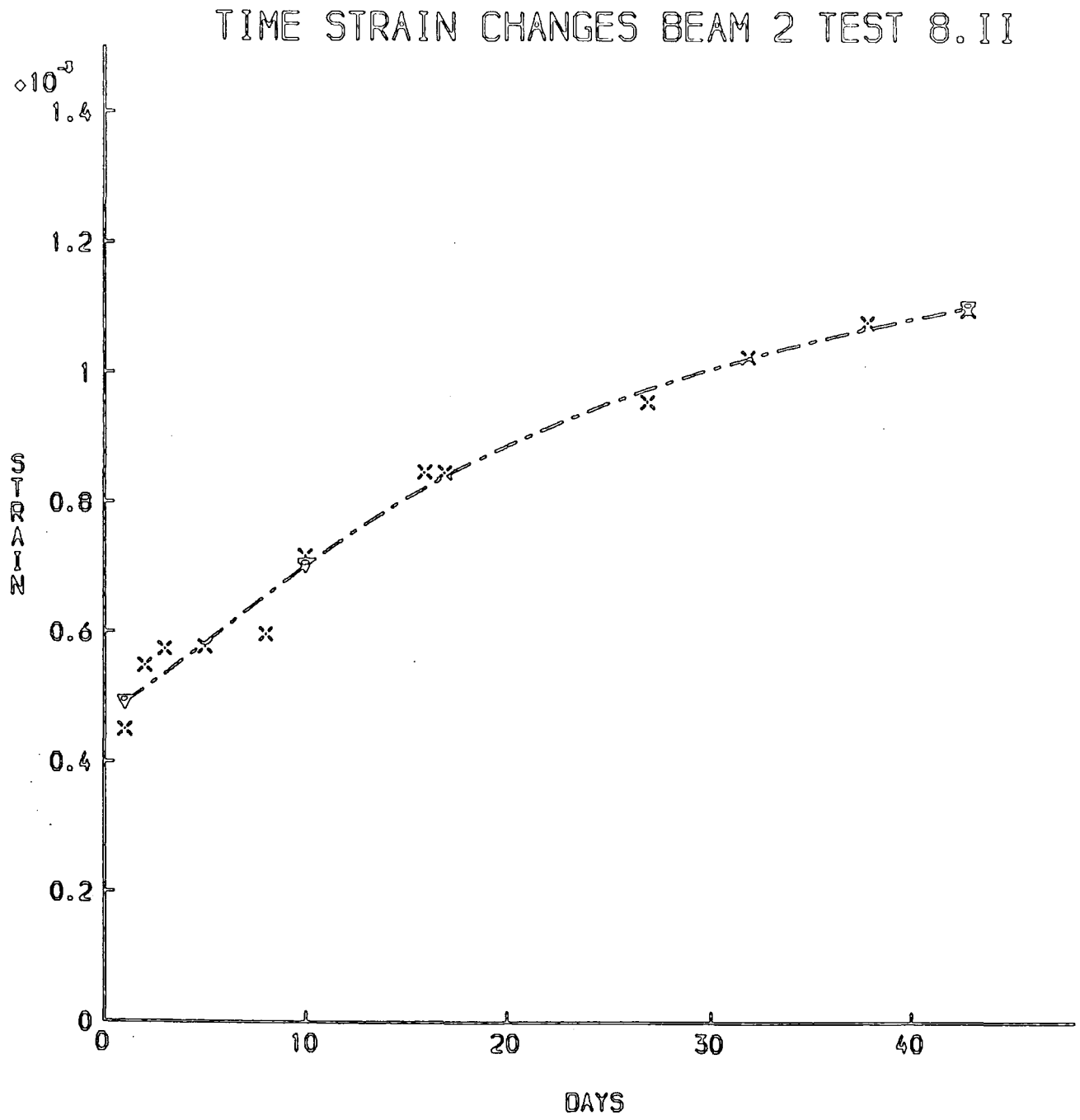
TIME STRAIN CHANGES BEAM 2 TEST 8.II
◇10⁻³
1.4
1.2
1
0.8
0.6
0.4
0.2
0
STRAIN
0
10
20
30
40
DAYS

FIG. 8.II.4.

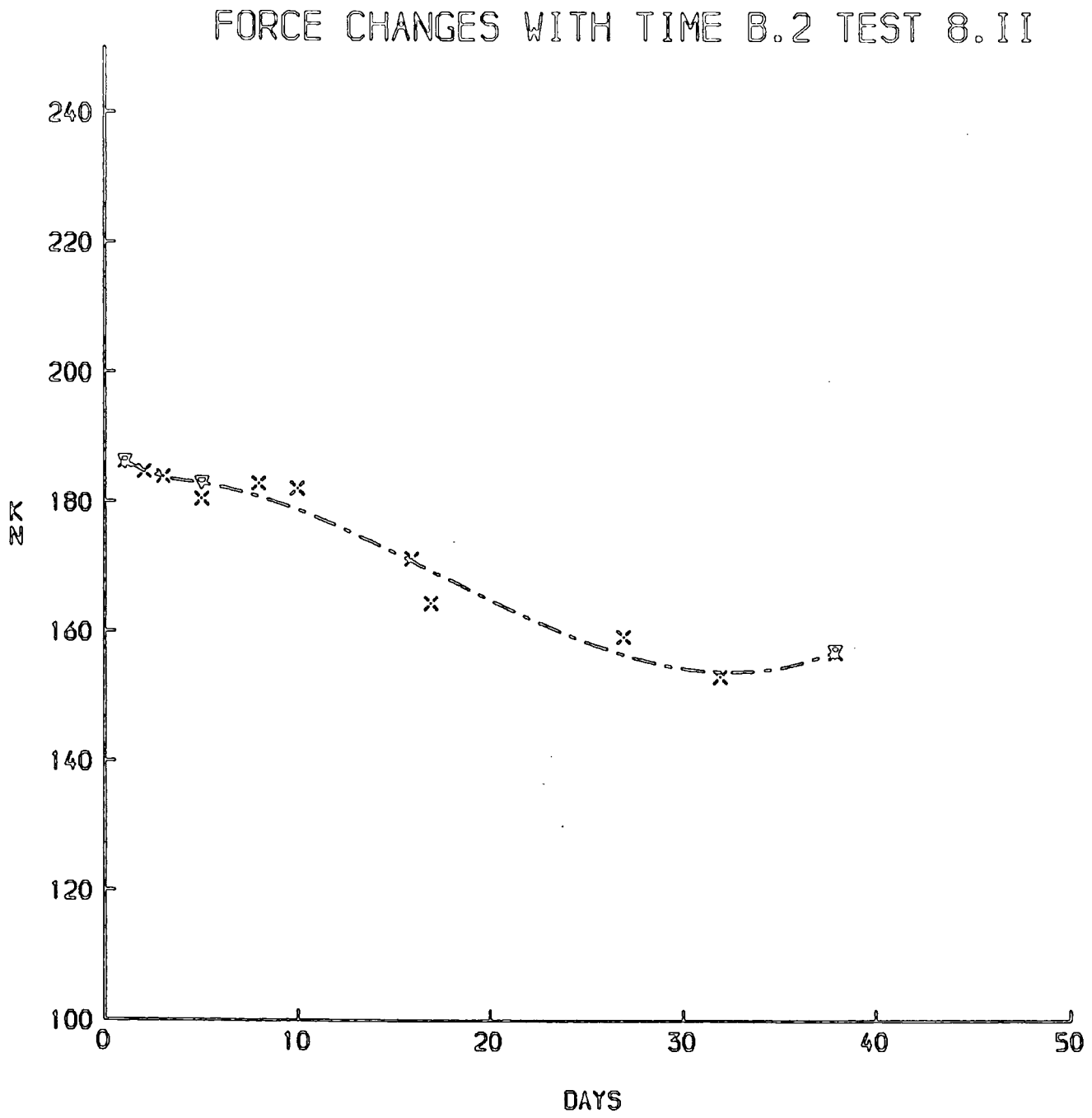
FORCE CHANGES WITH TIME B.2 TEST 8.II
240
220
200
180
160
140
120
100
KN
0
10
20
30
40
50
DAYS

FIG. 8.II.5

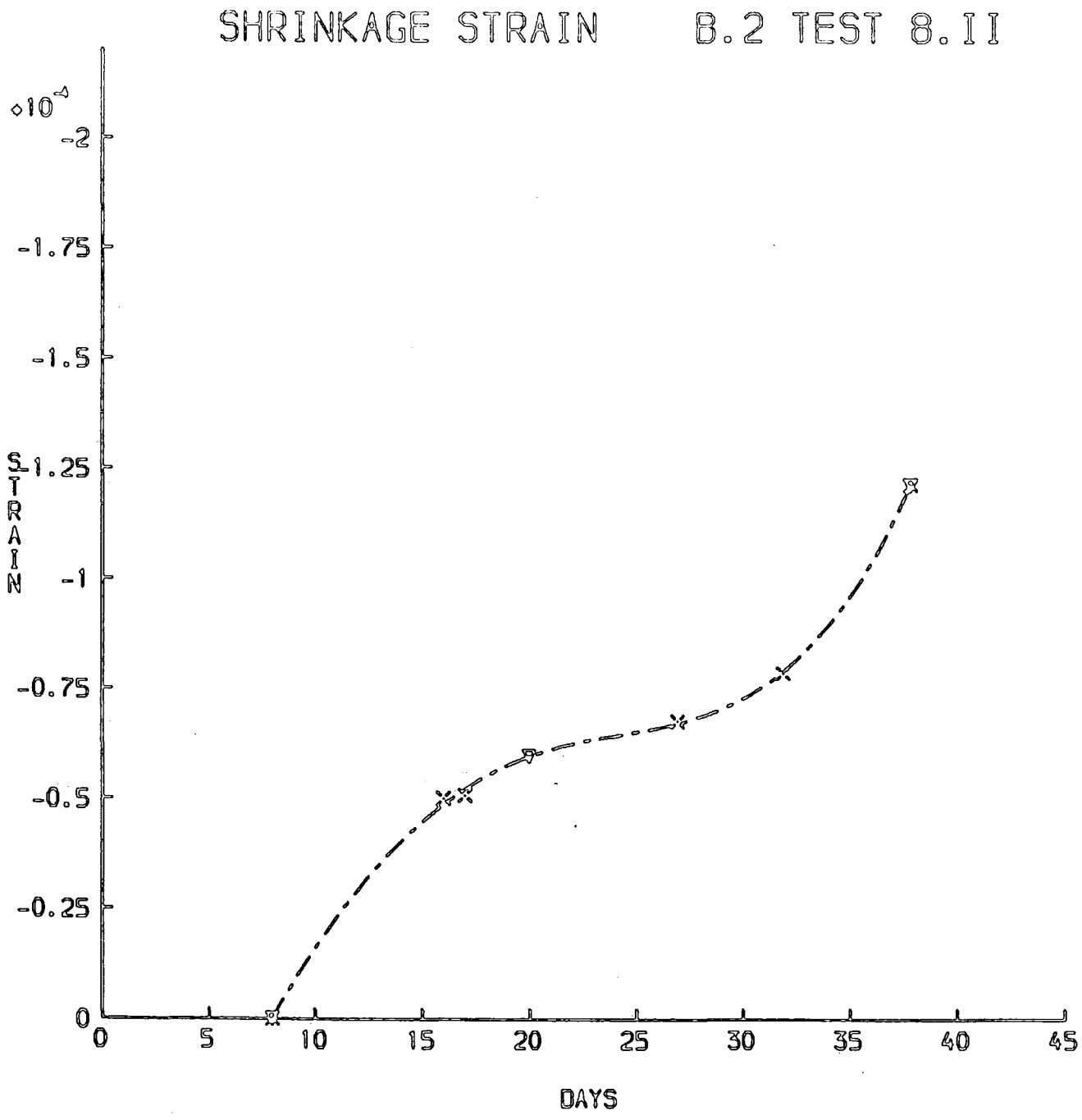
SHRINKAGE STRAIN B.2 TEST 8.II
$\times 10^{-4}$
-2
-1.75
-1.5
-1.25
-1
-0.75
-0.5
-0.25
0
STRAIN
0
5
10
15
20
25
30
35
40
45
DAYS

FIG. 8.11.6

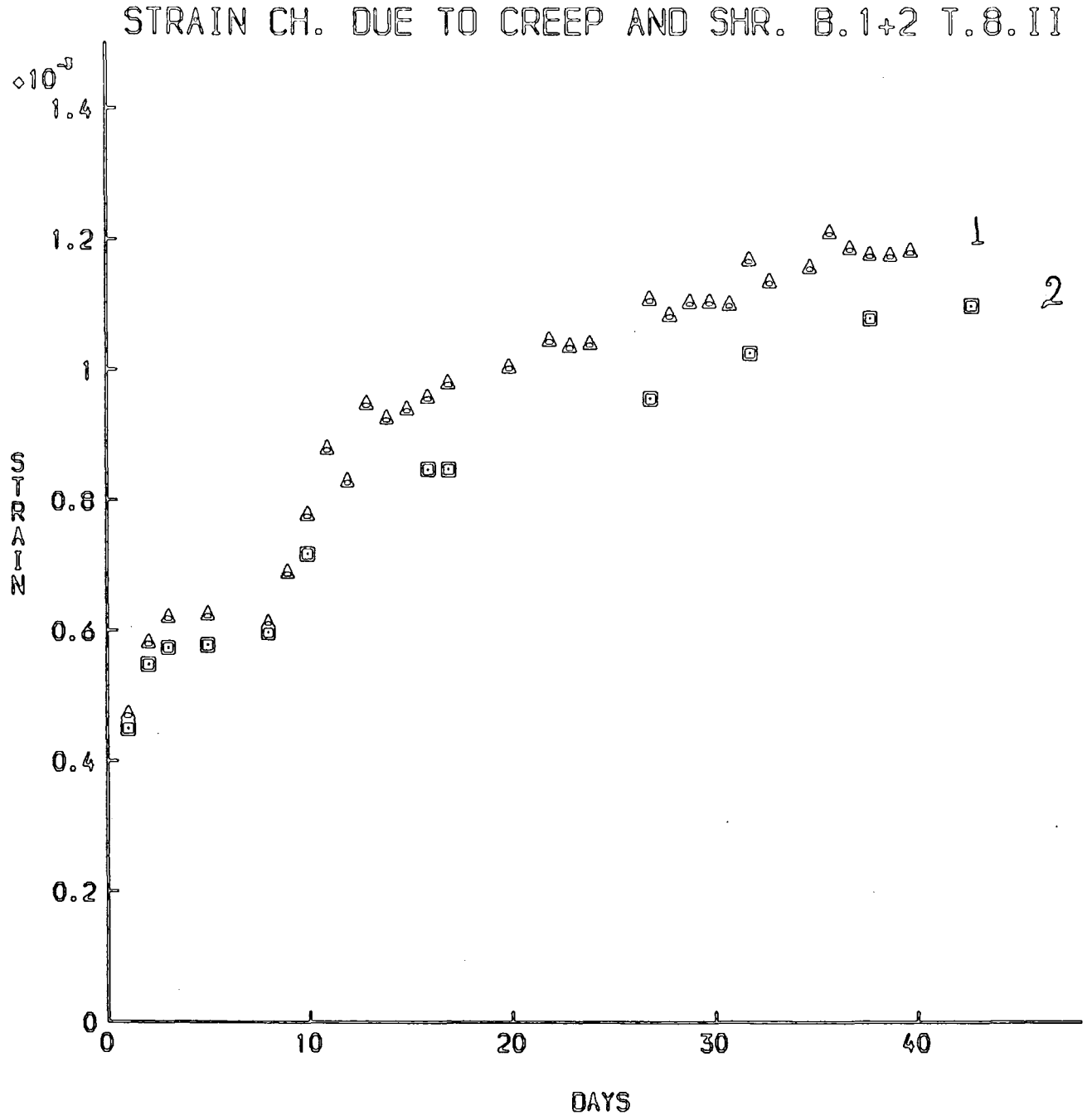
STRAIN CH. DUE TO CREEP AND SHR. B.1+2 T.8.II
◇10⁻⁵
1.4
1.2
1
0.8
0.6
0.4
0.2
0
STRAIN
0
10
20
30
40
DAYS
1
2

FIG. 8.11.7

CHAPTER 9

CONCLUSIONS AND RECOMMENDATIONS

CHAPTER 9 CONCLUSIONS AND RECOMMENDATIONS

9.1 Conclusions:

A number of reinforced and prestressed concrete beams was subjected to long-term loading and daily cycles of elevated temperature and low humidity values modelling the summer and late spring climate of central Saudi Arabia. Based upon the laboratory tests and analytical work presented, and pursuent to the limitations cited and time periods considered in these tests, the following conclusions are believed warranted:-

9.1.1 Tests on reinforced concrete beams

9.1.1.1 Long-term results

- When partly sealed beams were subjected to daily cycles of above normal temperature and low humidity prior to loading, their elastic deformations were reduced. However unsealed beams subjected to similar cycles before loading showed increased elastic deformation.
- The final creep deformations of beams, partly sealed and unsealed, subjected to diurnal environmental cycles prior to loading were less than creep deformations of partly sealed and unsealed beams subjected to similar cycles after loading.
- The benefits of sealing (and hence improved curing) were demonstrated in the values of elastic deflection. An increase of almost sixty per cent was observed in the value of the elastic deflection of the unsealed beam over the value of the completely sealed beam when both were subjected to the diurnal cycles for three days prior to loading.

- Partly sealed beams subjected to diurnal cycles showed rapid early-age creep deflections, thirty per cent more than that of fully sealed beams subjected to similar cycles. However the fully sealed beams had more creep deformation at later stages. The thirty two days creep of both sets was about equal.

- The first six days creep values for the unsealed beams subjected to the diurnal cycles were about 70% more than those of the fully sealed beams. However the increase was less for later creep. The total thirty two days creep value of the unsealed beams was about one and a half times that of the fully sealed beams.

- From limited evidence, indications are that final creep values might be derived as a simple factor of elastic values. Present experimental results show that the ratio of the thirty two days creep deformation to elastic deformation was about equal for all the cracked cyclically heated beams despite the different sealing conditions.

- Daily cycles of above normal temperature and low humidity values caused very large values of early age creep in some partly sealed beams. Up to 70% of the 32 day creep had occurred by the 6th day in some tests.

- Early-age creep values for partly sealed beams subjected to the diurnal cycles were about two times that of early-age creep values for beams exposed to normal laboratory conditions. However their later stage total creep values were about equal.

- Cyclic heating/cooling and low humidity values increased early-age creep of the unsealed beam to thirty per cent more than early-age creep of an unsealed beam exposed to normal

laboratory conditions. However the later creep value of the unsealed beam subjected to the daily cycles was markedly less than the later creep of the beam exposed to normal laboratory conditions, suggesting that the ultimate creep deformation value for the former beam might be less than the ultimate creep deformation value for the latter beam.

- There were only slight differences in the final values and the chronological development of creep for surface heated and insulated beams and for air heated and uninsulated beams.
- The elastic deflection predicted by the codes CP110, CEB-FIP and ACI was reasonably close to the measured values. However the creep deflection was generally underestimated by the codes CP110 and CEB-FIP (based on an effective modulus approach), while the use of the reduction factor method by the ACI 209 tended to overestimate slightly creep deflection values.
- The heating and humidity cycles had no marked influence on the magnitude of the recoverable creep after unloading.
- The use of the rate of creep method based upon specific thermal creep and a step by step approach gave in general satisfactory results. However experimental results showed that the assumption that creep increases with temperature at all times is not correct.
- Results showed that the value of the peak hogging shrinkage curvatures for the partly sealed beams subjected to the diurnal cycles were approximately equal to shrinkage curvature of the beam exposed to normal laboratory conditions.

The peak shrinkage value for the beam under normal conditions developed at a later time than the peak value for the beam under cyclic heating/humidity.

- The value of the maximum sagging shrinkage curvature for the unsealed beams of tests subjected to the daily cycles was three times as much as the maximum measured sagging shrinkage curvature for the beam exposed to normal laboratory conditions.

9.1.1.2 Effects of the Daily cycle

- Computed values of self-equilibrating stresses due to daily thermal cycle representing both summer and spring conditions (for central Saudi Arabia) of simply supported beams are generally small (e.g. about 1.5 N/mm^2) and can be ignored. This may not be so with deeper beams.

- Maximum measured curvature values due to daily thermal cycles representing both summer and spring conditions were small (typically about $0.8 \times 10^{-6} mm^{-1}$).

- The use of a simple iterative method based on the equilibrium of forces and moment change through the cross section can predict satisfactorily the curvature due to the daily thermal cycle. However the correlation is highly dependent on the value of coefficient of thermal expansion used in the analysis.

- The use of an uncracked section in the predictive analysis for curvature of the cracked beams due to the daily thermal cycle changes the correlation with measured curvature values only slightly, and is adequate for design.

9.1.2 Tests on prestressed beams

- The effects of heating/cooling and humidity cycles were to increase axial creep significantly for the first few days, but their effects at later stages were to reduce creep for both the partly sealed and the unsealed beams.
- The partly sealed beams experienced no increased creep and shrinkage losses in the prestressing force due to the applied daily cycles as compared to the beam exposed to normal laboratory conditions. The unsealed beam experienced only slight reduction in force as a result of cyclic heating/cooling and humidity values.
- In analysis of response to the daily cycle, the use of the simple iterative method based on the equilibrium of forces and moment change gave a better correlation of predicted curvature with measured values than was obtained for reinforced concrete beams. However the correlation (as was found for reinforced beams) was highly dependent on the value of coefficient of thermal expansion used in the analysis.
- Values of the self-equilibrating stresses due to the daily thermal cycle are small and can be ignored. This may not be so in deeper beams.
- The axial shrinkage for an unsealed block subjected to cyclic heating/cooling and humidity cycles was about two times that in the block exposed to normal laboratory conditions.

9.2 Recommendations for further research:

During the course of the present study it has been clear that several areas require particular attention in future investigation.

- In the present tests the boundary values of temperature were predicted using finite element analysis. There is a pressing need for field measurement of temperature distributions inside concrete members located in central Saudi Arabia.

- The combination of elevated temperature and low humidity on the material properties of concrete with different mix designs need to be investigated. Particularly important are the effects on the elastic modulus and the coefficient of thermal expansion. During the course of the present tests the variation of the value of the coefficient of thermal expansion was found to be of primary importance in the correlation between measured and predicted values of curvature due to daily thermal cycle. Thus an accurate me a surement of its value in relation to age and moisture distribution is vital in any predictive analysis.

- Tests conducted here were for positive temperature gradients. A useful extension would be to test the effect of reversed temperature gradients, such as occur during a cold clear night.

- Another useful work will be to extend this work to include beams with redundancies and to measure the effect of elevated temperature on the reaction forces at the supports.

- The effects of daily cycle should be investigated in relation to deeper beams.

- Lastly it is suggested that measurement should be conducted on partly and fully sealed beams over longer periods than what were considered here, and to include tests on beams subjected to environmental cycles and load at a younger age.

APPENDIX I

MATERIAL PROPERTIES OF THE CONCRETE

A. Compressive strength

Compressive strength was determined using 100 x 100 x 100 mm cubes. The cubes were demoulded one day after casting, and then cured in a water tank with a temperature of 18 ± 1°C until the time of testing. The values obtained are listed in the table below:-

Test Code	Age at test days	Number of cubes	Average N/mm ^{2}
5.I	21	10	41
	28	5	43
5.II	21	10	39
	28	5	41
5.III	21	10	42
	28	5	43.5
6.I	21	10	40.5
	28	5	43
6.II	21	10	43
	28	5	45
6.III	21	10	44.5
	28	5	45
7.I	21	10	41.5
	28	5	44

b. Cylinder splitting test

The Brazilian splitting test was conducted on 300 x 150 mm diameter cylinders. The average tensile strength from tests on two specimens three weeks old for the different tests are as follows:-

Test Code	Strength N/mm^2
5.I	3.5
5.II	3.5
5.III	3.3
6.I	4.1
6.II	3.0
6.III	4.2
7.I	3.3

c. Secant elastic modulus

This was measured in accordance with BS 1881 on 300 x 150 mm diameter cylinders, using three pairs of demec studs, parallel to the polar axis. The value reported here is the average of readings in two cylinders.

Test Code	Age at test days	Modulus Value KN/mm^2
5.I	21	24
	28	25.5
5.II	21	26
	28	26.5
5.III	21	24
	28	25.5
6.I	21	22
	28	25
6.II	21	27
	28	29
6.III	21	27
	28	29
7.I	21	24
	28	28

C. Coefficient of Thermal expansion

Concrete:

The value of the coefficient of thermal expansion was obtained from tests on small unreinforced cylinders (200 x 60 mm diameter).

A number of cylinders were sealed in a similar fashion to the beams, and kept in the cabin where, in addition to the air temperature variations, they were surface heated by a heating tape spread on their top surfaces. At the end of every week, one cylinder was taken out and completely sealed against moisture loss, then its coefficient of thermal expansion was measured by heating it in the oven to a temperature of 60°C and measuring strain change. At the end of the following week the coefficient of thermal expansion for another cylinder was obtained in a similar way, and so on until the end of the test period. The values reported here are the average values of all the cylinders for the particular test:-

Test Code	Coefficient of Thermal expansion x 10^{-6}/°C
5.I	10.88
5.II	11.63
5.III	11.24
6.I	10.4
6.II	12.2
6.III	12.72
7.I	11.85

Steel

The coefficient of thermal expansion was measured on a 300 mm long steel rod cut from the same material used in the tests. The rod was inserted into a water bath, where its temperature was raised to a known value and the expansion of the rod was measured, thus its coefficient was calculated.

APPENDIX II

THE USE OF CODES

CP110 : 1972

The British standard CP110 recommends that, for flexural members with partially cracked sections, the deflections should be obtained from curvatures calculated on the basis of linear strain distribution, with the tensile concrete contributing a fictitious triangluar stress block below the neutral axis. This fictitious force is defined by a stress of f_c N/mm^2 at the centroid of the tension reinforcement. It further assumes that the neutral axis depth is the same as that in a cracked section.

Hence the average tensile force in concrete = $\frac{1}{2} \frac{b(h-x)^2}{(d-x)} f_{ct}$ and the lever arm of this force about theneutral axis is $\frac{2}{3}(h - x)$; therefore moment due to concrete in tension = $\frac{1}{3} \frac{b(h-x)^3}{(d-x)} f_{ct}$

Thus when a moment M is applied to the partially cracked section, part of it is resisted by the concrete in tension; the net moment to be resisted by the concrete in compression and by the forces in the reinforcement is

$$M_{net} = M_{applied} - \frac{1}{3} \frac{b(h-x)^3}{(d-x)} f_{ct}$$

f_{ct} varies between a value of 1.0 for initial deflection to 0.55 for deflection at ultimate.

Curvature then = $\frac{M_{net}}{E_c I_c}$

Where E_c is the initial elastic modulus and I_c is the second moment of area for the cracked section.

For long term E_c can be replaced by E_t where E_t can be obtained from the effective modulus method

$$E_t = \frac{E_c}{1+\phi}$$

where ϕ is the creep coefficient and its value is given by the cement and concrete association (132) as a discontinuous function.

The calculation of the load-induced curvature according to CP110 requires successive approximations. As an alternative to the numerical integration of the curvatures, CP110 allows the calculation of the deflections from the standard expression

$$d = K L^2 \psi_b$$

where K depends on the shape of the bending moment diagram, L is the span, and ψ_b is the curvature at mid-span, calculated from

$$\frac{1}{r} = \frac{M_{net}}{E_c I_c} \qquad \text{for initial deflection}$$

and

$$\frac{1}{r} = \frac{M_{net}}{E_t I_c} \qquad \text{for long-term deflection}$$

The value of ϕ used for these tests was taken as 0.97 (obtained by interpolation), and the value for f_{ct} was taken as 0.85 (also by interpolation).

American Concrete Institute Method

ACI 209 have suggested that $\phi(t,to)$ can be evalued from:-

$$\phi(t,to) = \left[\frac{(t-to)^{0.6}}{10+(t-to)^{0.6}}\right] \phi_\infty(to)$$

where (t-to) = time since application of load, $\phi_\infty(to)$ = ultimate creep coefficient, and is given by:-

$$\phi_\infty(t_o) = 2.35\ K_H\ K_d\ K_s\ K_F\ K_{AC}\ K_{to}$$

where $\phi_\infty(t_o)$ = 2.35 for standard conditions, and each coefficient is a correction factor for conditions other than standard as follows:-

K_H = relative humidity

K_d = minimum member thickness

K_s = Fine aggregate content

K_F = Fine aggregate content

K_{AC} = Air content

K_{to} = Age of concrete at application of load.

K_H is given by

$K_H = 1.27 - 0.0067h \qquad (h \geq 40)$

where h is relative humidity per cent.

For humidities lower than 40%, values higher than 1.0 shall be used.

K_d for an average thickness between 150 and 380 mm is given by

$K_d = 1.14 - 0.00091\ d$ for $(t-to) \leq 1$ year where d is the average thickness of the concrete member under consideration (mm).

$K_s = 0.82 + 0.00264\ S_f$ where S_f = slump of fresh concrete (mm)

$K_f = 0.88 + 0.00\ 24\ \frac{s}{a}$

where s/a fine aggregate/total aggregate ratio by weight (per cent).

$K_{AC} = 0.46 + 0.09A \geq 1$

where A = air content

$K_{to} = 1.25\ t_o^{-0.118}$ (moist curing)

The following numerical values were used

K_H = 1.15 (by interpolation) for all the tests, except test 7.I

where K_H = 0.94

K_d = 0.96

K_s = 0.87

K_F = 0.96

K_{AC} = 1

$K_{to} = 1.25\ t_o^{-0.118}$

where t_o for the particular test was determined using the maturity expression suggested in CEB-FIP.

Comité Européen du Bèton (CEB-FIP), 1978

The CEP-FIP Model code 1978 divides creep into irreversible creep (plastic flow) and reversible creep (delayed elastic strain). The plastic flow is subdivided into a component representing flow for the first day under load (initial flow) and subsequent flow.

$$\phi(t,t_o) = \left[\frac{E_c(t_o)}{E_c(28)}\right] \phi_{28}(t,t_o)$$

where t is the time at which the creep coefficient is to be calculated.

t_o is age of loading.

$\phi_{28}(t,t_o)$ is the ratio of creep at any age t, after application of load at the age t_o, to the elastic strain at the age of 28 days and equal to

$$\phi_{28}(t,t_o) = \beta_a(t_o) + \phi_d\,\beta_d(t-t_o) + \phi_f\left[\beta_f(t) - \beta_f(t_o)\right] \ldots\ldots\ldots(1)$$

$\beta_a(t_o)$ is the initial flow and equal to

$$\beta_a(t_o) = 0.8\ \left[1 - \frac{F_c(t_o)}{F_{c\infty}}\right]$$

where $\frac{fc(t_o)}{fc_\infty}$ is the strength ratio, and

can be expressed as

$$\frac{f_c(t_o)}{fc\ \infty} = \frac{1}{1.276}\left(\frac{t_o}{4.2+0.85t_o}\right)^{\frac{3}{2}}$$

and

$$\phi_d\,\beta_d(t-t_o) = 0.4\ \{0.73\ [1-e^{-0.01(t-t_o)}] + 0.27\}$$

β_d in the above describes the development of delayed elastic strain with time and ϕ_d is the ratio of limiting delayed elastic strain to the initial elastic strain at the age of 28 days which is equal to 0.4. Equation (A.1) includes the term ϕ_f which is the flow coefficient = $\phi_{f1} \times \phi_{f2}$, where ϕ_{f1} is the ambient humidity coefficient and can be obtained from a table and is equal to 3.75 for a very dry atmosphere (< 40 per centR.H.) ϕ_{f2} is the notional thickness coefficient, which takes into account the member size by the notional thickness h_o which is given by

$h_o = \lambda \frac{2Ac}{u}$

A_c = cross-sectional area of the member (mm^2)

u = perimeter exposed to drying (mm)

λ = coefficient for ambient humidity, and is equal to 1.0 for very dry atmosphere (40% R.H.). ϕ_{f2} as a function of h_o can be obtained from a graph and for tests performed here under very dry atmosphere, the following values were used.

Partly sealed beams, $\phi_{f2} = 1.4$

and for the unsealed beams,

$$\phi_{f2} = 1.8$$

The expression $\phi_f \; [\beta_f(t) - \beta_f(t_o)]$

$$= \phi_f \left[\left(\frac{t}{t + H_f}\right)^{\frac{1}{3}} - \left(\frac{t_o}{t_o + H_f}\right)^{\frac{1}{3}} \right]$$

where H_f is a function of h_o and is given in a table, its value for the particular tests considered in this thesis is given by:

Partly sealed=870

Unsealed = 387

t_o is the age at application of load which can be corrected for the temperature applied before loading (maturity) by using this expression:

$$t_m = \frac{1}{30} \; (T + 10) \; (\Delta t) \; + t_o$$

where t_m is the equivalent time, Δt is the number of days under heated environment, t_o is the age at time of applying the heat, T is the main temperature occurring during a period Δt.

Hence T (age for beams heated before loading) = 23 days

$E_c(to)$ is related to E_c (28) by the following expression

$$E_c\ (to) = E_{c\ 28}\ \left(\frac{t_o}{4.2 + 0.85t_o}\right)^{\frac{1}{2}}$$

The creep coefficient obtained in this way is then used with the elastic modulus method to obtain $E_{effective}$, where

$$E_{eff} = \frac{E_c(t_o)}{1+\phi(t,t_o)}$$

E_{eff} obtained from here is used in the expression

$$d = K\frac{M^{max}\ L^2}{E_{t_o}\ I_{eff}}$$

to obtain deflection

For cracked section, Brangons' expression was used for I_{eff}, where for simply supported beams :

$$I_{eff} = \left(\frac{M_{cr}}{M^{max}}\right)^3 I_{uc} + \left[1 - \left(\frac{M_{cr}}{M^{max}}\right)^3\right] I_c$$

I_{uc} and I_c are second moment of area for transformed uncracked and cracked section respectively.

M_{cr} is the cracking moment =

$= I_{uc}\ F_{cm}/y$

where F_{cm} is modulus of rupture

y is distance from centroid of the transformed section to the extreme tension fibre

M^{max} = maximum moment ever applied to the member.

APPENDIX III

AIII.1 Deermining moments on the beams

a. Determining the ultimate moment using CP110.

$\frac{100\ As}{bd} = 1.37$

b = 100 mm

d = 165 mm

$f_{cu} \simeq 40\ N/mm^2$

$f_y = 460\ N/mm^2$

From charts (no.4)

$\frac{Mu}{bd^2} = 4.7$ $\quad \therefore \quad Mu = 12.8$ KN-m

b. Calculating the applied moments in tests 5.I and 5.II

Bottom beam:

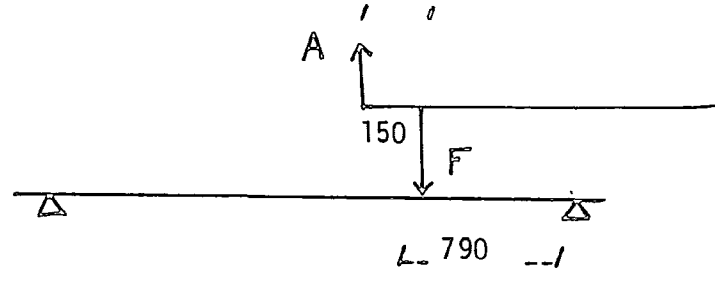

Weight of lever arm
= 57.5 kg.
Length of lever arm
= 1900 mm.

Taking moment about A

(57.5) (900) = F(150)

F = 345 Kg

$\therefore$ moment due to lever arm

= (345) (790) (9.81)

= 2.67 KN-m

dead load moment = 0.37 Kn-m

11 Kg were used at the end by taking moment of w' around A

(11) (1750) = F(150)

F = 128 Kg

moment = (128) (0.79) (9.81) = 0.99 KN-m

∴ total moment on bottom beam

= (2.67) + (0.99) + (0.37) = 4.03 KN-m

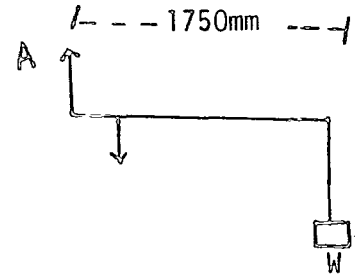

Top beam

From equilibrium of forces

F = (345 + 128) - (68.5 + 11)

= 393.5 Kg

∴ moment due to F

= (393.5) (950) (9.81)

= 3.67 KN-m

moment due to self weight ↓ = 0.37 Kn-m

Total moment on the beam = 3.67 - 0.37

= 3.3 KN-m

c. Calculating the used applied moment on tests 5.III, 6.I, 6.II, 6.III, 7.I

Bottom beam:

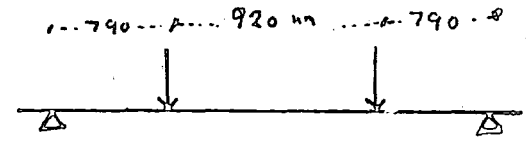

moment due to lever arm

= 2.67 KN-m

moment chosen = 48% of the ultimate (CP110)

= 6.1 KN-m

∴ moment due to the imposed weights

= (6.1) - (2.67 + 0.37)

= 3.06

$F = \frac{3060\ N}{(9.81)(0.79)}$ = 395 Kg

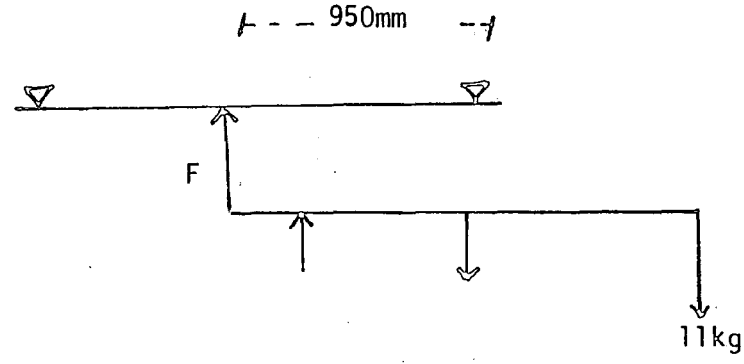

∴ W(1750) = (395) (150)

W = 34 Kg

Top beam:

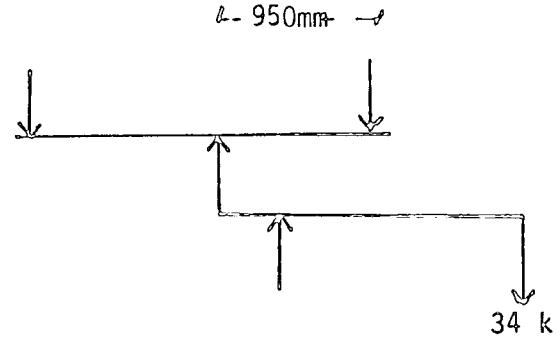

From equilibrium of forces

F = (345 + 395) - (68.5 + 34)

= 637.5 Kg

∴ moment due to F

= (637.5) (950)

= 5.9 KN -m

Total moment on top beam = 5.9 - 0.37

= 5.53 KN-m

≃ 43% of ultimate

(CP110)

AIII.2 Calculating deflection using the moment area theorem

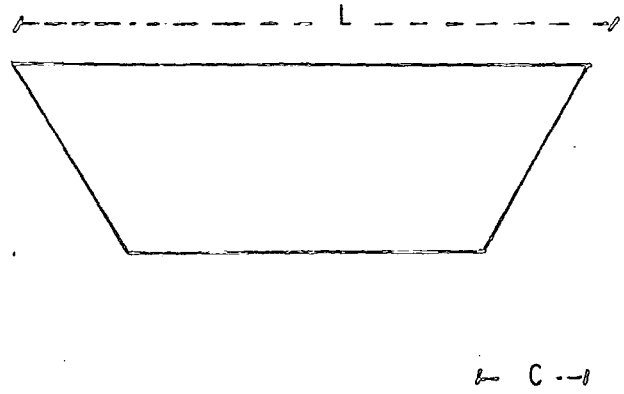

$\therefore$ deflection at midspan =

$$= \frac{L^2}{8}\left[1 - \frac{4}{3}\left(\frac{c}{L}\right)^2\right]\left(\frac{1}{r}\right)$$

($\frac{1}{r}$ is central curvature.)

which for the bottom beam

$$= (677\ 233.3)\left(\frac{1}{r}\right) \qquad \begin{bmatrix} L = 2500\ mm \\ c = 790\ mm \end{bmatrix}$$

and for the top beam:

$$= (630833.3)\left(\frac{1}{r}\right) \qquad \begin{bmatrix} L = 2500\ mm \\ c = 950\ mm \end{bmatrix}$$

A.III.3

Example on the Use of the Codes

Using the codes to determine the initial and long term deflection of beam 7.I/2 .

CEB - FIP

Initial deflection

$$\beta_a(to) = 0.8 \left[1 - \frac{1}{1.276} \left(\frac{21}{4.2 + 0.85\,(21)}\right)^{\frac{3}{2}}\right]$$

$$= 0.217$$

$$\phi_d \; \beta_d\,(t-to) = 0.4 \{0.73 \left[1 - e^{-0.01(36)}\right] + 0.27\}$$

$$= 0.196$$

$$\phi_{f_1} = 3 \;, \quad \phi_{f_2} = 1.4 \qquad \text{(from tables and chart)}$$

$$\therefore \quad \phi_f = \phi_{f_1} \times \phi_{f_2} = 4.2$$

$$H_f = 870$$

$$\phi_f \left[\beta_f(t) - \beta_f(to)\right] = \phi_f \left[\left(\frac{t}{t+H_f}\right)^{\frac{1}{3}} - \left(\frac{to}{to + H_f}\right)^{\frac{1}{3}}\right]$$

$$= 0.45$$

$$\therefore \quad \phi\,(t-to) = 0.217 + 0.196 + 0.45$$

$$= 0.86$$

$$E = 9.5\,(f_{cyl}(to))^{\frac{1}{3}}$$

$$= 30.0$$

$$\alpha = \frac{Es}{Ec} = 6.67$$

$$\rho = 0.0137$$

Neutral axis for cracked section =

$$X_1 = D_{st}\left[(-\alpha\rho) + (\alpha^2\rho^2 + 2\alpha\rho)^{1/2}\right]$$

$D_{st} = 165\text{mm}$

$= 56.7\text{mm}$

Neutral axis for uncracked section =

$$X_2 = \left[(A_c\, h/_2) + (\alpha\, A_{st}\, D_{st})\right] / (A_c + \alpha A_{st})$$

$h = 200$ mm

$A_{st} = 226\ mm^2$

$A_c = 2 \times 10^4 mm^2$

$= 104.7\text{mm}$

Modulus of rupture $(F_{cm}) = 0.3\, f_{c_y}^{2/3}(0.6 + 0.4h^{-1/4})$

$= 3.69\ N/mm^2$

$$I_{cracked} = \frac{B\,x^3}{3} + (A_{st}\,\alpha)\,(D_{st} - x)^2$$

$= 23.8 \times 10^6\ mm^4$

$$I_{uncracked} = \frac{Bh^3}{12} + Bh(X - \frac{h}{2})^2 + (A_{st}\,(\frac{E_s - E_c}{E_c}))(D_{st} - X)^2$$

$= 71.8 \times 10^6\ mm^4$

$$M_{cracked} = F_{cm}(I_{uncracked}) / (h - X_{un})$$

$= 2.78 \times 10^6$ N-mm

$$I_{effective} = I_{un}\left(\frac{M_{cr}}{M^{max}}\right)^3 + I_{crac}\left[1 - \left(\frac{M_{cr}}{M^{max}}\right)^3\right]$$

$$= (71.8 \times 10^6)\left(\frac{2.78}{6.1}\right)^3 + (23.8 \times 10^6)\left(1 - \left(\frac{2.78}{6.1}\right)^3\right)$$

$= 28.4 \times 10^6\ mm^4$

$\therefore$ Initial Deflection $= (677233.3)\left[\frac{(6.1 \times 10^6}{(3.\times 10^4)\,(28.4 \times 10^6)}\right]$

$= 4.8$ mm

Long term:

Using the effective modulus method, we have

$$E_t = \frac{Eo}{1 + \phi(t_o, t)}$$

$$= 15.79$$

$\therefore$ $X_1 = 72.2mm$

$X_2 = 108.0$ mm

$I_C = 36.8 \times 10^6$ mm^4

$I_{un} = 76.4 \times 10^6$ mm^4

$I_{eff} = 41.79 \times 10^6$ mm^4

Long term deflection = 6.2mm

creep deflection = 1.4mm

ACI:

Initial deflection:

$$E = (5.03)\,(f_{cy\ell_{28}})^{\frac{1}{2}}$$

$$= 29.66 \simeq 30\ KN/mm^2$$

$$F_{CM} = 0.6\,(f_{cy\ell})^{\frac{1}{2}}$$

$$= 3.44\ N/mm^2$$

using the same procedure as was done for the CEB-FIP calculation.

$\therefore$ Initial deflection =

= 5.0 mm

Long-term:

$$\phi = \frac{(t-to)^{0.6}}{10 + (t-to)^{0.6}}\ \phi_\infty\,(to)$$

$t_o = 21$, $t = 57$ days

$\phi_\infty\,(to) = 2.35\ K_H\ K_d\ K_s\ K_F\ K_{AC}\ K_{to}$

$K_H = 0.94$

$K_d = 0.96$

$K_s = 0.87$

$K_F = 0.96$

$K_{AC} = 1$

$K_{to} = 0.873$

$\therefore$ $\phi\,(t,to) = 0.716$

Creep deflection = $K\, d_o\, \phi\,(t, to)$

where K is a reduction factor = 0.85

do is the initial deflection

$\therefore$ creep deflection = (0.85) (5.0) (0.716)

= 3.0mm

CP110;

$E = 31.\ KN/mm^2$

$X = (165)\ \{(-6.67)\ (0.0137) + [(6.67)^2 (0.0137)^2 + 2(6.67)(0.0137)]^{1/2}\}$

$= 57.15mm$

$$M_{net} = M_{applied} - \frac{1}{3}\left[\frac{(100)\ (200-57.15)^2}{(165-57.15)}\right] \quad (1.0)$$

$= 5.2 \times 10^6$ N-mm

$$I_c = \frac{B\, X^3}{3} + \left(A_{st}\left(\frac{E_s}{E_c}\right)\right)(d - X)^2$$

$= 23.7 \times 10^6\ mm^4$

$$d_o \text{ (initial deflection)} = (677233.3)\left[\frac{5.2 \times 10^6}{(30 \times 10^4)(23.7 \times 10^6)}\right]$$

= 4.95 mm

Long term:

$\phi \simeq 0.97$ (by interpolation)[41]

$f_c \simeq 0.85$ (by interpolation)

$\therefore E_t = \frac{3. \times 10^4}{1 + 0.97}$

$= 15.2 \times 10^3$

$x = 73.73$ mm

$I_c = 38.1 \times 10^6$ mm^4

$M_{net} = 6.1 \times 10^6 - (\frac{1}{3}) [\frac{(100)(200-73.73)^3}{(165-73.73)}] (0.85)$

$= 5.47 \times 10^6$ N-mm

d (long term) = 6.39 mm

$\therefore$ creep deflection = 1.44 mm

REFERENCES

1. Rasheeduzzafar, Dakhil F.H., and Al-Gahtani A.S. Deterioration of concrete structures in the Environment of the Middle East. Journal of the American Concrete Institute. No proceedings, v.81; January-February 1984. pp.13-20.

2. ACI Committee 305. Hot weather concreting. Journal of the American Concrete Institute. Proceedings, vol.74, No.8, August 1977. pp.317-332.

3. Shirley, D.E. Concreting in Hot Weather. Cement and concrete Association Publication 45.013

4. The Institution of Civil Engineers. A guide to specifying concrete. Part 1 - Type 1 Specification 1963.

5. Brook, K.M. Problems of concreting in cold and hot weather. Cement and Concrete Association. TRA 412. May 1969.

6. Rosentröm, S. Experiences from the Salvage of ABU Simple Temples. Concrete in Hot Countries. International Seminar. Helsingor,1981. Arranged by SKANSKA.

7. The ciria Guide to concrete construction in the Gulf Region. CIRIA special publication 31, 1984.

8. Concrete in Hot Countries. International seminar. Helsingor 1981 arranged by SKANSKA.

9. Concrete in the Middle East. Part 1. A viewpoint Publication, Eyre and Spottiswoode Ltd., London 1982.

10. Building in Hot Climates. A selection of overseas building notes. Department of Environment. Building Research Establishment. London, H.M.S.O.,1980.

11. Pollock, J.D. and Kay, A.E. Concrete Construction in Hot Climate with particular reference to the Middle East. Handbook of Structural Concrete. Edited by Kong, F.K., Evans, R.H., Cohen, E. and Roll, F. Pittman Advanced Publishing Program. London,1983.

12. Concrete in the Middle East. Part 2. A viewpoint Publication. Eyre and Spottiswoode Ltd., 1982.

13. Altman,K. Shrinkage of Concrete in Extreme Climate. Fundamental Research on creep and shrinkage of Concrete. (papers presented at an International Conference, Lausanne. September 1980.) The Hague, Marinus Nifhoff Publishers, 1982.pp 203-212.

14. Al-Jazirah Daily Newspaper. April 21,1982. Riyadh, Saudi Arabia.

15. Udin, T. and Culver, C.G. Effects of Elevated Temperature on Structural Members. Journal of the Structural Division ST7. July 1975. pp 1531-1549.

16. Lankard, D.R., Birkimer, D.L., Fondriest,F.F., and Snyder, M.J. Effect of moisture content on the structural propeerties of Portland cement concrete exposed to temperatures up to 500°F. Temperature and concrete. A.C.I. Special publication SP.25, 1971.

17. Clark, J.L. Thermal Stress problems in offshore structures. Oceanology International 78 Brighton I.C.E. pp.19-24.

18. White, G.I. Non-linear differential temperature disibutions in concrete bridge structures : A review of the current literature. Cement and Concrete Association Technical Report 525, May 1979.

19. Emerson, M. The Calculation of the distribution of temperature in bridges. Crowthorne, Department of the Environment, 1973. TRRL Report LR 561.

20. Emerson, M. Bridge Temperatures and Movements in the British Isles. Crowthorne, Ministry of Tansport, 1968. LR228.

21. Emerson, M. Temperature differences in bridges: basis of design requirements. Crowthorne, Department of the Environment, 1977. TRRL Report 765.

22. Morlock, D.J. The instrumentation of bridges for the measurement of temperature and movement. Crowthorne, Department of the Environment, 1974. TRRL Report 641.

23. Emerson, M. Bridge temperatures estimated from the shade temperature Crowthorne, Department of the Environment, 1976. TRRL Report 695.

24. Emnerson, M. Bridge temperatures for setting bearings and expansion joints. Crowthorne, Department of the Environment,1979. TRRL Report 479.

25. Black, W., Moss, D.S. and Emerson, M. Bridge Temperatures derived from measurement of movement. Crowthorne, Department of the Environment. TRRL Report 748.

26. Emerson, M. Temperatures in Bridges during the hot summer of 1976. Crowthorne, Department of the Environment, TRRL Report 783.

27. Waine, N.D. A comparison between alternative methods of Representing Temperature Differences. Crowthorne, Department of the Environment, 1978 TRRL. Supplementary Report 442, pp.47-67.

28. Jones, M.R. Bridge temperatures calculated by a computer program Crowthorne, Department of the Environment, 1976. TRRL Report LR702.

29. Blythe, D.W.R., and Lunniss, R.C. Temperature Difference effects in Concrete Bridges. Crowthorne, Department of the Environment, 1978. TRRL Supplementary Report 442, pp.68-80

30. de la Pena, C., Shrinkage and creep specimens of thin section, RILEM Bulletin, Paris, No.3, July 1959, pp.60-70

31. Barber, S.E., "Calculation of Maximum Pavement Temperatures from Weather Reports". Highway Research Board Bulletin No.168, 1957

32. Zuk, W. Thermal Behaviour of Composite Bridges - Insulated and Uninsulated. Highway Research Record No.76. 1965, pp. 231-53.

33. Carslaw, H.S. and Jaeger, J.C., Conduction of heat in solids. Second edition, Oxford, Clarendon Press, 1973. pp.510.

34. Kehlbeck, F. and Bieger, K.W. Stresses in concrete bridges due to unsteady temperature. Conference of road bridge loading, Cambridge, April 1975.

35. Hunt, B. and Cooke, N. Thermal calculations for bridge design. Proceedings of the American Society of Civil Engineers, Journal of the Structural Division. Vol.101, No.ST9. September 1975, pp.1763-1800.

36. Priestley, M.J.N. and Thurston, S. Discussion of Reference 7. Proceedings of the American Society of Civil Engineers, Journal of the Structural Division. Vol.102, No.ST6. June 1976.

37. Berwanger, C. Transient Thermal Behaviour of Composite Bridges Journal of Structural Engineer. Vol.109. No.10, October 1983.

38. Elbadry, M.M., Ghali, A. Temperature variations in concrete bridges. Journal of Structural Engineer. Vol.109 No.10, October, 1983.

39. Emanual, J.H. and Hulsey, L.J. Temperature Distributions in Composite Bridges Journal of the Structural Division, ASCE, Vol. 104, No.ST1, Proc. paper 13474, January 1978. pp.65-78.

40. Priestley, M.J.N. Temperature gradients in bridges - some design considerations. New Zealand Engineering. Vol. 27, Part 7 July 1972, pp.228-233.

41. Priestley, M.J.N. Linear heat-flow and thermal stress analysis of concrete bridge decks. Christchurch, New Zealand, University of Canterbury, Department of Engineering, February 1976. Research Report No.7613.

42. British Standards Institution. Steel, concrete and composite bridges. London, 1978. Eight parts. BS. 5400.

43. Hambly, E.C. Temperature Distributions and stresses in concrete bridges. The Structural Engineer. Vol. 56A, No.5. May 1978. pp.143-148.

44. Churchward, A. and Sokal, Y. Prediction of Temperatures in Concrete Bridges. Journal of Structural Division ASCE, Vol. 107. No.11. November, 1981. pp.2163-2176.

45. Emerson, M. Bridge temperatures in the Arabian Gulf : theoretical predictions. Crowthorne, Department of the Environment, TRRL Supplementary Report 495.

46. Radolli, M. and Green, R. Thermal Stresses in concrete bridge superstructures under summer conditions. Transportation Research Record. No.547. 1975, pp.23-36.

47. Thurston, S.J., Priestley, M.J.N. and Cooke, N. Influence of Cracking on Thermal Response of Reinforced Concrete. Concrete International Vol.6, No.8 August,1984 pp 36-43.

48. Harada,T.,Takeda,J., Yamane, S. and Fuzumura,F. Strength, elasticity and thermal properties of concrete subjected to elevated temperatures. ACI SP-34, 1972. V.1 pp 377-407.

49. Nishizawa,N., Okamura,H. Strength and inelastic properties of concrete at elevated temperatures. ACI SP-34, 1972, V.1 pp.407-421.

50. Bertero, V.V., Polivka, M. Influence of thermal exposures on mechanical characteristics of concrete. ACI SP-34 V.1 pp.505-531.

51. Zoldners, N.G. Thermal properties of concrete under sustained elevated temperatures. ACI SP-25, 1971. pp.1-31.

52. Abrams, M.S. Compressive strength of concrete at temperatures to 1600°F. ACI SP-25 pp.33-57.

53. Sullivan, P.J., Poucher. The influence of temperature on the physical properties of concrete and mortar in the range 20 to 400°. ACI SP-25, 1971. pp.103-135.

54. Mears, A.P., Long term tests on the effect of moderate heating on the compressive strength and dynamic modulus of elasticity of concrete. ACI. SP-34, 1972, V.2. pp. 355-375.

55. Kaplan, M.F. and Roux, F.J.P. Effects of elevated temperature on the properties of concrete for the containment and shielding of Nuclear Reactors. ACI.SP-34, 1972. V.1 pp.437-441.

56. Marechal, J.G. Variations in the modulus of elasticity and Poisson's ratio with temperature. ACI. SP-34, 1972. Vol.1. pp.495-503.

57. Crispino,E. Studies on the technology of concrete under thermal conditions. ACI-34, 1972. Vol.1. pp 443-479.

58. Hannant,Strain behaviour of concrete up to 95°C under compressive stresses. Proc. Conf. on PCPV, Group C, paper 17, London 1967.

59. Weigler, H., Fischer, R. Influence of high temperature on strength and deformations of concrete. ACI. SP-34, 1972 Vol.1, pp.481-493.

60. Hannant, D.J. Effects on the strength of various concretes of sustained temperatures near 100 dg C. Civil Engineering and Public Works Review 1957. pp.665-667.

61. Neville, A.M. Properties of Concrete. Pittman Publishing. Third edition, 1981.

62. Marshall, A.L. The Thermal properties of concrete. Building Science V.7. pp.167-174. Pergamon Press,1972.

63. Marechal, J.C. Thermal conductivity and thermal coefficients of concrete as a function of temperature and humidity. ACI Special Pub., SP-34, 1972, Vol. 2, pp. 47-57.

64. Mayers, S.L. How Temperature and Moisture changes may affect the durability of concrete. Rock products. August 1951, pp.153-157.

65. Bonnell, D.G.R. and Harper, F.C. The thermal expansion of concrete. Nat.Bldg.Studies. Techn. paper No.7, HMSO,1951.

66. Berwanger, C. and SARKAR, F. Thermal Expansion of concrete and reinforced concrete. A.C.I. journal, November 1976, pp. 618-21.

67. Brown, R.D. Thermal Movement of Concrete. Concrete (current practice sheet) Nov.1972. pp.51-53.

68. Wittman, F. and Lukas J. Experimental study of Thermal expansion of hardened cement paste. Materials and structure, 7 No. 40, pp.247-52 (Paris, July 1974).

69. Walker, S., Bloem, D.L. and Mullen, W.G. Effects of Temperature changes on concrete as influenced by aggregates. J. American Concrete Institute 48, pp.661-79.

70. Mitchell, L.J. Hardened Concrete - Thermal properties of concrete-making materials. ASTM, STP 169-1, 202, 1966.

71. Concrete Society Technical Report No.101. The Creep of structural concrete. Report of a Working Party of the Materials Technology Divsional Committee. 1973.

72. England, G.L., Ross, A.D. Shrinkage, moisture and pore pressures in heated concrete. ACI special publication sp.34, 1972, Vol.2, pp.883-907.

73. Mcdonald, J.E. An experimental study of moisture migration in concrete. ACI special publication SP-34, 1972, Vol.2, pp 957-929.

74. England, G.L., Sharp, T.J. Migration of moisture and pore pressure in heated concrete. Proc. of the 1st Int.Conf. on SMIRT, Berlin, Sept.1972. Vol.4-part H.

75. Chapman, D.A., England,G.L. Effects of Moisture Migration on shrinkage, pore pressure and other concrete properties. Conf. on SMIRT, San Francisco, Aug.1977, paper No.H 4/d.

76. Poitevin,P. Water migration in concrete under a sustained temperature gradient. ACI Special publication, SP-34, 1972. Vol.2, pp.957-929.

77. Troxell, G.E., Raphael, J.M. and Davis, R.E. Long-time creep and shrinkage tests on plain and reinforced concrete, Proc. ASTM,58,1958,pp 1101-20.

78. Pihlagavaara, S.E. Estimation of Drying of concrete at different Relative Humidities and Temperatures of Ambient Air with Special discussion about fundamental features of Drying and Shrinkage. Creep and Shrinkage in concree structures. Edited by Z.P. Bazant and F.H.Wittman. pp 87-108.

79. Bažant,Z.,Wu,T. Creep anmd shrinkage for concrete at Variable Humidity. Journal of the Engineering Mechanics Division., Dec.1974, pp.1183-1209.

80. Bažant,Z. Mathematical Models for creep and shrinkage of concrete creep and shrinkage in concrete structures. Edited by Z.Bazant and F.H.Wittman. John Wiley & Sons Ltd.,1982, pp.363.

81. Hansen, T.C. and Mattock, A.HJ. Influence of size and shape of Member on shrinkage and creep of concrete. ACI Journal proc. vol.63, No.2, Feb. 1966, pp.267-90.

82. Hughes, B.P., Lowe, I.R.E., and Walker,J. The diffusion of Water in concrete at temperatures between 50° and 95°C. Brit. J.Appl.Phys., vol.17, 1966, pp 1545-52.

83. Lowe, I.R.G.,Hughes,B.P. and Walker,J. The diffusion of water in concrete at 30°C. Cement and Concrete Research,Vol.1, 1971,pp 547-57.

84. Bazant, Z.P. and Naggar, L.J.(1972). 'Non-linear water diffusion in nonsaturated concrete'. Materials and Structures, (RILEM, Paris) 5, 3-20.

85. Hobbs, D.W. and Parrott, L.J. Prediction of drying shrinkage. Concrete.Vol.13 No.2, February 1979, pp 19-24.

86. Hobbs, D.W. Shrinkage-induced curvature of reinforced concrete members. C & CA Development Report Nov.1979.

87. Branson, D.E. Deformation of concrete structures. New York. McGraw-Hill International Book Co. 1977, pp.546.

88. Hobbs, D.W. Shrinkage and load induced curvature of reinforced concrete beams. Fundamental Research on creep and shrinkage of concrete. (Papers presented at an International Conference Lausanne. Sept.1980). The Hague, Martinus Nijhoff Publishers,1982, pp.439-449.

89. Neville,M.A., Mayers,L. Creep of Concrete: Influencing Factors and Prediction. Symposium on creep of concrete. American Concrete Institute special publication No.9, 1964 pp.1-31.

90. Evans, R.H., Kong, F.K. Creep of prestressed concrete - 1, edited by F.Sawko., Chap.3. pp.95-124.

91. Ruetz, W. A hypothesis for the creep of hardened cement paste and the influence of simultaneous shrinkage. Proc. Int. Conf. on Structure of concrete, Cement and Concrete Association : Lonondon, 1968, pp.365-87.

92.Glucklish, J. and Ishai, O. Creep mechanisms in cement mortar, ACI Journal,59, 1962, pp.923-48.

93. Ali, I. and Kesler, E.C. Mechanisms of creep in concrete. Symposium on Creep of Concrete. American Concrete Institute Special Publication No.9, 1964, pp.35-57.

94. Neville, M.A. Dilger, H.W., Brookes, J.J. Creep of plain and structural concrete. Construction Press Publishing

95. England, G.L. and Mohrram, A. Designing for creep and temperature in concrete off-shore structures. Oceanology International.

96. Hansen, T.C. Creep of concrete : The influence of variations in the humidity of the ambient atmosphere, sixth Congress

97. Gamble, W. Creep of concrete in variable environments. Journal of structural Division, ASCE. Vol.108, No.ST10, October 1982 pp.2211-222.

98. Gamble, B.R. and Parrot, L.J. Creep of concrete in compression during drying and welting. Magazine of Concrete Research, 30, No.104, Sept.1978, pp.129-38.

99. Meyers, B.L. and Slate, F.O. Creep and creep recovery of plain concrete as influenced by moisture conditions and associated variables. Magazine of Concrete Research, 22. No.70, 1970, pp.37-41

100. Hansen, T.C. Effect of wind on creep and drying shrinkage of hardened cement, mortar and concrete. Materials Research and Standards, 6, No.1, 1966, pp.16-19.

101 Parrot, L.J. Increase in creep of hardened cement paste due to carbonation under load. Magazine of Concrete Research 27, No.92, 1975.

102. Serafim, L.J. and Gluviero, M.Q. Influence of emperature on the creep of mass concrete, RILEM Bulletin, Paris, No.6, March 1960, pp.23-32.

103. Arthanari, S and Yu, C.W. Creep of concree under uniaxial and biaxial stresses at elevated temperatures, Magazine of Concrete Research 19, No.60, 1967, pp.149-56.

104. England, L.G. and Ross, A.D. Reinforced concrete under thermal gradients. Magazine of Concrete Research, 14, No.40, 1962, pp.5-12

105. Nasser, K.W. and Neville, A.M. Creep of old concrete at normal and elevated temperatures. ACI Journal, 64, 1967, pp.97-103

106. Zielinski, J.L. and Sadowski, A. The influence of moisture content on the creep of concrete at elevated temperatures. 2nd Int. Conf. on SMIRT, Berlin Sept.1973 paper H6/3 pp.1-7.

107. Hansen, R. & C. and Erikson, L. Temperature change effect on behaviour of cement paste, mortar and concrete under load, ACI Journal, 63, 1966, pp.489-504.

108. Illston, J.M., Sanders, P.D. Characteristics and prediction of creep of a saturated mortar under variable temperature, Magazine of Concrete Research, 26, No.88, 1974, pp.169-79.

109. Parrott, L.J. and Symmons, R.M. Deformation Properties of an oil storage vessel concrete subjected to fluctuating stresses and temperatures, C & CA, Concrete in the Oceans, Report No.P3/14, Dec. 1977.

110. Parrott, L.J. A Study of Transitional Thermal Creep in hardened cement paste. Magazine of Concrete Research, Vol.31, Part 107, pp.99-103.

111. Rainford, E.C. and Timusk, J. The Creep of hardened Portland cement paste under cyclic temperature, J.Amer.Ceramic Soc., 61, Nos.9-10, 1978, pp.380-5

112. Fahmi, H.M., Polivka, M. and Bresler, B. Effect of sustained and cyclic elevated temperature on creep of concrete, cement and concrete research, 2, 1972, pp.591-606.

113. Swamy, N. and Arumugasaamy, P. A simple aid for predicting shrinkage and creep stains in buildings and bridges. The Structural Engineer/volume 59A/No.3/March 1981.

114. Bazant, P.Z. and Chern, J-C. Comment on the use of Ross's Hyperbolas and Recent Comparisons of various practical creep prediction models. Cement and Concrete Research, Vol.12, No.4, July, 1982.

115. England, G.L. and Ross, A.D. Reinforced concrete under thermal gradients, Magazine of Concrete Research, Vol.14, No.40 Mach 1962, pp.5-12.

116. Ross, A.D., England, G.L. and Swan, R.H. Prestressed concrete beams under a sustained temperature crossfall. Mahgazine of Concrete Research. Vol.17, No.52,September 1965, pp.117-126.

117. Arthanary, S. and Yu, C.W. An analysis of the creep and shrinkage effects upon pressed concrete members under temperature gradient and its application. Magazine of Concrete Research. Vol.19, No.60. Sept.1967.

118. Nielsen, L.F. The improved Dischinger Method as related to other methods and practical applicability. Designing for creep and shrinkage in concrete structures. American Concrete Institute. SP-76.

119. Bazant, Z. and Cherm, J-C. Bayesian Statistical Prediction of concrete creep and shrinkage. Journal of the American Concrete Institute July-August 1984, proc.v.81. pp.319-329.

120. Gilbert, I. and Warner, R.F. Tension Stiffening in Reinforced concrete slabs. Journal of the Structural Division, December 1979, pp.1885-1899.

121. PAFEC LTD., Theory Nottingham, U.K.

122. Zienkwicz, O.C. The Finite Element Method, 3rd Edition, McGraw-Hill Book Company (UK) Limited, Maidenhead, Berkshire, England, 1977, pp.787.

123. Mayer, G.E. Analytical Method in Conduction Heat Transfer, McGraw-Hill Book Co., Inc., New York, 1971.

124. Segerlind, L.J. Applied Finite Element Analysis, John Wiley and Sons, Inc., 1976.

125. PAFEC LTD. PAFEC 75 Data Preparation, 1978.

126. Potocki, F.P. Road temperatures and climatological observations in the Enmirate of Abu Dhabi. Department of the Environment. Crowthorne, 1978. TRRRL Report SR 412.

127. Meterological Record (Climate section). Kingdom of Saudi Arabia.

128. Gloyne, R.W. The Diurnal variation of Global Radiation on a horizontal surface - with special reference to Aberdeen-Meterological Magazine 101,1972, pp.44-51.

129. Guttman, I., Wilks, S.S. and Hunter, J.S. Introductory Engineering Statistics, 3rd edition, John Wiley & Sons, 1982.

130. Cox, M.G. The Numerical Evaluation of a sSpline from its B-Spline Representation. National Physical Laboratory, Division of Numerical Analyss and Computing. NPL Report NAC 68, July, 1976.

131. British Standards Institution. The structural use of concrete, Part I; Design, mnaterials, workmanship. London pp.155. CP110: Part 1:1972.

132. Bate, S.C.C. et al. Handbook on the Unified Code for structural concrete (CP110:1972). London, Cement and Concrete Association, 1972. pp153

133. ACI Committee 435. Deflections of reinforced concrete flextural members. Journal of the American Concrete Institute. Proceedings Vol.63, No.6. June 1966. pp.637-674.

134. ACI Committee 209. Prediction of creep, shrinkage and temperature effects in concrete structures. Designing for effects of creep, shrinkage, temperature in concrete structures. Detroit, American Concrete Institute, 1971, ACI Sp.27-3 pp.51-93.

135. Comite Euro-International du Beton an Federation Internationale de la precontrainte. Model code for concrete structures. Third edition. London, Cement and Concrete Association, 1978, pp.384.

136. Brook, T.J. Accuracy of estimating long-term strains in concrete. Magazine of Concrete Research. vol.36. No.128,Sept. 1984. pp.131-145

137. Muller, H.S. and Hilsdorf, H.K. Comparison of prediction methods for creep coefficients of structural concrete with experimental data. Fundamental Research on creep and shrinkage of concrete. (Papers presented at an International Conference, Lausanne, Sept.1980). The Hague, Martinus Nijhoff Publishers, 1982, pp.269-278.

138. Hambly, E.C. Bridge Deck behaviour, Chapman and Hall Pub., 1976. pp.187-194.

LISTS OF THE COMPUTER PROGRAMS USED IN THE ANALASIS.

```
C PROGRAM TO CALCULATE THE STRESSES IN A CRACKED SECTION
C DUE TO APPLIED TEMPERATURES AND MOMENTS
DIMENSION TEMP(100), FRSRN(100), STRL(100), DPLAY(100), AXST(100),
1          TMST(100), FINST(100), DELT(100), APMST(100),
2          CHECK(100), STNCH(100), TOSNCH(100)
C NOTE COMPRESSION IS +VE AND TENSION IS -VE
C B=BREADTH OF SECTION,D=DEPTH OF SECTION
C DST=DEPTH TO STEEL,AST=AREA OF STEEL
C NLAY=NUMBER OF LAYERS
C FCU=CUBE STRENGTH(+VE),FTU=TENSILE STRENGTH OF CONCRETE(-VE)
C EC=MODULUS FOR CONCRETE,ES=MODULUS FOR STEEL
C ALPC=COEFF. OF THERMAL EXPANSION FOR CONCRETE
C ALPS=COEFF. OF THERMAL EXPANSION FOR STEEL
C ****START NEW LINE IN DATA FILE****
C D1=DEPTH TO TEMPERATURE T2
C D2=DEPTH TO TEMPERATURE T3
C D3=DEPTH TO TEMPERATURE T4
C D4=DEPTH TO TEMPERATURE T5  ETC FOR REMAINING LAYERS
C T1=TEMPERATURE AT TOP OF BEAM
C T9=TEMPERATURE AT BOTTOM OF BEAM
C ****START NEW LINE IN DATA FILE****
C KK=NUMBER OF ENTERIES OF THE APPLIED MOMENT
C ****EACH ENTER FOR THE APPLIED MOMENT MUST BE ON A NEW LINE****
C APMOM=APPLIED MOMENT
   REAL NLAY
   READ (1,*) B, D, DST, AST, NLA, FCU, FTU, EC, ES, ALPC, ALPS, NN
   READ (1,*) D1, D2, D3, D4, D5, D6, D7, D8
   READ (1,*) APMOM, IK, KM
   IF (IK .EQ. 1) GO TO 10
   IF (IK .EQ. 2) GO TO 30
   IF (IK .EQ. 3) GO TO 50
   IF (IK .EQ. 4) GO TO 70
   IF (IK .EQ. 5) GO TO 90
   IF (IK .EQ. 6) GO TO 110
 10 WRITE (6,20)
 20 FORMAT (35X, ' CURVATURE VALUES FOR EXPERMINT ONE')
   GO TO 130
 30 WRITE (6,40)
 40 FORMAT (35X, ' CURVATURE VALUS FOR EXPERMINT TWO')
   GO TO 130
 50 WRITE (6,60)
 60 FORMAT (35X, ' CURVATURE VALUES FOR EXPERMINT THREE')
   GO TO 130
 70 WRITE (6,80)
 80 FORMAT (35X, ' CURVATURE VALUES FOR EXPERMINT FOUR')
   GO TO 130
 90 WRITE (6,100)
100 FORMAT (35X, ' CURVATURE VALUES FOR EXPERMINT FIVE')
   GO TO 130
110 WRITE (6,120)
120 FORMAT (35X, ' CURVATURE VLUES FOR EXPERMINT SIX')
   GO TO 130
130 CONTINUE
   IF (KM .EQ. 1) GO TO 140
   IF (KM .EQ. 2) GO TO 160
140 WRITE (6,150)
150 FORMAT (//40X, ' BEAM ONE LOADED AND HEATED')
   GO TO 180
160 WRITE (6,170)
170 FORMAT (//40X, ' BEAM FOUR HEATED ONLY ')
```

```
    GO TO 180
180 CONTINUE
    DO 540 II = 1, NN
      READ (1,*) T1, T2, T3, T4, T5, T6, T7, T8, T9, T10, TI
      DO 190 I = 1, NLA
        CHECK(I) = 1.0
190   CONTINUE
      NS = -10E+05
200   CONTINUE
      AXTC = 0.
      TMOMC = 0.0
      DO 300 I = 1, NLA
        THICK = D / NLA
        DLAY = THICK * (I - 0.5)
        DPLAY(I) = DLAY
        IF (DLAY .LE. D1) GO TO 210
        IF (DLAY .LE. D2) GO TO 220
        IF (DLAY .LE. D3) GO TO 230
        IF (DLAY .LE. D4) GO TO 240
        IF (DLAY .LE. D5) GO TO 250
        IF (DLAY .LE. D6) GO TO 260
        IF (DLAY .LE. D7) GO TO 270
        IF (DLAY .LE. D8) GO TO 280
        TLAY = T10 + (T9 - T10) * (D - DLAY) / (D - D8)
        GO TO 290
210     TLAY = T2 + (T1 - T2) * (D1 - DLAY) / D1
        GO TO 290
220     TLAY = T3 + (T2 - T3) * (D2 - DLAY) / (D2 - D1)
        GO TO 290
230     TLAY = T4 + (T3 - T4) * (D3 - DLAY) / (D3 - D2)
        GO TO 290
240     TLAY = T5 + (T4 - T5) * (D4 - DLAY) / (D4 - D3)
        GO TO 290
250     TLAY = T6 + (T5 - T6) * (D5 - DLAY) / (D5 - D4)
        GO TO 290
260     TLAY = T7 + (T6 - T7) * (D6 - DLAY) / (D6 - D5)
        GO TO 290
270     TLAY = T8 + (T7 - T8) * (D7 - DLAY) / (D7 - D6)
280     TLAY = T9 + (T8 - T9) * (D8 - DLAY) / (D8 - D7)
290     CONTINUE
        TEMP(I) = TLAY
        DT = TLAY - TI
        DELT(I) = DT
        FRSN = ALPC * DT
        FRSRN(I) = FRSN
        REST = FRSN * EC
        STRL(I) = REST
300   CONTINUE
      DO 310 I = 1, NLA
        AXTC = AXTC + STRL(I) * B * THICK * CHECK(I)
        TMOMC = TMOMC + STRL(I) * B * THICK * DPLAY(I) * CHECK(I)
310   CONTINUE
      ST = T6 + (T5 - T6) * (D - DST) / (D - D4)
      STSTN = ALPS * (ST - TI)
      AXTOT = AXTC + AST * ES * STSTN
      TMOM = TMOMC + DST * AST * ES * STSTN
      ASUM = 0.0
      AYSUM = 0.0
      DO 320 I = 1, NLA
        AY = B * THICK * DPLAY(I) * CHECK(I)
```

```
        A = B * THICK * CHECK(I)
        ASUM = ASUM + A
        AYSUM = AYSUM + AY
320   CONTINUE
      AYSUM = AYSUM + AST * DST * ES / EC
      ASUM = ASUM + AST * ES / EC
      YBAR = AYSUM / ASUM
      SECTI = 0.0
      DO 330 I = 1, NLA
        SI = B * THICK ** 3 * CHECK(I) / 12 + B * THICK * CHECK(I) * (
     1    DPLAY(I) - YBAR) ** 2
        SECTI = SECTI + SI
330   CONTINUE
      SECTI = SECTI + AST * (ES/EC) * (DST - YBAR) ** 2
      TMT = 0.0
      DO 340 I = 1, NLA
        AXST(I) = AXTOT * CHECK(I) / ASUM
        TM = AXST(1) * B * THICK * CHECK(I) * DPLAY(I)
        TMT = TMT + TM
340   CONTINUE
      TMT = TMT + AXST(1) * DST * AST * ES / EC
      DO 350 I = 1, NLA
        TMST(I) = (TMT - TMOM) * (YBAR - THICK*(I - 0.5)) * CHECK(I) /
     1     SECTI
        APMST(I) = APMOM * (YBAR - THICK*(I - 0.5)) * CHECK(I) / SECTI
        FINST(I) = (STRL(I) - AXST(I) - TMST(I) + APMST(I)) * CHECK(I)
        STNCH(I) = (AXST(1) + TMST(I)) / EC
        TOSNCH(I) = STNCH(I) - APMST(I) / EC
350   CONTINUE
      DO 360 I = 1, NLA
        IF (CHECK(I) .LT. 0.1) GO TO 360
        IF (FINST(I) .GT. FTU) GO TO 360
        CHECK(I) = 0.0
360   CONTINUE
      NSUM = 0.0
      DO 370 I = 1, NLA
370   NSUM = NSUM + CHECK(I)
      IF (NSUM .EQ. NS) GO TO 380
      NS = NSUM
      GO TO 200
C IF NUMBER OF UNCRACKED LAYERS REDUCES,GO TO 42 AND REPEAT
C UNTIL NUMBER OF LAYERS IS UNCHANGED
380   CONTINUE
      STSR = STSTN * ES
      STSAV = AXST(1) * ES / EC
      STSMR = (TMT - TMOM) * (YBAR - DST) * ES / (SECTI*EC)
      STSAP = APMOM * (YBAR - DST) * ES / (SECTI*EC)
      FSTS = STSR - STSAV - STSMR + STSAP
      STSNTH = (STSAV + STSMR) / ES
      TOSST = STSNTH - STSAP / ES
      NLS = 0
      DO 390 I = 1, NLA
        IF (CHECK(I) .LT. 0.1) GO TO 390
        NLS = 1 + NLS
390   CONTINUE
      DC = THICK * (NLS - 0.5)
C LOOPS TO 44&45 IS THE INTERPOLATION OF STRAIN BETWEEN
C THAT IN THE LOWEST UNCRACKED LAYER AND STEEL STRAIN.
      DO 400 I = 1, NLA
        IF (CHECK(I) .GT. 0.1) GO TO 400
```

```
        STNCH(I) = STNCH(NLS) + (STSNTH - STNCH(NLS)) * (I - NLS) *
     1    THICK / (DST - DC)
400   CONTINUE
      WRITE (6,410) APMOM
410   FORMAT ('0', 'APPLIED MOMENT=', F15.1)
      WRITE (6,420)
420   FORMAT ('0', ' I    CHECK(I)  RESTRAINED    AVERAGE',
     1          '      MOMENT      APPLIED      RESIDUAL      THERMAL')
      WRITE (6,430)
430   FORMAT (' ', '                      STRESS  - COMPRESSIVE',
     1          ' - RELEASE  + MOMENT   =   STRESS       STRAIN')
      WRITE (6,440)
440   FORMAT (' ', '                                      STRESS',
     1          '                    STRESS')
      DO 460 I = 1, NLA
        WRITE (6,450) I, CHECK(I), STRL(I), AXST(I), TMST(I),
     1    APMST(I), FINST(I), STNCH(I)
450     FORMAT ('0', I3, 5X, F3.1, 5X, 5(F7.2,5X), E12.4)
460   CONTINUE
      WRITE (6,470) STSR, STSAV, STSMR, STSAP, FSTS, STSNTH
470   FORMAT ('0', 'REINFORCEMENT:', /, 18X, 5(F7.2,5X), E12.4)
      NLAY = 1.0 * NLA
      CURV = (STNCH(1) - STNCH(NLAY)) / (THICK*(NLAY - 1.))
      WRITE (6,480) CURV
480   FORMAT ('0', 'CURVATURE,1/R, =    ', E12.4)
      WRITE (6,490)
490   FORMAT ('0', ' I      TEMP   CHANGE IN  DEPTH',
     1          '       FREE SLICE')
      WRITE (6,500)
500   FORMAT (' ', '                      TEMP    TO EACH',
     1          '        STRAINS')
      WRITE (6,510)
510   FORMAT (' ', '                                LAYER')
      DO 530 I = 1, NLA
        WRITE (6,520) I, TEMP(I), DELT(I), DPLAY(I), FRSRN(I)
520     FORMAT ('0', I3, 5X, F4.1, 5X, F4.1, 5X, F5.1, 5X, E12.6)
530   CONTINUE
540 CONTINUE
    STOP
    END
```

```
=    PROGRAM CPCR =

C      PROGRAM TO CALCULAE CURVATURE USING THE RATE OF CREEP
C      METHOD WITH SPECIFIC THERMAL CREEP AND STEP BY STEP
C      APPROACH. S.T.C. VALUES ARE OBTAINED FROM SMALL
C      UNREINFORCED CYLINDER.
   REAL MST
   INTEGER S
   DIMENSION TEMP(100,100), SN(100,100), CURV(100), CHECK(50),
  1          AXTC(100), TMOM(100), DPLAY(100), AXST(100,100),
  2          TLAY(100), APMST(100), SES(100,100), MST(100,100),
  3          CRPS(100), STSN(100), SPTC(100), CRPSM(100,100),
  4          TAXC(100), TMCR(100), ST(100), CAXST(100,100),
  5          TMOMC(100), CRP(100,100), T(100,100), AXTOT(100),
  6          CTMT(100), CTMST(100,100), ESLN(100), TSN(100,100),
  7          TM(100); STML(100), STS(100), STM(100), STSTC(100),
  8          TMC(100), Y1(100)
C NOTE COMPRESSION IS +VE AND TENSION IS -VE
C B=BREADTH OF SECTION,D=DEPTH OF SECTION
C DST=DEPTH TO STEEL,AST=AREA OF STEEL
C NLAY=NUMBER OF LAYERS
C FCU=CUBE STRENGTH(+VE),FTU=TENSILE STRENGTH OF CONCRETE(-VE)
C EC=MODULUS FOR CONCRETE,ES=MODULUS FOR STEEL
C ALPC=COEFF. OF THERMAL EXPANSION FOR CONCRETE
C ALPS=COEFF. OF THERMAL EXPANSION FOR STEEL
C ****START NEW LINE IN DATA FILE****
C D1=DEPTH TO TEMPERATURE T2
C D2=DEPTH TO TEMPERATURE T3
C D3=DEPTH TO TEMPERATURE T4
C D4=DEPTH TO TEMPERATURE T5  ETC. FOR REMAINING LAYERS
C T1=TEMPERATURE AT TOP OF BEAM
C T9=TEMPERATURE AT BOTTOM OF BEAM
C ****START NEW LINE IN DATA FILE****
C M=NUMBER OF DAYS.
C J= NUMBER OF THERMOCOUPLESL.
C APMOM=APPLIED MOMENT.
C SPTC = SPECIFIC THERMAL CREEP.
C FCM= MODOLUS OF RUPTURE.
C MCR= CRACKING MOMENT.
   READ (1,*) B, D, DST, AST, NLA, FCU, FTU, EC, ES, ALPC, ALPS, M, J
   READ (1,*) D1, D2, D3, D4, D5, D6, D7, D8
   READ (1,*) APMOM
   S = M - 1
   DO 10 K = 1, M
10 READ (2,*) (T(K,N),N=1,J)
   DO 20 I = 1, NLA
20 CHECK(I) = 1.0
   NS = -10.0E+5
30 CONTINUE
   DO 140 K = 1, S
     DO 130 I = 1, NLA
       THICK = D / NLA * 1.0
       DLAY = THICK * (I - 0.5)
       DPLAY(I) = DLAY
       IF (DLAY .LE. D1) GO TO 40
       IF (DLAY .LE. D2) GO TO 50
       IF (DLAY .LE. D3) GO TO 60
       IF (DLAY .LE. D4) GO TO 70
```

```
      IF (DLAY .LE. D5) GO TO 80
      IF (DLAY .LE. D6) GO TO 90
      IF (DLAY .LE. D7) GO TO 100
      IF (DLAY .LE. D8) GO TO 110
      DPLAY(I) = DLAY
      TLAY(K) = T(K,10) + (T(K,9) - T(K,10)) * (D - DLAY) / (D - D8)
      GO TO 120
 40   TLAY(K) = T(K,2) + (T(K,1) - T(K,2)) * (D1 - DLAY) / D1
      GO TO 120
 50   TLAY(K) = T(K,3) + (T(K,2) - T(K,3)) * (D2 - DLAY) / (D2 - D1)
      GO TO 120
 60   TLAY(K) = T(K,4) + (T(K,3) - T(K,4)) * (D3 - DLAY) / (D3 - D2)
      GO TO 120
 70   TLAY(K) = T(K,5) + (T(K,4) - T(K,5)) * (D4 - DLAY) / (D4 - D3)
      GO TO 120
 80   TLAY(K) = T(K,6) + (T(K,5) - T(K,6)) * (D5 - DLAY) / (D5 - D4)
      GO TO 120
 90   TLAY(K) = T(K,7) + (T(K,6) - T(K,7)) * (D6 - DLAY) / (D6 - D5)
      GO TO 120
100   TLAY(K) = T(K,8) + (T(K,7) - T(K,8)) * (D7 - DLAY) / (D7 - D6)
      GO TO 120
110   TLAY(K) = T(K,9) + (T(K,8) - T(K,9)) * (D8 - DLAY) / (D8 - D7)
      GO TO 120
120   CONTINUE
      TEMP(I,K) = (5*(TLAY(K) + T(K,J)) + 19*(TLAY(K) + T(K + 1,J)))
     1     / 48
130   CONTINUE
140 CONTINUE
    ASUM = 0.0
    AYSUM = 0.0
    DO 150 I = 1, NLA
      AY = B * THICK * DPLAY(I) * CHECK(I)
      A = B * THICK * CHECK(I)
      ASUM = ASUM + A
      AYSUM = AYSUM + AY
150 CONTINUE
    AYSUM = AYSUM + AST * DST * ES / EC
    ASUM = ASUM + AST * ES / EC
    YBAR = AYSUM / ASUM
    R = ES / EC
    P = AST / (B*DST)
    X1 = DST * (-R*P + ((P*R)**2 + 2*R*P)**0.5)
    AC = B * D
    X2 = ((AC*D/2) + R*AST*DST) / (AC + R*AST)
    SI1 = (B*X1**3) / 3. + (AST*ES/EC) * (DST - X1) ** 2
    ECST = AST * (ES - EC) / EC
    SI2 = (B*D**3) / 12. + B * D * (X2 - 0.5*D) ** 2 + ECST * (X2 -
   1DST) ** 2
    FCM = -1.33 * FTU
    MCR = SI2 * FCM / (D - X2)
    SECTI = SI2 * (MCR/APMOM) ** 3 + SI1 * (1 - (MCR/APMOM)**3)
    DO 160 I = 1, NLA
160 APMST(I) = APMOM * (YBAR - THICK*(I - 0.5)) / SECTI
    DO 170 I = 1, NLA
      IF (CHECK(I) .LT. 0.1) GO TO 170
      IF (APMST(I) .GT. FTU) GO TO 170
      CHECK(I) = 0.0
170 CONTINUE
    NSUM = 0.0
    DO 180 I = 1, NLA
```

```
180 NSUM = NSUM + CHECK(I)
    IF (NSUM .EQ. NS) GO TO 190
    NS = NSUM
    GO TO 30
190 DO 280 K = 1, S
      READ (3,*) SPTC(K)
      TAXC(K) = 0.0
      TMCR(K) = 0.0
      IF (K .EQ. 1) GO TO 210
      DO 200 I = 1, NLA
        SN(I,K) = -SPTC(K) * TEMP(I,K) * MST(I,K)
200   CONTINUE
      GO TO 230
210   DO 220 I = 1, NLA
        MST(I,K) = APMST(I)
        SN(I,K) = -(SPTC(K)*TEMP(I,K)*MST(I,K))
220   CONTINUE
230   DO 240 I = 1, NLA
        TAXC(K) = TAXC(K) + SN(I,K) * EC * B * THICK * CHECK(I)
        TMCR(K) = TMCR(K) + SN(I,K) * EC * B * THICK * DPLAY(I) *
   1    CHECK(I)
240   CONTINUE
      STS(K) = SN(16,K) * ES
      AXTOT(K) = TAXC(K) + STS(K) * AST
      TMOM(K) = TMCR(K) + STS(K) * AST * DST
      CTMT(K) = 0.0
      DO 250 I = 1, NLA
        CAXST(I,K) = AXTOT(K) * CHECK(I) / ASUM
        TM(K) = CAXST(1,K) * B * THICK * CHECK(I) * DPLAY(I)
        CTMT(K) = CTMT(K) + TM(K)
250   CONTINUE
      CTMT(K) = CTMT(K) + CAXST(1,K) * DST * AST * ES / EC
      DO 260 I = 1, NLA
        CTMST(I,K) = (CTMT(K) - TMOM(K)) * (YBAR - THICK*(I - 0.5)) *
   1    CHECK(I) / SECTI
        SES(I,K) = (-CAXST(I,K) - CTMST(I,K) + SN(I,K)*EC)
260   CONTINUE
      DO 270 I = 1, NLA
        MST(I,K + 1) = (SES(I,K) + MST(I,K))
270   CONTINUE
280 CONTINUE
    DO 290 I = 1, NLA
      CRPS(I) = 0.0
      DO 290 K = 1, S
        CRP(I,K) = -(CAXST(1,K) + CTMST(I,K)) / EC
        CRPS(I) = CRPS(I) + CRP(I,K)
        CRPSM(I,K) = CRPS(I)
290 CONTINUE
    DO 300 K = 1, S
      DO 300 I = 1, NLA
        ESLN(I) = APMST(I) * CHECK(I) / EC
        TSN(I,K) = ESLN(I) + CRPSM(I,K)
300 CONTINUE
    CURVO = (ESLN(1) - ESLN(NS)) / (THICK*(NS - 1.))
    DO 310 K = 1, S
      CURV(K) = (TSN(1,K) - TSN(NS,K)) / (THICK*(NS - 1))
310 CONTINUE
    WRITE (6,320) CURVO
320 FORMAT (/, 'CURVATURE,1/R= ', E12.4)
    WRITE (6,330) (CURV(K),K=1,S)
```

```
330 FORMAT (/, 'CURVATURE,1/R= ', E12.4)
    WRITE (4,340)
340 FORMAT (//'APPLIED MOMENT STRESS')
    WRITE (4,350) (APMST(I),I=1,NLA)
350 FORMAT (F12.4)
    WRITE (4,360)
360 FORMAT (//'B D DST FTU EC ES ALPC ALPS ')
    WRITE (4,370) B, D, DST, FTU, EC, ES, ALPC, ALPS
370 FORMAT (8E20.5)
    WRITE (4,380)
380 FORMAT (//'NLA M J ')
    WRITE (4,390) NLA, M, J
390 FORMAT (3I2)
    STOP
    END
```

```
C     PROGRAM TO CALCULATE CURVATURE USING LEAST SQUARE FIT
C     I=NUMBER OF DAYS
C     K=DEMEC NUMBER
C     SI(N)=INITIAL STRAIN OF THE N DEMEC
C     SF(M,N)=STRAN OF THE N DEMEC ON THE M DAY
C     IK=1 EXPECTED VALUE OF CURVATURE
C       =2 THE HIGH RANGE OF CURVATURE
C       =3 THE LOWER RANGE OF CURVATURE
C       =5 SHRINKAGE CURVATURE
C     KM=6 EXP.6 ,NO SHRINKAGE
C     LM=1 TOP STRAN
C       =2 STRAIN AT THE STEEL LEVEL
C       =3 NEUTRAL AXIS POSITION
C       =4 DEFLECTION
C       =  ANY OTHER NUMBER GIVES CURVATURE RANGES
C     LI=1 HIGHER RANGE OF TOP STRAIN
C       =2 LOWER RANGE OF TOP STRAIN
C       =ANY OTHER NUMBER IS THE EXPECTED VALUE FOR TOP STRAIN
C     LL=1 HIGHER RANGE OF STRAIN AT STEEL LEVEL
C       =2 LOWER RANGE  OF STRAIN AT STEEL LEVEL
C       = ANY OTHER NUMBER GIVES THE EXPECTED VALUE FOR STRAIN
C        AT ST.L
C       TN=THE t DISTRIBUTION VALUE
      DIMENSION SI(100), SF(100,100), SN(100,100), SSTN(100),
     1          SSN(100),PN2(100),
     1          B(100), C(100), A(100), E(100), R1(100), R2(100),
     2          RA(100), SNSQ(100), SY(100), Q(100), F(100), T(100),
     3          H(100), R(100), SSD(100), P(100), H1(100), H2(100),
     4          DC(100), DM(100), R8(100), B0(100), U(100), WR1(100),
     5          WR2(100), G(100), S(100), W(100), PR1(100), R0(100),
     6          PR2(100), Y1(100), Y2(100), S1(100), S2(100),
     7          SE(100,100), R9(100), SU(100,100), TF(100), K3(100),
     8          F2(100), G3(100), ZR(100), R3(100), PN1(100),
     9          PT1(100), PT2(100), PS1(100), PS2(100), PD0(100),
     *          PD1(100), PD2(100), G4(100), E0(100), TC(100)
      READ (1,*) I, K, TI, V, IK, KM, LM, LI, LL, MN
      READ (1,*) (DC(N),N=1,K)
      READ (1,*) (SI(N),N=1,K)
      READ (1,*) (TF(M),M=1,I)
      READ (2,*) ((SF(M,N),N=1,K),M=1,I)
      DO 10 M = 1, I
        DO 10 N = 1, K
          SU(M,N) = (SF(M,N) - SI(N)) * .81E-05
          TC(M) = (TF(M) - TI) * 10.E-06
          SN(M,N) = SU(M,N) - TC(M)
   10 CONTINUE
      QS = 0.0
C      D=SUM OF X
      D = 0.0
      DO 20 N = 1, K
        D = D + DC(N)
   20 CONTINUE
      DO 30 M = 1, I
        SSTN(M) = 0.0
        DO 30 N = 1, K
          SSTN(M) = SSTN(M) + SN(M,N)
C       SSTN(M)=SUM OF Y FOR DAY M
   30 CONTINUE
      DO 40 M = 1, I
        SSN(M) = 0.0
```

```
          DO 40 N = 1, K
            SSN(M) = SSN(M) + DC(N) * SN(M,N)
C         SSN(M)=SUM OF XY FOR DAY M
   40   CONTINUE
C         SD=SUM OF X SQUARES
        SD = 0.0
        DO 50 N = 1, K
          SD = SD + DC(N) * DC(N)
   50   CONTINUE
        DO 60 M = 1, I
          R(M) = 0.0
          SNSQ(M) = 0.0
          DO 60 N = 1, K
            SNSQ(M) = SNSQ(M) + (SN(M,N)*SN(M,N))
   60   CONTINUE
        SX = SD - (D*D/K)
        READ (1,*) TN
C         RL=NUMBER OF DAYS FOR THE LOADED BEAMS.
        READ (1,*) RL
        DO 70 M = 1, I
          SY(M) = SNSQ(M) - (SSTN(M)*SSTN(M)/K)
C         B(M)= THE SLOPE OF THE LINE AT DAY M
          B(M) = (SSN(M) - D*SSTN(M)/K) / (SD - D**2/K)
          R3(M) = B(M) * SX ** .5 / SY(M) ** 0.5
C         C(M)=THE Y INTERCEPT ON DAY M
          C(M) = (SSTN(M)/K) - B(M) * D / K
          E(M) = (677233.30) * B(M)
          Q(M) = SY(M) - (B(M)*B(M)*SX)
          SSD(M) = Q(M) / (K - 2)
          QS = QS + SSD(M)
          F(M) = 4.303 * (SSD(M)/SX) ** 0.5
          F2(M) = -100 * (F(M)/B(M))
          R1(M) = B(M) - F(M)
          R2(M) = B(M) + F(M)
          Z = (D/K) * (D/K) / SX
          T(M) = 4.303 * ((((1.0/K) + Z)*SSD(M))**0.5)
          H1(M) = C(M) - T(M)
          H2(M) = C(M) + T(M)
          G(M) = -C(M) / B(M)
          WR1(M) = H2(M) / R2(M)
          WR2(M) = H1(M) / R1(M)
          U(M) = -WR1(M) - G(M)
          G3(M) = 100 * (U(M)/G(M))
          S(M) = C(M) + (200*B(M))
          W(M) = 4.303 * (((1.0/K + ((200 - D/K)**2)/SX)*SSD(M))**0.5)
          PR1(M) = S(M) - W(M)
          PR2(M) = S(M) + W(M)
          Y1(M) = V * PR1(M)
          Y2(M) = V * PR2(M)
          G4(M) = C(M) + (35*B(M))
          S1(M) = V * H1(M)
          S2(M) = V * H2(M)
          ZR(M) = E(M) / E(1)
   70   CONTINUE
        QSA = QS / RL
        PN = TN * (QSA/SX) ** 0.5
C         S(M) IS STRAIN AT TOP FACE
        PT = TN * ((1.0/K + ((200. - D/K)**2)/SX)*QSA) ** 0.5
        PS = TN * ((1.0/K + ((35. - D/K)**2)/SX)*QSA) ** 0.5
        DO 80 M = 1, I
```

```
      PN1(M) = B(M) - PN
      PN2(M) = B(M) + PN
      PT1(M) = S(M) - PT
      PT2(M) = S(M) + PT
      PS1(M) = G4(M) - PS
      PS2(M) = G4(M) + PS
 80 CONTINUE
    KK = I - 3
    IF (LM .EQ. 1) GO TO 770
    IF (LM .EQ. 2) GO TO 860
    IF (LM .EQ. 3) GO TO 950
    IF (KM .EQ. 6) GO TO 560
    IF (IK .EQ. 1) GO TO 410
    IF (IK .EQ. 2) GO TO 110
    IF (IK .EQ. 3) GO TO 260
    DO 100 M = 1, I
      WRITE (6,90) B(M)
 90   FORMAT (E20.5)
100 CONTINUE
    GO TO 980
110 DO 170 M = 1, 3
      IF (LM .EQ. 4) GO TO 130
      WRITE (6,120) PN1(M)
120   FORMAT (E20.5)
130   IF (MM .EQ. 1) GO TO 140
      PD1(M) = (677233.3) * PN1(M)
      GO TO 150
140   PD1(M) = (630833.3) * PN1(M)
150   WRITE (6,160) PD1(M)
160   FORMAT (E20.5)
170 CONTINUE
    DO 250 M = 1, KK
      READ (5,*) R8(M)
      IF (R8(M) .LE. 0) GO TO 180
      RO(M) = PN1(M + 3) + R8(M)
      GO TO 190
180   RO(M) = PN1(M + 3) - R8(M)
      IF (LM .EQ. 4) GO TO 210
190   WRITE (6,200) RO(M)
200   FORMAT (E20.5)
      IF (MN .EQ. 1) GO TO 220
210   PDO(M) = (677233.3) * RO(M)
      GO TO 230
220   PDO(M) = (630833.3) * RO(M)
230   WRITE (6,240) PDO(M)
240   FORMAT (E20.5)
250 CONTINUE
    GO TO 980
260 DO 320 M = 1, 3
      IF (LM .EQ. 4) GO TO 280
      WRITE (6,270) PN2(M)
270   FORMAT (E20.5)
280   IF (MN .EQ. 1) GO TO 290
      PD2(M) = (677233.3) * PN2(M)
      GO TO 300
290   PD2(M) = (630833.3) * PN2(M)
300   WRITE (6,310) PD2(M)
310   FORMAT (E20.5)
320 CONTINUE
    DO 400 M = 1, KK
```

```
      READ (5,*) R9(M)
      IF (R9(M) .LE. 0) GO TO 330
      RO(M) = PN2(M + 3) + R9(M)
      GO TO 340
330   RO(M) = PN2(M + 3) - R9(M)
      IF (LM .EQ. 4) GO TO 360
340   WRITE (6,350) RO(M)
350   FORMAT (E20.5)
360   IF (MN .EQ. 1) GO TO 370
      PDO(M) = (677233.3) * RO(M)
      GO TO 380
370   PDO(M) = (630833.3) * RO(M)
380   WRITE (6,390) PDO(M)
390   FORMAT (E20.5)
400 CONTINUE
    GO TO 980
410 DO 470 M = 1, 3
      IF (LM .EQ. 4) GO TO 430
      WRITE (6,420) B(M)
420   FORMAT (E20.5)
430   IF (MN .EQ. 1) GO TO 440
      E(M) = (677233.3) * B(M)
      GO TO 450
440   E(M) = (630833.3) * B(M)
450   WRITE (6,460) E(M)
460   FORMAT (E20.5)
470 CONTINUE
    DO 550 M = 1, KK
      READ (5,*) RA(M)
      IF (RA(M) .LE. 0) GO TO 480
      BO(M) = B(M + 3) + RA(M)
      GO TO 490
480   BO(M) = B(M + 3) - RA(M)
      IF (LM .EQ. 4) GO TO 510
490   WRITE (6,500) BO(M)
500   FORMAT (E20.5)
510   IF (MN .EQ. 1) GO TO 520
      EO(M) = (677233.3) * BO(M)
      GO TO 530
520   EO(M) = (630833.3) * BO(M)
530   WRITE (6,540) EO(M)
540   FORMAT (E20.5)
550 CONTINUE
    GO TO 980
560 IF (IK .EQ. 2) GO TO 630
    IF (IK .EQ. 3) GO TO 700
    DO 620 M = 1, I
      IF (LM .EQ. 4) GO TO 580
      WRITE (6,570) B(M)
570   FORMAT (E20.5)
580   IF (MN .EQ. 1) GO TO 590
      E(M) = (677233.3) * B(M)
      GO TO 600
590   E(M) = (630833.3) * B(M)
600   WRITE (6,610) E(M)
610   FORMAT (E20.5)
620 CONTINUE
    GO TO 980
630 DO 690 M = 1, I
      IF (LM .EQ. 4) GO TO 650
```

```
      WRITE (6,640) PN1(M)
640   FORMAT (E20.5)
650   IF (MN .EQ. 1) GO TO 660
      PD1(M) = (677233.3) * PN1(M)
      GO TO 670
660   PD1(M) = (630833.3) * PN1(M)
670   WRITE (6,680) PD1(M)
680   FORMAT (E20.5)
690 CONTINUE
    GO TO 980
700 DO 760 M = 1, I
      IF (LM .EQ. 4) GO TO 720
      WRITE (6,710) PN2(M)
710   FORMAT (E20.5)
720   IF (MN .EQ. 1) GO TO 730
      PD2(M) = (677233.3) * PN2(M)
      GO TO 740
730   PD2(M) = (630833.3) * PN2(M)
740   WRITE (6,750) PD2(M)
750   FORMAT (E20.5)
760 CONTINUE
770 DO 790 M = 1, I
      IF (LI .EQ. 1) GO TO 800
      IF (LI .EQ. 2) GO TO 830
      WRITE (6,780) S(M)
780   FORMAT (E20.5)
790 CONTINUE
    GO TO 980
800 DO 820 M = 1, I
      WRITE (6,810) PT1(M)
810   FORMAT (E20.5)
820 CONTINUE
    GO TO 980
830 DO 850 M = 1, I
      WRITE (6,840) PT2(M)
840   FORMAT (E20.5)
850 CONTINUE
    GO TO 980
860 IF (LL .EQ. 1) GO TO 890
    IF (LL .EQ. 2) GO TO 920
    DO 880 M = 1, I
      WRITE (6,870) G4(M)
870   FORMAT (E20.5)
880 CONTINUE
    GO TO 980
890 DO 910 M = 1, I
      WRITE (6,900) PS1(M)
900   FORMAT (E20.5)
910 CONTINUE
    GO TO 980
920 DO 940 M = 1, I
      WRITE (6,930) PS2(M)
930   FORMAT (E20.5)
940 CONTINUE
950 DO 970 M = 1, I
      WRITE (6,960) G(M)
960   FORMAT (E20.5)
970 CONTINUE
980 STOP
    END
```

```
(    1)  TITLE TEMP PROFILES, D=.2  0800-1200                                .6
(    2)  NODES
(    3)  AXIS.NUMBER=1
(    4)  NODE X     Y
(    5)  1    0.00 -.1
(    6)  2    0.05 -.1
(    7)  3    0.1  -.1
(    8)  4    0.00 0.00
(    9)  5    0.05 0.00
(   10)  6    0.1  0.00
(   11)  7    0.00 0.05
(   12)  8    0.1  .05
(   13)  9    0.00 0.1
(   14)  10   0.05 0.1
(   15)  11   0.1  0.1
(   16)  12   0.00 0.15
(   17)  13   0.1  0.15
(   18)  14   0.00 0.2
1                                                          PAFEC PAGE     2
(   19)  15   0.05 0.2
(   20)  16   0.1  0.2
(   21)  17   .00  0.3
(   22)  18   0.05 0.3
(   23)  19   0.1  0.3
(   24)  ELEMENTS
(   25)  NUMBER ELEM     PROP TOPOLOGY
(   26)  1      39310    1    1 3 4 6 2 5
(   27)  2      39210    2    4 6 9 11 5 7 8 10
(   28)  3      39210    2    9 11 14 16 10 12 13 15
(   29)  4      39310    3    19 17 16 14 18 15
(   30)  PLATES.AND.SHELLS
(   31)  PLATE MATERIAL THICKNESS
(   32)  1     11       1.0
(   33)  2     12       1.0
(   34)  3     13       1.0
(   35)  MATERIAL
(   36)  MATE RO     K      SH
(   37)  11   0.0    9.0    0.0
(   38)  12   2400   1.4    960
(   39)  13   0.0    23.0   0.0
(   40)  TEMP
(   41)  TEMP   START   FINISH STEP
(   42)  32.0    4      16     1
(   43)  UNSTEADY.THERMAL.TIMES
(   44)  TIME.STEP  MAX.TIME   NUMBER.
(   45)  1800       14400      1
(   46)  THERMAL.SHOCK
(   47)  NODE  TEMP.TIME.LIST
(   48)  1     32.0  0.0   56.0  14400
(   49)  2     32.0  0.0   56.0  14400
(   50)  3     32.0  0.0   56.0  14400
(   51)  4     32.0  0.0   48.0  14400
(   52)  5     32.0  0.0   48.0  14400
```

```
(    53)  6     32.0  0.0   48.0  14400
(    54)  17    32.0  0.0   56.0  14400
(    55)  18    32.0  0.0   56.0  14400
(    56)  19    32.0  0.0   56.0  14400
(    57)  NODAL.FLUX.SHOCK
(    58)  NODE  FLUX.TIME.LIST.
(    59)  14    5.1   0.0   10.22 14400
(    60)  15    20.4  0.0   40.88 14400
(    61)  16    5.1   0.0   10.22 14400
(    62)  CONTROL
(    63)  CALC.TRANS.TEMP
(    64)  SAVE.TEMPS.TO.STORE8
(    65)  ECON
(    66)  CONTROL.END
(    67)  END.OF.DATA.
0END OF DATA          0 ERRORS
```


NO ERRORS OR WARNINGS IN VALIDATION

DATA MODULES STORED ON THE BACKING STORE FILE

ELEMENTS

NUMBER	GROUP.	ELEMEN	PROPER	INE	TOPOLOGY							
1	1	39310	1	6	1	3	4	6	2	5		
2	1	39210	2	8	4	6	9	11	5	7	8	10
3	1	39210	2	8	9	11	14	16	10	12	13	15
4	1	39310	3	6	19	17	16	14	18	15		

GLOBAL COORDINATES

NODE	X	Y	Z
1	0.0000	-0.1000	0.0000
3	0.1000	-0.1000	0.0000
5	0.0500	0.0000	0.0000
7	0.0000	0.0500	0.0000
9	0.0000	0.1000	0.0000
11	0.1000	0.1000	0.0000
13	0.1000	0.1500	0.0000
15	0.0500	0.2000	0.0000
17	0.0000	0.3000	0.0000
19	0.1000	0.3000	0.0000

NODE	X	Y	Z
2	0.0500	-0.1000	0.0000
4	0.0000	0.0000	0.0000
6	0.1000	0.0000	0.0000
8	0.1000	0.0500	0.0000
10	0.0500	0.1000	0.0000
12	0.0000	0.1500	0.0000
14	0.0000	0.2000	0.0000
16	0.1000	0.2000	0.0000
18	0.0500	0.3000	0.0000

MATERIAL

MATERI	E	NU	RO	ALPHA	MU	K	SH	BULK.MODULUS
1	0.209E 12	0.3000	7800.0000	0.110E-04	0.500E-02	48.0000	452.0000	0.174E 12
2	0.195E 12	0.3000	7700.0000	0.120E-04	0.500E-02	24.5000	440.0000	0.162E 12
3	0.125E 12	0.2500	7100.0000	0.120E-04	0.500E-02	54.0000	586.0000	0.833E 11
4	0.685E 11	0.3300	2695.0000	0.240E-04	0.0100	238.0000	900.0000	0.672E 11
5	0.700E 11	0.3300	2800.0000	0.220E-04	0.0100	190.0000	879.0000	0.686E 11
6	0.750E 11	0.3300	3000.0000	0.200E-04	0.0100	180.0000	858.0000	0.735E 11
7	0.110E 12	0.3000	4533.0000	0.850E-05	0.500E-02	168.6000	582.0000	0.132E 12
8	0.610E 11	0.2500	2224.0000	0.720E-05	0.0200	0.8400	795.0000	0.915E 11
9	0.345E 10	0.4500	1230.0000	0.600E-04	0.0500	0.2000	800.0000	0.345E 11
10	0.300E 11	0.2000	2400.0000	0.100E-04	0.0500	1.5000	653.0000	0.167E 11
11	0.0000	0.0000	0.0000	0.0000	0.0000	9.0000	0.0000	0.0000
12	0.0000	0.0000	2400.0000	0.0000	0.0000	1.4000	960.0000	0.0000
13	0.0000	0.0000	0.0000	0.0000	0.0000	23.0000	0.0000	0.0000

NODAL.FLUX.SHOCK

NODE.N	FLUX.TIME.LI			
14	5.1000	0.0000	10.2200	0.144E 05
15	20.4000	0.0000	40.8800	0.144E 05
16	5.1000	0.0000	10.2200	0.144E 05

PLATES

PLATE.	MATERI	THICKN	FACING	OUTER.	RAD1	RAD2
1	11	1.0000	0	0.0000	0.0000	0.0000
2	12	1.0000	0	0.0000	0.0000	0.0000
3	13	1.0000	0	0.0000	0.0000	0.0000

TEMPERATURE

LOAD.C	TEMPER	START	FINISH	STEP	LIST.OF.NODE
1	32.0000	4	16	1	0

THERMAL.SHOCK

NODE.N	TEMP.TIME.LI			
1	32.0000	0.0000	56.0000	0.144E 05
2	32.0000	0.0000	56.0000	0.144E 05
3	32.0000	0.0000	56.0000	0.144E 05
4	32.0000	0.0000	48.0000	0.144E 05
5	32.0000	0.0000	48.0000	0.144E 05
6	32.0000	0.0000	48.0000	0.144E 05
17	32.0000	0.0000	56.0000	0.144E 05
18	32.0000	0.0000	56.0000	0.144E 05
19	32.0000	0.0000	56.0000	0.144E 05

UNSTEADY.THERMAL.TIMES

TIME.S	MAX.TI	NUMBER	ITABLE
1800.0000	0.144E 05	1	0

NO ERRORS OR WARNINGS IN GEOMETRY CHECK

E S T I M A T E O F B A S E A N D F I L E S I Z E R E Q U I R E M E N T S (A)

NOTE – (1) AN ASTERISK * DENOTES AN OVERESTIMATE

PHASE	BASE/FILE	SINGLE PRECISION NUMBERS.
3	BASE	458
4	BASE	5474*

C O N T E N T S

DATA MODULES STORED ON THE BACKING STORE FILE 4

ESTIMATE OF BASE AND FILE SIZE REQUIREMENTS (A) 6

NO ERRORS OR WARNINGS IN THIS PHASE

**** MAXIMUM SIZE OF BASE IN THIS PHASE WAS 477 WORDS ****

+++ END OF PHASE 1 +++

PHASE NO. 7
STARTS HERE

TITLE TEMP PROFILES, D=.2 0800-1200

****
* *
* THERMAL ANALYSIS *
* *
* DOUBLE PRECISION SOLUTION *
* *
* TRANSIENT SOLUTION WITH INITIAL TEMPERATURE FIELD *
* TO BE READ FROM THE TEMPERATURE MODULE *
* *
****

INITIAL TEMPERATURE FIELD

TEMPERATURES AT STRUCTURAL NODES

NODE NUMBER	GLOBAL CO-ORDINATES X	Y	Z	TEMPERATURE

1	0.0	-0.100	0.0	0.0
2	0.050	-0.100	0.0	0.0
3	0.100	-0.100	0.0	0.0
4	0.0	0.0	0.0	32.000
5	0.050	0.0	0.0	32.000
6	0.100	0.0	0.0	32.000
7	0.0	0.050	0.0	32.000
8	0.100	0.050	0.0	32.000
9	0.0	0.100	0.0	32.000
10	0.050	0.100	0.0	32.000
11	0.100	0.100	0.0	32.000
12	0.0	0.150	0.0	32.000
13	0.100	0.150	0.0	32.000
14	0.0	0.200	0.0	32.000
15	0.050	0.200	0.0	32.000
16	0.100	0.200	0.0	32.000
17	0.0	0.300	0.0	0.0
18	0.050	0.300	0.0	0.0
19	0.100	0.300	0.0	0.0

1 PAFEC PAGE 17

SPECIFIED HEAT FLUXES FOR TRANSIENT CALCULATION AT TIME 0.0

NODE	HEAT FLUX	FLUX GRADIENT

1 PAFEC PAGE 18

SPECIFIED TEMPERATURES FOR TRANSIENT CALCULATION AT TIME 1800.

NODE	TEMPERATURE	TEMPERATURE GRADIENT
1	35.0	0.167E-02
2	35.0	0.167E-02
3	35.0	0.167E-02
4	34.0	0.111E-02
5	34.0	0.111E-02
6	34.0	0.111E-02
17	35.0	0.167E-02
18	35.0	0.167E-02
19	35.0	0.167E-02

1 PAFEC PAGE 19

SPECIFIED HEAT FLUXES FOR TRANSIENT CALCULATION AT TIME 1800.

NODE	HEAT FLUX	FLUX GRADIENT

14	5.74	0.356E-03
15	23.0	0.142E-02
16	5.74	0.356E-03

T I M E = 1800.000

TEMPERATURES AT STRUCTURAL NODES

NODE	TEMPERATURE	NODE	TEMPERATURE	NODE	TEMPERATURE	NODE	TEMPERATURE	NODE	TEMPERATURE
1	35.000	2	35.000	3	35.000	4	34.000	5	34.000
6	34.000	7	32.236	8	32.236	9	32.458	10	32.458
11	32.458	12	32.833	13	32.833	14	40.219	15	40.219
16	40.219	17	35.000	18	35.000	19	35.000		

SPECIFIED TEMPERATURES FOR TRANSIENT CALCULATION AT TIME 3600.

NODE	TEMPERATURE	TEMPERATURE GRADIENT
1	38.0	0.167E-02
2	38.0	0.167E-02
3	38.0	0.167E-02
4	36.0	0.111E-02
5	36.0	0.111E-02
6	36.0	0.111E-02
17	38.0	0.167E-02
18	38.0	0.167E-02
19	38.0	0.167E-02

SPECIFIED HEAT FLUXES FOR TRANSIENT CALCULATION AT TIME 3600.

NODE	HEAT FLUX	FLUX GRADIENT
14	6.38	0.356E-03
15	25.5	0.142E-02
16	6.38	0.356E-03

T I M E = 3600.000

TEMPERATURES AT STRUCTURAL NODES

NODE	TEMPERATURE	NODE	TEMPERATURE	NODE	TEMPERATURE	NODE	TEMPERATURE	NODE	TEMPERATURE
1	38.000	2	38.000	3	38.000	4	36.000	5	36.000
6	36.000	7	33.137	8	33.137	9	32.528	10	32.528
11	32.528	12	35.457	13	35.457	14	41.672	15	41.672
16	41.672	17	38.000	18	38.000	19	38.000		

1 PAFEC PAGE 24

SPECIFIED TEMPERATURES FOR TRANSIENT CALCULATION AT TIME 5400.

NODE	TEMPERATURE	TEMPERATURE GRADIENT
1	41.0	0.167E-02
2	41.0	0.167E-02
3	41.0	0.167E-02
4	38.0	0.111E-02
5	38.0	0.111E-02
6	38.0	0.111E-02
17	41.0	0.167E-02
18	41.0	0.167E-02
19	41.0	0.167E-02

1 PAFEC PAGE 25

SPECIFIED HEAT FLUXES FOR TRANSIENT CALCULATION AT TIME 5400.

NODE	HEAT FLUX	FLUX GRADIENT
14	7.02	0.356E-03
15	28.1	0.142E-02
16	7.02	0.356E-03

1 PAFEC PAGE 26

T I M E = 5400.000

TEMPERATURES AT STRUCTURAL NODES

NODE	TEMPERATURE	NODE	TEMPERATURE	NODE	TEMPERATURE	NODE	TEMPERATURE	NODE	TEMPERATURE
1	41.000	2	41.000	3	41.000	4	38.000	5	38.000
6	38.000	7	34.289	8	34.289	9	34.235	10	34.235
11	34.235	12	37.175	13	37.175	14	45.757	15	45.757

16	45.757	17	41.000	18	41.000	19	41.000

SPECIFIED TEMPERATURES FOR TRANSIENT CALCULATION AT TIME 7200.

NODE	TEMPERATURE	TEMPERATURE GRADIENT
1	44.0	0.167E-02
2	44.0	0.167E-02
3	44.0	0.167E-02
4	40.0	0.111E-02
5	40.0	0.111E-02
6	40.0	0.111E-02
17	44.0	0.167E-02
18	44.0	0.167E-02
19	44.0	0.167E-02

SPECIFIED HEAT FLUXES FOR TRANSIENT CALCULATION AT TIME 7200.

NODE	HEAT FLUX	FLUX GRADIENT
14	7.66	0.356E-03
15	30.6	0.142E-02
16	7.66	0.356E-03

T I M E = 7200.000

TEMPERATURES AT STRUCTURAL NODES

NODE	TEMPERATURE	NODE	TEMPERATURE	NODE	TEMPERATURE	NODE	TEMPERATURE	NODE	TEMPERATURE
1	44.000	2	44.000	3	44.000	4	40.000	5	40.000
6	40.000	7	35.904	8	35.904	9	35.587	10	35.587
11	35.587	12	39.568	13	39.568	14	48.557	15	48.557
16	48.557	17	44.000	18	44.000	19	44.000		

SPECIFIED TEMPERATURES FOR TRANSIENT CALCULATION AT TIME 9000.

NODE	TEMPERATURE	TEMPERATURE GRADIENT

1	47.0	0.167E-02
2	47.0	0.167E-02
3	47.0	0.167E-02
4	42.0	0.111E-02
5	42.0	0.111E-02
6	42.0	0.111E-02
17	47.0	0.167E-02
18	47.0	0.167E-02
19	47.0	0.167E-02

1 PAFEC PAGE 31

SPECIFIED HEAT FLUXES FOR TRANSIENT CALCULATION AT TIME 9000.

NODE	HEAT FLUX	FLUX GRADIENT
14	8.30	0.356E-03
15	33.2	0.142E-02
16	8.30	0.356E-03

1 PAFEC PAGE 32

T I M E = 9000.000

TEMPERATURES AT STRUCTURAL NODES

NODE	TEMPERATURE	NODE	TEMPERATURE	NODE	TEMPERATURE	NODE	TEMPERATURE	NODE	TEMPERATURE
1	47.000	2	47.000	3	47.000	4	42.000	5	42.000
6	42.000	7	37.620	8	37.620	9	37.545	10	37.545
11	37.545	12	41.869	13	41.869	14	52.132	15	52.132
16	52.132	17	47.000	18	47.000	19	47.000		

1 PAFEC PAGE 33

SPECIFIED TEMPERATURES FOR TRANSIENT CALCULATION AT TIME 0.1080E+05

NODE	TEMPERATURE	TEMPERATURE GRADIENT
1	50.0	0.167E-02
2	50.0	0.167E-02
3	50.0	0.167E-02
4	44.0	0.111E-02
5	44.0	0.111E-02
6	44.0	0.111E-02
17	50.0	0.167E-02
18	50.0	0.167E-02
19	50.0	0.167E-02

1 SPECIFIED HEAT FLUXES FOR TRANSIENT CALCULATION AT TIME 0.1080E+05

NODE	HEAT FLUX	FLUX GRADIENT
14	8.94	0.356E-03
15	35.8	0.142E-02
16	8.94	0.356E-03

1 T I M E = 0800.000

TEMPERATURES AT STRUCTURAL NODES

NODE	TEMPERATURE	NODE	TEMPERATURE	NODE	TEMPERATURE	NODE	TEMPERATURE	NODE	TEMPERATURE
1	50.000	2	50.000	3	50.000	4	44.000	5	44.000
6	44.000	7	39.522	8	39.522	9	39.511	10	39.511
11	39.511	12	44.475	13	44.475	14	55.446	15	55.446
16	55.446	17	50.000	18	50.000	19	50.000		

1 SPECIFIED TEMPERATURES FOR TRANSIENT CALCULATION AT TIME 0.1260E+05

NODE	TEMPERATURE	TEMPERATURE GRADIENT
1	53.0	0.167E-02
2	53.0	0.167E-02
3	53.0	0.167E-02
4	46.0	0.111E-02
5	46.0	0.111E-02
6	46.0	0.111E-02
17	53.0	0.167E-02
18	53.0	0.167E-02
19	53.0	0.167E-02

1 SPECIFIED HEAT FLUXES FOR TRANSIENT CALCULATION AT TIME 0.1260E+05

NODE	HEAT FLUX	FLUX GRADIENT

14	9.58	0.356E-03
15	38.3	0.142E-02
16	9.58	0.356E-03

T I M E = 2600.000

TEMPERATURES AT STRUCTURAL NODES

NODE	TEMPERATURE	NODE	TEMPERATURE	NODE	TEMPERATURE	NODE	TEMPERATURE	NODE	TEMPERATURE
1	53.000	2	53.000	3	53.000	4	46.000	5	46.000
6	46.000	7	41.507	8	41.506	9	41.734	10	41.734
11	41.734	12	47.156	13	47.156	14	59.034	15	59.034
16	59.034	17	53.000	18	53.000	19	53.000		

SPECIFIED TEMPERATURES FOR TRANSIENT CALCULATION AT TIME 0.1440E+05

NODE	TEMPERATURE	TEMPERATURE GRADIENT
1	56.0	0.167E-02
2	56.0	0.167E-02
3	56.0	0.167E-02
4	48.0	0.111E-02
5	48.0	0.111E-02
6	48.0	0.111E-02
17	56.0	0.167E-02
18	56.0	0.167E-02
19	56.0	0.167E-02

SPECIFIED HEAT FLUXES FOR TRANSIENT CALCULATION AT TIME 0.1440E+05

NODE	HEAT FLUX	FLUX GRADIENT
14	10.2	0.356E-03
15	40.9	0.142E-02
16	10.2	0.356E-03

T I M E = 4400.000

TEMPERATURES AT STRUCTURAL NODES

NODE	TEMPERATURE	NODE	TEMPERATURE	NODE	TEMPERATURE	NODE	TEMPERATURE	NODE	TEMPERATURE
1	56.000	2	56.000	3	56.000	4	48.000	5	48.000
6	48.000	7	43.589	8	43.589	9	44.039	10	44.039
11	44.039	12	50.002	13	50.002	14	62.604	15	62.604
16	62.604	17	56.000	18	56.000	19	56.000		

C O N T E N T S

NO ERRORS OR WARNINGS IN THIS PHASE

**** MAXIMUM SIZE OF BASE IN THIS PHASE WAS 4757 WORDS ****

+++ END OF PHASE 7 +++

SYSTEM LEVEL 5.2
JUNE 1984

PHASE NO. 9
STARTS HERE

TITLE TEMP PROFILES, D=.2 0800-1200

DEFAULT STRESS.ELEMENTS MODULE CREATED.
SUBROUTINE R89010 ISOPARAMETRIC THERMAL DERIVATIVE ROUTINE
CALCULATES MAXIMUM GRADIENT IN PLANE
ALPHA IS THE ANGLE OF MAX. GRAD. MEASURED + TO THE ELEMENT Y-AXIS FROM ELEMENT X AXIS
BETA IS THE ANGLE RELATIVE TO THE GLOBAL X-AXIS AND IS SET TO 9999.0 IF THE ELEMENT IS NOT IN THE GLOBAL XY PLANE

ELE NO.	TEMPERATURE VALUE	MAXIMUM GRADIENT	ANGLE ALPHA	ANGLE BETA	DERIVATIVES W.R.T. GLOBAL X-AXIS	DERIVATIVES W.R.T. GLOBAL Y-AXIS	GLOBAL COORDINATES X	Y	Z	
2	0.4000E+01	0.9017E+07	240.84	60.84	-0.4393E+07	-0.7875E+07	0.0	0.0	0.0	4
2	-0.2570E+06	0.5853E+07	-24.28	-24.28	0.5335E+07	-0.2406E+07	0.0	0.0500	0.0	5
2	-0.2406E+06	0.1542E+08	11.45	11.45	0.1511E+08	0.3062E+07	0.0	0.1000	0.0	6
2	-0.1669E+06	0.2588E+07	208.09	28.09	-0.2284E+07	-0.1219E+07	0.0500	0.0	0.0	7
2	-0.8985E+05	0.4508E+07	72.55	72.55	0.1352E+07	0.4301E+07	0.0500	0.0500	0.0	-2
2	0.2632E+06	0.1104E+08	62.84	62.84	0.5038E+07	0.9820E+07	0.0500	0.1000	0.0	8
2	-0.2283E+06	0.6781E+06	255.12	75.12	-0.1741E+06	-0.6553E+06	0.1000	0.0	0.0	9
2	-0.1219E+06	0.5575E+07	118.17	-61.83	-0.2632E+07	0.4915E+07	0.1000	0.0500	0.0	10
2	0.2632E+06	0.1163E+08	115.66	-64.34	-0.5038E+07	0.1049E+08	0.1000	0.1000	0.0	11
3	-0.2406E+06	0.1613E+08	20.40	20.40	0.1511E+08	0.5622E+07	0.0	0.1000	0.0	9
3	-0.3993E+05	0.7503E+07	18.71	18.71	0.7107E+07	0.2406E+07	0.0	0.1500	0.0	10
3	0.7000E+01	0.1855E+07	-25.85	-25.85	0.1669E+07	-0.8089E+06	0.0	0.2000	0.0	11
3	0.2632E+06	0.5416E+07	-21.52	-21.52	0.5038E+07	-0.1986E+07	0.0500	0.1000	0.0	12
3	0.1477E+06	0.2662E+07	-81.37	-81.37	0.3994E+06	-0.2632E+07	0.0500	0.1500	0.0	-3
3	0.1500E+02	0.3677E+07	243.01	63.01	-0.1669E+07	-0.3277E+07	0.0500	0.2000	0.0	13
3	0.2632E+06	0.8009E+07	231.02	51.02	-0.5038E+07	-0.6226E+07	0.1000	0.1000	0.0	14
3	0.1000E+02	0.7635E+07	214.29	34.29	-0.6308E+07	-0.4301E+07	0.1000	0.1500	0.0	15
3	-0.1669E+06	0.5543E+07	205.38	25.38	-0.5008E+07	-0.2376E+07	0.1000	0.2000	0.0	16

UNAVERAGED STRESSES FOR ELEMENTS WRITTEN TO BLOCKS   2 TO   2
OF THE STRESS FILE

AVERAGED STRESSES FOR NODES WRITTEN TO BLOCKS   3 TO   3
OF THE STRESS FILE

C O N T E N T S

NO ERRORS OR WARNINGS IN THIS PHASE

**** MAXIMUM SIZE OF BASE IN THIS PHASE WAS   4550 WORDS ****

+++ END OF PHASE 9 +++